Phylogeny, paleobiogeography, and paleophysiology of the Triassic dicynodonts (Therapsida, Anomodontia) : contributions of the Laotian and Moroccan forms

Chloé Olivier

▶ **To cite this version:**

Chloé Olivier. Phylogeny, paleobiogeography, and paleophysiology of the Triassic dicynodonts (Therapsida, Anomodontia) : contributions of the Laotian and Moroccan forms. Paleontology. Sorbonne Université, 2020. English. NNT : 2020SORUS399 . tel-03590277

HAL Id: tel-03590277
https://theses.hal.science/tel-03590277v1

Submitted on 27 Feb 2022

HAL is a multi-disciplinary open access archive for the deposit and dissemination of scientific research documents, whether they are published or not. The documents may come from teaching and research institutions in France or abroad, or from public or private research centers.

L'archive ouverte pluridisciplinaire **HAL**, est destinée au dépôt et à la diffusion de documents scientifiques de niveau recherche, publiés ou non, émanant des établissements d'enseignement et de recherche français ou étrangers, des laboratoires publics ou privés.

Sorbonne Université

ED 398 - Géosciences, Ressources Naturelles et Environnement

Centre de Recherche en Paléontologie - Paris / Equipe Phylogénie et diversification des métazoaires

Phylogeny, paleobiogeography, and paleophysiology of the Triassic dicynodonts (Therapsida, Anomodontia)

Contributions of the Laotian and Moroccan forms

Par Chloé OLIVIER

Thèse de doctorat de Paléontologie

Dirigée par Jorge CUBO et Nour-Eddine JALIL

Présentée et soutenue publiquement le 25 février 2020

Devant un jury composé de :

Botha-Brink Jennifer, Professeure, Rapporteure

Kammerer Christian F., Research Curator of Paleontology, Rapporteur

Vignes-Lebbe Régine, Professeure, Examinatrice

Fröbisch Jörg, Professeur, Examinateur

Laurin Michel, Directeur de recherche, Examinateur

Except where otherwise noted, this work is licensed under http://creativecommons.org/licenses/by-nc-nd/3.0/

("*There are some things that it is better to begin than to refuse, even though the end may be dark*.") (J.R.R. Tolkien)

"*Happiness is when what you think, what you say, and what you do are in harmony.*" (Mahatma Gandhi)

ACKNOWLEDGMENTS

Firslty, I extend my gratitude to my supervisors Prof. Jorge Cubo and Prof. Nour-Eddine Jalil, without whom, my PhD would have not been proposed. I met Nour-Eddine as an undergraduate when I was initiated to the vast world of paleontology and discovered a strong passion for these seemingly strange animals that are the dicynodonts. Jorge largely participated in my introduction to the complex and fascinating field of bone histology. I thank them for their encouragement, support, and driving me on to do my best. They enabled me to be self-reliant in my work pushing me to always argue my opinion.

Funding was also a very important part to the success of this PhD, so I am very grateful to my doctoral school for accepting to finance my PhD project, and my two laboratories the Institut des Sciences de la Terre de Paris (ISTeP, Paris) and Centre de Recherche Paléontologie – Paris (CR2P), which funded most of my travels to visit different dicynodont collections and to participate to the congress IMERP (Lesvos, Greece, 2017). I also thank the GDRI PalBioDiv SEA project, the association Société des Amis du Muséum, and the funded project SYNTHESYS for their supplementary financial supports.

For helping me with the administrative complexity and the organisation of missions, I thank A. Bastos, S. Colas, M.J. Queyroy, L. Pastor, D. Tristani, M. Lages, and E. Tourneur.

Thanks to many curators who welcomed me in the different institutions: E. Butler (National Museum, Bloemfontein, South Africa), J. D. Cundiff (Museum of Comparative Zoology, Cambridge, Massachusetts, U.S.A.), S. Chapman (Natural History Museum, London, United Kingdom), B. Zipfel (Evolutionary Studies Institute, Johannesburg, South Africa), C. Mehling (American Museum of Natural History, New York City, New York, U.S.A), J. Liu (Institute of Vertebrate Paleontology and Paleoanthropology, Beijing, China), and the Ministry of Information and Culture of Laos P.D.R. (Savannakhet Dinosaur Museum, Laos).

Submitting my papers would not be possible without support from many collaborators, in addition to my supervisors. I thus would like to thank the geologist colleagues S. Bourquin and C. Rossignol, histologist A. Houssaye, statisticians L. Legendre and Y. Desdevises, and paleontologists M. Faure-Brac, J.-S. Steyer, and B. Battail.

For their technical support that allowed me to better study the fossils and to best figure them despite a poor preservation, I am very grateful to C. Bouillet, P. Richir, and H. Bourget for the preparation of fossils and moulds, H. Lamrous and S. Morel for the histological sections, S. Fernandez for drawings, P. Loubry and L. Cazes for the pictures, and M.A. Angel for guiding me in the paleontological library.

To improve my work and enrich the discussions by their relevant remarks, I give thanks to J. Botha-Brink, K. Brink, V. Barriel, J. Camp, C. Kammerer, K.D. Angielczyck, J. Bardin, A. Meade, J. Liu, A. Huttenlocker, R. Allain, B. Khalloufi, L. Villier, D. Germian, M. Laurin, M. Pickford, K. Rey, K. Leverger, T. Arbez, O.Bethoux, G. Billet, G. Clément, and anonymous reviewers.

Thanks to J. Botha-Brink and C. Kammerer to review my PhD thesis, and R. Vigne-Lebbe, J. Fröbisch, and M. Laurin to be jury members of my thesis.

Staying enduring and positive during this adventure strewn with pitfalls would not be achievable without the support of my supervisors and the “chatering” break shared with friends T. Alloul, C. Bronnert, S. Toussaint, M. Tanrattana, L. Bento Da Costa, N. Robin, M. Faure-Brac, M. Plasse, T. Arbez, L. Rozada, R. Allemand, C. Del Rio, F. Clarac, and, in particular, V. Barriel.

Finally, I will always be grateful to my family and its encouragement to achieve my goal and support me in the darkest moments of my PhD work.

TABLE OF CONTENTS

RÉSUMÉ DÉTAILLÉ DE LA THÈSE

Introduction

Les dicynodontes sont des thérapsides plantivores du Permo-Trias. Ils costituent une composante majeure des faunes continentales des écosystèmes terrestres, qu'ils ont dominés sur une période d'environ 70 millions d'années, du Permien moyen au Trias supérieur. Ce travail de thèse s'intéresse tout particulièrement aux formes triasiques. Ces dernières sont principalement représentées par le grand clade des Kannemeyeriiformes qui inclut plus de 90% de des formes triasiques. Les Lystrosauridae (avec le genre multipsécifique *Lystrosaurus*) et les Emydopoidae (avec les genres *Kombuisia* et *Myosaurus*) forment les deux autres clades contenant des dicynodontes du Trias. Alors que la position phylogénétique de *Myosaurus* et *Kombuisia* au sein des Emydopoidae est consensuelle, les relations phylogénétiques au sein des Kannemeyeriiformes et des Lystrosauridae sont encore fortement débattues. De plus, la validité taxonomique de nombreux genres kannemeyeriiformes et d'espèces de *Lystrosaurus* est remise en cause.

Le clade des dicynodontes est connu pour avoir été l'un des rares groupes de vertébrés terrestres à avoir survécu à la crise biologique majeure du Permo-Trias (P-Tr). Les relations phylogénétiques au sein des dicynodontes montrent que plusieurs groupes auraient franchi cette crise, comme c'est le cas des Lystrosauridae et des Emydopoidae. L'âge Permien du groupe-frère des Kannemeyeriiformes, par ailleurs absents au Trias inférieur, a conduit certains auteurs à supposer une lignée fantôme pour ce clade, interprétée comme étant un biais stratigraphique. La rareté des restes de dicynodontes a longtemps supposé une diversification post-crise tardive des dicynodontes, repoussée au Trias moyen, du fait des rudes conditions environnementales au Trias inférieur. Néanmoins, la découverte relativement récente des genres *Kombuisia*, *Myosaurus*, et *Sungeodon,* s'ajoutant à *Lystrosaurus* au Trias inférieur appuierait plutôt l'hypothèse d'une résilience post-crise des dicynodontes bien plus rapide. Au Trias moyen, les dicynodontes connaissent une importante radiation évolutive avec l'apparition d'une vingtaine de nouveaux genres. Malgré cette grande diversification ils s'éteignent au cours du Trias supérieur. Les formes les plus tardives, *Lisowicia* (Pologne) et *Pentasaurus* (Afrique du Sud), très récemment décrites, datent de la fin Norien-début Rhétien. D'un point de vue paléogéographique, les dicynodontes

sont principalement connus au Trias inférieur au sud du Gondwana (Inde, Afrique du Sud, Zambie et Antarctique) avec également quelques formes en Eurasie (Russie et Chine du Nord). Leurs occurrences se multiplient au Trias moyen pour s'étendre jusqu'en Chine du Sud. Au Trias supérieur, les dicynodontes connaissent une répartition cosmopolite. En plus du sud du Gondwana (Afrique du Sud, Namibie, Brésil et Argentine) et de la Chine, leurs restes vont être retrouvés en Laurentia (Etats-Unis), au nord du Gondwana (Maroc) et à l'ouest de l'Eurasie (Pologne).

L'organisation histologique osseuse, conservée au cours de la fossilisation, peut être utilisée comme '*proxy*' pour connaitre la physiologie d'organismes fossiles. La description qualitative de l'histologie osseuse a seulement été renseignée chez cinq genres de dicynodontes triasiques : *Lystrosaurus*, *Placerias*, *Wadiasaurus*, *Dinodontosaurus*, et *Kannemeyeria*. Chez ces dicynodontes, le taux de croissance et le mode de vie ont pu être inférés, bien que ce dernier soit encore débattu. Une organisation osseuse de type fibro-lamellaire retrouvée chez ces formes a permis de conclure à un fort taux de croissance de l'os. Une corrélation entre le taux de croissance osseuse et le taux métabolique au repos a été proposée, suggérant un fort métabolisme chez ces organismes. Néanmoins, de l'os fibro-lamellaire a été observé chez des organismes ectothermes actuels, remettant alors en cause la précédente corrélation. Récemment, une inférence quantitative du taux métabolique au repos, issue de modèles statistiques paléohistologiques, a été effectuée chez des archosauromorphes fossiles.

Par une approche multidisciplinaire, cette thèse vise à améliorer nos connaissances sur l'anatomie, le métabolisme, l'écologie, la phylogénie, et l'histoire biogéographique des dicynodontes au cours du Trias. Elle se fonde sur l'étude de restes inédits de formes laotiennes et marocaines.

Apports des nouvelles formes laotiennes

Les premières découvertes de restes de dicynodontes au Laos remontent à la fin du 19ème siècle, quand Counillon a récolté en 1896 un crâne partiel dans le Bassin de Luang-Prabang. Etudié par Répelin en 1923, l'attribution taxonomique de ce crâne a longtemps été débattu (*Dicynodon* ou *Lystrosaurus*). L'absence d'illustrations et de descriptions anatomiques détaillées ne permet pas de clore ce débat et l'attribution taxinomique de ce crâne aujourd'hui perdu demeure énigmatique. De nombreuses missions franco-laotiennes (menées par P. Taquet) ont mis à jour un abondant matériel

crânien et post-crânien de dicynodontes au sein la formation des argiles violettes du Bassin de Luang-Prabang (Laos). Les trois crânes les mieux conservés, provenant de ce matériel, ont été préparés et brièvement décrits par Battail (2009) et attribué au genre *Dicynodon*. Néanmoins, aucune analyse phylogénétique n'a été effectuée pour tester leurs relations au sein des dicynodontes. De plus, une large révision taxonomique a été récemment réalisée pour le genre *Dicynodon*. En plus d'une meilleure connaissance de leur anatomie et des questions taxonomique et phylogénétique, l'étude des dicynodontes laotiens présente deux grands intérêts : (1) l'ajout de nouvelles formes d'âge fin Permien-début Trias enrichit notre compréhension de l'évolution du groupe autour de la crise P-Tr, et (2) la découverte de dicynodontes sur le bloc Indochinois alimente le débat actuel sur la collision de ce bloc avec le reste de la Pangée.

La description détaillée des trois crânes et la comparaison avec les autres dicynodontes a permis de les attribuer à deux nouveaux genres monospécifiques de dicynodontes : *Counillonia superoculis* et *Repelinosaurus robustus*. L'analyse phylogénétique a mis en évidence une proche parentée entre *Repelinosaurus* et les Kannemeyeriiformes, ainsi qu'entre *Counillonia* et les dicynodontidés permiens. Bien que cela reste débattu, la formation des argiles violettes incluant les dicynodontes laotiens serait plus probablement datée du Trias inférieur. La découverte de deux nouvelles formes de dicynodontes juste après la crise P-Tr appuie l'hypothèse d'une résilience post-crise plus rapide. De plus, la proximité phylogénétique entre *Counillonia* et des dicynodontidés permiens ajouterait un autre groupe de dicynodontes connu de par et d'autre de la limite P-Tr, en plus des Lystrosauridae et des Emydopoidae. Enfin, la présence de dicynodontes presque exclusivement terrestres sur le bloc Indochinois au Trias inférieur supposerait une collision du bloc avec le reste de la Pangée datée au moins de cette époque.

Révision taxonomique des dicynodontes marocains et description de matériel postcrânien inédit

En plus des restes crâniens du Trias supérieur (Carnien), décrits par J.M. Dutuit dans les années 1980, un abondant matériel postcrânien de dicynodontes a été récolté dans les mêmes sites au sein du Bassin d'Argana (Maroc). L'étue des restes crâniens a permis à Dutuit (1988, 1989), de définir trois espèces: *Moghreberia nmachouensis*, *Azarifeneria barrati*, et *A. robustus*. J.M. Dutuit distingue ces deux genres

principalement par l'importante robustesse des os d'*Azarifeneria*. Cependant, la validité taxonomique des genres marocains a été remise en question depuis par certains auteurs, suggérant une synonymie entre *Moghreberia* et le genre nord-américain *Placerias*, et entre *Azarifeneria* et *Moghreberia* ou le genre sud-américain *Ischigualastia*. De ce fait, *Azarifeneria*, représenté par des restes incomplets, est encore considéré *nomen dubium* et *Moghreberia* n'a été inclu dans une analyse phylogénétique que très récemment (Kammerer et al. 2011), mais ce fut sur la base d'un codage très partiel. Les objectifs de cette étude ont été : (1) de décrire une grande partie du matériel postcrânien inédit retrouvé dans le Bassin d'Argana ; (2) de ré-étudier les restes crâniens de *Moghreberia* et *Azarifeneria* ; (3) de discuter de la validité taxonomique des deux genres et (4) de compléter la matrice phylogénétique de Kammerer et al. (2011).

Moghreberia nmachouensis étant connu par la majorité des restes crâniens du Bassin d'Argana, le morphotype le plus fréquent retrouvé dans les restes postcrâniens lui a été attribué. Il est principalement caractérisé par une scapula avec une extrémité dorsale relativement large et un processus acromial réduit, une crête deltopectorale humérale bien développée formant un angle obtus entre son bord antérieur et distal, une insertion du muscle *latissimus dorsi* sur l'humérus en forme de pavillon, et la présence d'un processus supinateur sur l'ectépicondyle de l'humérus. L'étude des restes crâniens et postcrâniens de *Moghreberia* a permis une meilleure connaissance de son anatomie et, par conséquent, d'améliorer son codage dans la matrice phylogénétique préexistante. Contrairement à ce qui est généralement admis, notre analyse a montré que *Moghreberia* était phylogénétiquement plus proche du genre polonais *Lisowicia* que de *Placerias*. Les restes crâniens très fragmentaires des deux espèces d'*Azarifeneria* n'ont pas permis de les distinguer significativement de *Moghreberia* ou des autres kannemeyeriiformes. De plus, bien qu'il n'y ait pas de caractères diagnostiques significatifs, un deuxième morphotype pourrait être mis en évidence dans le matériel postcrânien du fait de son importante robustesse, rappelant celle du matériel crânien d'*Azarifeneria*.

Paléophysiologie des dicynodontes

L'endothermie correspond au maintien de la température corporelle par la production de chaleur non-frissonnante. Elle se caractérise par un fort taux métabolique au repos. On retrouve ce mécanisme physiologique chez les mammifères

et les oiseaux actuels. Cette acquisition par convergence chez les deux groupes constitue un évènement évolutif majeur puisqu'il modifie la relation énergétique de l'organisme avec son environnement. De nombreux '*proxy*' (comme la présence de pelage ou d'os turbinaux chez les mammifères) sont utilisés pour inférer une stratégie endotherme aux organismes fossiles. Comme mentionné précédemment, l'organisation histologique osseuse peut également être utilisée. Néanmoins, la relation entre le taux de croissance osseuse observable sur une coupe histologique et le taux métabolique au repos présente certaines exceptions. Des modèles d'inférence paléohistologiques ont été récemment proposés pour inférer quantitativement le taux métabolique au repos chez des archosauromorphes fossiles. Cela a permis de mieux contraindre temporellement et phylogénétiquement l'acquisition de l'endothermie chez les sauropsides. L'étude de la paléophysiologie des dicynodontes s'est donc basée sur la construction des premiers modèles paléohistologiques d'inférence incluant des synapsides fossiles.

Premièrement, des modèles suivant la méthode de Guénard et al. (2013) et Legendre et al. (2016) ont été construits en se servant de l'approche des Phylogenetic Eigenvector Maps (PEMs) pour prendre en compte la phylogénie. La variable expliquée était le taux métabolique au repos (RMR) et les variables explicatives, la densité, l'aire, et la forme des lacunes ostéocytaires. Deux modèles distincts ont été créés, l'un basé sur le fémur et l'autre sur l'humérus, pour inférer le RMR de trois synapsides fossiles (dicynodontes permien *Oudenodon baini*, et triasiques *Lystrosaurus* sp., et *Moghreberia nmachouensis*). La construction des modèles passe, d'une part, par la sélection de la meilleur combinaison de vecteurs phylogénétiques propres et, d'autre part, du choix d'une ou d'aucune des variables explicatives selon le critère d'Akaike (AICc). Les modèles paléohistologiques ont inféré un fort RMR chez les trois dicynodontes, corroborant l'observation qualitative d'un fort taux de croissance osseuse (os fibro-lamellaire) chez ces trois taxons. Plus généralement, cette étude montre une acquisition unique de l'endothermie mammalienne il y a au moins 260 millions d'années au nœud des Neotherapsida.

Du fait du faible échantillonnage de dicynodontes et de certaines limites méthodologiques dans l'approche de Legendre et al. (2016), d'autres modèles d'inférence ont ensuite été construits en utilisant un échantillonnage plus large et la méthode des Phylogenetic Generalised Least Squares (PGLS). La nouvelle méthodologie présente plusieurs avantages dont ceux de prendre en compte une

combinaison de variables histologiques et de paramétrer un modèle d'évolution plus explicite. Dans un but de comparaison, des modèles utilisant l'approche des PEMs ont également été créés sur le nouvel échantillonnage. De même que pour la première étude, les modèles basés sur le fémur et l'humérus ont été traités séparément. Les variables histologiques ont porté sur la densité, l'aire, et la forme des lacunes ostéocytaires, et sur la densité d'ostéones primaires. L'échantillonnage de dicynodontes s'est élargi par rapport à la première étude : formes permiennes *Daptocephalus*, *Endothiodon*, *Oudenodon baini*, et *Tropidostoma*, et triasiques *Kannemeyeria simocephalus*, *Lystrosaurus murrayi*, *Moghreberia nmachouensis*, et *Myosaurus gracilis*. Un haut taux métabolique au repos a été inféré pour l'ensemble des dicynodontes étudiés avec les deux méthodes, excepté pour *Myosaurus* et *Endothiodon* avec les PEMs (due à une variation méthodologique). Ces résultats confirment les premières inférences quantitatives chez les dicynodontes et les observations histologiques qualitatives documentées dans la littérature. Ils supportent également une apparition unique de l'endothermie au moins au nœud des Neotherapsida. Cependant, la découverte d'un fort taux métabolique chez des dicynodontes permiens et triasiques tend à infirmer l'hypothèse de l'avantage sélectif d'un taux élevé pour survivre à la crise P-Tr.

Conclusions et perspectives

Ce travail a mis en évidence l'apport des formes laotiennes et marocaines dans notre compréhension de l'évolution des dicynodontes au cours du Trias. En effet, les deux nouvelles formes laotiennes *Counillonia superoculis* et *Repelinosaurus robustus*, très probablement du Trias inférieur, confirment, d'une part, une résilience post-crise des dicynodontes plus rapide que précédemment supposée et, d'autre part, la survie d'un plus grand nombre de clades à la crise P-Tr. De plus, la présence au Laos de ces dicynodontes complètement adaptés à un mode de vie terrestre suppose un lien continental entre le bloc Indochinois et le reste de la Pangée, dès le Trias inférieur. Néanmoins, les relations phylogénétiques de ces dernières varient entre les Kannemeyeriiformes, Lystrosauridae, et Dicynodontidae, très probablement à cause de leur combinaison particulière de caractères. Une étude, après préparation, de l'ensemble du matériel crânien et postcrânien disponible et inédit de dicynodontes récoltés dans le Bassin de Luang Prabang permettrait de compléter nos connaissances sur la faune de dicynodontes au Laos.

La révision taxonomique du genre marocain *Moghreberia* a montré sa validité au sein des dicynodontes, et de nombreux caractères le distinguent, notamment de *Placerias*. L'étude du postcrânien inédit provenant du Bassin d'Argana (Maroc) a permis d'en attribuer la majorité à *Moghreberia*, améliorant notre connaissance de cette espèce et complétant ainsi sa diagnose. Cependant, le robuste *Azarifeneria* n'a pas pu être significativement distingué des autres dicynodontes. Il est alors toujours considéré *nomen dubium*. Bien qu'il n'ait pas de caractères diagnostiques, un deuxième morphotype robuste a été mis en évidence au sein du matériel postcrânien. La taille imposante de *Moghreberia* et de ce deuxième morphotype confirment l'hypothèse de l'augmentation de la taille chez les dicynodontes au cours du Trias, jusqu'aux plus grandes formes au Trias supérieur. Des fouilles supplémentaires, notamment dans les niveaux équivalents du gisement XII encore peu prospectés, pourrait apporter de nouvelles découvertes sur les dicynodontes nord-africains. Contrairement à *Lisowicia* ou *Pentasaurus*, *Moghreberia* qui est d'âge Carnien, n'apporte pas d'information sur les dernières formes de dicynodontes connus. Cependant, un squelette complet inédit de dicynodonte (en cours de préparation) a été retrouvé dans la formation des argiles rouges du Bassin de Luang-Prabang (Laos) et daté du Norien. Son étude présente plusieurs intérêts : (1) la description du premier dicynodonte complet (crâne et restes post-crâniens en connexion) connu au Trias supérieur, (2) une meilleure compréhension de la distribution des dicynodontes au cours du Trias supérieur, s'agit-il d'une nouvelle forme du Trias supérieur ou l'extension stratigraphique d'une espèce déjà décrite ? et (3) l'apport des nouveaux éléments à notre connaissance de la biodiversité au Trias supérieur et des conditions d'extinction des dicynodontes.

Les modèles d'inférence paléophysiologiques basés sur l'histologie osseuse ont permis d'inférer un métabolisme endotherme à tous les dicynodontes permiens et triasiques étudiés. Plus généralement, cela suppose une apparition unique de l'endothermie mammalienne au moins au nœud des Neotherapsida, il y a environ 260 millions d'années. L'utilisation en parallèle de deux méthodes, les PEMs et PGLS pour construire les modèles, a mis en évidence certaines limites méthodologiques dans les deux approches. Afin d'améliorer ces modèles, l'ajout de taxons actuels semble primordial pour pouvoir augmenter l'échantillonnage fossile et couvrir une plus grande échelle de l'évolution du thermométabolisme chez les Synapsides.

CHAPTER I

GENERAL INTRODUCTION

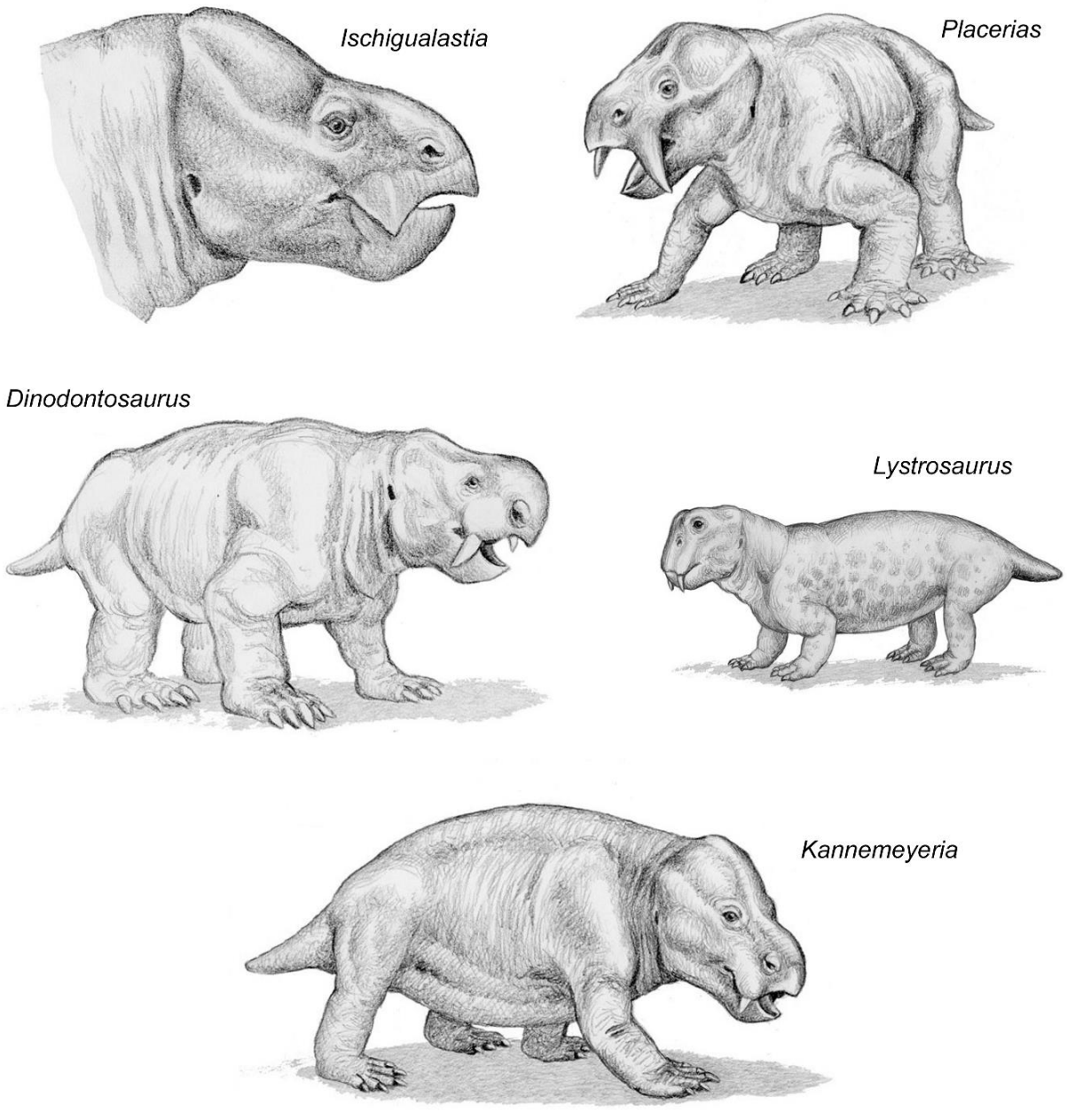

Triassic dicynodonts © WillemSvdMerwe (www.deviantart.com)

Dicynodontia

The first mention of dicynodont remains is due to Bain (1845) who reported near Fort Beaufort town (Karoo basin in South Africa) the discovery of a “reptile” skull with only two large teeth, which he named “Bidental”. The same year witnessed the first description of a dicynodont by Owen (1845) (Fig. I.1), which he attributed to a new genus *Dicynodon* within Reptilia. Dicynodontia (meaning “δις”, twice and “κυνόδους”, canine-tooth) were first named by Owen (1860b) after the long maxillary tusk. Further studies also presented dicynodont forms with vestigial tusks in *Placerias* (Camp and Welles, 1956) even tuskless as in *Myosaurus* (Cluver, 1974), *Kombuisia* (Fröbisch, 2007), or *Stahleckeria* (Maisch, 2001). In some cases, the presence or absence of tusk seems to be related to sexual dimorphism (e.g., Bandyopadhyay, 1988: *Wadiasaurus*). Another remarkable character in the dicynodonts is the presence of an osseous toothless beak that was probably encased in a keratinized sheath (i.e., ramphoteca according to Benoit et al., 2018), identified as soon as the end of the 19th century by Owen (1845) in *Dicynodon testudiceps* (Fig. I.1) (considered as *nomen dubium* since the taxonomic revision of Kammerer et al., 2011).

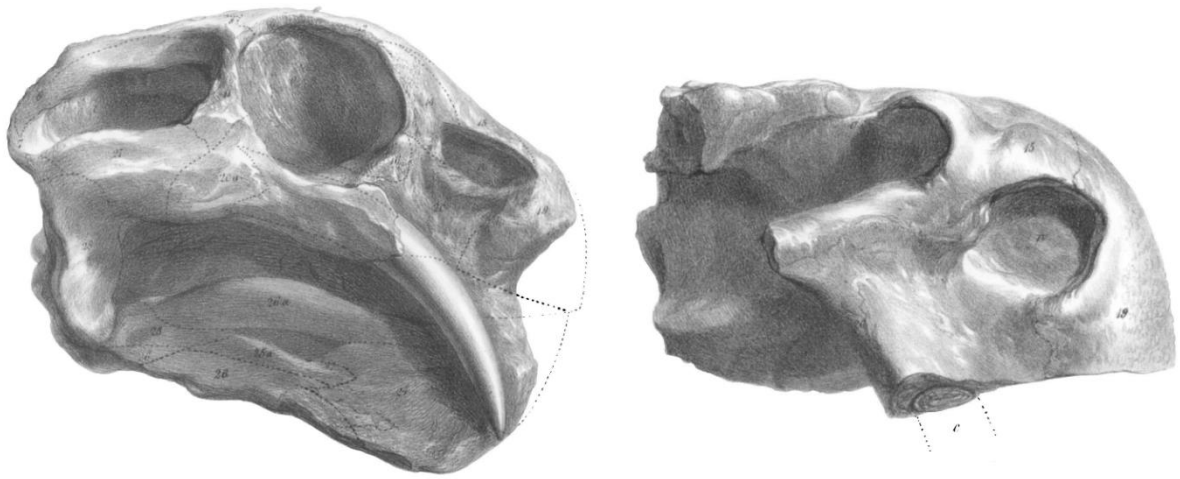

Figure I.1. Lateral view of the skulls of *Dicynodon lacerticeps* (left) and “*Dicynodon testudiceps*” (right) (modified from Owen, 1845). The illustrations are not in scale.

Dicynodontia are included in Anomodontia (Owen, 1860b), within Therapsida (Broom, 1905). They have colloquially been attributed to “mammal-like reptiles”, a paraphyletic group comprising all non-mammalian synapsid taxa (including the paraphyletic “pelycosaurs” and the non-mammalian therapsids) (e.g., Benton, 2005). As indicated by their name, the “mammal-like reptiles” have long been considered as

stem-mammals that arose from a hypothetical stem-reptile (e.g., Kemp, 1980), placing them in this way at an intermediate position between the reptiles and mammals. With the advent of cladistic analysis and the use of phylogenetic analysis, the term “mammal-like reptiles” is outdated and inaccurate, and should be avoided. All non-mammalian clades include extinct taxa, the only extant synapsids today are thus mammals (Marsupialia, Placentalia and Monotremata). In term of taxonomic diversity, abundance, and stratigraphic and geographic distributions, Dicynodontia represent the most successful clade of synapsids after Mammalia. They comprise around well-characterized 50 Permian and 30 Triassic genera (e.g., Fröbisch, 2009; Kammerer et al., 2011, 2013; Cox and Angielczyk, 2015; Angielczyk and Kammerer, 2017; Angielczyk et al., 2018; Kammerer et al., 2019; Sulej and Niedźwiedzki, 2019).

The oldest known dicynodonts *Eodicynodon oosthuizeni* (Barry, 1974) and “*Eodicynodon*” *oelofseni* (Rubidge, 1990) are dated of Wordian (Middle Permian) and come from the *Eodicynodon* Assemblage Zone (AZ) from South Africa. The youngest definite dicynodont remains are those of *Pentasaurus* from the lower Elliot Formation of South Africa (Kammerer, 2018) and of *Lisowicia* from the terrestrial sequence at Lisowicie in Poland (Sulej and Niedźwiedzki, 2019). They extend the stratigraphic range of the dicynodonts to the latest Norian–early Rhaetian (e.g., Knoll, 2004; Sulej and Niedźwiedzki, 2019). This gives Dicynodontia a temporal range of about 60 millions years surviving to the Permo-Triassic mass extinction, the largest mass extinction in Earth history that occurred about 250 million years ago (e.g., Fröbisch, 2007).

They were the dominant herbivores in their ecosystems and the major component of primary consumers from late Permian (with the pareiasaurs and captorhinids) (e.g., Bernardi et al., 2017) to Middle Triassic. They were widespread with a cosmopolitan distribution. Their remains were found in Africa (South Africa, Madagascar, Malawi, Morocco, Mozambique, Namibia, Tanzania, Zambia, Zimbabwe), Antarctica, Asia (China, India, Laos), Europe (Poland, Russia, Scottland), and North (U.S.A.) and South (Argentina, Brazil) America (e.g., Fröbisch, 2009; Sulej and Niedźwiedzki, 2019). They represent an emblematic terrestrial vertebrate that play an important role in assessing the impact of the end-Permian extinction on the terrestrial fauna.

More than half of the known dicynodont specimens are originated from the South African Karoo Basin (e.g., Fröbisch, 2009; Smith et al., 2012). In addition to the

fossil potential of this site, this probably highlights a clear geographic bias in studies of dicynodont. Some geographic area are significantly more studied (South Africa) (e.g., Ward et al., 2005; Smith and Botha-Brink, 2014; Viglietti et al., 2018) than others (Laos, Morocco, or Poland).

Position of the Triassic forms within the phylogeny of Dicynodontia

Kannemeyeriiformes

The kannemeyeriiform subclade includes the majority of the Triassic dicynodonts with the following 27 valid genera: *Angonisaurus* (Cox and Li, 1983), *Dinodontosaurus* (Romer, 1943), *Dolichuranus* (Keyser, 1973), *Eubrachiosaurus* (Williston, 1904), *Ischigualastia* (Cox, 1962), *Jachaleria* (Bonaparte, 1970), *Lisowicia* (Sulej and Niedźwiedzki, 2019), *Kannemeyeria* (Seeley, 1908), *Moghreberia* (Dutuit, 1980), *Parakannemeyeria* (Sun, 1960), *Pentasaurus* (Kammerer, 2018), *Placerias* (Lucas, 1904), *Rabidosaurus* (Kalandadze, 1970), *Rechnisaurus* (Roy-Chowdhury, 1970), *Rhadiodromus* (Efremov, 1951), *Rhinodicynodon* (Kalandadze, 1970), *Sangusaurus* (Cox, 1969), *Shaanbeikannemeyeria* (Cheng, 1980), *Shansiodon* (Yeh, 1959), *Sinokannemeyeria* (Young, 1937), *Stahleckeria* (Huene, 1935), *Tetragonias* (Cruickshank, 1967), *Ufudocyclops* (Kammerer et al., 2019), *Uralokannemeyeria* (Danilov, 1971), *Vinceria* (Bonaparte, 1969), *Wadiasaurus* (Roy-Chowdhury, 1970), *Xiyukannemeyeria* (Liu and Li, 2003), and *Zambiasaurus* (Cox, 1969) (e.g., Kammerer et al., 2011, 2013; Kammerer and Smith, 2017; Angielczyk et al., 2018; Kammerer, 2018; Kammerer et al., 2019). The inclusion of Middle and Late Triassic forms in a same clade has been previously assumed by Huene (1948), who defined six families within Anomodontia (Endothiodontidae, Dicynodontidae, Cistecephalidae, Geikiidae, Lystrosauridae and Kannemeyeridae). However, while the monophyly of Kannemeyeriiformes is consensual in recent literature, they have not always been considered belonging to a distinct and unique clade. Within the Middle and Late Triassic forms, Cox (1965) thus distinguished three distinct families: (1) Kannemeyeriidae (*Sinokannemeyeria*, *Parakannemeyeria*, *Kannemeyeria*, *Ischigualastia*, *Placerias*, and *Barysoma* a synonym of *Stahleckeria* (Lucas, 1993)), (2) Shansiodontidae (*Shansiodon* and '*Dicynodon*' *njalilus* a synonym of *Tetragonias* (Kammerer et al., 2013)), and (3) Stahleckeriidae (*Stahleckeria* and *Dinodontosaurus*). Romer (1956) placed Triassic forms such as *Dinodontosaurus*, *Eubrachiosaurus*, *Kannemeyeria*, *Placerias*, *Rhadiodromus*, *Sinokannemeyeria*, and *Stahleckeria* within

Dicynodontidae including the Permian forms. The same year, Camp (1956) supported that *Stahleckeria*, *Kannemeyeria*, and *Placerias* belong to the same family of Kannemeyeriidae. Then, Keyser and Cruickshank (1979) revised the taxonomy of the Triassic dicynodonts (excluding Lystrosauridae, and the genera *Myosaurus* and *Kombuisia*) and grouped them in four subfamilies (Kannemeyerinae, Dinodontosaurinae, Stahleckerinae, and Jachelerinae) within the Kannemeyeridae. Keyser and Cruickshank (1979) also supposed that the Middle and Late Triassic dicynodonts would be closely related to the Permian *Rhachiocephalus*, *Daptocephalus*, and *Dinamodon*. It was not until the work of Maisch (2001) who redefined Kannemeyeriiformes as the clade of the Triassic non-lystrosaurid dicynodontoids, and clearly broke from studies considering this group as a dicynodontid. As previously mentioned, the monophyly of Kannemeyeriiformes has not been subjected to much doubt in all subsequent phylogenetic analyses (e.g., Damiani et al., 2007; Kammerer et al., 2011; Boos et al., 2016; Angielczyk and Kammerer, 2017; Angielczyk et al., 2018; Kammerer et al., 2019; Sulej and Niedźwiedzki, 2019). In parallel to the “stratigraphic” definition of Maisch (2001), Kammerer et al. (2013) proposed a more comprehensive taxonomic definition of Kannemeyeriiformes comprising of *Kannemeyeria simocephalus* and all taxa more closely related to it than to *Lystrosaurus murrayi* or *Dicynodon lacerticeps*.

Despite, the phylogenetic relationships within Kannemeyeriiformes and their alpha taxonomy are raising issues, as shown by the absence of consensus in the literature (e.g., Vega-Dias et al., 2004; Govender and Yates, 2009; Kammerer and Angielczyk, 2009; Domnanovich and Marsicano, 2012; Maisch and Matzke, 2014; Kammerer and Smith, 2017; Angielczyk et al., 2018; Kammerer et al., 2019). For instance, the exhaustive taxonomic definitions of the kannemeyeriiform families by Cox (1965) have been contested by most phylogenetic analyses in literature (e.g., Kammerer et al., 2011, 2013; Cox and Angielczyk, 2015; Boos et al., 2016; Angielczyk and Kammerer, 2017; Kammerer and Smith, 2017; Angielczyk et al., 2018; Kammerer et al., 2019; Sulej and Niedźwiedzki, 2019). Kammerer et al. (2013) then proposed a comprehensive taxonomic definition for Stahleckeriidae including the last common ancestor of *Placerias hesternus* and *Stahleckeria potens*, and all of its descendants, excluding *Shansiodon wangi* or *Kannemeyeria simocephalus*. Uncertainties likewise persisted about the validity of some kannemeyeriiform genera such as *Shaanbeikannemeyeria* (synonym of *Rechnisaurus*), *Rechnisaurus* (junior synonym of

Kannemeyeria), *Uralokannemeyeria* (synonym of *Kannemeyeria*), or *Moghreberia* (junior synonym of *Placerias*) (e.g., Keyser and Cruickshank, 1979; Cox, 1991; Hunt and Lucas, 1991; Lucas and Wild, 1995). Some Middle and Late Triassic dicynodont taxa may be considered nomen dubia due to their fragmentary associated material: the Chinese *Fukangolepis* (Lucas and Hunt, 1993a) and *Sungeodon* (Maisch and Matzke, 2014), the North American *Brachybrachium* (Williston, 1904), the North African *Azarifeneria* (Dutuit, 1989a, 1989b), the South African *Ptychocynodon* (Seeley, 1904), and numerous Russian forms such as *Calleonasus* (Kalandadze and Sennikov, 1985), *Cristonasus* (Surkov, 1999a), *Edaxosaurus* (Kalandadze and Sennikov, 1985), *Elatosaurus* (Kalandadze and Sennikov, 1985), *Elephantosaurus* (Vjuschkov, 1969), *Nasoplanites* (Surkov, 1999a), *Parvobestiola* (Surkov, 1999a), *Planirostris* (Surkov, 1999b), *Putillosaurus* (Surkov, 2005), and *Rhinocerocephalus* (Vjuschkov, 1969) (e.g., Lucas and Hunt, 1993b; Lucas, 1995; Lucas and Wild, 1995; Fröbisch, 2009). Most of these taxa have been closely related or attributed to Kannemeyeriiformes.

Lystrosauridae and the emydopoids *Kombuisia* and *Myosaurus*

Lystrosaurus (Cope, 1870) is the main representative genus of Lystrosauridae. It is particularly prominent since it is one of the scarce terrestrial vertebrate to be known from both sides of the Permo-Triassic boundary (e.g., Smith and Ward, 2001; Ray et al., 2005; Botha and Smith, 2006; Fröbisch, 2009). *Lystrosaurus* is also a relevant stratigraphic tool (Rubidge, 1990) by the abundance of its Triassic remains, its Pangean repartition (South of Africa, India, Antarctica, Russia, China, and probably Laos), and its short temporal distribution (Fröbisch, 2009; Jasinoski et al., 2014). Lystrosauridae are the only family of dicynodonts whose monophyly has not been questionned (e.g., Keyser and Cruickshank, 1979), particularly because the genus *Lystrosaurus* is distinguished from all other dicynodonts by the peculiar and distinct specialization of the skulls with a deep dorsoventrally-projected snout. Following the comprehensive definition of Kammerer and Angielczyk (2009), Lystrosauridae are all taxa more closely related to *Lystrosaurus murrayi* (Huxley, 1859), than to *Dicynodon lacerticeps* (Owen, 1845), or to *Kannemeyeria simocephala* (Weithofer, 1888).

A proliferation of species were attributed to *Lystrosaurus* between 18th and 19th centuries. However, most of these species were named on the basis of poorly preserved fossils and thus questionable diagnostic criteria (Grine et al., 2006). A major taxonomic revision of the South African species of *Lystrosaurus* has been conducted

by Grine et al. (2006) using multivariate allometry analyses. They reduced their number from 27 to 4 valid species: *L*. *maccaigi* (Seeley, 1898), *L*. *murrayi* (Huxley, 1859), *L*. *declivis* (Owen, 1860a), and *L*. *curvatus* (Owen, 1876). A recent morphological study of the skulls attributed to *L. murrayi* and *L. declivis* by Thackeray (2018) supposed a synonymy of these two species. The Indian dicynodont specimens, attributed to *L. murrayi* (Huxley, 1859), *L. platyceps* (Seeley, 1898), *L. maccaigi* (Seeley, 1898), and *L. rajurkari* (Tripathi and Satsangi, 1963) by Tripathi and Satsangi (1963), have been re-evaluated by multivariate allometry analyses (Ray et al., 2005). They finally only concluded to the presence of a single species *L. murrayi* (Huxley, 1859). Seven *Lystrosaurus* species have been described in China: *L. broomi* (Young, 1939), *L. hedini* (Young, 1935), *L. robustus* (Sun, 1973)*, L. shichanggouensis* (Cheng, 1986)*, L. weidenreichi* (Young, 1939), and *L. youngi* (Sun, 1964). In addition, Battail (1997) raised a further concern about the taxonomic validity of *L. broomi* (= *L. murrayi*?), *L. shichanggouensis* (= *L. maccaigi*?), and *L. youngi* (= *L. curvatus*?). Few forms attributed to *Lystrosaurus* were also discovered in Russia and Laos. The Laotian specimen discovered by Counillon (1896) in the Luang Prabang Basin has originally been assigned to a new species of *Dicynodon, D. incisivum* (Répelin, 1923), closely related to *D. orientalis* (Huxley, 1865). It was then attributed by Das Gupta (1922) to *Lystrosaurus*. The specimen is now lost, and we cannot rely on the illustrations from the original description to confirm or invalidate the attribution of the Laotian form to *Lystrosaurus* (e.g., Colbert, 1982; Kammerer et al., 2011). '*Dicynodon incisivum*' is then considered nomen dubium (e.g., Battail, 2009; Fröbisch, 2009; Kammerer et al., 2011).

Lystrosauridae are mostly assumed as sister-group of Kannemeyeriiformes within Dicynodontoidea (e.g., Angielczyk, 2007; Fröbisch and Reisz, 2008; Angielczyk and Rubidge, 2010; Kammerer et al., 2011; Cox and Angielczyk, 2015; Boos et al., 2016; Kammerer and Smith, 2017; Angielczyk et al., 2018; Kammerer, 2018; Kammerer et al., 2019; Sulej and Niedźwiedzki, 2019). However, Angielczyk and Kurkin (2003) found the "*Dicynodon*-like" taxa *Peramodon* and *Vivaxosaurus* more closely related to Kannemeyeriiformes than to *Lystrosaurus*. The taxon *Vivaxosaurus* was also the sister-taxa of *Kannemeyeria* in the phylogenetic analysis of Angielczyk (2007). Moreover, in the analysis of Angielczyk and Kammerer (2017), *Dicynodon*, and the "*Dicynodon*-like" taxa *Delectosaurus*, *Vivaxosaurus*, *Jimusaria*, *Gordonia*, *Sintocephalus*, *Euptychognathus*, *Daptocephalus*, *Peramodon*, *Dinanomodon*, and

Turfanodon are more closely related to Kannemeyeriiformes than to Lystrosauridae. Kammerer (2019a) and Kammerer et al. (2019) even assumed the Permian "*Dicynodon*-like" taxa *Gordonia* and *Jimusaria* as kannemeyeriiforms (according the comprehensive definition of Kammerer et al., 2013).

In addition to Kannemeyeriiformes and Lystrosauridae, the Triassic dicynodonts also include *Myosaurus* and *Kombuisia*. These two are the only Triassic non-dicynodontoid dicynodonts. In the phylogenetic analyses, *Myosaurus* and *Kombuisia* are consistently related to the Permian cistecephalids within Emydopoidae (Cox and Angielczyk, 2015; Boos et al., 2016; Kammerer and Smith, 2017; Angielczyk et al., 2018; Kammerer, 2018, 2019b; Kammerer et al., 2019).

Temporal evolution of the Triassic dicynodonts

The dicynodonts have strongly been impacted by the Permian-Triassic crisis (Fig. I.2; e.g., Fröbisch, 2007). As mentioned above, Lystrosauridae represent the most emblematic group of dicynodonts to have survived this crisis (e.g., Fröbisch, 2007; Botha-Brink et al., 2016). In addition, as suggested by the phylogenetic relationships recovered herein, other clades would appear to have crossed the Permian-Triassic boundary (Fig. I.2; e.g., Angielczyk, 2001; Fröbisch, 2007; Fröbisch et al., 2010; Kammerer et al., 2011). The affiliation of the Triassic genera *Kombuisia* and *Myosaurus* within Emydopoidae indicates the survival of the clade to the crisis. The close relationships of Kannemeyeriiformes with the Permian dicynodontoids implies a ghost lineage extending to the Permian (Kammerer et al., 2011). Many authors have interpreted this ghost lineage as stratigraphic gaps explained by geographic biases (e.g., Angielczyk, 2001; Fröbisch et al., 2010; Kammerer et al., 2011). This hypothesis has notably been consolidated by the discovery of Early Triassic dicynodonts in poorly-studied geographic areas: the emydopoid *Kombuisia* (previously known in Middle Triassic in South Africa) in Antarctica (Fröbisch et al., 2010) and the kannemeyeriiform *Sungeodon* in China (Maisch and Matzke, 2014).

Untill recently, *Lystrosaurus*, *Myosaurus*, and *Kombuisia* have been the only known genera in the Early Triassic (e.g., Fröbisch, 2007, 2009). This led to the hypothesis of a delayed recovery of the dicynodonts after the Permian-Triassic crisis (e.g., Sahney and Benton, 2008; Chen and Benton, 2012; Irmis and Whiteside, 2012) until the Middle Triassic that witnessed the radiation of Kannemeyeriiformes (e.g., Fröbisch, 2009). Sun et al. (2012) have indeed described an "equatorial tetrapod gap"

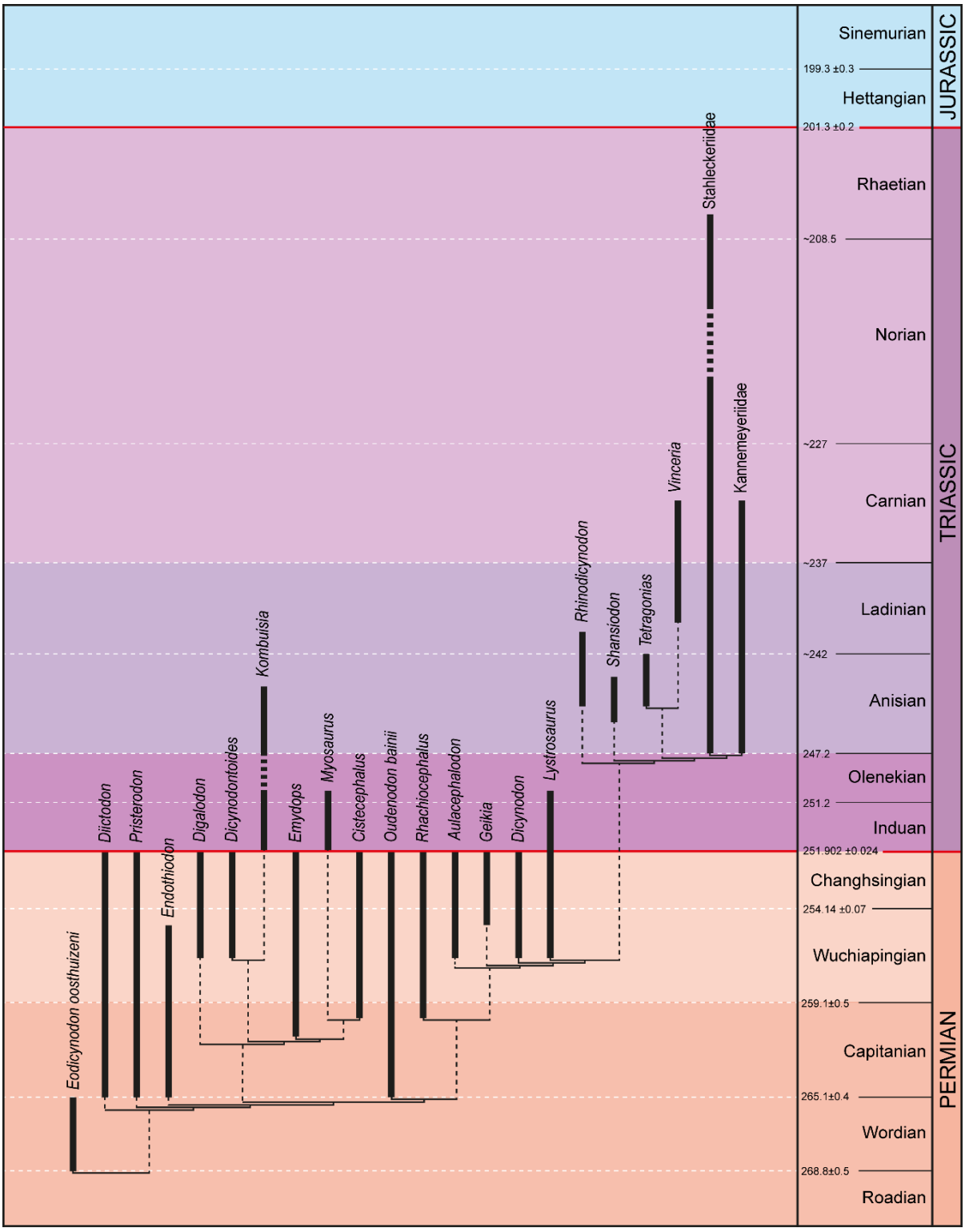

Figure I.2. Phylogeny of Dicynodontia modified from Kammerer (2018) with stratigraphic ranges (modified from Fröbisch, 2009 after the international chronostratigraphic chart v2019/05 and the results from Knoll, 2004; Fröbisch et al., 2010; Angielczyk et al., 2014; Ottone et al., 2014; Sidor et al., 2014; Kammerer et al., 2015, 2019; Viglietti et al., 2016; Kammerer, 2018; Liu et al., 2018; Sulej and Niedźwiedzki, 2019). The recent *Ufudocyclops* and *Lisowicia* were considered in stratigraphic ranges (Kammerer et al., 2019; Sulej and Niedźwiedzki, 2019).

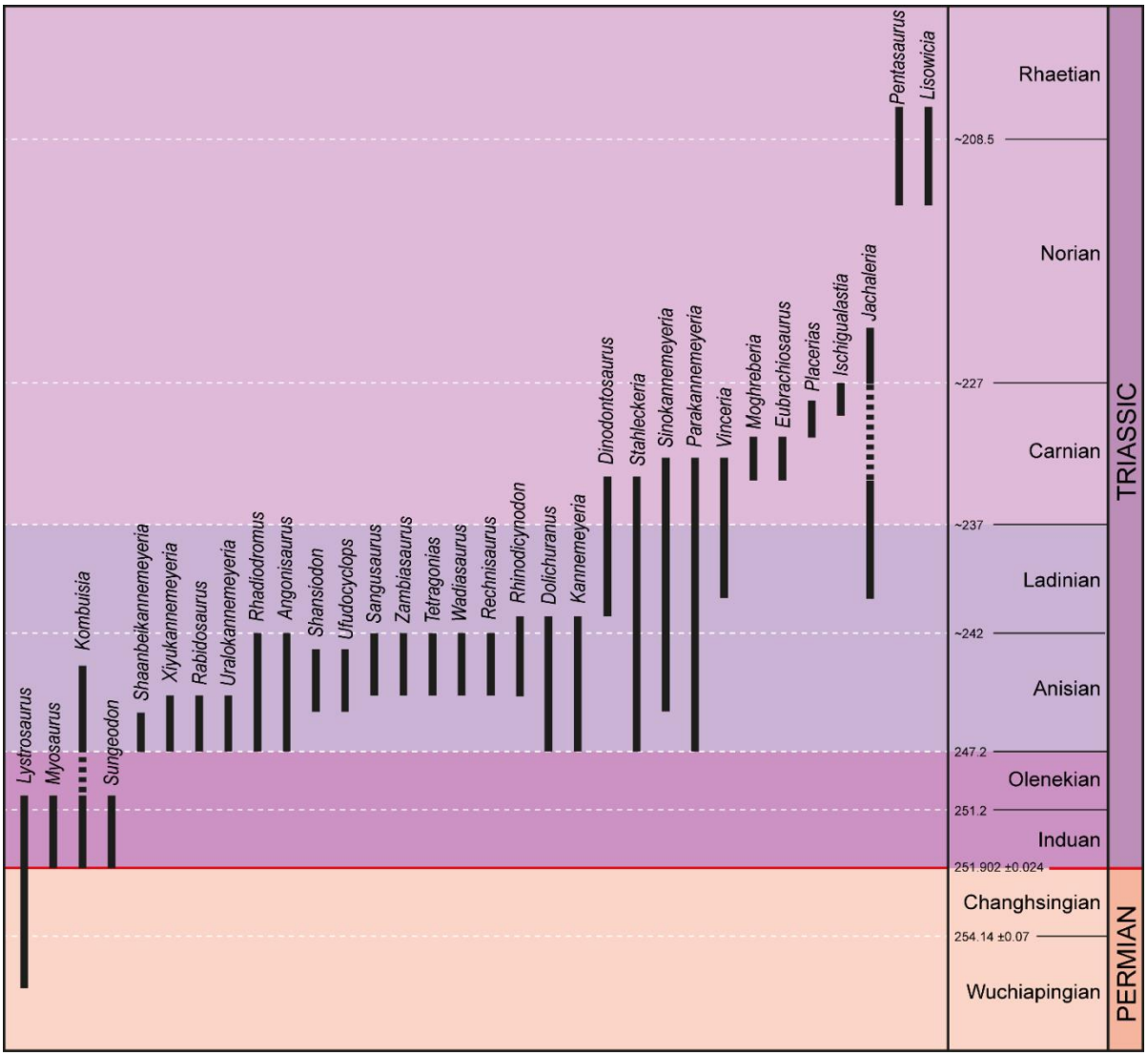

Figure I.3. Stratigraphic ranges of the Triassic dicynodont genera (modified from Fröbisch, 2009 after the international chronostratigraphic chart v2019/05 and the results from Knoll, 2004; Fröbisch et al., 2010; Angielczyk et al., 2014; Maisch and Matzke, 2014; Ottone et al., 2014; Sidor et al., 2014; Kammerer et al., 2015, 2019; Viglietti et al., 2016; Kammerer, 2018; Liu et al., 2018; Sulej and Niedźwiedzki, 2019).

during Early Triassic, caused by excessive equatorial paleotemperatures. On one hand, thee recent discovery of a Chinese Early Triassic dicynodont *Sungeodon* (Maisch and Matzke, 2014) reduced the Kannemeyeriiformes stratigraphic gap previously supposed (e.g., Kammerer et al., 2011). It also suggested an earlier recovery of the dicynodont fauna from the end Permian event (Fig. I.3; e.g., Botha and Smith, 2006; Maisch and Matzke, 2014). In addition, the work of Bernardi et al. (2018) explained the “equatorial tetrapod gap” of Sun et al. (2012) by a massive migration of tetrapod fauna to cooler region in higher latitudes, during the earliest Triassic. However, the taxonomic validity of the *Sungeodon* is nevertheless still questioned (Kammerer et al., 2019).

Despite the great diversification of Kannemeyeriiformes during the Triassic with more than forty new genera (Kammerer et al., 2013), they became extinct during Late Norian-Early Rhaetian, with the latest forms from the Norian (*Jachaleria colorata,* Los Colorados Formation of Argentina) (Fig. I.2; Kent et al., 2014), up to latest Norian–earlier Rhaetian (*Pentasaurus* from the lower Elliot Formation of South Africa (Knoll, 2004; Kammerer, 2018), and *Lisowicia* from the terrestrial sequence at Lisowicie in Poland (Sulej and Niedźwiedzki, 2019)) (Fig. I.3). Cranial remains have been excavated in the Early Cretaceous Rolling Downs Group in Australia and attributed to a dicynodont by Thulborn and Turner (2003). These interpretations raised many questions, Lucas (2015) and Fröbisch (2009) thus attributed these remains to Dicynodontia gen. et sp. indet. A recent study using X-ray synchrotron microtomography reassesed the anatomy of the cranial remains that appear most closely related to the late Cenozoic mammalian megafauna (Knutsen and Oerlemans, 2020).

Spatial distribution of the Triassic dicynodonts

In Early Triassic, the dicynodonts were known in the South of Gondwana and Eurasia (North China and Russia), with the oldest kannemeyeriiforms *Sungeodon* in China (Maisch and Matzke, 2014) (Fig. I.4). During the Middle Triassic, the geographic distribution of the dicynodonts then further extends in South of Gondwana (Argentina, Brazil, South of Africa, Namibia, Zambia, Tanzania, and India) and Eurasia (North and South China, and Russia) (Fig. I.4). In Late Triassic, the dicynodonts are always found in South of Gondawana (Argentina, Brazil, Namibia) and Eurasia (South China), but also in Laurentia (United States of America) and North of Gondwana (Morocco) (Fig. I.4). The youngest occurences of dicynodont representatives (Poland and South Africa) have not been figured in Figure I.4, because of their late Norian-early Rhaetian in age.

The Triassic was the theater of the first premises of fragmentation of the supercontinent Pangea. Despite some intracontinental geographical barriers, in view of the Pangean context, the continents would present similar fauna assemblages at a given time during this period (e.g., Cracraft, 1974). Different paleobiogeographic methods are used to study the correlation between the evolution of the biodiversity and the paleogeographic areas. For instance, in dicynodonts, two strategies are mostly used: (1) the “stratigraphic method” with correlation between the stratigraphic

Early Triassic (Onelekian) 232.9 My

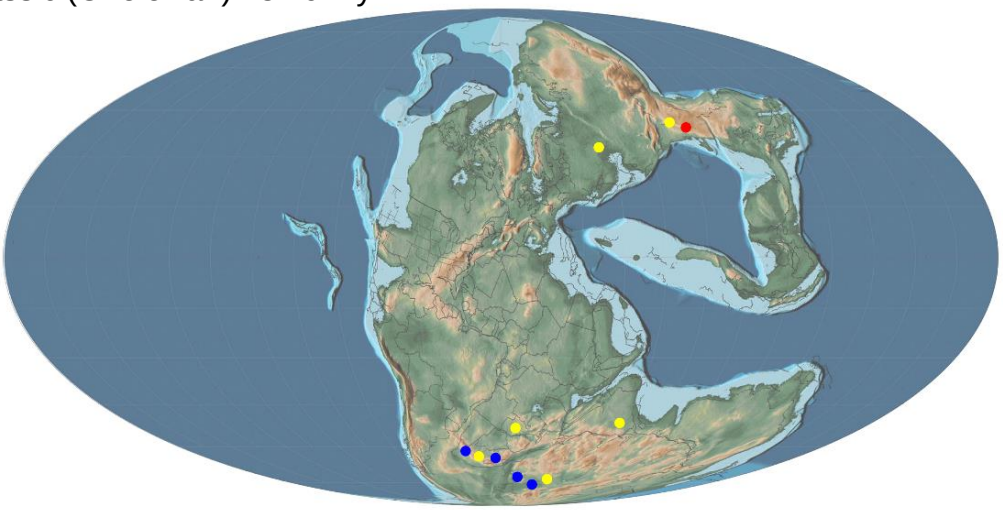

Middle Triassic (Anisian) 241.5 My

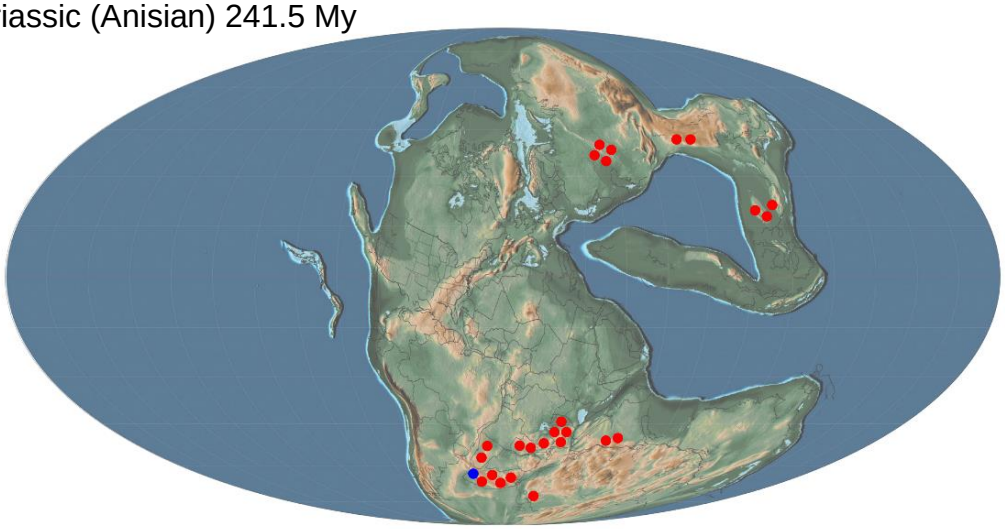

Late Triassic (Carnian) 248.5 My

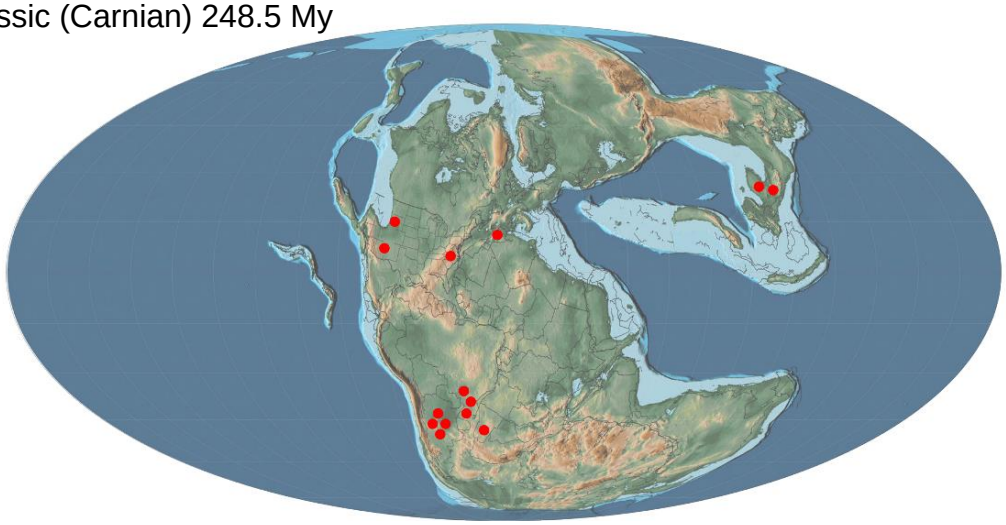

Figure I.4. Spatial distribution of dicynodonts during the Triassic (according the results from Fröbisch, 2009; Fröbisch et al., 2010; Abdala et al., 2013; Angielczyk et al., 2014; Maisch and Matzke, 2014; Ottone et al., 2014; Sidor et al., 2014; Kammerer, 2018; Liu et al., 2018). Maps are modified from Scotese (2014). The colored points indicate the locality of emydopoids (blue), lystrosaurids (yellow), and kannemeyeriforms (red).

occurences of taxa and the position of the geographic areas, and (2) the "phylogeography" (Cecca and Zaragüeta i Bagils, 2015) as a geographic interpretation resulted from the phylogenetic history of the taxa or population (i.e., group of individuals belonging to the same species). The paleobiogeography of the Triassic dicynodonts using the "stratigraphic method" has been studied in a few taxa: *Ischigualastia* (Elder, 2000) and *Stahleckeria* (Abdala et al., 2013). An extended paleobiogeographic approach including paleogeographic, stratigraphic, and phylogenetic data has been used by Hancox et al. (2013) for *Angonisaurus* and *Shansiodon*. The global work on the Triassic tetrapods of Ezcurra (2010) based its paleogeographic conclusions on "phylogeography" method. He briefly mentioned the evolution of the spatial distribution of the Triassic dicynodonts *Stahleckeria*, *Dolichuranus*, *Kannemeyeria*, *Vinceria*, *Tetragonias*, and *Shansiodon*. The tree reconciliation analyses of Ezcurra (2010) identified a cosmopolitan distribution in some tetrapod groups as the capitosaurid temnospondyles and the dicynodonts *Vinceria*, *Tetragonias*, and *Shansiodon* in Triassic. Some studies highlighted the spatial distribution of some tetrapod taxa highly impacted by the paleolatitudinal variations (i.e., provicialism) (e.g., Shubin and Sues, 1991; Irmis et al., 2007; Bernardi et al., 2018). In parallel, a paleolatitudinal distinction has been noticed between the plant assemblages in Laurasia and Gondwanna (e.g., Artabe et al., 2003; Ezcurra, 2010; Bernardi et al., 2018).

Histology and microanatomy of bone and the paleobiology of dicynodonts

The inner bone organization is preserved during the fossilisation and provide information, by comparison with bone of extant organisms, on the growth strategies, metabolism, and lifestyle of extinct organisms (e.g., Botha, 2003; Ray et al., 2005; Green et al., 2010; Ray et al., 2010; Green, 2012). The study of the bone organisation can be provided at two scales: a large one with the microanatomy (bone density, proportion of the cortex related to the medulla…), and a limited scale with the histology (organisation of the collagen fibers, osteocytes, bone remodelling…). The bone histology and microanatomy were only known for five Triassic dicynodonts: *Lystrosaurus* (e.g., Germain and Laurin, 2005; Ray et al., 2005), *Placerias* (Green et al., 2010; Green, 2012), *Wadiasaurus* (Ray et al., 2010), *Dinodontosaurus* (Bueno, 2015), and *Kannemeyeria* (e.g., Botha-Brink and Angielczyk, 2010).

The microanatomy of the dicynodonts suggested a diversity of lifestyle with terrestrial, semi-aquatic, and fossorial forms (e.g., Germain and Laurin, 2005; Ray et al., 2005; Green et al., 2010; Ray et al., 2010, 2012). However, the interpretations of the lifestyle of the dicynodonts based on the microanatomy raised issues. For instance, the lifestyle of *Lystrosaurus* is supposed to be: (1) semi-aquatic based on the bone microanatomy (Germain and Laurin, 2005: high bone density), morphoanatomie (Ray, 2006: forelimbs enlarged and flattened), and taphonomy (Germain and Laurin, 2005: abundance of rests and well preservation), and (2) terrestrial based on bone microanatomy (Botha-Brink and Angielczyk, 2010: an organization similar to the terrestrial *Kannemeyeria* and *Dicynodon*), paleoenvironment (King and Cluver, 1990: desertic environment), and the associated fauna (King and Cluver, 1990; Botha-Brink and Angielczyk, 2010: the remains of the amphibious fauna are sparse in comparison with those of *Lystrosaurus*). Indexes were used to quantify the bone thickness in the cortex that is supposed to be correlated to the lifestyle (Chinsamy-Turan, 2005). Wall (1983) proposed the RBT index (i.e., relative bone thickness), which indicates an organism at least semi-aquatic if exceeding 30%. However, some authors questioned the significance of the RBT when the bone thickness is medium or low developed, as in semi-aquatic or terrestrial organisms (e.g., Magwene, 1993; Ray et al., 2012). Another microanatomical index has been proposed, the cortico-diaphyseal index (i.e., mean cortical area relative to the external diameter of bone) measured by Bone Profiler (Girondot and Laurin, 2003) to be included in a paleobiological inference model (e.g., Germain and Laurin, 2005; Kriloff et al., 2008; Canoville and Laurin, 2010). Nonetheless, the software Bone profiler cannot measure the index without a clear medullar cavity.

The histological studies of the Triassic dicynodonts highlighted the presence of fibrolamellar bone ([FLB] primary osteons with lamellar bone within a woven bone matrix) and parallel fibers layer in the periphery of the cortex in *Lystrosaurus* (Ray et al., 2005), *Placerias* (Green et al., 2010), *Wadiasaurus* (Ray et al., 2010), *Dinodontosaurus* (Bueno, 2015), and *Kannemeyeria* (Botha-Brink and Angielczyk, 2010). These features indicate a high and cyclic bone growth rate that may be subject to environmental variations (e.g., Ricqlès et al., 1991; Chinsamy and Rubidge, 1993; Ray and Chinsamy, 2004). An external fundamental system has been indentified in *Placerias* (Green et al., 2010) and probably in *Dinodontosaurus* (Bueno, 2015), suggesting a complete or partial end in growth. Montes et al. (2007) deduced a

correlation between the bone growth rate and the resting metabolic rate (i.e., amount of energy used by an organism at rest per unit time). However, that correlation is questioned by Padian et al. (2004) that highlighted the presence of FLB in ectotherm organisms. The quantitative estimation of the resting metabolic rate fossil was first performed by Legendre et al. (2016) using a paleophysiological inference model, but only in extinct archosauromorphs.

Objectives

The large objective of this work is to better understand the evolution of the dicynodonts during the Triassic. We more particularly focus on the Laotian and Moroccan dicynodonts and their impact on paleobiogeographic, phylogenetic, and paleophysiologic issues.

Three well-preserved Laotian skulls discovered in the Luang Prabang Basin are described and added in a phylogenetic analysis to discuss about their taxonomic attribution and phylogenetic relationships. They have also briefly been described by Battail (2009) who attributed them to the genus *Dicynodon*. However, he never included them in a phylogenetic analysis and a comprehensive taxonomic revision of *Dicynodon* was recently made by Kammerer et al. (2011). The datation of the Purple Claystone Fm (bearing the dicynodonts) to latest Permian-earlier Triassic first brought interesting information about the still poorly-known evolution of the group around the major biological P-Tr crisis. Secondly, the presence of dicynodonts of late Permian-Early Triassic in age in the Indochina Block shed new light on the debate on the paleogeography of the South East Asia.

Three Moroccan species are currently known in the Argana Basin (Morocco): *Moghreberia nmachouensis*, *Azarifeneria barrati*, and *A*. *robustus*. However, uncertainties remain on their taxonomic validity. The dicynodont postcranial specimens discovered in the same basin are newly described to discuss about the presence of one or multiple Moroccan morphotypes. As well as the Laotian dicynodonts, the study of the Moroccan forms is also interested due to their occurrences in poorly-studied geographic areas.

First paleobiological inference models based on histological variables are built to infer thermometabolism in extinct synapsids: here, the dicynodonts. The inclusion of the largest sample of dicynodonts provides quantitative data on their metabolism and its evolution in this group during the Permian-Triassic. In a more broadly objective,

these inferences provides new evidence to better temporally and phylogenetically constrain the acquisition of the mammalian endothermy.

CHAPTER II

NEW LAOTIAN FORMS: ANATOMY, PHYLOGENY, AND IMPLICATIONS ON PALEOBIOGEOGRAPHY AND POST-PERMIAN DICYNODONT SURVIVORSHIP

Laotian dicynodont (M. Boulay & S. Lorrains © ADAGP – Paris 2006)

Laotian dicynodonts, a recent discovery that raises issues

A fragmentary skull has been discovered by Counillon (1896) and then studied by Répelin (1923) (Fig. II.1). As developed below, since its original description, its taxonomic attribution to the genus *Dicynodon* or *Lystrosaurus* has always been discussed (e.g., Das Gupta, 1922; Woodward, 1932; Yuan and Young, 1934; Piveteau, 1938; Battail, 2009; Kammerer et al., 2011). This question, unfortunately, remains unanswered due to the lost of the Counillon's specimen and the inaccuracy of the original description and the associated illustrations (Fig. II.5; e.g., Colbert, 1982; Battail et al., 1995; Kammerer et al., 2011).

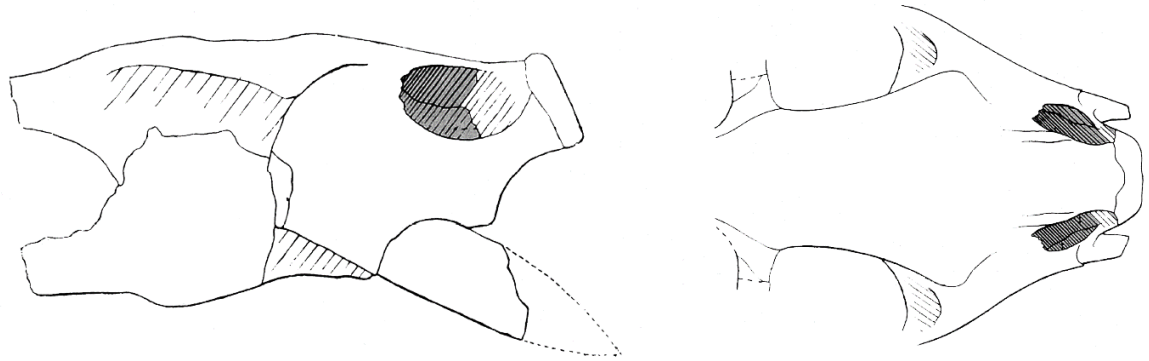

Figure II.1. Counillon's specimen reconstructed by Piveteau (1938) in lateral (left) and dorsal (right) view (modified from Piveteau, 1938). The illustrations are not in scale.

Later, an abundant and relatively well-preserved dicynodont cranial and post-cranian material was collected by Franco-Laotian expeditions (1993-2003) led by P. Taquet (Muséum national d'Histoire naturelle [MNHN], Paris, France) in the Purple Claystone Formation of the Luang Prabang Basin (Laos). Battail et al. (1995) first reported on the discovery of the Laotian dicynodont skulls on the basis of the two most-prepared skulls (LPB 1993-2 and 1993-3, illustrated in PAPER I). The noticeable characters highlighted by a preliminary description of the two skulls led them to attribute the specimens to two distinct species of *Dicynodon* (Battail et al., 1995). Later, Battail (2009) briefly redescribed LPB 1993-2 and 1993-3, plus a third specimen 1995-9 from the same locality. On the basis of the definitions of *Dicynodon* by Cluver and Hotton III (1981) and Cluver and King (1983), he confirmed the previous attribution to *Dicynodon* (Battail et al., 1995; Battail, 2009). However, until the comprehensive taxonomic revision of the genus *Dicynodon* by Kammerer et al. (2011), the validity of many species of *Dicynodon* was problematic (e.g., Broom, 1911; Watson, 1917).

Morphological variation were noticed between the three Laotian skulls, uncertainties thus persisted about their attributions to different and distinct species in regards to intraspecific (ontogeny, dimorphism) or taphonomic variation (Battail, 2009).

The revised study of the Laotian specimens presents several interests. First, the taxonomic attribution of the Laotian specimens and their phylogenetic positions have to be checked and settled. Then, while the age of the Purple Claystone Fm was largely debated (e.g., Counillon, 1896; Répelin, 1923; Piveteau, 1938; Saurin, 1962; Battail, 2009; Rossignol et al., 2016), the precise relationships of dicynodont forms supposed to be latest Permian-earlier Triassic in age would bring additional information about the evolution of the group around the major biological P-Tr crisis. Finally, their occurrence in Southeastern Asia (Laos) shed new light on the paleobiogeography of dicynodonts during the early Triassic-latest Permian and consequently on the debate about the timing of collision between the Indochina, the South China and the North China blocks.

The PAPER I dealed with these problematics and has been published in *Journal of Vertebrate Paleontology*. The Laotian dicynodonts are currently conserved in the Savannakhet Dinosaur Museum in Laos. Financial support granted by the GDRI PalBioDiv SEA project allowed me a first-hand study of the three skulls LPB 1993-2, 1993-3, and 1995-9 in the Laotian museum, where I described and photographed them. The morphological variation noticed between the Laotian forms has been discussed based on observations collected during the visits of dicynodont collections in the Evolutionary Studies Institute in Johannesburg (South Africa; financial support from CR2P), the Museum of Comparative Zoology in Cambridge (Massachusetts, U.S.A.; financial support from CR2P and ISTEP), and the Natural History Museum in London (United Kingdom; financial support from SYNTHESYS), and on the literature.
In PAPER I, I wrote the majority of the article except the “Geological Setting” part that has been provided by the geologist colleagues S. Bourquin (Université de Rennes, France) and C. Rossignol (Universidade de São Paulo, Brazil). The discussion parts “New Data Supporting the Survivorship of Multiple Lineages across the P-Tr Boundary?” and “Paleobiogeographic Implications of the Two Laotian Dicynodonts” resulted from joint discussions between all coauthors. I preformed the phylogenetic analyses and produced all figures except the figure 1 and the reconstruction in figures 2 to 4 drawn by S. Fernandez (MNHN, France).
The results have been presented during the International Meeting of Early-stage Researchers in Palaeontology (Lesvos, Greece, 2017).

PAPER I

New dicynodonts (Therapsida, Anomodontia) from near the Permo-Triassic boundary of Laos: implications for dicynodont survivorship across the Permo–Triassic mass extinction and the paleobiogeography of Southeast Asian Blocks

Chloé Olivier, *[1, 2] Bernard Battail, [2] Sylvie Bourquin, [3] Camille Rossignol, [4] J. - Sébastien Steyer [2], and Nour-Eddine Jalil [2]

[1]CR2P (Centre de Recherche en Paléontologie - Paris), Museum National d'Histoire Naturelle–CNRS–Sorbonne Université, 57 rue Cuvier, CP 38, F-75005, Paris, France, chloe.olivier@mnhn.fr; bernard.battail@mnhn.fr; jean-sebastien.steyer@mnhn.fr; nour-eddine.jalil@mnhn.fr;

[2]Univ Rennes, CNRS, Géosciences Rennes - UMR 6118, F-35000 Rennes, France, sylvie.bourquin@univ-rennes1.fr;

[3]Instituto de Astronomia, Geofísica e Ciências Atmosféricas, Departamento de Geofísica, Universidade de São Paulo, Rua do Matão, 1226, Cidade Universitária, Butantã, 05508-090 São Paulo, São Paulo, Brazil, camil.rossignol@gmail.com;

[4]Laboratoire Biodiversité et Dynamique des Ecosystèmes, Faculté des Sciences Semlalia, Université Cadi Ayyad, Boulevard Prince My Abdellah, 40000 Marrakech, Maroc

*Corresponding author

Published in *Journal of Vertebrate Paleontology* in 2019

Journal of Vertebrate Paleontology e1584745 (22 pages)
© by the Society of Vertebrate Paleontology
DOI: 10.1080/02724634.2019.1584745

Check for updates

ARTICLE

NEW DICYNODONTS (THERAPSIDA, ANOMODONTIA) FROM NEAR THE PERMO-TRIASSIC BOUNDARY OF LAOS: IMPLICATIONS FOR DICYNODONT SURVIVORSHIP ACROSS THE PERMO-TRIASSIC MASS EXTINCTION AND THE PALEOBIOGEOGRAPHY OF SOUTHEAST ASIAN BLOCKS

CHLOE OLIVIER, *[,1] BERNARD BATTAIL,[1] SYLVIE BOURQUIN,[2] CAMILLE ROSSIGNOL,[3] J.-SEBASTIEN STEYER,[1] and NOUR-EDDINE JALIL[1,4]

[1]CR2P (Centre de Recherche en Paléontologie - Paris), Museum National d'Histoire Naturelle–CNRS–Sorbonne Université, 57 rue Cuvier, CP 38, F-75005, Paris, France, chloe.olivier@mnhn.fr; bernard.battail@mnhn.fr; jean-sebastien.steyer@mnhn.fr; nour-eddine.jalil@mnhn.fr;

[2]Univ Rennes, CNRS, Géosciences Rennes - UMR 6118, F-35000 Rennes, France, sylvie.bourquin@univ-rennes1.fr;

[3]Instituto de Astronomia, Geofísica e Ciências Atmosféricas, Departamento de Geofísica, Universidade de São Paulo, Rua do Matão, 1226, Cidade Universitária, Butantã, 05508-090 São Paulo, São Paulo, Brazil, camil.rossignol@gmail.com;

[4]Laboratoire Biodiversité et Dynamique des Ecosystèmes, Faculté des Sciences Semlalia, Université Cadi Ayyad, Boulevard Prince My Abdellah, 40000 Marrakech, Maroc

ABSTRACT—The dicynodonts are an emblematic group of herbivorous therapsids that survived the Permo-Triassic (P-Tr) crisis. Laotian dicynodonts from stratigraphically constrained beds, recently dated using the U-Pb zircon method, yield new insights into terrestrial faunas of Southeast Asia during the latest Permian and earliest Triassic. Summarily described, they were originally attributed to the genus *Dicynodon*. We provide a new phylogenetic analysis for Laotian dicynodonts, based on three well-preserved skulls, indicating that they belong to two new taxa: *Counillonia superoculis*, gen. et sp. nov., and *Repelinosaurus robustus*, gen. et sp. nov. Our phylogenetic analysis of Dicynodontia indicates that (1) *Counillonia* is closely related to some '*Dicynodon*'-grade taxa and (2) *Repelinosaurus* is a kannemeyeriiform. The phylogenetic affinities of these new Laotian dicynodonts allow discussion of the survivorship of multiple lineages (Kannemeyeriiformes and '*Dicynodon*'-grade dicynodontoids) across the P-Tr crisis. The Laotian dicynodonts also shed new light on the paleobiogeography of Southeast Asia from the late Paleozoic to the early Mesozoic, particularly the timing of collisions between the Indochina, the South China, and the North China blocks. The presence of dicynodonts in Laos, most likely in the Early Triassic, thus implies that the connection between the Indochina Block and the South China Block occurred no later than the latest Permian or earliest Triassic (i.e., when the dicynodonts provide direct evidence for a connection).

http://zoobank.org/urn:lsid:zoobank.org:pub:FE310B53-41AA-4C13-B076-5D1CB91FC1BE

SUPPLEMENTAL DATA—Supplemental materials are available for this article for free at www.tandfonline.com/UJVP

Citation for this article: Olivier, C., B. Battail, S. Bourquin, C. Rossignol, J.-S. Steyer, and N.-E. Jalil. 2019. New dicynodonts (Therapsida, Anomodontia) from near the Permo-Triassic boundary of Laos: implications for dicynodont survivorship across the Permo-Triassic mass extinction and the paleobiogeography of Southeast Asian blocks. Journal of Vertebrate Paleontology. DOI: 10.1080/02724634.2019.1584745.

INTRODUCTION

The dicynodonts are emblematic Permian and Triassic (P-Tr) therapsids. They constitute an important component of the terrestrial P-Tr fauna and were the dominant herbivores in their ecosystems (Cluver and King, 1983). As such, dicynodonts represent a key group for understanding the impact of the P-Tr crisis on terrestrial environments. Known Early Triassic dicynodont genera include the cosmopolitan and speciose *Lystrosaurus*, the small-bodied emydopoids *Myosaurus* from South Africa/Antarctica and *Kombuisia* from Antarctica, and the Chinese kannemeyeriiform *Sungeodon* (Fröbisch et al., 2010; Maisch and Matzke, 2014).

In North China, Liu et al. (2013) used the U-Pb zircon method (based on zircon U-Pb sensitive high-resolution ion microprobe [SHRIMP] dating) within the Ermaying and Tongchuan dicynodont-bearing formations (with the kannemeyeriiform genera *Shansiodon* and *Sinokannemeyeria*) and dated them to Early to Middle Triassic. More recently, the higher-resolution chemical abrasion–thermal ionization mass spectrometry (CA-TIMS) dated these formations as Middle Triassic (Anisian–Ladinian) (Liu et al., 2018). Thus, the main kannemeyeriiform radiation seems to have occurred after the beginning of the Triassic, with ca. 40 species known by the Middle Triassic (Fröbisch, 2008).

The first record of dicynodonts in Laos (Southeast Asia) dates back to the 19th century: Counillon (1896) mentioned a poorly preserved and incomplete skull found in the Purple Claystone Formation of the Luang Prabang Basin, northern Laos (Fig. 1A). This specimen was first studied by Repelin (1923), who assigned it to a new species of *Dicynodon*, *D. incisivum*, which he considered to be closely related to *Dicynodon orientalis* from the Panchet Formation of India. Later, Das Gupta (1922)

*Corresponding author.

Color versions of one or more of the figures in the article can be found online at www.tandfonline.com/ujvp.

Published online 23 Apr 2019

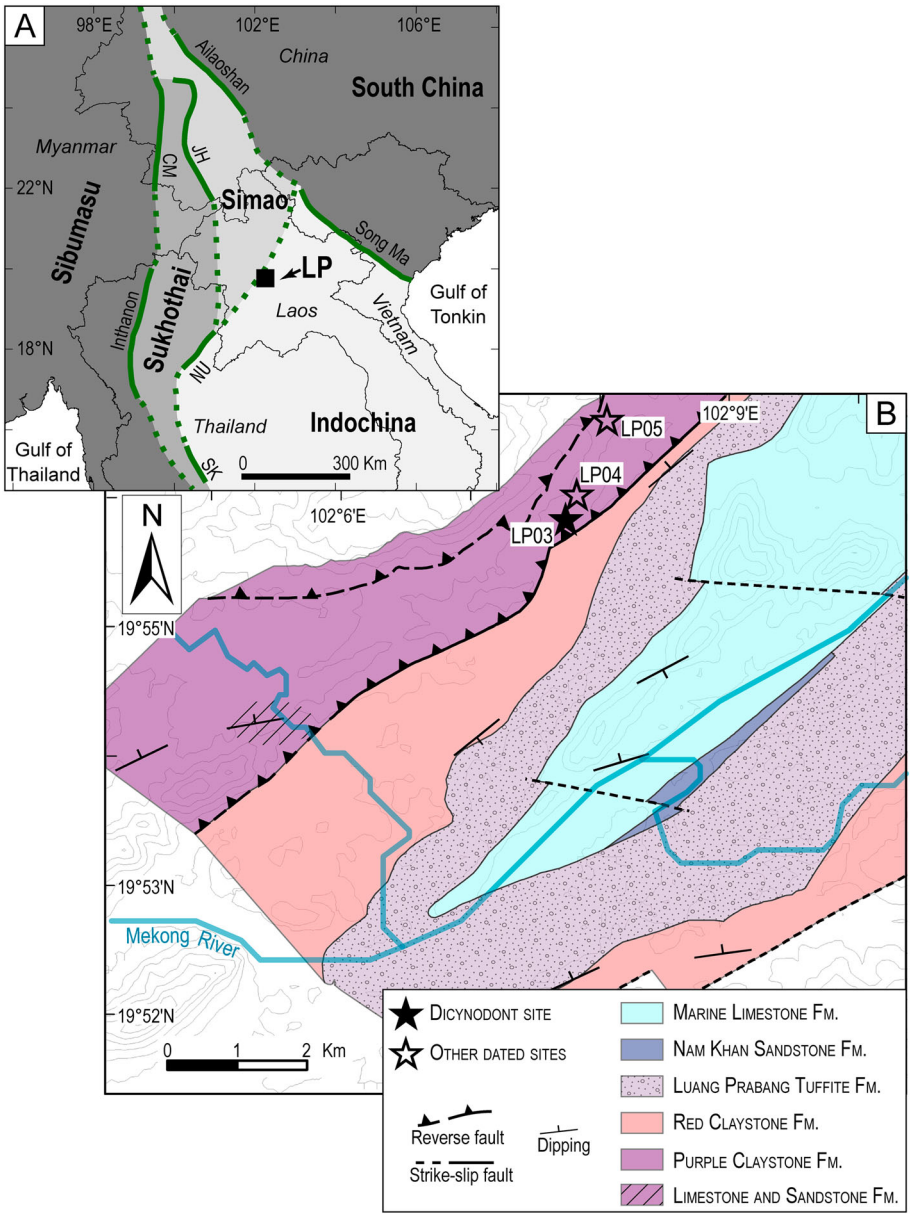

FIGURE 1. Continental blocks of Southeast Asia and geological map of the Luang Prabang Basin. **A**, tectonic subdivisions of Southeast Asia, after Metcalfe (2011). **B**, geological map of the Luang Prabang Basin with the emplacement of fossil sites and dated samples. Modified after Blanchard et al. (2013). Sample LP03 was collected at the dicynodont site, sample LP04 in an unfossiliferous site, and sample LP05 at the chroniosuchian site (Arbez et al., 2018). **Abbreviations**: **AL**, Ailaoshan suture zone; **CM**, Changning Menglian suture zone; **JH**, Jinghong suture zone; **LP**, emplacement of the Luang Prabang Basin; **NU**, Nan Uttaradit suture zone; **SK**, Sra Kaeo suture zone.

transferred *D. orientalis* to the genus *Lystrosaurus* and Woodward (1932), followed by Yuan and Young (1934), attributed Counillon's specimen to *Lystrosaurus*. Piveteau (1938) redescribed the specimen and reassigned it to *Dicynodon*. Based on this study, Battail (2009) and Kammerer et al. (2011) also favored this taxonomic attribution. Nevertheless, this specimen continued to be mentioned as *Lystrosaurus* without further comment (Keyser and Cruickshank, 1979; King, 1988). Counillon's specimen has unfortunately been lost, preventing further investigations. The illustrations accompanying the original description cannot be interpreted with confidence (Colbert, 1982; Kammerer et al., 2011). Accordingly, the taxon '*Dicynodon incisivum*' should be considered a nomen dubium (as pointed out by many authors, e.g., Battail, 2009; Fröbisch, 2009; Kammerer et al., 2011).

Between 1993 and 2003, Franco-Laotian expeditions led by P. Taquet (Museum National d'Histoire Naturelle [MNHN], Paris, France) collected abundant dicynodont remains from the Purple Claystone Formation of the Luang Prabang Basin. Among these fossils, three dicynodont skulls (LPB 1993-2, LPB 1993-3, and LPB 1995-9) were tentatively ascribed to the genus *Dicynodon* by Battail (2009). However, no phylogenetic analysis has been performed on these specimens, and their relationships with other dicynodonts remain equivocal.

The age of these specimens, collected in the Purple Claystone Formation, has long been a subject of debate. Indeed, this formation was first attributed to the Early Triassic (Counillon, 1896; Repelin, 1923; Piveteau, 1938) but was later considered to be Late Triassic to Middle Jurassic in age (Saurin, 1962). Based on the dicynodont skulls and their supposed attribution to the genus *Dicynodon* (Battail, 2009), this formation was considered to be late Permian in age (Battail, 2009). Recent geochronological analyses (based on U-Pb detrital zircons dated by laser ablation inductively coupled plasma mass spectroscopy [LA-ICP-MS]) performed on volcaniclastic rocks from the Purple Claystone

TABLE 1. Summary of the maximum depositional ages obtained by U-Pb laser ablation inductively coupled mass spectrometry (LA-ICP-MS) dating on detrital zircon grains from volcaniclastic rocks of the samples collected in the Purple Claystone Formation (LP03, LP04, LP05) (Rossignol et al., 2016).

				Maximum depositional age				
Sample	N_a	N_{zr}	N	Concordia age	± (2σ)	n	MSWD	Probability
LP03	105	102	25	252.0	2.6	6	0.89	0.55
LP04	41	36	7	300.5	3.7	4	0.73	0.65
LP05	96	95	39	251.0	1.4	21	0.55	0.99

LP03 was collected at the dicynodont fossil site. The MSWD and the probability given for the concordia ages are for both concordance and equivalence. **Abbreviations**: **MSWD**, mean square of weighted deviates; **n**, number of analyses used to calculate the maximum depositional age; **N**, number of concordant zircon grains; $\mathbf{N_a}$, number of analyses per sample; $\mathbf{N_{zr}}$, number of zircon grains analyzed per sample.

Formation suggest a maximum depositional age of 251.0 ± 1.4 Ma (Table 1) (Rossignol et al., 2016).

This temporal framework thus allows us to document dicynodont survivorship and post-extinction recovery in a P-Tr basin located outside the classic, extensively studied Russian (e.g., Benton et al., 2004) and South African (e.g., Ward et al., 2005; Smith and Botha-Brink, 2014; Viglietti et al., 2018) ones. The fauna preserved in the Luang Prabang Basin also offers new evidence concerning the paleobiogeography of dicynodonts.

Here, we provide detailed description of the three Laotian skulls (LPB 1993-2, LPB 1993-3, and LPB 1995-9), which represent two new taxa. Phylogenetic analysis is then performed to test the relationships of these new taxa within Dicynodontia.

Institutional Abbreviations—**BP**, Evolutionary Studies Institute (formerly the Bernard Price Institute for Palaeontological Research and the Institute for Human Evolution), Johannesburg, South Africa; **LPB**, Laotian specimens found in the Luang Prabang Basin, currently in the Savannakhet Dinosaur Museum, Savannakhet, Laos; **MCZ**, Museum of Comparative Zoology, Harvard University, Cambridge, Massachusetts, U.S.A.; **NHMUK**, Natural History Museum, London, United Kingdom.

Anatomical Abbreviations—**aPt**, anterior ramus of the pterygoid; **Bo**, basioccipital; **Ch**, choana; **EcPt**, ectopterygoid; **Eo**, exoccipital; **EpiPt**, epipterygoid; **Fm**, foramen magnum; **Fr**, frontal; **Ip**, interparietal; **Ipv**, interpterygoid vacuity; **Ju**, jugal; **La**, lacrimal; **Laf**, lacrimal foramen; **Lbf**, labial fossa; **mPt**, median plate of the pterygoid; **Mx**, maxilla; **Na**, nasal; **Oct**, occipital tuber; **Opt**, opisthotic; **Pa**, parietal; **Pal**, palatine; **Pant**, pila antotica; **Pbs**, parabasisphenoid; **Pi**, pineal foramen; **Pm**, premaxilla; **Po**, postorbital; **Pp**, preparietal; **PrF**, prefrontal; **Q**, quadrate; **Qj**, quadratojugal; **qPt**, quadrate ramus of the pterygoid; **Smx**, septomaxilla; **So**, supraoccipital; **Sq**, squamosal; **T**, tusk; **Tpf**, posttemporal fenestra; **Va**, vagus nerve aperture; **Vo**, vomer.

GEOLOGICAL SETTING

The Luang Prabang Basin, located in the Indochina Block (Fig. 1A), was originally studied by Counillon (1896) and consists of an asymmetric NE–SW (northeast–southwest) syncline with NE–SW thrusts separating the Purple Claystone Formation and the Limestone and Sandstone Formation to the north from younger formations to the south (Fig. 1B; Blanchard et al., 2013).

The Limestone and Sandstone Formation is made up of shallow marine deposits, dated to the late Changhsingian on the basis of its ammonoid remains (Blanchard et al., 2013). These marine deposits are overlain by black claystone layers, containing a typical Cathaysian flora (Bercovici et al., 2012).

The Limestone and Sandstone Formation is overlain by the Purple Claystone Formation, from which various fossil remains have been excavated (dicynodonts and a chroniosuchian; Steyer, 2009; Arbez et al., 2018). The Purple Claystone Formation is mainly composed of homogeneous silty claystones, silts, and more rarely clays (Bercovici et al., 2012). The formation also comprises volcaniclastic siltstones and sandstones, with millimeter- to centimeter-sized rounded and highly weathered volcaniclasts (up to about 20 vol.%). These volcaniclasts exhibit a variety of volcanic textures (microlithic, trachytic, porphyritic) and are sometimes embedded within lithic fragments, attesting to multiple reworking events for these volcaniclasts (Bercovici et al., 2012; Blanchard et al., 2013). The Purple Claystone Formation also contains subordinate amounts of coarser deposits, including sandstone and conglomeratic facies with three-dimensional megaripples typical of braided river deposits. The conglomeratic levels consist of rounded pebbles of highly fossiliferous limestones (foraminifers, corals, bryozoans), subangular to rounded pebbles of volcanic rocks, black cherts, red quartzites, red sandstones, and siltstones. Paleosols, sometimes exhibiting vertical root traces, are developed within this formation (Bercovici et al., 2012). The sedimentary facies association indicates braided river depositional environments, evolving vertically to alluvial plain environments, probably including ponds (Bercovici et al., 2012).

Three samples from the Purple Claystone Formation, including one collected at the dicynodont site (Fig. 1C), were dated using U-Pb geochronology on detrital zircon (Rossignol et al., 2016). The sample collected at the dicynodont fossil site yielded a maximum depositional age of 252.0 ± 2.6 Ma, whereas the other volcaniclastic samples collected in the same formation yielded maximum depositional ages of 251.0 ± 1.4 and 300.5 ± 3.7 Ma (Table 1). The various volcaniclastic textures, their roundness, and the relatively low volcaniclast content (below 20%) implying an important and protracted mixing with other detrital particles, as well as the fact that some of the volcaniclasts underwent at least two sedimentary cycles (Bercovici et al., 2012; Blanchard et al., 2013), suggest that these dates, obtained from zircon grains interpreted as being detrital in origin, represent maximum depositional ages. The actual age of deposition of the Purple Claystone Formation is therefore likely to be younger. Both youngest maximum depositional ages (i.e., 252.0 ± 2.6 and 251.0 ± 1.4 Ma) encompass the P-Tr boundary (251.902 ± 0.024 Ma; Burgess et al., 2014) within uncertainties. The consideration of a late Permian age, potentially plausible, would nonetheless imply that the reworking of the zircon grains took place within an unlikely brief time span. Given the age of the overlying formation (224.9 ± 1.0 Ma; Blanchard et al., 2013), an age up to the Carnian could be proposed as the theoretical upper age limit for the Purple Claystone Formation. However, the occurrence of a regional Middle Triassic unconformity (e.g., Racey, 2009), probably superimposed onto the reverse fault separating the Purple Claystone Formation from other sedimentary units to the southeast (Fig. 1B), reduces the likely time span for the deposition of the Purple Claystone Formation. Consequently, an Early Triassic age for the Purple Claystone Formation and its enclosed fossils is considered to be the most likely.

METHODS

The interpretation of the cranial bone contacts is based either on direct observations of the scarce preserved sutures or on relief differences. When possible, some sutures were deduced from the contacts between the surrounding bones.

SYSTEMATIC PALEONTOLOGY

THERAPSIDA Broom, 1905
ANOMODONTIA Owen, 1860
DICYNODONTIA Owen, 1860
DICYNODONTOIDEA Olson, 1944
COUNILLONIA, gen. nov.

Type Species—*Counillonia superoculis*, gen. et sp. nov., monotypic.

Etymology—In honor of the French geologist Jean-Baptiste-Henri Counillon, member of the Pavie Missions, who was the first to mention the occurrence of dicynodonts in the Luang Prabang Basin (Counillon, 1896; see Steyer, 2009, for a biography).

Diagnosis—See diagnosis of the type species.

COUNILLONIA SUPEROCULIS, gen. et sp. nov.
(Fig. 2)

Holotype—LPB 1993-3, a skull without mandible (basal length: 16.02 cm; maximum width: 13.41 cm). The posterior side of the left orbit, the quadrates, and the stapes are missing. The dorsal surfaces of the premaxilla, the nasals, the prefrontals, and the frontals are partially eroded. The prearietal, the prootic, and the epipterygoid are poorly preserved.

Geographic Distribution and Stratigraphic Range—LPB 1993-3 (19°55′59″N, 102°07′41″E) was discovered in the Purple Claystone Formation, Luang Prabang Basin (Laos). This formation was initially attributed to the Early Triassic by Counillon (1896) then to the late Permian by Battail (2009). Recent geochronological (U-Pb on detrital zircon; Rossignol et al., 2016) analyses suggest a maximum depositional age of 251.0 ± 1.4 Ma (see 'Geological Setting' above).

Etymology—From the Latin 'oculis' (dative plural of oculus, eye) and 'super' (upward), referring to its largely dorsally opening orbits due to an especially narrow interorbital bar.

Diagnosis—Medium-sized dicynodontoid characterized by the unique combination of the following character states: a reduced premaxillary secondary palate; a nasofrontal suture with a distinct posterior process; a narrow intertemporal bar; a reduced temporal fenestra; a pineal foramen located in the posterior quarter of the dorsal skull length; an acute angle of the squamosal wings in lateral view; zygomatic squamosal rami posteriorly inserted at mid-height of the occiput; a relatively large median pterygoid plate; high-angled posterior pterygoid rami; anterior rami of the pterygoids ventrally highly expanded; a long interpterygoid vacuity; no intertuberal ridge; distinct exoccipital and basioccipital contributions to the occipital condyle; and a very sharp and posteriorly directed lateral edge of the paroccipital process, which is distinctly offset from the surface of the occipital plate. The nasofrontal suture with a distinct posterior process distinguishes *Counillonia* from the Laotian *Repelinosaurus* and '*Dicynodon*'-grade taxa. Further distinguished from closely related '*Dicynodon*'-grade taxa by a pineal foramen located far posteriorly and a large median pterygoid plate. Further distinguished from *Repelinosaurus* by an anteriorly directed caniniform process, a narrow interorbital bar, a triangular occiput, and zygomatic squamosal rami posteriorly inserted at mid-height of the occiput.

Description

The skull is slender and short, with a short preorbital region and a narrow snout. In dorsal view, the skull is relatively broad, with laterally expanded zygomatic arches. The combination of the laterally bowed zygomatic arches and narrow interorbital results in notably dorsally directed orbits (Fig. 2A). The surfaces of the premaxilla, the maxillae, the nasals, the frontals, and the postorbitals are weathered. Because of this, the mid-nasal, naso-premaxillary, preparieto-frontal, and postorbito-parietal sutures are not visible (Fig. 2A). The absence of visible sutural contacts in the weathered narial region precludes determination of the possible presence of the septomaxillae (Fig. 2B). It is thus not clear whether the septomaxillae form part of the ventrolateral margin of the nares, which seems to be formed only by the premaxilla anteriorly, the nasals dorsolaterally, and the maxillae ventrolaterally. In addition, the bone contacts cannot be discerned on the occiput, nor along the medial partition of the temporal and orbital fossae (Fig. 2B, D).

The short premaxilla is fused and forms the anterior portion of the snout that constricts and ends in a squared tip. The tip of the snout shows weak ventral curvature in anterior view (not figured here) as in *Tropidostoma* and *Aulacephalodon* (Kammerer and Smith, 2017). However, this curvature and possible ridges or rugosities cannot be confirmed due to the poor preservation of the dorsal surface of the premaxilla. The premaxilla contributes to the external anterior edge of the naris. The large narial opening is situated near the anterior and ventral edges of the snout and contributes to more than a third of the surface of the snout (Fig. 2B). The external ventral margin of the naris is visible in dorsal view (Fig. 2A). The premaxilla contacts the nasals posterodorsally and the maxilla posterolaterally at the level of the anterior third of the nares. In ventral view, the premaxilla bears two thin, parallel longitudinal ridges (the anterior palatal ridges) that surround a wide, median longitudinal depression and extend beyond the anterior third of the palatal surface (Fig. 2C). This depression turns posteriorly into a sharp crest (the median palatal ridge), which extends to the vomer posteriorly and is flanked on either side by flat depressions. The height of this longitudinal ridge increases posteriorly. On the palatal surface, the premaxilla contacts the maxillae laterally. The absence of visible sutures between the premaxilla and the palatines yields no information about a potential contact (Fig. 2C). The nasals bear a median, rugose, and well-developed boss, which extends onto the bones bordered by two wide elongated depressions that broaden posteriorly and terminate on the frontals (Fig. 2A). However, as mentioned above, the poor preservation of the snout surface precludes firm conclusions about the original external relief of the nasals. The nasals are surrounded by the frontals and the prefrontals posteriorly, the premaxilla anteriorly, and the maxillae and lacrimals laterally (Fig. 2A, B).

The prefrontals form the anterodorsal edge of the orbits. On the external surface of the skull, they contact the frontals medially, the lacrimals laterally, and the nasals anteriorly (Fig. 2A). A single rugose boss is visible on each prefrontal. However, as already noted for the nasals, there is no reliable information about the original relief of the bones due to the poor preservation of their external surfaces.

The frontals form the major part of the skull roof (Fig. 2A). The sutures of the frontals can be discerned along their contact with the postorbitals, the prefrontals, and the nasals, as well as at the interfrontal contact (Fig. 2A). The external surface of the skull roof is poorly preserved; the presence of postfrontals cannot be confirmed in LPB 1993-3. The nasofrontal suture has a distinct posterior process. The dorsal margin of the orbits seems to be largely made up of the frontals. Apart from a small chip of bone missing on the right dorsal margin of the orbit, the rest of its margin appears to be preserved, with a symmetry of the lateral

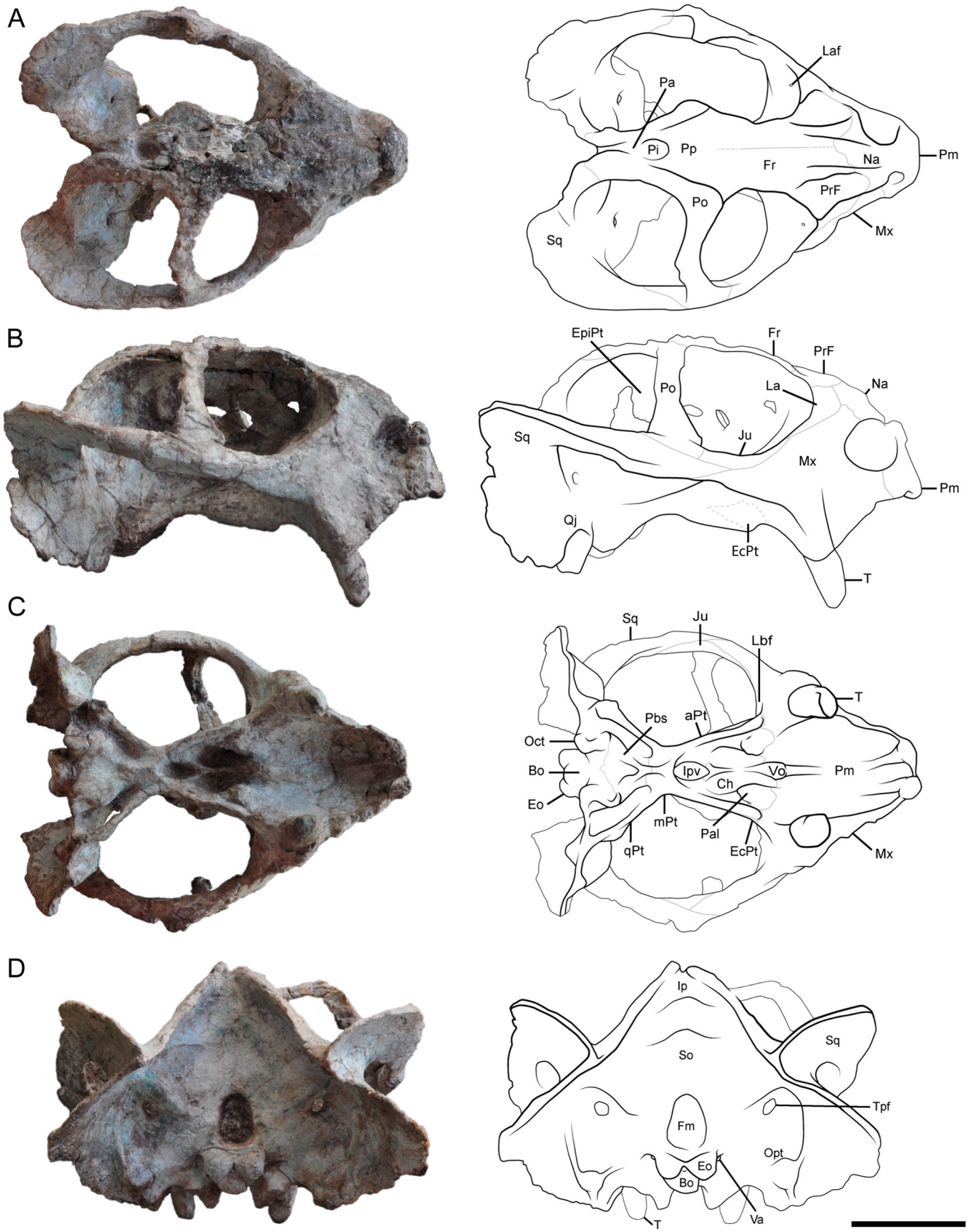

FIGURE 2. *Counillonia superoculis*, gen. et sp. nov., LPB 1993-3, holotype, photographs and interpretive drawings of skull in **A**, dorsal, **B**, right lateral, **C**, ventral, and **D**, occipital views. The thin gray lines represent sutures, and the bold black lines represent relief. The dotted line represents the authors' interpretation of sutures based on variation in bone texture. Scale bar equals 5 cm.

TABLE 2. Cranial measurements (in cm) of the three Laotian dicynodont skulls attributed to *Counillonia superoculis* and *Repelinosaurus robustus*, scaled with Image J 1.50i.

	1. *C. superoculis*	2. *R. robustus*	
Dimension	LPB 1993-3	LPB 1995-9	LPB 1993-2
Basal length (from the tip of snout to the occipital condyle)[a]	16.02	15.72	19.00
Maximum width[b]	13.41	NA	NA
Maximum orbital height[c]	4.82	4.19	5.79
Maximum orbital length[c]	5.67	4.73	6.82
Mediolateral diameter of the tusk root[a]	1.27	1.46	2.02
Anteroposterior diameter of the tusk root[a]	1.56	0.90	1.49
Pineal foramen length[b]	1.36	1.33	0.96
Pineal foramen width[b]	0.96	0.87	0.66

[a]In ventral view.
[b]In dorsal view.
[c]In lateral view.

margins of the orbits and continuous lateral borders. The interorbital region is broader than the intertemporal bar (Fig. 2A).

The prearietal is strongly weathered, and its anterior part is missing. However, its posterior region displays a small bulge anterior to the pineal foramen, the relief possibly being due to its poor preservation (Fig. 2A). The contact between the prearietal and neighboring bones (postorbitals and frontals) cannot be determined.

The dorsal exposure of the parietals is limited to a midline groove between the posterior postorbital processes (Fig. 2A). The parietals then contact the postorbitals laterally and dorsally. External sutural contacts between the parietals and the frontals are invisible due to the poor preservation of the prearietal and the eroded external surface of the skull roof. The pineal foramen is surrounded by the parietals posteriorly and by the prearietal anteriorly. The oval pineal foramen, with a length of 1.36 cm and a width of 0.96 cm (Table 2), has its long axis perpendicular to the axis of the intertemporal bar. It is located in the posterior quarter of the skull roof (continuous character 7, Appendix 1).

The slender postorbitals have lateral and posterior processes. The posterior postorbital process merges along the intertemporal bar, posterior to the pineal foramen (Fig. 2A). The temporal portion of the postorbitals appears to be oblique, with a dorsolateral orientation. However, the poor preservation of the external surface of the postorbital does not allow confirmation of this orientation with certainty. The posterior postorbital region is thinner than the preorbital one (Fig. 2A). The postorbitals extend along almost the entire intertemporal bar, bordering the temporal fossae medially and anteriorly (Fig. 2A). They thus constitute the posterior margin of the orbits. On their external surface, the posterior postorbital processes mainly contact the squamosals and to a lesser degree the interparietal posteriorly, the parietals medially, and the frontals anteriorly. As mentioned above, no reliable information can be provided on the contact between the postorbitals, the frontals, and the prearietal. The lateral postorbital processes have a sutural contact with the jugals anteroventrally and the zygomatic squamosal processes posteroventrally (Fig. 2B).

The maxillae form the largest part of the lateral surface of the snout. They contact the premaxilla anteriorly and the lacrimals and the nasals dorsally (Fig. 2B). The maxillonasal suture lies on the dorsal edge of the nares. There is no sutural contact between the maxillae and the prefrontals due to the anterior expansion of the lacrimals that contact the nasals. The maxillary zygomatic process is posteriorly pointed and contacts the squamosal posteriorly and the jugal dorsally (Fig. 2B). The maxillae bear short caniniform processes housing tusks. The dorsal edge of the erupted portion of the tusk is anterior to the anterior edge of the orbits. The caniniform processes and the tusks face anteriorly. The tusks have a subcircular basal section (Fig. 2C; Table 2). On the ventral surface, no maxillary teeth are observed except the tusks (Fig. 2C). The maxillae contact the anterior rami of the pterygoids and the ectopterygoids posteriorly and the jugals and the squamosals laterally. No boundaries are visible in front of the palatines, and nothing can be confirmed about the extension of medial maxillary processes posterior to the premaxilla. In *Lystrosaurus* (e.g., Cluver, 1971) and *Kannemeyeria lophorhinus* (e.g., the holotype, BP/1/3638, and the specimen formerly referred to *Rechnisaurus cristarhynchus*, NHMUK R11955 [Renaut et al., 2003; C. Olivier, pers. observ., 2018]), these processes exclude the contact between the premaxilla and the palatines. A depression lies on the suture between the maxillae and the pterygoids (Fig. 2B). A broad labial fossa opens posterior to the tusk (Fig. 2C). Its boundaries cannot be discerned; however, it is usually surrounded by the maxillae ventrally, the jugals dorsolaterally, and the palatines medially (e.g., Cluver, 1971). It is therefore not certain whether *Counillonia* has a true labial fossa (circumscribed by the maxillae, the palatines, and the jugals) or a comparable structure to the foramen in dicynodonts such as *Diictodon*, *Endothiodon*, or *Dicynodontoides* (e.g., Angielczyk and Kurkin, 2003).

The lacrimals are relatively triangular in lateral view (Fig. 2B). They contact the nasals and prefrontals dorsally, the maxillae ventrally, and the jugals posteriorly. Their anterior, well-developed expansions exclude a maxilloprefrontal sutural contact. Their sutures within the orbits are not visible. The lacrimals constitute the anterior margin of the orbits with the jugals anteroventrally and the prefrontals anterodorsally (Fig. 2B). Within the orbit, each lacrimal is perforated by a single foramen (Fig. 2A).

The jugals are longitudinally elongated and form the ventral edge of the orbits (Fig. 2B). However, their expansion within the orbits and their natural limits cannot be discerned due to the absence of visible sutures, as noted above. Visible sutures on the lateral side of the skull show a long scarf joint with the maxillae ventrally, a jugal posterior process contacting the postorbitals posteriorly, and a small contact with the zygomatic squamosal processes ventroposteriorly and the lacrimals anterodorsally (Fig. 2B).

The squamosals are triradiate, with zygomatic, temporal, and quadrate rami. The zygomatic ramus shapes the posterior region of the zygomatic arch (Fig. 2B). In dorsal view (Fig. 2A), it widens posteriorly into a wing-shaped structure without a folded edge. It becomes narrow in the pointed anterior region, without dorsoventral expansion posterior to the postorbital bar (Fig. 2B). The squamosal zygomatic processes contact the jugals, the postorbitals, and the maxillae anteriorly (Fig. 2B). They circumscribe the temporal fossae laterally and partly

posteriorly. The zygomatic squamosal rami show a relatively ventral insertion on the back of the skull, at mid-height on the occiput (Fig. 2D). On the lateral side, they do not reach the dorsal region of the occiput. The temporal processes delimit the temporal fossae posteromedially. On their external surface, they contact the postorbitals dorsally. On their occipital side, no contact between bones is visible (Fig. 2D). The absence of the limits of the tabulars does not allow us to determine whether the squamosals are separated from the supraoccipitals by the tabulars. The steep angle between the temporal and zygomatic processes of the squamosal slightly exceeds 90° (Fig. 2D). The wide lateral extensions of the squamosal make an angle of less than 90° with the occipital side. A part of the lateral edge of the occiput is thus hidden. The squamosals extend posteriorly to the occipital condyle (Fig. 2C).

The lateral surface of the braincase is strongly eroded, but bone structures can be noted. Although the sutural contacts of the prootics are not visible, the basal part of the left pila antotica (not figured here) is preserved. Only the dorsal region of the long and narrow epipterygoids, which contacts the ventral process of the parietals, is preserved. A strong anteroventral depression in the squamosals indicates the connection with the missing quadrates (Fig. 2B).

The vomer displays a tuberosity turning into a vertical blade, which narrows posteriorly and separates the two choanae (Fig. 2C). The width of the median blade is constant along its length. The vomer contacts the premaxilla anteriorly and the pterygoids posteriorly. It forms the anterior margin of an elongated and ovoid interpterygoid vacuity (Fig. 2C).

The palatines border the choanae anterolaterally. The anterior palatine expansions form rugose and textured pads, indicating a keratinized covering (Fig. 2C). They narrow posteriorly to form relatively smooth processes. The palatines contact the anterior rami of the pterygoids along their entire lateral scarf joint and are anteriorly bordered by the maxillae. However, as mentioned above, due to the uncertainties about their anterior sutural contact, it is not clear whether they contact the premaxilla. A lateral palatine foramen is present alongside each anterior expanded pad (Fig. 2C).

Each pterygoid has an anterior ramus and a posterior (or quadrate) ramus. A single median plate connects the two bones and links the four rami. The pterygoids contact the secondary palate and the basicranium (Fig. 2C). Their ventral projections extend strongly anteroventrally, such that they form an anterior depression with the maxillae (Fig. 2B). These anterior pterygoid keels extend along most of the length of the anterior rami. Nevertheless, this extension cannot be precisely measured because the sutures are not visible laterally (Fig. 2B). The anterior rami of the pterygoids merge from the median plate, posterior to the interpterygoid vacuity. The interpterygoid vacuity is thus bordered by the pterygoids posteriorly and the vomer anteriorly. The posterior margin of the vacuity rises flush with the median plate of the pterygoids. The ventral surface of the narrow median plate bears a thin crista oesophagea (Fig. 2C). The median plate of the pterygoids contacts the parabasisphenoid posteriorly and the vomer anteriorly. In addition, a possible contribution of the parabasisphenoid to the interpterygoid vacuity cannot be proved. Two posterior rami of the pterygoids contact the squamosal fossa posteriorly and probably the medial condyles of the quadrates laterally.

Despite the absence of visible sutural contacts on the lateral side of the skull, the presence of the ectopterygoids is indicated by variation in bone texture on the lateral border of the anterior rami of the pterygoids (Fig. 2B). The ectopterygoids have a slender leaf shape and expand laterally along the anterior rami of the pterygoids. They do not expand posterior to the palatines in palatal view (Fig. 2C).

The crista oesophagea continues onto the parabasisphenoid and then diverges posteriorly to form the ridges leading to the basitubera (Fig. 2C). The contribution of the parabasisphenoid to the fenestra ovalis of the tubera is considerably restricted in comparison with the basioccipital. The stapedial facet is ventrolaterally directed, and its narrow margin mostly extends anteroposteriorly. The paired carotid canals, located in the anterior region of the parabasisphenoid in many dicynodonts (e.g., Maisch, 2002; Surkov and Benton, 2004), are not visible here. No intertuberal ridge is visible. The basioccipital extends onto the occipital plate and with the exoccipitals forms a tripartite occipital condyle (Fig. 2D). The exoccipitals and the basioccipital appear not to be fused in the condyle. A circular central depression is located between the three occipital subcondyles. Medially, the exoccipitals border the aperture of the vagus nerves (Dutuit, 1988).

The contacts between the interparietal and the other bones forming the occipital side and the posterior region of the skull roof cannot be discerned (Fig. 2D). Despite the eroded surface of the posterior postorbital processes, the interparietal does not seem to contribute to the skull roof (Fig. 2A).

The occiput is triangular in posterior view (Fig. 2D). Although sutures are not clearly preserved, the overall similarity of the occiputs of the *Counillonia* type specimens to those of other dicynodonts (*Lystrosaurus*: Cluver, 1971; *Dicynodon* and *Diictodon*: Cluver and Hotton, 1981) suggests that they shared a similar construction of the occiput. The teardrop-shaped foramen magnum may be laterally bordered by the exoccipitals, which overhang the basioccipital as in other dicynodonts. They would also contact the supraoccipital dorsally, the opisthotics laterally, and the basioccipital ventrally. A central depression on the supraoccipitals overhangs the foramen magnum and is dorsally bordered by a weak transverse nuchal crest, which extends upward toward the interparietal. The extent of the tabulars cannot be determined. The broad oval posttemporal fenestrae are located dorsal to the level of the occipital condyle, at the transverse level of the mid-height of the foramen magnum (Fig. 2D). They are oriented in the ventromedial-dorsolateral axis and would be delimited by the squamosal laterally, the supraoccipital dorsomedially, and the opisthotic ventromedially as in most dicynodonts. An oblique ridge on the supraoccipital extends over the fenestra. This ridge continues, below the fenestra, on the opisthotics and terminates in a sharp tuberosity.

KANNEMEYERIIFORMES Maisch, 2001

REPELINOSAURUS, gen. nov.

Type Species—*Repelinosaurus robustus*, gen. et sp. nov., monotypic.

Etymology—In honor of the French geologist Joseph Répelin, member of the Pavie Missions, who described and named Counillon's dicynodont skull '*Dicynodon incisivum*' (Répelin, 1923; see Steyer, 2009, for a biography). Also from the latinized Greek 'saurus' (a lizard) often used for nonmammalian synapsids, colloquially known as 'mammal-like reptiles.'

Diagnosis—See diagnosis of the type species.

REPELINOSAURUS ROBUSTUS, gen. et sp. nov. (Figs. 3–5)

Holotype—LPB 1993-2, a partial skull without mandible (basal length: 19 cm). The left postorbital bar, the zygomatic arch, the dorsolateral wing of the squamosal, the left quadratojugals, the quadrates, more than half of the left part of the occipital side, the external portion of the tusks, and the stapes are missing. The palatal surface is strongly eroded: most of the sutures

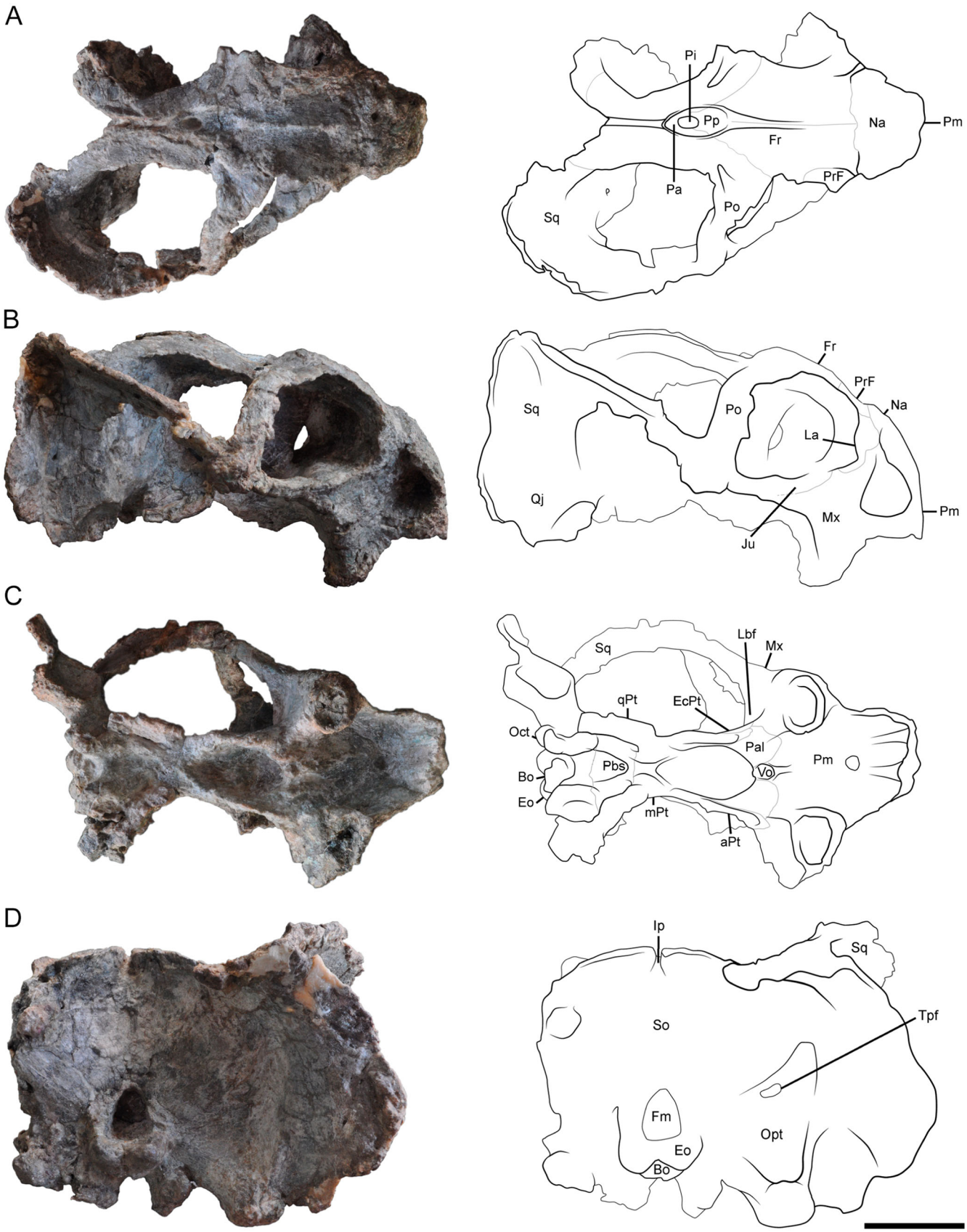

FIGURE 3. *Repelinosaurus robustus*, gen. et sp. nov., LPB 1993-2, holotype, photographs and interpretive drawings of skull in **A**, dorsal, **B**, right lateral, **C**, ventral, and **D**, occipital views. The thin gray lines represent the sutures, and the bold black lines represent relief. Scale bar equals 5 cm.

FIGURE 4. *Repelinosaurus robustus*, gen. et sp. nov., LPB 1995-9, referred specimen, photographs and interpretive drawings of skull in **A**, dorsal, **B**, right lateral, **C**, ventral, and **D**, occipital views. The thin gray lines represent the sutures, and the bold black lines represent relief. The dotted line represents the authors' interpretation of sutures based on variation in bone texture. Scale bar equals 5 cm.

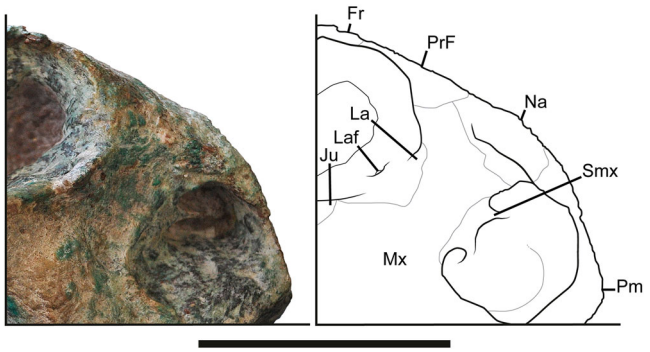

FIGURE 5. Close-up photograph and interpretive drawing of the lateral snout region of the referred skull LPB 1995-9, attributed to *Repelinosaurus robustus*, gen. et sp. nov. The thin gray lines represent sutures, and the bold black lines represent relief. Scale bar equals 5 cm.

cannot be made out and some bones are poorly preserved or are missing.

Referred Material—LPB 1995-9 is a skull (basal length: 15.72 cm) lacking the mandible, the right quadrate ramus of the pterygoid, the left stapes, the quadrates, and the left quadratojugal. The right stapes and the epipterygoids are poorly preserved. The specimen was subjected to lateral compression. However, the left orbit seems to have maintained its original shape.

Geographic Distribution and Stratigraphic Range—Same as for *Counillonia* (see above), LPB 1993-2 (19°55′59″N, 102°07′41″E) and LPB 1995-9 (19°55′16″N, 102°06′27″E) were collected in the Purple Claystone Formation, Luang Prabang Basin (Laos).

Etymology—From the Latin 'robustus' (robust), referring to its robust cranial appearance.

Diagnosis—Medium-sized dicynodontoid characterized by the unique combination of the following character states: a reduced preorbital region; a notch on the dorsal edge of the narial opening; nasal bosses present as a median swelling with a continuous posterior margin; a straight frontonasal suture; parietals exposed in midline groove; a relatively flat temporal portion of the postorbital, so that most of the exterior surface of the bone faces dorsally; a vertical caniniform process; and high insertion of the zygomatic squamosal rami on the occiput posteriorly. Distinguished from all dicynodontoids by a very small preorbital region. Further distinguished from all kannemeyeriiforms by a median nasal swelling with a continuous posterior margin and a flat temporal portion of the postorbital. Further distinguished from the Laotian *Counillonia* by a wide interorbital bar, a straight frontonasal suture, a vertical caniniform process, a rectangular occiput, and a high insertion of the zygomatic squamosal rami on the occiput posteriorly.

Remarks—Some differences distinguish LPB 1993-2 and LPB 1995-9, such as (1) the position of the pineal foramen on the skull roof that is more posterior in LPB 1993-2 (continuous character 6, Appendix 1); (2) a higher angulation between the occiput and the palate in LPB 1993-2 (continuous character 13, Appendix 1); (3) a relatively flat palatal surface of the premaxilla in LPB 1993-2 or with marked depressions on either side of the median crest in LPB 1995-9 (discrete character 29, Appendix 1); (4) a sutural contact between the maxillae and the prefrontals present in LPB 1995-9 and absent in LPB 1993-2 (discrete character 49, Appendix 1); (5) a preparietal depressed in LPB 1993-2 or flush with the skull roof in LPB 1995-9 (discrete character 68, Appendix 1); (6) a bigger pineal foramen in LPB 1995-9 (Table 2); (7) tusk basal section compressed mediolaterally in LPB 1995-9 and anteroposteriorly in LPB 1993-2 (Table 2); and (8) more developed ornamentation on the frontals in LPB 1993-2. However, each character-state variation noted could be due to taphonomic deformation, ontogeny, sexual dimorphism or other intraspecific variability (discussed below). Moreover, LPB 1995-9 and LPB 1993-2 were found in the same geological formation, suggesting conspecificity.

Description

The skulls are narrow and robust, with a wide and short snout that narrows slightly anteriorly and terminates in a squared tip. *Repelinosaurus* has a wider interorbital region (Figs. 3A, 4A) than *Counillonia* (Fig. 2A). The orbits are thus open mainly laterally. The dorsal surfaces of the premaxilla, the maxillae, and the nasals of LPB 1995-9 are weathered, but the preservation of these surfaces in LPB 1993-2 displays strong rugosities on the snout (Figs. 3A, 4A). Nevertheless, the nasopremaxillary and the mid-nasal sutures cannot be traced in LPB 1993-2. The septomaxilla is well preserved in LPB 1995-9, unlike in LPB 1993-2 where the poor preservation of the naris does not yield information about this bone (Figs. 3B, 4B, 5). Sutures are not visible on the occiput of either specimen, except for the connection of the right quadrate in LPB 1995-9. The scarf joints also cannot be discerned on the medial portion of the temporal and orbital fossae, but the dorsal head of the epipterygoid and the basal region of the pila antotica are preserved in LPB 1995-9 (Fig. 4B). The palatal surface of LPB 1993-2 is poorly preserved; few sutures are thus visible.

As mentioned above, lots of pits and strong rugosities mark the dorsal surface of the premaxilla in LPB 1993-2 and extend onto the nasals before stopping abruptly at the nasoprefrontal and nasofrontal sutures (Fig. 3A). These rugosities are thought to indicate a keratinized covering (e.g., Angielczyk et al., 2018). The premaxilla contributes to the external anterior edge of the nares. In lateral view, the well-developed nares of both LPB 1995-9 and LPB 1993-2 represent more than half of the length of the snout (Figs. 3B, 4B). Their ventral edges are close to the ventral border of the snout. The premaxilla is toothless and anteriorly bears two short parallel longitudinal ridges, which are separated by a shallow depression and overlie the anterior quarter of the premaxilla (Figs. 3C, 4C). An anterior rounded pit of medium size in LPB 1993-2, visible posterior to the premaxillary longitudinal crest, could be of taphonomic origin (Fig. 3C). Posterior to this depression, a sharp median ridge extends onto two-thirds of the premaxilla. In LPB 1993-2, the premaxilla is relatively flat. However, this median ridge is surrounded by two depressions, which deepen in the posterior region of the secondary palate in LPB 1995-9. These depressions may be caused by taphonomic lateral compression (discussed below). The premaxilla contacts the nasals posterodorsally and the maxillae posterolaterally at the level of the anterior third of the nares in LPB 1995-9 (Figs. 3B, 4B). However, the sutures of the premaxilla with the nasals and maxillae are not visible in LPB 1993-2. In both LPB 1995-9 and LPB 1993-2, the premaxilla contacts the maxillae and their caniniform processes laterally on the palatal surface. However, the suture between the premaxilla, the maxillae, and the palatines are not clearly preserved (Figs. 3C, 4C).

The well-developed nasal bosses terminate laterally in a posterodorsal notch at the dorsal edge of the nares and are separated from the frontals and prefrontals by a shallow depression (Figs. 3B, 4B). The notch on the posterodorsal edge of the naris is formed by a thick expansion of the nasal bosses, which hides the external ventral narial edge in dorsal view. The bosses form a median swelling that is more marked in LPB 1993-2 than in LPB 1995-9 (Figs. 3B, 4B). The nasals are bordered by the frontals and the prefrontals posteriorly, the premaxilla anteriorly, and the maxillae laterally. However, the nasals do not contact the lacrimals in LPB 1995-9, in contrast to the condition in LPB 1993-2 (Figs. 3B, 4B, 5).

The prefrontals form the edge of the orbits with the lacrimals anteriorly, the jugals ventrally, the postorbitals posteriorly, and

the frontals dorsally (Figs. 3A, B, 4A, B). As for the nasals, the prefrontal extension is broader in dorsal than in lateral view. The prefrontals bear a weak boss, distinct from the nasals. The prefrontals contact the maxillae ventrally in LPB 1995-9 (Figs. 4B, 5).

The interorbital region of *Repelinosaurus* (Figs. 3A, 4A) is clearly wider than that of *Counillonia* (Fig. 2A). In *Repelinosaurus*, it is mainly formed by the frontals constituting the dorsal margin of the orbits, which rise slightly laterally. In addition, as mentioned above, the prefrontals bear bosses in both specimens. The interorbital region obscures the orbits in dorsal view; their orientation is thus mainly lateral, whereas it is dorsolateral in *Counillonia*. In LPB 1993-2, the frontals are separated by a sharp median ridge bordered by two deep depressions (Fig. 3A). In LPB 1995-9, the preparietal, the parietals, and the posterior region of the frontals show a depression. The frontals contact the nasals anteromedially, the prefrontals laterally, the postorbitals posterolaterally, and the preparietal posteromedially (Figs. 3A, 4A). The nasofrontal suture is relatively straight in *Repelinosaurus* (Figs. 3A, 4A), whereas it has a distinct posterior process in *Counillonia* (Fig. 2A). No postfrontals are observed in LPB 1995-9 (Fig. 4A), but as in *Counillonia*, we cannot determine whether they were absent or present in LPB 1993-2 because of the eroded external bone surface (Figs. 2A, 3A).

In LPB 1993-2, the preparietal is depressed and bordered anteriorly by a ridge (Fig. 3A), which continues into the median frontal ridge. The surface of the preparietal is flush with the depressed surface of the frontals in LPB 1995-9 (Fig. 4A). The preparietal contacts the postorbitals posterolaterally, the short parietals posteriorly, and the frontals anteriorly (Figs. 3A, 4A).

The parietal contribution of the skull roof in LPB 1993-2 is limited to a midline groove between the posterior postorbital processes (Fig. 3A). These posterior parietal processes are thus slender. Noticeable lateral compression has modified the angulation of the postorbitals in LPB 1995-9. This taphonomic deformation may have resulted in artificial contact of the postorbitals in the midline of the intertemporal bar (Fig. 4A). The posterior expansion of the parietals is dorsally hidden by the posterior processes of the postorbitals or cannot be determined due to the lack of a clear suture between the parietal and the interparietal. However, the anterior part of the parietals is preserved. In both specimens of *Repelinosaurus*, the anterolateral processes of the parietals, bordering the pineal foramen, are more anteroposteriorly elongate than broad (Figs. 3A, 4A), but their posterior end is not visible. The external dorsal surface of the parietals contacts the interparietal posteriorly, the postorbitals posterolaterally, and the preparietal anteriorly. The parietals and the preparietal surround the pineal foramen posteriorly and anteriorly, respectively. The oval pineal foramen is clearly smaller in LPB 1993-2 (length: 0.96 cm; width: 0.66 cm) than in LPB 1995-9 (length: 1.33 cm; width: 0.87 cm) (Table 2). In both specimens, the foramen is perpendicular to the intertemporal bar and flush with the skull roof. The pineal foramen is also more anterior in LPB 1995-9 than in LPB 1993-2 (continuous character 6, Appendix 1). In lateral view, the poor preservation of the specimens of *Repelinosaurus* does not allow observation of the sutural contact between the parietals and the prootic (Figs. 3B, 4B).

The lateral postorbital bars possess tuberosities in LPB 1993-2, in contrast to LPB 1995-9 (Figs. 3A, B, 4A, B). The posterior postorbital processes of *Repelinosaurus* extend over the entire narrow intertemporal bar as in *Counillonia* (Figs. 2D, 3B, 4B). The temporal portion of the postorbitals is flat and dorsally directed in LPB 1993-2 (Fig. 3A). We consider that its slightly oblique direction in LPB 1995-9 is due to lateral compression (Fig. 4A). This horizontal expansion of the posterior processes of the postorbitals in *Repelinosaurus* is linked to a large fossa formed by the postorbitals and the parietals below the intertemporal bar. The posterior processes of the postorbitals, widened in both LPB 1993-2 and LPB 1995-9, contact the squamosals and the interparietal posteriorly. Anteriorly, they are separated from the preparietal and the parietals by a sharp ridge in LPB 1995-9 (Fig. 4A). The postorbital surface has a triangular depression between the posterior and lateral processes (Figs. 3A, 4A). The lateral processes of the postorbitals constitute the posterior margin of the orbits. These processes are wider in LPB 1993-2 than in LPB 1995-9 (Figs. 3B, 4B). In LPB 1995-9, they have a sutural contact with the jugals anteroventrally and the zygomatic squamosal processes posteroventrally (Fig. 4A). The state of preservation of the zygomatic arches of LPB 1993-2 does not provide information about the location of the scarf joints. In dorsal view, the lateral expansion of the postorbital bars is smaller in *Repelinosaurus* than in *Counillonia*, giving the skull of *Repelinosaurus* a narrower appearance (Figs. 2A, 3A, 4A).

The lateral surface of the maxilla displays stronger rugosities in LPB 1993-2 than in LPB 1995-9 (Figs. 3B, 4B), but it is difficult to determine the degree to which these rugosities are a real feature. In both skulls, the maxillae contact the premaxilla anteriorly and the lacrimals and nasals dorsally. However, in LPB 1993-2, the maxillae do not contact the prefrontals because the anterior process of the lacrimals intervenes, in contrast to LPB 1995-9 (Figs. 3B, 4B, 5). In LPB 1993-2, a notch on the palatal rim is visible on the right side of the skull but not on its left, suggesting a taphonomic origin. The poor preservation of the lateral surface of LPB 1993-2 does not provide information about the sutures in the zygomatic arch. Nevertheless, these contacts are visible in LPB 1995-9 (Fig. 4B). The zygomatic processes of the maxillae comprise a bifid tip embedded in the squamosals and dorsally bordered by the jugals. The maxillae are relatively robust, especially in LPB 1993-2. In addition, the caniniform process is more developed in LPB 1993-2 than in LPB 1995-9 (Figs. 3B, 4B). In *Repelinosaurus* (Figs. 3B, 4B), the caniniform process is vertical, whereas it is anteriorly directed in *Counillonia* (Fig. 2B). The external part of the tusks is missing in LPB 1993-2, but the tusk roots are anteroposteriorly flattened, whereas they are mediolaterally compressed in LPB 1995-9 (Table 2). In LPB 1995-9, the tusks are posteriorly directed and turn medially, forming a medial concavity (Fig. 4B). The lack of fractures and the direction of the main taphonomic distortion (see above) suggest that the tusks have not been deformed, but the space left between the tusks would not be sufficient for inserting a jaw (J. Camp, pers. comm., 2017). Moreover, the distinct wear facet (formed as the mandible slides, e.g., Cluver, 1971; K. Angielczyk, pers. comm., 2018) observed on the inner surface of the left tusk is backwardly directed, indicating distortion. The distal part of the right tusk is too eroded to reach any conclusion. On the ventral orbital edge, a rounded labial fossa is visible posterior to the caniniform process (Figs. 3C, 4C). Nevertheless, as noted in *Counillonia*, the sutural contacts cannot be discerned; therefore, we cannot conclude whether *Repelinosaurus* has a true labial fossa (circumscribed by maxillae, palatines, and jugals) or just a labial foramen (e.g., Angielczyk and Kurkin, 2003).

In LPB 1995-9, the well-preserved septomaxillae bear a sharp ridge, which partly divides the nares, and form the posteroventral part of the margin of the nares with the maxillae (Figs. 4B, 5). The septomaxillae also contact the nasal dorsally and the premaxillae anteriorly.

The lacrimals are limited by the nasals anteriorly, the prefrontals dorsally, the maxillae anteroventrally, and the jugals posterolaterally in LPB 1993-2 (Fig. 3B). Their anterior, well-developed expansion does not allow a sutural contact between the maxillae and the prefrontals. On the lateral surface of LPB 1995-9, the lacrimals are only limited by the maxillae anteriorly and slightly by the jugals posterolaterally (Fig. 4B). A sutural contact between the maxillae and the prefrontals is also reported in some dicynodonts, such as *Kombuisia* (e.g., Fröbisch, 2007) or *Kannemeyeria* (e.g., Renaut, 2000). Nevertheless, the antorbital margin formed by the prefrontals, the lacrimals, and the maxillae

(Figs. 4B, 5) seems to be unique to LPB 1995-9 within dicynodonts. We therefore cannot rule out the possibility that the limits of the lacrimals may be inaccurate due to taphonomic deformation. Additionally, the left lateral side of the skull is too eroded, and this particular bone contact cannot be confirmed. On both skulls of *Repelinosaurus*, the bone sutures of the orbits are not visible (Figs. 3A, 4A). In LPB 1995-9, the lacrimals show a tuberosity on the antorbital rim, which forms the anterior border of the lacrimal foramen.

The jugal makes a small contribution to the lateral surface of the skull (Figs. 3B, 4B). In LPB 1993-2, the sutures with the other bones on the zygomatic arches (except the maxillae and lacrimals) cannot be determined because of poor preservation. The zygomatic arches of LPB 1995-9 show a sutural contact between the jugals and the postorbitals posteriorly, and the squamosals posteroventrally (Fig. 4B).

The zygomatic squamosal processes form the posterior regions of the zygomatic arches and circumscribe the temporal fossae laterally and partly posteriorly. They widen posteriorly into a wing-shaped process and become narrow, without dorsoventral expansion posterior to the postorbital bar (Fig. 3A, B). The right zygomatic arch of LPB 1993-2 presents a ventral expansion at the intersection between the descending bar of the postorbital and the zygomatic arch (Fig. 3B), somewhat reminiscent of the ventrally directed convexity of the squamosal in *Aulacephalodon* (e.g., Tollman et al., 1980). However, the absence of the left zygomatic arch and of visible sutures in the right zygomatic arch do not permit us to conclude whether it is of natural or taphonomic origin. Specimen LPB 1995-9 does not exhibit this type of ventral expansion on its zygomatic arches (Fig. 4B). The edge of the zygomatic squamosal wing is flat and straight in LPB 1993-2 (Fig. 3B). The lateral compression affecting LPB 1995-9 has distorted the edge of the zygomatic arch. The squamosal zygomatic processes of LPB 1995-9 contact the jugals and the postorbitals dorsally and the maxillae in the pointed anterior region (Fig. 4B). In contrast to *Counillonia* (Fig. 2D), the squamosal zygomatic processes of *Repelinosaurus* are inserted dorsally on the back of the skull, well above the dorsal edge of the foramen magnum (Figs. 3D, 4D). They extend slightly onto the dorsal region of the occiput in LPB 1993-2 but not in LPB 1995-9 (Figs. 3B, 4B) because of lateral compression. This compression also raised the intertemporal region and crushed the zygomatic squamosal processes in LPB 1995-9. The temporal squamosal processes of *Repelinosaurus*, delimiting the temporal fossae posteromedially, are shorter than in *Counillonia*. They contact the postorbitals dorsally and the interparietal medially. As already noted, the bone contact on the occipital side cannot be traced (Figs. 3D, 4D). No conclusion is thus possible concerning the limits of the tabulars and the potential separation of the squamosals and supraoccipitals. The quadrate rami of the squamosals are laterally expanded in *Repelinosaurus*. Compared with *Counillonia* (Fig. 2D), they are in the same plane as the occiput surface in LPB 1993-2 (Fig. 3D). This structure cannot be compared in LPB 1995-9 because of deformation and because the left quadrate ramus of the squamosal is missing.

The lateral surface of the skulls is eroded, but some structures can be made out: a deep anteroventral depression in the squamosal may indicate their contact with the missing quadrate in LPB 1993-2 and in the left side in LPB 1995-9 (Figs. 3B, 4B). In addition, the dorsal head of the epipterygoid contacting the parietals and the basal region of the pila antotica are preserved in LPB 1995-9 (Fig. 4B).

The vomer is missing in LPB 1993-2, but its poorly preserved anterior region can be observed (Fig. 3C). It displays a median blade separating the choanae in LPB 1995-9 (Fig. 4C). The width of this blade is constant throughout its length. Anteriorly, the vomer shows a tuberosity following the posteromedial ridge of the premaxilla (Figs. 3C, 4C). The vomer is divided posteriorly and delimits the anterior edge of the interpterygoid vacuity, where it contacts the median plate of the pterygoids (Fig. 4C).

The palatines are bordered by the anterior rami of the pterygoids laterally (Figs. 3C, 4C) and the maxillae anteriorly. Because of the poor preservation, the morphology of the palatine-premaxillary contact is uncertain. Only the wide anterior region of the palatines is preserved in LPB 1993-2 (Fig. 3C), but their poor preservation does not provide relevant information about their texture. In LPB 1995-9, the palatines widen anteriorly, forming a rugose textured pad (Fig. 4C). No foramen is observed within the palatines, and we cannot determine whether there is a foramen between these palatines and the anterior rami of the pterygoids because of lateral compression of the palate.

Due to the multiple breaks and the missing bone in some areas, nothing can be said about the presence of pterygoid keels in LPB 1993-2 (Fig. 3B). The ventral projection of the anterior rami of the pterygoids does not extend strongly ventrally in LPB 1995-9 (Fig. 4B), in contrast to *Counillonia* (Fig. 2B) where this extension projects strongly ventrally. However, as in *Counillonia*, the absence of sutures in lateral view prevents measurements of the ventral expansion of the pterygoid keel from being taken. The thin anterior rami of the pterygoids contact the ectopterygoids anterolaterally, in the form of a slender leaf in LPB 1995-9. The ectopterygoids do not expand further posterior to the palatines in palatal view. In LPB 1993-2, they are not preserved but a shallow depression on the anterolateral edge of the pterygoids marks their presence. In LPB 1995-9, the teardrop-shaped interpterygoid vacuity is bordered by the median plate of the pterygoids posteriorly and the vomer anteriorly (Fig. 4C). The anterior margin of the interpterygoid vacuity is not defined in LPB 1993-2 because the major portion of the vomer is missing. As in *Counillonia*, the ventral surface of the median plate bears a thin crista oesophagea in LPB 1995-9, which turns into two ridges posteriorly on the parabasisphenoid (Fig. 4C). However, the bone surface of LPB 1993-2 is eroded. The poor preservation of the two skulls of *Repelinosaurus* excludes any comments about a potential contribution of the parabasisphenoid to the interpterygoid vacuity. The posterior rami of the pterygoids are poorly preserved in LPB 1993-2 and are missing in LPB 1995-9 (Figs. 3C, 4C).

Two ridges extend onto the parabasisphenoid, from the crista oesophagea, and widen posteriorly (Figs. 3C, 4C). They delimit a broad triangular intertuberal depression. The parabasisphenoid is mainly vertical and makes less contribution to the fenestra ovalis than the basioccipital. The stapedial facet in LPB 1993-2 is exposed ventrolaterally, and its narrow margin extends anteroposteriorly (Fig. 3C). In LPB 1995-9, the structure of the parabasisphenoid-basioccipital tubera is distorted, probably because of taphonomic deformation. As in *Counillonia*, the paired carotid canals, located in the anterior region of the parabasisphenoid, are not visible in either of the specimens of *Repelinosaurus*. No intertuberal ridge is visible. In LPB 1993-2, the basioccipital extends onto the occipital plate and with the exoccipital forms a tripartite occipital condyle (Fig. 3D). The occipital condyle is too poorly preserved in LPB 1995-9 to be precisely described (Fig. 4D).

Only the right quadrate is preserved in LPB 1995-9 (Fig. 4C, D). It is ventrally bifid, with lateral and medial condyles separated by a median groove. The lateral condyle is more anteroposteriorly elongated than the medial one. However, the dorsal lobe was laterally crushed.

The contact between the interparietal and the other bones forming the occiput and the posterior region of the skull roof cannot be discerned (Figs. 3D, 4D). However, it seems that the interparietal does not contribute to the skull roof. In both LPB 1993-2 and LPB 1995-9, the interparietal seems to form a deep longitudinal notch, which is mainly overhung by the postorbitals dorsally. However, the interparietal-parietal suture is not clearly visible.

The occiput is rectangular in LPB 1993-2 (Fig. 3D) but distorted in LPB 1995-9 (Fig. 4D). The insertion of the squamosals on the occiput makes an obtuse angle in LPB 1993-2 (Fig. 3D): most of the lateral squamosal expansion is thus visible in occipital view, in contrast to the condition in *Counillonia* (Fig. 2D). The lateral compression of LPB 1995-9 may explain the sharper angle of the lateral squamosal expansions and their asymmetry. As mentioned above, sutures are not clearly preserved. Nevertheless, as in *Counillonia*, the overall similarity of the occiputs of *Repelinosaurus* (Figs. 3D, 4D) to *Lystrosaurus* (Cluver, 1971), *Dicynodon*, or *Diictodon* (Cluver and Hotton, 1981) suggests that they shared a similar construction of the occiput. However, the dorsoventral expansion of the tabular cannot be determined. In LPB 1995-9, a short nuchal crest, ventrally bordered by a depression, extends onto the most dorsal region of the supraoccipital (Fig. 4D). No nuchal crest is visible in LPB 1993-2. A very wide triangular depression extends laterally to the foramen magnum and surrounds the posttemporal fenestrae (Figs. 3D, 4D). The anterior tip of this depression is located near the junction between the root of the squamosal wings and the supraoccipital. Its ventral base extends between the basal tubera and the oblique opisthotic crest, which turns into a sharp process.

PHYLOGENETIC ANALYSIS

Methodology

A phylogenetic analysis was conducted to test the systematic position of the three Laotian dicynodont specimens. This analysis is based on an augmented version of the matrix of Angielczyk and Kammerer (2017), which is one of the most recent and comprehensive analyses of dicynodonts. Our final data set (Supplemental Data 1) thus includes 106 operational taxonomic units and 194 characters: 171 discrete characters (treated as of equal weight and as unordered, except for characters 81, 84, 102, 163, 173, and 174, following Angielczyk and Kammerer, 2017) and 23 continuous characters (Appendix S1 in Supplemental Data 2). All new measurements and codings, made for the Laotian specimens studied (Appendix 1), are defined using procedures mentioned in Kammerer et al. (2011) and personal communications from C. F. Kammerer (2017) and K. D. Angielczyk (2017). The treatment of the continuous characters is additive (ordered), following Goloboff et al. (2006). Unknown and/or inapplicable states of discrete and continuous characters are coded as '?' (Strong and Lipscomb, 1999). In order to treat the continuous characters with a continued and ordered evolution permitted by Goloboff's algorithm (Goloboff et al., 2006), we analyzed the data set using TNT 1.1 (December 2013 version) (Goloboff et al., 2008). We performed two analyses: a New Technology search that analyzes different parts of the tree separately (Goloboff, 1999) and a traditional search. In the first case, we did a driven search with the initial search level set to check every three hits. One hundred replications were chosen as the starting point for each hit, and the search was set to find the most parsimonious trees 20 times. We did the phylogenetic analysis using sectorial search (default settings) and tree-drifting (default settings but the number of cycles was three) to produce a nearly optimal tree, which could be used for tree-fusing (default settings, but a global fuse every three hits was input; Goloboff, 1999). In the second search, we used a traditional search of tree bisection reconnection (TBR) branch swapping with 11,111 replications and nine trees saved per replication. *Biarmosuchus* was used as the outgroup. We obtained the same most parsimonious tree with both methods (1,156.346 steps, consistency index = 0.236, retention index = 0.712) (Fig. 6). We indicate the Bremer values as a node support index (Fig. 6; Bremer, 1988). According to the recommendations of Goloboff et al. (2008), we performed successive traditional searches using the most parsimonious trees as a starting point. We increased the value of suboptimal trees each step to avoid overestimation of the value of the Bremer support. We saved successively larger sets of suboptimal trees ('stop when maxtrees hit' selected). The resulting trees were checked to discard duplicate cladograms each search. Once the optimal and suboptimal trees stored (99,999 unique cladograms), we tested the score differences to lose each node using the 'Bremer support' function.

Results and Comparisons with Previous Dicynodont Phylogenies

The most parsimonious tree is shown in Figure 6. The clade Dicynodontoidea is weakly supported. However, some clades within Dicynodontoidea are well supported, such as Rhachiocephalidae and Lystrosauridae (Fig. 6).

We hereafter follow the comprehensive taxonomy of Kammerer and Angielczyk (2009). Our results are in accordance with the strict consensus cladogram of Angielczyk and Kammerer (2017), except for some relationships within Dicynodontoidea. Our phylogenetic analysis indicates that Pylaecephalidae is distinct from Emydopoidea, not recovered within Therochelonia, and placed in a comparable position to that proposed by Angielczyk and Kurkin (2003), Fröbisch (2007), Angielczyk and Rubidge (2013), Boos et al. (2016), Angielczyk and Kammerer (2017), and Angielczyk et al. (2018). Additionally, the Kingoriidae are here included in the Kistecephalia within Emydopoidea as previously proposed (e.g., Angielczyk and Kurkin, 2003; Angielczyk and Rubidge, 2013; Castanhinha et al., 2013; Cox and Angielczyk, 2015; Angielczyk et al., 2016, 2018; Angielczyk and Kammerer, 2017; Kammerer and Smith, 2017). Within dicynodontoids, the relationships within Cryptodontia (here compositionally equivalent to Oudenodontidae), Rhachiocephalidae, and Lystrosauridae are consistent with the results of Angielczyk and Kammerer (2017). In contrast to previous studies (e.g., Angielczyk and Rubidge, 2013; Castanhinha et al., 2013; Kammerer et al., 2013; Cox and Angielczyk, 2015; Kammerer and Smith, 2017), Rhachiocephalidae and Geikiidae are not included in Cryptodontia, but in Dicynodontoidea (as defined by Kammerer and Angielczyk, 2009), as proposed by Boos et al. (2016), Angielczyk and Kammerer (2017), and Angielczyk et al. (2018).

As mentioned by Kammerer and Angielczyk (2009), no consensus exists on a taxonomic definition of Kannemeyeriiformes, probably because the alpha taxonomy of the Triassic forms is still unresolved. If we consider the definition of Kannemeyeriiformes sensu Maisch (2001) to be the clade of Triassic non-lystrosaurid dicynodontoids, in our current results the Laotian *Repelinosaurus* may thus be considered to be a kannemeyeriiform. However, the other Laotian Triassic genus, *Counillonia*, is a non-kannemeyeriiform dicynodontoid, closely related to Permian '*Dicynodon*'-grade taxa (i.e., most taxa previously attributed to *Dicynodon* before the taxonomic revision by Kammerer et al., 2011): *Daptocephalus*, *Peramodon*, *Dinanomodon*, *Turfanodon*, *Euptychognathus*, *Sintocephalus*, *Jimusaria*, *Gordonia*, *Delectosaurus*, *Vivaxosaurus*, and the two valid species of *Dicynodon* (Fig. 6; Kammerer et al., 2011). The stratigraphic definition of Kannemeyeriiformes sensu Maisch (2001) is thus challenged by the phylogenetic position of *Counillonia*. We therefore follow the phylogenetic definition of Kannemeyeriiformes sensu Kammerer et al. (2013) as the clade comprising *Kannemeyeria simocephalus* and all taxa more closely related to it than to *Lystrosaurus murrayi* or *Dicynodon lacerticeps*. Under this definition, *Repelinosaurus* is recovered as a kannemeyeriiform. In contrast to recent studies, our phylogeny recovers a large clade of

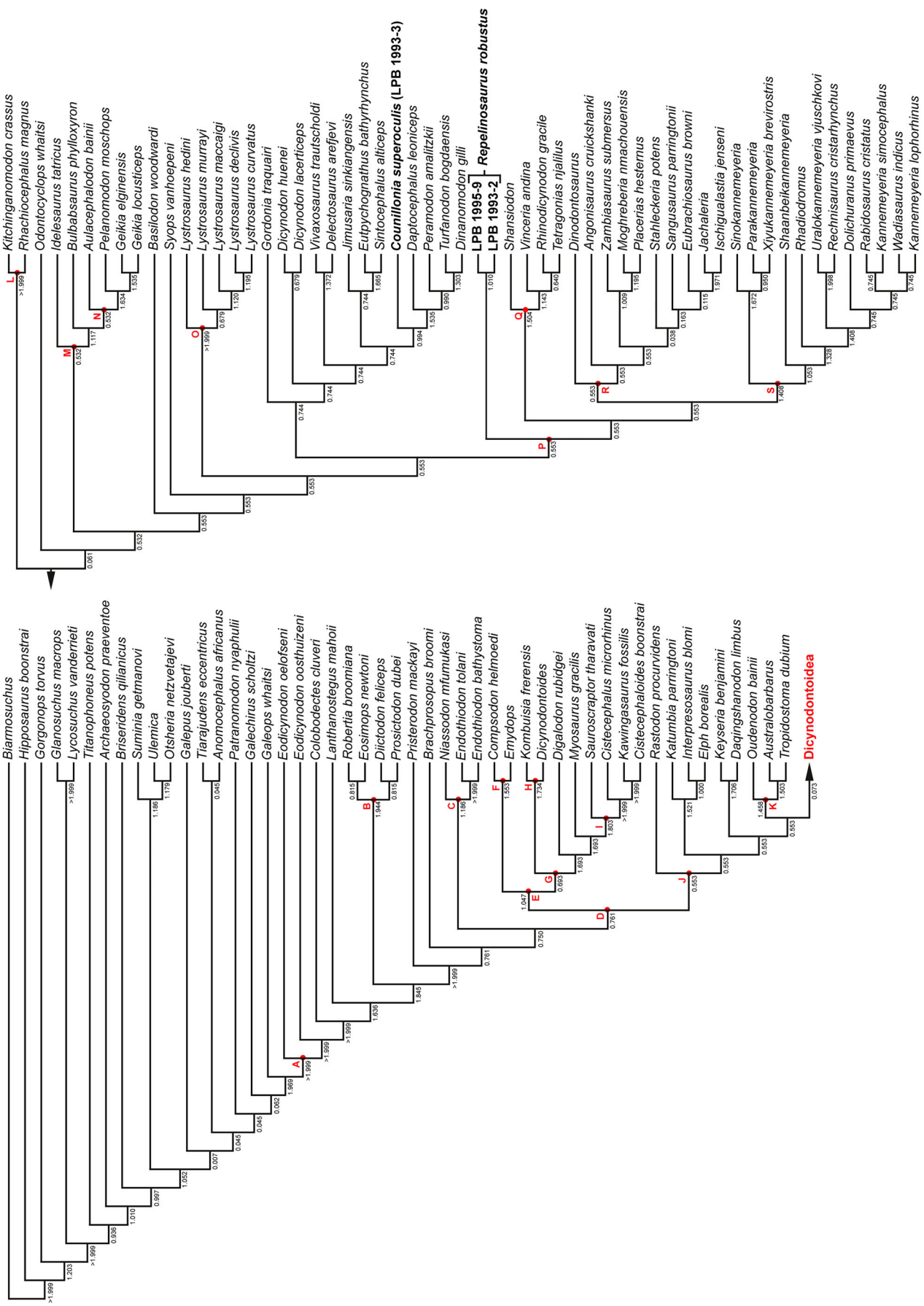

FIGURE 6. The most parsimonious cladogram. See text for tree statistics. Numbers at nodes represent Bremer support values. Capital letters indicate the following clades (Maisch, 2001; Kammerer and Angielczyk, 2009): A, Dicynodontia; B, Pylaecephalidae; C, Endothiodontia; D, Therochelonia; E, Emydopoidea; F, Emydopidae; G, Kistecephalia; H, Kingoriidae; I, Cistecephalidae; J, Bidentalia; K, Cryptodontia; L, Rhachiocephalidae; M, Geikiidae; N, Geikiinae; O, Lystrosauridae; P, Kannemeyeriiformes; Q, Shansiodontidae; R, Stahleckeriidae; S, Kannemeyeriidae.

'*Dicynodon*'-grade taxa uniting *Daptocephalus*, *Peramodon*, *Dinanomodon*, *Turfanodon*, *Euptychognathus*, *Sintocephalus*, *Jimusaria*, *Gordonia*, *Delectosaurus*, *Vivaxosaurus*, and the two valid species of *Dicynodon* (Kammerer et al., 2011). These '*Dicynodon*'-grade taxa and *Counillonia* form a clade with Kannemeyeriiformes characterized by two unambiguous synapomorphies: (1) a lacrimal not in contact with the septomaxilla (60[0]) and (2) a dorsal process on the anterior end of the epipterygoid footplate (127[1]). The results of Angielczyk and Kurkin (2003) also recovered *Peramodon* and *Vivaxosaurus* as more closely related to Kannemeyeriiformes than to *Lystrosaurus*. Within Kannemeyerii formes, our phylogenetic results indicate that *Repelinosaurus* is sister to the rest of Kannemeyeriiformes, which is divided into three relatively well-supported clades: Shansiodontidae, Kannemeyeriidae, and Stahleckeriidae. Shansiodontidae, as defined by Maisch (2001), includes *Shansiodon*, *Vinceria, Rhinodicynodon*, and *Tetragonias*. They are sister group to all other kannemeyeriiforms but *Repelinosaurus*, a position previously recovered by Castanhinha et al. (2013), Kammerer et al. (2013), Cox and Angielczyk (2015), Boos et al. (2016), and Kammerer and Smith (2017). Despite the fact that Shansiodontidae sensu Maisch (2001) is paraphyletic in the analyses of Kammerer and Angielczyk (2017) and Angielczyk et al. (2018), *Shansiodon*, *Vinceria, Rhinodicynodon*, and *Tetragonias* are also more basal than all other kannemeyeriiforms in their studies. The compositions of the clades Kannemeyeriidae and Stahleckeriidae are similar in the current analysis to those of Kammerer and Angielczyk (2017) and Angielczyk et al. (2018). Stahleckeriidae, as the last common ancestor of *Placerias hesternus* and *Stahleckeria potens*, and all of its descendants, excluding *Shansiodon wangi* or *Kannemeyeria simocephalus* (Kammerer et al., 2013), are characterized by six unambiguous synapomorphies: (1) a short interpterygoid vacuity (continuous character 10); (2) a very reduced minimum width of the scapula (continuous character 17); (3) a very long anterior iliac process (continuous character 21); (4) a smooth and flat median pterygoid plate (115[1]); (5) the presence of six sacral vertebrae (165[3]); and (6) the M. latissimus dorsi inserted on a rugose tuberosity on the posteroventral surface of the humerus (175[0]). Kannemeyeriidae may therefore be defined here as the clade comprising *Kannemeyeria simocephalus* and all taxa more closely related to it than to *Stahleckeria potens*, *Placerias hesternus*, or *Shansiodon wangi*. This clade is supported by six unambiguous synapomorphies: (1) a high preorbital region (continuous character 1); (2) a high trochanteric crest on the femur (continuous character 22); (3) a very narrow scapula (the narrowest in dicynodontoids; continuous character 23); (4) a dorsal edge of the erupted portion of the canine tusk anterior to the anterorbital margin (55[0]); (5) a temporal portion of the skull roof angled dorsally with a strong break in slope near its anterior end (67[1]); and (6) a lateral edge of the paroccipital process distinctly offset from the surface of the occipital plate (135[1]).

Positions of the Three Laotian Specimens

Our results indicate that the Laotian specimens LPB 1993-2 and LPB 1995-9 form a relatively well-supported clade, characterized by five unambiguous synapomorphies: (1) the most reduced preorbital region in dicynodontoids (continuous character 1); (2) a notch on the dorsal edge of the narial opening (41[1]); (3) nasal bosses present as a median swelling with a continuous posterior margin (57[1]); (4) parietals exposed in the midline groove (72[1]); and (5) a relatively flat temporal portion of the postorbitals, such that most of the external surface of the bone faces dorsally (74[0]). This supports our attribution of these Laotian specimens to the single new taxon *Repelinosaurus robustus*, gen. et sp. nov., erected above. This Laotian clade is included in Kannemeyeriiformes, which are thus defined by three derived character states: (1) the absence of postfrontal (64[1]); (2) no converging ventral keels on the posterior portion of the anterior pterygoid rami (114[0]); and (3) the absence of the intertuberal ridge (126[0]).

As mentioned above, the third Laotian specimen LPB 1993-3 is close to some '*Dicynodon*'-grade taxa: *Daptocephalus*, *Peramodon*, *Dinanomodon*, *Turfanodon*, *Euptychognathus*, *Sintocephalus*, *Jimusaria*, *Gordonia*, *Delectosaurus*, *Vivaxosaurus*, and the two valid species of *Dicynodon* (Kammerer et al., 2011). All these taxa form a clade supported by four unambiguous synapomorphies: (1) the highest temporal fenestra within dicynodontoids (continuous character 5); (2) a weakly developed distal end of the radius, in contrast to the condition in other dicynodontoids (continuous character 19); (3) a rounded anterior tip of the snout (35[0]); and (4) a raised circumorbital rim (62[1]). Within this clade, LPB 1993-3 is sister to the clade formed by the late Permian South Gondwanan *Daptocephalus* and *Dinanomodon*, Chinese *Turfanodon*, and Russian *Peramodon* (Fröbisch, 2009).

Battail (2009) previously compared the three Laotian specimens with *Lystrosaurus* and *Dicynodon*. Based on a morphological study, he attributed them to *Dicynodon* as previously defined by Cluver and Hotton (1981), before the taxonomic revision of *Dicynodon* by Kammerer et al. (2011). Our phylogenetic results do not contradict this preliminary assignment because the Laotian specimens show closer affinities with '*Dicynodon*'-grade taxa and the two valid species of *Dicynodon* (Kammerer et al., 2011) than with *Lystrosaurus*.

DISCUSSION

Morphological Variation in *Repelinosaurus robustus*

Specimens LPB 1995-9 and LPB 1993-2 are found in the same clade as *Repelinosaurus*, which is an early kannemeyeriiform (Fig. 6). As noted above, a variety of features distinguishes these two specimens. However, these differences could be related to postmortem distortion, ontogeny, sexual dimorphism, or other intraspecific variation.

Specimen LPB 1995-9 is distinguished by well-defined depressions lateral to the median ridge of the premaxilla, in contrast to the flat surface in LPB 1993-2 (discrete character 29, Appendix 1). Nevertheless, it is clear that LPB 1995-9 was affected by lateral compression, as indicated by the lack of symmetry in ventral view, the tusks turned inward, the more anterior position of the left tusk with respect to the right one, and breaks in the compressed zygomatic arches. In addition, the angulation between the occipital plate and the palate is less in LPB 1995-9 than in LPB 1993-2 (continuous character 13, Appendix 1) and could be linked to taphonomic distortion. The latter could also explain other differences such as (1) the direction of the posterior processes of the postorbitals (slightly oblique in LPB 1995-9 but horizontal in LPB 1993-2); (2) the insertion of the squamosal wings in the occipital plate (reaching the dorsal margin of the occiput in LPB 1993-2 but not in LPB 1995-9); and (3) the dorsal expansion of the parietals in the intertemporal bar (as a midline groove in LPB 1993-2 but mostly overlapped by the postorbitals in LPB 1995-9). In addition, although only two specimens of *Repelinosaurus* are currently known, it cannot be excluded that the other morphological differences between the two specimens could be related to ontogenetic, dimorphic, or other intraspecific variation.

Indeed, the negative allometry measured in the length of the pineal foramen versus skull size in *Repelinosaurus* (Table 2) could be interpreted as ontogenetic variability, as observed in *Colobodectes cluveri* (Angielczyk and Rubidge, 2009). In this taxon, Angielczyk and Rubidge (2009) also noted well-developed caniniform processes, with a disappearance of the palatal rim notch in the largest skull. Here, the large LPB 1993-2 shows a

deeper lateral convexity of the caniniform processes, yet no palatal rim notch is present. A greater length of the intertemporal bar posterior to the pineal foramen is also noted in the smaller LPB 1995-9 (continuous character 6, Appendix 1), as is the case in the Middle Triassic *Dolichuranus primaevus* (C. Olivier, pers. observ., on BP/1/4570 vs. BP/1/4573). This could suggest that the position of the pineal foramen may be related to ontogeny.

Specimen LPB 1995-9 is less robust than LPB 1993-2, which bears more-developed ornamentations: (1) its frontals bear a sharp frontal ridge; (2) high rugosities are noted on its premaxilla, maxillae, lateral processes of the postorbitals, and the squamosal zygomatic arch; and (3) its nasal bosses are more laterally developed. Variations in width, depth, and rugosity of skulls of the Middle–Late Triassic *Dinodontosaurus turpior* appear to be related to ontogeny (e.g., C. Olivier, pers. observ.; Lucas and Harris, 1996): the large specimen MCZ 1679 bears frontal, prefrontal, and postorbital bosses, which contrasts with the smaller MCZ 1677 (C. Olivier, pers. observ.). The development of cranial ridges and ornamentations is indeed related to skull size in *Lystrosaurus*, but only up to a size threshold (Grine et al., 2006). In addition, the size variation of ridges and ornamentation differs according to the species of *Lystrosaurus* (Grine et al., 2006). More developed ornamentation is also observed in the largest skulls of *Lystrosaurus*, but Ray (2005) proposed a sexually dimorphic variation, with inferred male individuals more ornamented than females. In addition, a more developed cranial ornamentation in adult males has been evidenced in *Diictodon* (Sullivan et al., 2003) and in *Pelanomodon*, which may be linked to the 'armament' in the context of sexual selection (Kammerer et al., 2016). The relative form and size of the nasal bosses also appears to be related to sexual dimorphism in the Permian *Aulacephalodon* (e.g., Keyser, 1969; Tollman et al., 1980). However, the quantitative analyses of Tollman et al. (1980) indicated a positive allometry in the width of the nasal bosses, instead suggesting an ontogenetic effect in *Aulacephalodon*. Moreover, as seen in LPB 1993-2, a ventrally directed convexity of the squamosal zygomatic arch in large specimens of *Aulacephalodon* are observed only in males (e.g., Tollman et al., 1980).

The basal section of the tusk of LPB 1993-2 (anteroposteriorly compressed) is different from that of LPB 1995-9 (mediolaterally compressed) (Table 2). Angielczyk and Rubidge (2009) noted the fact, that the smallest specimen of *Colobodectes cluveri* has less-developed and newly erupted tusks, is related to ontogeny. In *Repelinosaurus*, the tusks of LPB 1995-9 are well erupted and in the same proportion as in the larger LPB 1993-2. This variation in the basal section of the tusk thus appears unlikely to be linked to ontogeny. The mediolateral compression of the tusks in LPB 1995-9 could not be explained by lateral postmortem compression because of the excellent preservation of the tusks. Another intraspecific variation (i.e., related neither to sex nor to ontogeny) may thus explain the differences in tusk basal sections. This may also be the case for the prepariental that is depressed or flush with the skull roof (discrete character 68, Appendix 1) and for the maxilloprefrontal suture, which is present only in some of the specimens (discrete character 49, Appendix 1).

Most morphological variation within *Repelinosaurus robustus* may therefore be related to ontogeny and/or sexual dimorphism, as demonstrated to occur in other dicynodonts (e.g., Keyser, 1969; Tollman et al., 1980; Ray, 2005; Angielczyk and Rubidge, 2009), taphonomic distortion, or other intraspecific variation. Nevertheless, as mentioned above, the number of specimens of *Repelinosaurus* is too low to assess which kind of intraspecific variation (sexual dimorphism, ontogeny, etc.) is present.

Taxonomic Validity of *Repelinosaurus* and *Counillonia*

Phylogenetic affinities are found between the Laotian *Counillonia* and the late Permian *Peramodon*, *Delectosaurus*, *Vivaxosaurus, Turfanodon*, *Jimusaria*, *Gordonia*, *Euptychognathus*, *Daptocephalus*, *Dinanomodon*, *Sintocephalus,* and the two valid species of *Dicynodon* (Fig. 6; Kammerer et al., 2011). Within the clade formed by *Counillonia* and these '*Dicynodon*'-grade taxa, the following autapomorphies distinguish the Laotian dicynodont: (1) a relatively large median pterygoid plate (continuous character 8, Appendix 1); (2) the absence of an intertuberal ridge; and (3) opisthotics with distinct posteriorly directed processes (Fig. 2C, D). As in *Delectosaurus*, the occipital condyle of *Counillonia* is not fused, whereas the other cited '*Dicynodon*'-grade taxa have a co-ossified single unit. The nasofrontal suture is either straight, as in *Dicynodon huenei* and *Jimusaria*, or has an anterior process as in the other cited '*Dicynodon*'-grade taxa, unlike the clear posterior process in *Counillonia* (Fig. 2A). Overall, most morphological characters distinguish *Counillonia* from its closely related '*Dicynodon*'-grade taxa. If we focus on the geographically close taxa such as the Russian *Peramodon*, *Delectosaurus* and *Vivaxosaurus* and the Chinese *Turfanodon* and *Jimusaria*, other differences can be highlighted. *Peramodon* and *Turfanodon* have a rounded dorsal margin of the squamosal wings in lateral view (Kammerer et al., 2011), whereas the dorsal margin is more acute in *Counillonia* because of a lower lateral opening (Fig. 2B). The interorbital region in *Turfanodon* is wider than in *Counillonia* (Fig. 2A; Kammerer et al., 2011). *Counillonia* also has an interpterygoid vacuity and temporal squamosal processes longer than in *Jimusaria* (Kammerer et al., 2011); the squamosals therefore do not reach the dorsal region of the occiput in this Laotian genus (Fig. 2B). In contrast to *Vivaxosaurus*, the caniniform processes are less anteriorly projected in *Counillonia* and its maxillae do not bear a rounded boss anterior to the tusks (Fig. 2B; Kammerer et al., 2011). In *Counillonia*, the anterior rami of the pterygoids are ventrally highly expanded and therefore not in the same plane as the more dorsal palatines (Fig. 2C), in contrast to the condition in *Delectosaurus.*

Repelinosaurus is recovered as a kannemeyeriiform. Only one genus of kannemeyeriiform was previously known near the Permo-Triassic boundary: the Early Triassic *Sungeodon* (Maisch and Matzke, 2014). *Repelinosaurus* differs from all kannemeyeriiforms by the strong reduction of the preorbital region (Figs. 3A, 4A). This character state is shared to a lesser degree with *Counillonia* (Fig. 2A) and the kistecephalian *Kombuisia* (Fröbisch, 2007). As in the Early Triassic *Kombuisia* and *Myosaurus*, the nasal bosses of *Repelinosaurus* form a single median swelling in dorsal view (Figs. 3A, 4A), in contrast to currently known kannemeyeriiforms, which have a pair of bosses. In *Repelinosaurus*, the parietals, weakly exposed on the skull roof, are inserted between the two wide posterior processes of the postorbitals (Figs. 3A, 4A), in contrast to the majority of kannemeyeriiforms except *Sangusaurus*, *Uralokannemeyeria*, and *Rechnisaurus.* Kannemeyeriiformes are known for their temporal crest, generally associated with laterally directed posterior processes of the postorbitals. This is not the case in *Repelinosaurus* (Figs. 3A, B, 4A, B), where the postorbitals mainly face dorsally.

New Data Supporting the Survivorship of Multiple Lineages across the P-Tr Boundary?

The latest Permian terrestrial biomes were dominated by herbivorous pareiasaurs and dicynodonts and carnivorous gorgonopsians and therocephalians (e.g., Steyer, 2012; Benton and Newell, 2014). A recent study (Bernardi et al., 2017) evidenced a link between the distribution of herbivore tetrapods, phytoprovinces, and latitudinal climatic zonation. More specifically, dicynodonts were predominant only in high paleolatitude biomes. The dicynodonts were strongly affected by the P-Tr crisis (e.g., Fröbisch, 2007). The lystrosaurids are the emblematic clade to have survived the P-Tr event (e.g., Fröbisch, 2007; Botha-Brink et al., 2016). However, as indicated by the dicynodont

phylogenetic relationships recovered herein (e.g., Angielczyk, 2001; Fröbisch, 2007; Fröbisch et al., 2010; Kammerer et al., 2011), other lineages also appear to cross the end-Permian boundary. Fröbisch (2007) previously highlighted the interesting phylogenetic position of the Triassic *Kombuisia*, belonging to kingoriids and closely related to the Permian *Dicynodontoides*. *Kombuisia* is known from the probable Middle Triassic of South Africa and also the Early Triassic of Antarctica (e.g., Fig. 6; Fröbisch, 2007; Fröbisch et al., 2010). The stratigraphic positions of the two *Kombuisia* species imply lengthy ghost lineages, stretching back into the Permian. The Early Triassic *Myosaurus* is also closely related to Permian dicynodonts and is sister taxon to the cistecephalids (e.g., Fig. 6; Fröbisch, 2007). In addition, most previous studies assumed a ghost lineage for Kannemeyeriiformes (e.g., Fröbisch, 2007; Fröbisch et al., 2010; Kammerer et al., 2011). Kammerer et al. (2011) indeed inferred Permian forms (such as lystrosaurids or '*Dicynodon*'-grade taxa) as sister groups to the kannemeyeriiforms. They thus assumed a ghost lineage for the kannemeyeriiforms that spans at least part of the late Permian and the earliest Triassic.

Most previous studies noted the impact of a potential geographic bias on the presence of ghost lineages in dicynodonts (e.g., Angielczyk, 2001; Fröbisch et al., 2010; Kammerer et al., 2011). Their hypothesis was supported by the discovery of specimens of *Kombuisia* (formerly known from the Karoo Basin in South Africa, dated to the Middle Triassic) from the Early Triassic Fremouw Formation in Antarctica (Fröbisch et al., 2010). In addition, the assumption of Kammerer et al. (2013) regarding the occurrence of kannemeyeriiforms in the Early Triassic gained support by the recent description of *Sungeodon* from the Junggar Basin in China (Maisch and Matzke, 2014). Despite relatively weak node support, the phylogenetic position of the Laotian *Repelinosaurus* also helps to shorten the ghost lineage between the kannemeyeriiforms and the other dicynodontoids, extending the first appearance of Kannemeyeriiformes to near the P-Tr boundary. In addition, the discovery of the earliest kannemeyeriiforms in an understudied geographic area such Laos, with *Repelinosaurus*, and China, with *Sungeodon* (Maisch and Matzke, 2014), strengthens these suggestions, underlining a geographic bias in dicynodont sampling. The phylogenetic position of *Counillonia* makes it the first known '*Dicynodon*'-grade dicynodontoid that could have survived the P-Tr extinction (maximum depositional age of 251.0 ± 1.4 Ma).This supports the survivorship of multiple dicynodont lineages across the P-Tr event, as previously suggested (e.g., Angielczyk, 2001; Fröbisch, 2007; Fröbisch et al., 2010; Kammerer et al., 2011)

The dicynodont postextinction recovery was thought to be have been relatively delayed (e.g., Sahney and Benton, 2008; Chen and Benton, 2012), starting in the Middle Triassic when the kannemeyeriiforms underwent a large adaptive radiation (Fröbisch, 2009). Sun et al. (2012) described an 'equatorial tetrapod gap' and attributed the delayed recovery to excessive paleotemperatures during the Early Triassic, especially at the warmer equatorial paleolatitudes. However, other studies have supported a rapid recovery (e.g., Botha and Smith, 2006; Maisch and Matzke, 2014). The occurrence in the Early Triassic of the kannemeyeriiform *Sungeodon* (Maisch and Matzke, 2014) and potentially of a new Laotian kannemeyeriiform *Repelinosaurus* (maximum depositional age of 251.0 ± 1.4 Ma; Rossignol et al., 2016) would support a rapid recovery of the group after the P-Tr mass extinction event. In addition, Bernardi et al. (2018) explained the 'equatorial tetrapod gap' defined by Sun et al. (2012) by invoking a northward tetrapod distribution shift during the Induan. Besides, as for Antarctica (Fröbisch et al., 2010), the presence of dicynodonts (*Repelinosaurus* and *Counillonia*) and a chroniosuchian (*Laosuchus naga*, Arbez et al., 2018) in Laos near the Permo-Triassic boundary may also indicate a refuge zone where the dicynodont and chroniosuchian (and possibly other tetrapod faunas) were not strongly affected by the P-Tr crisis. However, the available data on the Laotian fauna of the Permo-Triassic period are not yet sufficient to draw firm conclusions on this point.

As mentioned above, Bernardi et al. (2017) demonstrated a significant correlation between the distribution of the dicynodonts and phytoprovinces, indicating that the resilience and survivorship of dicynodonts after the crisis may be linked to plant diversity. Indeed, Gastaldo et al. (2017) described an uninterrupted plant cover of glossopterids and sphenophytes in the *Lystrosaurus* Assemblage Zone, across the P-Tr boundary. A full recovery of plants is also attested from the Middle Triassic (e.g., Benton and Newell, 2014). An Early Triassic flora is well documented in South China, combining the late Permian relict *Gigantopteris* and pioneer taxa dominated by the lycopsid *Annalepsis* (Yu et al., 2015). This Chinese paleoflora has been shown to be stable across the P-Tr boundary, with the highest turnover rates occurring during the Induan (Xiong and Wang, 2011). Even if documented in a distinct and somewhat remote area from the Luang Prabang Basin at that time (Fig. 1), a rich and diversified paleoflora (Bercovici et al., 2012) has been evidenced above the strata correlated to the late Changhsingian (Blanchard et al., 2013) and below the Purple Claystone Formation (Rossignol et al., 2016). The occurrence of paleosols with root traces (Bercovici et al., 2012) attests to the presence of plants during the deposition of the Purple Claystone Formation.

Paleobiogeographic Implications of the Two Laotian Dicynodonts

The occurrence of new dicynodonts in the Luang Prabang Basin (Laos), located in the Indochina Block (e.g., Fig. 1A; Cocks and Torsvik, 2013), provides interesting new insights into the controversial paleogeography of Southeast Asia.

Like all the other East and Southeast Asian continental blocks, the Indochina Block originates from the eastern Gondwana margin (e.g., Metcalfe, 2013; Burrett et al., 2014). The separation of this block from the Gondwana mainland, by the opening of the Paleotethyan Ocean, is dated to the Early Ordovician (e.g., Cocks and Torsvik, 2013) or the Devonian (e.g., Metcalfe, 2011, 2013; Thanh et al., 2011; Lai et al., 2014). The collision between the Indochina and South China blocks has been variously dated: Silurian to Devonian (e.g., Thanh et al., 2011), Carboniferous (e.g., Metcalfe, 2011; Vượng et al., 2013; Zhang et al., 2014), late Permian to Early Triassic (Halpin et al., 2016), Early Triassic (e.g., Lepvrier et al., 2004; Kamvong et al., 2014), Middle Triassic (e.g., Nakano et al., 2008; Zhang et al., 2013, 2014; Faure et al., 2014; Rossignol et al., 2018), or even Late Triassic (e.g., Liu et al., 2012).

Microanatomical studies, analyzing the distribution of the bone tissues and morphological and taphonomic evidence, support an essentially terrestrial lifestyle for most dicynodonts (e.g., Wall, 1983; King and Cluver, 1990; Ray et al., 2005, 2010, 2012; Botha-Brink and Angielczyk, 2010). *Lystrosaurus* is one of the rare dicynodonts supposed to be semiaquatic based on its microanatomy, morphology, and taphonomic preservation (e.g., Germain and Laurin, 2005; Ray, 2006). However, these conclusions have been questioned, and a terrestrial lifestyle has been proposed for *Lystrosaurus* based on its microanatomy, associated faunas, and paleoenvironment (e.g., King and Cluver, 1990; Botha-Brink and Angielczyk, 2010). The bone microstructure in *Lystrosaurus* is similar to that of *Placerias*, *Wadiasaurus,* and *Kannemeyeria* (Wall, 1983; Ray et al., 2005, 2012). However, whereas a semiaquatic lifestyle based on microanatomy is proposed for *Placerias* (Green et al., 2010), *Kannemeyeria* and *Wadiasaurus* were supposed to be terrestrial (Ray et al., 2010, 2012). Evidence for the dicynodont lifestyle remains equivocal, but even if some taxa did have a semiaquatic

but freshwater lifestyle, this would be unlikely to allow dispersal across a wide oceanic domain.

The presence of dicynodonts in Laos highlights a connection between the Indochina Block and the South China Block (SCB). U-Pb geochronology on detrital zircon suggested that the connection may occur not later than 251.0 ± 1.4 Ma, the maximum depositional age. Two different hypotheses can be proposed to account for such a connection.

Firstly, the Indochina Block could have been connected with the North China Block (NCB), via the SCB. This hypothesis requires that the contact between the NCB and the SCB was effective at 251.0 ± 1.4 Ma, i.e., slightly before the Middle to Late Triassic age generally considered plausible for the collision between these blocks (Li, 1994; Weislogel et al., 2006; Chang and Zhao, 2012; Torsvik and Cocks, 2017). It also implies a connection between the Indochina Block and the SCB before or during the latest Permian or earliest Triassic, as proposed by Lepvrier et al. (2004), Metcalfe (2011), Kamvong et al. (2014), Scotese (2014), and Halpin et al. (2016). However, other interpretations support a continental connection between the SCB and the Indochina Block later than the Early Triassic (see references above). A diachronous continental collision between the SCB and the Indochina Block (Halpin et al., 2016), beginning during the late Permian to the east (present day coordinates) and continuing toward the west up to the Middle Triassic, has recently been put forward. Such a hypothesis reconciles an Early to Middle Triassic collision between the SCB and the Indochina Block with the paleobiogeographic distribution of dicynodonts. This is further corroborated with the discovery of a new chroniosuchian in nonmarine rocks in the Purple Claystone Formation (Arbez et al., 2018). This form is inferred to have had an amphibious lifestyle (e.g., Buchwitz et al., 2012; Golubev, 2015; Arbez et al., 2018) and supports a connection between Eurasia and the Indochina Block at that time.

Secondly, another hypothesis to account for the presence of dicynodont remains in the Indochina Block consists of an indirect connection with other landmasses via a string of microcontinents. Indeed, a connection between Pangea and the Indochina Block, involving the western Cimmerian continental strip before or during the Early Triassic, was also suggested (Buffetaut, 1989; Metcalfe, 2006, 2011). Laos is characterized by a Cathaysian flora, also found in China, Korea, Japan, Thailand, Indonesia, and Malaysia (e.g., Bernardi et al., 2017). The strong affinities between Cathaysian and Cimmerian faunas and floras suggest geographic proximity (Wang and Sugiyama, 2002; Torsvik and Cocks, 2017). Nevertheless, this proximity is based on plants and marine faunas (Wang and Sugiyama, 2002; Ueno, 2003; Shen et al., 2013; Torsvik and Cocks, 2017), which are less constrained for dispersion by oceanic barriers than terrestrial faunas are. Moreover, the presence of marine faunas and a majority of limestone deposits during the late Permian in the Sibumasu Block (e.g., Ueno, 2003; Chaodumrong et al., 2007; Shen et al., 2013; Wang et al., 2013) indicates a largely submerged land (Metcalfe, 2011). Furthermore, the collision between the Sibumasu or Simao block and the Indochina Block is considered to have occurred after the Norian (e.g., Metcalfe, 2011; Rossignol et al., 2016). The Cimmerian option also supposes proximity between the Cimmerian blocks and Pangea. The collision between Iran and Eurasia is latest Triassic–Jurassic in age (e.g., Wilmsen et al., 2009; Zanchi et al., 2009). However, Zanchi et al. (2015) suggest an affinity and probable proximity between Eurasia and Central Iran as early as late Paleozoic. These uncertainties render difficult the involvement of the Cimmerian blocks during the Permian–Triassic in the role of an indirect connection and suggest the existence of other microcontinents to explain this second hypothesis.

The aforementioned two hypotheses are based on a maximum depositional age of 251.0 ± 1.4 Ma for the Laotian dicynodonts. Such a maximum depositional age is also compatible with a deposition of the Purple Claystone Formation in the Middle Triassic (Rossignol et al., 2016). This maximum depositional age is therefore consistent with paleogeographic results indicating collisions between the NCB and the SCB (Li, 1994; Weislogel et al., 2006; Chang and Zhao, 2012; Torsvik and Cocks, 2017) in the Middle Triassic and between the Indochina Block and the SCB in the Middle to Late Triassic (e.g., Liu et al., 2012; Zhang et al., 2013; Faure et al., 2014; Rossignol et al., 2018). This implies the survival of a '*Dicynodon*'-grade taxon *Counillonia superoculis* through the P-Tr crisis. This work brings new insights to ongoing debates about the paleobiogeographic and geodynamic evolution of Southeast Asia from the late Paleozoic to the early Mesozoic. It warrants further field expeditions in late Permian and Early Triassic formations in the former Indochina block to confirm or reject our hypotheses.

ACKNOWLEDGMENTS

We thank the Ministry of Information and Culture of Lao P.D.R. and the Savannakhet Dinosaur Museum (Laos) for their authorization to study the material. We also thank C. Bouillet and P. Richir (CR2P, MNHN, Paris, France) for their help during the preparation of the material; S. Fernandez (MNHN) for the drawings; T. Arbez (CR2P, MNHN) for his comments on the Laotian chroniosuchian; B. Khalloufi (CR2P, MNHN) and R. Zaragüeta (ISYEB, MNHN) for their discussion on paleobiogeographic issues; R. R. Allain, V. Barriel, O. Bethoux, G. Billet, and M. Laurin (CR2P, MNHN), A. K. Huttenlocker (University of Southern California, Los Angeles, California, U.S.A.), C. Kammerer (North Carolina Museum of Natural Sciences, Raleigh, North Carolina, U.S.A.), K. D. Angielczyk (Field Museum of Natural History, Chicago, Illinois, U.S.A.), J. Camp (University of California, Riverside, County California, U.S.A.), and an anonymous reviewer for their relevant and constructive remarks; and M. Pickford (CR2P, MNHN) and M. Laurin (CR2P, MNHN) for improving the English. C.O. benefited from the financial support of the GDRI PalBioDiv SEA project, which allowed her to consult the dicynodonts material in Savanaketh (Laos). C.R. acknowledges the financial support of the São Paulo Research Foundation (FAPESP [Fundação Amparo à Pesquisa do Estado de São Paulo]; processo 2018/02645-2 and processo 2015/16235-2).

ORCID

Chloe Olivier http://orcid.org/0000-0003-1466-6535

LITERATURE CITED

Angielczyk, K. D. 2001. Preliminary phylogenetic analysis and stratigraphic congruence of the dicynodont anomodonts (Synapsida: Therapsida). Palaeontologia africana 37:53–79.

Angielczyk, K. D., and C. F. Kammerer. 2017. The cranial morphology, phylogenetic position and biogeography of the upper Permian dicynodont *Compsodon helmoedi* van Hoepen (Therapsida, Anomodontia). Papers in Palaeontology 3:513–545.

Angielczyk, K. D., and A. A. Kurkin. 2003. Phylogenetic analysis of Russian Permian dicynodonts (Therapsida: Anomodontia): implications for Permian biostratigraphy and Pangaean biogeography. Zoological Journal of the Linnean Society 139:157–212.

Angielczyk, K. D., and B. S. Rubidge. 2009. The Permian dicynodont *Colobodectes cluveri* (Therapsida, Anomodontia), with notes on its ontogeny and stratigraphic range in the Karoo Basin, South Africa. Journal of Vertebrate Paleontology 29:1162–1173.

Angielczyk, K. D., and B. S. Rubidge. 2013. Skeletal morphology, phylogenetic relationships and stratigraphic range of *Eosimops newtoni* Broom, 1921, a pylaecephalid dicynodont (Therapsida, Anomodontia) from the middle Permian of South Africa. Journal of Systematic Palaeontology 11:191–231.

Angielczyk, K. D., P. J. Hancox, and A. Nabavizadeh. 2018. A redescription of the Triassic kannemeyeriiform dicynodont *Sangusaurus* (Therapsida, Anomodontia), with an analysis of its feeding system; pp. 189–227 in C. A. Sidor and S. J. Nesbitt (eds.), Vertebrate and Climatic Evolution in the Triassic Rift Basins of Tanzania and Zambia. Society of Vertebrate Paleontology Memoir 17. Journal of Vertebrate Paleontology 37(6, supplement).

Angielczyk, K. D., B. S. Rubidge, M. O. Day, and F. Lin. 2016. A reevaluation of *Brachyprosopus broomi* and *Chelydontops altidentalis*, dicynodonts (Therapsida, Anomodontia) from the middle Permian *Tapinocephalus* Assemblage Zone of the Karoo Basin, South Africa. Journal of Vertebrate Paleontology. doi: 10.1080/02724634.2016.1078342.

Arbez, T., C. A. Sidor, and J. S. Steyer. 2018. *Laosuchus naga* gen. et sp. nov., a new chroniosuchian from South-East Asia (Laos) with internal structures revealed by micro-CT scan and discussion of its palaeobiology. Journal of Systematic Palaeontology. doi: 10.1080/14772019.2018.1504827.

Battail, B. 2009. Late Permian dicynodont fauna from Laos. Geological Society, London, Special Publications 315:33–40.

Bernardi, M., F. M. Petti, and M. J. Benton. 2018. Tetrapod distribution and temperature rise during the Permian–Triassic mass extinction. Proceedings of the Royal Society B: Biological Sciences 285:20172331. doi: 10.1098/rspb.2017.2331.

Bernardi, M., F. M. Petti, E. Kustatscher, M. Franz, C. Hartkopf-Fröder, C. C. Labandeira, T. Wappler, J. H. A. van Konijnenburg-van Cittert, B. R. Peecook, and K. D. Angielczyk. 2017. Late Permian (Lopingian) terrestrial ecosystems: a global comparison with new data from the low-latitude Bletterbach Biota. Earth-Science Reviews 175:18–43.

Benton, M. J., and A. J. Newell. 2014. Impacts of global warming on Permo–Triassic terrestrial ecosystems. Gondwana Research 25:1308–1337.

Benton, M. J., V. P. Tverdokhlebov, and M. V. Surkov. 2004. Ecosystem remodelling among vertebrates at the Permian–Triassic boundary in Russia. Nature 432:97–100.

Bercovici, A., S. Bourquin, J. Broutin, J.-S. Steyer, B. Battail, M. Véran, R. Vacant, B. Khenthavong, and S. Vongphamany. 2012. Permian continental paleoenvironments in Southeastern Asia: new insights from the Luang Prabang Basin (Laos). Journal of Asian Earth Sciences 60:197–211.

Blanchard, S., C. Rossignol, S. Bourquin, M.-P. Dabard, E. Hallot, T. Nalpas, M. Poujol, B. Battail, N.-E. Jalil, J.-S. Steyer, R. Vacant, M. Véran, A. Bercovici J. B. Diez, J.-L. Paquette, B. Khenthavong, and S. Vongphamany. 2013. Late Triassic volcanic activity in South-East Asia: new stratigraphical, geochronological and paleontological evidence from the Luang Prabang Basin (Laos). Journal of Asian Earth Sciences 70–71:8–26.

Boos, A. D. S., C. F. Kammerer, C. L. Schultz, M. B. Soares, and A. L. R. Ilha. 2016. A new dicynodont (Therapsida: Anomodontia) from the Permian of southern Brazil and its implications for bidentalian origins. PLoS ONE 11:e0155000.

Botha, J., and R. M. H. Smith. 2006. Rapid vertebrate recuperation in the Karoo Basin of South Africa following the End-Permian extinction. Journal of African Earth Sciences 45:502–514.

Botha-Brink, J., and K. D. Angielczyk. 2010. Do extraordinarily high growth rates in Permo–Triassic dicynodonts (Therapsida, Anomodontia) explain their success before and after the end-Permian extinction? Zoological Journal of the Linnean Society 160:341–365.

Botha-Brink, J., D. Codron, A. K. Huttenlocker, K. D. Angielczyk, and M. Ruta. 2016. Breeding young as a survival strategy during Earth's greatest mass extinction. Scientific Reports 6:24053. doi: 10.1038/srep24053.

Bremer, K. 1988. The limits of amino acid sequence data in angiosperm phylogenetic reconstruction. Evolution 42:795–803.

Broom, R. 1905. On the use of the term Anomodontia. Albany Museum Records 1:266–269.

Buchwitz, M., F. Witzmann, S. Voigt, and V. Golubev. 2012. Osteoderm microstructure indicates the presence of a crocodylian-like trunk bracing system in a group of armoured basal tetrapods. Acta Zoologica 93:260–280.

Buffetaut, E. 1989. The contribution of vertebrate palaeontology to the geodynamic history of South East Asia; pp. 645–653 in A. M. C. Şengör (ed.), Tectonic Evolution of the Tethyan Region. Kluwer Academic Publishers, Dordrecht, The Netherlands.

Burgess, S. D., S. A. Bowring, and S.-Z. Shen. 2014. High-precision timeline for Earth's most severe extinction. Proceedings of the National Academy of Sciences of the United States of America 111:3316–3321.

Burrett, C., K. Zaw, S. Meffre, C. K. Lai, S. Khositanont, P. Chaodumrong, M. Udchachon, S. Ekins, and J. Halpin. 2014. The configuration of Greater Gondwana—evidence from LA ICPMS, U-Pb geochronology of detrital zircons from the Palaeozoic and Mesozoic of Southeast Asia and China. Gondwana Research 26:31–51.

Castanhinha, R., R. Araújo, L. C. Júnior, K. D. Angielczyk, G. G. Martins, R. M. S. Martins, C. Chaouiya, F. Beckmann, and F. Wilde. 2013. Bringing dicynodonts back to life: paleobiology and anatomy of a new emydopoid genus from the upper Permian of Mozambique. PLoS ONE 8:e80974.

Chang, K.-H., and X. Zhao. 2012. North and South China suturing in the east end: what happened in Korean Peninsula? Gondwana Research 22:493–506.

Chaodumrong, P., X.-D. Wang, and S.-Z. Shen. 2007. Permian lithostratigraphy of the Shan–Thai Terrane in Thailand: revision of the Kaeng Krachan and Ratburi groups; pp. 229–236 in W. Tantiwanit (ed.) Prooceedings of the International Conference on Geology of Thailand (GEOTHAI'07): Towards Sustainable Development and Sufficiency Economy, Bangkok, 21–22 November 2007.

Chen, Z.-Q., and M. J. Benton. 2012. The timing and pattern of biotic recovery following the end-Permian mass extinction. Nature Geoscience 5:375–383.

Cluver, M. A. 1971. The cranial morphology of the dicynodont genus *Lystrosaurus*. Annals of the South African Museum 56:155–274.

Cluver, M. A., and N. Hotton III. 1981. The genera *Dicynodon* and *Diictodon* and their bearing of classification of the Dicynodontia (Reptilia, Therapsida). Annals of the South African Museum 83:99–146.

Cluver, M. A., and G. M. King. 1983. A reassessment of the relationships of Permian Dicynodontia (Reptilia, Therapsida) and a new classification of dicynodonts. Annals of the South African Museum 91:195–273.

Cocks, L. R. M., and T. H. Torsvik. 2013. The dynamic evolution of the Palaeozoic geography of eastern Asia. Earth-Science Reviews 117:40–79.

Colbert, E. H. 1982. The distribution of *Lystrosaurus* in Pangaea and its implications. Geobios 15:375–383.

Counillon, H. 1896. Documents pour servir à l'étude géologique des environs de Luang–Prabang (Cochinchine). Comptes rendus de l'Académie des sciences 123:1330–1333.

Cox, C. B., and K. D. Angielczyk. 2015. A new endothiodont dicynodont (Therapsida, Anomodontia) from the Permian Ruhuhu Formation (Songea Group) of Tanzania and its feeding system. Journal of Vertebrate Paleontology. doi: 10.1080/02724634.2014.935388.

Das Gupta, H. C. 1922. Notes on the Panchet reptile; pp. 237–241, Sir Asutosh Mukherjee Silver Jubilee Volumes, Volume 2. University Press, Calcutta, India. Das Gupta, 1922. Name of publisher correct/complete? Or '[xxx] University Press'; 'University [of xxx] Press'?

Dutuit, J. M. 1988. Ostéologie crânienne et ses enseignements, apports géologique et paléoécologique, de *Moghreberia nmachouensis*, Dicynodonte (Reptilia, Therapsida) du Trias supérieur marocain. Bulletin du Muséum national d'histoire naturelle, Section C, Sciences de la terre, paléontologie, géologie, minéralogie 10:227–285.

Faure, M., C. Lepvrier, V. V. Nguyen, T. V. Vu, W. Lin, and Z. Chen. 2014. The South China block-Indochina collision: where, when, and how? Journal of Asian Earth Sciences 79:260–274.

Fröbisch, J. 2007. The cranial anatomy of *Kombuisia frerensis* Hotton (Synapsida, Dicynodontia) and a new phylogeny of anomodont therapsids. Zoological Journal of the Linnean Society 150:117–144.

Fröbisch, J. 2008. Global taxonomic diversity of anomodonts (Tetrapoda, Therapsida) and the terrestrial rock record across the Permian-Triassic boundary. PLoS ONE 3:e3733.

Fröbisch, J. 2009. Composition and similarity of global anomodont-bearing tetrapod faunas. Earth-Science Reviews 95:119–157.

Fröbisch, J., K. D. Angielczyk, and C. A. Sidor. 2010. The Triassic dicynodont *Kombuisia* (Synapsida, Anomodontia) from Antarctica, a refuge from the terrestrial Permian-Triassic mass extinction. Naturwissenschaften 97:187–196.

Gastaldo, R. A., J. Neveling, C. V. Looy, M. K. Bamford, S. L. Kamo, and J. W. Geissman. 2017. Paleontology of the Blaauwater 67 and 65 farms, South Africa: testing the *Daptocephalus*/*Lystrosaurus* biozone boundary in a stratigraphic framework. Palaios 32:349–366.

Germain, D., and M. Laurin. 2005. Microanatomy of the radius and lifestyle in amniotes (Vertebrata, Tetrapoda). Zoologica Scripta 34:335–350.

Goloboff, P. A. 1999. Analyzing large data sets in reasonable times: solutions for composite optima. Cladistics 15:415–428.

Goloboff, P. A., J. S. Farris, and K. C. Nixon. 2008. TNT, a free program for phylogenetic analysis. Cladistics 24:774–786.

Goloboff, P. A., C. I. Mattoni, and A. S. Quinteros. 2006. Continuous characters analyzed as such. Cladistics 22:589–601.

Golubev, V. K. 2015. Dinocephalian stage in the history of the Permian tetrapod fauna of Eastern Europe. Paleontological Journal 49:1346–1352.

Green, J. L., M. H. Schweitzer, and E.-T. Lamm. 2010. Limb bone histology and growth in *Placerias hesternus* (Therapsida: Anomodontia) from the Upper Triassic of North America. Palaeontology 53:347–364.

Grine, F. E., C. A. Forster, M. A. Cluver, and J. A. Georgi. 2006. Cranial variability, ontogeny and taxonomy of *Lystrosaurus* from the Karoo Basin of South Africa; pp. 432–503 in M. T. Carrano, T. J., Gaudin, R. W. Blob, and J. R. Wible (eds.), Amniote Paleobiology: Perspectives on the Evolution of Mammals, Birds, and Reptiles. University of Chicago Press, Chicago, Illinois.

Halpin, J. A., H. T. Tran, C.-K. Lai, S. Meffre, A. J. Crawford, and K. Zaw. 2016. U-Pb zircon geochronology and geochemistry from NE Vietnam: a "tectonically disputed" territory between the Indochina and South China blocks. Gondwana Research 34:254–273.

Kammerer, C. F., and K. D. Angielczyk. 2009. A proposed higher taxonomy of anomodont therapsids. Zootaxa 2018:1–24.

Kammerer, C. F., and R. M. H. Smith. 2017. An early geikiid dicynodont from the *Tropidostoma* Assemblage Zone (late Permian) of South Africa. PeerJ 5:e2913.

Kammerer, C. F., K. D. Angielczyk, and J. Fröbisch. 2011. A comprehensive taxonomic revision of *Dicynodon* (Therapsida, Anomodontia) and its implications for dicynodont phylogeny, biogeography, and biostratigraphy. Journal of Vertebrate Paleontology 31(6, Supplement). Society of Vertebrate Paleontology Memoir 11:1–158.

Kammerer, C. F., K. D. Angielczyk, and J. Fröbisch. 2016. Redescription of the geikiid *Pelanomodon* (Therapsida, Dicynodontia), with a reconsideration of '*Propelanomodon*.' Journal of Vertebrate Paleontology. doi: 10.1080/02724634.2015.1030408.

Kammerer, C. F., J. Fröbisch, and K. D. Angielczyk. 2013. On the validity and phylogenetic position of *Eubrachiosaurus browni*, a kannemeyeriiform dicynodont (Anomodontia) from Triassic North America. PLoS ONE 8:e64203.

Kamvong, T., K. Zaw, S. Meffre, R. Maas, H. Stein, and C.-K. Lai. 2014. Adakites in the Truong Son and Loei fold belts, Thailand and Laos: genesis and implications for geodynamics and metallogeny. Gondwana Research 26:165–184.

Keyser, A. W. 1969. A re-evaluation of the systematics and morphology of certain anomodont Therapsida. Ph.D. dissertation, University of the Witwatersrand, Johannesburg, South Africa, 325 pp.

Keyser, A. W., and A. R. I. Cruickshank. 1979. The origins and classification of Triassic dicynodonts. Transactions of the Geological Society of South Africa 82:81–108.

King, G. M. 1988. Anomodontia. Handbuch der Paläoherpetologie, 17C. Gustav Fischer Verlag, Stuttgart, Germany, 174 pp.

King, G. M., and M. A. Cluver. 1990. The aquatic *Lystrosaurus*: an alternative lifestyle. Historical Biology 4:323–341.

Lai, C.-K., S. Meffre, A. J. Crawford, K. Zaw, C.-D. Xue, and J. A. Halpin. 2014. The Western Ailaoshan Volcanic Belts and their SE Asia connection: a new tectonic model for the Eastern Indochina Block. Gondwana Research 26:52–74.

Lepvrier, C., H. Maluski, V. Van Tich, A. Leyreloup, P. Truong Thi, and N. Van Vuong. 2004. The Early Triassic Indosinian orogeny in Vietnam (Truong Son Belt and Kontum Massif); implications for the geodynamic evolution of Indochina. Tectonophysics 393:87–118.

Li, Z.-X. 1994. Collision between the North and South China blocks: a crustal-detachment model for suturing in the region east of the Tanlu fault. Geology 22:739–742.

Liu, J., L. Li, and X.-W. Li. 2013. SHRIMP U-Pb zircon dating of the Triassic Ermaying and Tongchuan formations in Shanxi, China and its stratigraphic implications. Vertebrata PalAsiatica 51:162–168.

Liu, J., J. Ramezani, L. Li, Q.-H. Shang, G.-H. Xu, Y.-Y. Wang, and J.-S. Yang. 2018. High-precision temporal calibration of Middle Triassic vertebrate biostratigraphy: U-Pb zircon constraints for the *Sinokannemeyeria* Fauna and Yonghesuchus. Vertebrata PalAsiatica 56:16–24.

Liu, J., M.-D. Tran, Y. Tang, Q.-L. Nguyen, T.-H. Tran, W. Wu, J. Chen, Z. Zhang, and Z. Zhao. 2012. Permo-Triassic granitoids in the northern part of the Truong Son belt, NW Vietnam: geochronology, geochemistry and tectonic implications. Gondwana Research 22:628–644.

Lucas, S. G., and S. K. Harris. 1996. Taxonomic and biochronological significance of specimens of the Triassic dicynodont *Dinodontosaurus* Romer 1943 in the Tübingen collection. Paläontologische Zeitschrift 70:603–622.

Maisch, M. W. 2001. Observations on Karoo and Gondwana vertebrates. Part 2: a new skull-reconstruction of *Stahleckeria potens* von Huene, 1935 (Dicynodon, Middle Triassic) and a reconsideration of kannemeyeriiform phylogeny. Neues Jahrbuch für Geologie und Paläontologie, Abhandlungen, 220:127–152.

Maisch, M. W. 2002. A new basal lystrosaurid dicynodont from the Upper Permian of South Africa. Palaeontology 45:343–359.

Maisch, M. W., and A. T. Matzke. 2014. *Sungeodon kimkraemerae* n. gen. n. sp., the oldest kannemeyeriiform (Therapsida, Dicynodontia) and its implications for the early diversification of large herbivores after the P/T boundary. Neues Jahrbuch für Geologie und Paläontologie, Abhandlungen 272:1–12.

Metcalfe, I. 2006. Palaeozoic and Mesozoic tectonic evolution and palaeogeography of East Asian crustal fragments: the Korean Peninsula in context. Gondwana Research 9:24–46.

Metcalfe, I. 2011. Tectonic framework and Phanerozoic evolution of Sundaland. Gondwana Research 19:3–21.

Metcalfe, I. 2013. Gondwana dispersion and Asian accretion: tectonic and palaeogeographic evolution of eastern Tethys. Journal of Asian Earth Sciences 66:1–33.

Nakano, N., Y. Osanai, N. T. Minh, T. Miyamoto, Y. Hayasaka, and M. Owada. 2008. Discovery of high-pressure granulite-facies metamorphism in northern Vietnam: constraints on the Permo–Triassic Indochinese continental collision tectonics. Comptes Rendus Geoscience 340:127–138.

Olson, E. C. 1944. Origin of mammals based upon cranial morphology of the therapsid suborders. Geological Society of America Special Papers 55:1–136.

Owen, R. 1860. On the orders of fossil and recent Reptilia, and their distribution in time. Report of the Twenty-Ninth Meeting of the British Association for the Advancement of Science 1859:153–166.

Piveteau, J. 1938. Un therapside d'Indochine. Remarques sur la notion de continent de Gondwana. Annales de Paléontologie 27:137–152.

Racey, A. 2009. Mesozoic red bed sequences from SE Asia and the significance of the Khorat Group of NE Thailand. Geological Society, London, Special Publications 315:41–67.

Ray, S. 2005. *Lystrosaurus* (Therapsida, Dicynodontia) from India: taxonomy, relative growth and cranial dimorphism. Journal of Systematic Palaeontology 3:203–221.

Ray, S. 2006. Functional and evolutionary aspects of the postcranial anatomy of dicynodonts (Synapsida, Therapsida). Palaeontology 49:1263–1286.

Ray, S., S. Bandyopadhyay, and R. Appana. 2010. Bone histology of a kannemeyeriid dicynodont *Wadiasaurus*: palaeobiological implications; pp. 73–89 in S. Bandyopadhyay (ed.), New Aspects of Mesozoic Biodiversity. Springer, Heidelberg and Berlin, Germany.

Ray, S., J. Botha-Brink, and A. Chinsamy-Turan. 2012. Dicynodont growth dynamics and lifestyle adaptations; pp. 121–148 in A. Chinsamy-Turan (ed.), Forerunners of Mammals. Indiana University Press, Bloomington, Indiana.

Ray, S., A. Chinsamy, and S. Bandyopadhyay. 2005. *Lystrosaurus murrayi* (Therapsida, Dicynodontia): bone histology, growth and lifestyle adaptations. Palaeontology 48:1169–1185.

Renaut, A. 2000. A re-evaluation of the cranial morphology and taxonomy of the Triassic dicynodont genus *Kannemeyeria*. Ph.D.

dissertation, University of the Witwatersrand, Johannesburg, South Africa, 214 pp.
Renaut, A. J., R. J. Damiani, A. M. Yates, and P. J. Hancox. 2003. A taxonomic note concerning a dicynodont (Synapsida: Anomodontia) from the Middle Triassic of East Africa. Palaeontologia africana 39:93–94.
Repelin, J. 1923. Sur un fragment de crâne de *Dicynodon*, recueilli par H. Counillon dans les environs de Luang-Prabang (Haut-Laos). Bulletin du Service Géologique de l'Indochine 12:1–7.
Rossignol, C., S. Bourquin, M. Poujol, E. Hallot, M.-P. Dabard, and T. Nalpas. 2016. The volcaniclastic series from the Luang Prabang Basin, Laos: a witness of a triassic magmatic arc? Journal of Asian Earth Sciences 120:159–183.
Rossignol, C., S. Bourquin, E. Hallot, M. Poujol, M.-P. Dabard, R. Martini, M. Villeneuve, J.-J. Cornée, A. Brayard, and F. Roger. 2018. The Indosinian orogeny: a perspective from sedimentary archives of north Vietnam. Journal of Asian Earth Sciences 158:352–380.
Sahney, S., and M. J. Benton. 2008. Recovery from the most profound mass extinction of all time. Proceedings of the Royal Society of London B: Biological Sciences 275:759–765.
Saurin, E. 1962. Luang Prabang Est. Carte géologique du Vietnam, Cambodge, Laos 1:500,000. Service géographique national, Dalat, Vietnam.
Scotese, C. R. 2014. Atlas of middle and late Permian and Triassic paleogeographic maps: Early Triassic. Paleomap Project, Department of Geology, University of Texas at Arlington. Available at www.scotese.com. Accessed March 9, 2017.
Shen, S.-Z., H. Zhang, G. R. Shi, W. Li, J. Xie, L. Mu, and J. Fan. 2013. Early Permian (Cisuralian) global brachiopod palaeobiogeography. Gondwana Research 24:104–124.
Smith, R. M. H., and J. Botha-Brink. 2014. Anatomy of a mass extinction: sedimentological and taphonomic evidence for drought-induced die-offs at the Permo-Triassic boundary in the main Karoo Basin, South Africa. Palaeogeography, Palaeoclimatology, Palaeoecology 396:99–118.
Steyer, J.-S. 2009. The geological and palaeontological exploration of Laos; following in the footsteps of J. B. H. Counillon and A. Pavie. Geological Society, London, Special Publications 315:25–32.
Steyer, J.-S. (ed.). 2012. Earth Before the Dinosaurs. Indiana University Press, Bloomington, Indiana, 182 pp.
Strong, E. E., and D. Lipscomb. 1999. Character coding and inapplicable data. Cladistics 15:363–371.
Sullivan, C., R. R. Reisz, and R. M. H. Smith. 2003. The Permian mammal-like herbivore *Diictodon*, the oldest known example of sexually dimorphic armament. Proceedings of the Royal Society of London B: Biological Sciences 270:173–178.
Sun, Y., M. M. Joachimski, P. B. Wignall, C. Yan, Y. Chen, H. Jiang, L. Wang, and X. Lai. 2012. Lethally hot temperatures during the Early Triassic greenhouse. Science 338:366–370.
Surkov, M. V., and M. J. Benton. 2004. The basicranium of dicynodonts (Synapsida) and its use in phylogenetic analysis. Palaeontology 47:619–638.
Thanh, N. X., M. T. Tu, T. Itaya, and S. Kwon. 2011. Chromian-spinel compositions from the Bo Xinh ultramafics, Northern Vietnam: implications on tectonic evolution of the Indochina block. Journal of Asian Earth Sciences 42:258–267.
Tollman, S. M., F. E. Grine, and B. D. Hahn. 1980. Ontogeny and sexual dimorphism in *Aulacephalodon* (Reptilia, Anomodontia). Annals of the South African Museum 8:159–186.
Torsvik, T. H., and J. R. M. Cocks (eds). 2017. Earth History and Palaeogeography. Cambridge University Press, Cambridge, U.K., 332 pp.
Ueno, K. 2003. The Permian fusulinoidean faunas of the Sibumasu and Baoshan blocks: their implications for the paleogeographic and paleoclimatologic reconstruction of the Cimmerian Continent. Palaeogeography, Palaeoclimatology, Palaeoecology 193:1–24.
Viglietti, P. A., R. M. H. Smith, and B. S. Rubidge. 2018. Changing palaeoenvironments and tetrapod populations in the *Daptocephalus* Assemblage Zone (Karoo Basin, South Africa) indicate early onset of the Permo-Triassic mass extinction. Journal of African Earth Sciences 138:102–111.
Vượng, N. V., B. T. Hansen, K. Wemmer, C. Lepvrier, V. Tích, and T. Trọng Thắng. 2013. U/Pb and Sm/Nd dating on ophiolitic rocks of the Song Ma suture zone (northern Vietnam): evidence for upper Paleozoic paleo-tethyan lithospheric remnants. Journal of Geodynamics 69:140–147.
Wall, W. P. 1983. The correlation between high limb-bone density and aquatic habits in recent mammals. Journal of Paleontology 57:197–207.
Wang, X.-D., and T. Sugiyama. 2002. Permian coral faunas of the eastern Cimmerian Continent and their biogeographical implications. Journal of Asian Earth Sciences 20:589–597.
Wang, X.-D., W. Lin, S.-Z. Shen, P. Chaodumrong, G. R. Shi, X. Wang, and Q. Wang. 2013. Early Permian rugose coral *Cyathaxonia* faunas from the Sibumasu Terrane (Southeast Asia) and the southern Sydney Basin (Southeast Australia): paleontology and paleobiogeography. Gondwana Research 24:185–191.
Ward, P. D., J. Botha, R. Buick, M. O. De Kock, D. H. Erwin, G. H. Garrison, J. L. Kirschvink, and R. M. H. Smith. 2005. Abrupt and gradual extinction among late Permian land vertebrates in the Karoo Basin, South Africa. Science 307:709–714.
Weislogel, A. L., S. A. Graham, E. Z. Chang, J. L. Wooden, G. E. Gehrels, and H. Yang. 2006. Detrital zircon provenance of the Late Triassic Songpan-Ganzi complex: sedimentary record of collision of the North and South China blocks. Geology 34:97.
Wilmsen, M., F. T. Fürsich, K. Seyed-Emami, M. R. Majidifard, and J. Taheri. 2009. The Cimmerian Orogeny in northern Iran: tectono-stratigraphic evidence from the foreland. Terra Nova 21:211–218.
Woodward, A. S. 1932. Dicynodontidae; pp. 257–260 in K. A. von Zittel (ed.), Textbook of Palaeontology. Macmillan, London.
Xiong, C., and Q. Wang. 2011. Permian–Triassic land-plant diversity in South China: was there a mass extinction at the Permian/Triassic boundary? Paleobiology 37:157–167.
Yu, J. X., J. Broutin, Z.-Q Chen, X. Shi, H. Li, D. Chu, and Q. Huang. 2015. Vegetation changeover across the Permian–Triassic Boundary in Southwest China: extinction, survival, recovery and palaeoclimate: a critical review. Earth-Science Reviews 149:203–224.
Yuan, P. L., and C. C. Young. 1934. On the Occurrence of *Lystrosaurus* in Sinkiang. Bulletin of the Geological Society of China 12:575–580.
Zanchi, A., S. Zanchetta, F. Berra, M. Mattei, E. Garzanti, S. Molyneux, A. Nawab, and J. Sabouri. 2009. The Eo-Cimmerian (Late? Triassic) orogeny in North Iran. Geological Society, Special Publications 312:31–55.
Zanchi, A., N. Malaspina, S. Zanchetta, F. Berra, L. Benciolini, M. Bergomi, A. Cavallo, H. R. Javadi, and M. Kouhpeyma. 2015. The Cimmerian accretionary wedge of Anarak, Central Iran. Journal of Asian Earth Sciences 102:45–72.
Zhang, R. Y., C.-H. Lo, X.-H. Li, S.-L. Chung, T. T. Anh, and T. Van Tri. 2014. U-Pb dating and tectonic implication of ophiolite and metabasite from the Song Ma suture zone, northern Vietnam. American Journal of Science 314:649–678.
Zhang, R. Y., C.-H. Lo, S.-L Chung, M. Grove, S. Omori, Y. Iizuka, J. G. Liou, and T. Van Tri. 2013. Origin and Tectonic Implication of Ophiolite and Eclogite in the Song Ma Suture Zone between the South China and Indochina Blocks. Journal of Metamorphic Geology 31:49–62.

Submitted June 1, 2017; revisions received January 24, 2019;
accepted January 27, 2019.
Handling editor: Adam Huttenlocker.

APPENDIX 1. Continuous and discrete codings in the Laotian dicynodonts used in the phylogenetic analysis; en dash (–) indicates missing values. The character-taxon matrix is available as Supplemental Data 1.

Continuous codings (characters 1 to 23)

LPB 1993-3 (holotype of *Counillonia superoculis*)
0.2975.068 – – 0.276 0.134–0.131 8.333 0.140–9.616 0.876 – – – – – – – – – –

LPB 1993-2 (holotype of *Repelinosaurus robustus*)
0.200–0.295–0.408 0.281 – – – – – 14.698 0.829 – – – – – – – – – – – –

LPB 1995-9 (attributed to *Repelinosaurus robustus*)
0.205–0.254 – – 0.316–0.124–0.101 – – 0.935 – – – – – – – – – – – –

Discrete codings (characters 24 to 194)

LPB 1993-3 (holotype of *Counillonia superoculis*)
120022121010000???00022??1101000??2????????0???
????0?0100211002011?0??11111210301??10121010211
0?022?120?????01011??????????????????????????????
????????????????????????????

LPB 1993-2 (holotype of *Repelinosaurus robustus*)
1200221210?10000?100?22??1101001?100?10??100201
11000001002110020l??0??????1????????1012??10?11
??022?120?????01??1??????????????????????????????
????????????????????????????

LPB 1995-9 (attributed to *Repelinosaurus robustus*)
12002012101?000??100022??0101001?10001001?0010?11
00000100211?02??1?0??1111121030???1012101?2110?
02???20????????1??????????????????????????????
????????????????????????????

CHAPTER III

TAXONOMIC REVISION OF THE MOROCCAN DICYNODONTS WITH DESCRIPTION OF NEW DICYNODONT POSTCRANIAL REMAINS FROM THE ARGANA BASIN (MOROCCO)

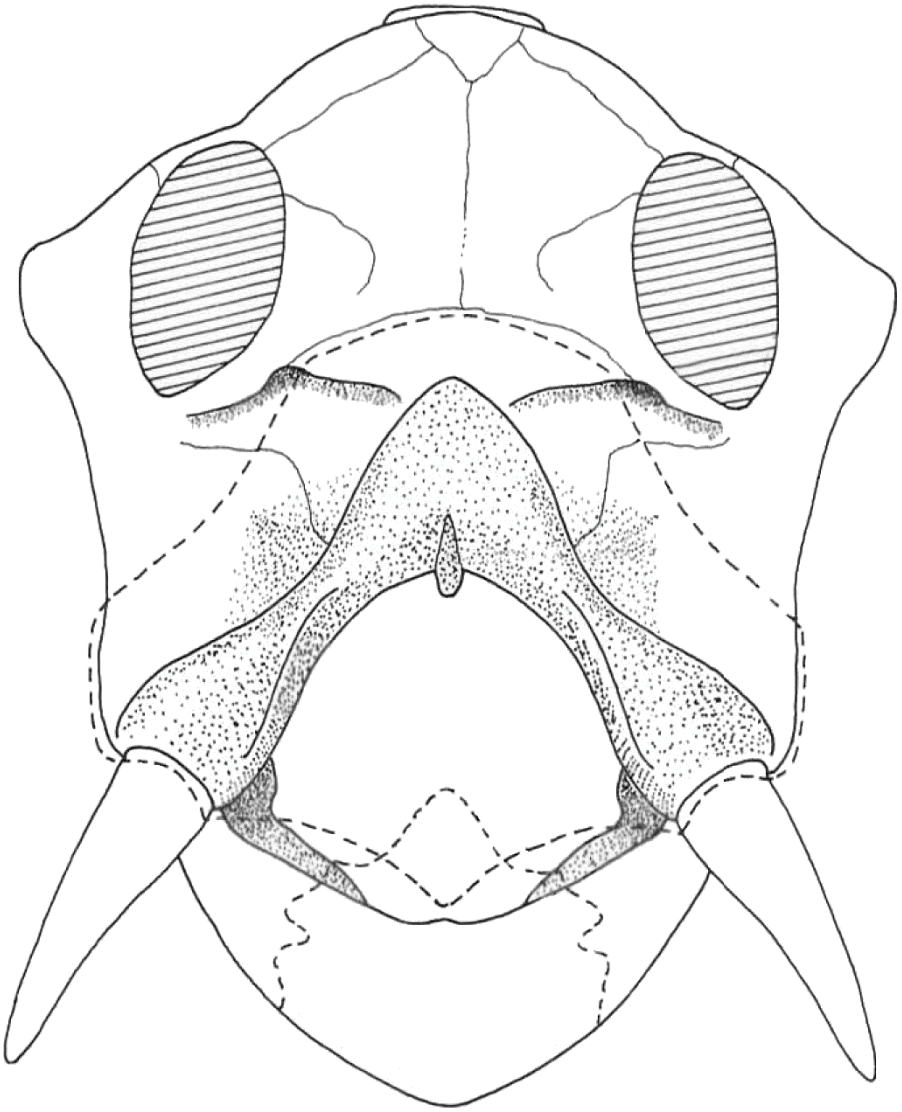

Reconstructed skull of *Moghreberia nmachouensis* in anterior view by Dutuit (1988)

Uncertain taxonomy of Moroccan dicynodonts

The first mention of therapsids in the Argana Basin dated back to 1960 by Arambourg (*in* Arambourg and Duffaud, 1960). He reported on the presence of a large canine (probably dicynodont remain), that he recognised as belonging to a therapsid. Later, Dutuit (1965) first mentioned the presence of dicynodonts in the Argana Basin (Morocco). Dutuit (1976) briefly reported on the discoveries of the dicynodont remains in the localities XI and XII. In the collection catalogue edited by J.M. Dutuit, he also notified the presence of a unique dicynodont bone in the locality XIII. The localities XI, XII, and XIII are located at the base of the Irohalene Member (lithostratigraphic unit t5) in the Argana Basin or the lithostratigraphic level t5 according Tixeront's nomenclature (Fig. III.1).

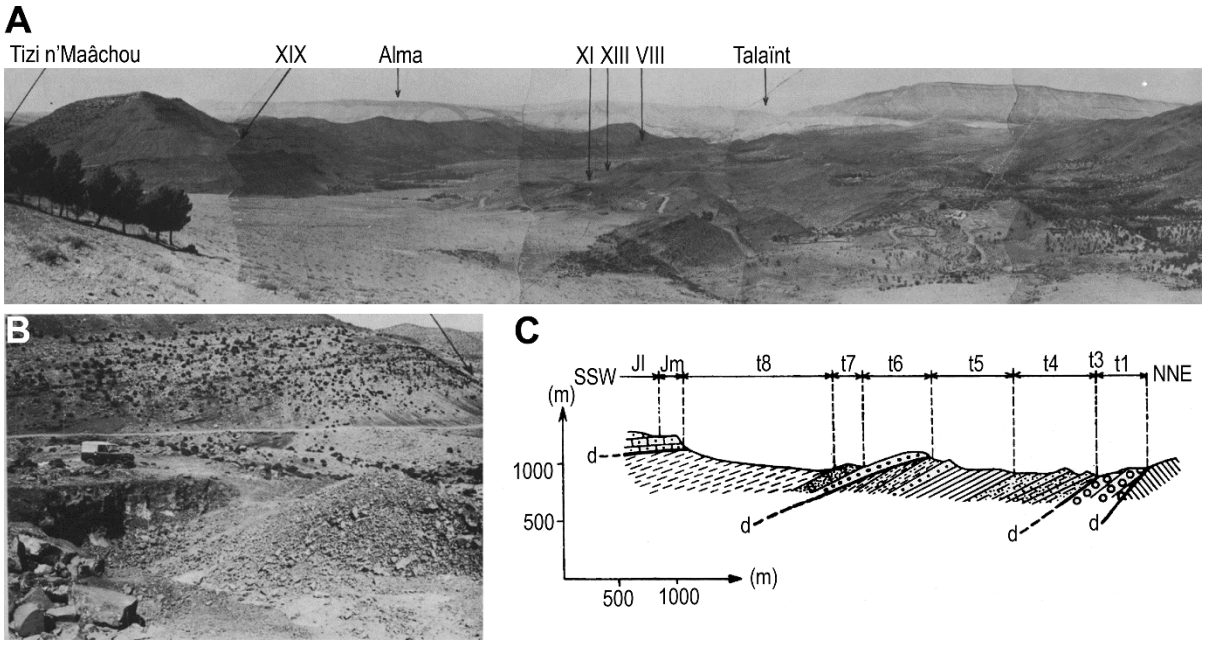

Figure III.1. Illustrations of the Irohalene Member t5 (according the nomenclature of M. Tixeront) and stratigraphic log of the Argana Basin modified from Dutuit (1976). A, panorama of the Irohalen valley oriented ESE-WNW; B, picture of the locality XI; and C, stratigraphic log of the North of the Argana Basin provided by M. Tixeront. Abbreviations: d, unconformity; Jl, Late Jurassic; Jm, Middle Jurassic.

The major part of the dicynodont remains have been excavated from the locality XI comprising three levels: (1) lower level XIa (= "layer 1" of the locality XI) including a big dicynodont form only known by postcranial remains, (2) middle level XIb (= "layer 2" of the locality XI) with remains describing an almost complete skeleton of a dicynodont genus, associated with rests of the pseudosuchian *Arganasuchus dutuiti*, and (3) upper level XIc (= "layer 1" of the locality XI or "XIp" for "fishes" level) including actinopterygians, dipnoi, and the temnospondyl *Almasaurus habbazi* and

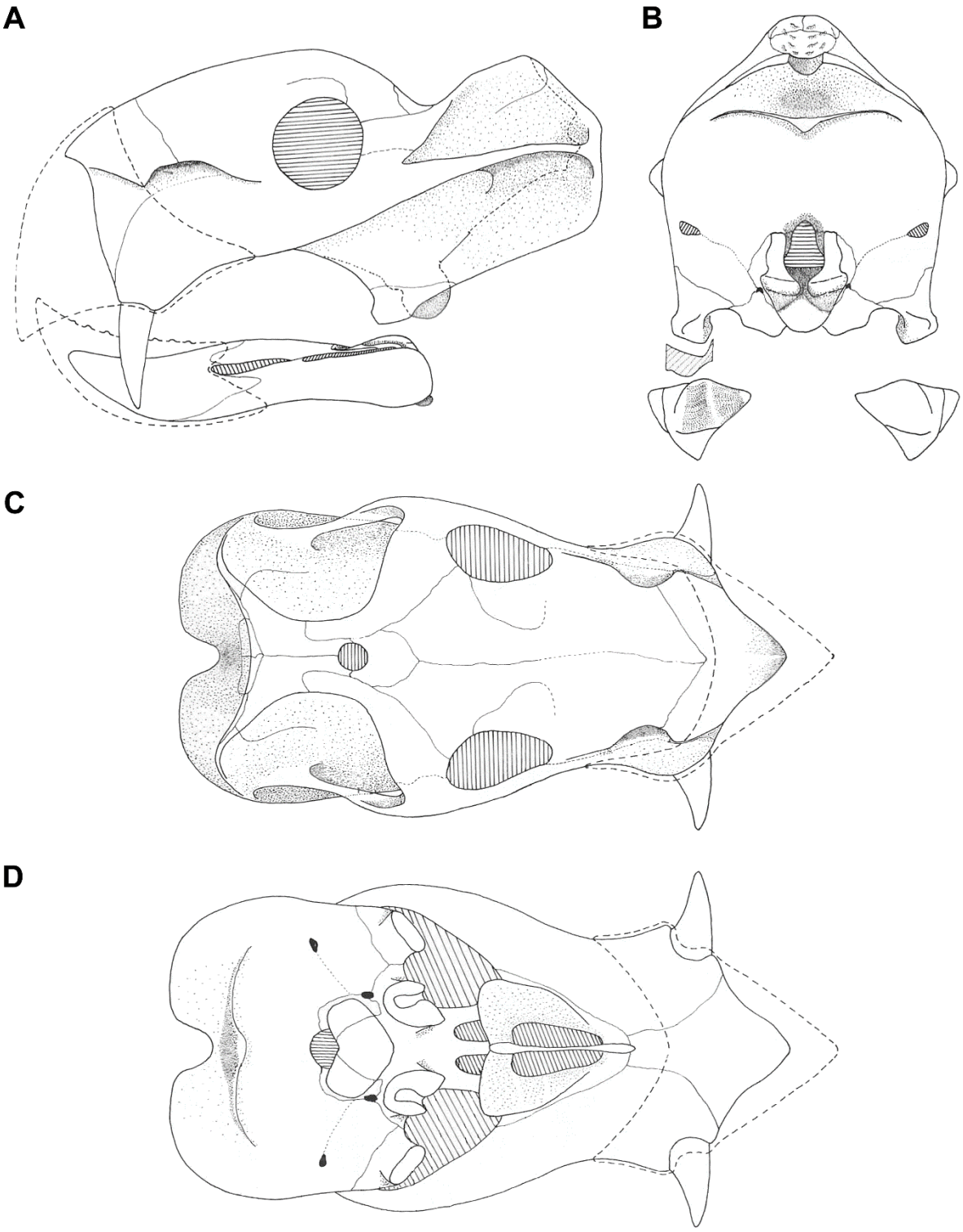

Figure III.2. Reconstructed skull of *Moghreberia nmachouensis* by Dutuit (1988) in left lateral (A), occipital (B), dorsal (C), and ventral (D) view

Dutuitosaurus ouazzoui (Dutuit, 1976, 1980; Khaldoune et al., 2017). While the locality XII has been poorly studied, Dutuit (1976) mentioned the discovery of a partial dicynodont skull with associated vertebrae and potential limb bone. The locality XIII of

the Argana Basin is noticeable by the abundant and well-preserved rests of *Dutuitosaurus ouazzoui*.

Moghreberia nmachouensis, recovered in the locality XIb, was first named by Dutuit (1980) on the basis of the two skulls MNHN.F.ALM 280 and 281 that he briefly described. Dutuit (1980) highlighted similarities between the Moroccan genus and the kannemeyerids (sensu Huene, 1948) *Placerias*, *Rabidosaurus*, and *Parakannemeyeria*. However, he did not establish the diagnosis of *Moghreberia* that distinguishes the Moroccan genus from others. A more detailed description was later provided by Dutuit (1988) (Fig. III.2), based on the two previous skulls and additional partial cranial remains discovered in the same locality. Dutuit (1988) attributed the Moroccan genus to Kannemeyeridae (sensu Huene, 1948). He considered *Moghreberia* more closely related to the North American genus *Placerias* than to other dicynodonts (Dutuit, 1988). However, the taxonomic validity of *Moghreberia* was questioned by some authors (e.g., Cox, 1991; Hunt and Lucas, 1991; Lucas and Wild, 1995; Lucas, 2018). Kammerer et al. (2011) first introduced the Moroccan genus in a phylogenetic analysis and placed it as a sister-taxa of *Placerias*, as the following phylogenetic studies (e.g., Kammerer et al., 2013; Angielczyk and Kammerer, 2017; Kammerer et al., 2019).

Two other Moroccan species were also added by Dutuit (1989a, 1989b) within the new genus *Azarifeneria*. The first species, *A. barrati*, was defined based on a partial dicynodont skull (MNHN.F.AZA 366.1-2-3) excavated from the locality XII (Dutuit, 1989a). A partial mandible (MNHN.F.ALM 167) from the locality XIb allowed Dutuit (1989b) to define the second species *A. robustus*. However, the taxonomic validity of these two species have been questioned by succeeding studies (e.g., Cox, 1991; Lucas and Wild, 1995; Fröbisch, 2009; Kammerer et al., 2013) due to the lack of relevant diagnostic features that would distinguish *Azarifeneria* from *Moghreberia* (e.g., Lucas and Wild, 1995; Lucas, 2018) or other dicynodonts such as *Ischigualastia* (Cox, 1991). No more study has been done done since Dutuit's work (1989a, 1989b) and *Azarifeneria* is still considered nomen dubium.

Dutuit (1980, 1988, 1989a, 1989b) focused his studies on cranial remains, but abundant postcranial dicynodont specimens have been discovered in the same localities XI, XII, and XIII, according to the collection catalogue edited by J.M. Dutuit. As highlighted by Kammerer et al. (2011), the potential importance of missing data and the lacks of post-cranial data shadow the phylogenetic position of *Moghreberia*. The

study of the post-cranial material would increase our knowledge of *Moghreberia nmachouensis* known only by its cranial remains. It would lead to better define its phylogenetic relationships and characterise it by comparison to the other dicynodonts and particularly to *Placerias*. Moreover, it would provide information on the presence of one or more distinct morphotypes morphotypes and consequently whether one or more distinct dicynodont taxa are present in the Argana Basin. Finally, the abundance of the rests would allow us to discuss on the potential morphological variation in the postcranial skeleton in dicynodonts.

The study of the postcranial dicynodont remains from the Argana Basin and its implications have been developed in PAPER II. All the cranial and postcranial material is currently preserved in the collections of the Muséum national d'Histoire naturelle in Paris (France). Due to the abundance of the postcranial material, the description focused on the most preserved bones, while the study covers a large part of the available material comprising around a hundred specimens (7 connected or isolated vertebrae, 10 ribs, 22 scapulae, 8 interclavicles, 1 sternum, 13 humeri, 5 radii, 9 ulnae, 1 complete pelvic girdle, 1 ilium, 3 ischia, 1 pubis, 9 femora, 3 tibiae, and 1 fibula). Even focused on the post-cranium, the cranial material (including holotypes), has been briefly re-evaluated in order to discuss the validity of the Moroccan genera *Moghreberia* and *Azarifeneria*, and check the coding of *Moghreberia* in the previous phylogenetic matrices. The morphological variation noticed in the cranial and postcranial material has been discussed based on first hand examination of dicynodont specimens during my visits of collections in the American Museum of Natural History in New York (New York City, U.S.A.; financial support from CR2P and ISTEP), the Evolutionary Studies Institute in Johannesburg (South Africa; financial support from CR2P), the Institute of Vertebrate Paleontology and Paleoanthropology in Beijing (China; financial supports from CR2P and the Société des Amis du Muséum), the Museum of Comparative Zoology in Cambridge (Massachusetts, U.S.A.; financial support from CR2P and ISTEP), and the Natural History Museum in London (United Kingdom; financial support from SYNTHESYS). I also relied on the literature and pictures provided by the colleagues J. Liu (Institute of Vertebrate Paleontology and Paleoanthropology, Beijing, China) and C.F. Kammerer (North Carolina Museum of Natural Sciences, Raleigh, North Carolina, U.S.A.), In PAPER II, I wrote the wole of the article, produced all figures except the pictures took by Lilian Cazes and Philippe Loubry (CR2P, MNHN, France), and performed the phylogenetic analyses.

First description of dicynodont postcranial material from the Argana Basin (Late Triassic, Morocco) and taxonomic revision of the two Moroccan genera *Moghreberia* and *Azarifeneria*

Chloé Olivier [1*] and Nour-Eddine Jalil [1,2]

[1]Centre de Recherche en Paléontologie (CR2P, UMR 7207), Sorbonne Université, MNHN, CNRS, Muséum national d'Histoire naturelle, Département Origines et Évolution, case postale 38, 57 rue Cuvier, F-75231 Paris cedex 05 (France)
chloe.olivier@upmc.fr; nour-eddine.jalil@mnhn.fr

[2]Department of Geology, Faculté des Sciences Semlalia, Université Cadi Ayyad, Boulevard Prince My Abdellah, 40000 Marrakech, Maroc

*Corresponding author

PAPER II

Considering submission to *Geodiversitas*

European Journal of Taxonomy

First description of dicynodontian postcranial material from the Argana Basin (Late Triassic, Morocco) and taxonomic revision of the two Moroccan genera *Moghreberia* and *Azarifeneria*

Chloé Olivier [1*] and Nour-Eddine Jalil [1,2]

[1]Centre de Recherche en Paléontologie (CR2P, UMR 7207), Sorbonne Université, MNHN, CNRS, Muséum national d'Histoire naturelle, Département Origines et Évolution, case postale 38, 57 rue Cuvier, F-75231 Paris cedex 05 (France)
chloe.olivier@upmc.fr; nour-eddine.jalil@mnhn.fr

[2]Department of Geology, Faculté des Sciences Semlalia, Université Cadi Ayyad, Boulevard Prince My Abdellah, 40000 Marrakech, Maroc

*Corresponding author

Abstract

Three dicynodont species have been described in the Triassic of the Argana Basin (Carnian; base of the Irohalen Member, Morocco): *Moghreberia nmachouensis*, *Azarifeneria b*arrati, and *A. robustus*. While an abundant postcranial material have been also collected in the same locality, only the cranial remains were studied and used to diagnose the three species. The Moroccan species are then poorly known and have always been questioned. The revised study of the cranial specimens attributed to *Azarifeneria* did not emphasized significant differences distinguishing *Azarifeneria barrati* and *A. robustus* from other Triassic dicynodonts, especially *Moghreberia nmachouensis*. The present study provided the first description of the rich dicynodont postcranial material from the Argana Basin. An almost complete skeleton attribuable to *M. nmachouensis* enhanced our understanding of this species and completed the gap in the phylogenetic matrix. Unlike previous studies that allied *Moghreberia* and the North American *Placerias*, our phylogenetic analysis concluded that the Moroccan species is more closely related to the Polish *Lisowicia*. Moreover, significant morphological variations have been noticed in the postcranial material and discussed. Despite a lack of diagnostic characters, at least a second more massive morphotype can be likely interpreted in the postcranial material.

Introduction

Dicynodontia represent an emblematic taxa of the Permian-Triassic (P-Tr) period to have survived the most important biological crisis. Considering the recent phylogenetic analyses and their stratigraphic range implying ghost lineages, multiple dicynodont clades would have crossed the P-Tr boundary: Lystrosauridae, Emydopoidae, Dicynodontidae, and Kannemeyeriiformes (e.g., Angielczyk 2001; Fröbisch 2007; Fröbisch *et al.* 2010; Kammerer *et al.* 2011; Olivier *et al.* 2019). They highly diversified during the Middle Triassic whit the occurences of around twenty new genera (Kammerer et al., 2013), to finally become extinct at the end of Triassic. During this period, they were worldwide with a cosmopolitain distribution: *Dinodontosaurus* (Chañares Formation [Fm] in Argentina, and Santa Maria Fm in Brazil), *Stahleckeria* (Santa Maria Fm in Brazil), *Eubrachiosaurus* (Popo Agie Fm in USA), *Ischigualastia* (Ischigualasta Fm in Argentina), *Jachaleria* (Chañares Fm and Los Colorados Fm in Argentina, and Caturrita Fm in Brazil), *Moghreberia* (Argana Basin in Morocco), *Placerias* (Blue Mesa Member of Petrified Forrest Fm, Bluewater Creek Fm, and Pekin Fm in USA), *Vinceria* (Puesto Viejo Fm and Cerro de Las Cabras Fm in Argentina), and the two youngest forms *Lisowicia* (Lipie Śląskie clay-pit at Lisowice village in Poland) and *Pentasaurus* (Elliot Fm in South Africa) (e.g., Fröbisch, 2009; Kammerer, 2018; Sulej and Niedźwiedzki, 2019).

The Moroccan dicynodont *Moghreberia nmachouensis* has been originally and briefly described by Dutuit (1980) based on two poorly-preserved skulls, collected in the locality XIb (Dutuit's nomenclature) of the Argana Basin and dated to the Late Triassic. Later, a more detailed description of *Moghreberia* was published (Dutuit, 1988), based on the two above-cited skulls and isolated but well-preserved cranial remains. Abundant postcranial remains have also been excavated but have never been described. Dutuit (1988) highlighted anatomical similarities between the cranial remains of *Moghreberia* and the skulls of *Kannemeyeria* and *Stahleckeria*, and especially with the North American *Placerias*. He then attributed the Moroccan dicynodont to Kannemeyeridae (Huene, 1948). *Moghreberia* has been distinguished from other dicynodonts by (1) a relative low, dorsoventrally and laterally, expanded occipital surface, (2) a lateral mandibular branches mainly horizontal, (3) a dorsal margin of the erupted portion of the canine tusk anterior to the nasal cavity and, (4) a very pointed triangular anterior tip of snout (Dutuit, 1988). The same year, King (1988)

attributed the Moroccan form to Kannemeyeriini (Lehman, 1961) that included the genera *Kannemeyeria*, *Shaanbeikannemeyeria*, *Dolichuranus*, *Wadiasaurus*, and *Rabidosaurus*. Dutuit (1988) has already alluded to a synonymy between *Moghreberia* and the North American *Placerias*, while he accepted the validity of the Moroccan genus. Later, several authors considered *Moghreberia* as a junior synonym of *Placerias* (e.g., Cox, 1991; Hunt and Lucas, 1991; Lucas and Wild, 1995; Lucas, 2018), delaying the inclusion of the Moroccan form up to the phylogenetic study of Kammerer et al. (2011). Kammerer et al. (2011), followed by later analyses (e.g., Kammerer et al., 2013, 2019; Angielczyk and Kammerer, 2017), placed *Moghreberia* as sister-group of *Placerias.* They definitely distinguished these two genera by several cranial morphological characters. Kammerer et al. (2011) also highlighted the potential impact of missing data on the phylogenetic position of the Moroccan form and the need to study its postcranial remains.

Two other endemic species were discovered in the Argana Basin: *Azarifeneria barrati* and *A*. *robustus* (Dutuit, 1989a, 1989b). *A*. *barrati* has been described on the basis of two cranial specimens from the same individual (the parietosquamosal structure MNHN.F.AZA 366.1 and the posterior part of the basicranium MNHN.F.AZA 366.2), found in the locality XII (Dutuit's nomenclature). Only a fragmentary mandible (MNHN.F.ALM 167) from the locality XIb (Dutuit's nomenclature) is known for *A*. *robustus*. However, considerable uncertainties remain about the validity of the second Moroccan genus, particularly because of an obvious lack of diagnostic character in the available material (e.g., Cox, 1991; Lucas and Wild, 1995; Fröbisch, 2009; Kammerer et al., 2013). Indeed, the cranial remains attributed to *Azarifeneria,* (Dutuit, 1989a, 1989b) mainly highlighted a big size, high robustness and similarities with the Brazilian *Stahleckeria*. *Azarifeneria* was sometimes considered synonym of *Moghreberia* (e.g., Lucas and Wild, 1995; Lucas, 2018), *Ischigualastia* (Cox, 1991), or a *nomen dubium* (e.g., Fröbisch, 2009).

The Moroccan dicynodonts represent the only North African therapsids. Our main purpose was to describe the rich dicynodont postcranial remains collected in the Argana Basin. On one hand, we completed our understanding about the anatomy of *Moghreberia nmahcouensis* and checked its phylogenetic relationships and taxonomic validity. On the other hand, due to the obvious lack of diagnostic character in

Azarifeneria, we revised the description of its cranial remains and discussed about its validity.

Institutional Abbreviations—**AMNH**, American Museum of Natural History, New York City, New York, U.S.A.; **BP**, Evolutionary Studies Institute (formerly the Bernard Price Institute for Palaeontological Research and the Institute for Human Evolution), Johannesburg, South Africa; **BSPG**, Bayerische Staatssammlung für Paläontologie und Geologie, Munich, Germany; **GSN**, Geological Survey of Namibia, Namibia; **GPIT**, Institut und Museum für Geologie und Paläontologie, Tübingen, Germany; **IVPP**, Institute of Vertebrate Paleontology and Paleoanthropology, Beijing, China; **MCZ**, Museum of Comparative Zoology, Harvard University, Cambridge, Massachusetts, U.S.A.; **MNHN**, Muséum national d'Histoire naturelle, Paris, France; **NHMUK**, Natural History Museum, London, United Kingdom; **NHMW**, Naturhistorisches Museum Wien, Vienna, Austria ; **UCMP**, University of California Museum of Paleontology, Berkeley, California, U.S.A.; **USNM**, National Museum of Natural History, Washington, District of Columbia, U.S.A.; **ZPAL**, Institute of Paleobiology, Polish Academy of Sciences, Warsaw, Poland.

Anatomical Abbreviations—**A**, angular; **Acetf**, actebular facet; **Acr**, acromion process; **Aip**, anterior process of the ilium; **Bo**, basioccipital; **Cnc**, cnemial crest; **Corfor**, coracoid foramen; **Csp**, caudal neural spine; **Ct**, centrum; **D**, dentary; **Delt**, insertion of the *deltoideus* muscle; **Dpc**, deltopectoral crest; **DRadf**, distal radial facet; **Dt**, dentary table; **Ect**, ectepicondyle; **Ent**, entepicondyle; **Entefor**, entepicondylar foramen; **Eo**, exoccipital; **Femf**, femoral facet; **Fh**, hemoral head; **Fibf**, fibular facet; **Fr**, frontal; **Ft**, insertion site of the *flexores tibiales*; **Glef**, glenoid facet; **Hd**, humeral head; **Hrb**, head of rib; **Il**, ilium; **IntF**, intercondylar fossa; **Ip**, interparietal; **Isch**, ischium; **Itroch**, insertion site of *ischio-trochantericus* muscle; **LatdorDFK**, insertion for the *latissimus dorsi* muscle according to King (1981) and Defauw (1986); **LatdorR**, insertion for the *latissimus dorsi* muscle according to Romer (1976); **Ldr**, lateral dentary ridge; **Lra**, reflected angular lamina; **Mdr**, median dentary ridge; **Mf**, Meckel fossa; **Mfor**, magnum foramen; **Nc**, neural canal; **Obtfor**, obturator foramen; **OleF**, olecranon fossa; **Olep**, olecranon process; **Opt**, opisthotic; **Pa**, parietal; **Par**, parapophyse; **Pbs**, parabasisphenoid; **Pds**, posterior dentary sulcus; **Pfor**, pineal foramen; **Pip**, posterior process of the ilium; **Po**, postorbital; **Pof**, postorbital facet; **PopF**, popliteal fossa; **Poz**, postzygapophyse; **Pp**, preparietal; **PPt**, posterior pterygoid

branch; **PRadf**, proximal radial facet; **Prsf**, prespinous fossa; **Prz**, prezygapophyse; **Pubt**, pubic tubercle; **Q**, quadrate, **Radc**, radial condyle; **Rpr**, posterior ridge on the rib; **S**, splenial; **Sct**, sacral centrum; **Serasup**, insertion of the *serratus anterior superficialis* muscle; **Sf**, sacral facet; **Sigf**, sigmoidal facet; **So**, supraoccipital; **Sp**, neural spine; **Sq**, squamosal; **Srb**, fused sacral rib; **SSp**, sacral neural spine; **Subco**, insertion for the *subcoracoscapularis* muscle; **Sup**, supinator process; **Supco**, insertion of the *supracoracoideus* muscle; **T**, tusk; **Tcr**, trochanteric crest; **Tidf**, tibial facet; **Tm**, minor trochanter; **Tri**, insertion of the *triceps* muscle; **Trif**, triangular flattened facet; **Troch**, ulnar trochlea; **Trp**, transverse process; **Tth**, third trochanter; **Tub**, parabasisphenoid-basioccipital tuber; **Vo**, vomer.

Material and methods

Geological setting and palaeoenvironment

The Argana Basin is located in the western part of the High Atlas of Morocco between Im'N'Tanout village in the North and Ameskroud in the South (Fig. 1). The Basin comprises three formations subdivided in eight lithostratigraphic units (T1 to T8): (1) the lower Ikakern Fm (Members T1 and T2), (2) the middle Timezgadiouine Fm (Members T3 to T5), and (3) the upper Bigoudine Fm (Members T6 to T8) (e.g., Tixeront, 1973; Jalil, 1999). The cranial and postcranial dicynodont remains have been excavated from the localities XI, XII, and XIII (Dutuit's nomenclature), located at the base of the Irohalene Member T5 in the Timezgadiouine Fm (Argana Basin, Morocco) (Fig. 1; Tixeront, 1973; Dutuit, 1988, 1989a, 1989b).

In addition to the dicynodonts, the lower part of the Irohalene Member has yielded the actinopterygians (*Dipteronotus gibbosus*, *Mauritanichthys rugosus*, cf. *Ischnolepis*, cf. *Procheirichthys*, cf. *Atopocephala*), the dipnoi *Arganodus*, a probable latimerioid, the amphibian temnospondyls *Almasaurus* and *Dutuitosaurus*, the phytosaur *Arganarhinus*, the aetosaur *Longosuchus*, the archosauromorph *Azendohsaurus*, and the silesaurid dinosauromorph *Diodorus* (e.g., Gauffre, 1993; Lucas, 1998; Jalil, 1999; Kammerer et al., 2012; Khaldoune et al., 2017). The top of the member present a more aquatic faunal assemblage with the amphibians *Metoposaurus* and *Arganasaurus*, and the phytosaur *Angistorhinus* (e.g., Dutuit, 1976; Jalil, 1999; Sulej, 2002; Khaldoune et al., 2017). Lucas (2018) correlated the faunal assemblage of the Irohalene Member (T5) (phytosaurs '*Parasuchus*' (=*Arganarhinus*; Kammerer et al., 2016b) and *Angistorhinus*, the aetosaur *Longosuchus*, and the

dicynodont '*Placerias*' (considering synonym of *Moghreberia* in his study)) to the Otischalkian land-vertebrate faunachron, supposed to be Carnian in age (e.g., Lucas, 1998, 2018; Jalil, 1999). A similar faunal assemblage has also been described in North America (Popo Agie Fm, Colorado City Fm, Salitral Fm, and Newark Supergroup), Germany (Stuttgart Fm), and India (Maleri Fm) (e.g., Lucas, 1998, 2018). Nevertheless, Kammerer et al. (2012) recommended to consider these biostratigraphic interpretations with caution. Indeed, on one hand, the index taxa supporting the Otischalkian land-vertebrate faunachron (*Paleorhinus* and *Metoposaurus*), as traditionally defined, have been shown to represent non-monophyletic groups; on the other hand, *Azendohsaurus* recovered in the Irohalene Member is also known in the late Middle or early Late Triassic Makay Fm (Isalo Group, Madagascar) (e.g., Flynn et al., 1999, 2000; Kammerer et al., 2010). Moreover, tetrapod footprints discovered in the Irohalene Member have been attributed by Lagnaoui et al. (2012, 2016) to the archosaur ichnogenera *Apatopus* (phytosaur), *Atreipus-Grallator* (dinosauromorph), *Brachychirotherium* (crocodylian-stem archosaur), *Eubrontes* (theropod), *Parachirotherium* (? dinosauriform), and *Synaptichnium*, and the non-archosaur ichnogenus *Rhynchosauroides* (lepidosauromorph or archosauromorph). The presence of *Apatopus*, *Eubrontes*, *Atreipus-Grallator*, and *Brachychirotherium* is indicative of Late Triassic *Brachychirotherium* biochron (Klein and Lucas, 2010). However, *Parachirotherium* has only been recorded in the Middle Triassic Benk Fm (Germany). Its presence in the Irohalene Member would then suppose either the youngest occurrence of this ichnotaxa (Lagnaoui et al., 2012), or support an earlier age of the member as in the case of *Azendohsaurus*. A stratigraphic extention of the Irohalene Member T5 in the late Middle Triassic does not contradict the previous studies conluding to a Middle Triassic age of the underlying Aglegal Member T4 (e.g., Medina et al., 2001; Jalil et al., 2009). However, the occurrence of a Late Triassic rhynchosaur in the basalmost Irohalene Member would indicate a later age for the member (N.-E. Jalil, pers. comm., 2019). The magnetostratigraphy and radioisotopic analyses of Irmis et al. (2010) suggest a longer Norian that would fully or partly include the Otischalkian land-vertebrate faunachron. However, their conclusions are not supported by the palynomorphic analyses of Tourani et al. (2000) that interpreted a Late Carnian age for the Tadart Ouadou T6 and Sidi Mansour T7 Members, and an early Norian age for the Hasseine Member T8. Also, the studies of Argana Basalt, a

volcanic sequence associated with the Central Atlantic Magmatic Province (CAMP) underlying the Bigoudine Fm, suggested a Norian even early Jurassic age for the upperpart of the formation (e.g., Olsen et al., 2000; Marzoli et al., 2004; Whiteside et al., 2007; Deenen et al., 2011). A stratigraphic extention of the Irohalene Member T5 to the Norian appears less likely in regards to the palynology and geochronology. Under the light of the previous results, a Late Triassic age for the Irohalene Member appears most likely.

Most of the dicynodont remains have been discovered in the mid-level of the locality XI (locality XIb according to Dutuit, 1976). The examination of the external surface of the dicynodont bones (eroded, cracked, and peeling) related to the taphonomic works of Behrensmeyer (1975), suggested to Dutuit and Heyler (1983) a warm and relatively dry climate as a depositional environment of the Irohalene Member. These latter is interpreted as an alluvial plain sandstones and mudstones with a well-developed cyclical lacustrine sequence in the base of the member (e.g., Olsen et al., 2000). Furthermore, Olsen et al. (2000) assumed a relatively humid environment in the Irohalene Member with shallow lacustrine water at the base and even fluvial at the top. The faunal assemblage composed of aquatic, semi-aquatic, and terrestrial forms would support a well-irrigated soil with lakes of fresh even brackish water (e.g., Dutuit and Heyler, 1983).

New Moroccan dicynodont postcranial material

As mentioned above, an abundant dicynodont postcranial material has been discovered in the localities XIa, XIb, and XIII of the Argana Basin. Almost every skeletal element is represented within this material, only the atlas-axis complex, cleithrum, clavicle, and autapodia have not been collected. The present study focused on the well-preserved specimens (see Table 1S for more details about their preservation and locality).

Vertebrae—Most of the specimens are discovered in the locality XIb. The locality of MNHN.F.ALM 198, 274 and two unnumbered connected vertebrae (named ‘Vunknb 1 and 2’ from front to back) are unknown. Three specimens (MNHN.F.ALM 198, 288, and Vunknb 1 and 2) are proably the last cervical or first dorsal vertebrae. MNHN.F.ALM 120, 159, and 265 are probably the middorsal vertebrae. MNHN.F.ALM 120 consists of four vertebrae preserved in the same block and labelled ‘MNHN.F.ALM 120-1, -2, -3, and -4’ from front to back. MNHN.F.ALM 159 are two articulated

vertebrae named ‘MNHN.F.ALM 159-1 and -2’ (from front to back). MNHN.F.ALM 274 corresponds to the two pelves of a same individual, connected to sacral and first caudal vertebrae, with two associated but disconnected posterior dorsal vertebrae (named ‘MNHN.F.ALM 274-1 and -2’). MNHN.F.ALM 136 composed of five vertebrae (labelled ‘MNHN.F.ALM 136-1, -2, -3, -4, and -5 from front to back) presents peculiar features of sacral vertebrae.

Ribs—Seven ribs MNHN.F.ALM 86, 90, 91, 95, 96, 97, and 296, and three proximal costal heads (MNHN.F.ALM 163, 272, and an unnumbered specimen) were stored in collection. All have been excavated from the locality XIb, but the unknown locality of the unnumbered costal head.

Scapulae, coracoids, and precoracoids—Twenty-one isolated dicynodont scapulae (MNHN.F.ALM 17, 19, 29, 30, 83, 98, 108, 113, 114, 132, 153, 155, 259, 263, 283, 292, 299, and three unnumbered scapulae) have been discovered in the Argana Basin. Most of scapulae have been excavated from the locality XIb, except MNHN.F.ALM 17, 113, 114, and 299 from the locality XIa. Two unnumbered scapulae (labelled ‘Sunknb 1 and 2’) are also found in the locality XI, but the level is unknown. The locality of the third unnumbered scapula is unknown (labelled ‘Sunknb 3’). MNHN.F.AZA 365 is the only dicynodont specimen from the locality XIII. Two scapulocoracoid complexes (MNHN.F.ALM 92 and 298) were also found in collection and come from the locality XIb.

Interclavicles—Eight interclavicles are known (MNHN.F.ALM 93, 94, 158, 260, 278, 295, and two unnumbered specimens), mainly in the locality XIb. The level of the locality is unknown for MNHN.F.ALM 295 and the two unnumbered interclavicles (labelled ‘Intunknb 1 and 2’).

Sternum—MNHN.F.ALM 134 is the only sternum of the collection. It comes from the locality XIb.

Humeri—Eight complete (MNHN.F.ALM 24, 25, 101, 102, 105, 115, 275, and 297) and five fragmentary (MNHN.F.ALM 121, 133, 147, and two unnumbered specimens labelled ‘Humunknb 1 and 2’) dicynodont humeri are found in collection. Most of them are found in the locality XIb of the basin. MNHN.F.ALM 115 and 275 have been located in the lower level of XI (locality XIa). The level in the locality XI is unknown for

Humunknb 1. Humunknb 2 is supposed to be collected in the localities X, XI or XVI, according to the collection catalogue edited by J.M. Dutuit.

Radii—Three nearly complete radii (MNHN.F.ALM 84, 131, 287, and 289) are found in collection. They have been discovered in the locality XIb. An unnumbered specimen contains the distal regions of a radius and ulna. Its locality is unknown.

Ulnae—Eight ulnae entirely or partly preserved (MNHN.F.ALM 18, 27, 28, 35, 87, 126, 154, and 261). All the specimens have been excavated from the locality XIb, except MNHN.F.ALM 154 which is from the locality XIa. No supplementary information is known about the stratigraphical level of MNHN.F.ALM 35 in the locality XI.

Pelves—One complete pelvic girdle MNHN.F.ALM 274 is preserved. It is associated with a posterior dorsal, sacral, and caudal vertebrae (mentioned above). As noticed above, the locality of MNHN.F.ALM 274 is unknown. In addition, an ilium (MNHN.F.ALM 104), three ischia (MNHN.F.ALM 123, 125, and 138), and a pubis (MNHN.F.ALM 122) are found isolated in the locality XIb.

Femora—Nine partly (MNHN.F.ALM 34 and 290) or entirely (MNHN.F.ALM 21, 22, 23, 26, 85, 100, and 284) preserved dicynodont femora are preserved. All come from the locality XIb, except MNHN.F.ALM 284, which is from the locality XIa.

Tibiae—Three tibiae are found in collection. They have been discovered in the locality XI, at the lowest stratigraphical level XIa (MNHN.F.ALM 291) and the middle one XIb (MNHN.F.ALM 33 and unnumbered specimen).

Fibula—Only one dicynodont fibula is found in collection (detailed location is unknown).

Phylogenetic method

As a result of the description of the new postcranial material attributed to the Moroccan dicynodont *Moghreberia nmachouensis*, a phylogenetic analysis was conducted to test its phylogenetic position. This analysis was based on the matrix from Kammerer (2018), the most recent and comprehensive matrix published for dicynodonts. The final phylogenetic dataset thus included 111 operational taxonomical units and 197 characters: 23 continuous characters and 174 discrete characters (of equal weight and unordered, except for characters 81, 84, 102, 163, 173, and 174, following Angielczyk and Kammerer, 2017). The Permian dicynodont *Dicynodon huenei* is deleted and the two taxa *Dicynodon angielczyki* and *Daptocephalus huenei*

were added and coded, according to the recent taxonomic revision and phylogenetic analysis of Kammerer (2019a). The coding of *Compsodon* and *Sangusaurus* was modified according to the modifications suggested by Kammerer et al. (2019). The new Polish dicynodont *Lisowicia bojani* (Sulej and Niedźwiedzki, 2019) has been added in the phylogenetic analysis. The coding of this taxa followed the study of Sulej and Niedźwiedzki (2019), but the characters 195 to 197 in the present study were newly coded on the basis of the supplementary descriptions and figures from Sulej and Niedźwiedzki (2019).

The coding of the cranial and mandibular characters of *Moghreberia nmachouensis* has been revised using the cranial specimens MNHN.F.ALM 10, 12, 37, 168, 280, and 281, and the mandible MNHN.F.ALM 38 (see Supplementary data). The attribution of the mandible MNHN.F.ALM 80 to *Moghreberia* is doubtful especially on the basis of the particular form of the tip of the dentary symphysis (pointed tip of snout; not figured here), while it appears more rounded or squared off in MNHNF.ALM 38. A more detailed comparison of this mandible and discussion about its phylogenetic affinities were not the aim of the present analysis and will be provided in a future study. Consequently, the specimen MNHN.F.ALM 80 has not been included in the analysis. The description of the new postcranial remains filled gap in our knowledge of the anatomy of *Moghreberia* and allowed a more comprehensive coding of its characters-states than in Kammerer (2018). The attribution of the massive specimens (MNHN.F.ALM 27, 96, 154, 275, 291, 299, and 365) to *Moghreberia* is still doubtful and has been discussed below. As well for the femur MNHN.F.ALM 22, its peculiar morphology (discussed below) significantly differs from all other femora attributed to *Moghreberia*. These specimens have thus not been considered in the phylogenetic analysis. As mentioned below, the revised study of the specimens attributed to *Azarifeneria barrati* (MNHN.F.AZA 366.1 and 366.2) and *A. robustus* did not emphasize significant differences between *Azarifeneria* and *Moghreberia*, even with other kannemeyriiforms (discussed below). The two species previously attributed to *Azarifeneria* by Dutuit (1989a, 1989b) have thus not been included in the analysis.

Following the phylogenetic method of Olivier et al. (2019) using TNT 1.1 (December 2013 version) (Goloboff et al., 2008), we performed a New Technology search and a driven search with the initial search level set to check every three hits. One hundred replications were chosen as the starting point for each hit, and the search

was set to find the most parsimonious trees 20 times. We did the phylogenetic analysis using a sectorial search (default settings) and tree-drifting (default settings but the number of cycles was three) to produce a nearly optimal tree, which was used for tree-fusing (default settings, but a global fuse every three hits was input) (Goloboff, 1999). In parallel, we did a traditional search of tree bisection reconnection (TBR) branch swapping with 11,111 replications and nine trees saved per replication. The continuous character were treated as ordered following the method from Goloboff et al. (2006). Unknown and/or inapplicable states of discrete and continuous characters are coded as '?' (Strong and Lipscomb, 1999). *Biarmosuchus* was used as outgroup. We obtained the same most parsimonious tree (1202.936 steps, consistency index= 0.229, retention index= 0.712) with the two phylogenetic analyses. The Bremer indexes (BS) were calculated to measure the node support according to the method detailed by Olivier et al. (2019) following the recommendations of Goloboff et al. (2008).

Systematic palaeontology

THERAPSIDA Broom, 1905

ANOMODONTIA Owen, 1860

DIYCNODONTIA Owen, 1860

KANNEMEYERIIFORMES Maisch, 2001

MOGHREBERIA Dutuit, 1980

Type Species—*Moghreberia nmachouensis* (Dutuit, 1988)

Diagnosis (modified from (Dutuit, 1988)—Large-sized kannemeyeriiform with skull over 40 cm but narrow with small lateral expansion of the squamosals. It can be distinguished from all other adequately known dicynodonts by the following combination of character-states: no posterior ridge of the palatal region of the premaxilla, absenceof teeth except well-developed paired of tusks, preparietal deeply depressed, small contribution of the posterior processes of the postorbitals to the intertemporal bar, parietals flat and well exposed on the intertemporal bar with slender and elongate posterior parietal processes, intertemporal bar highly angled in lateral view with a strong break in slope between the pre- and post-pineal region, reduced fossa on the ventral surface of the intertemporal bar, small contribution of the interparietal bone to the intertemporal skull roof, no distinct notch below the zygomatic process of the squamosal in posterior view, relatively large expansion of the dorsal

region of the scapula, acromion process low developed to absent, well-developed deltopectoral crest, obtuse angle between the anterior and distal edges of the deltopectoral crest, insertion of the m. *latissimus dorsi* onto a pinna-like process, and supinator process present on the ectepicondyle.

MOGHREBERIA NMACHOUENSIS Dutuit, 1980

Holotype—Dutuit (1980) did not mention a holotype in the original publication of *Moghreberia nmachouensis*. In disagreement with the International Code of Zoological Nomenclature (ICZN) rules, Dutuit (1988) later designated MNHN.F.ALM 280 as the holotype and MNHN.F.ALM 281 as the syntype for *M. nmachouensis*. In accordance with ICZN rules, we here proposed the lectotype MNHN.F.ALM 280 (Fig. 2) and the paralectotype MNHN.F.ALM 281 for *M. nmachouensis*.

Geographic Distribution and Stratigraphic range of the types—The locality XIb (according Dutuit's nomenclature) of the Argana Basin in Morocco. The locality XI (GPS coordinates: 161°8'E, 456°9'N) is located at the basis of the Irohalene Member T5, according to the nomenclature of Tixeront (1973). While the age of the Irohalene Member is still debated, a Carnian age appears most likely (discussed above).

Referred material—An abundant material is available in the collection of MNHN. It comes from the same locality as the cranial elements attributed to *Moghreberia* and was collected at the same time as the latter. It contains almost all elements of a complete postcranial skeleton, including:

- eight connected or isolated vertebrae: MNHN.F.ALM 120, 136, 159, 198, 265, 288, and two unnumbered specimens in connection named here 'Vunknb 1 and 2';
- nine ribs: MNHN.F.ALM 86, 90, 91, 95, 97, 296, and the three costal heads MNHN.F.ALM 163, 272, and an unnumbered specimen;
- nineteen isolated scapulae: MNHN.F.ALM 17, 19, 29, 30, 83, 98, 108, 113, 114, 132, 153, 155, 259, 263, 283, 292, and three unnumbered specimens;
- two scapulocoracoid complexes: MNHN.F.ALM 92 and 298;
- seven intercalvicles: MNHN.F.ALM 93, 94, 158, 278, 295, and two unnumbered specimens;
- one sternum: MNHN.F.ALM 134;
- twelve humeri: MNHN.F.ALM 24, 25, 101, 102, 105, 115, 121, 133, 147, 297, and two unnumbered specimens;

- four radii: MNHN.F.ALM 84, 131, 287, and 289;
- six ulnae: MNHN.F.ALM 18, 28, 35, 87, 126, and 261;
- one isolated ilium: MNHN.F.ALM 104;
- three isolated ischia: MNHN.F.ALM 123, 125, and 138;
- one isolated pubis: MNHN.F.ALM 122;
- one complete pelvis: MNHN.F.ALM 274 connected with sacral and caudal vertebrae;
- seven femora: MNHN.F.ALM 21, 23, 26, 34, 85, 100, and 290;
- two tibiae: MNHN.F.ALM 33 and an unnumbered specimen;
- one fibula: MNHN.F.ALM 32.

Geographic Distribution and Stratigraphic range of the referred material—The dicynodont postcranial remains were found in the localities XIa, XIb, and XIII (according Dutuit's nomenclature) of the Argana Basin in Morocco (see Table 1S for more details; Dutuit 1976, 1980, 1988). The localities XI (GPS coordinates: 161°8'E, 456°9'N) and XIII (GPS coordinates: 161°E, 458°N) are located on the basis of the Irohalene Member T5, according the nomenclature of Tixeront (1973). While the age of the Irohalene Member is still debated, a Carnian age appears most likely (discussed above).

Diagnosis—See the generic diagnosis

THERAPSIDA Broom, 1905

ANOMODONTIA Owen, 1860

DIYCNODONTIA Owen, 1860

KANNEMEYERIIFORMES Maisch, 2001

AZARIFENERIA Dutuit, 1989b

Type Species—*Azarifeneria barrati* (Dutuit, 1989b)

Status—Nomen dubium (Dicynodontoidea indet.)

AZARIFENERIA BARRATI Dutuit, 1989b

Holotype—MNHN.F.AZA 366.1 and 366.3 in connection: the parieto-squamosal and the right anterolateral region of skull, and MNHN.F.AZA 366.2: the occipital plate most likely belonging to a same big skull, according to Dutuit (1989b) (Fig. 3A-C).

Geographic Distribution and Stratigraphic range—The locality XII (according Dutuit's nomenclature; GPS coordinates: 160°7'E, 458°6'N) of the Argana Basin in Morocco. It is located at the basis of the Irohalene Member T5 (Dutuit, 1989b). While the age of the Irohalene Member is still debated, a Carnian age appears most likely (discussed above).

Status—Nomen dubium

Remarks—MNHN.F.AZA 366.1 and 366.2 present morphological similarities with the *Moghreberia nmachouensis* cranial remains, like the postorbitals that do not extend on the entire length of the intertemporal crest and the absence of an intertuberal crest. Nevertheless, the holotype of *Azarifeneria barrati* from *M. nmachouensis* by: (1) greater skull robustness, (2) longer intertemporal crest, (3) larger occipital condyle, and (4) higher contribution of the postorbitals to the intertemporal bar. However, the diagnostic features highlighted by Dutuit (1988) for *Moghreberia* could not be verified in MNHN.F.AZA 366.1 and 366.2, and the noticeable differences are not sufficient to firmly distinguish *A. barrati* from *M. nmachouensis* (discussed above).

AZARIFENERIA ROBUSTUS Dutuit, 1989a

Holotype—MNHN.F.ALM 167 (Fig. 4D-F), a fragmentary mandible with the anterior extremity eroded and broken, almost the whole right hemi-mandible and only the two-thirds of the left distorted hemi-mandible are preserved.

Geographic Distribution and Stratigraphic range—The locality XIb (according Dutuit's nomenclature) of the Argana Basin in Morocco. The locality XI (GPS coordinates: 161°8'E, 456°9'N) is located at the basis of the Irohalene Member T5 (Dutuit, 1989a). While the age of the Irohalene Member is still debated, a Carnian age appears most likely (discussed above).

Status—Nomen dubium

Remarks—The short anteroposterior expansion of the angular, abruptly curved dorsally, distinguishes the mandible MNHN.F.ALM 167 from MNHN.F.ALM 38 attributed to *Moghreberia*. However, intraspecific variation of this feature has been observed in *Stahleckeria potens*, thus supposing *Azarifeneria robustus* a synonym of *Moghreberia nmachouensis* (discussed below). Nonetheless, MNHN.F.ALM 167 presents relevant similarities with the mandible of *Stahleckeria potens* as previously

assumed by Dutuit (1989a), but also with other kannemeyeriiforms as *Angonisaurus* or *Xiyukannemeyeria*. As well as *A. barrati*, these only mandibular features are not sufficient to firmly support the taxonomic validity of *A. robustus* (discussed below).

Restudy of the cranial material attributed to *Azarifeneria* in relation to *Moghreberia*

Holotype of A. barrati: MNHN.F.AZA 366.1 and 366.2

According to Dutuit (1989b), there is no doubt that MNHN.F.AZA 366.1 and 366.2 belong to the same individual (Fig. 3A-C), while there is no bone contact between the two specimens after preparation. They constitute a very massive skull in comparison with *Moghreberia* (MNHN.F.ALM 280 (Fig. 2) and 281). A third specimen MNHN.F.AZA 366.3 forms the right anterolateral region of the big skull, associated with MNHN.F.ALM 366.1 (Fig. 3C). This specimen deserves more preparation and was not described in the present study.

MNHN.F.AZA 366.1 constitutes the posterior region of the skull that it formed with MNHN.F.AZA 366.3 (Fig. 3C). Only the dorsal region comprised of part of squamosal wings and the highly eroded intertemporal crest is preserved (Fig. 3A-C). The relief of the intertemporal crest cannot be interpreted due to the poor preservation, while the bone contacts can be studied. As mentioned by Dutuit (1989b), the posterior expansions of the postorbitals in MNHN.F.AZA 366.1 extend far beyond the pineal foramen and constitute more than half of the intertemporal crest. The posterior expansions of the postorbitals are more anteroposteriorly restricted in *Moghreberia* (MNHN.F.ALM 280 and 281; Figs 2A, 3C; Dutuit, 1988). However, in MNHN.F.ALM 10 attributed to *Moghreberia*, the postorbitals also cover more than half of the intertemporal crest as well as MNHN.F.AZA 366.1 (Figs 3C, E). As opposed to the interpretations of Dutuit (1989b), the poor preservation of the posterior end of the intertemporal crest in MNHN.F.AZA 366.1 does not provide firm conclusions about the contribution of the interparietal to the crest as observed in *Moghreberia* (Dutuit, 1988).

MNHN.F.AZA 366.2 is a part of the lower half of the occiput and the posterior region of the basicranium (Fig. 3A, C). Most of the supraoccipital and opisthotics, and all the quadratojugals are missing, the interpretation of their structures thus remains difficult. The large and rounded foramen magnum overhangs a highly distorted and poorly preserved occipital condyle. The occipital condyle is therefore largely covered by sediment. Despite the poor preservation of the condyle and a right exoccipital

condyle missing, the exoccipitals and basioccipital appear fused posteriorly to form a slightly tripartite condyle as in *Moghreberia* (Fig. 3A, D; Dutuit, 1988). In MNHN.F.AZA 366.2, the exoccipitals form narrow dorsal expansions that run along the lateral margin of the foramen magnum. They bear marked reliefs as in MNHN.F.ALM 268 and 280, attributed to *Moghreberia* (Figs 2C, 3A, D). The right opisthotic condyle is well preserved and presents a similar morphology to *Moghreberia* (Fig. 3A, D). On ventral view, the basioccipital predominantly forms the parabasisphenoid-basioccipital tubera, relatively narrow as in *Moghreberia* (MNHN.F.ALM 268 and 280; Figs 2B, C, F). The parabasisphenoid, nearly vertical, only contributes to the anterior margin of the stapedial facet of the tuber that is ventrolaterally exposed. The right opisthotic of MNHN.F.AZA 366.2 (Fig. 2C) appears to border the stapedial fossa posterolaterally, as in *Moghreberia* (MNHN.F.ALM 268 and 280; Fig. 3A, D), as opposed to the previous interpretation of Dutuit (1988). No intertuberal ridge is observed in MNHN.F.AZA 366.2 (Fig. 3C). A deep and rounded depression on the parabasisphenoid of MNHN.F.AZA 366.2 (Fig. 3C) is observed in the intertuberal groove, close to the suture with the basioccipital. A similar depression is noticed in MNHN.F.ALM 280 (Fig. 2B) as opposed to MNHN.F.ALM 268 and 281 (Fig. 3F; C. Olivier pers. observ.). The two observed depressions are partly filled by sediment. Nonetheless, these depressions cannot correspond to the single carotid foramen described in *Diictodon feliceps* (Surkov and Benton, 2004; previously *D. testudirostris* according the taxonomic revision of Kammerer et al., 2011), this latter being located more anteriorly on the parabasisphenoid and close to the suture with the pterygoid mid-plate. Most of the pterygoids are missing with the proximal part of the posterior pterygoid rims and the median plate highly eroded.

MNHN.F.ALM 167, holotype of A. robustus

MNHN.F.ALM 167 is a fragmentary mandible without its right rim and the third posterior part of the left rim (Fig. 4D-F). As already mentioned, Dutuit (1989a) mainly focused on the morphological similarities with the Brazilian *Stahleckeria*, without clearly mentioned them and briefly described the anatomy of the mandible.

As noticed by Dutuit (1989a), the dentaries are fused and robust (Fig. 4D-F). In dorsal view, the symphyseal region is deeply curved and bordered by two large swellings as in *Moghreberia* (Fig. 4A, D). Nothing can be said about the presence of dentary table (as defined by Angielczyk and Rubidge, 2013), because of the poor

preservation of these two reliefs. Despite sediment remaining, a distinct posterior dentary sulcus (Fig. 4D), obviously narrow, is noticeable in dorsal view of the anterior expansion of the left mandibular rim in MNHN.F.ALM 167. The anterior region of a slight swelling is preserved and border the medial margin of the left dentary sulcus. The sulcus runs on the dorsal surface of the dentary far beyond the anterior margin of the Meckel fossa, as opposed to *Moghreberia* where the sulcus terminates at the level of the anterior margin of the fossa (Fig. 4A, D). Thick but eroded lateral dentary ridges are observed on both lateral sides of the dentary (Fig. 4F). Despite the lack of bone at the anterior tip of the mandible, a median and thick ridge is noticeable on the dentary in anterior view, indicating an anterior bone erosion relatively slight. As noticed by Dutuit (1989a), the dentary appears more expanded lateromedially than anteroposteriorly (Fig. 4D, F), in comparison with *Moghreberia* (Fig. 4A, C), giving it a massive aspect. In addition, the tip of the lower jaw of MNHN.F.ALM 167 would most likely be more rounded or squared-off (Fig. 4D). The lower jaw is highly constricted just posterior to the lateral dentary ridges. In lateral view, the left posterodorsal expansion of the dentary appears highly eroded. Most of the left surangular is missing. The posterior expansion of the dentary delimits the anterior margin of the Meckel fossa. The poor preservation of the lateral side of the left mandibular rim does not provide information about the form of a lateral dentary shelf or a potential occlusion of the fossa by a dentary sheet. However, if the Meckel fossa is laterally opened, its anteroposteriorly expansion would appear significantly smaller than in *Moghreberia* (Fig. 4C, F).

Posterior to the dentary symphysis, the fused splenial form a deep depression on its posterior surface. An anterior triangular expansion of the splenial points on the ventral surface of the dentary (Fig. 4E).

In dorsal view, the angle formed between the left mandibular rim and the long axis of its symphyseal region appears more opened than in *Moghreberia* (Fig. 4A, D). The posterior end of the angular and almost whole the reflected lamina are missing in the left rim. Also, the surangular and the articular are not preserved. The angular mainly forms the lateral border of the preserved region of the mandibular rim. Posteriorly to the posterodorsal expansion of the dentary, the angular abruptly raises up to reach the level of the dentary dorsally (Fig. 4F). In *Moghreberia*, the angular slightly points dorsally and far beyond the posterior end of the dentary (Fig. 4C). As well as for the

ascending branch of the angular, the reflected angular lamina sharply curves ventrally posterior to the short Meckel fossa (Fig. 4F). Potential ornementations could not be studied on the external surface of the reflected lamina due to the poor preservation of external bone surface and sediment remaining. Only a large median depression has been interpreted between the ascending branch of the angular and the descending one of the reflected lamina (Fig. 4F). In ventral view, the angular and the reflected angular lamina split and diverge laterally and medially, respectively (Fig. 4E). The point of this separation is more anterior in MNHN.F.ALM 167 than in *Moghreberia* (Fig. 4B).

Description of the new dicynodont postcranial material from Argana Basin

The orientation of the limb bone was based on an increasingly erected posture of the dicynodonts as considered by the most recent studies (e.g., Ray, 2006; Sulej and Niedźwiedzki, 2019). The interpretation of the muscular insertion sites followed the studies of Camp and Welles (1956), Romer (1956a), Defauw (1986), and King (1988).

Axial skeleton

VERTEBRAE

Because of gradual changing of characters along the vertebral column, the attribution of the vertebrae to a specific region can be hard when they are isolated or found in small connected groups. We thus described the groups of specimens that present similar features.

Last cervical vertebrae and/or first dorsals MNHN.F.ALM 288, 198, Vunknb 1 and 2 (Fig. 5)—The two connected vertebrae Vunknb 1 and 2 (Fig. 5C-F) are identified to be the last cervical vertebrae and/or first dorsals especially because of (1) parapophyses clearly separated from the transverse processes in Vunknb 1, (2) neural spine of Vunknb 2 nearly dorsally directed, (3) transverse processes large and triangular in both vertebrae, and (4) obtuse angle between the prezygapophyses (e.g., Cox, 1959; King, 1981) (structures developed below). As previously mentioned, MNHN.F.ALM 288 is highly anteroposteriorly compressed (Fig. 5A-B). The proportions of their different structures may thus be altered. In addition, a sediment layer covers a part of the external bone surface probably hiding specific characters. Like Vunknb 1 and 2, MNHN.F.ALM 288 and 198 are supposed to be one of the last cervicals or first dorsals

because of the form of their transverse processes and the prezygapophyses largely spaced.

The centra of the two connected vertebrae Vunknb 1 and 2, and MNHN.F.ALM 288 are concave in the anterior and posterior sides, indicating amphicoelous vertebrae (Fig. 5A, B, C, E). While the sediment remains between the Vunknb 1 and 2, they have been considered similar in their structures. The oval centra of Vunknb 1 and 2, and MNHN.F.ALM 288 are higher than wide (Fig. 5A, B, C, E). Their lateral surfaces are concave and limited anteriorly and posteriorly by a bone thickening, bordering the anterior and posterior sides of the centra. The sediment and erosion prevent observation of these structures in MNHN.F.ALM 288. The centra and neural arches limit ovoid neural canals (almost or entirely filled by sediment). The ventral margin formed by the centrum is well observed in MNHN.F.ALM 288. It is concave anterodorsally and almost straight posterodorsally (Fig. 5A-B). The neural canal of MNHN.F.ALM 288 appears larger than in Vunknb 1 and 2, as well as the size of centrum that is higher in MNHN.F.ALM 288 (Fig. 5A, B, C, E). These differences are most likely due to the post-mortem compression in MNHN.F.ALM 288, but they also would define an individual with larger proportions.

Thick ovoid protuberances present in the lateral sides of the vertebrae Vunknb 1 and 2, in middle of the centra near to the anterior side, are interpreted as parapophyses (Fig. 5D, F). The parapophyses of Vunknb 1 are rounded whereas that of Vunknb 2 are ovoid and dorsoventrally elongated. The parapophyses of Vunknb 2 appear in continuity with transverse processes (=diapophyses) by a small ridge. However, the thin sediment layer remaining preclude this interpretation with certainty. However, the parapophyses of Vunknb 1 are clearly well separated from the transverse processes, indicating double-heads associated ribs. The parapophyses distinct from the transverse processes have also been observed in cervical vertebrae of most dicynodonts like *Dicynodontoides nowacki* (previously "*Kingoria*" *nowacki* by Cox, 1959; then *D. nowacki* by Angielczyk et al., 2009), *Dicynodon huenei* (previously *D.* "*trigonocephalus*" by King, 1981; then *D*. *huenei* by the taxonomic revision of Kammerer et al., 2011), *Placerias* (Camp and Welles, 1956), *Rhachiocephalus* (Maisch, 2004), and *Wadiasaurus* (Bandyopadhyay, 1988). However Cox (1959), King (1981), and Bandyopadhyay (1988) also mentioned separated parapohyses and transverse processes in the first two or three dorsals in *Dicynodontoides nowacki*,

Dicynodon huenei, and *Wadiasaurus*. The well-developed parapophyses in Vunknb 1 may indicate that the vertebra is one of the last cervicals or one of the first dorsals. Sediment remaining in the lateral sides of the centrum of MNHN.F.ALM 288 makes impossible the observation of parapophyses and their fusion with transverse processes.

The suture between the centra and neural arches are not visible on Vunknb 1 and 2, and MNHN.F.ALM 288, suggesting adult individuals. In these three vertebrae and MNHN.F.ALM 198, the triangular transverse processes are flattened anteroposteriorly and extended dorsally or slightly dorsolaterally to form a dorsal corner slightly posterior to the dorsal border of the prezygapophyses (Fig. 5A, B, C, E). The dorsal margins of the transvere processes are thus nearly horizontal and not clearly dorsolaterally oblique like in the dorsal vertebrae MNHN.F.ALM 120, 159, and 265 (Figs 6A, C, E, G, 7A, C). Moreover, the anterior and posterior surfaces of the large transverse processes are slightly concave. These depressions would be correlated to the insertion of a strong musculature supporting the head (King, 1981) and the pectoral girdle that has no solid connection with the backbone (Romer, 1956a). The lateral margins located at the dorsolateral corner of transverse processes are anteroposteriorly extended.

The flattened prezygapophyses present large articular surfaces directed mediodorsally (Fig. 5A, C). The angle between the prezygapophyses is obtuse indicating high lateral movements (e.g., King, 1981). The short postzygapophyses, located dorsally to the prezygapophyses, posteriorly arise from the basis of the neural spine (Fig. 5B, E). They are separated by a deep and narrow groove, which forms a “U”-shaped channel. Their articular surfaces are ventrolaterally directed. The neural spine abruptly merges dorsally to the prezygapopyses. It is almost complete and nearly vertical with a slight backward orientation in Vunknb 2(Fig. 5D), as opposed to the neural spines of most dorsal vertebrae that are clearly posteriorly directed in dicynodonts (e.g., Cox, 1959; Bandyopadhyay, 1988). In lateral view, the neural spine is partly presvered in MNHN.F.ALM 288, but it would indicate a slight posterior orientation of the process. The neural spine is missing in Vunknb 1.

Anterior dorsals MNHN.F.ALM 120, 159, and 265 (Figs 6, 7)—A dorsal position along the vertebral column is supposed for MNHN.F.ALM 120, 159, and 265. This interpretation of their position is based on the presence of (1) confluence of the

transverse processes and parapophyses, (2) narrow neural arches with the transverse processes mainly dorsally expanded, (3) prezygapophyses and postzygapophyses very closely spaced, and (4) neural spines strongly posteriorly directed.

All preserved centra of these vertebrae are higher than wide. Their anterior and posterior surfaces are clearly concave indicating amphicoelous vertebrae. A well-marked notochordal central pit is present on both anterior and posterior surfaces of MNHN.F.ALM 265 and on the anterior surface of MNHN.F.ALM 159-1 (Figs 6C, G, 7A, C). The lateral border of the centra is more concave than the ventral one, highlighting a high lateral constriction of the centra, clearly visible in MNHN.F.ALM 159 and 265 (Figs 6D, H, 7B, D). In MNHN.F.ALM 159 and 120 (Fig. 6A, C, F, G), the ovoid neural canal is ventrally limited by the centrum with a concave margin anteriorly and a straight one posteriorly, as in MNHN.F.ALM 288, Vunknb 1 and 2 (Fig. 5A, B, C, E). The ventral margin of the neural canal of MNHN.F.ALM 265 is almost straight in the posterior side, but also in the anterior side that is most likely due to postmortem distortion (Fig. 7A, C). The neural canal in the dorsal vertebrae MNHN.F.ALM 120, 159, and 265 (Figs 6A, C, F, G, 7A, C) does not appear narrower and higher than in the last cervical and/or first dorsal vertebrae Vunknb 1 and 2, and MNHN.F.ALM 288 (Fig. 5A, B, C, E); as opposed to the observations of Cox (1959) in *Dicynodontoides nowacki* and Maisch (2004) in *Rhachiocephalus magnus*.

No clear suture is observed between the centra and neural arches indicating that MNHN.F.ALM 120, 159, and 265 are adult. As opposed to the last cervical and/or first dorsal vertebrae Vunknb 1 and 2, and MNHN.F.ALM 288 (Fig. 5A, B, C, E), the transverse processes of the dorsal vertebrae appear narrower with expansions more dorsally projected than laterally (Figs 6A, C, F, G, 7A, C). The bone surface around the neural canal and prezygapophyses is then more reduced. The contact between the transverse processes and the neural spine extends far beyond the prezygapophyses in dorsal vertebrae (Figs 6A, C, F, G, 7A, C), as opposed to Vunknb 1 and 2, and MNHN.F.ALM 288 (Fig. 5A, B, C, E). In addition, the transverse processes are in continuity with the parapophyses indicating associated single-head ribs (Figs 6B, D, 7B, D). The parapophyses are more ovoid and elongated than in the last cervical/first dorsal vertebrae. They are also more dorsally located on the lateral side of the neural arches, while they are on the lateral side of the centra in Vunknb 1 and 2, and MNHN.F.ALM 288 (Fig. 5D, F).

The preserved prezygapophyses in MNHN.F.ALM 120-1, 120-4, and 159-1 (Fig. 6A, C, E) show thin layers that appear narrower and more dorsoventrally reduced than in Vunknb 1 and 2, and MNHN.F.ALM 288 (Fig. 5A, C). The zygapophyses between the dorsal vertebrae are set at a less obtuse angle to each other than in the last cervical and/or first dorsal vertebrae described above. The articulation between the dorsal vertebrae would then be less flexible permitting small lateral movements. In parallel, the observation of the well-preserved postzygapophyses of MNHN.F.ALM 120-3 and 265 (Figs 6E, F, 7C) indicates that they are closer than in the last cervical or first dorsal vertebrae Vunknb 2 and MNHN.F.ALM 288 (Fig. 5B, E).

The neural spine is well preserved in MNHN.F.ALM 265 but partly or entirely missing in the other dorsal vertebrae. The neural spines are clearly posteriorly directed (Figs 6B, D, H, 7B, D). The well-preserved neural spine in the last cervical or first dorsal vertebra Vunknb 2 (Fig. 5D) appears more anteroposteriorly expanded than in MNHN.F.ALM 120-1, 159-1, and 265 (Figs 6B, D, H, 7B, D). The neural spine of MNHN.F.ALM 265 shows a thickening in its dorsal end (Fig. 7C-D), as previously described in the mid-dorsal vertebrae of *D*. *huenei* (King, 1981). King (1981) explained this thickening as a higher insertion site for *interspinalis* muscle to connect more firmly the neural spines along the vertebral column.

Isolated posteriormost dorsals in MNHN.F.ALM 274 (a same block including a complete pelvic girdle connected to sacral and caudal vertebrae, and associated with two isolated vertebrae) (Fig. 8)—The structural similarity between these two isolated vertebrae and the sacral vertebrae in MNHN.F.ALM 274 indicate that they probably follow each other.

The centra of the two vertebrae are ovoid and amphicoelous with lateral concavities (Fig. 8A, C, E, G). Judging by their association with a pelvic girdle and the combination of characters (described below), the two vertebrae are supposed to be posteriormost dorsal vertebrae. Nonetheless, the two disconnected vertebrae MNHN.F.ALM 274 present similar features both with the last cervicals/first dorsals MNHN.F.ALM 288, Vunknb 1 and 2; and with more anterior dorsals MNHN.F.ALM 120, 159, and 265.

The transverse processes are largely projected beyond the prezygapophyses in the two isolated vertebrae MNHN.F.ALM 274 (Fig. 8A, C, E, G), a particular structure that has been highlighted in the more anterior dorsals MNHN.F.ALM 120, 159, and 265

(Figs 6A, C, E, G, 7A, C). Also, the rib facets of the parapophyses and transverse processes are continuous and the neural spines are largely directed posteriorly (Fig. 8B, D, F, H). The dorsal end of the neural spine is thick and roughened indicating muscular insertion (Fig. 8A, E), probably for the *interspinalis* muscle (King, 1981), as in MNHN.F.ALM 265 (Fig. 7C).

However, the large ovoid neural canal is laterally bordered by large lateral expansions of neural arches that fill in the angle between the transverse processes and the centra (Fig. 8A, C, E, G). These noticeable expansions have also been described in the last cervicals/first dorsals MNHN.F.ALM 288, Vunknb 1 and 2 (Fig. 5A, B, C, E). King (1981) also mentioned these lateral expansions of the neural arches in the posteriormost vertebrae of *Dicynodon huenei*. As in the last cervicals/first dorsals, large transverse processes anteriorly covered by a depression would indicate strong muscular insertions, probably due to the position close to the pelvic girdle. Also, like in MNHN.F.ALM 288, Vunknb 1 and 2 (Fig. 5A, B, C, E), the angle between both the prezygapophyses and postzygapophyses is largely open in the two isolated vertebrae MNHN.F.ALM 274 (Fig. 8A, C, E, G). This could be indicative of flexibility into the immediate presacral region (King, 1981), at the opposite of the relatively rigid trunk region with pre- and postzygapophyses closer in the dorsals (MNHN.F.ALM 120, 159, and 265; Figs 6A, C, E, G, 7A, C).

Sacral vertebrae MNHN.F.ALM 136 and 274 (Figs 9, 24)—The centra of the sacral vertebrae are fused together and their sutures are marked by small and roughened thickenings in ventral view (Figs 9B, 24C). They appear anteroposteriorly longer than the cervical and/or dorsal vertebrae. The lateral and ventral sides of the sacral vertebrae are slightly concave compared to the studied cervicals and/or dorsals. A sharp median crest can be observed on the ventral side of the second sacral centrum of MNHN.F.ALM 274 (Fig. 24C). However, the specimen appears to be highly distorted by a postmortem compression that crushed the centrum laterally and could generate that crest. The first sacral vertebra of MNHN.F.ALM 136 is poorly preserved (Fig. 9 A). Nonetheless, the centrum size appears to decrease from the first to the last sacral vertebrae in both specimens (Figs 9B, 24C).

While the posterior side is hidden by the following vertebra, the anterior side of the first sacral vertebra of MNHN.F.ALM 274 shows a large and dorsoventrally expanded centrum with an anterior concavity likely suggesting an amphicoelous

vertebra. In spite of the high compression of the specimen, the neural canal appears rounded and relatively reduced compared to the canals of cervical and/or dorsal vertebrae. The prezygapophyses are largely spaced (Fig. 24A-B) like in the last cervicals/first dorsals (Vunknb 1 and 2, and MNHN.F.ALM 288: Fig. 5A, C; the two isolated posteriomost dorsals in MNHN.F.ALM 274: Fig. 8A, C). In the first sacral vertebra of *Dicynodon huenei* (King, 1981) and *Dicynodontoides nowacki* (Cox, 1959), the prezygapophyses seem larger than in the rest of the sacrum. Indeed, the first sacral articulated with the last posterior dorsal vertebra that present a large angle between its postzgapophyses (as observed in the two isolated posteriomost dorsals in MNHN.F.ALM 274: Fig. 8E, G) suggesting high flexibility in this region. This flexibility then strongly diminishes along the sacrum due to the fused centra and closely-spaced zygapophyses as described in *Dicynodon huenei* (King, 1981). The quality of the preservation and preparation of the studied material prevent the description of the zygapophyses of the rest of the sacral vertebrae.

The sacral transverse processes are more robust but less laterally expanded, compared to the cervical and/or dorsal vertebrae. They extend laterally, not dorsally beyond the level of the dorsal margins of the prezygapophyses as in the first cervicals/last dorsals (Vunknb 1 and 2, and MNHN.F.ALM 288: Fig. 5A, B, C, E). However, as in the previous described last cervical/first dorsal and posteriormost dorsal vertebrae (Figs 5A, B, C, E, 8A, C, E, G), the lateral expansions of neural arches fill in the angle between the transverse processes and the centra. The lateral expansions of both sacral vertebrae fuse with short sacral ribs that are directed posteriorly in ventral view (Figs 9B, 24C). The suture between the sacral centra and ribs are marked by a roughened swelling.

The sacral ribs are twisted and constricted at the middle of their long axis (Figs 9B, 24C). Their lateral ends are anteroposteriorly expanded and anteroventrally oriented to contact the ilium. The lateral expansion of the first and second sacral ribs of MNHN.F.ALM 136 and 274, has a “spatulate”-like form marked by anterior and posterior swellings. The lateral expansions of the other preserved sacral ribs are also thicker but more rounded in lateral view. A fragment of left fused ribs is visible posteriorly to the fourth sacral ribs, indicating at least five sacral vertebrae in MNHN.F.ALM 136 (Fig. 9A). Five sacral ribs could be distinguished in MNHN.F.ALM 274 supposing at least five sacral vertebrae (Fig. 24A). That corroborates the presence

of five sacral vertebrae in MNHN.F.ALM 136 (Fig. 9A). The poor preservation and high sediment remaining in MNHN.F.ALM 274 make difficult to distinguish the boundary between the sacral and caudal vertebrae. Nevertheless, a count of five sacral ribs appears the most likely. The preserved part of the distal end of the first right sacral ribs associated with four sacral articular facets in the ilium MNHN.F.ALM 104 (described below; Fig. 25B) confirm the hypothesis of five sacral vertebrae in *Moghreberia*.

Only the neural spine of the first sacral vertebra of MNHN.F.ALM 136 can be is preserved, while highly eroded. It is crushed and lies against the dorsal side of the second sacral vertebrae. In MNHN.F.ALM 274, it is almost entirely preserved and distinct from the sediment remaining (Fig. 24B). It is short and posteriorly directed. Its distal end widens dorsally, probably for a strong epaxial muscular insertion.

Caudal vertebrae in MNHN.F.ALM 274 (Fig. 24B)—The caudal vertebrae reach the posterior margin of the ischia. The unusual angle of the caudal vertebrae (Fig. 24B) is probably du to a postmortem distortion. Most of caudal centra are still in the sediment matrix. Judging by the number of the neural spines visible and the most posterior visible centrum in lateral view, five caudal vertebrae can be observed. The centrum of the first caudal vertebra is larger and longer than the fifth caudal one indicating that size of caudal vertebrae strongly decreases posteriorly along the vertebral column. The more posterior preserved caudal vertebra presents a small and rounded centrum with a posterior concavity. The caudal ribs appear to be associated with vertebrae, but their poor preservation does not provide more information.

RIBS

All the studied ribs are anteroposteriorly flattened. Judging by the angulation of the transverse processes (Figs 6D, 7B, 8B, D), the anterior side of the ribs would be anterodorsally faced. None ribs present an accentuated curvature. This feature, often used to identify the position of the ribs could not be used in the present study. The position has thus been concluded from the shape of the rib head and the distal end when preserved, and the size of the crest located at the dorsal margin of the bone close to the rib head.

MNHN.F.ALM 91 and the unnumbered rib head are attributed to an anterior dorsal position along the vertebral column (Fig. 10A-B, I-J). As in the anterior dorsal ribs of *Jachaleria* (Vega-Dias and Schultz, 2004) and *Dicynodontoides nowacki* (Cox, 1959), the two specimens present two well-developed articular facets (tuberculum and

capitelum) in proximal view of their heads, clearly separated by a marked incision (Fig. 10A-B, I-J). The dorsal turbeculum is dorsoventrally higher than the capitelum. Distinct tuberculum and capitulum have also been described on cervicals ribs of most dicynodonts like *Dicynodon huenei* (King, 1981), *Dicynodontoides nowacki* (Cox, 1959), and *Jachaleria* (Vega-Dias and Schultz, 2004). The rib heads of MNHN.F.ALM 91 and the unnumbered specimen being similar in size, they thus should have similar size. These specimens appear too long to be cervical ribs. A large swelling merges from the dorsal margin of the tuberculum on the anterior side of the ribs and extends until the distal end of the rib. It dorsally protrudes to form a sharp crest that runs on the dorsal margin of the one fifth third of MNHN.F.ALM 91 (Fig. 10B). This crest would participate to the insertion site of the epaxial muscle *ilio-costalis* that extend until the transverse processes (Romer, 1956a; King, 1981). A second narrower swelling forms the ventral margin of the rib, parallel to the dorsal one. A groove separates the two swellings and becomes deeper along the bone until the distal end (Fig. 10B). While the distal end of MNHN.F.ALM 91 is highly eroded, a rounded and roughened extremity is clearly visible. Except a small depression marked by the dorsal crest, the posterior side of the rib is flat.

The head of MNHN.F.ALM 96 presents two well-developed tuberculum and capitulum but only partly separated by a slight constriction (Fig. 10G, H). This continuity would indicate an associated vertebra with fused transverse process and parapophysis. This rib could thus be more posterior along the vertebral column than MNHN.F.ALM 91 and the unnumbered rib head. While the rib head of MNHN.F.ALM 90 is poorly preserved, a marked crest protrudes on the proximal region of the dorsal margin like in MNHN.F.ALM 96 (Fig. 10D, H). The dorsal margin of the other ribs MNHN.F.ALM 86, 95, and 97 appears continuous without merging crest (Fig. 11B, D, F). This would indicate that MNHN.F.ALM 90 and 96 are closer to MNHN.F.ALM 91 and the unnumbered rib head than the other ribs. The anterior surface of MNHN.F.ALM 90 is similar to MNHN.F.ALM 91 with parallel dorsal and ventral swellings, running along the entire bone and becoming flattened close to the distal end (Fig. 10B, D). MNHN.F.ALM 96 appears one of the most robust ribs (Fig. 10G, H). Compared to MNHN.F.ALM 91 and the unnumbered rib head (Fig. 10A, B, I, J), MNHN.F.ALM 96 presents more developed tuberculum and capitulum (Fig. 10G, H). On the anterior side, its dorsal crest is clearly thicker than in MNHN.F.ALM 90 and 91 (Fig. 10B, D, G).

In addition, the dorsal swelling becomes flattened before reaching the middle of the long bone axis and no distinct ventral swelling is visible. The distal end of MNHN.F.ALM 96 is dorsoventrally expanded, thick and rounded that could indicate an articulation with the sternum, directly or by cartilaginous continuation (King, 1981).

The rib head MNHN.F.ALM 163 seems as robust and expanded as the head of MNHN.F.ALM 96 (Fig. 10G, K). A slight constriction may be interpreted in proximal view but the poor preservation of the articular facets does not allow firmly concluding. A slight inflexion toward an anterodorsal direction of the dorsal margin of the bone could suggest the initiation of the dorsal crest (Fig. 10L), as described in MNHN.F.ALM 90, 91, and 96 (Fig. 10A, C, H). These features would attribute MNHN.F.ALM 163 to an anterior dorsal position along the vertebral column.

The head of MNHN.F.ALM 97 is as dorsoventrally expanded as in MNHN.F.ALM 91, 96, and the unnumbered rib head (Figs 10B, G, J, 11E). No clear incision is present between the tuberculum and capitulum. However, the posterior side of the head is highly eroded, and because of the poor preservation it is not possible to conclude with certainty about the presence of a constriction between the two proximal articular facets as in MNHN.F.ALM 96. As well as the most previous described ribs, two large swellings border the dorsal and ventral margins of the anterior side (Fig. 11E). While the dorsal swelling becomes thinner dorsally to form a crest, this latter does not set off the dorsal margin of the rib as mentioned above in MNHN.F.ALM 90, 91, and 96 (Figs 10A, C, H, 11E). King (1981) suggested an insertion site of the muscle *ilio-costalis* increasingly reduced more posteriorly in the vertebral column of *Dicynodon huenei*. If we consider that the size of the dorsal crest is tied to that of the muscle *ilio-costalis*, we could suggest the position of MNHN.F.ALM 97 more posterior than that of MNHN.F.ALM 90, 91, 96, and the unnumbered rib head. The size and shape of the head of MNHN.F.ALM 96 and 97 being mainly similar, another hypothesis would explain the morphological differences (robustness, developed dorsal crest) by dimorphism or polymorphism (discussed below).

MNHN.F.ALM 86 and 95 do not show dorsal crest in proximal region as in MNHN.F.ALM 97 (Fig. 11B, D, E). The two swellings run along the dorsal and ventral margins of the bones, but they seem less pronounced than in MNHN.F.ALM 97. In addition, the groove separating the two ridges appears shallower than in most of the other previously described ribs (Figs 10B, D, F, 11B, D, E). The heads of MNHN.F.ALM

86 and 95 are also less dorsoventrally expanded than in MNHN.F.ALM 91, 96, 97, and the unnumbered rib head (Figs 10A, G, J, 11B, D, E). MNHN.F.ALM 86 and 95 are poorly preserved, but it is clear that they are single-headed. The less developed articular surfaces and reliefs, and the smaller size in MNHN.F.ALM 86 and 95 suggest a more posterior position than the previous described ribs. These ribs were probably associated to posterior dorsal vertebrae. A decrease of articular surfaces is also described in posterior dorsal ribs in *Jachaleria* (Vega-Dias and Schultz, 2004) and *Dicynodon huenei* (King, 1981), and from the mid-dorsal region in *Diictodon* (Ray and Chinsamy, 2003). In addition, Ray and Chinsamy (2003) also noticed ribs with single heads from the posterior dorsal region in dicynodonts.

The rib heads of MNHN.F.ALM 87 and 272 are as robust as in MNHN.F.ALM 96 and 163 (Figs 10G, K, 11G, 23E). Like in MNHN.F.ALM 86, 95, and 97 (Fig. 11B, D, E), they do not present a pronounced crest in their dorsal margins (Fig. 11G, 23E). In addition, the tuberculum and capitelum are continuous. These features would suggest a posterior dorsal position along the vertebral column. However, most of MNHN.F.ALM 87 and 27 are missing, except the more proximal region. Consequently, their relative position along the column is still uncertain.

The head of MNHN.F.ALM 296 is missing (Fig. 10E, F). However, a distinct crest sets off from the dorsal margin at proximal region of the bone as in MNHN.F.ALM 90, 91, and 96 (Fig. 10B, D, F, G). Also, two marked parallel swelling run along the dorsal and ventral margins of the anterior side, with a median deep groove like in MNHN.F.ALM 90, 91, and 97. A thick median ridge merges at the first third of posterior side to flatten in the last third nearby the ventral margin of the rib (Fig. 10E). Judging by its location on the ribs and its posteroventral orientation (supposing ribs directed anterodorsally as mentioned above), the ridge could be the insertion site for intercostal muscles. This feature distinguishes this specimen from all other. Similar ridges are also observed in MNHN.F.ALM 90 and 97 but less developed (Figs 10C, 11F), the posterior surface is almost flattened in MNHN.F.ALM 96 (Fig. 10H), and the posterior sides of MNHN.F.ALM 86 and 96 are too poorly preserved to conclude. If we consider the presence of a dorsal crest at the proximal side as a specific feature of the anterior dorsal ribs in *Moghreberia*, MNHN.F.ALM 296 could be interpreted as such. The median thick ridge on the posterior side could thus be attributed to variation of the size of the insertion site for muscles along the vertebral column (like for the dorsal crest, a

probable insertion site for the *iliocostalis* muscle) and/or intraspecific variation (ontogeny, dimorphism, and/or polymorphism) (discussed below).

Pectoral girdle

There is no trace of cleithrum nor clavicle attributed to dicynodont in postcranial material found in the Argana Basin.

SCAPULOCORACOID

The scapula is an elongated bone with enlarged dorsal and ventral regions. The ventral expansion is larger than the dorsal one. In posterior view, the scapulae are more or less concave medially and convex laterally depending on the quality of the preservation of specimens. MNHN.F.ALM 292 presents the highest medial concavity, probably of taphonomic origin. This postmortem distortion is also evidenced by the anterior blade of the ventral region highly medially directed. The dorsal expansion of MNHN.F.ALM 17 and 30, and Sunknb 3 is mainly straight in posterior view. Marks of crushing are observed on these scapulae with many cracks and fractures that may reduce the original concavity, especially at the limit between the middle and dorsal regions. The posterior margin of scapulae is much thicker than the anterior one forming a crest.

The dorsal region of scapula is mediolaterally flattened to form a narrow and elongated scapular blade (Figs 12-16). All well-preserved scapulae (MNHN.F.ALM 17, 29, 83, 153, 155, 259, and 298) present a distinct swelling that runs along the posterior border of the dorsal expansion (Figs. 12A, E, 13C, 14C). This swelling borders the large insertion site of the *deltoidus* muscle posteriorly and a small shallow fossa anteriorly where the *serratus anterior superficialis* muscle inserts (Figs 12A, E, 13A, C; e.g., King, 1981; Ray, 2006). On the medial side of MNHN.F.ALM 29, 83, and 298 (Figs 12B, F, 14D), a large and weak swelling anteriorly borders a rounded shallow fossa, probably the insertion site for the *subcorascapularis* muscle (e.g., King, 1981; Ray, 2006).

A flat surface extends in all specimens on the posterior margin at the middle region of scapula. It is medially limited by a sharp ridge that is accentuated by a deep medial fossa at the ventral region. The flat surface extends ventrally to be anteriorly bordered by a pronounced posterior tuberosity in all well-preserved scapulae. This

corresponds to the site of the insertion of *triceps* muscle (Figs 12-16; e.g., Camp and Welles, 1956).

The anterior margin of the scapulae is characterized by a weakly-developed and hemispherical acromion process (Figs 12A, C, E, 14C, 15F, C), while it is reduced to a flat roughened surface in MNHN.F.ALM 17 (Fig. 13C). In the other specimens, no acromion process could be clearly observed, either due to a poor preservation of the external bone surface or to the size of the process, extremely reduced even flat. The acromion process laterally delimits a reduced prespinous fossa (e.g., Camp and Welles, 1956; Cruickshank, 1975). In scapulae with well-preserved acromion and *triceps* muscle tuberosities (MNHN.F.ALM 17, 29, 30, 83, 132, and 259), the first one is usually more developed than the second one (Figs 12, 13C, D, 14C, D, 15C, D). The acromion process overhangs a large expansion of the anterior margin of the ventral region. This rectangular expansion dorsally projects (MNHN.F.ALM 29, 30, 83, 113, 132, 292, 298, 299, and Sunknb 3) (Figs 12, 13A, E, 14C, 15C, 16A) forming an ovoid and roughened surface (MNHN.F.ALM 83, 113, 132, and Sunknb 3: Figs 12F, 13F, 15C, 16B). The broad expansion of the anteroventral region of the scapula may indicate a large insertion of the *supracoracoideus* muscle on the lateral side. Together with the *deltoideus* muscle, this muscle would perform the elevation and protraction of the humerus, as suggested by Ray (2006) in *Wadiasaurus indicus* and *Lystrosaurus murrayi*.

The ventral region of the scapula fuses with the coracoid and precoracoid anteriorly, and articulates with the humerus posteriorly. In ventral view, the glenoid facet is ovoid and mediolaterally expanded. It narrows anteriorly to be followed by the thin co,tact zone with the coracoid. The well-preserved glenoid articular surfaces (MNHN.F.ALM 29, 83, 92, 114, 132, 259, 283 and MNHN.F.AZA 365) are curved and present two facets, the anterior one ventrally faced and the posterior one posteroventrally faced (Figs 12B, F, 14B, 15D, F, I). The posterior articular facet of the glenoid is more developed than the anterior one. The posterior margin of the glenoid facet forms a rounded swelling that sets off from the rest of the posterior border of most of the scapulae (MNHN.F.ALM 17, 29, 83, 92, 98, 113, 114, 132, 283, 298, and Sunknb 1 and 3: Figs 12A, E, 13C, E, 14A, C, 15A, C, F, 16A, C).

MNHN.F.ALM 92 and 298 are the only scapulae with preserved precoracoids and coracoids (Fig. 14). These latter are better preserved in MNHN.F.ALM 298 than in

MNHN.F.ALM 92. However, only the medial side of the coracoid and precoracoid of MNHN.F.ALM 298 can be observed. In ventral view, the coracoid appears thicker than the precoracoid. The suture between the precoracoid and coracoid cannot be observed in both specimens, the participation of the precoracoid to the glenoid cavity cannot thus be determined. The suture between the scapula and precoracoid is clearly visible in lateral view in MNHN.F.ALM 92, where it forms a weak and narrow swelling anteriorly (Fig. 14A). This suture is also visible in the medial side of MNHN.F.ALM 298 but not marked by a particular relief (Fig. 14D). The precoracoid and coracoid are poorly preserved in MNHN.F.ALM 92 and sediment covers their external surface of the both specimens MNHN.F.ALM 92 and 298. However, a coracoid foramen is noticeable and entirely surrounded by the precoracoid (Fig. 14B, D). It is located on the posterodorsal corner of the precoracoid. Below the coracoid foramen, the posteroventral region of the precoracoid is concave. The dorsal margin of the coracoid is posterolaterally faced and mainly constitutes the posteroventral margin of the glenoid fossa (Fig. 14B, D). As for the scapula, the glenoid facet of the coracoid is surrounded by a ridge on the lateral side of MNHN.F.ALM 92. This ridge runs posteriorly ending in a posteriorly pointed and thick tip (Fig. 14B). It flattens posterodorsally to form a small facet facing posterodorsally, which is surrounded by two sharp ridges projecting laterally and medially (Fig. 14B). A posterior rounded process sets off from the posterior margin of the coracoid and faces medially in MNHN.F.ALM 92. The poor preservation of the glenoid facets, as well as, the posterior margin of the coracoid in MNHN.F.ALM 298 excludes any description.

INTERCLAVICLE

The interclavicle is a flattened T-shaped bone. It is divided in two regions separated by a small constriction: a triangular anterior part extended laterally and an elongated posterior one ending by a rounded extremity (Fig. 17). The posterior region is longer than the anterior one, forming the two-thirds of the bone. In lateral view, the anterior region turns dorsally to form an angle with the rest of the bone, marked by a ventral median tuberosity. This angle is high in MNHN.F.ALM 93 and 158, as opposed to MNHN.F.ALM 278 where it is almost plate. Intermediate states were observed in MNHN.F.ALM 94, 260, and 295.

In ventral view, the triangular anterior region bears two shallow triangular fossae separated from each other by a weak swelling, clearly visible in MNHN.F.ALM 260 and

295 (Fig. 17C, H). These two fossae would accomodate the two clavicles. Two thick ridges run along the two lateral margins of the anterior region. They medially converged to a pronounced median tuberosity (MNHN.F.ALM 93, 158, and 260: Fig. 17A, H). This tuberosity is less developed in MNHN.F.ALM 94 and Intunknb 2 (Fig. 17G, J), even almost absent in MNHN.F.ALM 278 and 295 (Fig. 17C, I). The size variation of the interclavicular median tuberosity appears to be related to the angle between the anterior and posterior regions of the interclavicle. Higher is the angle between the two regions of interclavicle in lateral view, more pronounced is the interclavicular median tuberosity. No lateral ridges are observed in ventral view of Intunknb 1, and the interclavicular tuberosity is reduced to a roughened ovoid surface (Fig. 17E). The angle between the two lateral ridges merging from the interclavicular median tuberosity slightly varied from the different specimens, except in MNHN.F.ALM 260 where it is significantly more obtuse (Fig. 17). As in ventral view, the lateral margins of the anterior region of MNHN.F.ALM 93, 295 and Intunknb 1 are dorsally bordered by ridges delimiting a shallow triangular fossa (Fig. 17B, D, F).

A constriction separates the anterior and posterior regions, especially in Intunknb 1 (Fig. 17 E, F). The posterior region is flattened. It slightly widens posteriorly and ends with a flat and rounded extremity, which is articulated with the sternum. In ventral view, a large swelling arises from the interclavicular median tuberosity and posteriorly runs along the long axis of the bone to flatten at the end. The relief of this swelling seems to be related to the relief of the interclavicular process (Fig. 17C, G, H, I, J). The lateral margins of the shallow fossae extend on either side of the swelling. Nothing can be said about thus character on MNHN.F.ALM 93 because of the poor. No noticeable character is present on the dorsal side of the posterior region of the interclavicle except a short, deep, and median groove at the posterior end (Fig. 17B, D).

STERNUM

The sternum presents anterior and posterior regions bordered by sternal bosses on each lateral side (Fig. 11I). Despite the poor preservation of the posterior region, the anterior margin of the sternum appears thicker. The anterior region extends on the first third of the sternum and bears a large ovoid fossa posteriorly delimited by the sternal bosses. In fact, the thickened anterior margin medially turns in both lateral sides to form a unique pair of sternal bosses. These bosses present a rounded surface facing

anterodorsally. Two sharp crests arising from the sternal bosses to run to the posterior region along the long axis of the bone would represent articulation surfaces with ribs (e.g., Ray and Chinsamy, 2003). A large median swelling, formed by the two mentioned narrow ridges, is also observed in the posterior region as in *Placerias* (Camp and Welles, 1956) or *Dinodontosaurus* (MCZ 1692, C. Olivier pers. observ.).

Forelimb

HUMERUS

The humeri were mainly formed by two large triangular proximal and distal regions joined by a twisted short shaft. The angle of twist of humeri is variable ranging from 30° (MNHN.F.ALM 24 and 25) to 60° (MNHN.F.ALM 102, 101, and 115) with intermediate values. We assumed that this character state is highly constrained by the quality of the preservation of the bone and was affected by postmortem compression. The anteroposterior expansion of the proximal region of the humerus varies between the specimens. MNHN.F.ALM 24 presents the most expanded proximal region of the sample, in comparison with the less expanded one in MNHN.F.ALM 102 (Figs 18B, 19D). Intermediate stages have been observed in the relatively well-preserved MNHN.F.ALM 25, 101, and 115 (Figs 18E, 19E, F). Nothing can be said for MNHN.F.ALM 275 due to the postmortem compression.

On the anterodorsal margin, the humeral head forms a prominent and thick expansion onto the proximal border, clearly visible in MNHN.F.ALM 21, 25, 101, 102, 121, and 297 (Fig. 18F, K, 19G, H). The articular surface with the glenoid fossa appears triangular in shape. While well-preserved, the proximal end is missing in MNHN.F.ALM 24. The poor preservation of MNHN.F.ALM 275 does not provide information about the shape of its humeral head. The proximal expansion of the humeri is concave in posterior view (i.e., biccipital fossa) and convex in anterior one.

The dorsal margin of the proximal humeral region of most specimens (MNHN.F.ALM 24, 25, 101, 102, 121, 297 and Humunknb 1) bears the insertion for the muscle *subcoracoscapularis*, in a pinna-like process on the dorsomedial corner (Figs 18B, E, G, J, 19A, E). In posterior view, a thick tuberosity is located anterior to the insertion of m. *subcoracoscapularis* in MNHN.F.ALM 25 and 102 (Figs 18F, 19G), while there is no noticeable swelling in MNHN.F.ALM 24, 25, and Humunknb 1. As in *Dimetrodon* (Romer 1956a), this tuberosity could be the insertion site of the muscle *latissimus dorsi*. However, King (1981) and Defauw (1986) reconstructed the insertion

of this muscle in *Robertia* and *Diictodon* respectively, in a tuberosity close to the mid-shaft on the dorsodistal margin of the proximal expansion. A pinna-like process is observed at the same location in *Kannemeyeria simocephalus* (AMNH 5591/5592/5593, C. Olivier pers. observ.) and *Parakannemeyeria* (IVPP V979, C. Olivier pers. observ.). A pinna-like process is also present on the dorsal margin of the distal part of the proximal expansion in MNHN.F.ALM 24 and 102 (Figs 18B, 19D). A distinct fractured zone on the posterior margin of MNHN.F.ALM 25 is also noticeable (Fig. 18E) at the same location. According to the definition of King (1981) and Defauw (1986), this pinna-like process could be the insertion site of m. *latissimus dorsi*.

The proximal expansion is anteroventrally bordered by a well-developed deltopectoral crest, thinner in MNHN.F.ALM 24, 25, 115, and 297 than in MNHN.F.ALM 102 making it the most robust humerus. Sediment covers almost the whole posterior surface of the proximal expansion of MNHN.F.ALM 101 that needs to be more prepared to check this character. In all humeri where it is well-preserved, the deltopectoral crest is longer than 50 % of the maximal length of humeri (Figs 18B, E, 19D, E, F). The distal angle of the deltopectoral crest is more curved in MNHN.F.ALM 102 and 197 (Fig. 19D) than in MNHN.F.ALM 24, 25, and 115 (Figs 18B, E, 19E). A thick hemispherical tuberosity is observed close to the proximoventral margin of the deltopectoral crest, in posterior view of MNHN.F.ALM 24, 102, and 115 (Figs 18B, 19D, E). This bone tuberosity could participate to the insertion the m. *pectoralis* (e.g., King, 1981; Ray, 2006). The deltopectoral crest may also participate to the insertion of m. *scapulohumeralis anterior*, m. *supracoracoideus*, and m. *deltoidus*, from the proximal to distal end of the crest (e.g., Ray, 2006).

The distal expansion of humeri is formed by the entepicondyle anteriorly and the ectepicondyle posteriorly. The ectepicondyle is dorsoventrally thicker than the entepicondyle, while the entepicondyle is more anteroposteriorly elongated in ventral view forming a rectangular process clearly visible in MNHN.F.ALM 24 and 102 (Figs 18C, 19G). This well-developed and rectangular process probably offers attach zone to the flexor muscle of the forearm (Romer, 1956b). The ectepicondyle of MNHN.F.ALM 102 and 101 bears a sharp and subvertical supinator process (Fig. 19A, B) such as in *Placerias* (AMNH 4990, C. Olivier pers. observ.) and *Lisowicia* (Sulej and Niedźwiedzki, 2019). A similar process is also present in MNHN.F.ALM 121 and Humunknb 2 but more broadly elongated along the anterior border of the ectepicondyle

(Fig. 18H, K). Also, only a slight hemispherical supinator process, less marked than in MNHN.F.ALM 121, is identified in MNHN.F.ALM 24 and 25 (Fig. 18A, D). The external surfaces of these latter do not seem entirely eroded; but the ectepicondyle of MNHN.F.ALM 24 appears crushed. The ectepicondyle and entepicondyle circumscribe a deep triangular ventral fossa and a shallow triangular dorsal olecranon fossa. While the ventral fossa is clearly visible in most specimens, the olecranon fossa is unambiguously and only noticeable in MNHN.F.ALM 101 (Fig. 19H). Nothing can be said about the presence of a marked olecranon fossa in the highly eroded MNHN.F.ALM 297 and MNHN.F.ALM 24 that is affected by taphonomic compression. Sediment remains and hides the dorsal side of the distal expansion of MNHN.F.ALM 102. The entepicondylar foramen crosses the shaft and is anterodistally oriented. This foramen opens in the posterior margin of the mid-shaft and terminates in the ventral fossa of the distal humeral expansion (Figs 18A, D, J, 19A). No ectepicondilar foramen was observed. The distal expansion of the humeri bears two continuous articular surfaces: the posterior trochlea (articulation with ulna) and the anterior radial condyle (Figs 18A, D, 19A, B). This latter is entirely extended in ventral view. The articular surface of the trochlea is more developed in dorsal view than in ventral one. On the dorsal side of the distal expansion, the trochlea forms a small triangular surface marked by a sharp and anteroproximally-directed ridge. It dorsally extends in a flat hemispherical surface that borders the base of the ventral distal fossa.

RADIUS

The radii have a slender shaft and two proximal and distal regions, anteroposteriorly and mediolaterally expanded. As most of dicynodonts, the proximal expansion is slightly smaller than the distal one, clearly noticeable in MNHN.F.ALM 131 and 289 (Figs 20C, 21A). The posterior surface of the proximal and distal expansions is slightly concave as opposed to the convexity of the anterior surface. In dorsal view, the proximal articular surface is narrower laterally. The articular surfaces of the specimens are poorly preserved, making difficult more detailed description.

The posterior surface of the shaft is flat as opposed to the anterior one that presents a large swelling close to the medial border. This oblique swelling makes the medial side of the shaft looking thicker than the lateral border. It is more developed in MNHN.F.ALM 84, 287, and the unnumbered radius. On the posterior surface, a crest, runs along the long axis of the shaft, on the opposite side of the described swelling. A

thin crest also extends along of the lateral margin on the posterior surface (Figs 20B, D, F, 21B, D). The lateral margin of MNHN.F.ALM 84, 289, and the unnumbered radius is more concave than the medial border (Figs 20A, 21A, C). The distal expansion of these radii laterally projects to form a slightly squared off tubercle, clearly visible in MNHN.F.ALM 289 and the unnumbered radius (Fig. 21 A, C). While the distal expansion of MNHN.F.ALM 131 is highly crushed, the lateral margin of the long axis of the bone appears more curved than the medial one (Fig. 20C).

On the posterior surface, a roughened surface is located on the medial border of the proximal expansion of MNHN.F.ALM 131 (Fig. 20C) and could be interpreted as the insertion area for the *biceps radialis* tendon as suggested by Camp and Welles (1956). This localized insertion could not be observed in MNHN.F.ALM 289 due to a large roughened surface extended on the whole posterior side of the proximal region. The poor preservation of the proximal expansion of MNHN.F.ALM 287 and 84 precludes any dascription of this feature.

ULNA

The ulnae are mediolaterally flattened and anteroposteriorly expanded. In all completely preserved ulnae, the distal end and shaft are reduced compared to the great expansion of the proximal region. The olecranon process is well expanded beyond the articulation for humerus.

On the medial side of the ulnae, a large ovoid fossa extends on over the half of the long axis of bone, mainly in dorsal region. This fossa is deeper in MNHN.F.ALM 154 than in other specimens (Figs 22, 23). However, the deepness of this fossa may depend onto the quality of the preservation of the surrounding swellings. These latter appear highly eroded and/or fractured in most specimens. The dorsal expansion extends anteroposteriorly with a thick posterior margin and a narrow anterior one that forms a crest directed anteriorly. This crest starts on the dorsal part of the shaft and dorsally forms the anterior margin of the radial facet (Figs 22A, 23A, D). The articular surface with the radius represents a deep triangular fossa located below the anterolateral margin of the sigmoidal facet. As its anterior border, the posterior border of the radial facet is sharply demarcated by a lateral crest. This crest is more or less anteriorly directed depending on the specimens and the quality of preservation (Figs 22A, 23A, D). A second fossa is observed posteriorly to this lateral crest (Figs 22A, 23A, D). It is thus more or less expanded depending on the projection angle of the

crest. According to Ray (2006), this depression would be the insertion for m. *triceps*. The sigmoidal facet constitutes the articular surface of the olecranon process with the humerus. It forms a triangular surface with a rounded posterior corner and two anterior sharp corners: (1) the lateral corner formed by the crest limiting the radial facet posteriorly and (2) the anterior one formed by the anterior proximal crest of ulna (Figs 22A, 23A, D). The sigmoidal facet is anterolaterally faced. There is no evidence of cartilaginous suture between the olecranon process and the rest of ulna, as described in *Placerias hesternus* (Camp and Welles, 1956). The structures are difficult to observe on the lateral side of MNHN.F.ALM 126 and 154 due to their poor preservation.

The hemispherical distal articulation, relatively well preserved in MNHN.F.ALM 15, 18, 87, 126, 154, and 261 (Figs 22B, F, G, 23E), is more medially expanded than laterally. Moreover, the articular process mainly appears posteriorly directed. In ventral view, the articular surface is broader posteriorly and becomes narrower anteriorly to form a ridge. This sharp ridge starts from the distal articular surface and vanishes along the shaft in medial view. This relief is only visible in MNHN.F.ALM 15 and 87 (Fig. 23E). The erosion of the distal epiphyses of MNHN 18, 126, 154, and 261 excludes any description of these peculiar features. In anterior view, a triangular fossa is present above the distal articular process. It is dorsally pointed and clearly visible in MNHN.F.ALM 18, 154, and especially in MNHN.F.ALM 87 (Figs 22A, G, 23D). The fossa is limited by a sharp ridge, previously mentioned, medially and a second one laterally (clearly visible in MNHN.F.ALM 87). It is most likely the distal contact area with the radius. The lateral ridge, shallower than the medial one, continues the anterior proximal crest and runs along the anterior margin to posteriorly end on the distal articular process (Fig. 23D).

Pelvic girdle

A complete pelvic girdle MNHN.F.ALM 274 and isolated pelvic bones (an ilium, three ischia, and a pubis) are preserved. Distinct sutures between the three pelvic bones can clearly be observed on the right side of MNHN.F.ALM 274 (Fig. 24D). Also, the well-preserved articular surfaces of the isolated bones indicate that the three pelvic bones are not fused in *Moghreberia* (if we consider the specimen adult). This feature would indicate a flexibility of the pelvis during the life as mentioned by Cox (1959) and King (1981).

ILIUM

The ilia MNHN.F.ALM 104 and 274 are constituted by a thin dorsal iliac blade that narrows ventrally before widening to form a thick and stout articular process (Figs 24B, D, 25). The complete pelvis MNHN.F.ALM 274 shows that the ilium articulates with the ischium posteriorly and the pubis anteriorly by its ventral process. Areas of contact with the sacral ribs are visible on the medial side of the iliac plate (Fig. 25B).

The iliac blades expand anteroposteriorly to form two asymmetrical processes: a longer anterior process and a reduced posterior one (Figs 24B, 25). The right ilium of MNHN.F.ALM 274 is too poorly preserved to observe the anterior iliac process. The posterior iliac process is dorsoventrally narrower and thus appears more pointed than the anterior one. The anterior process of the left ilium of MNHN.F.ALM 274 appears less expanded than in MNHN.F.ALM 104, likely due to the postmortem distortion of the pelvis. The iliac blades are mainly concave laterally, with the iliac anterior and posterior processes curving laterally in MNHN.F.ALM 104 and the left ilium of MNHN.F.ALM 274 (Figs 24B, 25). The lateral surface of MNHN.F.ALM 104 is well preserved unlike the iliac surfaces of MNHN.F.ALM 274. While the lateral surface is mostly flat, a shallow and large ovoid fossa can be observed on the whole anterior iliac process. This fossa would correspond to the large insertion site of the anterior bundle of m. *iliofemoralis* (King, 1981). A smaller shallow depression also covers the lateral side of the posterior iliac process and would be the insertion site of the posterior bundle of m. *iliofemoralis* (King, 1981). These two large bundles of m. *iliofemoralis* would extend to the trochanter major of the femur (King, 1981). The medial side of the ilia of MNHN.F.ALM 274 is hidden by the connected sacrum. In MNHN.F.ALM 104, the incomplete and expanded distal end of the first sacral rib remains connected with the ilium (Fig. 25B). While highly eroded, the traces of the articular facets of four succeeding sacral ribs are preserved on the external surface of the medial side of the iliac blade. They are situated ventroposteriorly to the first described sacral rib (Fig. 25). Each presumed facet is marked by striations and ventrally limited by a bone thickening increasingly developed from the second to the fourth facet. Low striations marked the fifth smallest facet. Its presence is deduced from a small horizontal ridge located on the same oblique axis connecting the other bone thickenings.

The iliac blade thickens ventrally and constricts anteroposteriorly to form a neck. This latter slightly widens ventrally to constitute the dorsal region of the acetabulum

(Figs 24B, 25). Dorsally to the acetabulum facet, a roughened and thick swelling vertically runs along the neck. A similar relief has been observed in *Sangusaurus paringtonii* (Angielczyck et al., 2018). On the medial side of the neck in MNHN.F.ALM 104, the ventral limits of the fourth and fifth rib facets overhang a deep and rounded fossa (Fig. 25B).

In lateral view, a thick swelling forms the well-developed supraacetabular buttress that overhangs the acetabulum. This buttress is laterally and ventrally directed on the lateral and medial sides, respectively. (Fig. 25). A small and pointed tuberosity merges from the posterior margin of the supraacetabular buttress. The anterior part of the buttress is not preserved in both studied ilia. A notch marks the posterior corner of the supraacetabular buttress on the right ilium in MNHN.F.ALM 274. However it appears to be of taphonomic origin and no noticeable feature is observed on the buttress of MNHN.F.ALM 104 and on the left ilium in MNHN.F.ALM 274. The acetabular facet formed by the ilia is ventrally oriented. The ilium connects the puboischiatic plate ventrally to form acetabulum, a rounded and deep facet that receives the femoral head (Fig. 24 B, D). The suture between the ilium and the puboischiatic plate is oblique and anteroventrally oriented.

ISCHIUM

As well as the described ilia, the ischia MNHN.F.ALM 123, 125, 138, and 274 present three different successive regions from dorsal to ventral: an acetabular facet, an anteroposteriorly constricted neck, and a ventral region anteroposteriorly expanded. The ischium constitutes the posteroventral corner of the acetabulum. This latter is dorsolaterally oriented and ovoid (Figs 24B, D, 26A, B). A thick swelling limits the lateral margin of the acetabular facet to form a well-developed posteroventral buttress of the acetabulum. Medially, a flat surface borders the anterior corner of the dorsal articular process of the ischia (MNHN.F.ALM 123 and 125: Fig. 26B, D). This surface extends along the two thirds of the medial margin of the acetabular facet. It is anteriorly and slightly dorsally directed to articulate with the pubis. Medially, the anterior side of the acetabular facet is separated from the dorsal articular facet by a sharp ridge (Fig. 26B, D). The suture between the ilium and ischium crosses the acetabulum at mid-height (MNHN.F.ALM 274: Fig. 24B, D).

The stout dorsal articular process of the ischia only contributes to the first quarter of the dorsoventral axis of the bone. It constricts ventrally to form the posterior

margin of the ovoid obturator foramen (Fig. 24B, D, 26A, C). The ischia then abruptly widen to a large bone plate anteroposteriorly expanded. While the anterior and posterior margins of the ischiatic expansions are fractured or eroded in MNHN.F.ALM 125 (Fig. 26C), the anterior expansion clearly appears to be more anteroposteriorly expanded than the posterior one, clearly visible. The medial side of the ischia MNHN.F.ALM 123, 125, and 138 are strongly concave with the anterior and posterior expansions medially curved. The curvature of the ischia of MNHN.F.ALM 274 are less marked than in the three other specimens, most likely due to the quality of conservation. In ventral view, the bone is mediolaterally thick in its median axis and becomes thin to form the flattened anterior and posterior expansions (Fig. 26A, C). The posterior expansion is fan-shaped and seems thinner than the anterior one. In MNHN.F.ALM 123, a hemispherical tuberosity is located ventrally to the median swelling and would correspond to the insertion of m. *flexores tibiales* (Fig. 26A), as supposed by Ray (2006) in *Wadiasaurus*. A shallow depression is present on the lateral surface of the posterior ischiatic expansion. It is anteriorly limited by the thick median swelling. A flat triangular surface, located on the posterior side of the lateral region of the neck, overhangs this depression from which it is separated by a shallow swelling (Fig. 26A, C). This surface would correspond to the lateral insertion site of m. *ischio-trochantericus* (e.g., King, 1981; Ray, 2006). This muscle then turns medially to insert on the medial side of the ischium (e.g., King, 1981; Ray, 2006). The lateral side of the anterior plate expansion would contribute to the insertion of m. *pubo-ischiofemoralis externus* that also extends on the pubis (e.g., King, 1981; Ray, 2006).

PUBIS

As well as the ischia, the pubes MNHN.F.ALM 122 and 274 present a short and stout dorsal process that ventrally constricts in a neck that expands anteroposteriorly (Figs 24D, 26E). The pubis constitutes the anteroventral corner of the acetabulum and faces dorsolaterally. It is laterally bordered by a low swelling as opposed to the well-developped lateral buttresses present in the ilia and ischia. A drop-shaped and flat surface is observed close to the anteromedial corner of the acetabular facet (MNHN.F.ALM 122: Fig. 26E). As described in *Sangusaurus* (Angielczyk, 2019), it would dorsally connect the iliac supraacetabular. A second surface is present in MNHN.F.ALM 122. It is ovoid, flat, and faces posteriorly bordering the posterior margin

of the acetabular facet. This small articular surface most likely connects the dorsal process of the ischium (Fig. 26E).

Ventrally to the dorsal articular process of pubis, the bone constricts to form the anterior margin of the obturator foramen. In all preserved pubes (MNHN.F.ALM 274 and 122), a thick process merges from the neck and extends anteroventrally to constitute the pubic tubercle (Figs 24D, 26E). This tubercle bears an elongated articular surface anteroventrally facing. Laterally, a roughened surface extends from the anterodorsal corner of the lateral side to the anterior side of the pubic tubercle in MNHN.F.ALM 122 (Fig. 26E). Angielczyk et al. (2019) described a similar pitting area on the anterior edge of the pubic tubercle in *Sangusaurus*. This area has been interpreted differently by other authors, as the insertion zone of m. *ambiens* (e.g., King, 1981; Ray, 2006) or a zone contributing to the pubic symphysis covered by cartilage (Angielczyk et al., 2019). Posteriorly to the pubic tubercle, a thin bone expansion posteriorly extends to connect the ischium and form the puboischiatic plate. This latter laterally offers a large insertion zone for m. *pubo-ischiofemoralis externus* (e.g., King, 1981; Ray, 2006). The medial side of the pubes is hidden by sediment or too eroded in MNHN.F.ALM 274 and 122 respectively, preventing the interpretation of muscular insertion sites.

Hindlimb

FEMUR

The femurs are relatively robust and anteroposteriorly flat. Constricted at the shaft, the femur widens both proximally and distally to form a proximal region more developed than distal one (Figs 27, 28). The medial border of the femur is thick and straight, while the lateral one bears a narrow crest in its proximal region, the trochanteric crest. As opposed to the other preserved femurs, MNHN.F.ALM 22 presents a sigmoid border in medial view, probably caused by post-mortem compression (Fig. 27C, F, I, 28D, H). This taphonomic distortion may also explain the dorsoventral crushing of both proximal and distal ends of MNHN.F.ALM 22 (discussed below).

The femoral head is a rounded swelling that dorsally offsets from the anterior side of the proximal region (MNHN.F.ALM 21, 23, 26: Fig. 27). While the femoral heads are more or less preserved depending on specimens, all of them are anteromedially oriented. The dorsal margin is thus not continuous between the femoral head and the

great trochanter (or trochanter major), but in MNHN.F.ALM 23 most likely due to postmortem erosion. Due to a bad state of preservation, the femoral head forms a hemispherical tuberosity in MNHN.F.ALM 22 (preservation discussed above) and 284 (Fig. 28C, F), or even a weak swelling in MNHN.F.ALM 100 and 290 (Fig. 28A). Both proximal and distal epiphyses of MNHN.F.ALM 100 and 290 (two of the smallest specimens) are weakly preserved suggesting a juvenile ontogenetic stage (e.g., Gale, 1988) or because of taphonomic erosion (discussed below).

A broad and shallow ovoid fossa extends below the proximal femoral head (Figs 27B, E, H, 28B, D, G). It is dorsomedially limited by a weak swelling forming the incipient minor trochanter, posteriorly located in MNHN.F.ALM 22, 23, and 284, and more medially in MNHN.F.ALM 21 and 26. Moreover, this fossa is more or less marked depending to the specimens: deeper in MNHN.F.ALM 23, 26, and 284 than in MNHN.F.ALM 21, 22, 85, and 100. Nothing can be said about this fossa on MNHN.F.ALM 290 besause of poor preservation. The great trochanter is present in the lateral border of the femurs. It extends along more than a third of the femur, forming a distinct trochanteric crest that is almost parallel to the long axis of the bone (Figs 27, 28). Nothing can be said on the morphology of the minor and great trochanters, and the trochanteric crest of MNHN.F.ALM 85 and 290 because of the poor preservation of their proximal region. A third trochanter is present in MNHN.F.ALM 22 (Fig. 28C, D, E). It is clearly separated from the great trochanter forming a thick swelling, as in *Dolichuranus* (BP/1/4578, C. Olivier pers. observ.), *Tetragonias* (GPIT 292, C. Olivier pers. observ.) and *Dinodontosaurus* (MCZ VPRA-3105, C. Olivier pers. observ.) (Fig. 31I, J, K). However, the lateral shape of the trochanteric crest in MNHN.F.ALM 21, 23, 26, and 284 do not suggest a distinct third trochanter (Figs 27B, E, H, 28D, G). Nothing can be said about the presence of a third trochanter in MNHN.F.ALM 100 due to the poor preservation of the lateral margin of its trochanteric crest.

Two posteriorly-directed condyles constitute the distal region of the femur. The articular surface of the medial condyle is smaller than the lateral one (Figs 27, 28F). As opposed to the medial border that is continuous with the rest of the femur, the lateral margin of the distal end offsets laterally by a rectangular (MNHN.F.ALM 21, 26, 290, and 284: Figs 27A, D, 28F) tuberosity reaching the level of the lateral expansion of the trochanteric crest. The pointed shape of the tuberosity of the distal region of MNHN.F.ALM 22, 23, 100 (Figs 27G, 28A, C) appears most likely due to the erosion.

The articular condyles are distinctly separated by a shallow ventral groove that runs on the posterior side to form the intercondylar fossa. It is more clearly noticeable in MNHN.F.ALM 26 (Fig. 27E) than in MNHN.F.ALM 21, 23 and 284. The poor conservation of the distal ends of MNHN.F.ALM 85, 100, and 22 prevents the observation of this structure. Except in MNHN.F.ALM 85 and 100, all femurs present the popliteal fossa that deepens from the distal part of the shaft to the intercondylar fossa on posterior side (Figs 27B, E, H, 28D, G).

TIBIA

On both extremities of the almost rounded shaft, the proximal and distal ends are expanded with the proximal region larger than the distal one (Fig. 29A, C, E). In medial view, the tibia looks sigmoidal with a proximal and distal ends projecting anteriorly and posteriorly, respectively.

In the unnumbered tibia, the proximal articular surface is triangular in dorsal view with two concave facets for the medial and lateral condyles of the femur, and the hemispherical dorsal expansion of the cnemial crest. The proximal regions of MNHN.F.ALM 33 and 291 are too eroded to be described, in particular the shape of the articular surface. The anterior side of the proximal end is characterized by a large, median, and longitudinal cnemial crest that disappears before the mid-length of the tibia (Fig. 29A, C, E). This crest is clearly visible in the unnumbered tibia, it is highly eroded. Due to a taphonomic distortion, the cnemial crest of the unnumbered tibia (Fig. 29C) is constituted by the large proximal median tuberosity and the anteromedial thin ridge separated from each other by a narrow groove. The anterior surface of the proximal end of the cnemial crest is roughened indicating the insertion of m. *tibialis anterior* (e.g., Ray, 2006). The cnemial crest is highly eroded in MNHN.F.ALM 33 and 291. Medial and lateral fossae circumscribe on both sides of the cnemial crest in the three tibiae. In the unnumbered tibia, a lateral fossa extends proximally forming a notch in dorsal view, between the facet for the lateral condyle of the femur posterolaterally and the cnemial crest anteromedially (Fig. 29C). Medially to the cnemial crest, a shallow and triangular fossa allows the posteromedially-directed site of contact with the fibula (Fig. 29A, C).

In MNHN.F.ALM 291 (Fig. 29F), a wide crest extends on the posterior side of the tibia and flattens to the distal expansion. The proximal and distal ends of this crest

are not preserved in the unnumbered tibia and MNHN.F.ALM 33 (Fig. 29B, D). This crest runs along the long bone axis, close to the medial margin.

In anterior view, the medial margin of the distal expansion of the tibia is straighter than the lateral margin, which is more concave with a lateral process (Fig. 29B, D). A small depression marks the lateral rim and is overhung by a triangular flattened surface. The distal ends of the unnumbered tibia and MNHN.F.ALM 33 are poorly preserved. While MNHN.F.ALM 291 appears to have 'rolled' with smoothed reliefs, the round distal articulation with the femur looks a convex surface directed ventrally (Fig. 29F).

FIBULA

The fibula MNHN.F.ALM 32 consists of a spherical shaft that flattens in two large and flattened expansions (Fig. 29G). The proximal and distal articular surfaces face anterodorsally and anteroventrally, respectively. A thin longitudinal crest extends along the anterior margin of the middle of shaft. In medial view, the posterior margin is almost entirely straight compared to the anterior one, highly concave.

A shallow and large groove extends on most of the lateral side of the proximal expansion. Two flat articular surfaces, poorly preserved, extend on the proximal end: (1) the anterior tibial condyle and (2) the posterior femoral one (Fig. 29H). A large fossa, overhung by these condyles, extends on most of the proximal expansion. The anterior border of this fossa is mediolaterally thinner than the posterior one.

As for the proximal expansion, a fossa extends on the distal expansion that is anteriorly limited by a crest. While part of the distal articular condyle is missing, it appears anteromedially faced (Fig. 29H).

Phylogenetic relationships within Dicynodontia and phylogenetic position of *Moghreberia*

We hereafter follow the comprehensive taxonomic definitions of Angielczyk et al. (2009), Kammerer et al. (2013), and Olivier et al. (2019) to identify the dicynodont clades. Most of the clades in Dicynodontia are well supported, especially within Dicynodontoidae, such as Geikiidae, Kannemeyeriiformes, or Lystrosauridae.

Most of the non-dicynodontoid dicynodonts interrelationships of the present analysis are congruent with the recent phylogenetic studies (Fig. 30; e.g., Angielczyk and Kammerer, 2017; Angielczyk et al., 2018; Kammerer et al., 2019; Olivier et al.,

2019), but Emydopoidae that are not included in Endothiodontia as in Kammerer (2019b) and not the sister taxa of Phylaecephalidae as in Cox and Angielczyk (2015), Kammerer and Smith (2017), and Kammerer et al. (2017). As opposed to Cox and Angielczyk (2015), Kammerer et al. (2017, 2019), and Kammerer (2018), Cryptodontia do not comprise Rhachiocephalidae and Geikiidae, that are both considered as dicynodontoids (Fig. 30), as in Angielczyk and Kammerer (2017), Angielczyk et al. (2018), and Kammerer (2019a, 2019b). The present phylogenetic analysis resulted in Rhachiocephalidae as sister taxa of Geikiidae (Fig. 30), while they are more closely related to Lystrosauridae and Kannemeyeriiformes than to Geikiidae in Angielczyk and Kammerer (2017) and Angielczyk et al. (2018).

In all previous phylogenetic studies, the Late Permian *Australobarbarus* from Russia is placed in Oudenotontidae (e.g., Cox and Angielczyk, 2015; Angielczyk and Kammerer, 2017; Kammerer and Smith, 2017; Angielczyk et al., 2018; Kammerer, 2018, 2019b, 2019a; Kammerer et al., 2019; Olivier et al., 2019). However, our phylogeny shows a position of *Australobarbarus* more closely related to some "*Dicynodon*"-grade taxa (*Basilodon*, *Sintocephalus*, and *Euptychognathus*; i.e., taxa previously attributed to *Dicynodon* before the taxonomic revision of Kammerer et al., 2011), Kannemeyeriiformes, and Lystrosauridae than to *Rhachiocephalus*, *Oudenodon*, or *Geikia* (Fig. 30). The well-supported clade uniting *Australobarbarus* with some "*Dicynodon*"-grade taxa, Lystrosauridae, and Kannemeyeriiformes is characterized by (1) a low-developed anterior pterygoid keel (continuous character 7), (2) the posterior pterygoid rami weakly spread (continuous character 9), (3) a broadly expanded scapula (continuous character 17), (4) a posterior iliac process highly developed (continuous character 20), and (5) a contact between the pterygoids and the maxilla anteriorly (113[1]).

The clade comprising Kannemeyeriiformes, Lystrosauridae, and most of "*Dicynodon*"-grade taxa is well supported (Fig. 30) and is especially characterized by the posterior edges of the interpterygoid vacuity that flush with the median pterygoid plate (117[1]). All taxa of this clade present this character-state except the two species of *Dicynodon* (*D. angielczyki* and *D. lacerticeps*), where the vacuity is dorsal to the pterygoid mid-plate (117[0]) that constitutes a synapomorphy of the genus in the present study. However, the monophyly of the genus "*Daptocephalus*" is not supported here (Fig. 30), as opposed to Kammerer (2019a). Indeed, *D. huenei* appears more

closely related to *Dinanomodon gilli* than to *Daptocephalus leoniceps* (Fig. 30) based on: (1) a relatively larger intertemporal bar (continuous character 4), (2) a relatively longer temporal fenestra (continuous character 5), (3) a more obtuse angle between the occipital plate and the palate (continuous character 13), and (4) a notch on the dorsal edge of the naris (41[1]).

Multiple extensive definitions of the family Dicynodontidae have been proposed (e.g., Van Hoepen, 1934; Toerien, 1953; Romer, 1956b), while they are not consensual. We hereafter consider the family Dicynodontidae as the group including all taxa more related to *Dicynodon lacerticeps* (Owen, 1845) than to *Lystrosaurus murrayi* (Huxley, 1859) and to *Kannemeyeria simocephalus* (Weithofer, 1888). Dicynodontidae thus here unit *Dicynodon* and some of "*Dicynodon*"-grade taxa: *Vivaxosaurus*, *Delectosaurus*, "*Daptocephalus*", *Peramodon*, and *Dinanomodon* (Fig. 30). They constitute a well-supported clade defined by (1) an interpterygoid vacuity relatively long comparatively with other dicynodontoids like Kannemeyeriiformes and Lystrosauridae (continuous character 10), (2) long deltopectoral crest in humerus (continuous character 18), (3) a rounded snout (35[0]), (4) the presence of a circumorbital rim (62[1]), and (5) no contribution of the splenial to the dentary symphysis (154[1]). In the most phylogenetic studies (e.g., Kammerer et al., 2011; Boos et al., 2016; Angielczyk and Kammerer, 2017; Angielczyk et al., 2018; Kammerer, 2018), Dicynodontidae only include *Dicynodon lacerticeps* and *D. huenei* (= *Daptocephalus huenei* here, according to the recent taxonomic revision of Kammerer, 2019a). As well as the present study (Fig. 30), the analyses of Kammerer (2019a, 2019b) and Kammerer et al. (2019) showed *Dicynodon*, *Vivaxosaurus*, *Delectosaurus*, "*Daptocephalus*", *Peramodon*, *Dinanomodon*, and *Turfanodon* within Dicynodontidae. Olivier et al. (2019) placed the same quoted genera in Dicynodontidae; but also *Gordonia*, *Jimusaria*, *Euptychognathus*, *Sintocephalus*, and *Counillonia*.

Lystrosauridae only comprised the different species of the genus *Lystrosaurus* in Angielczyk and Kammerer (2017), Kammerer (2019a, 2019b), Kammerer et al. (2019), and Olivier et al. (2019). As well as the present study, Kammerer (2018) has also placed *Syops* in Lystrosauridae (Fig. 30), in addition to *Euptychognathus*, *Sintocephalus*, *Gordonia*, and *Jimusaria*. As opposed to Olivier et al. (2019) who placed the Loatian taxa *Counillonia* in Dicynodontidae and *Repelinosaurus* in Kannemeyeriiformes, the present analysis included them in Lystrosauridae (Fig. 30).

The two specimens attributed to *Repelinosaurus* form a clade supporting the monophyly of the genus, as previously assumed by Olivier et al. (2019). Among the synapomorphies supporting Lystrosauridae, the relatively straight suture between the frontals and nasals (58[0]), the presence of rugosities and thickenings on the postorbital bars (65[1]), and the distinct contributions of the basioccipital and exoccipitals to the occipital condyle (132[0]), distinguish *Counillonia* and *Repelinosaurus* from Kannemeyeriiformes and Dicynodontidae. The different phylogenetic positions of the Laotian dicynodonts by the present study (Fig. 30) and Olivier et al. (2019) remind the debate around the taxonomic attribution (*Lystrosaurus* or *Dicynodon*) of the lost dicynodont Counillon's (1896) specimen discovered in Laos (e.g., Das Gupta, 1922; Woodward, 1932; Yuan and Young, 1934; Piveteau, 1938; Battail, 2009; Kammerer et al., 2011).

The large clade of Kannemeyeriiformes is sister taxa of the clade uniting Dicynodontidae, Lystrosauridae, and *Turfanodon* (Fig. 30). According to the comprehensive definition of Kannemeyeriiformes proposed by Kammerer et al. (2013) as all taxa more closely related to *Kannemeyeria simocephalus* (Weithofer, 1888) than to *Lystrosaurus murrayi* (Huxley, 1859) or to *Dicynodon lacerticeps* (Owen, 1845), the late Permian *Gordonia* and *Jimusaria* are here included in this clade (Fig. 30), as in Kammerer (2019a, 2019b) and Kammerer et al. (2019). Kannemeyeriiformes are here a well-supported clade, defined by: a raised circumorbital rim (62[1]) (while absent in most kannemeyeriiforms) and a contact between the periotic and parietal (119[1]) (while uncoded in most kannemeyeriiforms). Other previous studies also placed some Permian taxa in Kannemeyeriiformes, such as *Vivaxosaurus* and *Peramodon* (Angielczyk and Kurkin, 2003; Angielczyk, 2007). Also, the analysis of Angielczyk and Kammerer (2017) placed *Dicynodon*, and the "*Dicynodon*"-grade taxa *Delectosaurus*, *Vivaxosaurus*, *Jimusaria*, *Gordonia*, *Sintocephalus*, *Euptychognathus*, *Daptocephalus*, *Peramodon*, *Dinanomodon*, and *Turfanodon* more closely related to Kannemeyeriiformes than to Lystrosauridae and to *Dicynodon lacerticeps*. The phylogenetic interrelationships of Stahleckeridae and Kannemeyeridae are mainly congruent with recent phylogenetic analyses (Fig. 30; e.g., Angielczyk and Kammerer, 2017; Kammerer et al., 2017, 2019; Angielczyk et al., 2018; Kammerer, 2018, 2019b, 2019a; Olivier et al., 2019). The two genera *Tetragonias* and *Vinceria* form a clade (Fig. 30) as in Angielczyk and Kammerer (2017), Angielczyk et al. (2018), and

Kammerer (2018), but are not included in a larger clade with *Rhinodicynodon* and *Shansiodon*, as in Olivier et al. (2019). As opposed to all recent phylogenetic studies, the kannemeyerid *Shaanbeikannemeyeria* is placed more closely related to the Chinese *Parakannemeyeria*, *Sinokannemeyeria*, and *Xiyukannemeyeria*, than to other kannemeyerids (Fig. 30). The two recently described *Pentasaurus* (Kammerer, 2018) and *Ufudocyclops* (Kammerer et al., 2019) are confirmed as members of Stahleckeridae, as in Kammerer (2018, 2019a) and Kammerer et al. (2019). Also, Sulej and Niedźwiedzki (2019) described the genus *Lisowicia* and placed it sister taxa of the clade *Moghreberia* + *Placerias*. As these previous results, the present analysis considered these three recent genera as stahleckerids (Fig. 30).

The Moroccan genus *Moghreberia* was firstly included in a computer-assisted phylogenetic analysis by Kammerer et al. (2011) who have highlighted its close relatives with the North American *Placerias* within Stahleckeridae. This phylogenetic hypothesis was accepted by subsequent studies (e.g., Castanhinha et al., 2013; Kammerer et al., 2013, 2017; Cox and Angielczyk, 2015; Boos et al., 2016; Angielczyk and Kammerer, 2017; Kammerer and Smith, 2017; Angielczyk et al., 2018; Olivier et al., 2019; Sulej and Niedźwiedzki, 2019). In the recent analyses of Kammerer (2018, 2019a, 2019b) and Kammerer et al. (2019), *Moghreberia* forms a clade with *Placerias*, *Pentasaurus*, and *Zambiasaurus*, but the phylogenetic relationships between these genera remain unresolved (i.e., polytomy). The Moroccan genus *Moghreberia* was here placed within a well-supported clade formed by *Placerias*, *Pentasaurus*, *Lisowicia*, and *Zambiasaurus* (Fig. 30), and characterized by four synapomorphies: (1) the palatal surface of premaxilla not exposed in lateral view (44[0]), (2) absence of a distinct lateral caniniform buttress (52[0]), (3) the insertion site of the *triceps* muscle developed into a prominent posterior projection (169[1]), and (4) a tall and subvertical supinator process close to the base of the humerus shaft (197[1]). As opposed to all previous studies, the present result shows that the North American *Placerias* is more closely relative to *Pentasaurus* than to *Moghreberia.* The clade *Pentasaurus* + *Placerias* is supported by the absence of curved lateral ridge between the anterior and lateral surfaces of the dentary (145[1]), as opposed to all other stahleckeriids. *Moghreberia* is here closer to *Lisowicia* than to *Placerias* (Fig. 30) forming a clade strongly supported by (1) the longest deltopectoral crest in Stahleckeridae but

Ischigualastia (continuous character 18), (2) a small contribution of the interparietal to the intertemporal skull roof (80[1]), and (3) a low-developed acromion process (170[0]).

Morphological variations in the postcranial material

The great majority of the cranial remains have been recovered in the locality XIb of the Argana Basin and attributed to *Moghreberia nmachouensis*. Also, most of the postcranial remains described here have been excavated from the locality XIb. The taphonomic data, the quality of preservation excluding any transport before fossilisation, and the concordance in size between the cranial and postcranial remains suggest that the most of postcranial remains could be attributed to the same taxon *Moghreberia nmachouensis* (Table 1). Nonetheless, we also discussed about the alternative morphotypes. Indeed, few morphological variations were highlighted in the description of the postcranial remains. First, some postcranial bones clearly appear more robust than their homologues. Then, variations in the development of bone structures have also been observed, especially on the humeri (shape of the supinator process) and femora (presence or not of a third trochanter and high erosion of articular regions). Finally, variations are noticed in the humeral twist angle, the ventral curve of the deltopectoral crest, and the shape of the proximal region of the interclavicle. These variations could be explained either by (1) intraspecific variation such as dimorphism or ontogeny, by (2) postmortem alteration, or (3) by the evidence of a distinct form from *Moghreberia* in the postcranial material. These variations are discussed under the light of the geographic locations of the sites, intraspecific variations known among dicynodonts, cranial features of the two Moroccan dicynodonts, *Moghreberia* and *Azarifeneria*, and postmortem deformation.

Dutuit (1976) mentioned the presence of a big dicynodont form, only known by postcranial material, in the lowest level of the locality XI (the locality XIa), with the scapula MNHN.F.ALM 299 (Fig. 13A-B), the humerus MNHN.F.ALM 275 (Fig. 18G), the ulna MNHN.F.ALM 154 (Fig. 22G), the femur MNHN.F.ALM 284 (Fig. 28F-H), and the tibia MNHN.F.ALM 291 (Fig. 29G-H). These specimens present big proportions and a noticeable massive appearance in comparison with their homologous bones. Nonetheless, the locality XIa also provided dicynodont postcranial remains comparable in proportions and appearance to most of the postcranial material from the locality XIb (the scapulae MNHN.F.ALM 17, 113, and 114: Fig. 13C-F; and the humerus MNHN.F.ALM 115: Fig. 19C, F, I). In parallel, postcranial remains of massive

appearance have also been excavated from the locality XIb (the rib MNHN.F.ALM 96: Fig. 10G-H; femur MNHN.F.ALM 22: Fig. 28C-E; and ulna MNHN.F.ALM 27: Fig. 23G-I) and from the locality XIII (the scapula MNHN.F.AZA 365: Fig. 15H-J).

First, a massive appearance could be explained by intraspecific variation such as ontogeny or dimorphism. Indeed, in some dicynodonts, bigger skulls appear more robust than the smaller one, as in *Repelinosaurus robustus* (Olivier et al., 2019), *Dinodontosaurus turpior* (e.g., C. Olivier pers. observ.; Lucas and Harris, 1996), and *Lystrosaurus* (e.g., Grine et al., 2006). However, this more massive appearance of the skull is frequently correlated to a more-developed ornamentations that is not the case in the massive postcranial bones from Argana. Moreover, while the humerus MNHN.F.ALM 275 (Fig. 18G), ulnae MNHN.F.ALM 27 and 154 (Figs 22G, 23G-I), and femur MNHN.F.ALM 284 (Fig. 28F-H) are bigger than their homologues, the sizes of the robust rib MNHN.F.ALM 96 (Fig. 10G-H), scapulae MNHN.F.ALM 299 (Fig. 13A-B) and MNHN.F.AZA 365 (Fig. 13A-B), femur MNHN.F.ALM 22 (Fig. 28C-E), and tibia MNHN.F.ALM 291 (Fig. 29G-H) are similar even lower than their more gracile homologous bones (Figs 10-11, 13-15, 27-29). Variation in robustness in similar size could thus be explained, on the one hand, by sexual dimorphism, as observed in *Lystrosaurus* (Ray et al., 2005), *Diictodon* (Sullivan et al., 2003), or *Pelanomodon* (Kammerer et al., 2016a). On the other hand, a distinct morphotype from *Moghreberia*, more massive, could finally be supposed to explain the clear distinction of robustness. The second Moroccan genus *Azarifeneria* is indeed distinguished from *Moghreberia* by its relevant bigger and more massive appearance. The hypothesis suggesting the association between the cranial remains of *Azarifeneria* and a massive postcranial material appears likely and it can also be observed in the highly robust humerii of *Dinodontosaurus*, be they are the smallest (e.g., MCZ 4230, C. Olivier pers. observ.) or the biggest specimen (e.g., MCZ 1687, C. Olivier pers. observ.). Nonetheless, the restudy of the cranial material of *Azarifeneria* did not emphasized significant differences distinguishing it from other Triassic genera. In addition, the cranial remains attributed to *Azarifeneria* have been excavated from the localities XIb and XII (Dutuit, 1976, 1989a, 1989b). The attribution of the massive second morphotype from the localities XIa and XIII to *Azarifeneria* could thus not be firmly concluded. In addition, except for the specimens MNHN.F.ALM 22 and 96, no diagnostic characters permit to

clearly distinguish the second morphotype from the postcranial material of *Moghreberia*.

Within the femora sample, both proximal and distal epiphyses of MNHN.F.ALM 100 and 290 (two of the smallest specimens attributed to *Moghreberia*) are highly eroded, suggesting a weak ossification and a probable juvenile ontogenetic stage (e.g., Gale, 1988). Their morphologies are similar to the femur attributed to *Zambiasaurus submersus* (Fig. 31A, B, D) that was identified as a juvenile individual (e.g., Angielczyk et al., 2014). Nevertheless, the microanatomical study of MNHN.F.ALM 100 (Olivier et al., 2017) highlighted the presence of an intense remodeling without external fundamental system (usually indicating a partially or complete arrest of growth), thus suggesting a subadult individual (e.g., Ray et al., 2005, 2010). A taphonomic origin may thus be proposed to explain the erosion of proximal and distal ends in MNHN.F.ALM 100 and 290. Similarly, the hypothesis of a juvenile ontogenetic stage of the femur NHMUK R9118 of *Zambiasaurus submersus* (e.g., Angielczyk et al., 2014) should be checked by microanatomical analysis.

The femur MNHN.F.ALM 22 is different from other specimens. It is relatively more robust (thicker shaft and larger proximal and distal regions) and presents a third trochanter. Indeed, a rugose process clearly sets off from the lateral margin of the trochanteric crest of MNHN.F.ALM 22 (Fig. 28C-D) compared to the continuous lateral margin of the femora in *Moghreberia nmachouensis* (Fig. 27), *Ischigualastia jenseni* (MCZ 378-58M, C. Olivier pers. observ.), *Kannemeyeria simocephalus* (NHMUK R3740, C. Olivier pers. observ.), *Parakannemeyeria* (IVPP V985, C. Olivier pers. observ.), and *Shansiodon* (IVPP V2415, C. Olivier pers. observ.) (Fig. 31). However, the third trochanter is rectangular and more developed in *Dolichuranus* (BP/1/4578, C. Olivier pers. observ.), *Tetragonias* (GPIT 292, C. Olivier pers. observ.), *Dinodontosaurus* (MCZ 3116, C. Olivier pers. observ.), and *Rhinodicynodon* (Surkov, 1998) than in MNHN.F.ALM 22 (Figs 28C-D, 31). A similar weak but distinct process is also present on the trochanteric crest of *Placerias hesternus* (Fig. 31; Camp and Welles, 1956; Kammerer et al., 2013), while the third trochanter have been coded ‘absent’ by Kammerer (2018). The weak but distinct third trochanteric of MNHN.F.ALM 22 and the femur of *Placerias hesternus* could be considered to represent an intermediate stage between the well-developed third trochanter of *Dolichuranus*, *Dinodontosaurus*, *Tetragonias*, and *Rhinodicynodon*, and the continuous trochanteric

crest described in all other dicynodonts known by their femurs (Fig. 31). Taphonomic erosion cannot be excluded to explain the absence of a clear third trochanter in the femurs attributed to *Moghreberia* (Figs 27-28). MNHN.F.ALM 22 is part of the smallest femurs with MNHN.F.ALM 100 and 290, the development of the third trochanter could be thus related to ontogeny. However, the previous studies supported a positive allometric relation between the development of the processes and the size of the dicynodonts (e.g., Lucas and Harris, 1996; Grine et al., 2006), as opposed to the previous assumption. In addition, while MNHN.F.ALM 22 present a similar size with MNHN.F.ALM 100, the shaft of MNHN.F.ALM 22 appears relatively larger than MNHN.F.ALM 100 and the other femora (Figs 27-28). At present, a distinct femoral morphotype (with MNHN.F.ALM 22) from *Moghreberia* appears the most likely, also supporting at least a second morphotype in the postcranial material more massive than *Moghreberia*.

The description of the humeri attributed to *Moghreberia* show a variation in the development and the shape of the supinator process. The distinct hemispherical and tab-like process is largely extended on the anterior margin of the ectepicondyle of MNHN.F.ALM 24, 25, 121, and Humunknb 2 (Fig. 18A, D, I, F), such as *Kannemeyeria simocephalus* (NHMUK R3741 and AMNH 5591/5592/5593, C. Olivier pers. observ.). *Angonisaurus cruickshanki* (NHMUK R9732, C. Olivier pers. observ.), *Stahleckeria potens* (Kammerer, 2018), and *Pentasaurus goggai* (Kammerer, 2018) (Fig. 32). However, the supinator process of MNHN.F.ALM 101 and 102 (Fig. 19A-B) is significantly more anteriorly developed but reduced along the ectepicondyle, such as *Lisowicia bojani* (Fig. 32). A similar variation of the shape of the supinator process can be noticed in *Placerias hesternus* with elongated (Fig. 32E) or reduced (Fig. 32D; e.g., Lucas, 1904; Camp and Welles, 1956; Kammerer et al., 2013) processes along the anterior margin of the ectepicondyle. Also, in *Zambiasaurus submersus*, the supinator process is either short (NHMUK R9140), or more elongated on the anterior margin of the ectepicondyle (NHMUK R9089) (Fig. 32I-J). This variation may be related to intraspecific variation, while a postmortem alteration would most likely explain it. Indeed, the supinator process is often altered during the fossilization in most of dicynodonts. Also, difference in the twist angle and the ventral curve of the deltopectoral crest in humeri may also be explained by intraspecific variation or postmortem distortion. A clearly more open twist angle of the shaft is noticed in

MNHN.F.ALM 24 and 25 (Fig. 18A, D) in regards to MNHN.F.ALM 102 and especially 101 (Fig.19A-B).

In the same way, the angle between the two lateral branches of the interclavicles differs depending on the specimen. The aperture angle is indeed clearly higher in MNHN.F.ALM 260 than in all other interclavicles (Fig. 17). Unlike the humeri, this variation is explained by intraspecific variation or by belonging to a distinct form instead of being due to a postmortem preservation.

Taxonomic revision of the Moroccan species

Distinction between Moghreberia and Placerias

Dutuit (1988) distinguished *Moghreberia* from all other dicynodonts by (1) a relatively narrow expansions of the occipital face, (2) lateral mandibular branches mainly horizontal, (3) dorsal margin of the erupted portion of the tusk anterior to the nasal cavity and, (4) a very pointed triangular anterior tip of snout. He noticed significant similarities that consider the Moroccan genus closer to *Placerias* than other forms, by (1) a similar organization of the snout, (2) premaxillae ending in a point, (3) highly reduced postorbitals and interparietal on the skull roof, and (4) convex skull roof with a high angulation of the occiput plate relative to the palate. However, *Moghreberia* has been considered synonym of the North American *Placerias* on the basis of the reconstruction of its skull by Dutuit (1988) (e.g., Cox, 1991; Hunt and Lucas, 1991; Lucas and Wild, 1995; Lucas, 2018). *Moghreberia nmachouensis* has first been included as a distinct species in the phylogenetic analyses of Kammerer et al. (2011). It was placed sister taxon of *Placerias* as originally assumed by Dutuit (1988). According to Kammerer et al. (2011), *Moghreberia* differs from *Placerias* by (1) large and elongated postnarial excavation (42[2]), (2) no caniniform depression (51[0]), (3) distinct lateral caniniform buttress with posteroventral furrow (52[2]), and (4) depressed preparietal (68[2]). The phylogenetic matrix of Kammerer et al. (2011) serves as a basis for the majority of the following phylogenetic studies in Dicynodontia. While it was continually adjusted by the authors, the coding of *Moghreberia* remains unchanged since the study of Kammerer et al. (2011) (e.g., Castanhinha et al., 2013; Kammerer et al., 2013, 2016b, 2019; Cox and Angielczyk, 2015; Boos et al., 2016; Angielczyk and Kammerer, 2017; Angielczyk et al., 2018; Kammerer, 2018). In addition, as well as in Kammerer et al. (2011), almost all the phylogenetic analyses supported *Moghreberia* closer related to *Placerias* (e.g., Castanhinha et al., 2013; Kammerer et

al., 2013, 2016b, 2019; Cox and Angielczyk, 2015; Boos et al., 2016; Angielczyk and Kammerer, 2017; Angielczyk et al., 2018). The recent inclusion of the Late Triassic *Pentasaurus* from the Elliot Fm (South Africa) in the phylogenetic analyses resulted in a polytomy between *Moghreberia*, *Placerias*, *Pentasaurus*, and *Zambiasaurus* (Kammerer, 2018, 2019a, 2019b; Kammerer et al., 2019) that Kammerer (2018) explained by the importance of the missing data for *Pentasaurus*.

As in all previous phylogenetic studies including *Moghreberia*, the present study placed the Moroccan genus in Stahleckeridae with *Angonisaurus*, *Dinodontosaurus*, *Eubrachiosaurus*, *Ischigualastia*, *Jachaleria*, *Lisowicia*, *Pentasaurus*, *Placerias, Sanguasaurus*, *Stahleckeria*, *Ufudocyclops*, and *Zambiasaurus*, especially on the basis of its narrower scapula compared to the other non-staleckeriids kannemeyeriiforms but *Tetragonias* (continuous character 17) (Fig. 30). As *Placerias*, the Moroccan genus here presents (1) a reduced fossa on the ventral surface of the intertemporal bar (76[1]), (2) stapedial facets of the parabasisphenoid-basioccipital tubera exposed ventrolaterally and open distally (122[2]; Figs 2B, 3F; Camp and Welles, 1956), (3) two sternal bosses (166[0]; Fig. 11I; Camp and Welles, 1956), (4) proeminent posterior process to insert the *triceps* muscle (169[1]; Figs 12-16; Camp and Welles, 1956), and (5) pubic plate anteroposteriorly and ventrodorsally shorter than ischium (184[1] and 185 [1]; Figs 24D, 26; Camp and Welles, 1956). However, as opposed to all previous studies, the Moroccan genus has been placed closer related to the Polish *Lisowicia* than to *Placerias* (Fig. 30). Indeed, as in Kammerer et al. (2011), *Moghreberia* differs here from *Placerias* by (1) large and elongated postnarial excavation (42[2]), (2) no caniniform depression (51[0]), (3) distinct lateral caniniform buttress with posteroventral furrow (52[2]), and (4) depressed preparietal (68[2]). The coding of some cranial and postcranial characters was revised in the present phylogenetic matrix in regards to the previous matrix of Kammerer (2018) (see Supplementary data). This highlighted the characteristics of the Moroccan genus compared to North American one by (1) low ventral expansion of the caniniform process (38[1]; Fig. 2A), (2) short internasals suture (56[1], visible in MNHN.F.ALM 37 no figured here), (3) small contribution of the interparietal to intertemporal bar (80[1]; Fig. 2A, 3E), (4) curved lateral ridge on the dentary (145[1]; Fig. 4C), (5) absent or very small acromion process (170[0]; Figs 12, 14-15), (6) insertion of the *latissimus dorsi* muscle as a pinna-like process (175[1]; Fig. 18B, E), and (7) obtuse angle between the

anterior and distal edges of the deltopectoral crest (176[1]; Figs 18B, E, 19F). Most of cranial and postcranial characters thus significantly distinguishe *Moghreberia* from *Placerias*, and unvalidate the previous hypotheses of synonymy between these two genera (e.g., Cox, 1991; Hunt and Lucas, 1991; Lucas and Wild, 1995; Lucas, 2018).

In addition, the genus *Placerias* was created and first diagnosed by Lucas (1904) on the basis of a right humerus (USNM 2198, holotype of *Placerias* type-species, *P. hesternus*). The second known species of *Placerias*, *P. gigas*, differs from *P. hesternus* on the basis of the robustness of its humerus that is more massive with broader distal condyles (Camp and Welles, 1956). The humerus of *Moghreberia* significantly differs from those of *Placerias* by an obtuse angle between the anterior and distal edges of the deltopectoral crest (Figs 18, 19, 32), as mentioned above. Moreover, the distal margin of the humeri of *Moghreberia* appears continuous between the trochlea and radial condyle (Fig. 18A, D, I, F), as opposed to *Placerias* where a distinct groove separates the two distal condyles (Fig. 32D-E; e.g., Camp and Welles, 1956; Kammerer et al., 2013). Despite the variation of the shape of the supinator in *Moghreberia* (discussed above), the supinator process of most of studied humeri represents a hemispherical and tab-like process largely extended on the anterior margin of the ectepicondyle (Fig. 18A, D, I, F). *P. gigas* and *P. hesternus* are characterized by a tall and subvertical supinator process with the dorsal margin close to the shaft (Fig. 32E; e.g., Camp and Welles, 1956; Kammerer et al., 2013). However, while poorly preserved, the pinna-like supinator process also appears on the ectepicondyle of the holotype of *Placerias* (USNM 2198: Fig. 32D; e.g., Lucas, 1904; Kammerer et al., 2013), reminding the humerus of *Moghreberia*. Nonetheless, the supinator process of USNM 2198 differs from *Moghreberia* because it is clearly more reduced and closer to the distal margin of the humerus (Figs 18A, D, I, F, 32D; e.g., Lucas, 1904; Kammerer et al., 2013).

Azarifeneria barrati

In the diagnosis of *Azarifeneria barrati*, Dutuit (1989b) highlighted the similarities of the skull roofs, occiputs, and basicrania of the Moroccan dicynodont and *Stahleckeria*. He detailed some differences between *Stahleckeria* and *A. barrati* that presents (1) a larger and longer intertemporal crest, (2) high contribution of the postorbitals to the intertemporal crest, (3) large occipital condyle, and (4) more

diverged tubers (Dutuit, 1989b). Nonetheless, Cox (1991) noticed very similar proportions between *Azarifeneria* and *Ischigualastia*.

The postorbitals have long posterior expansion in the intertemporal crest in MNHN.F.AZA 366.1. Nevertheless, they do not reach the entire length of the crest (Fig. 3B), as in *Angonisaurus* (BP 1/5530, C. Olivier pers. observ.), *Shansiodon* (IVPP V2416, C. Olivier pers. observ.), *Dinodontosaurus* (MCZ 3453, 1677, C. Olivier pers. observ.), *Ischigualastia* (Cox, 1965), and *Moghreberia* (Figs 2A, 3E), as opposed to *Stahleckeria* (e.g. Maisch, 2001; Vega-Dias et al., 2005). Moreover, like *Ischigualastia* (Cox, 1965) and *Moghreberia* (Figs 2B, 3F), the basicranium of MNHN.F.AZA 366.2 does not bear a distinct intertuberal crest (Fig. 3C), as opposed to *Stahleckeria* (AMNH 3857, C. Olivier pers. observ.). The shape of the parabasisphenoid-basioccipital tubera is distinctive in *Ischigualastia* and *Jachaleria*. They are thick, quadrangular and very close to each other (e.g., Cox, 1965; Vega-Dias and Schultz, 2004), whereas they are relatively narrower and more diverged in *Azarifeneria*, *Angonisaurus* (NHMUK R9732, C. Olivier pers. observ.), *Shansiodon* (IVPP V2416, C. Olivier pers. observ.), *Dinodontosaurus* (MCZ 1628 and 3454, C. Olivier pers. observ.), *Stahleckeria* (AMNH FARB 3857 and GSN OM-10, C. Olivier pers. observ.), and *Moghreberia* (Figs 2B, 3F). Despite the few data available on the anatomy of *A. barrati,* the morphologies of MNHN.F.AZA 366.1 and 366.2 suggest more similarities with *Moghreberia* than with *Stahleckeria* or *Ischigualastia*, as opposed to the previous conclusions of Dutuit (1989b) and Cox (1991).

Nonetheless, the revised study of MNHN.F.AZA 366.1 and 366.2 and their comparison with other kannemeyeriiforms emphasized only few even no significant differences between *A. barrati* and *Moghreberia*: (1) robustness, (2) length of intertemporal bar, (3) relative size of the occipital condyle, and (4) contribution of the postorbitals to the intertemporal bar. The major contrast between *Moghreberia* and *A. barrati* is the bone robustness. The variation of the bone thickness within dicynodont species is known in most taxa, and is mainly related to ontogeny or sexual dimorphism (e.g. Tollman et al., 1980; Lucas and Harris, 1996; Sullivan et al., 2003; Ray et al., 2005; Grine et al., 2006; Kammerer et al., 2016a; Olivier et al., 2019). This character is often associated to developed bone ornementations of dermal bones (bone rugosities, bosses and/or ridges in the nasals, frontals, prefrontals and/or postorbitals) that could not be evaluated in the present study due to the taphonomic erosion and

fragmentary skull in MNHN.F.AZA 366.1 and 366.2. The intertemporal bar of MNHN.F.AZA 366.1 appears longer than in *Moghreberia* (Figs 2A, 3B). Variations of the length of the intertemporal bar (i.e. measured from the posterior margin of the pineal foramen to the angle between the bar and the occiput) have already been noticed within some dicynodonts species. A relatively long crest has been observed in the smaller skulls in *Dolichuranus primaevus* (BP 1/4573 vs. BP 1/4570, C. Olivier pers. observ.), *Repelinosaurus robustus* (LPB 1995-9 vs. LPB 1993-2, (Olivier et al., 2019), but also in the bigger skull *Dinodontosaurus turpior* (MCZ 1679 vs. MCZ 1678, C. Olivier pers. observ.). In these cases, a negative or positive allometry may cause the variation of the relative length of the intertemporal. However, differences between skulls of almost equal size (measured from the tip of the snout to the angle between the intertemporal bar and the occiput) have also been observed in *Dinodontosaurus turpior* (AMNH 7806 and 7901; C. Olivier pers. observ.). A longer intertemporal crest in MNHN.F.AZA 366.1 may thus be due to ontogeny, sexual dimorphism, and/or intraspecific polymorphism. As noticed by Dutuit (1989b), the postorbitals of MNHN.F.AZA 366.1 cover more than half of the intertemporal length (Fig. 3B). Nevertheless, this feature can also be observed in the gracile MNHN.F.ALM 10 attributed to *Moghreberia* (Fig. 3E). The variation of the contribution of the posterior postorbital expansions to the intertemporal crest may be explained by intraspecific variation.

As mentioned above, the occipital condyle of MNHN.F.AZA 366.2 is partly filled by sediment that hides its dorsal margin and its right part made by the exoccipital. Despite its poor preservation, the relative size of the basioccipital condyle does not appear significantly different between MNHN.F.AZA 366.2 and MNHN.F.ALM 268 that was attributed to *Moghreberia* (Fig. 3A, D).

Most of the supposed differences distinguishing *A. barrati* from *Moghreberia* may thus be due to taphonomy or related to ontogeny, dimorphism, and/or intraspecific polymorphism. However, MNHN.F.AZA 366.1 and 366.2 could not be attributed with confidence to *Moghreberia nmachouensis*. Indeed, none of the diagnostic features of *Moghreberia* (Dutuit, 1988) can be checked in MNHN.F.AZA 366.1 and 366.2 due to the absence or poor preservation of the cranial structures.

Azarifeneria robustus

Dutuit (1989a) presumed the proportions of the different parts of the incomplete mandible of *Azarifeneria robustus* (MNHN.F.ALM 167) with reference to the mandible of *Stahleckeria*. He differentiated *A. robustus* from *Moghreberia* on the basis of the robustness and the inferred proportions of MNHN.F.ALM 167. Later, Cox (1991) supposed these proportions more similar to those of *Ischigualastia* mandible, than to those of *Moghreberia*.

As mentioned by Dutuit (1989a), similarities are noticeable between MNHN.F.ALM 167 and *Stahleckeria*; but also with other Triassic genera. Indeed, a massive lower jaw with a short anteroposterior expansion of the angular, abruptly curved dorsally is also observed in *Angonisaurus cruickshanki* (NHMUK R9732 and BP 1/452, C. Olivier pers. observ.), *Xiyukannemeyeria brevirostris* (IVPP V4457, C. Olivier pers. observ.), and *Stahleckeria potens* (AMNH FARB 3857, C. Olivier pers. observ.) (Fig. 33). A short and massive mandible has also been described in *Ischigualastia jenseni* (Fig. 33; Cox, 1965). In comparison, the mandible of *Moghreberia* is more gracile with a long Meckel fossa, and an angular more elongated and slightly dorsally curved (Fig. 4), as in *Kannemeyeria latirostris* (BP 1/3636, C. Olivier pers. observ.), *K. lophorhinus* (BP 1/3638, C. Olivier pers. observ.), *K. simocephalus* (NHMUK R3602, BP 1/4524 and 5624, C. Olivier pers. observ.), *Shaanbeikannemeyeria xilougouensis* (IVPP V11676, C. Olivier pers. observ.), and *Shansiodon* sp. (BP 1/5532, C. Olivier pers. observ.) (Fig. 33). Nonetheless, a variation of the anterodorsal expansion of the angular was noticed in *Stahleckeria potens* with a short and highly dorsally curved angular in AMNH FARB 3857, while it is more elongated and less curved in GSN OM-10 (Fig. 33C-D; Abdala et al., 2013).

The restudy of the mandible of *Azarifeneria robustus* highlighted three hypotheses: (1) *A. robustus* synonym of *Moghreberia nmachouensis* as supposed by Lucas and Wild (1995) and Lucas (2018), with intraspecific variation in angular as it is the case in *Stahleckeria potens*; (2) *A. robustus* distinct from *M. nmachouensis*, but synonym of another genus such as *Angonisaurus*, *Xiyukannemeyeria, Stahleckeria*, or *Ischigualastia* as supposed by Cox (1991) for this latter, or (3) *A. robustus* is a valid species. However, the poor preservation of the holotype and the only known specimen MNHN.F.ALM 167 does not allow to firmly distinguish *A. robustus* from *Moghreberia* or other kannemeyeriiforms such as *Angonisaurus*, *Xiyukannemeyeria*, *Ischigualastia*,

or *Stahleckeria*. In the absence of new data and material, *Azarifeneria robustus* should be considered a *nomen dubium*.

Acknowledgements

We want to thank the many curators and collection teams who have provided access to comparative materials: Jessica D. Cundiff (Museum of Comparative Zoology, Harvard University, Cambridge, Massachusetts, U.S.A.), Sandra Chapman (Natural History Museum, London, United Kingdom), Bernhard Zipfel (Evolutionary Studies Institute (formerly the Bernard Price Institute for Palaeontological Research and the Institute for Human Evolution), Johannesburg, South Africa), Jun Liu (Institute of Vertebrate Paleontology and Paleoanthropology, Beijing, China), and Carl Mehling (American Museum of Natural History, New York City, New York, U.S.A.). Kind thanks are also given to Jun Liu (Institute of Vertebrate Paleontology and Paleoanthropology, Beijing, China) and Christian F. Kammerer (North Carolina Museum of Natural Sciences, Raleigh, North Carolina, U.S.A.) for the pictures of the specimens GSN OM 10 and GPIT 295, respectively; and Lilian Cazes and Philippe Loubry (Centre de Recherche de Paléontologie - Paris, France) for the pictures of the Moroccan dicynodont material.

References

Abdala, F., C. A. Marsicano, R. M. H. Smith, and R. Swart. 2013. Strengthening Western Gondwanan correlations: A Brazilian Dicynodont (Synapsida, Anomodontia) in the Middle Triassic of Namibia. Gondwana Research 23:1151–1162.

Angielczyk, K. D. 2007. New specimens of the tanzanian dicynodont "*Cryptocynodon*" *parringtoni* Von Huene, 1942 (Therapsida, Anomodontia), with an expanded analysis of Permian dicynodont phylogeny. Journal of Vertebrate Paleontology 27:116–131.

Angielczyk, K. D., and A. A. Kurkin. 2003. Phylogenetic analysis of Russian Permian dicynodonts (Therapsida: Anomodontia): implications for Permian biostratigraphy and Pangaean biogeography. Zoological Journal of the Linnean Society 139:157–212.

Angielczyk, K. D., and B. S. Rubidge. 2013. Skeletal morphology, phylogenetic relationships and stratigraphic range of *Eosimops newtoni* Broom, 1921, a

pylaecephalid dicynodont (Therapsida, Anomodontia) from the Middle Permian of South Africa. Journal of Systematic Palaeontology 11:191–231.

Angielczyk, K. D., and C. F. Kammerer. 2017. The cranial morphology, phylogenetic position and biogeography of the upper Permian dicynodont *Compsodon helmoedi* van Hoepen (Therapsida, Anomodontia). Papers in Palaeontology 3:513–545.

Angielczyk, K. D., P. J. Hancox, and A. Nabavizadeh. 2018. A redescription of the Triassic kannemeyeriiform dicynodont *Sangusaurus* (Therapsida, Anomodontia), with an analysis of its feeding system. Journal of Vertebrate Paleontology 37:189–227.

Angielczyk, K. D., C. A. Sidor, S. J. Nesbitt, R. M. H. Smith, and L. A. Tsuji. 2009. Taxonomic revision and new observations on the postcranial skeleton, biogeography, and biostratigraphy of the dicynodont genus *Dicynodontoides*, the senior subjective synonym of *Kingoria* (Therapsida, Anomodontia). Journal of Vertebrate Paleontology 29:1174–1187.

Angielczyk, K. D., J.-S. Steyer, C. A. Sidor, R. M. H. Smith, R. L. Whatley, and S. Tolan. 2014. Permian and Triassic Dicynodont (Therapsida: Anomodontia) Faunas of the Luangwa Basin, Zambia: Taxonomic Update and Implications for Dicynodont Biogeography and Biostratigraphy; pp. 93–138 in Early Evolutionary History of the Synapsida. Springer, Dordrecht.

Bandyopadhyay, S. 1988. A Kannemeyeriid Dicynodont from the Middle Triassic Yerrapalli Formation. Philosophical Transactions of the Royal Society of London B: Biological Sciences 320:185–233.

Battail, B. 2009. Late Permian dicynodont fauna from Laos. Geological Society, London, Special Publications 315:33–40.

Behrensmeyer, A. K. 1975. The taphonomy and paleoecology of Plio-Pleistocene vertebrate assemblages east of Lake Rodolf, Kenya. Bulletin of the Museum of Comparative Zoology 146:473–573.

Boos, A. D. S., C. F. Kammerer, C. L. Schultz, M. B. Soares, and A. L. R. Ilha. 2016. A New Dicynodont (Therapsida: Anomodontia) from the Permian of Southern Brazil and Its Implications for Bidentalian Origins. PLoS ONE 11.

Camp, C. L., and S. P. Welles. 1956. Triassic dicynodont reptiles. Part I. The North American genus *Placerias*. Memories of the University of California 13:255–304.

Castanhinha, R., R. Araújo, L. C. Júnior, K. D. Angielczyk, G. G. Martins, R. M. S. Martins, C. Chaouiya, F. Beckmann, and F. Wilde. 2013. Bringing Dicynodonts Back to Life: Paleobiology and Anatomy of a New Emydopoid Genus from the Upper Permian of Mozambique. PLoS ONE 8:e80974.

Counillon, H. 1896. Documents pour servir à l'étude géologique des environs de Luang-Prabang (Cochinchine). Comptes Rendus de l'Académie Des Sciences, Paris 123:1330–1333.

Cox, C. B. 1959. On the anatomy of a new dicynodont genus with evidence of the position of the tympanum. Journal of Zoology 132:321–367.

Cox, C. B. 1965. New Triassic Dicynodonts from South America, Their Origins and Relationships. Philosophical Transactions of the Royal Society of London B 248:457–514.

Cox, C. B. 1991. The Pangaea dicynodont *Rechnisaurus* and the comparative biostratigraphy of Triassic dicynodont faunas. Palaeontology 34:767–784.

Cox, C. B., and K. D. Angielczyk. 2015. A New Endothiodont Dicynodont (Therapsida, Anomodontia) from the Permian Ruhuhu Formation (Songea Group) of Tanzania and Its Feeding System. Journal of Vertebrate Paleontology 35:e935388.

Cruickshank, A. R. 1975. The skeleton of the Triassic anomodont *Kannemeyeria wilsoni* Broom. Palaeontologica Africana 18:137–142.

Das Gupta, H. C. 1922. Notes on the Panchet Reptile; pp. 237–241 in Sir Asutosh Mukherjee Silver Jubilee Volumes, University Press. vol. 2. Calcutta.

Defauw, S. L. 1986. The Appendicular Skeleton of African Dicynodonts (therapsida, Dicynodontia, Permian, Triassic). unpublished PhD dissertation, Wayne State University, Detroit, USA, 248 pp.

Deenen, M., C. Langereis, W. Krijgsman, H. El Hachimi, and E. H. Chellai. 2011. Palaeomagnetic results from Upper Triassic red-beds and CAMP lavas of the Argana Basin, Morocco. Geological Society, London, Special Publications 357:195–209.

Dutuit, J. M. 1976. Introduction à l'étude paléontologique du Trias continental marocain: description des premiers stegocephales recueillis dans le couloir d'Argana (Atlas occidental). Éditions du Museum, Paris, 253 pp.

Dutuit, J. M. 1980. Principaux caractères d'un genre de Dicynodonte du Trias marocain. Comptes Rendus de l'Académie Des Sciences, Paris 290:655–658.

Dutuit, J. M. 1988. Ostéologie crânienne et ses enseignements, apports géologique et paléoécologique, de *Moghreberia nmachouensis*, Dicynodonte (Reptilia, Therapsida) du Trias supérieur marocain. Bulletin Du Muséum National d'histoire Naturelle. Section C, Sciences de La Terre, Paléontologie, Géologie, Minéralogie 10:227–285.

Dutuit, J. M. 1989a. Confirmation des affinités entre Trias supérieurs marocain et sud-américain: découverte d'un troisième Dicynodonte (Reptilia, Therapsida), *Azarifeneria robustus*, n. sp., de la formation d'Argana (Atlas occidental). Comptes Rendus de l'Académie Des Sciences. Série 2, Mécanique, Physique, Chimie, Sciences de l'univers, Sciences de La Terre 309:1267–1270.

Dutuit, J. M. 1989b. *Azarifeneria barrati*, un deuxieme genre de Dicynodonte du Trias supérieur marocain. Comptes Rendus de l'Académie Des Sciences. Série 2, Mécanique, Physique, Chimie, Sciences de l'univers, Sciences de La Terre 309:303–306.

Dutuit, J. M., and D. Heyler. 1983. Taphonomie des gisements de Vertébrés triasiques marocains (couloir d'Argana) et paléogéographie. Bulletin de La Societe Geologique de France 25:623–633.

Flynn, J. J., J. M. Parrish, B. Rakotosamimanana, W. F. Simpson, R. L. Whatley, and A. R. Wyss. 1999. A Triassic Fauna from Madagascar, Including Early Dinosaurs. Science 286:763–765.

Flynn, J. J., J. M. Parrish, B. Rakotosamimanana, L. Ranivoharimanana, W. F. Simpson, and A. R. Wyss. 2000. New Traversodontids (Synapsida: Eucynodontia) from the Triassic of Madagascar. Journal of Vertebrate Paleontology 20:422–427.

Fröbisch, J. 2009. Composition and similarity of global anomodont-bearing tetrapod faunas. Earth-Science Reviews 95:119–157.

Gale, T. M. 1988. Comments on a "nest" of juvenile dicynodont reptiles. Modern Geology 13:119–124.

Gauffre, F. 1993. The prosauropod dinosaur *Azendohsaurus laaroussii* from the Upper Triassic of Morocco. Palaeontology 36:897–908.

Goloboff, P. A. 1999. Analyzing large data sets in reasonable times: solutions for composite optima. Cladistics 15:415–428.

Goloboff, P. A., C. I. Mattoni, and A. S. Quinteros. 2006. Continuous characters analyzed as such. Cladistics 22:589–601.

Goloboff, P. A., J. S. Farris, and K. C. Nixon. 2008. TNT, a free program for phylogenetic analysis. Cladistics 24:774–786.

Grine, F. E., C. A. Forster, M. A. Cluver, and J. A. Georgi. 2006. Cranial variability, ontogeny and taxonomy of Lystrosaurus from the Karoo Basin of South Africa; pp. 432–503 in Amniote Paleobiology: Perspectives on the Evolution of Mammals, Birds, and Reptiles, University of Chicago Press. Carrano M. T., Gaudin T. J., Blob R. W. & Wible J. R., Chicago.

Huene, F. 1948. Short review of the lower tetrapods; pp. 65–106 in Robert Broom Commemorative Volume, Special Publications of theRoyal Society of South Africa. A. L. Du Toit (ed.), Cape Town.

Hunt, A. P., and S. G. Lucas. 1991. The Paleorhinus biochron and the correlation of the non-marine Upper Triassic of Pangaea. Palaeontology 34:487–501.

Huxley, T. H. 1859. On a new species of dicynodont (*D. murrayi*) from near Colesburg, South Africa; and on the structure of the skull in dicynodonts. Quarterly Journal of the Geological Society of London 15:649–659.

Irmis, R., J. Martz, W. Parker, and S. Nesbitt. 2010. Re-evaluating the correlation between Late Triassic terrestrial vertebrate biostratigraphy and the GSSP-defined marine stages. Albertiana 38:40–58.

Jalil, N. E. 1999. Continental Permian and Triassic vertebrate localities from Algeria and Morocco and their stratigraphical correlations. Journal of African Earth Sciences 29:219–226.

Jalil, N.-E., P. Janvier, and J. S. Steyer. 2009. A new cyclotosaurid (Amphibia, Temnospondyli) from the Triassic of Argana Basin (High Atlas Mountains, Morocco); biostratigraphic implications. 36–37.

Kammerer, C. F. 2018. The first skeletal evidence of a dicynodont from the lower Elliot Formation of South Africa. Palaeontologia Africana 52:102–128.

Kammerer, C. F. 2019a. Revision of the Tanzanian dicynodont *Dicynodon huenei* (Therapsida: Anomodontia) from the Permian Usili Formation. PeerJ 33.

Kammerer, C. F. 2019b. A new dicynodont (Anomodontia: Emydopoidea) from the terminal Permian of KwaZulu-Natal, South Africa. Palaeontologia Africana.

Kammerer, C. F., and R. M. H. Smith. 2017. An early geikiid dicynodont from the *Tropidostoma* Assemblage Zone (late Permian) of South Africa. PeerJ 5:e2913.

Kammerer, C. F., K. D. Angielczyk, and J. Fröbisch. 2011. A comprehensive taxonomic revision of "*Dicynodon*" (Therapsida, Anomodontia) and its implications for dicynodont phylogeny, biogeography, and biostratigraphy. Journal of Vertebrate Paleontology 31:1–158.

Kammerer, C. F., S. J. Nesbitt, and N. H. Shubin. 2012. The First Silesaurid Dinosauriform from the Late Triassic of Morocco. Acta Palaeontologica Polonica 57:277–284.

Kammerer, C. F., J. Fröbisch, and K. D. Angielczyk. 2013. On the Validity and Phylogenetic Position of *Eubrachiosaurus browni*, a Kannemeyeriiform Dicynodont (Anomodontia) from Triassic North America. PLoS ONE 8:e64203.

Kammerer, C. F., K. D. Angielczyk, and J. Fröbisch. 2016a. Redescription of the geikiid *Pelanomodon* (Therapsida, Dicynodontia), with a reconsideration of '*Propelanomodon*.' Journal of Vertebrate Paleontology 36:e1030408.

Kammerer, C. F., K. D. Angielczyk, and S. J. Nesbitt. 2017. Novel hind limb morphology in a kannemeyeriiform dicynodont from the Manda Beds (Songea Group, Ruhuhu Basin) of Tanzania. Journal of Vertebrate Paleontology 37:178–188.

Kammerer, C. F., J. J. Flynn, L. Ranivoharimanana, and A. R. Wyss. 2010. The first record of a probainognathian (Cynodontia: Chiniquodontidae) from the Triassic of Madagascar. Journal of Vertebrate Paleontology 30:1889–1894.

Kammerer, C. F., R. J. Butler, S. Bandyopadhyay, and M. R. Stocker. 2016b. Relationships of the Indian phytosaur *Parasuchus hislopi* Lydekker, 1885. Papers in Palaeontology 2:1–23.

Kammerer, C. F., P. A. Viglietti, P. J. Hancox, R. J. Butler, and J. N. Choiniere. 2019. A new kannemeyeriiform dicynodont (*Ufudocyclops mukanelai* , gen. et sp. nov.) from Subzone C of the *Cynognathus* Assemblage Zone, Triassic of South

Africa, with implications for biostratigraphic correlation with other African Triassic Faunas. Journal of Vertebrate Paleontology e1596921.

Khaldoune, F., N. E. Jalil, D. Germain, and J. S. Steyer. 2017. Les vertébrés du Permien et du Trias du Maroc (Bassin d'Argana, Haut Atlas occidental) : fenêtre ouverte sur l'évolution autour de la grande crise fin-paléozoïque. Mémoires de La Société Géologique de France 64p.

King, G. M. 1981. The functional anatomy of a Permian dicynodont. Philosophical Transactions of the Royal Society of London B: Biological Sciences 291:243–322.

King, G. M. 1988. Anomodontia; pp. 1–174 in Handbuch der Paläoherpetologie, 17. C, Fisher Verlag. G. Fisher, Stuttgart.

Klein, H., and S. Lucas. 2010. Tetrapod footprints – their use in biostratigraphy and biochronology of the Triassic. Geological Society London Special Publications 334:419–446.

Lagnaoui, A., H. Klein, H. Saber, A. Fekkak, A. Belahmira, and J. W. Schneider. 2016. New discoveries of archosaur and other tetrapod footprints from the Timezgadiouine Formation (Irohalene Member, Upper Triassic) of the Argana Basin, western High Atlas, Morocco – Ichnotaxonomic implications. Palaeogeography, Palaeoclimatology, Palaeoecology 453:1–9.

Lagnaoui, A., H. Klein, S. Voigt, A. Hminna, H. Saber, J. W. Schneider, and R. Werneburg. 2012. Late Triassic Tetrapod-Dominated Ichnoassemblages from the Argana Basin (Western High Atlas, Morocco). Ichnos 19:238–253.

Lehman, J.-P. 1961. Dicynodontia. Traité de Paléontologie 4:287–351.

Lucas, S. G. 1904. A new batrachian and a new reptile from the Triassic of Arizona. Proceeding of the U. S. National Museum 27:193–197.

Lucas, S. G. 1998. Global Triassic tetrapod biostratigraphy and biochronology. Palaeogeography, Palaeoclimatology, Palaeoecology 143:347–384.

Lucas, S. G. 2018. Late Triassic Terrestrial Tetrapods: Biostratigraphy, Biochronology and Biotic Events; pp. 351–405 in L. H. Tanner (ed.), The Late Triassic World. vol. 46. Springer International Publishing, Cham.

Lucas, S. G., and R. Wild. 1995. A Middle Triassic dicynodont from Germany and the biochronology of Triassic dicynodonts. Stuttgarter Beiträge Zur Naturkunde B 220:1–16.

Lucas, S. G., and S. K. Harris. 1996. Taxonomic and biochronological significance of specimens of the Triassic dicynodont *Dinodontosaurus* Romer 1943 in the Tübingen collection. Paläontologische Zeitschrift 70:603–622.

Maisch, M. W. 2001. Observations on Karoo and Gondwana vertebrates. Part 2: A new skull-reconstruction of *Stahleckeria potens* Von Huene, 1935 (Dicynodontia, Middle Triassic) and a reconsideration of kannemeyeriiform. Neues Jahrbuch Für Geologie Und Paläontologie - Abhandlungen 220:127–152.

Maisch, M. W. 2004. Postcranial morphology of *Rhachiocephalus* Seeley, 1898 (Therapsida: Dicynodontia) from the Upper Permian of Tanzania and the status of *Platypodosaurus robustus* Owen, 1880. Geologica et Palaeontologica 38:161–175.

Marzoli, A., H. Bertrand, K. B. Knight, S. Cirilli, N. Buratti, C. Vérati, S. Nomade, P. R. Renne, N. Youbi, R. Martini, K. Allenbach, R. Neuwerth, C. Rapaille, L. Zaninetti, and G. Bellieni. 2004. Synchrony of the Central Atlantic magmatic province and the Triassic-Jurassic boundary climatic and biotic crisis. Geology 32:973–976.

Medina, F., D. Vachard, J.-P. Colin, D. Ouarhache, and M. Ahmamou. 2001. Charophytes et ostracodes du niveau carbonaté de Taourirt Imzilen (Membre d'Aglegal, Trias d'Argana) ; implications stratigraphiques. Bulletin de l'Institut scientifique 23:21–26.

Olivier, C., A. Houssaye, N.-E. Jalil, and J. Cubo. 2017. First palaeohistological inference of resting metabolic rate in an extinct synapsid, *Moghreberia nmachouensis* (Therapsida: Anomodontia). Biological Journal of the Linnean Society 121:409–419.

Olivier, C., B. Battail, S. Bourquin, C. Rossignol, J.-S. Steyer, and N.-E. Jalil. 2019. New dicynodonts (Therapsida, Anomodontia) from near the Permo-Triassic boundary of Laos: implications for dicynodont survivorship across the Permo-Triassic mass extinction and the paleobiogeography of Southeast Asian blocks. Journal of Vertebrate Paleontology 0:e1584745.

Olsen, P. E., D. V. Kent, S. J. Fowell, R. W. Schlische, M. O. Withjack, and P. M. LeTourneau. 2000. Implications of a comparison of the stratigraphy and depositional environments of the Argana (Morocco) and Fundy (Nova Scotia, Canada) Permian-Jurassic basins. 165–183.

Owen, R. 1845. Report on the Reptilian Fossils of South Africa: PART I.-Description of certain Fossil Crania, discovered by AG Bain, Esq., in Sandstone Rocks at the South-eastern extremity of Africa, referable to different species of an Extinct genus of Reptilia (*Dicynodon*), and indicative of a new Tribe or Sub-order of Sauria. Proceedings of the Zoological Society of London 91:647–674.

Piveteau, J. 1938. Un Therapside d'Indochine. Remarques sur la notion de continent de Gondwana. Annales de Paléontologie 27:137–152.

Ray, S. 2006. Functional and evolutionary aspects of the postcranial anatomy of dicynodonts (Synapsida, Therapsida). Palaeontology 49:1263–1286.

Ray, S., and A. Chinsamy. 2003. Functional aspects of the postcranial anatomy of the Permian dicynodont *Diictodon* and their ecological implications. Palaeontology 46:151–183.

Ray, S., A. Chinsamy, and S. Bandyopadhyay. 2005. *Lystrosaurus murrayi* (Therapsida, Dicynodontia): bone histology, growth and lifestyle adaptations. Palaeontology 48:1169–1185.

Ray, S., S. Bandyopadhyay, and R. Appana. 2010. Bone Histology of a Kannemeyeriid Dicynodont *Wadiasaurus*: Palaeobiological Implications; pp. 73–89 in New Aspects of Mesozoic Biodiversity. vol. 132. Springer Berlin Heidelberg, Berlin, Heidelberg.

Romer, A. S. 1956a. The Vertebrate Body, Second edition. W.B. Saunders Company, Philadelphia, USA, 644 pp.

Romer, A. S. 1956b. Osteology of the Reptiles, University of Chicago Press, Chicago, Ill, 772 pp.

Strong, E. E., and D. Lipscomb. 1999. Character Coding and Inapplicable Data. Cladistics 15:363–371.

Sulej, T. 2002. Species discrimination of the Late Triassic temnospondyl amphibian *Metoposaurus diagnosticus*. Acta Palaeontologica Polonica 12.

Sulej, T., and G. Niedźwiedzki. 2019. An elephant-sized Late Triassic synapsid with erect limbs. Science 363:78–80.

Sullivan, C., R. R. Reisz, and R. M. H. Smith. 2003. The Permian mammal-like herbivore *Diictodon*, the oldest known example of sexually dimorphic armament. Proceedings of the Royal Society of London B: Biological Sciences 270:173–178.

Surkov, M. V. 1998. The postcranial skeleton of *Rhinodicynodon gracile* Kalandadze, 1970 (Dicynodontia). Paleontological Journal 32:402–409.

Surkov, M. V., and M. J. Benton. 2004. The basicranium of dicynodonts (Synapsida) and its use in phylogenetic analysis. Palaeontology 47:619–638.

Tixeront, M. 1973. Lithostratigraphie et minéralisation cuprifères et uranifères stratiformes syngénétiques et familières des formations detritiques permo-triasiques du Couloir d'Argana Haut-Atlas occidental (Maroc). Notes Service Geologique Maroc 33:147–177.

Toerien, M. J. 1953. The evolution of the palate in South African Anomodontia and its classificatory significance. Paleontologica Africana 1:49–117.

Tollman, S. M., F. E. Grine, and B. D. Hahn. 1980. Ontogeny and sexual dimorphism in *Aulacephalodon* (Reptilia, Anomodontia). Annals of the South African Museum 8:159–186.

Tourani, A., J. J. Lund, N. Benaouiss, and R. Graupp. 2000. Stratigraphy of Triassic syn-rift deposition in Western Morocco. Zentralblatt Für Geologie Und Paläontologie 9–10:1193–1215.

Van Hoepen, E. C. N. 1934. Oor die indeling van die Dicynodontidae na aanleiding van nuew vorme. Paleontologiese Navorsing van Die Nasionale Museum 2:67–101.

Vega-Dias, C., and C. L. Schultz. 2004. Postcranial material of *Jachaleria candelariensis* Araújo and Gonzaga 1980 (Therapsida, Dicynodontia), Upper Triassic of Rio Grande do Sul, Brazil. PaleoBios 24:7–31.

Vega-Dias, C., M. W. Maisch, and C. Schwanke. 2005. The taxonomic status of *Stahleckeria impotens* (Therapsida, Dicynodontia): redescription and discussion of its phylogenetic position. Revista Brasileira de Paleontologia 8:221–228.

Weithofer, A. 1888. Ueber einen neuen Dicynodonten (*Dicynodon simocephalus*) aus der Karrooformation Südafrikas. Annalen Des Naturhistorischen Museums in Wien 3:1–6.

Whiteside, J. H., P. E. Olsen, D. V. Kent, S. J.Fowell, and M. Et-Touhami. 2007. Synchrony between the Central Atlantic magmatic province and the Triassic–Jurassic mass-extinction event? Palaeogeography, Palaeoclimatology, Palaeoecology 244:345–367.

Woodward, A. S. 1932. Dicynodontidae; pp. 257–260 in Textbook of Palaeontology. vol. 2. Von Zittel, K. A. (ed.).

Yuan, P. L., and C. C. Young. 1934. On the Occurrence of *Lystrosaurus* in Sinkiang. Bulletin of the Geological Society of China 12:575–580.

Figure captions

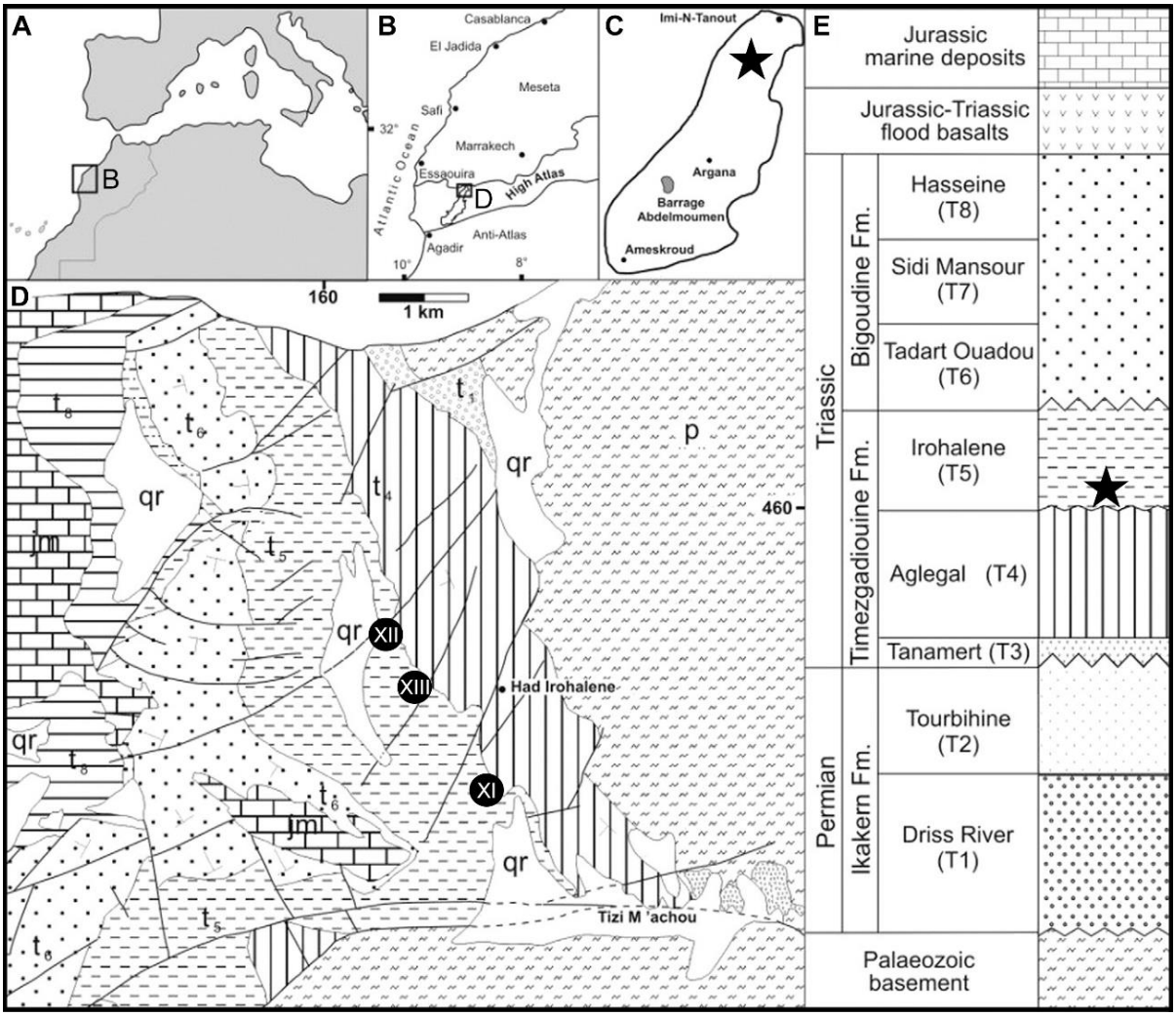

Figure 1. Geographic and stratigraphic position of dicynodont remains localities XI, XII, and XIII (Dutuit's nomenclature). A-C, Position in Morocco and in the Argana Basin of the two localities indicated by a star in C; D, Geological map with dicynodont localities XI, XII, and XIII; E, Stratigraphic section of the Argana Basin showing the level of the two localities indicated by a star. Geographic and geological maps, and stratigraphic section modified from Lagnaoui et al. (2016).

Figure 2. Lectotype of *Moghreberia nmachouensis* (MNHN.F.ALM 280), skull figured in dorsal (A), ventral (B), and posterior (C) views. The scale bar represents 5 cm.

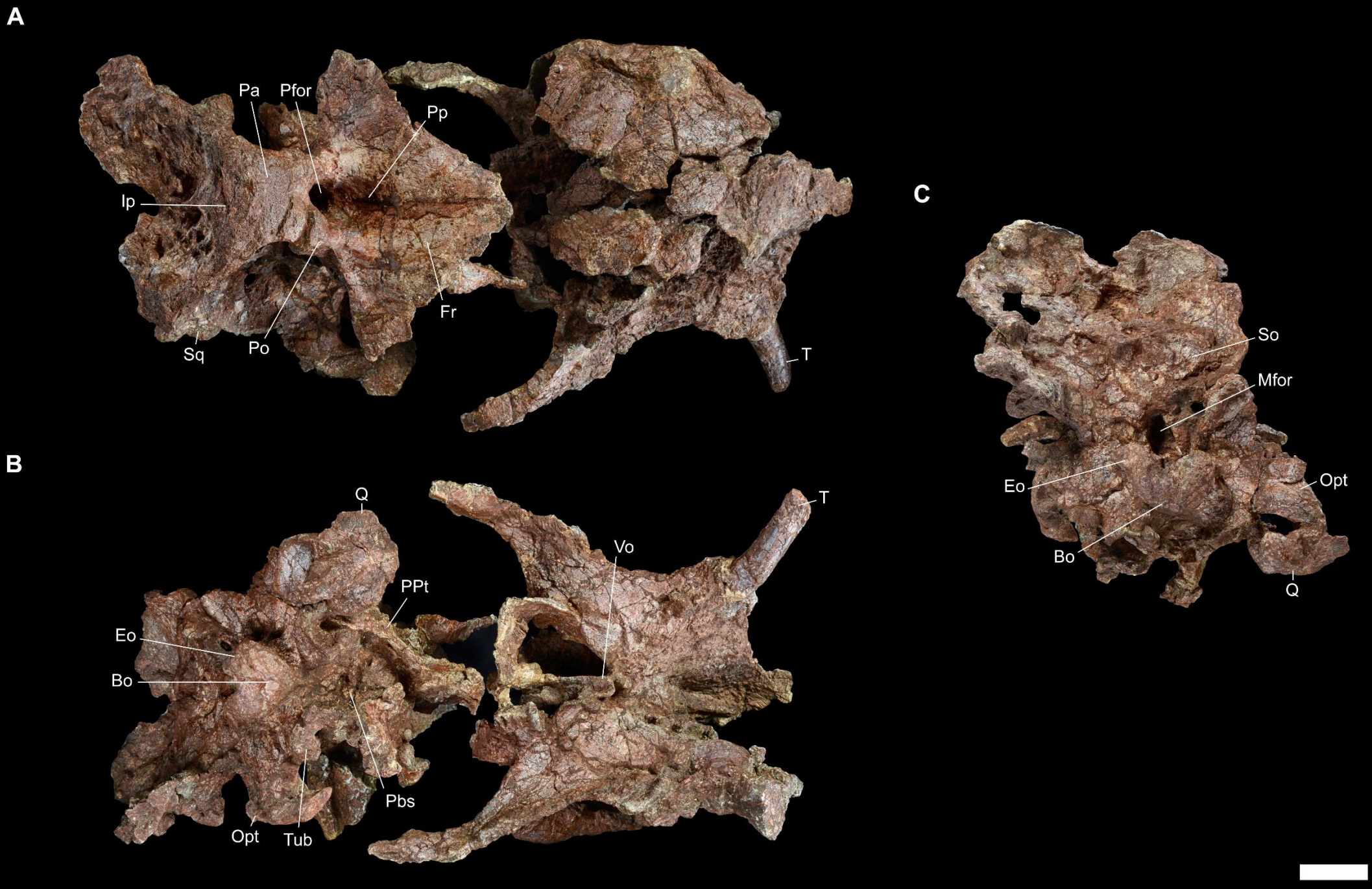
A
Pa
Pfor
Pp
Ip
Fr
Sq
Po
T
B
Q
T
Vo
PPt
Eo
Bo
Pbs
Opt
Tub
C
So
Mfor
Eo
Opt
Bo
Q

Figure 3. Holotypes of *Azarifeneria barrati* and cranial material attributed to *Moghreberia nmachouensis*, figured in posterior (A, D), dorsal (B, E), and ventral (C, F) views. **A, C**, MNHN.F.AZA 366.2: occipital plate of *A. barrati*; **B**, MNHN.F.AZA 366.1 and 366.3 connected forming the parieto-squamosal region of *A. barrati*; **D, F**, MNHN.F.ALM 268: occipital plate attributed to *M. nmachouensis*; **E**, MNHN.F.ALM 10: posterior region of the skull roof attributed to *M. nmachouensis*. The scale bars represent 5 cm.

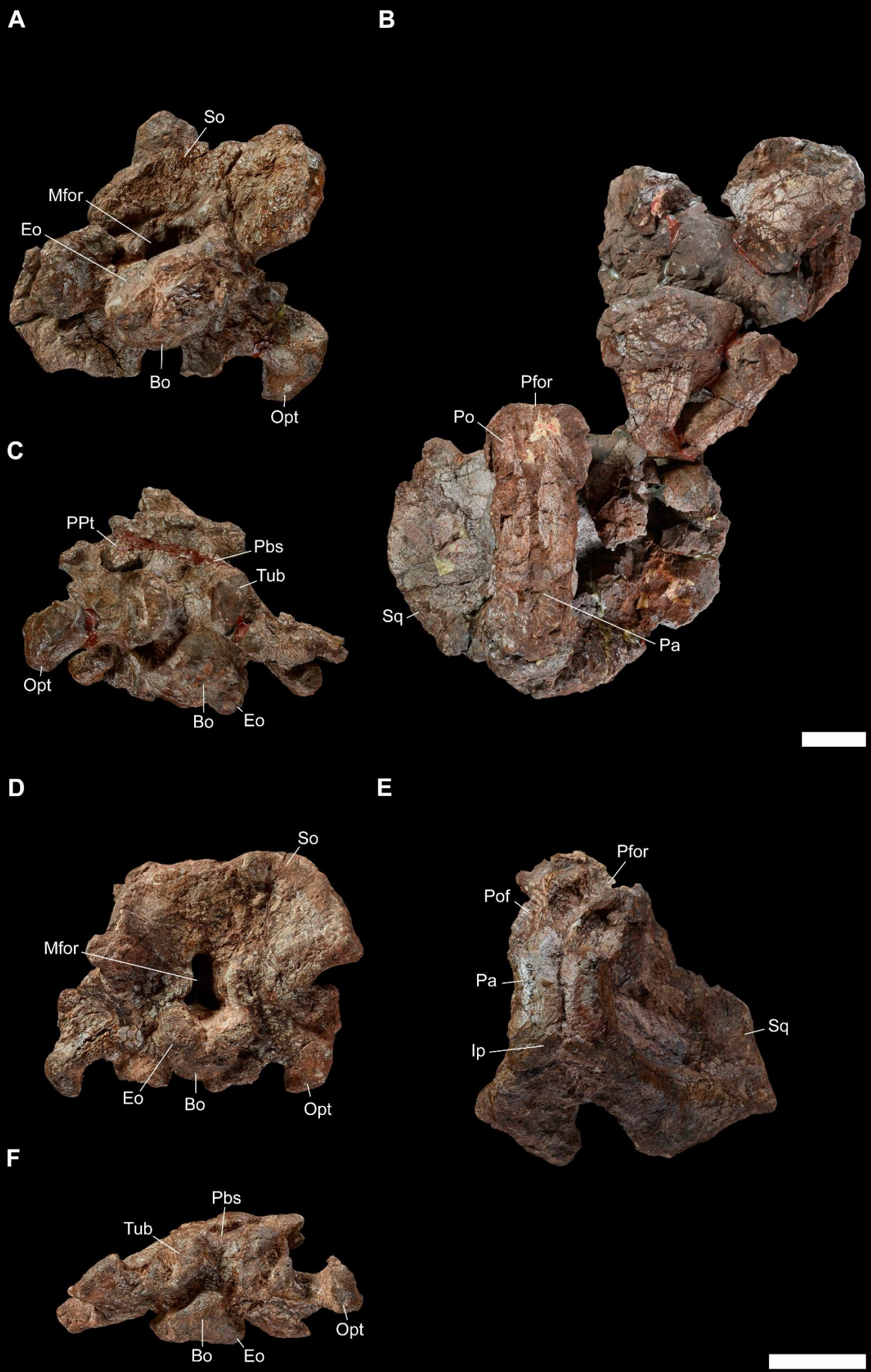
A
So
Mfor
Eo
Bo
Opt
B
Pfor
Po
Sq
Pa
C
PPt
Pbs
Tub
Opt
Bo
Eo
D
So
Mfor
Eo
Bo
Opt
E
Pfor
Pof
Pa
Sq
Ip
F
Pbs
Tub
Opt
Bo
Eo

Figure 4. Holotypes of *Azarifeneria robustus* and madibular material attributed to *Moghreberia nmachouensis*, figured in dorsal (A, D), ventral (B, E), and lateral (C, F) views. **A-C**, MNHN.F.ALM 38: mandible attributed to *M. nmachouensis*; **B-F**, MNHN.F.ALM 167: anterior portion of the mandible of *A. robustus*. The scale bar represents 5 cm.


A
D
Dt
Pds
S
A
B
D
Mdr
S
Lra
A
C
Mf
D
Ldr
A
Lra
D
D
Pds
A
E
D
S
Lra
A
F
D
Mf
Mdr
Ldr
A
Lra

Figure 5. Vertebrae attributed to *Moghreberia nmachouensis* and supposed to be last cervical and/or first dorsal vertebrae, figured in anterior (A, C), posterior (B, E), right lateral (D), and left lateral (F) views. **A-B**, MNHN.F.ALM 288; **C-F**, two unnumbered connected vertebrae called ‘Vunknb 1 and 2’, with the centra indicated by ‘Ct 1 and 2’ following the anteroposterior vertebral axis. The scale bar represents 5 cm.

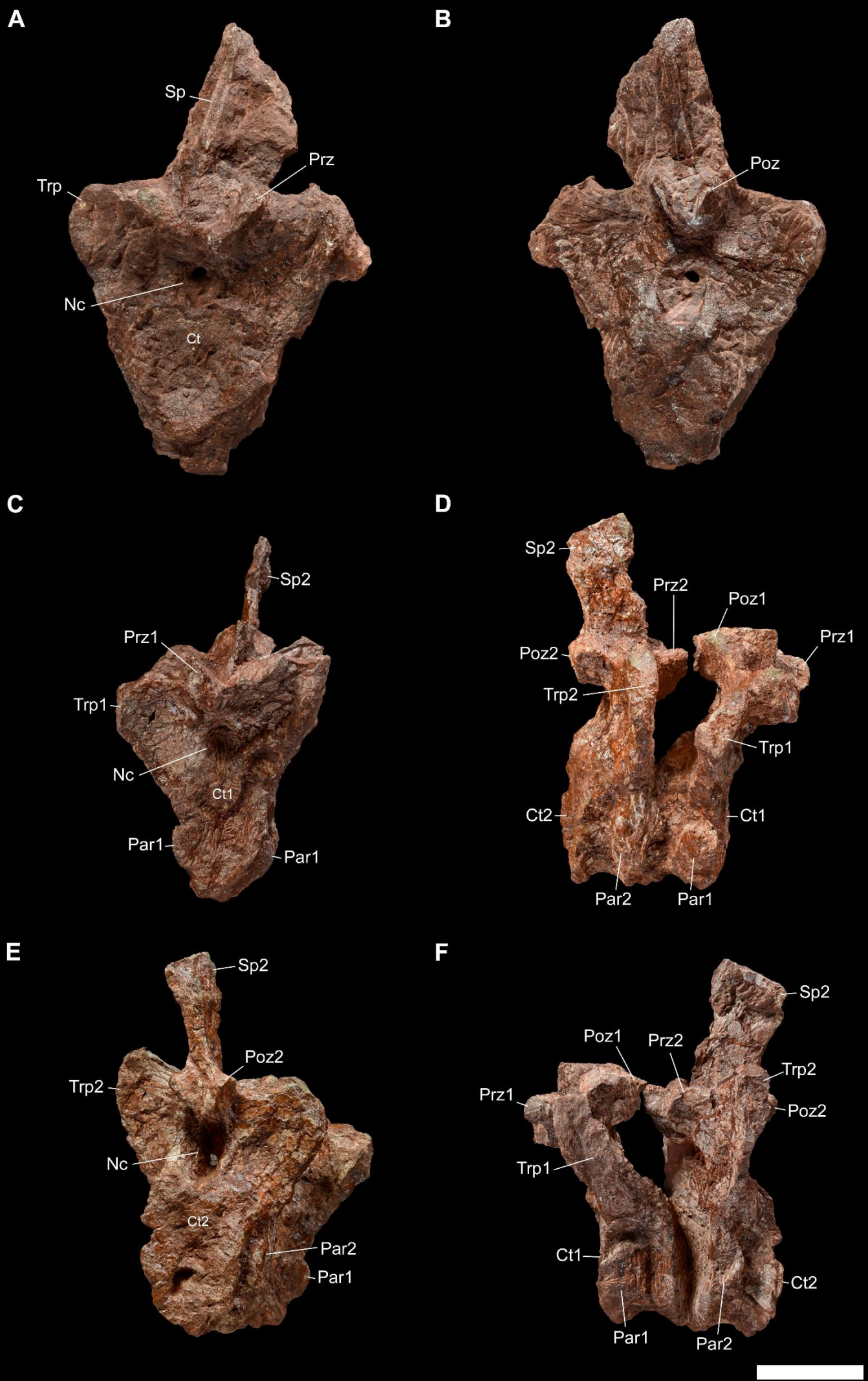
A
Sp
Prz
Trp
Nc
Ct
B
Poz
C
Sp2
Prz1
Trp1
Nc
Ct1
Par1
Par1
D
Sp2
Prz2
Poz1
Prz1
Poz2
Trp2
Trp1
Ct2
Ct1
Par2
Par1
E
Sp2
Poz2
Trp2
Nc
Ct2
Par2
Par1
F
Sp2
Poz1
Prz2
Trp2
Prz1
Poz2
Trp1
Ct1
Ct2
Par1
Par2

Figure 6. Dorsal vertebrae attributed to *Moghreberia nmachouensis*, figured in anterior (A, C), posterior (E, G), right anterolateral (F), right lateral (B, D), and left lateral (H) views. **A-B, E-F**, MNHN.F.ALM 120: four connected vertebrae, with the centra indicated by 'Ct 1, 2, 3, and 4' following the anteroposterior vertebral axis; **C-D, G-H**, MNHN.F.ALM 159: two connected vertebrae, with the centra indicated by 'Ct 1 and 2' following the anteroposterior vertebral axis. The scale bar represents 5 cm.

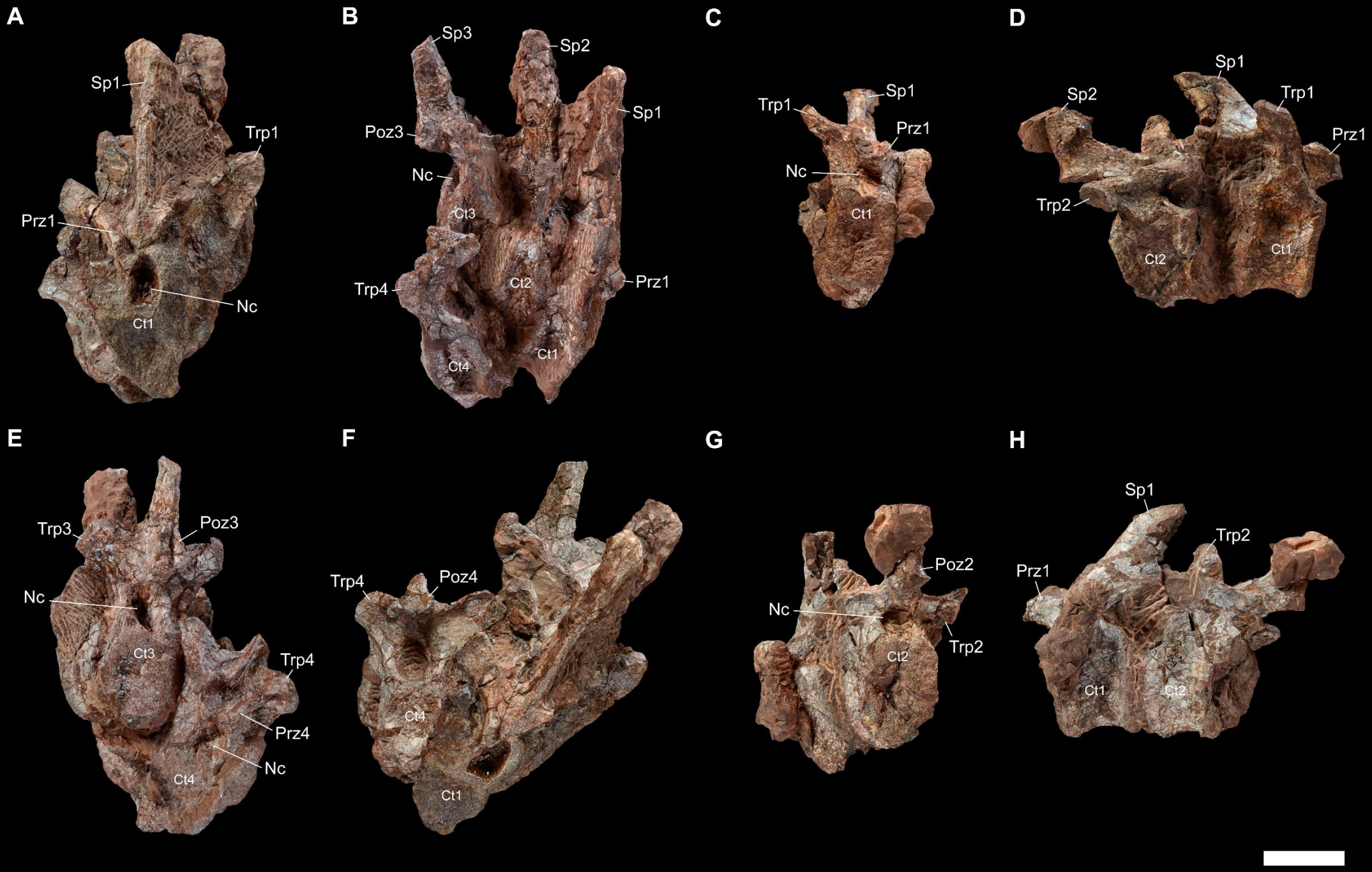
A
Sp1
Trp1
Prz1
Nc
Ct1
B
Sp3
Sp2
Sp1
Poz3
Nc
Ct3
Trp4
Ct2
Prz1
Ct4
Ct1
C
Sp1
Trp1
Prz1
Nc
Ct1
D
Sp1
Sp2
Trp1
Prz1
Trp2
Ct2
Ct1
E
Trp3
Poz3
Nc
Ct3
Trp4
Prz4
Nc
Ct4
F
Trp4
Poz4
Ct4
Ct1
G
Poz2
Nc
Trp2
Ct2
H
Sp1
Trp2
Prz1
Ct1
Ct2

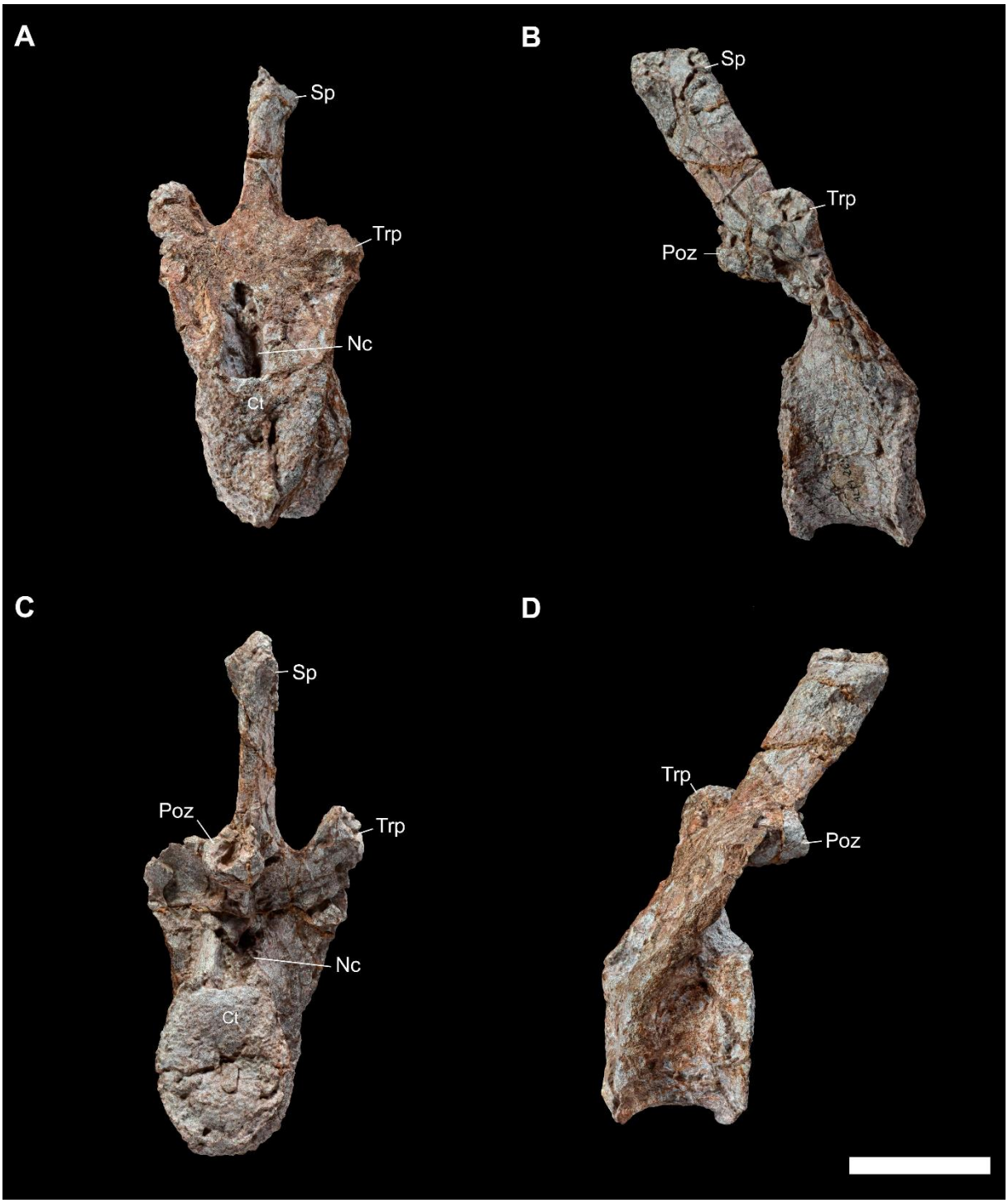

Figure 7. MNHN.F.ALM 265, dorsal vertebra attributed to *Moghreberia nmachouensis*, figured in anterior (A), posterior (C), right lateral (B), and left lateral (D) views. The scale bar represents 5 cm.

Figure 8. MNHN.F.ALM 274, two disconnected but associated posterior dorsal vertebrae attributed to *Moghreberia nmachouensis*, figured in anterior (A, C), posterior (E, G), right lateral (B, D), and left lateral (F, H) views. **A-B, E-F**, MNHN.F.ALM 274-1; **C-D, G-H**, MNHN.F.ALM 274-2. These two vertebrae were discovered in association with a complete pelvic girdle (with sacral and caudal vertebrae) represented in Fig. 24. The scale bar represents 5 cm.

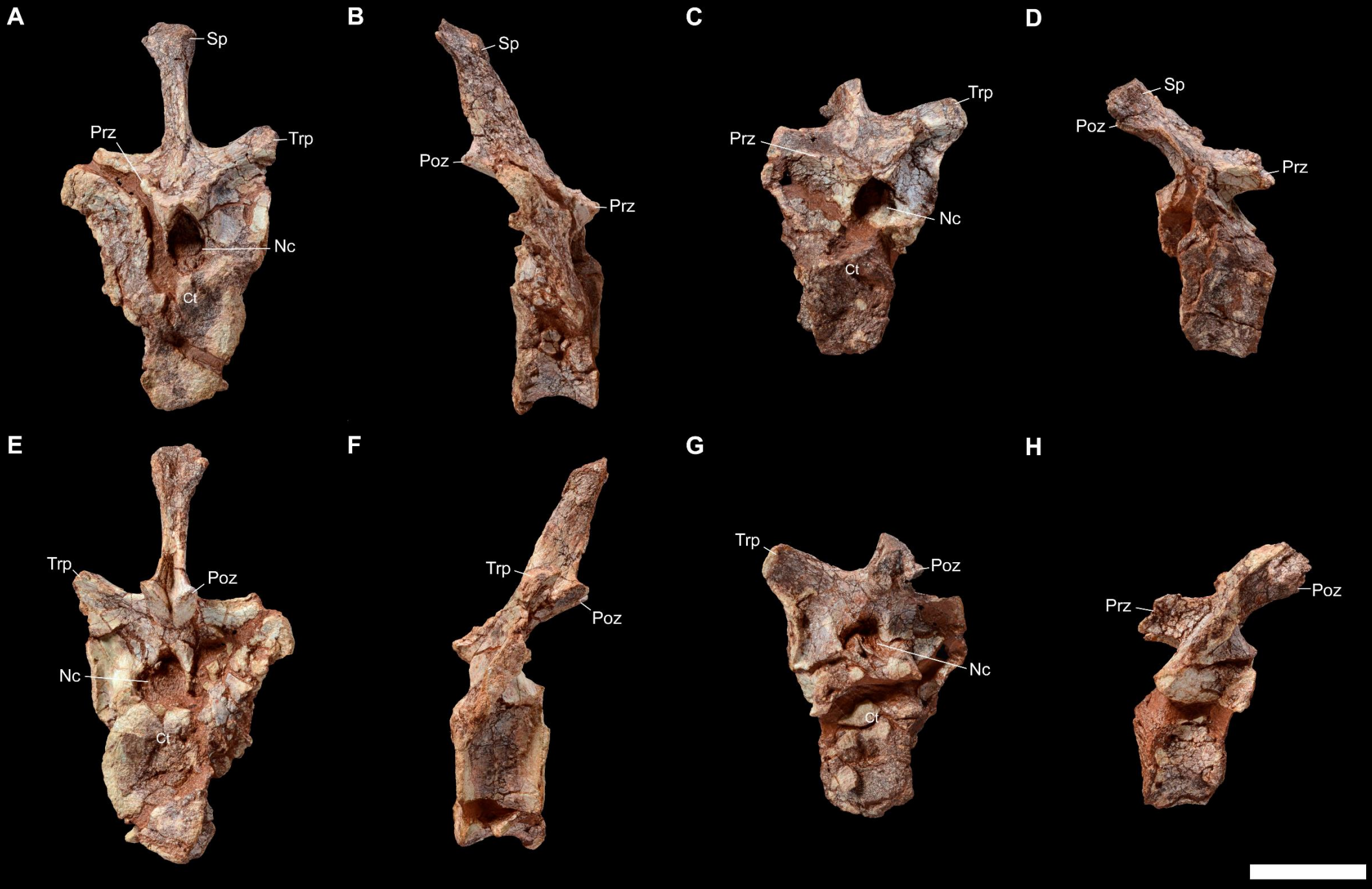
A
Sp
Prz
Trp
Nc
Ct
B
Sp
Poz
Prz
C
Trp
Prz
Nc
Ct
D
Sp
Poz
Prz
E
Trp
Poz
Nc
Ct
F
Trp
Poz
G
Trp
Poz
Nc
Ct
H
Prz
Poz

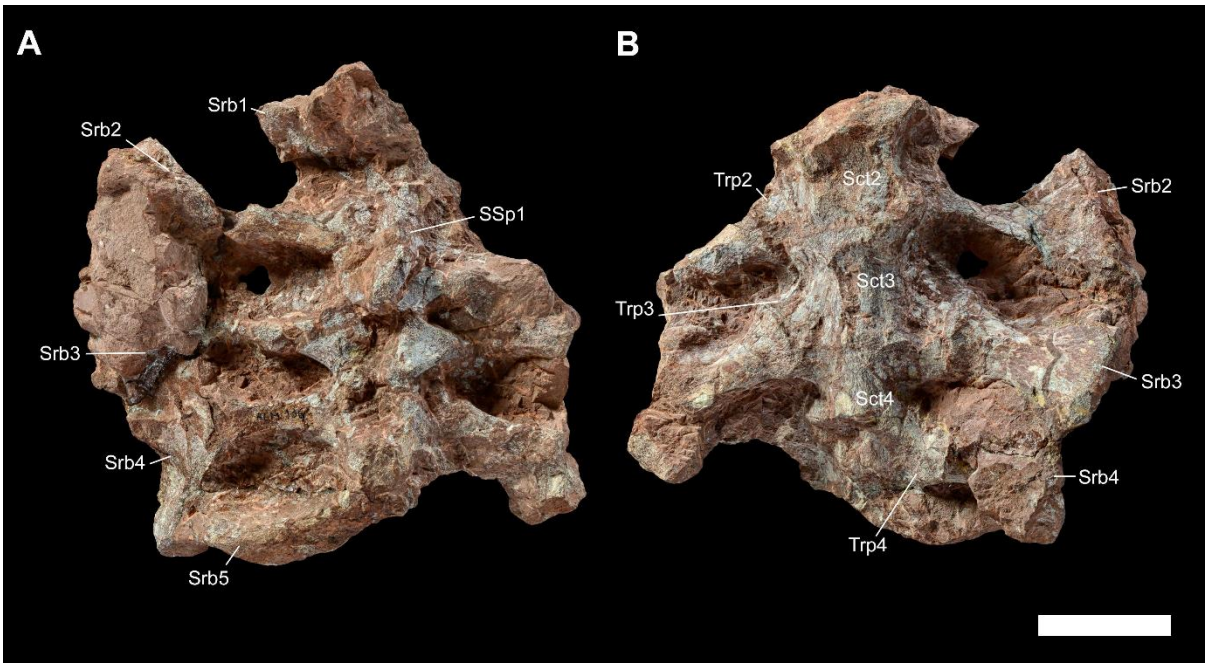

Figure 9. MNHN.F.ALM 136, incomplete sacrum attributed to *Moghreberia nmachouensis*, figured in dorsal (A) and ventral (B) views. The sacral centra were indicated by 'Sct 2, 3, and 4' following the anteroposterior vertebral axis. The scale bar represents 5 cm.

Figure 10. Anterior dorsal ribs and head ribs attributed to *Moghreberia nmachouensis* (except for MNHN.F.ALM 96 currently unattributed), figured in posterior (A, C, E, H, I, L) and anterior (B, D, F, G, J, K) views. **A-B**, MNHN.F.ALM 91: left rib; **C-D**, MNHN.F.ALM 90: left rib; **E-F**, MNHN.F.ALM 296: left rib; **G-H**, MNHN.F.ALM 96: right rib; **I-J**, left unnumbered head rib; **K-L**, MNHN.F.ALM 163: right head rib. The arrow head represents the marked constriction between the discontinuous tuberculm and capitelum. The scale bar represents 5 cm.


A
Crest
B
Crest
Groove
C
Crest
Rpr
D
Crest
Groove
E
Crest
Rpr
F
Crest
Groove
G
Crest
Groove
H
Crest
I
J
K
L

Figure 11. Sternum and posterior dorsal ribs and head rib attributed to *Moghreberia nmachouensis*, figured in posterior (A, C, F, H), anterior (B, D, E, G), and ventral (I) views. **A-B**, MNHN.F.ALM 86: left rib; **C-D**, MNHN.F.ALM 95: left rib; **E-F**, MNHN.F.ALM 97: right rib; **G-H**, MNHN.F.ALM 272: right head rib; **I**, MNHN.F.ALM 134: sternum. The scale bar represents 5 cm.


A
B
Groove
C
D
Groove
E
Groove
F
Rpr
G
H
I
boss

Figure 12. Scapulae attributed to *Moghreberia nmachouensis*, figured in lateral (A, C, E), and medial (B, D, F) views. **A-B**, MNHN.F.ALM 29: right scapula; **C-D**, MNHN.F.ALM 30: left scapula; **E-F**, MNHN.F.ALM 83: left scapula. The scale bar represents 5 cm.


A
Serasup
Delt
Acr
Supco
Glef
B
Subco
Tri
C
Acr
Supco
D
Tri
E
Serasup
Delt
Acr
Supco
Glef
F
Subco
Prsf
Tri

Figure 13. Scapulae attributed to *Moghreberia nmachouensis* (except for MNHN.F.ALM 299 currently unattributed), figured in lateral (A, C, E), and medial (B, D, F) views. **A-B**, MNHN.F.ALM 299: right scapula; **C-D**, MNHN.F.ALM 17: left scapula; **E-F**, MNHN.F.ALM 113: left scapula. The scale bar represents 5 cm.


A
Tri
B
Serasup
Delt
Supco
C
Serasup
Delt
Acr
Glef
D
Tri
E
Supco
Glef
F
Tri

Figure 14. Scapulocoracoids attributed to *Moghreberia nmachouensis*, figured in lateral (A, C), and medial (B, D) views. **A-B**, MNHN.F.ALM 92: left scapulocoracoid; **C-D**, MNHN.F.ALM 298: left scapulocoracoid. The scale bar represents 5 cm.


A
Corfor
Glef
B
Tri
facet
Corfor
C
Delt
Acr
Glef
D
Subco
Prsf
Tri
Corfor

Figure 15. Scapulae attributed to *Moghreberia nmachouensis* (except for MNHN.F.AZA 365 currently unattributed), figured in lateral (A, C, F, H), medial (B, D, G, I), and ventral (E, J) views. **A-B**, MNHN.F.ALM 98: left scapula; **C-E**, MNHN.F.ALM 132: left scapula; **F-G**, MNHN.F.ALM 283: right scapula; **H-J**, MNHN.F.AZA 365: right scapula. The scale bar represents 5 cm.


A
Glef
B
Tri
C
Acr
Supco
Glef
D
Tri
E
Glef
F
Acr
Glef
G
Subco
Prsf
Tri
H
Supco
Glef
I
Tri
J
Glef

Figure 16. Scapulae attributed to *Moghreberia nmachouensis*, figured in lateral (A, C, D) and medial (B, E, F) views. **A-B**, right unnumbered scapula called ‘Sunknb 3’; **C-F**, right unnumbered scapula called ‘Sunknb 1’; **D-E**, left unnumbered scapula called ‘Sunknb 2’. The scale bar represents 5 cm.


A
B
C
Supco
Glef
Tri
Glef
Supco
D
E
F
Delt
Supco
Tri

Figure 17. Interclavicles attributed to *Moghreberia nmachouensis* (except for MNHN.F.ALM 260 currently unattributed), figured in ventral (A, C, E, G-J) and dorsal (B, D) views. **A-B**, MNHN.F.ALM 93; **C-D**, MNHN.F.ALM 295; **E-F**, unnumbered interclavicle called 'Intunknb 1'; **G**, MNHN.F.ALM 94; **H**, MNHN.F.ALM 260; **I**, MNHN.F.ALM 278; **J**, unnumbered interclavicle called 'Intunknb 2'. The scale bar represents 5 cm.

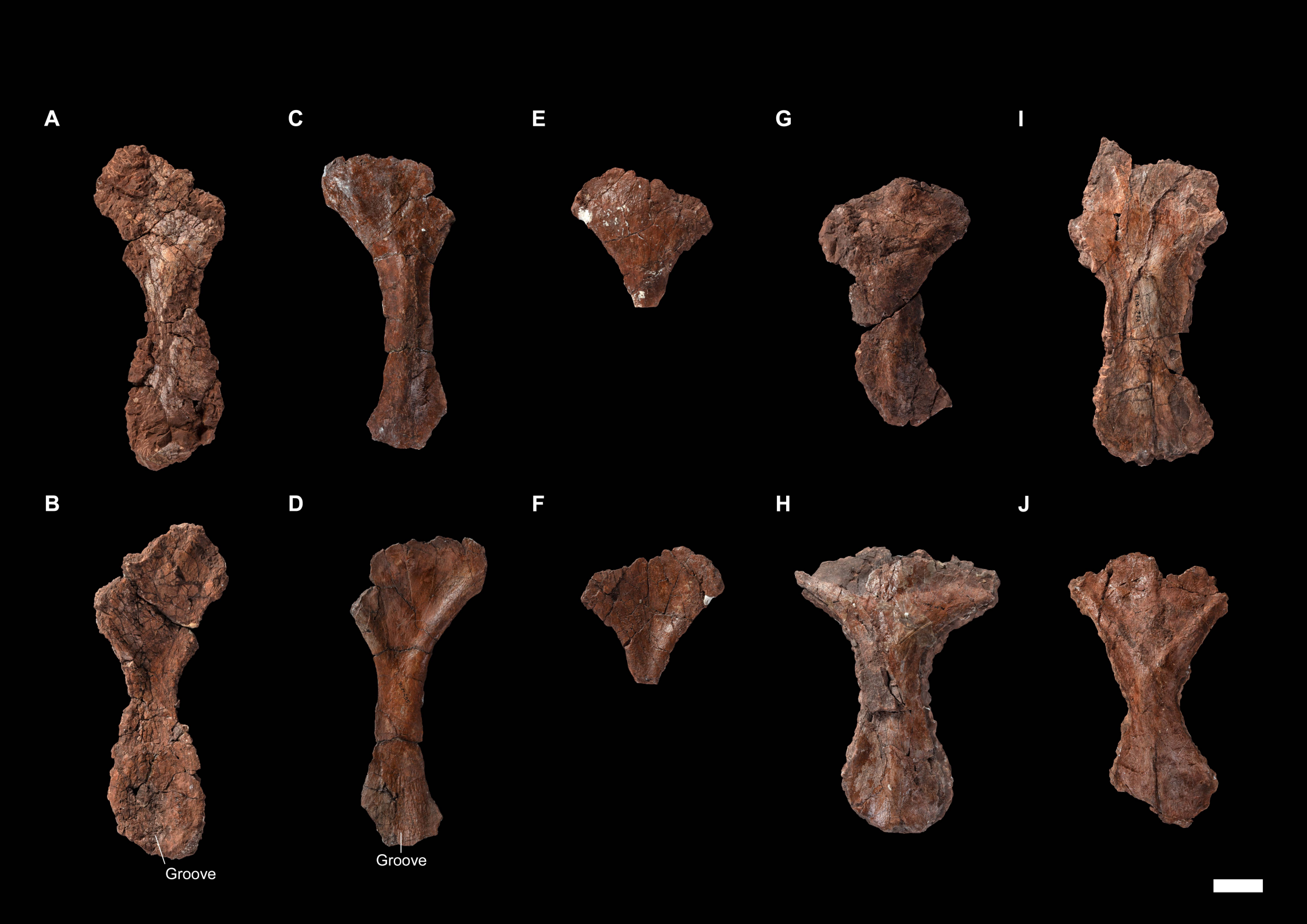
A
C
E
G
I
B
D
F
H
J
Groove
Groove

Figure 18. Humerii attributed to *Moghreberia nmachouensis* (except for MNHN.F.ALM 275 currently unattributed), figured in ventral (A, D, G, H, J), anteroventral (B, E), and dorsal (C, F, I, K) views. **A-C**, MNHN.F.ALM 24: left humerus; **D-F**, MNHN.F.ALM 25: left humerus; **G**, MNHN.F.ALM 275: left humerus; **H-I**, distal region of a right unnumbered humerus called ‘Humunknb 2’; **J-K**, MNHN.F.ALM 121: left humerus. The scale bar represents 5 cm.

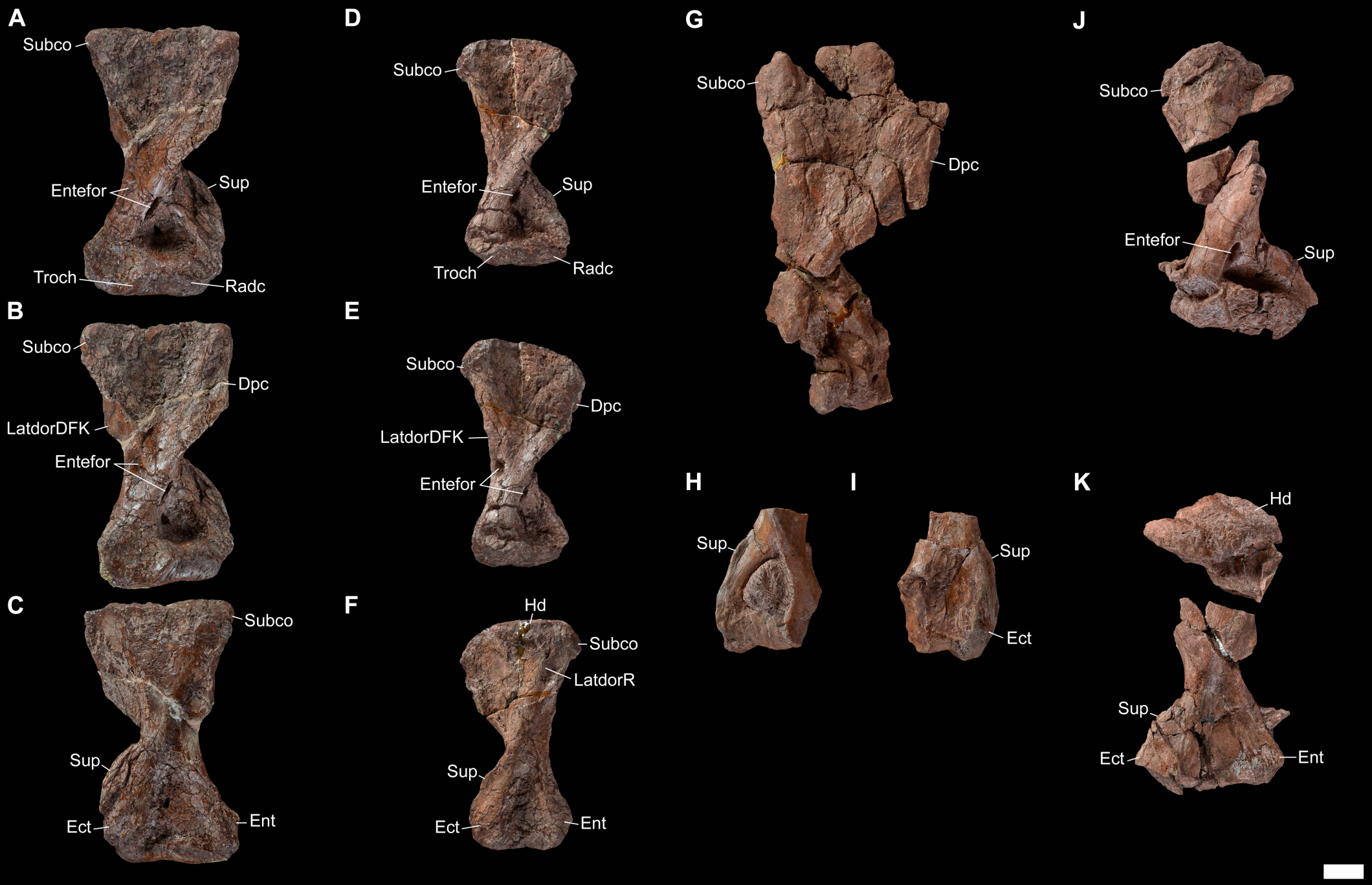
A
Subco
Entefor
Sup
Troch
Radc
B
Subco
Dpc
LatdorDFK
Entefor
C
Subco
Sup
Ect
Ent
D
Subco
Entefor
Sup
Troch
Radc
E
Subco
Dpc
LatdorDFK
Entefor
F
Hd
Subco
LatdorR
Sup
Ect
Ent
G
Subco
Dpc
H
Sup
I
Sup
Ect
J
Subco
Entefor
Sup
K
Hd
Sup
Ect
Ent

Figure 19. Humerii attributed to *Moghreberia nmachouensis*, figured in ventral (A-C), anteroventral (D-F), and dorsal (G-I) views. **A, D, G**, MNHN.F.ALM 102: left humerus; **B, E, H**, MNHN.F.ALM 101: right humerus; **C, F, I**, MNHN.F.ALM 115: right humerus. The scale bar represents 5 cm.

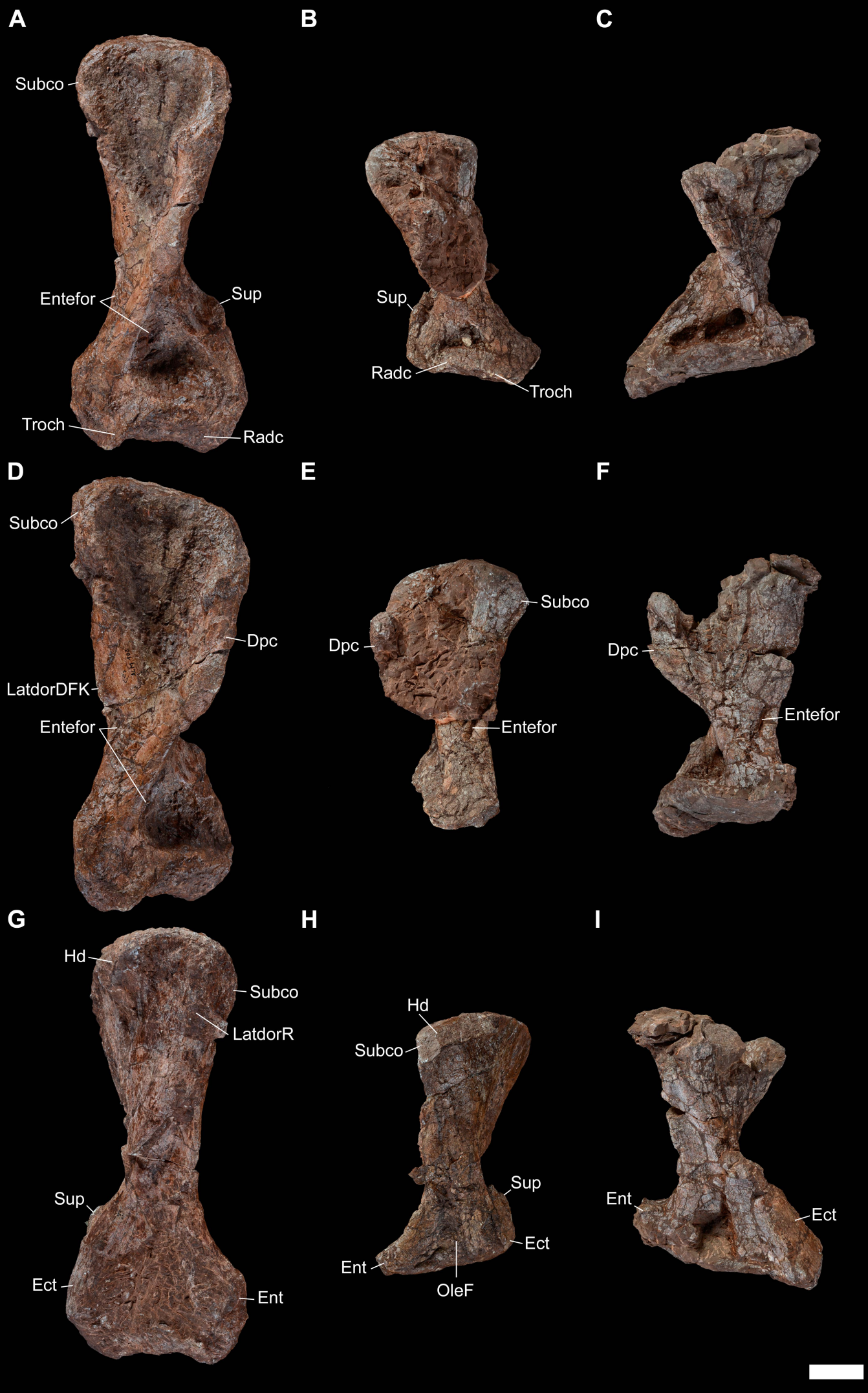
A
Subco
Entefor
Sup
Troch
Radc
B
Sup
Radc
Troch
C
D
Subco
Dpc
LatdorDFK
Entefor
E
Subco
Dpc
Entefor
F
Dpc
Entefor
G
Hd
Subco
LatdorR
Sup
Ect
Ent
H
Hd
Subco
Sup
Ect
Ent
OleF
I
Ent
Ect

Figure 20. Radii attributed to *Moghreberia nmachouensis*, figured in anterior (A, C, E) and posterior (B, D, F) views. **A-B**, MNHN.F.ALM 84: left radius; **C-D**, MNHN.F.ALM 131: left radius; **E-F**, MNHN.F.ALM 287: right radius. The scale bar represents 5 cm.


A
B
Crest
C
BicRad
D
Crest
E
F
Crest

Figure 21. Radii attributed to *Moghreberia nmachouensis*, figured in anterior (A, C) and posterior (B, D) views. **A-B**, MNHN.F.ALM 289: left radius; **C-D**, left unnumbered radius. The scale bar represents 5 cm.

Figure 22. Ulnae attributed to *Moghreberia nmachouensis* (except for MNHN.F.ALM 154 currently unattributed), figured in lateral (A, C, E, G) and medial (B, D, F) views. **A-B**, MNHN.F.ALM 18: right ulna; **C-D**, MNHN.F.ALM 28: left ulna; **E-F**, MNHN.F.ALM 261: left ulna; **G**, MNHN.F.ALM 154: left ulna. The scale bar represents 5 cm.

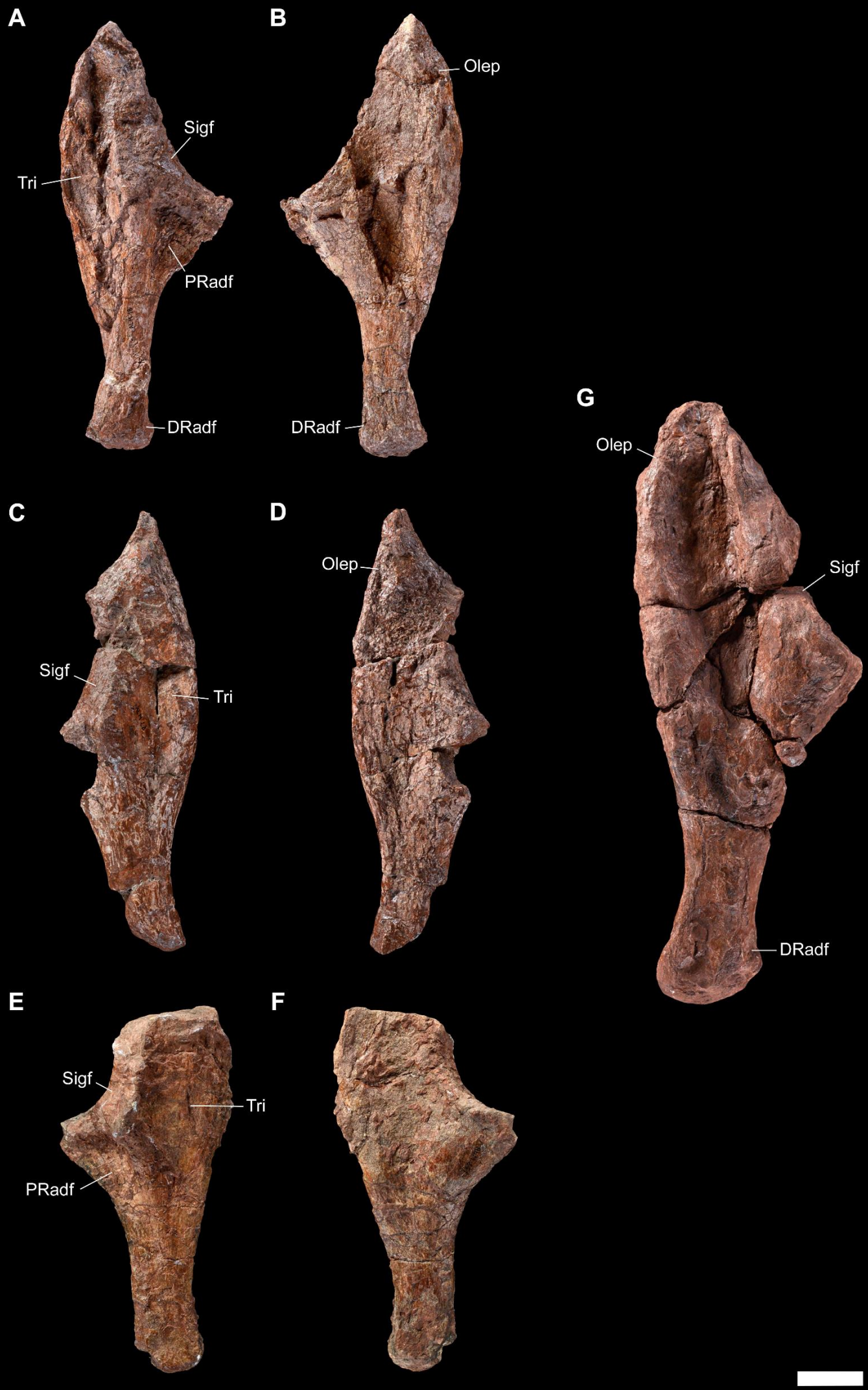
A
Sigf
Tri
PRadf
DRadf
B
Olep
DRadf
G
Olep
Sigf
DRadf
C
Sigf
Tri
D
Olep
E
Sigf
Tri
PRadf
F

Figure 23. Ulnae attributed to *Moghreberia nmachouensis* (except for MNHN.F.ALM 27 currently unattributed), figured in lateral (A, D, G), medial (B, E, H), and posterior (C, F, I) views. **A-C**, MNHN.F.ALM 35: right ulna; **D-F**, MNHN.F.ALM 87: right ulna associated with a left head rib; **G-I**, MNHN.F.ALM 27: right ulna. The scale bar represents 5 cm.


A
Sigf
Tri
PRadf
B
Olep
C
Olep
D
Sigf
Tri
PRadf
ridge
Hrb
DRadf
E
Olep
Hrb
ridge
F
Olep
Hrb
G
H
Olep
I

Figure 24. MNHN.F.ALM 274, complete pelvis attributed to *Moghreberia nmachouensis*, figured in dorsal (A), left lateral (B), ventral (C) and right lateral (D) views. The scale bar represents 5 cm.

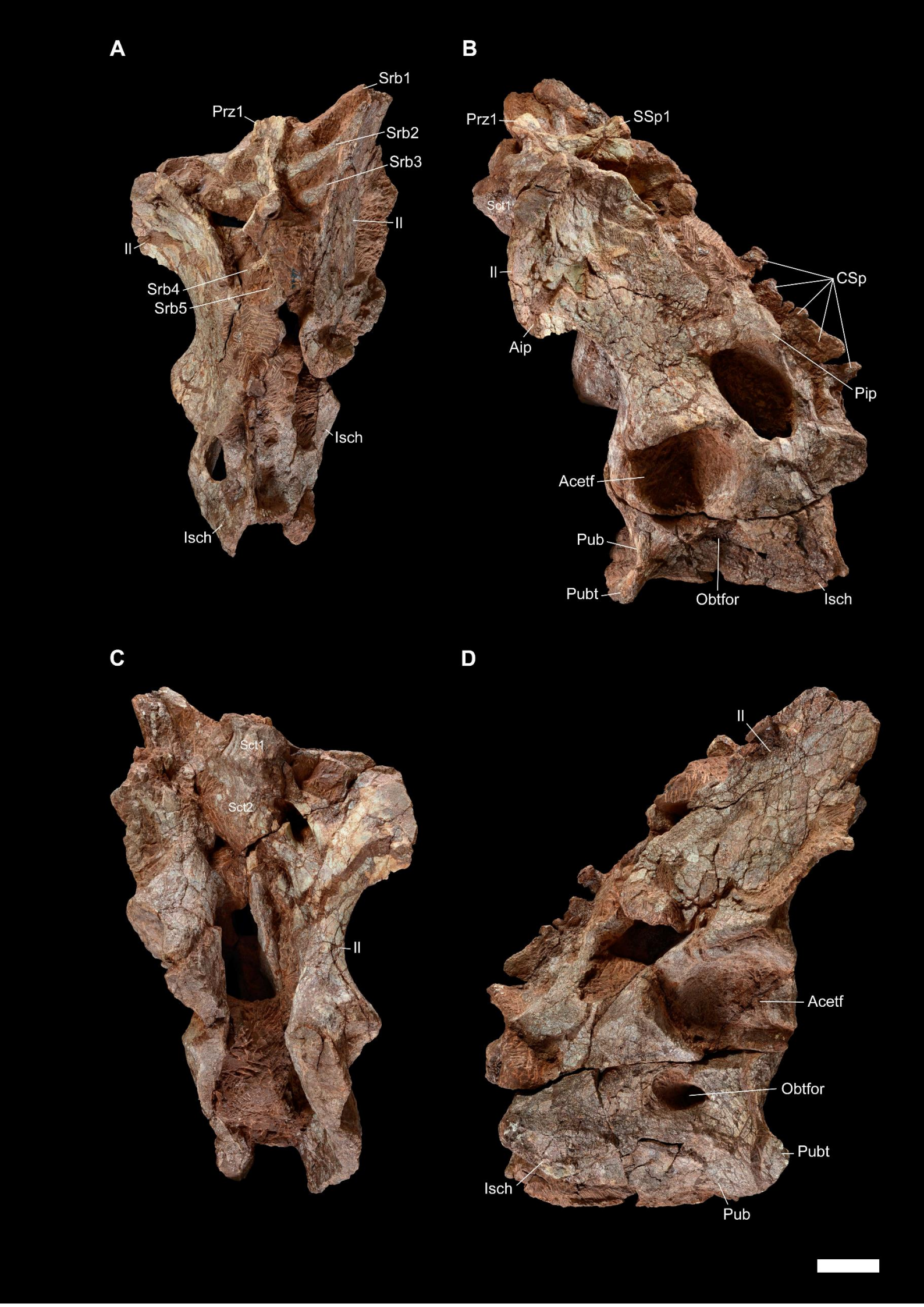
A
Srb1
Prz1
Srb2
Srb3
Il
Il
Srb4
Srb5
Isch
Isch
B
Prz1
SSp1
Sct1
Il
CSp
Aip
Pip
Acetf
Pub
Pubt
Obtfor
Isch
C
Sct1
Sct2
Il
D
Il
Acetf
Obtfor
Pubt
Isch
Pub

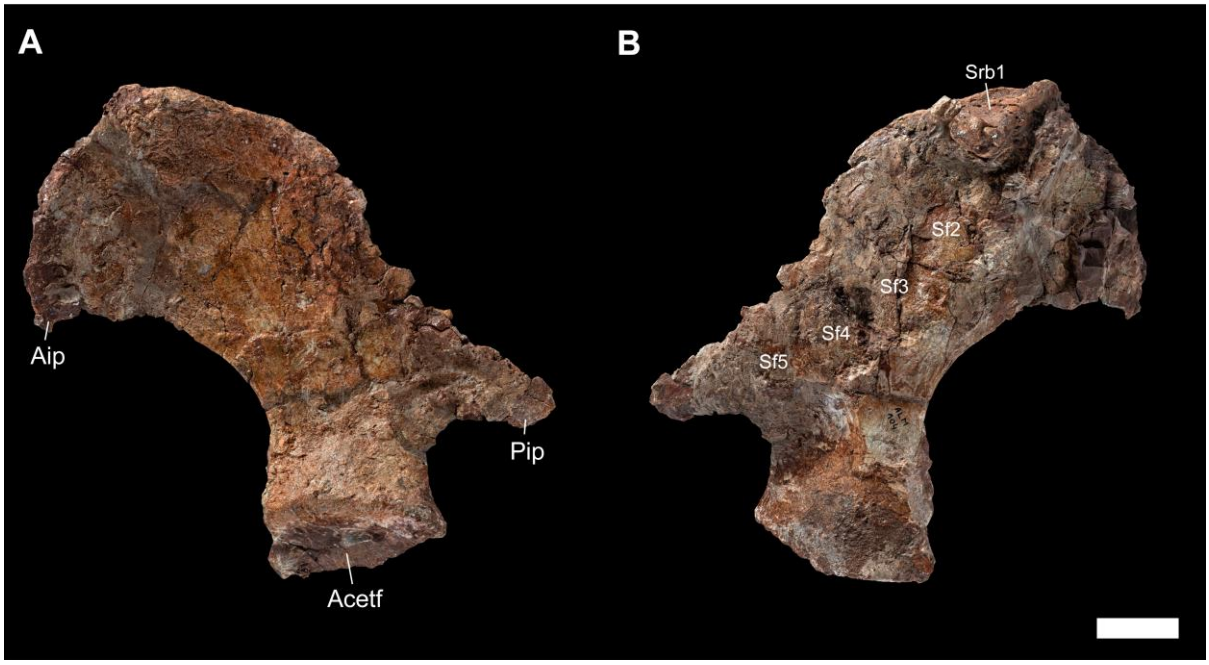

Figure 25. MNHN.F.ALM 104, left ilium attributed to *Moghreberia nmachouensis*, figured in lateral (A) and medial (B) views. The scale bar represents 5 cm.

Figure 26. Ischia and a pubis attributed to *Moghreberia nmachouensis*, figured in lateral (A, C, E) and medial (B, D, F) views. **A-B**, MNHN.F.ALM 123: right ischium; **C-D**, MNHN.F.ALM 125: right ischium; **E-F**, MNHN.F.ALM 122: left pubis. The scale bar represents 5 cm.

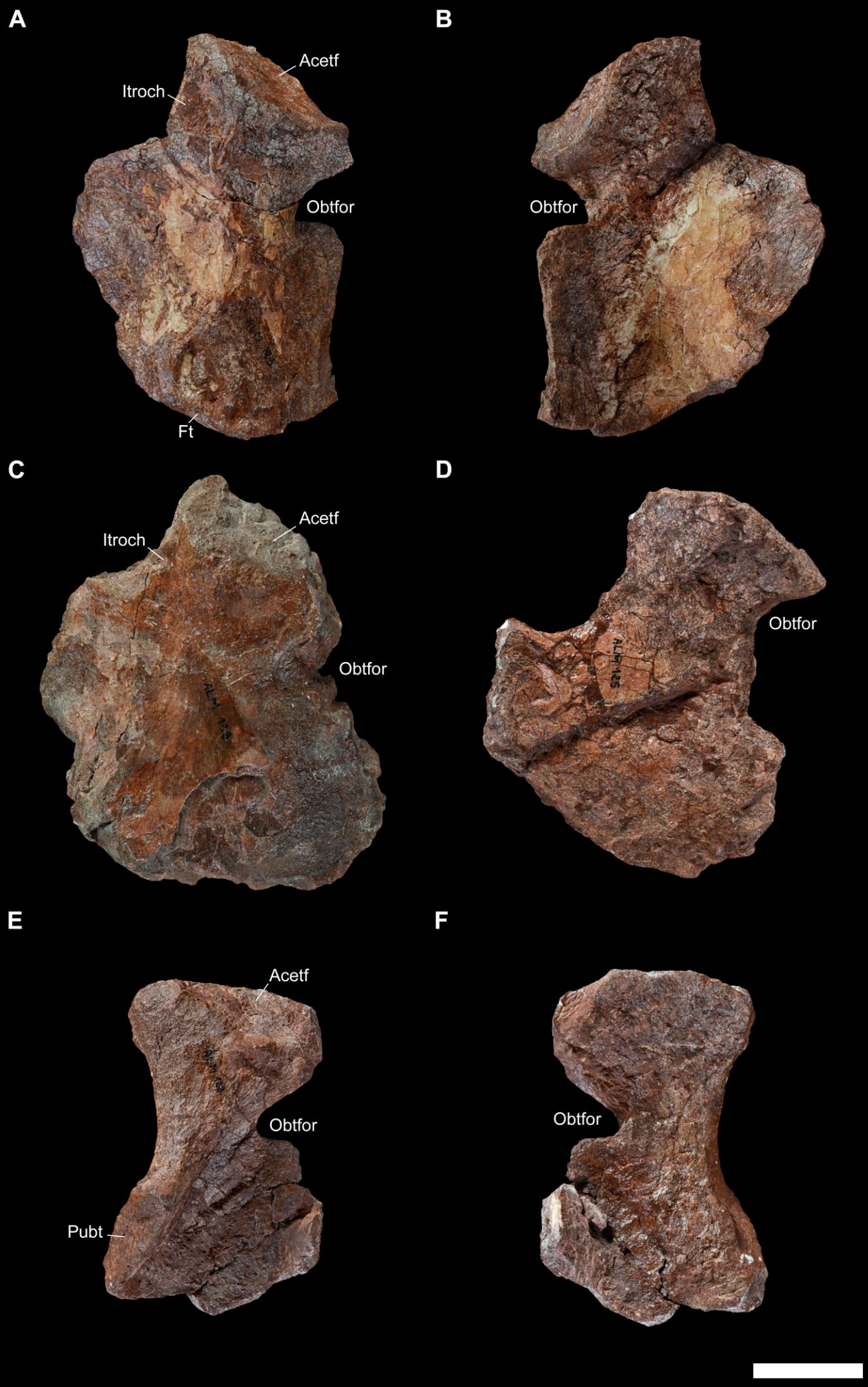
A
Acetf
Itroch
Obtfor
Ft
B
Obtfor
C
Acetf
Itroch
Obtfor
D
Obtfor
E
Acetf
Obtfor
Pubt
F
Obtfor

Figure 27. Femora attributed to *Moghreberia nmachouensis*, figured in anterior (A, D, G), posterior (B, E, H), and proximal (C, F, I) views. **A-C**, MNHN.F.ALM 21: left femur; **D-F**, MNHN.F.ALM 26: left femur; **G-I**, MNHN.F.ALM 23: right femur. The scale bar represents 5 cm.


A
Fh
Tcr
B
Fh
Tcr
Tm
PopF
IntF
C
Fh
D
Fh
Tcr
E
Fh
Tcr
Tm
PopF
IntF
F
Fh
G
Fh
Tcr
H
Tcr
Tm
PopF
IntF
I
Fh

Figure 28. Femora attributed to *Moghreberia nmachouensis* (except for MNHN.F.ALM 22 and 284 currently unattributed), figured in anterior (A, C, F), posterior (B, D, G), and proximal (E, H) views. **A-B**, MNHN.F.ALM 100: left femur; **C-E**, MNHN.F.ALM 22: right femur; **F-H**, MNHN.F.ALM 284: left femur. The scale bar represents 5 cm.

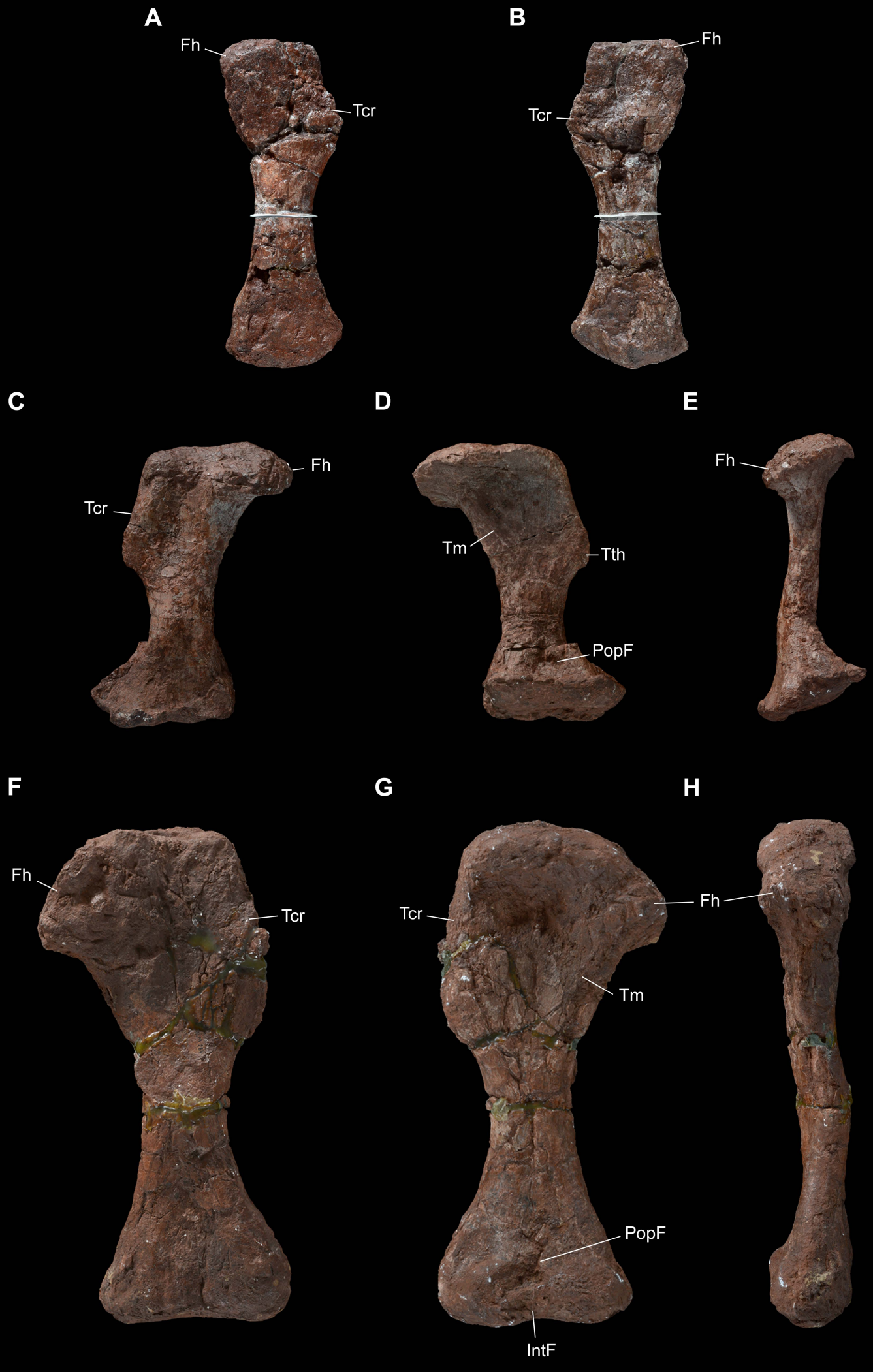
A
Fh
Tcr
B
Fh
Tcr
C
Fh
Tcr
D
Tm
Tth
PopF
E
Fh
F
Fh
Tcr
G
Tcr
Fh
Tm
PopF
IntF
H

Figure 29. Tibiae and a fibula attributed to *Moghreberia nmachouensis* (except for MNHN.F.ALM 291 currently unattributed), figured in anterior (A, C, E), posterior (B, D, F), lateral (G), and medial (H) views. **A-B**, MNHN.F.ALM 33: right tibia; **C-D**, right unnumbered tibia; **E-F**, MNHN.F.ALM 291: left tibia; **G-H**, MNHN.F.ALM 32: left fibula. The scale bar represents 5 cm.

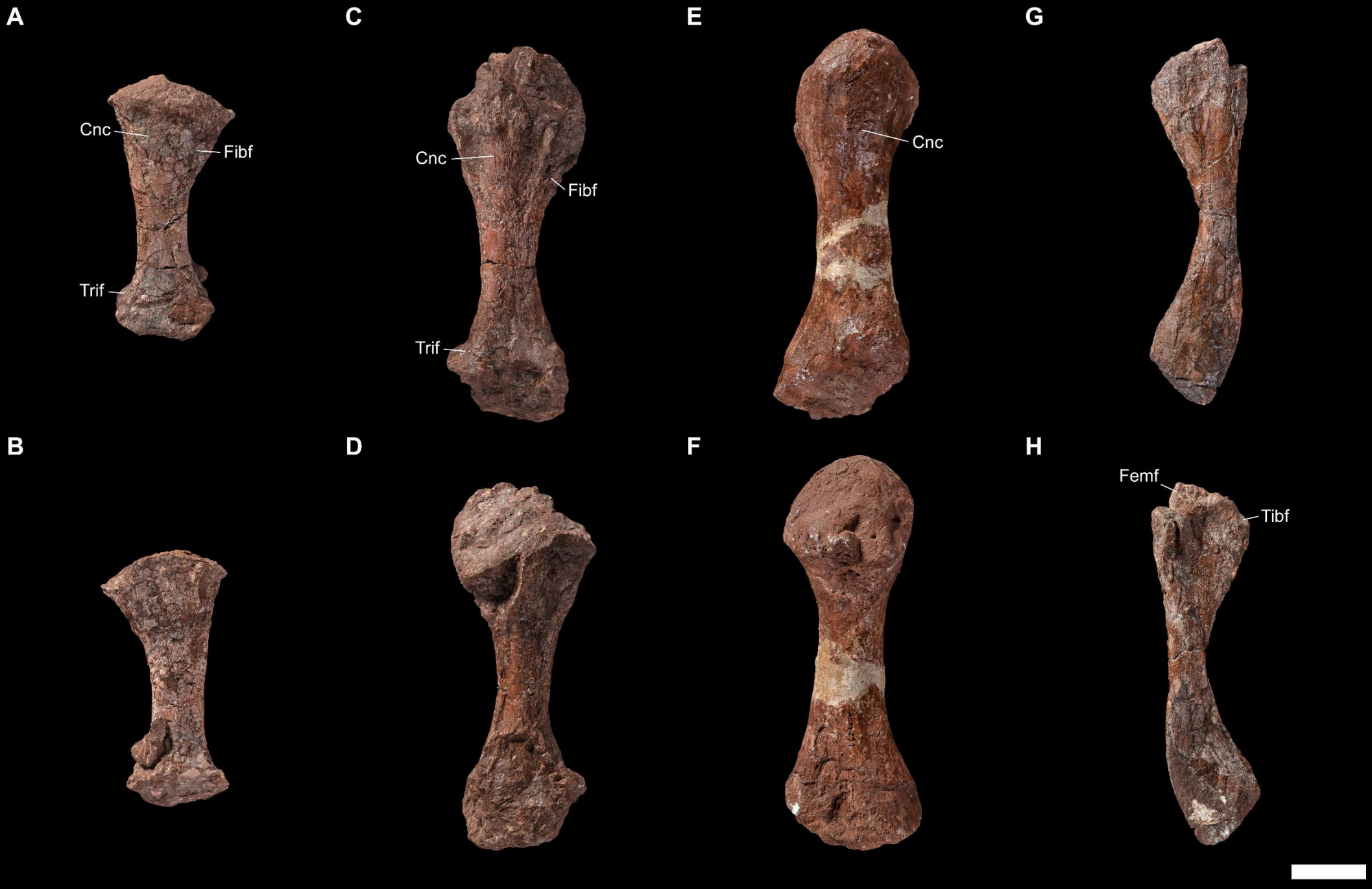
A
Cnc
Fibf
Trif
C
Cnc
Fibf
Trif
E
Cnc
G
B
D
F
H
Femf
Tibf

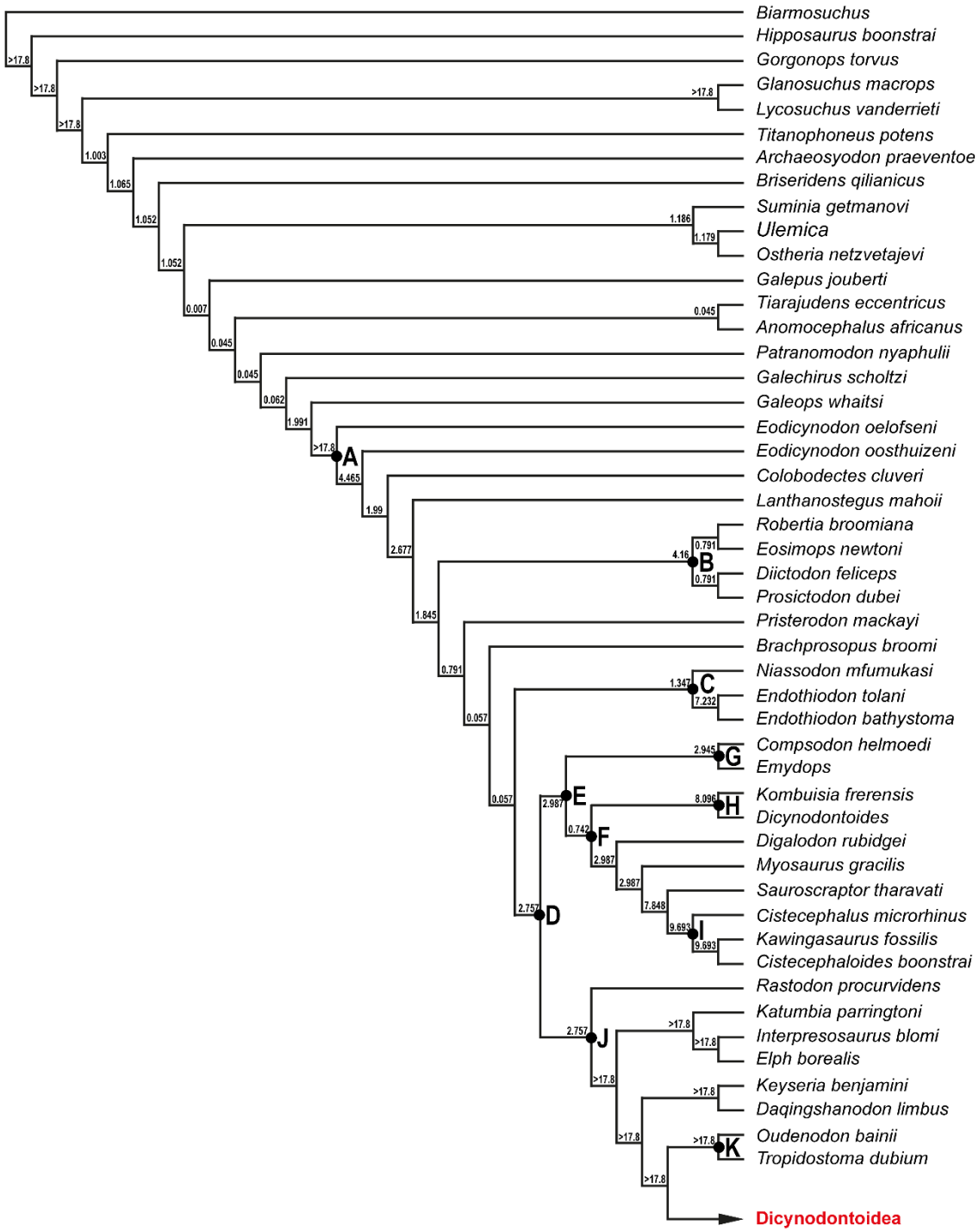

Figure 30. The most parsimonious cladogram (1202.936 steps, consistency index=0.229, retention index=0.712), with BS indicated above the branches and PBS (between the continuous [on right] and discrete [on left] characters) below. Capital letters indicate the following clades (Kammerer and Angielczyk, 2009; Kemmerer et al., 2013; Olivier et al., 2019): A, Dicynodontia; B, Pylaecephalidae; C, Endothiodontia; D, Therochelonia; E, Emydopoidea; F, Kistecephalia; G, Emydopidae; H, Kingoriidae; I, Cistecephalidae; J, Bidentalia; K, Cryptodontia; L, Geikiidae; M, Geikiinae; N, Rhachiocephalidae; O, Dicynodontidae ; P, Lystrosauridae; Q, Stahleckeriidae; R, Kannemeyeriidae.

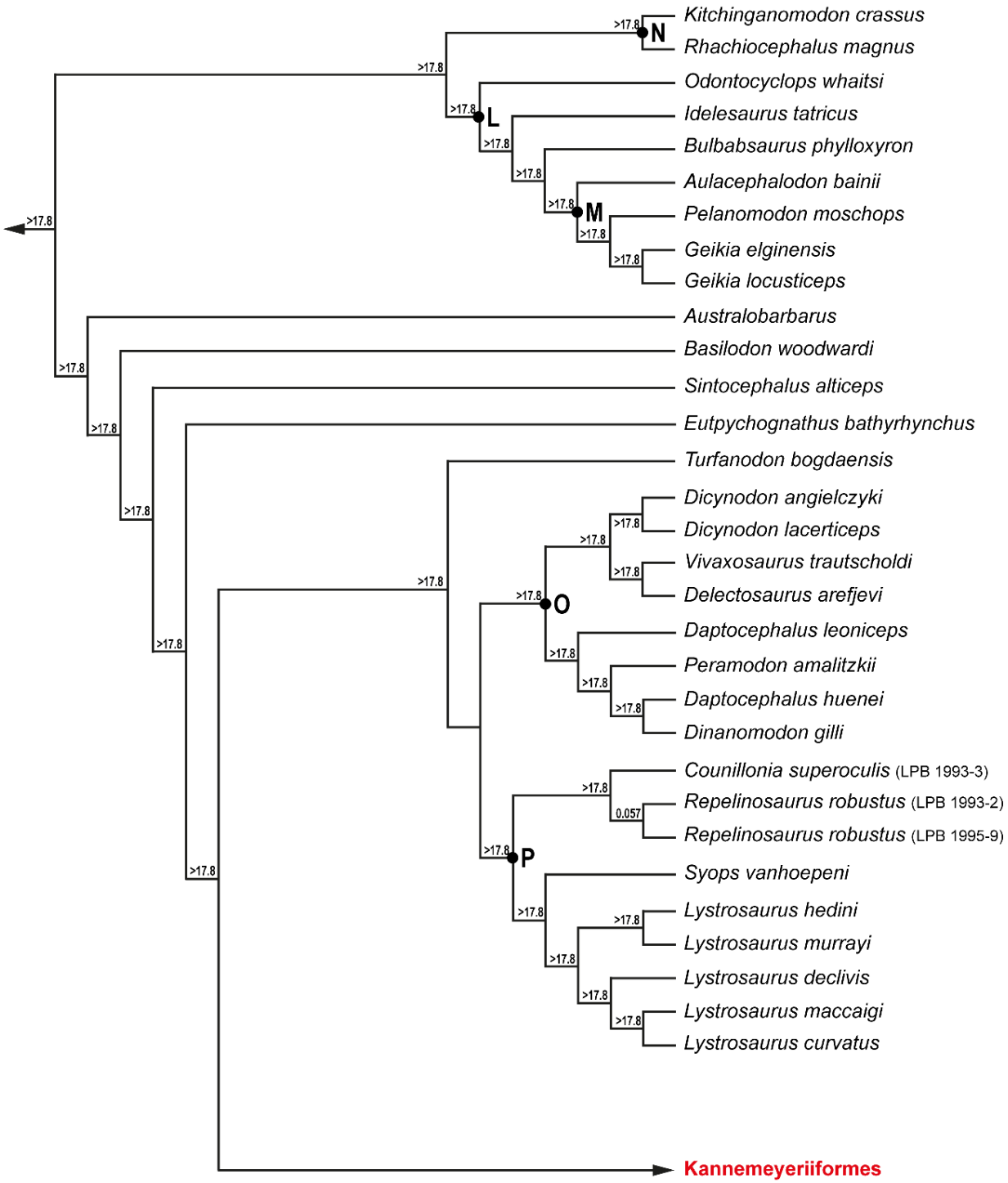

Figure 30. Continued.

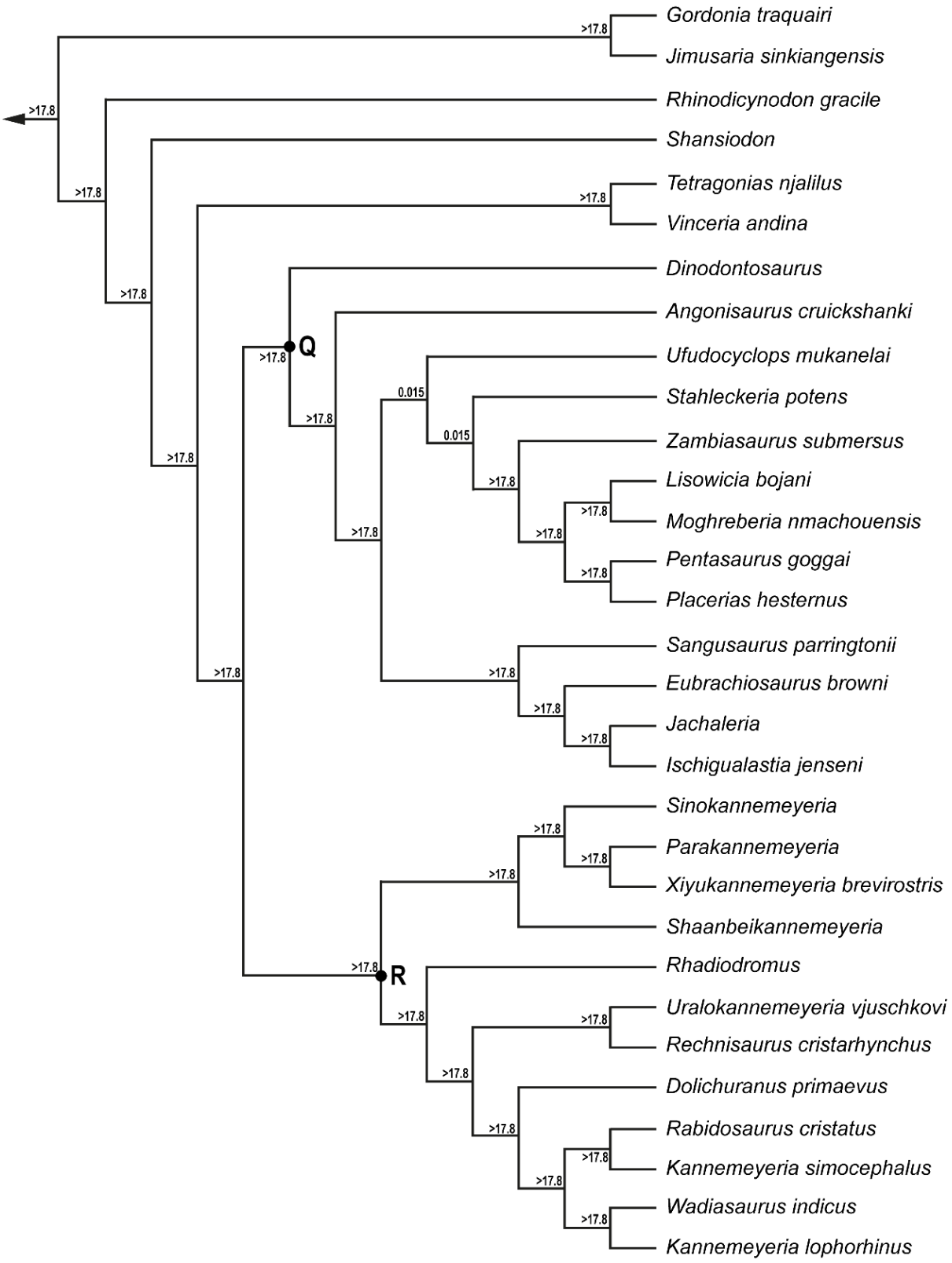

Figure 30. Continued.

Figure 31. Kannemeyeriiform femora in anterior view. **A-B**, *Moghreberia nmachouensis*: MNHN.F.ALM 21 and 100; **C**, MNHN.F.ALM 22, *incertae sedis*; **D**, *Zambiasaurus submersus*: NHMUK R9118; **E**, *Placerias hesternus*: UCMP 32394 (figured by Kammerer et al., 2013); **F**, *Parakannemeyeria dolichocephala*: IVPP V985; **G**, *Ischigualastia jenseni*: MCZ 378-58M; **H**, *Kannemeyeria simocephalus*: NHMUK R3740; **I**, *Tetragonias njalilus*: GPIT 292; **J**, *Dinodontosaurus turpior*: MCZ 3116; **K**, *Dolichuranis primaevus*: BP/1/4578. The specimens are left femora in A, B and E (reversed for comparative purposes), and right femora in C-D and F-K. The scale bars represent 5 cm.


A
B
C
Tth
D
E
Tth
F
G
H
I
Tth
J
Tth
K
Tth

Figure 32. Kannemeyeriiform humeri in dorsal (A-J) and ventral (K) view. **A, G**, *Moghreberia nmachouensis*: MNHN.F.ALM 102 (in A) and MNHN.F.ALM 24 (in G); **B**, *Lisowicia bojani*: ZPAL V.33/96 (modified from Sulej and Niedźwiedzki, 2019); **C**, *Angonisaurus cruickshanki*: NHMUK R9732; **D-E**, *Placerias hesternus*: USNM 2198 (in D) and UCMP 25361 (in E) (modified from Kammerer et al., 2013); **F**, *Pentasaurus goggai*: NHMW 1876-VII-B-123 (modified from Kammerer, 2018); **H**, *Kannemeyeria simocephalus*: NHMUK R3741; **I-J**, *Zambiasaurus submers*us: NHMUK R9089 and NHMUK R9140; **K**, *Stahleckeria potens*: BSPG AS-XXV-148 (modified from Kammerer, 2018). All the specimens are left humeri, except the right ones in C-E and K (reversed for comparative purposes). The scale bars represent 5 cm.

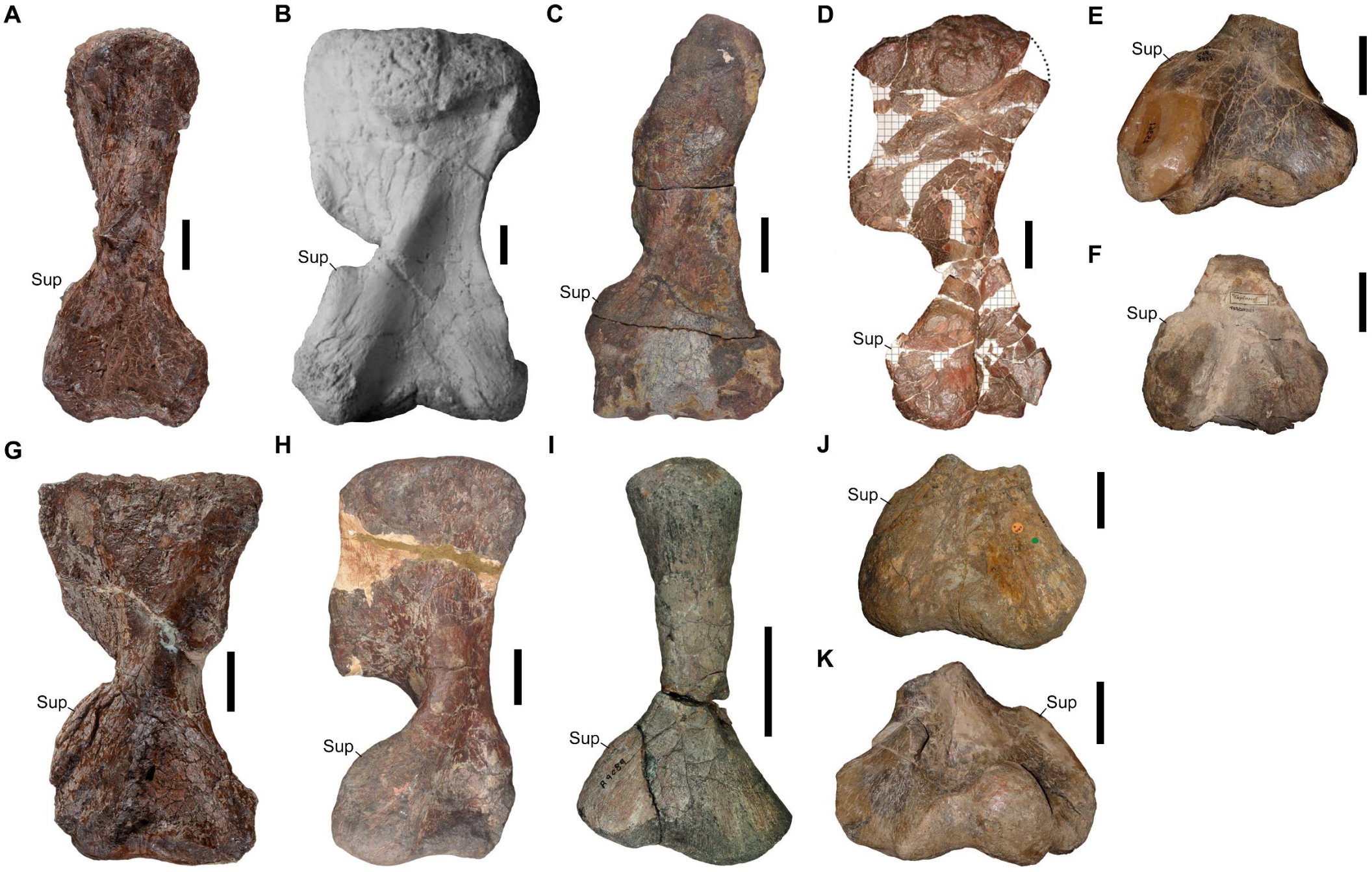
A
Sup
B
Sup
C
Sup
D
Sup
E
Sup
F
Sup
G
Sup
H
Sup
I
Sup
J
Sup
K
Sup

Figure 33. Kannemeyeriiform mandibles in lateral view. **A**, '*Azarifeneria robustus*': MNHN.F.ALM 167; **B**, *Moghreberia nmachouensis*: MNHN.F.ALM 38; **C-D**, *Stahleckeria potens*: cast AMNH FARB3857 (in C) and GSN OM 10 (in D); **E**, *Angonisaurus cruickshanki*: NHMUK R 9732; **F**, *Shaanbeikannemeyeria xilougouensis*: IVPP V11676; **G**, *Xiyukannemeyeria brevisrostris*: IVPP V4457; **H**, *Kannemeyeria simocephalus*: NHMUK R3602; **I**, *Ischigualastia jenseni*: MCZ 3120 figured by Cox (1965). All the specimens are in right lateral view (reversed for comparative purposes), except the mandibles in left lateral view in A, B, D, I. The scale bars represent 5 cm (specimen in I not in scale).

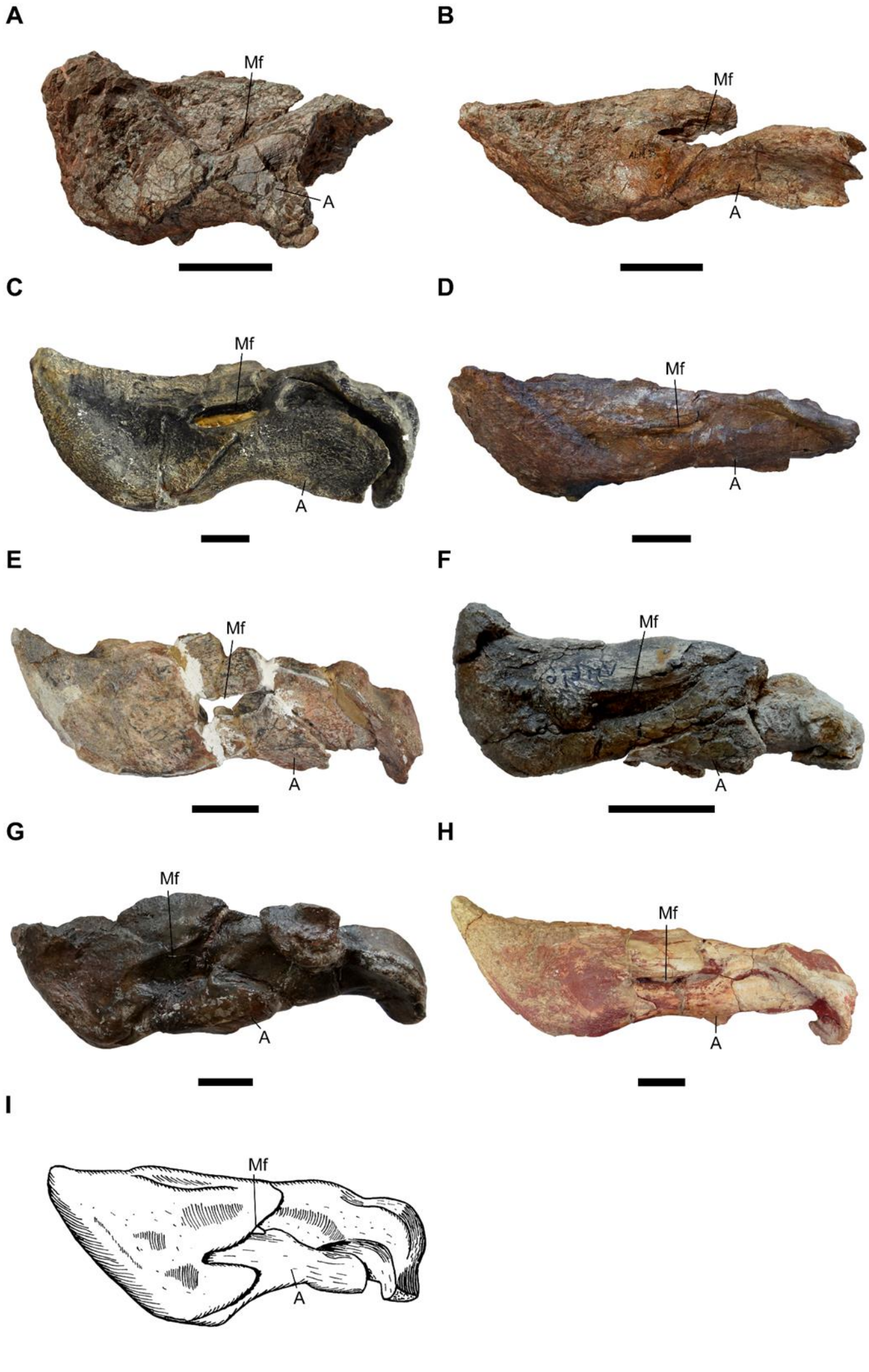
A
Mf
A
B
Mf
A
C
Mf
A
D
Mf
A
E
Mf
A
F
Mf
A
G
Mf
A
H
Mf
A
I
Mf
A

CHAPTER IV

PALEOPHYSIOLOGY OF THE DICYNODONTS AND MORE SPECIFICALLY THE TRIASSIC FORMS

Dicynodont © M. Boulay

Quantitative inference of the metabolic rate in extinct synapsid fossils

The energy expenditure is often studied by the ecologists to evaluate the adjustements made by the organisms to their environments. To be compared, we used the standardized “resting” metabolic rate defined as “the rate (1) in the zone of thermoneutrality when the individuals are (2) inactive, (3) postabsorptive, (4) adult (thereby eliminating the cost of growth), (5) nonreproductive (eliminating the cost of of pregnancy, lactation, egg formation, or incubation), and (6) regulating body temperature, and it is (7) measured during the inactive period” (McNab, 1997). Endothermy has evolved at least twice, in the mammals and birds. The acquisition of the mammalian endothermy is a major event in vertebrate evolution since it modified the energetic relationships between the organisms and their environment (Walter and Seebacher, 2009). In the classical definitions, an endothermic organism produces itself heat to control its body temperature. Clarke and Pörtner (2010) defined the endothermy as “the controlled maintenance of a relatively high and more or less constant internal body temperature, where the main source of heat is a high resting (basal) metabolic rate. […] Body temperature may exhibit circadian variability, with the amplitude typically inversely proportional to body size. Endothermy may also be suspended temporarly in periods of torpor or hibernation”. The studies of the role of muscles in the heat production led to propose a more detailed definition of endothermy as a non-shivering thermogenesis (e.g., Rowland et al., 2015; Nowack et al., 2017; Cubo and Jalil, 2019).

Many morphological proxies have been used to infer an endothermic metabolism in the synapsid fossil record such as the insulative fur (e.g., Ruben and Jones, 2000; Smith and Botha-Brink, 2011; Ruben et al., 2012; Benoit et al., 2018) and respiratory turbinates (e.g., Hillenius, 1992, 1994; Ruben et al., 1996; Crompton et al., 2015; Owerkowicz et al., 2015; Crompton et al., 2017). The inner bone organization is preserved during the fossilisation and would be also correlated with the bone growth rate and then the resting metabolic rate (e.g., Montes et al., 2007). A fibrolamellar bone (i.e., [FLB] primary osteons with lamellar bone within a woven bone matrix) thus indicates a high growth rate according to Francillon Vieillot et al. (1990) and Ricqlès et al. (1991). The qualitative histology (description of the inner organization of bone) of the synapsids was intensively studied and especially in dicynodonts. The presence of FLB was demonstrated in (1) cynodonts such as *Procynosuchus*, *Trucidocynodon* and

Langbergia (Botha-Brink et al., 2012), *Thrinaxodon* (Ricqlès, 1969; Ray et al., 2004; Chinsamy and Hurum, 2006; Botha-Brink et al., 2012), *Cynognathus* and *Diademodon* (Botha and Chinsamy, 2000; Botha-Brink and Angielczyk, 2010), *Trirachodon* (Botha and Chinsamy, 2004; Botha-Brink et al., 2012), and *Tritylodon* (Ricqlès, 1969; Ray et al., 2004; Chinsamy and Hurum, 2006; Botha-Brink et al., 2012), (2) therocephalians (Huttenlocker and Botha-Brink, 2014), (3) gorgonopsians (Chinsamy-Turan and Ray, 2012), (4) sphenacodontid *Dimetrodon* (Shelton et al., 2013), (5) ophiacodontid *Ophiacodon* (Shelton and Sander, 2017), (5) dromasaur Galeops (Botha-Brink and Angielczyk, 2010), and (6) dicynodonts *Eodicynodon*, *Diictodon*, *Endothiodon*, *Cistecephalus*, *Dicynodontoides*, *Rhachiocephalus*, *Aulacephalodon*, *Tropidostoma*, *Oudenodon*, *Dicynodon*, *Kannemeyeria*, *Placerias*, *Lystrosaurus declivis*, *L. murrayi* and *L. maccaigi* (e.g., Ray et al., 2005; Botha-Brink and Angielczyk, 2010; Green et al., 2010). These results would indicate an origin of FLB in Synapsida during the early Permian (Shelton and Sander, 2017). However, some extant ectotherms such as the alligators are able to produce FLB in captivity (Padian et al., 2004) and in wild (Tumarkin-Deratzian, 2007), that was been considered as an inherited feature from the endothermic ancestral state in archosaurs (Seymour et al., 2004).

Most of proxies used to infer metabolism of extinct oragnisms are qualitative. The qualitative histology being insufficient to rather precisely infer resting metabolic rates or physiological thermoregulation. A recent quantitative histological approach were thus first proposed by Legendre et al. (2016) to perform quantitative inferences of the resting metabolic rates on archosaur fossils using paleobiological models. These authors built their models based on microanatomical features (density, shape, and area of the osteocyte and vascular density) within a phylogenetic context (using the Phylogenetic Eigenvector Maps). Their study allowed to constrain both temporally and phylogenetically the acquisition of the avian endothermy assuming it at the archosauriform node. This method was then re-used by Fleischle et al. (2018) who inferred a high resting metabolic rate in plesiosaurs. However, these paleobiological inference models have never been applied to Synapsida.

This chapter comprises two studies dealing with the application of paleohistological inference models to infer the resting metabolic rate in synapsid fossils using the Phylogenetic Eigenvector Maps (PEMs) (PAPER III) and Phylogenetic Generalised Least Squares (PGLS) (PAPER IV) methods. They focused on a

dicynodont sample and highlighted on the implications on our understanding of the evolution of the acquisition of the mammalian endothermy.

The PAPER III has been started during my Master internship where I studied the qualitative histology of the humerus and femur of *Moghreberia nmachouensis*, and performed preliminary paleobiological inference models (based on humerus and femur) using PEMs. However, the extant sample of synapsids (including *Microcebus murinus*, *Cavia porcellus*, and *Mus musculus*) was not sufficient compared to the extinct sample (including the dicynodonts *M. nmachouensis*, *Lystrosaurus* sp., and *Oudenodon baini*). The first work of my PhD was to include three more extant synapsids (*Lepus europaeus*, *Oryctolagus cuniculus*, and *Capreolus capreolus*) and build new models. The bone sections were all conserved in MNHN. In this paper, J. Cubo, A. Houssaye, and I wrote the article. I made the description of the qualitative histology and the discussion “Growth Rate and Stage”. I measured the histological variables (density, shape, and area of the osteocyte) for both femur and humerus of the three fossils and the three added extant synapsids (Fig. IV.1). To smooth variations between the different regions of the bone, I took 30 measurements per region (anterior, posterior, lateral, and medial) of each bones (femur and humerus) for each histological variable (density, shape, and area of the osteocyte). Then, I performed the two statistical models (based on femur and humerus) using the R package MPSEM (Guénard et al., 2013), following the method of Legendre et al. (2016). I produced all the figures of the paper.

PAPER IV used the same extant sample as PAPER III but comprised a larger sample of dicynodonts with *Daptocephalus* (femur), *Endothiodon* (humerus), *Kannemeyeria simocephalus* (femur), *Lystrosaurus murrayi* (femur and humerus), *Moghreberia nmachouensis* (femur and humerus), *Myosaurus gracilis* (humerus), *Oudenodon baini* (femur and humerus), and *Tropidostoma* (femur and humerus). I visited the histological collection of the National Museum of Bloemfontein (South Africa; financial support from CR2P) to consult and photograph the bone sections of all cited dicynodont except those of *Moghreberia nmachouensis* and *Oudenodon baini* conserved in MNHN. As in the previous paper, the paleobiological models based on femur and humerus are distinct. As opposed to PAPER III, the main objective of this paper was to build models using a combination of histological variables and PGLS method. For comparative purposes, models using PEMs method have also been done. In PAPER IV, I wrote the whole of the article that has been improved by comments of all coauthors. I produced

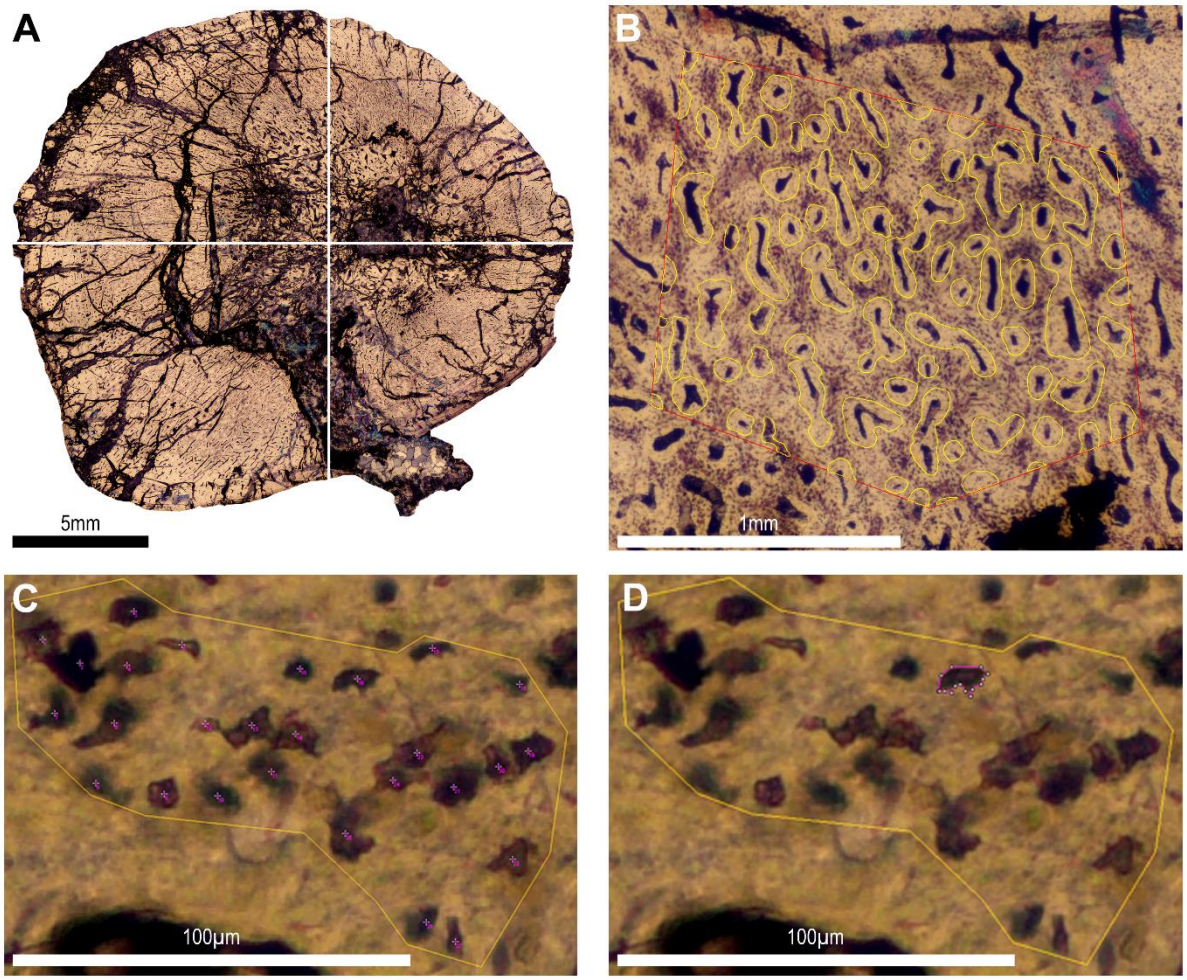

Figure IV.1. Measurements on the bone sections of the humerus NMQR 9960 of *Tropidostoma*. **A**, the surface of the mid-diaphyseal cross section of the bone divided in four parts; **B**, primary osteon density measured as the sum of areas of the osteons (yellow circled; i.e., primary osteons and the associated lamellar bone) compared to the total bone area (red limited); **C**, osteocyte density measured as the number of osteocytes (pink pointed) per bone area (yellow limited); **D**, osteocyte area (pink circled) and shape that is measured as the ratio between the major and the minor axes of the lacuna.

all the figures of the paper. Following the method of PAPER III and Fleischle et al. (2018), I measured all histological variables (density, shape, and area of the osteocyte, and primary osteon density) for femora and humeri of the fossil sample (except the primary osteon density of the femur of *Oudenodon* quantified by M. Faure-Brac), and the primary osteon density for humerus of the extant sample (Fig. IV.1). M. Faure-Brac quantified the primary osteon density of the femora of the extant species. The statistical methods have been discussed by Y. Desdevises, L. Legendre, and I. I built the models using PGLS (with BayesTraits V3.0.1; Pagel and Meade, 2016) and PEMs (with the R package MPSEM; Guénard et al., 2013) methods, and did the multiple tests of correlations, AICs, BayesFactor, and coss-validations.

First palaeohistological inference of resting metabolic rate in an extinct synapsid, *Moghreberia nmachouensis* (Therapsida: Anomodontia)

Chloe Olivier[1,2], Alexandra Houssaye[3], Nour-Eddine Jalil[2] and Jorge Cubo[1*]

[1]Sorbonne Universités, UPMC Univ Paris 06, CNRS, UMR 7193, Institut des Sciences de la Terre Paris (iSTeP), 4 place Jussieu, BC 19, Paris 75005, France

[2]Sorbonne Universités -CR2P -MNHN, CNRS, UPMC-Paris6. Muséum national d'Histoire naturelle, 57 rue Cuvier, CP38, Paris F-75005, France

[3]Département Écologie et Gestion de la Biodiversité, UMR 7179, CNRS/Muséum national d'Histoire naturelle, 57 rue Cuvier, CP55, Paris 75005, France

*Corresponding author

Published in *Biological Journal of Linnean Society* in 2017

PAPER III

Biological Journal of the Linnean Society, 2017, **121**, 409–419. With 4 figures.

First palaeohistological inference of resting metabolic rate in an extinct synapsid, *Moghreberia nmachouensis* (Therapsida: Anomodontia)

CHLOE OLIVIER[1,2], ALEXANDRA HOUSSAYE[3], NOUR-EDDINE JALIL[2] and JORGE CUBO1*

[1]*Sorbonne Universités, UPMC Univ Paris 06, CNRS, UMR 7193, Institut des Sciences de la Terre Paris (iSTeP), 4 place Jussieu, BC 19, Paris 75005, France*
[2]*Sorbonne Universités -CR2P -MNHN, CNRS, UPMC-Paris6. Muséum national d'Histoire naturelle, 57 rue Cuvier, CP38, Paris F-75005, France*
[3]*Département Écologie et Gestion de la Biodiversité, UMR 7179, CNRS/Muséum national d'Histoire naturelle, 57 rue Cuvier, CP55, Paris 75005, France*

Received 10 November 2016; revised 30 November 2016; accepted for publication 1 December 2016

The independent acquisition of endothermy in synapsids and diapsids are major events in vertebrate evolution since they were the driving force of a suite of correlated changes in anatomical, physiological, behavioural and ecological traits. While avian endothermy is assumed to have occurred at the archosauriform node, the acquisition of mammalian endothermy is poorly constrained both temporally and phylogenetically. Among the many unequivocal anatomical correlates of endothermy in synapsids, the presence of insulative pelage or respiratory turbinates only allows discrete inferences of presence/absence of endothermy. The analysis of bone histology allows richer palaeobiological inferences. We described the osteohistology and growth patterns of *Moghreberia nmachouensis* and two related taxa (*Lystrosaurus* and *Oudenodon*) for comparative purposes. Our observations suggest increasing growth rates from *Moghreberia* [the presence of incipient fibrolamellar bone (FLB) in humerus and femur], to *Lystrosaurus* (the presence of well-developed FLB in the femur but the presence of incipient FLB in the humerus), to *Oudenodon* (the presence of well-developed FLB in humerus and femur). However, qualitative histology does not allow reliable inferences about the occurrence of endothermy. We performed the first quantitative inferences of resting metabolic rates on fossil synapsids (*M. nmachouensis* as a model and *Lystrosaurus* and *Oudenodon* for comparative purposes) using quantitative histology (size, shape and density of osteocyte lacunae) combined with phylogenetic eigenvector maps. Our inferences are consistent with our qualitative histological observations: the mass-independent resting metabolic rate inferred for *M. nmachouensis* (2.58 $mLO_2\ h^{-1}\ g^{-0.67}$) is lower than the value inferred for *Lystrosaurus* (3.80 $mLO_2\ h^{-1}\ g^{-0.67}$), which is lower than that inferred for *Oudenodon* (4.58 $mLO_2\ h^{-1}\ g^{-0.67}$). Optimization of these inferences onto a phylogenetic tree of tetrapods using the parsimony method allowed us to better constrain the temporal (more than 260 Myr ago) and phylogenetic (Neotherapsida) frames of the acquisition of mammalian endothermy.

ADDITIONAL KEYWORDS: Dicynodontia – endothermy – fibrolamellar bone – palaeohistology – phylogenetic eigenvector maps.

INTRODUCTION

The acquisition of mammalian endothermy is a major event in vertebrate evolution since it modified the energetic relationships between organisms and their environment (Walter & Seebacher, 2009). To constrain the temporal and phylogenetic frames of this event, we need to identify unequivocal anatomical correlates of endothermy (Ruben *et al.*, 2012). Among them, the oldest evidence for an insulative pelage (through fossilized fur impressions) has been found in the Middle Jurassic non-mammalian therapsids (*Castorocauda*, Ji *et al.*, 2006; *Megaconus*, Zhou *et al.*, 2013; *Agilodocodon*, Meng *et al.*, 2015), but it seems that the acquisition of endothermy

*Corresponding author. E-mail: jorge.cubo_garcia@upmc.fr

© 2017 The Linnean Society of London,

based on increased aerobic capacity is older (Ruben *et al.*, 2012). The presence of respiratory turbinates is another anatomical feature linked to endothermy. Although these structures are rarely preserved in fossils, bone ridges of turbinate attachment are frequently preserved (Ruben *et al.*, 2012). These structures are first recognizable in therocephalians and in cynodonts (Ruben *et al.*, 2012), so they may have been acquired by the eutheriodonts. Thermic modelling (Florides *et al.*, 2001) and the isotopic composition of mineralized remains (Rey, 2016) have also been used to infer the physiological thermoregulation of nonmammalian synapsids.

Bone palaeohistology is a useful method to infer the bone growth rates and resting metabolic rates of extinct vertebrates. The bone histology of nonmammalian synapsids has been intensively studied in the last decade. Laurin & Buffrénil (2016) analysed the ophiacodont *Clepsydrops collettii* and concluded that the femur is made of woven-fibered tissue combined with parallel-fibered bone (PFB) in primary osteons. Shelton & Sander (2015) reported the presence of fibrolamellar bone (FLB) in *Ophiacodon retroversus*, *Ophiacodon uniformis* and *Ophiacodon mirus*. Shelton *et al.* (2013) reported 'incipient fibrolamellar bone' (iFLB) in the humerus and femur of *Dimetrodon natalis*. Botha-Brink & Angielczyk (2010) analysed a sample of Anomodontia and showed the presence of FLB in the dromasaur *Galeops* and the dicynodonts *Eodicynodon, Diictodon*, *Endothiodon*, *Cistecephalus*, *Dicynodontoides*, *Rhachiocephalus*, *Aulacephalodon*, *Tropidostoma*, *Oudenodon*, *Dicynodon*, *Kannemeyeria*, *Lystrosaurus declivis*, *Lystrosaurus murrayi* and *Lystrosaurus maccaigi*. Ray, Chinsamy & Bandyopadhyay (2005) analysed also the bone histology of *L. murrayi* and showed the presence of FLB in the humerus, femur, tibia and a proximal phalanx. Chinsamy & Ray (2012) reported FLB tissue in the long bones of two Gorgonopsia (*Scylacops* and *Aelurognathus*) and in the tibia and fibula of two undetermined Therocephalia. Huttenlocker & Botha-Brink (2014) concluded that basal therocephalians (e.g. *Lycosuchus*) are characterized by highly vascularized FLB, whereas Eutherocephalia (but *Moschorhinus*) lack this condition (e.g. *Theriognathus*). Some authors analysed the histological features of nonmammalian cynodonts and showed the presence of FLB in *Procynosuchus*, *Trucidocynodon* and *Langbergia* (Botha-Brink, Abdala & Chinsamy, 2012); *Thrinaxodon* (Botha & Chinsamy, 2005; Botha-Brink *et al.*, 2012; de Ricqlès, 1969); *Cynognathus* and *Diademodon* (Botha & Chinsamy, 2000; Botha-Brink *et al.*, 2012); *Trirachodon* (Botha & Chinsamy, 2004; Botha-Brink *et al.*, 2012); and *Tritylodon* (de Ricqlès, 1969; Ray, Botha & Chinsamy, 2004; Chinsamy & Hurum, 2006; Botha-Brink *et al.*, 2012). All these studies were carried out using classic qualitative histology. Results obtained using this approach are useful to infer bone growth rates assuming Amprino's rule (e.g. Montes, Castanet & Cubo, 2010), that is, considering that the organization of the collagenous wave and of the vascular network in the osseous tissue is strongly correlated with bone growth rate. However, they are not suitable to infer resting metabolic rates or physiological thermoregulation. Indeed, it has been shown that some extant ectotherms (e.g. the alligators) are able to form lamellar-zonal bone (de Ricqlès, Padian & Horner, 2003; Lee, 2004), but also FLB both in captivity (Padian, Horner & de Ricqlès, 2004) and in the wild (Tumarkin-Deratzian, 2007), probably an atavistic characteristic of an endothermic ancestry among archosaurs (Seymour *et al.*, 2004).

Recent developments in quantitative bone histology have facilitated the first direct inferences of resting metabolic rates in extinct diapsids (Legendre *et al.*, 2016). This study is aimed at performing the first quantitative inferences of resting metabolic rates on fossil synapsids, using three dicynodonts as models (*Moghreberia nmachouensis Lystrosaurus* and *Oudenodon*). Dicynodonts are among the most abundant terrestrial herbivores from the Middle Permian to Late Triassic. They were cosmopolitan and had a wide range of ecologies and morphologies represented by an abundant and diversified fossil record. *Myosaurus* and the species-rich genus *Lystrosaurus* survived the Permian/Triassic crisis (Maisch & Matzke, 2014). Therefore, dicynodonts are good models to gain a better understanding of the impact of this biotic crisis on terrestrial ecosystems. This survey is focused on the Moroccan Upper Triassic *M. nmachouensis* but includes the Permian *Oudenodon baini* and Triassic *Lystrosaurus* for comparative purposes. Only the cranial material of the monospecific genus *Moghreberia* was shortly described by Dutuit (1988). *Moghreberia* is a kannemeyeriiform, the most frequent group in the Triassic, but its phylogenetic position is discussed. Certain authors considered it as a synonym of the Upper Triassic North-American dicynodont *Placerias* (Cox, 1991), while others supposed they are sister-groups (Kammerer, Fröbisch & Angielczyk, 2013). In addition to inferring the resting metabolic rates of *M. nmachouensis*, we will describe the osteohistology and growth patterns of this taxon, using two related taxa (*Lystrosaurus* and *Oudenodon*) for comparative purposes.

MATERIAL AND METHODS

Materials

The materials used are humeral and femoral mid-diaphyseal transverse sections of the Moroccan Upper Triassic *M. nmachouensis* (femur MNHN.F.ALM 100 of 310 mm in length and humerus MNHN.F.ALM 297 of 375 mm in length; Fig. 1) and two additional

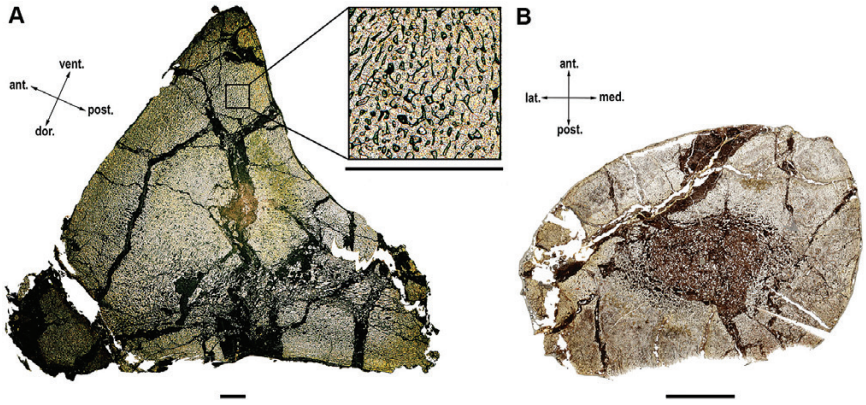

Figure 1. *Moghreberia nmachouensis* (Triassic, Argana basin, Morocco): Mid-diaphyseal cross sections of stylopodial bones. (A) Humerus MNHN.F.ALM 297; (B) femur MNHN.F.ALM 100. Abbreviations: ant., anterior side; dor., dorsal side; lat., lateral side; med., medial side; post., posterior side; vent., ventral side. Scale bars represent 5 mm.

dicynodonts from the personal collection of Armand de Ricqlès (research collection, Museum National d'Histoire Naturelle, Paris, France). On the one hand, *Lystrosaurus* sp. (humerus 24.1 of 131 mm in length and femur 11–15 of 90.7 mm in length without the proximal epiphysis) from the Triassic *Lystrosaurus* assemblage zone of the South African Karoo Basin (de Ricqlès, 1969), where *Lystrosaurus curvatus*, *L. declivis* and *L. murrayi* have been discovered (de Ricqlès, 1972; Smith & Botha, 2005; Botha & Smith, 2007; Fröbisch, 2009). On the other hand *Oudenodon baini* (humerus 292-1 of 119 mm in length and an unnumbered femur of 107 mm in length) from the *Cynognathus* assemblage zone of the South African Karoo Basin (de Ricqlès, 1969). Humerus and femur came from different specimens in all three taxa.

Histology

Bones were moulded prior to sectioning. All sections were made at the mid-diaphysis using standard procedures (e.g. Padian & Lamm, 2013; only the central part of the diaphysis has been embedded in a polyester resin). Sections were observed microscopically using Leica DM2700 P and Zeiss Axiovert 35 (Jena, Germany) microscopes under natural and polarized light and photographed using a DXM 1200 Digital Eclipse Camera System (Nikon, Japan) and an Olympus Digital Camera (Japan). Sections were also scanned using a high-resolution Epson V740 PRO scanner. The histological terminology follows Francillon-Vieillot *et al.* (1990).

Inference models

We constructed two resting metabolic rate inference models (for the humerus and for the femur) using phylogenetic eigenvector maps, a new powerful approach developed by Guenard, Legendre & Peres-Neto (2013) and recently used by Legendre *et al.* (2016). The interest of this approach lies in the fact that it takes into account both phylogenetic and phenotypic information (here bone quantitative histology) to perform palaeobiological inferences. We used a sample of 17 extant tetrapods (*Pleurodeles waltl*, *Microcebus murinus*, *Lepus europaeus*, *Oryctolagus cuniculus*, *Cavia porcellus*, *Mus musculus*, *Capreolus capreolus*, *Zootoca vivipara*, *Podarcis muralis*, *Varanus exanthematicus*, *Varanus niloticus*, *Chelodina oblonga*, *Pelodiscus sinensis*, *Trachemys scripta*, *Crocodylus niloticus*, *Gallus gallus* and *Anas platyrhynchos*) for which we know both the variable to be inferred in extinct taxa (resting metabolic rate) and the quantified histological features (size, shape and density of osteocyte lacunae in primary bone outside osteons). The bone histological data (size, shape and density of osteocyte lacunae in primary bone outside osteons) for all extant taxa but *L. europaeus*, *O. cuniculus* and *C. capreolus* were taken from Legendre *et al.* (2016). Bone histological data for the quoted three taxa were quantified in this study. Mass-independent resting metabolic rates (in mLO_2 h^{-1} $g^{-0.67}$) for all extant taxa but *Lepus*, *Oryctolagus* and *Capreolus* were experimentally quantified by Montes *et al.* (2007). Mass-independent resting metabolic rates for the quoted three taxa were taken respectively from Hackländer, Arnold & Ruf (2002), Seltmann, Ruf & Rödel (2009) and Mauget, Mauget & Sempéré (1999). We quantified the quoted bone histological variables in the humeri and femora of the taxa for which we aim to infer the resting metabolic rate (*M. nmachouensis*, *Lystrosaurus* and *Oudenodon*) using the procedure described by Legendre *et al.* (2016). Osteohistological data of extant growing tetrapod species taken from Legendre *et al.* (2016) were quantified in the outer

cortex, whereas osteohistological measurements performed in this study for three adult extant mammals (*L. europaeus*, *O. cuniculus* and *C. capreolus*) and three subadult or adult extinct synapsids (*M. nmachouensis*, *Lystrosaurus* and *Oudenodon*) were made in the deep cortex. In addition to this histological information, the structure of a phylogenetic tree was taken into account, expressed as a set of eigenfunctions, termed phylogenetic eigenvector maps. Afterwards, a subset of phylogenetic eigenfunctions and bone histological variables were selected to infer resting metabolic rates for species in the tree for which these trait data are otherwise lacking (*M. nmachouensis*, *Lystrosaurus* and *Oudenodon*). For each model (one constructed using femora and another using humeri), we calculated the Akaike information criterion (AIC) values to select the osteohistological variable (density, size or shape of osteocyte lacunae) that best fits with the phylogeny transcribed as eigenvectors. We choose the variable corresponding to the smallest AIC value. The combination of this selected variable and the eigenvectors (i.e. the phylogeny) allowed us to predict the dependent variable (metabolic rate) unknown in fossils. We performed the analyses using the R package MPSEM (Guénard et al., 2013) and constructed an inference model for each bone (humerus and femur). We selected the best set of variables among phylogenetic eigenvector maps plus one of the three histological characters, using their AIC corrected for finite sample sizes (Burnham, Anderson & Huyvaert, 2011), and cross-validated using leave-one-out cross-validation. Indeed, including more than one histological copredictor might have been a potential source of power loss considering our rather small sample size (Legendre *et al.*, 2016). In this way, we were able to infer the resting metabolic rates of *M. nmachouensis*, *Lystrosaurus* and *Oudenodon* with their 95% confidence intervals ($CI_{95\%}$). We obtained two resting metabolic rate values for each taxon, one using the humerus and the other using the femur. We used the highest estimation in our comparative analysis because a given specimen with the resting metabolic rate of an endotherm (e.g. *M. murinus*, Montes *et al.*, 2007) can grow slowly (*M. murinus*, Castanet *et al.*, 2004), but the contrary is not true (e.g. ectotherms including active animals such as *Varanus* have low resting metabolic rates and grow slowly; Montes *et al.*, 2007).

RESULTS

Microanatomical features

The humerus microstructure is relatively homogeneous with thin osseous trabeculae and reduced intertrabecular spaces occupying most of the section (Fig. 1A). The medullary area is difficult to distinguish from the cortex, although the tightness of the spongiosa becomes tighter (smaller intertrabecular spaces) away from the section centre.

The femur displays a thick compact cortex with a distinct medullary zone occupied by thin osseous trabeculae (Fig. 1B). Unfortunately the state of preservation prevents us to conclude whether an open medullary cavity occurred in the core of the section or whether the whole medullary area was occupied by a spongiosa.

Histological features

Moghreberia nmachouensis humerus. Bone is highly vascularized. An intense remodelling (i.e. process of bone resorption and the subsequent deposition of new bone over the resorption surfaces) extends from the inner to the outer cortex. It is of two types: (1) centripetal secondary bone platings on resorption lines (numerous cementing lines in various directions) with no formation of secondary osteons (Fig. 2A), on most of the section; and (2) Haversian remodelling, with secondary osteons (Fig. 2B), on the posterior and dorsal borders. Remains of primary bone are rare. They nevertheless suggest that primary bone consists in iFLB (sensu Klein [2010]; Fig. 2C), that is, with primary bone consisting of both PFB and woven bone and the vascular canals not being all primary osteons. Avascular PFB is observed at the periphery of the outer cortex locally along the posteroventral and posterodorsal borders. It is also observed as thin layers alternating with layers of iFLB, illustrating an alternation of zones (iFLB) and annuli (PFB; Fig. 2C). Important concentrations of Sharpey's fibres inserted rather perpendicularly to the collagen fibres are observed at the three pointed extremities of the section.

Moghreberia nmachouensis femur. As opposed to what is observed in the humerus, the femur is essentially composed of Haversian bone and remodelling extends up to the periphery of the outer cortex on the posteromedial and anterolateral borders, with only a few remains of primary bone on the periphery. The transition zone between the cortex and the medullary area is characterized by a loose spongiosa of secondary bone with only a few secondary osteons that show a large lumen (Fig. 2D). Bone vascularity is high in most of the cortex, but the vascular canal density decreases in the periphery of the anteromedial and anterolateral borders. Primary bone also consists of incipient FLB with some osteons aligned in concentric layers, alternating with thin layers of avascular PFB. Vascular canals are essentially longitudinal with circular and radial (even oblique) anastomoses. Sharpey's fibres are concentrated on the posterior border (less on the anterolateral and anteromedial borders). On

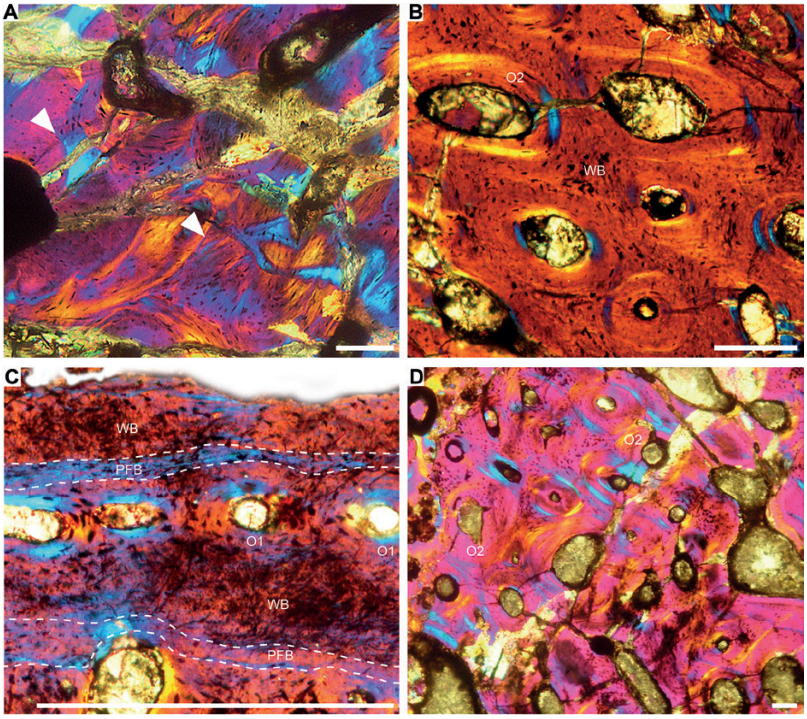

Figure 2. Qualitative histology of the *Moghreberia* humerus MNHN.F.ALM 297 (A–C) and femur MNHN.F.ALM 100 (D). (A) Secondary bone (remodelling with no formation of secondary osteons); arrowheads point to cementing lines; (B) secondary bone (Haversian remodelling) formed within a matrix of primary woven bone; (C) alternation of zones (mainly made of woven bone) and annuli (made of PFB). The incipient FLB observed within zones contains a bone matrix formed of woven and PFB and sparse vascular canals, some of which form primary osteons; (D) secondary osteons at the perimedullary zone. Abbreviations: O1, primary osteon; O2, secondary osteon; PFB, parallel-fibered bone; WB, woven bone. Scale bars represent 0.1 mm.

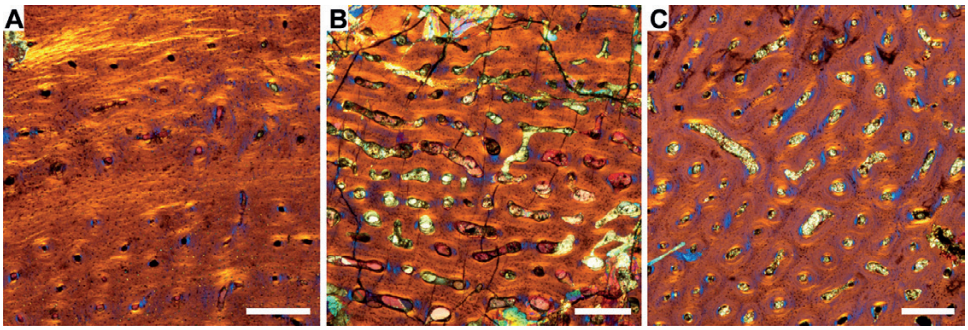

Figure 3. Occurrence of FLB and/or incipient FLB in *Lystrosaurus* sp. (A, B) and *Oudenodon baini* (C). (A) Humerus 24.1: primary bone consisting of parallel-fibered bone and woven bone (incipient FLB); (B) Femur 11–15: FLB; (C) unnumbered femur: FLB (also found in the humerus of this taxon). Scale bars represent 0.1 mm.

the posteromedial border, they are associated with a modification of the vascular canal orientation, the latter being oriented in the same direction as the fibres.

Neither the humerus nor the femur of *M. nmachouensis* shows a high concentration of growth marks or even a layer of PFB (thicker than an annulus) near the bone periphery.

Lystrosaurus and *Oudenodon* humeri and femora were analysed for comparative purposes. *Lystrosaurus* humerus shows incipient FLB (Fig. 3A), whereas *Lystrosaurus* femur shows well-developed FLB (Fig. 3B). *Oudenodon* femur (Fig. 3C) and humerus (not shown) are composed of well-developed FLB. *Lystrosaurus* and *Oudenodon* humeri and femora

show a lower quantity of secondary bone than the corresponding *Moghreberia* bones.

Resting metabolic rate inference models

For the humerus, the AIC suggests that the more accurate model includes the shape of osteocyte lacunae in addition to the selected phylogenetic eigenvector maps (R^2 = 0.9901686; AIC score = 18.66448). The mass-independent resting metabolic rate values (in $mLO_2\ h^{-1}\ g^{-0.67}$) inferred for the three taxa are: *Moghreberia*: 1.76 ($CI_{95\%}$ = [1.31, 2.37]); *Lystrosaurus*: 2.43 ($CI_{95\%}$ = [1.95, 3.03]); and *Oudenodon*: 1.09 ($CI_{95\%}$ = [0.88, 1.34]).

For the femur, the AIC suggests a model that includes the osteocyte lacunae density in addition to the selected phylogenetic eigenvector maps (R^2 = 0.993772; AIC score = 18.61558). The resting metabolic rate values (in $mLO_2\ h^{-1}\ g^{-0.67}$) inferred for the three taxa are: *Moghreberia*: 2.58 ($CI_{95\%}$ = [1.94, 3.43]); *Lystrosaurus*: 3.80 ($CI_{95\%}$ = [3.04, 4.76]); and *Oudenodon*: 4.58 ($CI_{95\%}$ = [3.63, 5.82]).

As stated in the 'Materials and methods' section, of the two mass-independent resting metabolic rate values inferred for each taxon (one using the model constructed using femora and the other using the model constructed using humeri), we used the higher one in our comparative analysis. In all three taxa, the higher value was inferred using the femora. These values are represented in Fig. 4 together with values experimentally measured in extant taxa. Dataset is available as supplementary information.

DISCUSSION

The parsimony method suggests that avian and mammalian endothermies are convergent (i.e. non-inherited from a common ancestor). These independent acquisitions of endothermy are major events in vertebrate evolution since they were the driving force of a suite of correlated changes in the respiratory and the circulatory systems, as well as in physiological, behavioural and ecological traits (Seymour *et al.*, 2004).

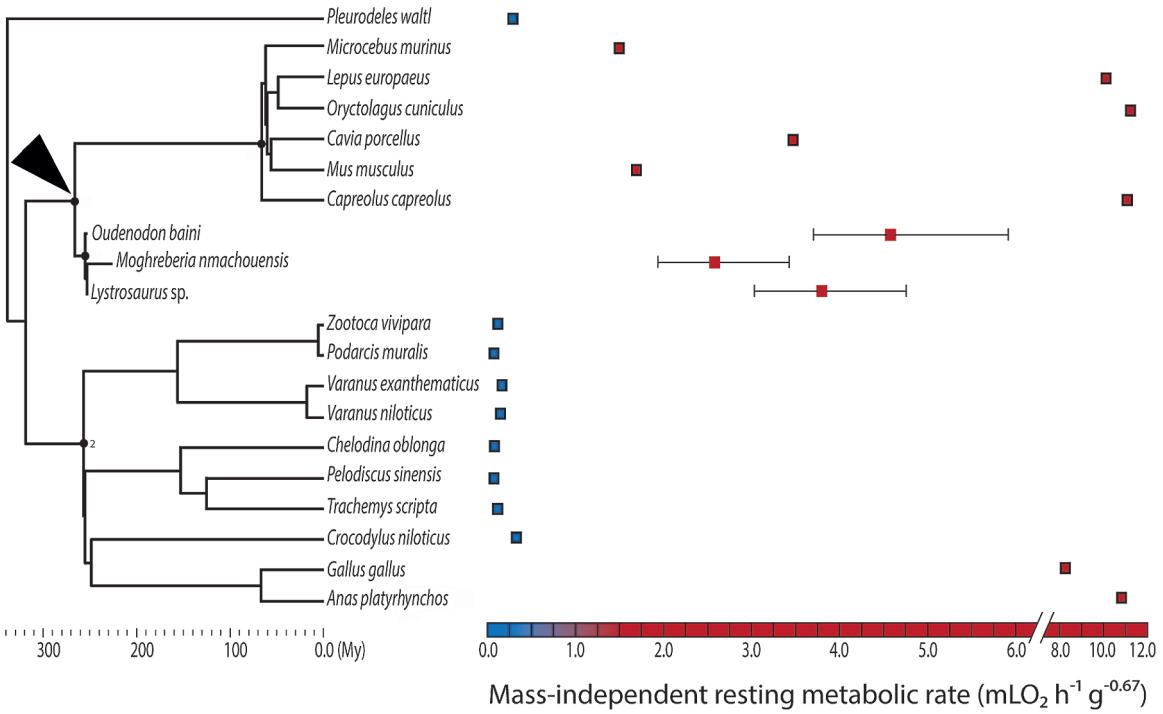

Figure 4. Mass-independent resting metabolic rate ($mLO_2\ h^{-1}\ g^{-0.67}$) for the species sampled in this study. For all extant taxa but *Lepus*, *Oryctolagus* and *Capreolus*, mass-independent resting metabolic rates (in $mLO_2\ h^{-1}\ g^{-0.67}$) were experimentally quantified by Montes *et al.* (2007) and histological data are taken from Legendre *et al.* (2016). For *Lepus*, *Oryctolagus* and *Capreolus*, mass-independent resting metabolic rates were taken respectively from Hackländer et al. (2002), Seltmann *et al.* (2009) and Mauget *et al.* (1999) and histological data were quantified in this study. For extinct taxa, histological data were quantified in this study, and mass-independent resting metabolic rates were estimated using phylogenetic eigenvector maps. For extant species, red dots correspond to endotherms (mammals and birds) and blue dots to ectotherms (all other taxa). We show inferred values for the fossil taxa with the corresponding 95% confidence intervals. Arrowhead shows the acquisition of endothermy by synapsids.

Bone palaeohistology is a reliable method that has been extensively used to infer the resting metabolic rates and physiological thermoregulation of extinct diapsids. Two approaches have been used. On the one hand, several authors performed *indirect* inferences of physiological thermoregulation assuming a relationship between bone growth rates and resting metabolic rate (Montes *et al.*, 2007). Indeed, de Ricqlès *et al.* (2003, 2008) inferred bone growth rates from bone tissue types using a qualitative approach and Amprino's rule (Montes *et al.*, 2010). Other authors performed quantitative palaeohistological inferences of bone growth rates (Cubo *et al.*, 2012; Legendre, Segalen & Cubo, 2013). On the other hand, some authors performed *direct* inferences of resting metabolic rates in extinct diapsids using bone palaeohistology and phylogenetic eigenvector maps (Legendre *et al.*, 2016). Here we used qualitative and quantitative histology to infer respectively growth patterns and resting metabolic rates of *M. nmachouensis*.

Growth rate and stage

(1) Ontogenetic stage. The *Moghreberia* humeral section shows a high remodelling activity and, in periphery, a cyclical growth with zones and annuli. Following the analysis of Ray *et al.* (2005) on *Lystrosaurus*, this would suggest, if *Moghreberia* grows in a similar way as *Lystrosaurus*, that the individual was at least subadult. Similarly, high remodelling has been tentatively interpreted as suggesting a nonjuvenile ontogenetic stage (Ray & Chinsamy, 2004; Ray *et al.*, 2004). This is consistent with the anatomy that suggests a subadult ontogenetic stage.

The femoral section shows again a high remodelling activity and an alternation of zones and annuli associated with a reduction in the degree of vascularization towards the bone periphery. Although the morphology suggests a juvenile ontogenetic stage (small size, loss of the epiphyses; Gale [1988]), the histology is rather in accordance with an at least subadult ontogenetic stage (Ray *et al.*, 2005; Ray, Bandyopadhyay & Appana, 2010).

(2) Growth rate. The occurrence of well-developed FLB and the very high vascularization observed in *Lystrosaurus* femur (Fig. 3B) and *Oudenodon* femur (Fig. 3C) and humerus (not shown) evoke previous observations made on the Permian dicynodonts *Endothiodon*, *Diictodon*, *Oudenodon*, and *Tropidostoma* (Chinsamy & Rubidge, 1993; Botha, 2003; Botha & Angielczyck, 2007; Botha-Brink & Angielczyk, 2010) and the Triassic dicynodonts *Placerias*, *Lystrosaurus*, *Wadiasaurus*, and *Kannemeyeria* (Botha-Brink & Angielczyck, 2010; Green, Schweitzer & Lamm, 2010; Ray *et al.*, 2005, 2010; Ray, Botha & Chinsamy, 2012; Green & Chinsamy-Turan, 2012). In contrast, *Moghreberia* humerus and femur and *Lystrosaurus* humerus lack a well-developed FLB but show incipient FLB. Fibrolamellar bone is generally observed in mammals and birds (e.g. Chinsamy & Elzanowski, 2001; Kolb *et al.*, 2015) and associated with rapid osteogenesis in extant and extinct taxa (e.g. Chinsamy & Rubidge, 1993; Padian, de Ricqlès & Horner, 2001; Ray & Chinsamy, 2004; Chinsamy & Tumarkin-Deratzian, 2009). As bone growth rate is associated, though indirectly, to metabolic rate (Reid, 1987; Padian *et al.*, 2001; Chinsamy-Turan, 2005; Montes *et al.*, 2007), FLB is generally associated with endothermy. Please keep in mind that although FLB is also observed in some ectothermic Crocodylia (Tumarkin-Deratzian, 2007; Woodward, Horner & Farlow, 2014), this presence is probably an atavistic characteristic inherited from the endothermic last common ancestor of archosaurs (Seymour *et al.*, 2004).

Incipient FLB, described by Klein (2010), has also been observed in temnospondyls (Konietzko-Meier & Schmitt, 2013), sauropterygians (pachypleurosaurs, nothosaurs; Klein, 2012; Klein *et al.*, 2016), phytosaurs (de Ricqlès *et al.*, 2003) and mosasaurs (Houssaye *et al.*, 2013), but also in the pelycosaur *Dimetrodon* (Shelton *et al.*, 2013). Considering that it has been shown that the PFB is formed at a lower growth rate than the woven bone, the presence of incipient FLB suggests a lower growth rate than the presence of well-developed FLB. Therefore, qualitative histological observations suggest increasing growth rates from *Moghreberia* (the presence of incipient FLB in humerus and femur) to *Oudenodon* (the presence of well-developed FLB in humerus and femur) and intermediate values for *Lystrosaurus* (the presence of well-developed FLB in the femur but presence of incipient FLB in the humerus). However, qualitative histology does not allow reliable inferences about the occurrence of endothermy.

(3) Bone remodelling. The strong remodelling in the long bones of *Moghreberia* evokes that observed in *Placerias* and *Kannemeyeria* (Green *et al.*, 2010; Ray *et al.*, 2012). It is, however, much more limited in other dicynodonts, where it essentially occurs in the medullary spongiosa and only extends up to the perimedullary region in adult specimens (Ray & Chinsamy, 2004; Ray *et al.*, 2005, 2012; Ray, Bandyopadhyay & Bhawal, 2009; Botha-Brink & Angielczyk, 2010) and where it is much scarcer in the rest of the cortex. Bone remodelling is interpreted as reflecting biomechanical constraints (Currey, 2003; Skedros *et al.*, 2007) but is also considered associated with an active metabolism (Currey, 2003), related to the blood flow of the bone vascular network (Seymour *et al.*, 2012) or to the size of the skeletal elements (Padian, Werning & Horner, 2016). This would be consistent with the hypothesis of a high metabolism in *Moghreberia*. However, comparative

data remain too limited to discuss further the possible physiological significance of bone remodelling.

Resting metabolic rate inference models

Palaeobiological inferences obtained using femoral quantitative histology (size, shape and density of osteocyte lacunae) and phylogenetic eigenvector maps suggest that the three taxa analysed – *M. nmachouensis*, *Lystrosaurus* and *Oudenodon baini* – had high mass-independent resting metabolic rates ($mLO_2\ h^{-1}\ g^{-0.67}$), similar to, or even higher than, those observed in some of the extant mammals from our sample (Fig. 4). These inferences are congruent with the conclusions obtained using qualitative histology (see above), according to which, assuming Amprino's rule, bone growth rates may increase from *Moghreberia* (characterized by the presence of incipient FLB in humerus and femur), to *Lystrosaurus* (the presence of incipient FLB in the humerus but the presence of well-developed FLB in the femur) to *Oudenodon* (the presence of well-developed FLB in both the humerus and the femur). Of the two mass-independent resting metabolic rate values inferred for each taxon (one using the femur and other using the humerus), we used the higher one (that obtained using the femur; cf. methods) in our comparative analysis. Of the three extinct taxa analysed, *Oudenodon* had the highest mass-independent resting metabolic rate. This result is the outcome of two facts: (1) the histological variable selected by the phylogenetic eigenvector maps for the femoral model was osteocyte lacunae density, and (2) *Oudenodon* shows the highest osteocyte lacunae density (0.00496 osteocyte lacunae/μm^2), followed by *Lystrosaurus* (0.00428 osteocyte lacunae/μm^2) and *Moghreberia* (0.00316 osteocyte lacunae/μm^2). Thus palaeobiological inferences performed in this study are robust because results obtained using quantitative histology and phylogenetic eigenvector maps are consistent with those obtained using qualitative histology.

Rey (2016) analysed the isotopic composition of mineralized tissues and concluded that endothermy was acquired twice among synapsids, by the non-*Dicynodon* Dicynodontoidea and the Eucynodontia. The optimization of our results onto the phylogeny using the parsimony method suggests a different pattern (Fig. 4): endothermy was acquired only once among synapsids, by the last common ancestor of Neotherapsida (i.e. the last common ancestor of mammals and *Oudenodon* more than 260 Myr ago). Once endothermy was acquired by the last common ancestor of Neotherapsida, taxa within this clade are expected to show high mass-independent resting metabolic rate values. Natural selection may have promoted slight variations in the mass-independent resting metabolic rate of *Oudenodon*, *Lystrosaurus* and *Moghreberia,* but the inferred values fall within the range of variation observed in extant mammals (Fig. 4).

In conclusion, quantitative histology and phylogenetic eigenvector maps developed by Guénard et al. (2013) and recently used by Legendre *et al.* (2016) allowed us to better constrain the temporal (more than 260 Myr ago) and phylogenetic (Neotherapsida) frames of the acquisition of mammalian endothermy.

ACKNOWLEDGEMENTS

We would like to express our gratitude to L. Legendre (Bloemfontein National Museum, South Africa) for helping us with statistical analyses, to A. de Ricqlès (Université Pierre et Marie Curie, Paris, France) and V. de Buffrénil (Muséum National d'Histoire Naturelle, Paris, France) for allowing access to collection specimens and to H. Lamrous (UPMC) and S. Morel (MNHN) for the preparation of the thin sections. We also thank H. Bourget (MNHN) for the execution of the moulds and L. Zylberberg (UPMC) for access to her microscope. Many thanks also to Jennifer Botha-Brink, Kirstin Brink and an anonymous reviewer for their helpful comments.

REFERENCES

Botha J. 2003. Biological aspects of the Permian dicynodont *Oudenodon* (Therapsida, Dicynodontia), deduced from bone histology and cross-sectional geometry. *Palaeontologia Africana* **39:** 37–44.

Botha J, Angielczyk KD. 2007. An integrative approach to distinguishing the Late Permian dicynodont species Oudenodon bainii and Tropidostoma microtrema (Therapsida: Anomodontia). *Palaeontology* **50**: 1175–1209.

Botha J, Chinsamy A. 2000. Growth patterns deduced from the bone histology of the cynodonts *Diademodon* and *Cynognathus*. *Journal of Vertebrate Paleontology* **20:** 705–711.

Botha J, Chinsamy A. 2004. Growth and life habits of the Triassic cynodont *Trirachodon*, inferred from bone histology. *Acta Palaeontologica Polonica* **49:** 619–627.

Botha J, Chinsamy A. 2005. Growth patterns of *Thrinaxodon liorhinus*, a non-mammalian Cynodont from the Lower Triassic of South Africa. *Palaeontology* **48:** 385–394.

Botha J, Smith RMH. 2007. *Lystrosaurus* species composition across the Permo-Triassic boundary in the Karoo Basin of South Africa: *Lystrosaurus* across the PTB. *Lethaia* **40:** 125–137.

Botha-Brink J, Angielczyk KD. 2010. Do extraordinarily high growth rates in Permo-Triassic dicynodonts (Therapsida, Anomodontia) explain their success before and after the end-Permian extinction? *Zoological Journal of the Linnean Society* **160:** 341–365.

Botha-Brink J, Abdala F, Chinsamy A. 2012. The radiation and osteohistology of nonmammaliaform cynodonts. In: Chinsamy-Turan A, ed. *Forerunners of Mammals: radiation, histology and biology*. Bloomington: Indiana University Press, 223–246.

Burnham KP, Anderson DR, Huyvaert KP. 2011. AIC model selection and multimodel inference in behavioral ecology: some background, observations, and comparisons. *Behavioral Ecology and Sociobiology* **65:** 3–35.

Castanet J, Croci S, Aujard F, Perret M, Cubo J, de Margerie E. 2004. Lines of arrested growth in bone and age estimation in a small primate: *Microcebus murinus*. *Journal of Zoology* **263:** 31–39.

Chinsamy A. 2012. The microstructure of bones and teeth of nonmammalian Therapsids. In: Chinsamy-Turan A, ed. *Forerunners of mammals: radiation, histology and biology*. Bloomington: Indiana University Press, 68–89.

Chinsamy A, Elzanowski A. 2001. Bone histology. Evolution of growth pattern in birds. *Nature* **412:** 402–403.

Chinsamy A, Hurum JH. 2006. Bone microstructure and growth patterns of early mammals. *Acta Palaeontologica Polonica* **51:** 325–338.

Chinsamy A, Ray S. 2012. Bone histology of some therocephalians and gorgonopsians, and evidence of bone degradation by fungi. In: Chinsamy-Turan A, ed. *Forerunners of mammals: radiation, histology and biology*. Bloomington: Indiana University Press, 199–221.

Chinsamy A, Rubidge BS. 1993. Dicynodont (Therapsida) bone histology: phylogenetic and physiological implications. *Palaeontologia Africana* **30:** 97–102.

Chinsamy A, Tumarkin-Deratzian A. 2009. Pathologic bone tissues in a Turkey vulture and a nonavian dinosaur: implications for interpreting endosteal bone and radial fibrolamellar bone in fossil dinosaurs. *Anatomical record (Hoboken, N.J.: 2007)* **292:** 1478–1484.

Chinsamy-Turan A. 2005. *The microstructure of dinosaur bone: deciphering biology with fine-scale techniques*. Baltimore: Johns Hopkins University Press.

Cox CB. 1991. The Pangaea dicynodont *Rechnisaurus* and the comparative biostratigraphy of Triassic dicynodont faunas. *Palaeontology* **34:** 767–784.

Cubo J, Le Roy N, Martinez-Maza C, Montes L. 2012. Paleohistological estimation of bone growth rate in extinct archosaurs. *Paleobiology* **38:** 335–349.

Currey JD. 2003. The many adaptations of bone. *Journal of Biomechanics* **36:** 1487–1495.

de Ricqlès A. 1969. Recherches paléohistologiques sur les os longs des Tétrapodes: Quelques observations sur la structure des os longs des Thériodontes. *Annales de Paléontologie* **55:** 1–52.

de Ricqlès A. 1972. Recherches paléohistologiques sur les os longs des Tétrapodes: Titanosuchiens, Dinocéphales et Dicynodontes. *Annales de Paléontologie* **58:** 1–78.

de Ricqlès A, Meunier FJ, Castanet J, Francillon-Vieillot H. 1991. Comparative microstructure of bone. *Bone* **3:** 1–78.

de Ricqlès A, Padian K, Horner JR. 2003. On the bone histology of some Triassic pseudosuchian archosaurs and related taxa. *Annales de Paléontologie* **89:** 67–101.

de Ricqlès A, Padian K, Knoll F, Horner JR. 2008. On the origin of high growth rates in archosaurs and their ancient relatives: complementary histological studies on Triassic archosauriforms and the problem of a 'phylogenetic signal' in bone histology. *Annales de Paléontologie* **94:** 57–76.

Dutuit JM. 1988. Ostéologie crânienne et ses enseignements, apports géologique et paléoécologique, de *Moghreberia nmachouensis*, Dicynodonte (Reptilia, Therapsida) du Trias supérieur marocain. *Bulletin du Muséum National d'Histoire Naturelle* **3:** 227–285.

Florides GA, Kalogirou SA, Tassou SA, Wrobel L. 2001. Natural environment and thermal behaviour of Dimetrodon limbatus. *Journal of Thermal Biology* **26:** 15–20.

Francillon-Vieillot H, de Buffrénil V, Castanet J, Géraudie J, Meunier FJ, Sire JY, Zylbeberg L, de Ricqlès A. 1990. Microstructure and mineralization of vertebrate skeletal tissues. In: Carter JG, ed. *Skeletal biomineralization: patterns, processes and evolutionary trends*. New York: Van Nostrand Reinhold, 471–530.

Fröbisch J. 2007. The cranial anatomy of *Kombuisia frerensis* Hotton (Synapsida, Dicynodontia) and a new phylogeny of anomodont therapsids. *Zoological Journal of the Linnean Society* **150:** 117–144.

Fröbisch J. 2009. Composition and similarity of global anomodont-bearing tetrapod faunas. *Earth-Science Reviews* **95:** 119–157.

Gale TM. 1988. Comments on a 'nest' of juvenile dicynodont reptiles. *Modern Geology* **13:** 119–124.

Green J, Chinsamy-Turan A. 2012. Bone and dental histology of Late Triassic dicynodonts from North America. In: Chinsamy-Turan A, ed. *Forerunners of mammals: radiation, histology and biology*. Bloomington: Indiana University Press, 178–196.

Green JL, Schweitzer MH, Lamm ET. 2010. Limb bone histology and growth in *Placerias hesternus* (Therapsida: Anomodontia) from the Upper Triassic of North America. *Palaeontology* **53:** 347–364.

Guenard G, Legendre P, Peres-Neto P. 2013. Phylogenetic eigenvector maps: a framework to model and predict species traits. *Methods in Ecology and Evolution* **4:** 1120–1131.

Hackländer K, Arnold W, Ruf T. 2002. Postnatal development and thermoregulation in the precocial European hare (Lepus europaeus). *Journal of Comparative Physiology. B, Biochemical, Systemic, and Environmental Physiology* **172:** 183–190.

Houssaye A, Lindgren J, Pellegrini R, Lee AH, Germain D, Polcyn MJ. 2013. Microanatomical and histological features in the long bones of Mosasaurine mosasaurs (Reptilia, Squamata)–implications for aquatic adaptation and growth rates. *PLoS ONE* **8:** e76741.

Huttenlocker AK, Botha-Brink J. 2014. Bone microstructure and the evolution of growth patterns in Permo-Triassic therocephalians (Amniota, Therapsida) of South Africa. *PeerJ* **2:** e325.

Ji Q, Luo ZX, Yuan CX, Tabrum AR. 2006. A swimming mammaliaform from the Middle Jurassic and ecomorphological diversification of early mammals. *Science (New York, N.Y.)* **311:** 1123–1127.

Kammerer CF, Fröbisch J, Angielczyk KD. 2013. On the validity and phylogenetic position of Eubrachiosaurus browni, a kannemeyeriiform dicynodont (Anomodontia) from Triassic North America. *PLoS One* **8:** e64203.

Klein N. 2010. Long bone histology of sauropterygia from the lower Muschelkalk of the Germanic basin provides unexpected implications for phylogeny. *PLoS One* **5:** e11613.

Klein N. 2012. Postcranial morphology and growth of the pachypleurosaur *Anarosaurus heterodontus* (Sauropterygia) from the Lower Muschelkalk of Winterswijk, The Netherlands. *Paläontologische Zeitschrift* **86:** 389–408.

Klein N, Sander PM, Krahl A, Scheyer TM, Houssaye A. 2016. Diverse aquatic adaptations in Nothosaurus spp. (Sauropterygia)-inferences from humeral histology and microanatomy. *PLoS One* **11:** e0158448.

Kolb C, Scheyer TM, Veitschegger K, Forasiepi AM, Amson E, Van der Geer AA, Van den Hoek Ostende LW, Hayashi S, Sánchez-Villagra MR. 2015. Mammalian bone palaeohistology: a survey and new data with emphasis on island forms. *PeerJ* **3:** e1358.

Konietzko-Meier D, Sander PM. 2013. Long bone histology of *Metoposaurus diagnosticus* (Temnospondyli) from the Late Triassic of Krasiejów (Poland) and its paleobiological implications. *Journal of Vertebrate Paleontology* **33:** 1003–1018.

Konietzko-Meier D, Schmitt A. 2013. A histological study of a femur of *Plagiosuchus*, a Middle Triassic temnospondyl amphibian from southern Germany, using thin sections and micro-CT scanning. *Netherlands Journal of Geosciences* **92:** 97–108.

Laurin M, de Buffrenil V. 2016. Microstructural features of the femur in early ophiacodontids: a reappraisal of ancestral habitat use and lifestyle of amniotes. *Comptes Rendus Palevol* **15:** 115–127.

Lee AH. 2004. Histological organization and its relationship to function in the femur of Alligator mississippiensis. *Journal of Anatomy* **204:** 197–207.

Legendre LJ, Guénard G, Botha-Brink J, Cubo J. 2016. Palaeohistological evidence for ancestral high metabolic rate in Archosaurs. *Systematic Biology* **65:** 989–996.

Legendre LJ, Segalen L, Cubo J. 2013. Evidence for high bone growth rate in *Euparkeria* obtained using a new paleohistological inference model for the humerus. *Journal of Vertebrate Paleontology* **33:** 1343–1350.

Maisch MW, Matzke AT. 2014. *Sungeodon kimkraemerae* n. gen. n. sp., the oldest kannemeyeriiform (Therapsida, Dicynodontia) and its implications for the early diversification of large herbivores after the P/T boundary. *Neues Jahrbuch für Geologie und Paläontologie* **272:** 1–12.

Mauget C, Mauget R, Sempéré A. 1999. Energy expenditure in European roe deer fawns during the suckling period and its relationship with maternal reproductive cost. *Canadian Journal of Zoology-Revue Canadienne De Zoologie* **77:** 389–396.

Meng QJ, Ji Q, Zhang YG, Liu D, Grossnickle DM, Luo ZX. 2015. Mammalian evolution. An arboreal docodont from the Jurassic and mammaliaform ecological diversification. *Science (New York, N.Y.)* **347:** 764–768.

Montes L, Castanet J, Cubo J. 2010. Relationship between bone growth rate and bone tissue organization in amniotes: first test of Amprino's rule in a phylogenetic context. *Animal Biology* **60:** 25–41.

Montes L, Le Roy N, Perret M, de Buffrenil V, Castanet J, Cubo J. 2007. Relationships between bone growth rate, body mass and resting metabolic rate in growing amniotes: a phylogenetic approach. *Biological Journal of the Linnean Society* **92:** 63–76.

Padian K, de Ricqlès AJ, Horner JR. 2001. Dinosaurian growth rates and bird origins. *Nature* **412:** 405–408.

Padian K, Horner JR, de Ricqlès A. 2004. Growth in small dinosaurs and pterosaurs: the evolution of archosaurian growth strategies. *Journal of Vertebrate Paleontology* **24:** 555–571.

Padian K, Lamm ET. 2013. *Bone histology of fossil tetrapods: advancing methods, analysis, and interpretation*. Berkeley: University of California Press.

Padian K, Werning S, Horner JR. 2016. A hypothesis of differential secondary bone formation in dinosaurs. *Comptes Rendus Palevol* **15:** 40–48.

Ray S, Bandyopadhyay S, Appana R. 2010. Bone histology of a kannemeyeriid dicynodont *Wadiasaurus*: palaeobiological implications. In: Bandyopadhyay S, ed. *New aspects of mesozoic biodiversity*. Berlin: Springer Berlin Heidelberg, 73–89.

Ray S, Bandyopadhyay S, Bhawal D. 2009. Growth patterns as deduced from bone microstructure of some selected neotherapsids with special emphasis on dicynodonts: phylogenetic implications. *Palaeoword* **18:** 53–66.

Ray S, Botha J, Chinsamy A. 2004. Bone histology and growth patterns of some nonmammalian therapsids. *Journal of Vertebrate Paleontology* **24:** 634–648.

Ray S, Botha J, Chinsamy A. 2012. Dicynodont growth dynamics and lifestyle adaptations. In: Chinsamy-Turan A, ed. *Forerunners of mammals: radiation, histology and biology*. Bloomington: Indiana University Press, 121–148.

Ray S, Chinsamy A. 2004. *Diictodon feliceps* (Therapsida, Dicynodontia): bone histology, growth, and biomechanics. *Journal of Vertebrate Paleontology* **24:** 180–194.

Ray S, Chinsamy A, Bandyopadhyay S. 2005. *Lystrosaurus murrayi* (Therapsida, Dicynodontia): bone histology, growth and lifestyle adaptations. *Palaeontology* **48:** 1169–1185.

Reid REH. 1987. Bone and dinosaurian 'endothermy'. *Modern Geology* **11:** 133–154.

Rey K. 2016. *Thermophysiologie des thérapsides et changements climatiques du Permien et du Trias (300-200 Ma)*. PhD thesis, Université de Lyon, France.

Ruben J, Hillenius W, Kemp T, Quick D. 2012. The evolution of mammalian endothermy. In: Chinsamy-Turan A, ed. *Forerunners of mammals: radiation, histology and biology*. Bloomington: Indiana University Press, 273–288.

Rubidge BS, Sidor CA. 2001. Evolutionary patterns among Permo-Triassic therapsids. *Annual Review of Ecology and Systematics* **32:** 449–480.

Seltmann MW, Ruf T, Röedel HG. 2009. Effects of body mass and huddling on resting metabolic rates of post-weaned

European rabbits under different simulated weather conditions. *Functional Ecology* **23:** 1070–1080.

Seymour RS, Bennett-Stamper CL, Johnston SD, Carrier DR, Grigg GC. 2004. Evidence for endothermic ancestors of crocodiles at the stem of archosaur evolution. *Physiological and Biochemical Zoology: PBZ* **77:** 1051–1067.

Seymour RS, Smith SL, White CR, Henderson DM, Schwarz-Wings D. 2012. Blood flow to long bones indicates activity metabolism in mammals, reptiles and dinosaurs. *Proceedings of the Royal Society B-Biological Sciences* **279:** 451–456.

Shelton C, Sander PM. 2015. *Ophiacodon* long bone histology: the earliest occurrence of FLB in the mammalian stem lineage. *PeerJ PrePrints* **3:** e1262.

Shelton CD, Sander PM, Stein K, Winkelhorst H. 2013. Long bone histology indicates sympatric species of *Dimetrodon* (Lower Permian, Sphenacodontidae). *Earth and Environmental Science Transactions of the Royal Society of Edinburgh* **103:** 217–236.

Skedros JG, Sorenson SM, Hunt KJ, Holyoak JD. 2007. Ontogenetic structural and material variations in ovine calcanei: a model for interpreting bone adaptation. *Anatomical record (Hoboken, N.J.: 2007)* **290:** 284–300.

Smith R, Botha J. 2005. The recovery of terrestrial vertebrate diversity in the South African Karoo Basin after the end-Permian extinction. *Comptes Rendus Palevol* **4:** 623–636.

Tumarkin-Deratzian AR. 2007. Fibrolamellar bone in wild adult *Alligator mississippiensis*. *Journal of Herpetology* **41:** 341–345.

Walter I, Seebacher F. 2009. Endothermy in birds: underlying molecular mechanisms. *The Journal of Experimental Biology* **212:** 2328–2336.

Woodward HN, Horner JR, Farlow JO. 2014. Quantification of intraskeletal histovariability in *Alligator mississippiensis* and implications for vertebrate osteohistology. *PeerJ* **2:** e422.

Zhou CF, Wu S, Martin T, Luo ZX. 2013. A Jurassic mammaliaform and the earliest mammalian evolutionary adaptations. *Nature* **500:** 163–167.

Palaeophysiological inference models using Phylogenetic Generalised Least Squares applied to the evolution of endothermy in dicynodonts (Synapsida, Therapsida)

Chloé Olivier[1*], Yves Desdevises[2], Lucas Legendre[3], Mathieu Faure-Brac[1] and Jorge Cubo[1]

[1]Sorbonne Université, Museum National d'Histoire Naturelle, CNRS, Centre de Recherche en Paléontologie – Paris (CR2P), 4 pl Jussieu, CP 104, F-75005, Paris, France; e-mails: chloe.olivier@upmc.fr, mathieu.faure-brac@edu.mnhn.fr, jorge.cubo_garcia@upmc.fr

[2]Sorbonne Universités, Sorbonne Université, CNRS, Biologie Intégrative des Organismes Marins (BIOM), Observatoire Océanologique de Banyuls/Mer, F-66650, Banyuls/Mer, France; e-mails: desdevises@obs-banyuls.fr

[3]Jackson School of Geosciences, The University of Texas at Austin, Austin, TX, USA; e-mail: lucasjlegendre@gmail.com

*Corresponding author

Reject with option to resubmit in *Palaeontology* in December 2019

PAPER IV

Palaeophysiological Inference Models Using Phylogenetic Generalised Least Squares Applied to the Evolution of Endothermy in Dicynodonts (Synapsida, Therapsida)

CHLOÉ OLIVIER[1*], YVES DESDEVISES[2], LUCAS LEGENDRE[3], MATHIEU FAURE-BRAC[1] *and* JORGE CUBO[1]

[1]Sorbonne Université, Museum National d'Histoire Naturelle, CNRS, Centre de Recherche en Paléontologie – Paris (CR2P), 4 pl Jussieu, CP 104, F-75005, Paris, France; e-mails: chloe.olivier@upmc.fr, mathieu.faure-brac@edu.mnhn.fr, jorge.cubo_garcia@upmc.fr

[2]Sorbonne Universités, Sorbonne Université, CNRS, Biologie Intégrative des Organismes Marins (BIOM), Observatoire Océanologique de Banyuls/Mer, F-66650, Banyuls/Mer, France; e-mails: desdevises@obs-banyuls.fr

[3]Jackson School of Geosciences, The University of Texas at Austin, Austin, TX, USA; e-mail: lucasjlegendre@gmail.com

*Corresponding author

Abstract: Palaeobiological inference modelling is increasingly used to infer biological or ecological traits in extinct taxa and understand their evolution. Recently, many studies have used palaeohistological inference models to infer the resting metabolic rate of sauropsids and synapsids and investigate the origin and evolution of endothermy independently acquired in these two clades. The inclusion of the phylogeny as predictive variables was recently performed using Phylogenetic Eigenvector Maps. In the present study, we used the phylogenetic generalised least squares in a Monte Carlo Markov Chain framework that enables the introduction of a combination of histological variables and the modelling of a more accurate evolutionary model. We built palaeohistological inference models based on Phylogenetic Generalised Least Squares to understand the evolution of endothermy in synapsids. For comparative purpose, inference models using Phylogenetic Eigenvector Maps methods were also performed. We used these models to infer the mass-independent resting metabolic rate in a broader sample of dicynodonts than in previous studies. A high resting metabolic rate was inferred for all Permian and Triassic dicynodonts included, corroborating previous qualitative and quantitative histological studies. Optimisation of these inferred values onto a calibrated phylogeny recovered a unique acquisition of endothermy in Synapsida at the Neotherapsida node, at least in the middle Permian (around 260 My). Within Dicynodontia, the inferred values of metabolic rate do not efficiently explain the differential survival rates across the Permo-Triassic boundary, as inferred in the literature.

Key words: dicynodonts, endothermy, palaeohistology, Phylogenetic Generalised Least Squares, Phylogenetic Eigenvector Maps

Dicynodonts survived to the Permo-Triassic crisis and were the most abundant terrestrial herbivores from the middle Permian to the Late Triassic (e.g. Cluver & King 1983). Many studies have focused on qualitative histology to understand their palaeophysiology (e.g. Ricqlès 1972; Chinsamy & Rubidge 1993; Ray & Chinsamy 2004; Botha & Angielczyk 2007; Green *et al.* 2010; Ray *et al.* 2010; Olivier *et al.* 2017). Amprino's rule (Amprino 1947) considers that the inner organisation of bone tissue (orientation of collagen fibers and vascularisation) reflects its bone growth rate. Therefore, the fibrolamellar bone (FLB, i.e., abundant primary osteons infilled with lamellar bone included in a woven bone matrix) is traditionally considered to indicate a high bone growth rate (e.g. Francillon Vieillot *et al.* 1990; Ricqlès *et al.* 1991). A high growth rate has thus been inferred for dicynodonts due to FLB or 'incipient' FLB described in all specimens studied to date: the middle Permian *Eodicynodon* (Botha-Brink & Angielczyk 2010), the late Permian *Aulacephalodon* (Ricqlès 1972; Chinsamy & Rubidge 1993; Botha-Brink and Angielczyk 2010), *Cistecephalus* (Chinsamy & Rubidge 1993; Botha-Brink & Angielczyk 2010), *Dicynodontoides* (Botha-Brink & Angielczyk 2010), *Diictodon* (Chinsamy & Rubidge 1993; Ray & Chinsamy 2004; Botha-Brink & Angielczyk 2010), *Endothiodon* (Chinsamy & Rubidge 1993; Ray *et al.* 2009, 2012; Botha-Brink and Angielczyk 2010), *Oudenodon* (Ricqlès 1972; Chinsamy & Rubidge 1993; Botha 2003; Botha & Angielczyk 2007; Botha-Brink & Angielczyk 2010; Ray *et al.* 2012), *Rhachiocephalus* (Botha-Brink & Angielczyk 2010), and *Tropidostoma* (Botha & Angielczyk 2007; Botha-Brink & Angielczyk 2010), the late Permian-Early Triassic *Lystrosaurus* (Chinsamy & Rubidge 1993; Ray *et al.* 2005, 2012; Botha-Brink & Angielczyk 2010), the Early Triassic *Myosaurus* (Botha-Brink *et al.* 2016), the Middle Triassic *Dinodontosaurus* (Enlow & Brown 1957), *Kannemeyeria* (Enlow & Brown 1957; Chinsamy & Rubidge 1993; Botha-Brink & Angielczyk 2010; Ray *et al.* 2012), and *Wadiasaurus* (Ray *et al.* 2010), and the Late Triassic *Moghreberia* (Olivier *et al.* 2017) and *Placerias* (Green *et al.* 2010; Green 2012). A significant relationship between bone growth rate (BGR) and resting metabolic rate (RMR) has been shown by Montes *et al.* (2007) in amniotes. However, a given bone tissue type (i.e., FLB) used to deduce BGR does not always appear to be associated with a given RMR. For instance, ectothermic alligators are able to form FLB in the wild (Tumarkin-Deratzian 2007), a capacity which could result from a potentially ancestral endothermy in archosaurs (e.g. Seymour *et al.* 2004; Legendre *et al.* 2016).

These relationships have been used to perform palaeobiological inferences. Palaeobiological inference modelling using quantitative histological data in a phylogenetic context is increasingly used to infer the palaeophysiology of extinct taxa and provide elements to understand the evolution of endothermy in sauropsids and synapsids (e.g. Legendre *et al.* 2016; Olivier *et al.* 2017; Fleischle *et al.* 2018; Cubo & Jalil, 2019). A strong phylogenetic signal in bone microstructural features has been described in many studies (e.g. Cubo *et al.* 2005; Germain & Laurin 2005; Botha-Brink & Angielczyk 2010; Legendre *et al.* 2013). Cubo *et al.* (2012) and Legendre *et al.* (2013) built statistical palaeobiological models using histological data to estimate the bone growth rate of extinct archosauromorphs and reconstructed its evolution using a calibrated phylogeny. Then, following the Phylogenetic Eigenvector Maps (PEMs) approach of Guénard *et al.* (2013), Legendre *et al.* (2016) improved these palaeobiological inference models based on histological variables by including phylogeny as a predictive variable for the first time. Olivier *et al.* (2017) built two inference models (humerus and femur), following the method of Legendre *et al.* (2016), and inferred a high RMR in three dicynodonts (*Moghreberia*, *Lystrosaurus* and *Oudenodon*). Except for the Permian *Oudenodon*, the geochemical analysis of Rey *et al.* (2017) also recovered an endotherm-like thermoregulation for all studied Triassic therapsids (e.g. *Moghreberia* and *Lystrosaurus*).

The Phylogenetic Generalised Least Squares approach (PGLS) (Grafen 1989; Martins & Hansen 1997; Pagel 1999) with Monte Carlo Markov Chain (MCMC) method (Gilks *et al.* 1995), using the software BayesTraits V3.0.1 (Pagel & Meade 2016), have been used to predict morphological and ecological variables in extinct species (e.g. Organ *et al.* 2007, 2011). On one hand, compared with PEMs, PGLS allow to apply an explicit evolutionary model with multiple parameters to model phylogenetic relationships (e.g. branch length scaling parameters: lambda, kappa, delta, and OU [Ornstein-Uhlenbeck model] parameters) and the evolution of the independent variables (e.g. distribution of coefficients of regression). On the other hand, the selection of the best model in Legendre *et al.* (2016) is solely based on one histological predictive variable, which may not reflect the whole histological information that could be used to predict RMR. Using the PGLS method, Organ *et al.* (2007) performed multiple regressions and included several independent variables to infer the unknown value of the dependent variable.

Few comparative studies with a large phylogenetic bracket have investigated evolutionary patterns of bone histological features (and resting metabolic rate) in dicynodonts (Botha-Brink & Angielczyk 2010; Green 2012; Olivier *et al.* 2017). The main objective of this study is to build palaeophysiological inference models using a combination of histological variables and PGLS methods. Models using PEMs were also built to be compared with the inferred RMR obtained with PGLS and the estimations from previous studies. We used these palaeohistological models to infer resting metabolic rate for a larger sample of dicynodonts and discussed the evolution of RMR within Dicynodontia and more widely in Synapsida.

MATERIAL AND METHODS

Histological and phylogenetic data on the extant and extinct species

Taxa sample. The palaeobiological models were built using the femora and humeri of 16 extant species (including six synapsids, nine sauropsids, and a salamander) with known values of mass-independent resting metabolic rate: *Capreolus capreolus*, *Cavia porcellus*, *Lepus europaeus*, *Microcebus murinus*, *Mus musculus*, *Oryctolagus cuniculus*, *Anas platyrhynchos, Chelodina oblonga, Pelodiscus sinensis, Trachemys scripta, Crocodylus niloticus, Podarcis muralis, Varanus exanthematicus, Varanus niloticus, Zootoca vivpara*, and *Pleurodeles waltl* (Tables 1–2; Appendix 1). Except for *Lepus*, *Oryctolagus*, and *Capreolus*, RMR values were taken from Montes *et al.* (2007). RMR values of *Capreolus, Lepus*, and *Oryctolagus* were respectively taken from Hackländer *et al.* (2002), Seltmann *et al.* (2009), and Mauget *et al.* (1999). Our extinct species sample includes *Daptocephalus* (femur), *Endothiodon* (humerus), *Kannemeyeria simocephalus* (femur), *Lystrosaurus murrayi* (femur and humerus), *Moghreberia nmachouensis* (femur and humerus), *Myosaurus gracilis* (humerus), *Oudenodon baini* (femur and humerus), and *Tropidostoma* (femur and humerus) (Tables 1–2; Appendix 1). This is a larger dicynodont sample than that used by Olivier *et al.* (2017), which included only three dicynodonts (*Lystrosaurus sp.*, *Moghreberia nmachouensis*, and *Oudenodon baini*). Our dicynodont sample ranges from the late Permian (*Endothiodon*, *Daptocephalus*, *Tropidostoma*, and *Oudenodon baini*), Early Triassic (*Lystrosaurus murrayi* and *Myosaurus gracilis*), Middle Triassic (*Kannemeyeria simocephalus*), to Late Triassic (*Moghreberia nmachouensis*) (Dutuit 1988; Fröbisch 2009; Botha-Brink & Angielczyk 2010; Kammerer *et al.* 2011; Viglietti 2016) (Appendix 1).

Histological variables. The effect of body mass on physiological variables, e.g. RMR, has long been established (e.g. Schmidt-Nielsen 1984; Peters 1986; Glazier 2005). The debate about an universal value of the allometric scaling exponent is ongoing, mainly arguing about the limits and benefits of two exponents: a 3/4 (Kleiber's law) or 2/3 (Rubner's rule) power scaling (Schmidt-Nielsen 1984; Dodds *et al.* 2001). Previously calculated RMR of birds and mammals were reviewed by Dodds *et al.* (2001), who did not find evidence in favour of one or the other power scaling exponent. Farrell-Gray & Gotelli (2005) used a likelihood analysis approach to compare the two exponents for RMR of mammals, birds, reptiles, and insects. The 95% confidence intervals of allometric exponent was from 0.72 to 0.73 and from 0.70 to 0.75 for birds and mammals, respectively. However, the confidence interval was from 0.55 to 0.93 for reptiles. The authors thus supported an universal 3/4 power scaling exponent only for endotherms. The meta-analysis of White *et al.* (2007) concluded significant differences between the estimated scaling exponents and a lack of support of a single power scaling exponent model. The results were later supported by the results in mammals of Sieg *et al.* (2009) and Capellini *et al.* (2010). Recently, the results of White *et al.* (2019) also confirmed the previous assumptions and showed an empirical variation of allometric exponents ranging from around 0.55 to 0.76, 0.63 to 0.88, and 0.74 to 1 for birds, mammals and ectotherms (insects, fishes amphibians, reptiles), respectively. Since the influence of mass on biological processes and the lack of consensus on a single allometric exponent law, we used the 2/3-power scaling for the RMR (in $mLO_2\ h^{-1}\ g^{-0.67}$), for comparative purposes, as in Legendre *et al.* (2016), Olivier *et al.* (2017), Fleischle *et al.* (2018), and Cubo & Jalil (2019).

The area, shape, and density of osteocyte lacunae in between primary osteons were quantified by Olivier *et al.* (2017) for *Capreolus, Lepus*, and *Oryctolagus*, and by Legendre *et al.* (2016) for all other extant taxa (Tables 1–2). These histological variables were taken from Olivier *et al.* (2017) for the extinct taxa *Mogreberia nmachouensis* and *Odenodon baini*, and were measured following the procedure proposed by Cubo *et al.* (2012) for *Daptocephalus*, *Endothiodon*, *Kannemeyeria simocephalus*, *Lystrosaurus murrayi*, *Myosaurus gracilis*, and *Tropidostoma* (Tables 1–2; Appendix 1). Fleischle *et al.* (2018) proposed a new histological variable that we included in our analyses, primary osteon density (defined as the proportion of the areas of primary osteons canals and the associated lamellar bone to the whole bone area),

to avoid underestimating vascular density in bones when the canals are mainly running perpendicular to the cutting plane. Primary osteon density was measured in this study for all extant and extinct taxa, following the procedure of Fleischle *et al.* (2018) (Tables 1–2; Appendix 1).

Phylogenetic context. For extant species, the topology and branch lengths were taken from the previous analyses of Benton *et al.* (2015) and Legendre *et al.* (2016). The authors in the literature agree on most phylogenetic relationships between the dicynodont taxa used in the study except for the position of the late Permian dicynodont *Daptocephalus*. Lystrosaurids (including *Lystrosaurus* in our study) are more closely related to kannemeyeriiforms (including *Moghreberia* and *Kannemeyeria* in our study) in the most recent studies, e.g. Cox & Angielczyk (2015), Boos *et al.* (2016), Angielczyk & Kammerer (2017), Kammerer & Smith (2017), and Angielczyk *et al.* (2018). However, *Daptocephalus* is more closely related to kannemeyeriiforms than lystrosaurids in the recent analysis of Olivier *et al.* (2019). The dating of the extinct clades was based on the oldest and youngest known fossils. The youngest appearance and disappearance ages were preferred. Branch lengths were calculated using the studies of Dutuit (1988), Fröbisch (2009), Kammerer *et al.* (2011), and Viglietti (2016). For comparative purposes, we applied models, using PGLS and PEMs methods, within two reference phylogenies: (1) considering the clade (((*Moghreberia*, *Kannemeyeria*), *Daptocephalus*), *Lystrosaurus*) (Olivier *et al.* 2019); and (2) the clade (((*Moghreberia*, *Kannemeyeria*), *Lystrosaurus*), *Daptocephalus*) (e.g. Cox & Angielczyk 2015; Boos *et al.* 2016; Angielczyk & Kammerer 2017; Kammerer & Smith 2017; Angielczyk *et al.* 2018).

Inference models using PGLS

Correlation between RMR and histological variables. The palaeobiological models based on the femur and the humerus were built upon the correlation between the predicted variable RMR (unknown in fossils) and four predictive histological variables (the area, shape, and density of osteocyte lacunae in between primary osteons and the primary osteon density). The data were ln-transformed to meet normality and homoscedasticity requirements.

The contribution of femoral and humeral histological data to predict RMR was assessed using Bayes Factors (Gilks *et al.* 1995) comparing two hypotheses: (1) a regression model where the regression coefficients β of the histological predictive

variables were estimated by the model; and (2) a regression model where the regression coefficients β of the histological predictive variables were forced to be zero (Organ *et al.* 2007). The histological predictive variables (taken one by one and/or in combination with others) explained a significant part of the variance of the RMR (Supplementary data), verified by a Bayes Factor superior to 2.

We also confirmed a significant correlation (Supplementary data) between the humeral and femoral predictive variables (taken one by one and/or in combination with others, for each bone) and RMR in a phylogenetic context using the R package caper and the *pgls* function (Orme 2018). We fixed the evolutionary parameters lambda at 0.7, kappa at 2.5, and delta at 1.5 (values justified below).

Relative significance of the independent variables to the RMR. We analysed the percentage of the variance in the RMR explained by the predictive variables. Considering all four humeral and femoral predictive variables to explain the RMR, the multiple regression, performed with the R package caper and the *pgls* function (Orme 2018), suggested that only the primary osteon density was significantly related to RMR. We evaluated the best selection of variables to build the best multiple regression models comparing their Akaike information criterion (AIC) (Sakamoto *et al.* 1986). The lower AICs were obtained when excluding the osteocyte area and shape for the femur, and the osteocyte area and density for the humerus (Supplementary data). However, as mentioned above, considering histological predictive variables for the femur and humerus one by one, all of them significantly explained a part of the variance of RMR (Supplementary data). We thus built the predictive regression models with all independent variables. Using BayesTraits V3.0.1 (Pagel & Meade 2016) and Bayes Factors, we posteriorly compared models including different combinations of histological variables using the selected model for the femur and the selected model for the humerus (discussed below). Each test yielded a Bayes Factor lower than 2 (Supplementary data), indicating no significant differences between the different combinations of histological variables and thus low risk of overparametrisation in the selected models.

Predictive modelling and model checking with BayesTraits. We followed the method used by Organ *et al.* (2007) to estimate unknown values for fossil taxa using a combination of variables (where values were known for all taxa) within a phylogenetic context. We constructed the inference models using multiple regressions with MCMC

(Gilks *et al.* 1995) and PGLS (Grafen 1989; Martins & Hansen 1997; Pagel 1999). We used the software BayesTraits V3.0.1 (Pagel & Meade 2016) to build the two palaeobiological inference models (respectively based on the femur and the humerus). The number of iterations to run the converged chain was defined at 10,000,000 and the burnin set at 2,000,000. To estimate the marginal likelihood, we used the stepping stone sampler (Xie *et al.* 2011) using 100 stones with 10,000 iterations for each.

We did not want to only focus on the priors and branch length scaling parameters (kappa, lambda, delta, and OU) automatically determined by BayesTraits and performed numerous tests to estimate the best priors of the Bayesian analyses and branch length scaling parameters. We evaluated the adequacy of the regression models by a leave-one-out cross validation, removing all the extant taxa one by one and inferring their RMR (Supplementary data). The posterior predictive modelling were derived from the posterior distributions estimated from the regression models. Overall, the best inferred RMR based on the femur and the humerus of extant taxa was provided with a lambda of 0.7 (i.e., a strong phylogenetic signal in data), kappa of 2.5 (i.e., gradual evolution with more change occurring in longer branches), delta of 1.5 (i.e., longer branches that contribute more to trait evolution indicating an accelerating evolution as time spans), and an exponential β distribution (useful when small regression coefficients are more likely than large ones according to Pagel & Meade (2016), with a mean of 5). In addition, the construction of the two inference models based on the same branch length scaling parameters and exponential β distributions indicated close evolutionary models of the femoral and humeral histological variables and allowed comparison between the results of the two models built.

Inference models using PEMs

For comparative purposes, we built two inference models for the femur and the humerus using PEMs, following the method of Guénard *et al.* (2013), then applied on archosaurs by Legendre *et al.* (2016). We used the four described predictive histological variables (osteocyte area, density, and shape, and primary osteon density) to predict the RMR values of studied dicynodonts. We performed the analyses using the R package MPSEM (Guénard *et al.* 2013).

In the method of PEMs used by Legendre *et al.* (2016), the best models have been selected (using the AICc) relative to: (1) the best set of variables among PEMs; and (2) one of the histological variables that best fit with the predicted variable. Using

the consensus phylogeny (see above; e.g. Cox & Angielczyk 2015; Boos *et al.* 2016; Angielczyk & Kammerer 2017; Kammerer & Smith 2017; Angielczyk *et al.* 2018), the AICc suggested that the more accurate models excluded all histological variables (adjusted R^2= 0.97; AIC score= 29.38) for the humerus and included the osteocyte density (adjusted R^2= 0.99; AIC score= 25.18) for the femur. Considering *Daptocephalus* sister-group of kannemeyeriiformes (Olivier *et al.* 2019), the model for the femur, selected by the AICc, included the osteocyte density (adjusted R^2= 0.99; AIC score= 25.18). In both models, the selected evolutionary model was close to a strict Brownian one. In the same way as for the inference models constructed with PGLS, we checked the predictive power of the selected models using leave-one-out cross-validation.

RESULTS

For each statistical method (PGLS and PEMs), different results were obtained in the models using femoral and humeral histological variables that may be attributed to intra-individual variability (e.g. Castanet *et al.* 2004). We used the highest estimations of RMR in each statistical method, because an ectotherm has a low growth rate most of the time, as opposed to endotherm that can grow slowly or fast (e.g. Castanet *et al.* 2004; Montes *et al.* 2007; Olivier *et al.* 2017). There is very little difference between the highest inferred values of RMR (Tables 3–5) from models using the two phylogenetic contexts: the clades (((*Moghreberia*, *Kannemeyeria*), *Daptocephalus*), *Lystrosaurus*) (Olivier *et al.* 2019) and (((*Moghreberia*, *Kannemeyeria*), *Lystrosaurus*), *Daptocephalus*) (e.g. Cox & Angielczyk 2015; Boos *et al.* 2016; Angielczyk & Kammerer 2017; Kammerer & Smith 2017; Angielczyk *et al.* 2018).

Except for *Endothiodon* and *Myosaurus*, the analyses using PEMs and PGLS both inferred high RMR values for fossils (i.e. values superior to the lowest RMR values of the endotherm extant species, Tables 3–4; Figs 1–2), that we thus supposed endotherms: *Daptocephalus* ($\bar{x}RMR_{Femur}$= 5.6081 $mLO_2\ h^{-1}\ g^{-0.67}$ using PGLS and $\bar{x}RMR_{Femur}$= 3.0039 $mLO_2\ h^{-1}\ g^{-0.67}$ using PEMs), *Kannemeyeria simocephalus* ($\bar{x}RMR_{Femur}$= 8.2487 $mLO_2\ h^{-1}\ g^{-0.67}$ using PGLS and $\bar{x}RMR_{Femur}$= 2.5697 $mLO_2\ h^{-1}\ g^{-0.67}$ using PEMs), *Lystrosaurus murrayi* ($\bar{x}RMR_{Femur}$= 6.4263 $mLO_2\ h^{-1}\ g^{-0.67}$ using PGLS and $\bar{x}RMR_{Femur}$= 3.1099 $mLO_2\ h^{-1}\ g^{-0.67}$ using PEMs), *Moghreberia nmachouensis* ($\bar{x}RMR_{Femur}$= 5.4165 $mLO_2\ h^{-1}\ g^{-0.67}$ using PGLS and $\bar{x}RMR_{Femur}$=

2.3782 $mLO_2\ h^{-1}\ g^{-0.67}$ using PEMs), *Oudenodon baini* ($\bar{x}RMR_{Humerus}$= 3.5929 $mLO_2\ h^{-1}\ g^{-0.67}$ using PGLS and $\bar{x}RMR_{Femur}$= 3.5050 $mLO_2\ h^{-1}\ g^{-0.67}$ using PEMs), and *Tropidostoma* ($\bar{x}RMR_{Humerus}$= 6.1707 $mLO_2\ h^{-1}\ g^{-0.67}$ using PGLS and $\bar{x}RMR_{Femur}$= 2.4354 $mLO_2\ h^{-1}\ g^{-0.67}$ using PEMs). High RMR values were predicted for *Endothiodon* ($\bar{x}RMR_{Humerus}$= 5.4032 $mLO_2\ h^{-1}\ g^{-0.67}$) and *Myosaurus* ($\bar{x}RMR_{Humerus}$= 4.3141 $mLO_2\ h^{-1}\ g^{-0.67}$) by PGLS methods, as opposed to PEMs methods that inferred intermediate RMR values (i.e., variance comprised between the lowest RMR of included endotherm extant taxa and the higher included ectotherm extant taxa) (Fig. 2; Table 4).

DISCUSSION

Selection of the best predictive models using PGLS and their predictive power

As mentioned in the 'Material and Methods' section, the inference models (based on the femur and the humerus) were selected checking the adequacy between the known values of RMR of the studied extant taxa and those predicted by the regression models (i.e., test of the 'predictive power') (Supplementary data). The coefficient of determination R^2 is the most popular measure to assess the fit of a regression model to the data. However, the R^2 of the two 'by hand' selected models (based on the femur and the humerus) was around 0.68 that is not the best value compared to the other evaluated models (Supplementary data). The simultaneous estimations of the branch length scaling parameters (lambda, kappa, delta, and/or OU) by BayesTraits resulted in models with a higher R^2. However, the models based on these automatically estimated parameters more under- or overestimated RMR than the 'by hand' selected models, especially in extant taxa with low RMR values (Supplementary data). The R^2 does not contain much valuable information on the predictive power of a regression model, as already noticed in literature (e.g. Gelman *et al.* 2018).

The 'by hand' selected humeral and femoral regression models using a lambda of 0.7, kappa of 2.5, delta of 1.5, and an exponential β distribution (with a mean of 5) presented the best 'predictive power'. However, the RMR of several extant taxa were strongly under- (*Anas*) or overestimated (*Chelodina*, *Varanus niloticus*, *Microcebus*) by the 'by hand' selected predictive models (Supplementary data). A lambda fixed at 0.7 indicates a strong phylogenetic signal in predictive variables. Given that *Anas* was the only extant avian, and hence the only endothermic sauropsid included in analysis, its

phylogenetic position may explain its underestimated RMR value ($\bar{x}RMR_{Femur}$= 0.798 $mLO_2\ h^{-1}\ g^{-0.67}$ and $\bar{x}RMR_{Humerus}$= 0.680 $mLO_2\ h^{-1}\ g^{-0.67}$). While their known RMR values are equal ($RMR_{\textit{Microcebus}}$= 1.526 $mLO_2\ h^{-1}\ g^{-0.67}$ and $RMR_{\textit{Mus}}$= 1.696 $mLO_2\ h^{-1}\ g^{-0.67}$), the values of the histological variables of *Microcebus* are higher than those of *Mus*, notably for the primary osteon density that appears to be strongly correlated to the RMR (see above) (Tables 1–2). In addition, a kappa fixed at 2.5 and delta at 1.5 means that longer branches more contribute to trait evolution that may explain why the predicted RMR value of *Microcebus* is overestimated and higher than in *Mus* (Fig. I.1; Supplementary data). As for *Microcebus*, the predicted RMR value of *Chelodina* was overestimated and higher than in *Pelodiscus,* probably due to the value of kappa and delta (Fig. I.1; Tables 1–2; Supplementary data). The predicted RMR value of *Varanus niloticus* ($\bar{x}RMR_{Femur}$= 0.324 $mLO_2\ h^{-1}\ g^{-0.67}$ and $\bar{x}RMR_{Humerus}$= 0.328 $mLO_2\ h^{-1}\ g^{-0.67}$) was more overestimated than in *Varanus exanthematicus* ($\bar{x}RMR_{Femur}$= 0.197 $mLO_2\ h^{-1}\ g^{-0.67}$ and $\bar{x}RMR_{Humerus}$=0.195 $mLO_2\ h^{-1}\ g^{-0.67}$), while the known RMR of *V*. *niloticus* (RMR= 0.157 $mLO_2\ h^{-1}\ g^{-0.67}$) is lower than in *V*. *exanthematicus* (RMR= 0.173 $mLO_2\ h^{-1}\ g^{-0.67}$). These two species of *Varanus* present the same branch lengths (Fig. I.1), but the histological variables values are mainly higher in *V. niloticus*, which may explain its higher RMR value than that of *V. exanthematicus* (Tables 1–2).

Inferred RMR values using PEMs or PGLS and comparison

Fibrolamellar or ‘incipient’ fibrolamellar bone, functionally associated with a high bone growth rate, was described in *Daptocephalus* (Botha-Brink & Angielczyk (2010): formerly *Dicynodon* until the taxonomic revision of Kammerer *et al.* (2011)), *Endothiodon* (Chinsamy & Rubidge 1993; Ray *et al.* 2009, 2012; Botha-Brink & Angielczyk 2010), *Kannemeyeria* (Ricqlès 1972; Chinsamy & Rubidge 1993; Botha-Brink & Angielczyk 2010; Ray *et al.* 2012), *Lystrosaurus* (Ricqlès 1972; Chinsamy & Rubidge 1993; Ray *et al.* 2005, 2005, 2012; Botha-Brink and Angielczyk 2010), *Moghreberia* (Olivier *et al.* 2017), *Myosaurus* (Botha-Brink *et al.* 2016), *Oudenodon* (Ricqlès 1972; Chinsamy & Rubidge 1993; Botha 2003; Botha & Angielczyk 2007; Botha-Brink & Angielczyk 2010; Ray *et al.* 2012), and *Tropidostoma* (Botha & Angielczyk 2007).

The palaeobiological inferences of Olivier *et al.* (2017) are congruent with the results of the present study that suggest a high RMR for the three dicynodonts *Moghreberia*, *Lystrosaurus*, and *Oudenodon*. Olivier *et al.* (2017) suggested a RMR

value lower in *Moghreberia* (2.58 $mLO_2\ h^{-1}\ g^{-0.67}$) than in *Oudenodon* (4.58 $mLO_2\ h^{-1}\ g^{-0.67}$), with an intermediate state in *Lystrosaurus* (3.80 $mLO_2\ h^{-1}\ g^{-0.67}$), as in the models using PEMs in this study (2.3782 $mLO_2\ h^{-1}\ g^{-0.67}$ for *Moghreberia*, 3.1099 $mLO_2\ h^{-1}\ g^{-0.67}$ for *Lystrosaurus*, and 3.505 $mLO_2\ h^{-1}\ g^{-0.67}$ for *Oudenodon*) (Table 4). However, some differences can be observed between the RMR values from the two studies. First, as opposed to *Moghreberia* and *Oudenodon*, the studied specimens of *Lystrosaurus* analysed here were different from those of Olivier *et al.* (2017), the inter-individual variability may explain this difference. Then, keeping the highest estimations of the RMR from the present study and Olivier *et al.* (2017), the predicted values using the PEMs methods for *Moghreberia*, *Oudenodon*, and *Lystrosaurus* were both dependent of the density of the osteocyte in femur that could explain the similar results. The differences between the inferred RMR from the present study and Olivier *et al.* (2017) may mainly be due to variation in branch lengths that were not exactly the same in the two studies. As mentioned above, the inference models using PEMs were built based solely on one of the histological variables that best fit with the predicted variable or on none of these. Using PEMs methods, the present RMR of *Myosaurus* and *Endothiodon* were predicted from a humeral model solely based on phylogeny (best AIC score without histological variables). The qualitative histological pattern of *Myosaurus* has never been published, but fibrolamellar bone has been described in *Endothiodon* (Chinsamy & Rubidge 1993; Ray *et al.* 2009, 2012; Botha-Brink & Angielczyk 2010). The RMR values of these dicynodonts just resulted in an optimisation onto the phylogeny (only depending on the branch lengths and the evolutionary model), explaining the close predicted RMR values for the humeral model in all dicynodonts using PEMs (Table 4). Concerning *Moghreberia*, *Oudenodon*, and *Lystrosaurus*, the predicted RMR from PEMs methods were closely related to the density of the femur osteocytes, explaining a higher RMR in *Oudenodon* than in *Moghreberia*, and an intermediate state in *Lystrosaurus* (Tables 1–3).

As opposed to Olivier *et al.* (2017) and the present RMR values resulting from PEMs, the models using PGLS predicted a lower RMR for *Oudenodon* (3.593 $mLO_2\ h^{-1}\ g^{-0.67}$) than for *Moghreberia* ($\bar{x}RMR_{Femur}$= 5.417 $mLO_2\ h^{-1}\ g^{-0.67}$) and *Lystrosaurus* ($\bar{x}RMR_{Femur}$= 6.426 $mLO_2\ h^{-1}\ g^{-0.67}$). Also, high differences can be observed between the predicted RMR values resulting from PEMs and PGLS in the other studied dicynodonts (Tables 3–4). Several hypotheses may be envisaged to explain the

difference between the results from PEMs and PGLS approaches. First, as previously mentioned, the models using PGLS take into account a combination of predictive histological variables, with low risk of overparametrisation. The RMR values predicted from PEMs approaches in the present study and Olivier *et al.* (2017) are only based on one predictive histological variable even none, depending on the AICc criterion. Then, the PGLS and PEMs methods differently implement the phylogenetic components. The PGLS directly incorporate the phylogenetic context in the error term of the model, then implying non-independent data; while the phylogenetic eigenvector regression (PVR), from which the PEMs is derived, adds the phylogeny as a predictive variable thus supposing independently distributed error among taxa (e.g. Adams & Church 2011; Freckleton *et al.* 2011). In addition, the selection of the best combination of eigenvector maps to characterise the phylogenetic relationships (e.g. Legendre *et al.* 2016) implies partial ignoring of them. While the PEMs improves the PVR in better taking account the phylogenetic signal in trait evolution (e.g. Diniz Filho *et al.* 2015) and adding a more complex evolutionary model, the evolutionary model resulted from the PEMs and PGLS remain different with a more explicit parametrisation in PGLS. These methodological differences between the two used statistical methods most likely imply differences in the predicted RMR values.

Evolution of endothermy in dicynodonts

As already noted, except for *Endothiodon* and *Myosaurus* (discussed above), the palaeobiological inference models suggested a high resting metabolic rate in all studied dicynodonts (Figs. 1–2; Tables 3–4) and are consistent with the qualitative histological studies. The results of the present study suggest a unique acquisition of endothermy in Synapsida at the Neotherapsida node (Fig. 1), at least at the middle Permian (around 260 My), as previously inferred by Olivier *et al.* (2017).

Rey *et al.* (2017) analysed, in the bone and teeth of Permo-Triassic therapsids, the oxygen isotopic compositions ($\delta^{18}O$) related to the $\delta^{18}O$ of body water (derived from the ingested water that depends on the environmental conditions) and the body temperature. They concluded that endothermy appeared either (1) twice in Synapsida within Lystrosauridae + Kannemeyeriiformes and Eucynodontia clades; or (2) once at the Dicynodontia node that may confirm our results. An endotherm-like metabolism was inferred in the Triassic dicynodonts as *Moghreberia*, *Kannemeyeria*, and *Lystrosaurus*, confirming our conclusions. However, an ectotherm-like metabolism was

predicted in the Permian dicynodonts *Oudenodon* and *Tropidostoma*, as opposed to the present results from the PGLS and PEMs methods and the qualitative histology studies (Ricqlès 1972; Chinsamy & Rubidge 1993; Botha 2003; Botha & Angielczyk 2007; Botha-Brink & Angielczyk 2010; Ray *et al.* 2012). The metabolic interpretations of Rey *et al.* (2017) were based on the inferred body temperature. In the present study, we assumed the endothermy as the result of any mechanism of non-shivering thermogenesis (NST) (e.g. Lowell & Spiegelman 2000; Rowland *et al.* 2015; Nowack *et al.* 2017) that increases both the body temperature and resting metabolic rate. Regional endothermy was described in species of lamnid shark, billfishes, opah, and tunas that were capable of conserving metabolic derived heat thus increasing regional temperature tissues (e.g. Dickson & Graham 2004; Runcie *et al.* 2009). In addition, the body temperature of the echidna, usually referred to as a 'protoendotherm', has a mode of 32°C, but can range over 10°C in activity (Grigg *et al.* 2004). The body temperature thus does not always reflect the resting metabolic rate of animals.

Some authors explained the resistance and resilience of some therapsids to environmental perturbations during the Permo-Triassic boundary (e.g. Benton & Newell 2014; Rey *et al.* 2016), by multiple biological and ecological characters, like the presence of a high bone growth rate (e.g. Botha-Brink & Angielczyk 2010) and an elevated thermometabolism (e.g. Rey *et al.* 2017). High RMR values, ranging from 4.31 to 8.25 $mLO_2\ h^{-1}\ g^{-0.67}$ in studied dicynodonts (Fig. 1), supported the hypothesis of a high growth strategy at least at the Dicynodontia node, as assumed by Botha-Brink & Angielczyk (2010). However, high bone growth and metabolic rate are not the sole explaining factor of differential success across the Permo-Triassic boundary for survival within dicynodonts. In fact, except for *Endothiodon* and *Myosaurus* (discussed above), high values of resting metabolic rate were found in all Permian and Triassic dicynodonts using PGLS and PEM methods (Figs. 1–2).

Our sample of dicynodont taxa is still not large enough to describe accurately the evolution of resting metabolic rate in this clade and more broadly in synapsids. All included dicynodonts presented a relative high bone growth rate (Botha-Brink & Angielczyk, 2010: supposed by a high mean channel density); the addition of genera with low bone growth rate (e.g. *Dicynodontoides*, *Cistecephalus*) may confirm or not if a fast growth rate is definitely related to the elevated metabolic capabilities of endothermy in dicynodonts. Extending the inference palaeophysiological models to

other “mammal-like reptile” taxa could allow lead to a broader understanding of the evolution of endothermy in synapsids. In addition, it would be noteworthy to investigate if the high growth rate supposed in several ophiacodonts (e.g. *Ophiacodon*, *Clepsydrops*) (Shelton & Sander 2015; Laurin & De Buffrénil 2016), sphenacodonts (e.g. *Dimetrodon*) (Shelton *et al.* 2013), dromasaurs (e.g. *Galeops*) (Botha-Brink & Angielczyk 2010), basal therocepalians (e.g. *Lycosuchus*) (Huttenlocker & Botha-Brink 2014), and gorgonopsians (e.g. *Scylacops* and *Aelurognathus*) (Chinsamy-Turan & Ray 2012) is related to high inferred RMR values.

CONCLUSIONS

1. Keeping the highest values of RMR from each statistical method (PEMs and PGLS), a high resting metabolic rate were inferred for the late Permian *Endothiodon*, *Daptocephalus*, *Tropidostoma*, and *Oudenodon baini*, the Early Triassic *Lystrosaurus murrayi* and *Myosaurus gracilis*, the Middle Triassic *Kannemeyeria simocephalus*, and the Late Triassic *Moghreberia nmachouensis*. These results confirmed the previous quantitative and qualitative histological studies.
2. A high RMR value inferred in all studied Permian and Triassic dicynodonts, mainly known for a high bone growth rate too, does not confirm an unique and important role of the acquisition of the endothermy on the differential survival success across the Permo-Triassic boundary within dicynodonts, as previously supposed in literature. However, a high RMR value inferred in all studied synapsids suggests an unique appearance of the acquisition of the endothermy in Synapsida, at the Neotherapsida node, at least at the middle Permian. The increase of taxa sample with dicynodonts known by their low bone growth rate and more basal synapsids may confirm or not the present results.
3. The automatic selection of the priors and branch length scaling parameters (kappa, lambda, delta, and OU) by BayesTraits V3.0.1 (Pagel & Meade 2016) is based on the coefficient of determination R^2 that would not efficiently inform about the ‘predicitve power’ of an inference model. The ‘by hand’ selection of the parameters of the regression models have thus been preferred.
4. Differences of RMR values are noticed if we used the PEMs or PGLS approach. They most be likely due to methodological variations between the two statistical

approaches, like taking into account the phylogenetic components or the parametrisation of the evolutionary model.

Acknowledgments. We want to thank J. Bardin (CR2P, MNHN, France) and A. Meade (University of Reading, Berkshire, UK) for discussions on PGLS methods. We thank J. Botha-Brink (National Museum, Bloemfontein, South Africa) for her help in histological data acquisition and her relevant comments. We thank D. Germain (CR2P, MNHN, France) for his help in histological collections of MNHN and E. Butler of the National Museum of Bloemfontein (South Africa) for the histological collections access.

REFERENCES

ADAMS, D. C. and CHURCH, J. O. 2011. The evolution of large-scale body size clines in Plethodon salamanders: evidence of heat-balance or species-specific artifact? *Ecography*, **34**, 1067–1075.

AMPRINO, R. 1947. La structure du tissu osseux envisagée comme expression de différences dans la vitesse de l'accroissement. *Archives de biologie*, **58**, 315–330.

ANGIELCZYK, K. D. and KAMMERER, C. F. 2017. The cranial morphology, phylogenetic position and biogeography of the upper Permian dicynodont *Compsodon helmoedi* van Hoepen (Therapsida, Anomodontia). *Papers in Palaeontology*, **3**, 513–545.

———, HANCOX, P. J. and NABAVIZADEH, A. 2018. A redescription of the Triassic kannemeyeriiform dicynodont *Sangusaurus* (Therapsida, Anomodontia), with an analysis of its feeding system. *Journal of Vertebrate Paleontology*, **37**, 189–227.

BENTON, M. J. and NEWELL, A. J. 2014. Impacts of global warming on Permo-Triassic terrestrial ecosystems. *Gondwana Research*, **25**, 1308–1337.

———, DONOGHUE, P. C. J., ASHER, R. J., FRIEDMAN, M., NEAR, T. J. and VINTHER, J. 2015. Constraints on the timescale of animal evolutionary history. *Palaeontologia Electronica*, **18**, 1–106.

BOOS, A. D. S., KAMMERER, C. F., SCHULTZ, C. L., SOARES, M. B. and ILHA, A. L. R. 2016. A New Dicynodont (Therapsida: Anomodontia) from the Permian of Southern Brazil and Its Implications for Bidentalian Origins. *PLoS ONE*, **11**.

BOTHA, J. 2003. Biological aspects of the Permian dicynodont *Oudenodon* (Therapsida: Dicynodontia) deduced from bone histology and cross-sectional geometry. *Palaeontologica africana*, **39**, 37–44.

BOTHA, J. and ANGIELCZYK, K. D. 2007. An integrative approach to distinguishing the Late Permian dicynodont species *Oudenodon bainii* and *Tropidostoma microtrema* (Therapsida: Anomodontia). *Palaeontology*, **50**, 1175–1209.

BOTHA-BRINK, J. and ANGIELCZYK, K. D. 2010. Do extraordinarily high growth rates in Permo-Triassic dicynodonts (Therapsida, Anomodontia) explain their success before and after the end-Permian extinction ? *Zoological Journal of the Linnean Society*, **160**, 341–365.

———, CODRON, D., HUTTENLOCKER, A. K., ANGIELCZYK, K. D. and RUTA, M. 2016. Breeding Young as a Survival Strategy during Earth's Greatest Mass Extinction. *Scientific Reports*, **6**, 24053.

BOUVIER, M. 1977. Dinosaur Haversian Bone and Endothermy. *Evolution*, **31**, 449–450.

CAPELLINI, I., VENDITTI, C. and BARTON, R. A. 2010. Phylogeny and metabolic scaling in mammals. *Ecology*, **91**, 2783–2793.

CASTANET, J., CROCI, S., AUJARD, F., PERRET, M., CUBO, J. and DE MARGERIE, E. 2004. Lines of arrested growth in bone and age estimation in a small primate: *Microcebus murinus*. *Journal of Zoology*, **263**, 31–39.

CHINSAMY, A. and RUBIDGE, B. S. 1993. Dicynodont (Therapsida) bone histology: phylogenetic and physiological implications. *Palaeontologica africana*, **30**, 97–102.

——— and HURUM, J. H. 2006. Bone microstructure and growth patterns of early mammals. *Acta Palaeontologica Polonica*, **51**, 325–338.

CHINSAMY-TURAN, A. and RAY, S. 2012. Bone histology of some Therocephalians and Gorgonopsians, and evidence of bone degradation by fungi. *In Forerunners of Mammals*, Chinsamy-Turan, A. (ed.), 199–222 pp.

CLUVER, M. A. and KING, G. M. 1983. A reassessment of the relationships of Permian Dicynodontia (Reptilia, Therapsida) and a new classification of dicynodonts. *Annals of South African Museum*, **91**, 195–273.

COX, C. B. and ANGIELCZYK, K. D. 2015. A New Endothiodont Dicynodont (Therapsida, Anomodontia) from the Permian Ruhuhu Formation (Songea Group) of Tanzania and Its Feeding System. *Journal of Vertebrate Paleontology*, **35**, e935388.

CUBO, J. and JALIL, N.-E. 2019. Bone histology of *Azendohsaurus laaroussii*: Implications for the evolution of thermometabolism in Archosauromorpha. *Paleobiology*, **45**, 317–330.

———, LE ROY, N., MARTINEZ-MAZA, C. and MONTES, L. 2012. Paleohistological estimation of bone growth rate in extinct archosaurs. *Paleobiology*, **38**, 335–349.

CUBO, J., PONTON, F., LAURIN, M., MARGERIE, E. de and CASTANET, J. 2005. Phylogenetic Signal in Bone Microstructure of Sauropsids. *Systematic Biology*, **54**, 562–574.

DICKSON, K. A. and GRAHAM, J. B. 2004. Evolution and consequences of endothermy in fishes. *Physiological and biochemical zoology: PBZ*, **77**, 998–1018.

DINIZ FILHO, J. A. F., VILLALOBOS, F., BINI, L. M., DINIZ FILHO, J. A. F., VILLALOBOS, F. and BINI, L. M. 2015. The best of both worlds: Phylogenetic eigenvector regression and mapping. *Genetics and Molecular Biology*, **38**, 396–400.

DODDS, P. S., ROTHMAN, D. H. and WEITZ, J. S. 2001. Re-examination of the '3/4-law' of metabolism. *Journal of Theoretical Biology*, **209**, 9–27.

DUTUIT, J. M. 1988. Ostéologie crânienne et ses enseignements, apports géologique et paléoécologique, de Moghreberia nmachouensis, Dicynodonte (Reptilia, Therapsida) du Trias supérieur marocain. *Bulletin du Muséum national d'histoire naturelle. Section C, Sciences de la terre, paléontologie, géologie, minéralogie*, **10**, 227–285.

FARRELL-GRAY, C. C. and GOTELLI, N. J. 2005. Allometric exponents support 3/4-power scaling law. *Ecology*, **86**, 2083–2087.

FLEISCHLE, C. V., WINTRICH, T. and SANDER, P. M. 2018. Quantitative histological models suggest endothermy in plesiosaurs. *PeerJ*, **6**, e4955.

FRANCILLON VIEILLOT, H., DE BUFFRÉNIL, V., CASTANET, J., GÉRAUDIE, J., MEUNIER, F. J., SIRE, J. Y., ZYLBERBERG, L. and DE RICQLÈS, A. 1990. Microstructure and mineralization of vertebrate skeletal tissues. *In Skeletal*

Biomineralization : Patterns, Process and Evolutionary Trends, Carter, J. G. (ed.), 471–530 pp.

FRECKLETON, R. P., COOPER, N. and JETZ, W. 2011. Comparative Methods as a Statistical Fix: The Dangers of Ignoring an Evolutionary Model. *The American Naturalist*, **178**, E10–E17.

FRÖBISCH, J. 2009. Composition and similarity of global anomodont-bearing tetrapod faunas. *Earth-Science Reviews*, **95**, 119–157.

GELMAN, A., GOODRICH, B., GABRY, J. and VEHTARI, A. 2018. R-squared for Bayesian regression models. *The American Statistician*, **73**, 307–309.

GERMAIN, D. and LAURIN, M. 2005. Microanatomy of the radius and lifestyle in amniotes (Vertebrata, Tetrapoda). *Zoologica Scripta*, **34**, 335–350.

GILKS, W. R., RICHARDSON, S. and SPIEGELHALTER, D. J. 1995. Introducing Markov chain Monte Carlo. *In Markov Chain Monte Carlo in Practice*, W. R. Gilks, S. Richardson and D. J. Spiegelhalter, London, 1–19 pp.

GLAZIER, D. S. 2005. Beyond the '3/4-power law': variation in the intra- and interspecific scaling of metabolic rate in animals. *Biological Reviews*, **80**, 611–662.

GRAFEN ALAN. 1989. The phylogenetic regression. *Philosophical Transactions of the Royal Society of London. B, Biological Sciences*, **326**, 119–157.

GREEN, J. L. 2012. Bone and Dental Histology of Late Triassic Dicynodonts from North America. *In Forerunners of Mammals*, Chinsamy-Turan, A. (ed.), 179–198 pp.

———, SCHWEITZER, M. H. and LAMM, E.-T. 2010. Limb bone histology and growth in *Placerias hesternus* (Therapsida: Anomodontia) from the Upper Triassic of North America. *Palaeontology*, **53**, 347–364.

GRIGG, G. C., BEARD, L. A. and AUGEE, M. L. 2004. The Evolution of Endothermy and Its Diversity in Mammals and Birds. *Physiological and Biochemical Zoology*, **77**, 982–997.

GUÉNARD, G., LEGENDRE, P. and PERES-NETO, P. 2013. Phylogenetic eigenvector maps: a framework to model and predict species traits. *Methods in Ecology and Evolution*, **4**, 1120–1131.

HACKLÄNDER, K., ARNOLD, W. and RUF, T. 2002. Postnatal development and thermoregulation in the precocial European hare (*Lepus europaeus*). *Journal of Comparative Physiology B*, **172**, 183–190.

HUTTENLOCKER, A. K. and BOTHA-BRINK, J. 2014. Bone microstructure and the evolution of growth patterns in Permo-Triassic therocephalians (Amniota, Therapsida) of South Africa. *PeerJ*, **2**, e325.

KAMMERER, C. F. and SMITH, R. M. H. 2017. An early geikiid dicynodont from the *Tropidostoma* Assemblage Zone (late Permian) of South Africa. *PeerJ*, **5**, e2913.

———, ANGIELCZYK, K. D. and FRÖBISCH, J. 2011. A comprehensive taxonomic revision of '*Dicynodon*' (Therapsida, Anomodontia) and its implications for dicynodont phylogeny, biogeography, and biostratigraphy. *Journal of Vertebrate Paleontology*, **31**, 1–158.

LAURIN, M. and DE BUFFRÉNIL, V. 2016. Microstructural features of the femur in early ophiacodontids: A reappraisal of ancestral habitat use and lifestyle of amniotes. *Comptes Rendus Palevol*, **15**, 115–127.

LEGENDRE, L. J., SEGALEN, L. and CUBO, J. 2013. Evidence for high bone growth rate in *Euparkeria* obtained using a new paleohistological inference model for the humerus. *Journal of Vertebrate Paleontology*, **33**, 1343–1350.

———, GUÉNARD, G., BOTHA-BRINK, J. and CUBO, J. 2016. Palaeohistological Evidence for Ancestral High Metabolic Rate in Archosaurs. *Systematic biology*, **65**, 989–996.

LOWELL, B. B. and SPIEGELMAN, B. M. 2000. Towards a molecular understanding of adaptive thermogenesis. *Nature*, **404**, 652–660.

MARTINS, E. P. and HANSEN, T. F. 1997. Phylogenies and the Comparative Method: A General Approach to Incorporating Phylogenetic Information into the Analysis of Interspecific Data. *The American Naturalist*, **149**, 646–667.

MAUGET, C., MAUGET, R. and SEMPÉRÉ, A. 1999. Energy expenditure in European roe deer fawns during the suckling period and its relationship with maternal reproductive cost. *Canadian Journal of Zoology*, **77**, 389–396.

MONTES, L., LE ROY, N., PERRET, M., DE BUFFRENIL, V., CASTANET, J. and CUBO, J. 2007. Relationships between bone growth rate, body mass and resting

metabolic rate in growing amniotes: a phylogenetic approach. *Biological Journal of the Linnean Society*, **92**, 63–76.

NOWACK, J., GIROUD, S., ARNOLD, W. and RUF, T. 2017. Muscle Non-shivering Thermogenesis and Its Role in the Evolution of Endothermy. *Frontiers in Physiology*, **8**, 889.

OLIVIER, C., HOUSSAYE, A., JALIL, N.-E. and CUBO, J. 2017. First palaeohistological inference of resting metabolic rate in an extinct synapsid, *Moghreberia nmachouensis* (Therapsida: Anomodontia). *Biological Journal of the Linnean Society*, **121**, 409–419.

———, BATTAIL, B., BOURQUIN, S., ROSSIGNOL, C., STEYER, J.-S. and JALIL, N.-E. 2019. New dicynodonts (Therapsida, Anomodontia) from near the Permo-Triassic boundary of Laos: implications for dicynodont survivorship across the Permo-Triassic mass extinction and the paleobiogeography of Southeast Asian blocks. *Journal of Vertebrate Paleontology*, **0**, e1584745.

ORGAN, C., NUNN, C. L., MACHANDA, Z. and WRANGHAM, R. W. 2011. Phylogenetic rate shifts in feeding time during the evolution of Homo. *Proceedings of the National Academy of Sciences*, **108**, 14555–14559.

ORGAN, C. L., SHEDLOCK, A. M., MEADE, A., PAGEL, M. and EDWARDS, S. V. 2007. Origin of avian genome size and structure in non-avian dinosaurs. *Nature*, **446**, 180–184.

ORME, D. 2018. The caper package: comparative analysis of phylogenetics and evolution in R. 36.

PAGEL, M. 1999. Inferring the historical patterns of biological evolution. *Nature*, **401**, 877–884.

PAGEL, M. and MEADE, A. 2016. BayesTraits V3 Manual. .

PETERS, R. H. 1986. *The ecological implications of body size*. Cambridge, Massachussetts.

RAY, S. and CHINSAMY, A. 2004. *Diictodon feliceps* (Therapsida, Dicynodontia): bone histology, growth, and biomechanics. *Journal of Vertebrate Paleontology*, **24**, 180–194.

———, ——— and BANDYOPADHYAY, S. 2005. *Lystrosaurus murrayi* (Therapsida, Dicynodontia): bone histology, growth and lifestyle adaptations. *Palaeontology*, **48**, 1169–1185.

———, BANDYOPADHYAY, S. and BHAWAL, D. 2009. Growth patterns as deduced from bone microstructure of some selected neotherapsids with special emphasis on dicynodonts: Phylogenetic implications. *Palaeoworld*, **18**, 53–66.

———, ——— and APPANA, R. 2010. Bone Histology of a Kannemeyeriid Dicynodont *Wadiasaurus*: Palaeobiological Implications. *In New Aspects of Mesozoic Biodiversity*, Vol. 132. Springer Berlin Heidelberg, Berlin, Heidelberg, 73–89 pp.

———, BOTHA-BRINK, J. and CHINSAMY-TURAN, A. 2012. Dicynodont growth dynamics and lifestyle adaptations. *In Forerunners of Mammals*, Chinsamy-Turan, A. (ed.), 121–148 pp.

REVELL, L. J. 2012. Phytools: an R package for phylogenetic comparative biology (and other things). *Methods in Ecology and Evolution*, **3**, 217–223.

REY, K., AMIOT, R., FOUREL, F., ABDALA, F., FLUTEAU, F., JALIL, N.-E., LIU, J., RUBIDGE, B. S., SMITH, R., STEYER, J.-S., VIGLIETTI, P. A., WANG, X. and LÉCUYER, C. 2017. Oxygen isotopes suggest elevated thermometabolism within multiple Permo-Triassic therapsid clades. *ELife*, e28589.

———, ———, ———, RIGAUDIER, T., ABDALA, F., DAY, M. O., FERNANDEZ, V., FLUTEAU, F., FRANCE-LANORD, C., RUBIDGE, B. S., SMITH, R. M., VIGLIETTI, P. A., ZIPFEL, B. and LÉCUYER, C. 2016. Global climate perturbations during the Permo-Triassic mass extinctions recorded by continental tetrapods from South Africa. *Gondwana Research*, **37**, 384–396.

RICQLÈS, A. 1972. Recherches paléohistologiques sur les os longs des Tétrapodes. Part III. Titanosuchiens, Dinocephales, Dicynodontes. *Annales de Paléontologie (Vertébrés)*, **58**, 17–60.

———, MEUNIER, F. J., CASTANET, J. and FRANCILLON-VIEILLOT, H. 1991. Comparative microstructure of bone. *Bone*, **3**, 1–78.

ROWLAND, L. A., BAL, N. C. and PERIASAMY, M. 2015. The role of skeletal-muscle-based thermogenic mechanisms in vertebrate endothermy. *Biological Reviews of the Cambridge Philosophical Society*, **90**, 1279–1297.

RUNCIE, R. M., DEWAR, H., HAWN, D. R., FRANK, L. R. and DICKSON, K. A. 2009. Evidence for cranial endothermy in the opah (*Lampris guttatus*). *The Journal of Experimental Biology*, **212**, 461–470.

SAKAMOTO, Y., ISHIGURO, M. and KITAGAWA, G. 1986. *Akaike information criterion statistics*. Vol. 81. D. Reidel Publishing Company.

SCHMIDT-NIELSEN, K. 1984. *Scaling: Why is animal size so important?*. Cambridge University Press, Cambridge, Massachussetts.

SELTMANN, M. W., RUF, T. and RÖDEL, H. G. 2009. Effects of body mass and huddling on resting metabolic rates of post-weaned European rabbits under different simulated weather conditions. *Functional Ecology*, **23**, 1070–1080.

SEYMOUR, R. S., BENNETT-STAMPER, C. L., JOHNSTON, S. D., CARRIER, D. R. and GRIGG, G. C. 2004. Evidence for Endothermic Ancestors of Crocodiles at the Stem of Archosaur Evolution. *Physiological and Biochemical Zoology: Ecological and Evolutionary Approaches*, **77**, 1051–1067.

SHELTON, C. and SANDER, P. M. 2015. *Ophiacodon* long bone histology: the earliest occurrence of FLB in the mammalian stem lineage. PeerJ PrePrints.

SHELTON, C. D., SANDER, P. M., STEIN, K. and WINKELHORST, H. 2013. Long bone histology indicates sympatric species of *Dimetrodon* (Lower Permian, Sphenacodontidae). *Earth and Environmental Science Transactions of The Royal Society of Edinburgh*, **103**, 217–236.

SIEG, A. E., O'CONNOR, M. P., MCNAIR, J. N., GRANT, B. W., AGOSTA, S. J. and DUNHAM, A. E. 2009. Mammalian Metabolic Allometry: Do Intraspecific Variation, Phylogeny, and Regression Models Matter? *The American Naturalist*, **174**, 720–733.

TUMARKIN-DERATZIAN, A. R. 2007. Fibrolamellar Bone in Wild Adult Alligator Mississippiensis. *Journal of Herpetology*, **41**, 341–345.

VIGLIETTI, P. A. 2016. Stratigraphy and sedimentary environments of the Late Permian *Dicynodon* Assemblage Zone (Karoo Supergroup, South Africa) and implications for basin development. Ph.D. dissertation, University of the Witwatersrand, Johannesburg, South Africa, 272pp.

WHITE, C. R., CASSEY, P. and BLACKBURN, T. M. 2007. Allometric Exponents Do Not Support a Universal Metabolic Allometry. *Ecology*, **88**, 315–323.

———, MARSHALL, D. J., ALTON, L. A., ARNOLD, P. A., BEAMAN, J. E., BYWATER, C. L., CONDON, C., CRISPIN, T. S., JANETZKI, A., PIRTLE, E., WINWOOD-SMITH, H. S., ANGILLETTA, M. J., CHENOWETH, S. F., FRANKLIN, C. E., HALSEY, L. G., KEARNEY, M. R., PORTUGAL, S. J. and ORTIZ-BARRIENTOS, D. 2019. The origin and maintenance of metabolic allometry in animals. *Nature Ecology & Evolution*, **3**, 598.

XIE, W., LEWIS, P. O., FAN, Y., KUO, L. and CHEN, M.-H. 2011. Improving marginal likelihood estimation for Bayesian phylogenetic model selection. *Systematic Biology*, **60**, 150–160.

FIG. 1. Mass-independent resting metabolic rate (in $mLO_2\ h^{-1}\ g^{-0.67}$) for the extant and extinct species of the study using MCMC and PGLS methods, considering the consensus clade (((*Moghreberia*, *Kannemeyeria*), *Lystrosaurus*), *Daptocephalus*) (e.g. Cox & Angielczyk 2015; Boos *et al.* 2016; Angielczyk & Kammerer 2017; Kammerer & Smith 2017; Angielczyk *et al.* 2018). The RMR values gradient extends from ectotherms (indicated by blue dots) to endotherms (indicated by red dots). We show highest inferred values for the fossil taxa using models. The corresponding 95% confidence intervals (Table 3) could not be represented because of the scale.

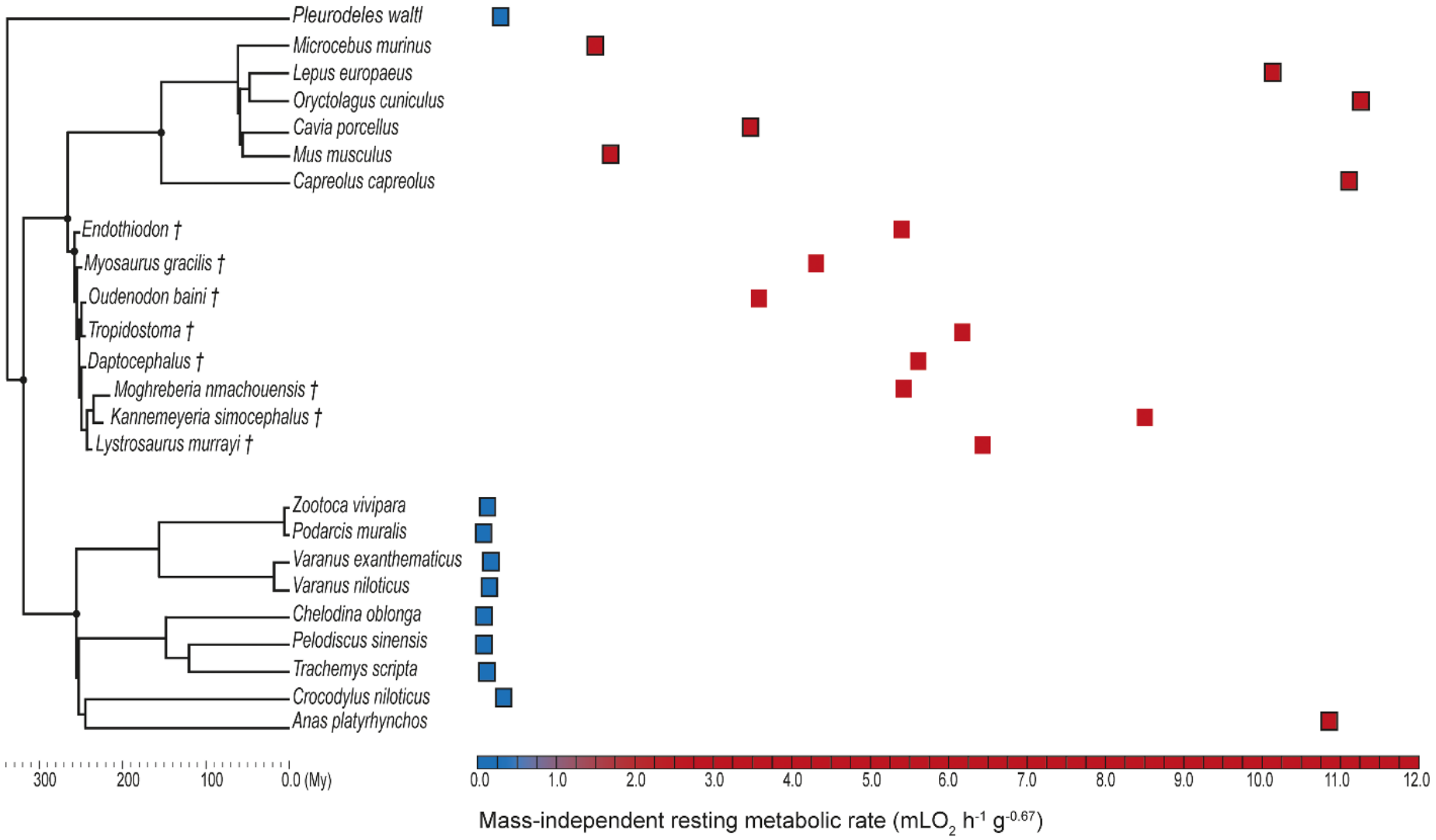
Pleurodeles waltl
Microcebus murinus
Lepus europaeus
Oryctolagus cuniculus
Cavia porcellus
Mus musculus
Capreolus capreolus
Endothiodon †
Myosaurus gracilis †
Oudenodon baini †
Tropidostoma †
Daptocephalus †
Moghreberia nmachouensis †
Kannemeyeria simocephalus †
Lystrosaurus murrayi †
Zootoca vivipara
Podarcis muralis
Varanus exanthematicus
Varanus niloticus
Chelodina oblonga
Pelodiscus sinensis
Trachemys scripta
Crocodylus niloticus
Anas platyrhynchos
300
200
100
0.0 (My)
0.0
1.0
2.0
3.0
4.0
5.0
6.0
7.0
8.0
9.0
10.0
11.0
12.0
Mass-independent resting metabolic rate (mLO2 h-1 g-0.67)

FIG. 2. Mass-independent resting metabolic rate (in $mLO_2\ h^{-1}\ g^{-0.67}$) for the extant and extinct species of study using PEMs, considering the consensus clade (((*Moghreberia*, *Kannemeyeria*), *Lystrosaurus*), *Daptocephalus*) (e.g. Cox & Angielczyk 2015; Boos *et al.* 2016; Angielczyk & Kammerer 2017; Kammerer & Smith 2017; Angielczyk *et al.* 2018). The RMR values gradient extends from ectotherms (indicated by blue dots) to endotherms (indicated by red dots). We show highest inferred values for the fossil taxa using models. The ambiguous inferred RMR values were represented by a question mark. The corresponding 95% confidence intervals (Table 4) are represented for the predicted value of extinct taxa.

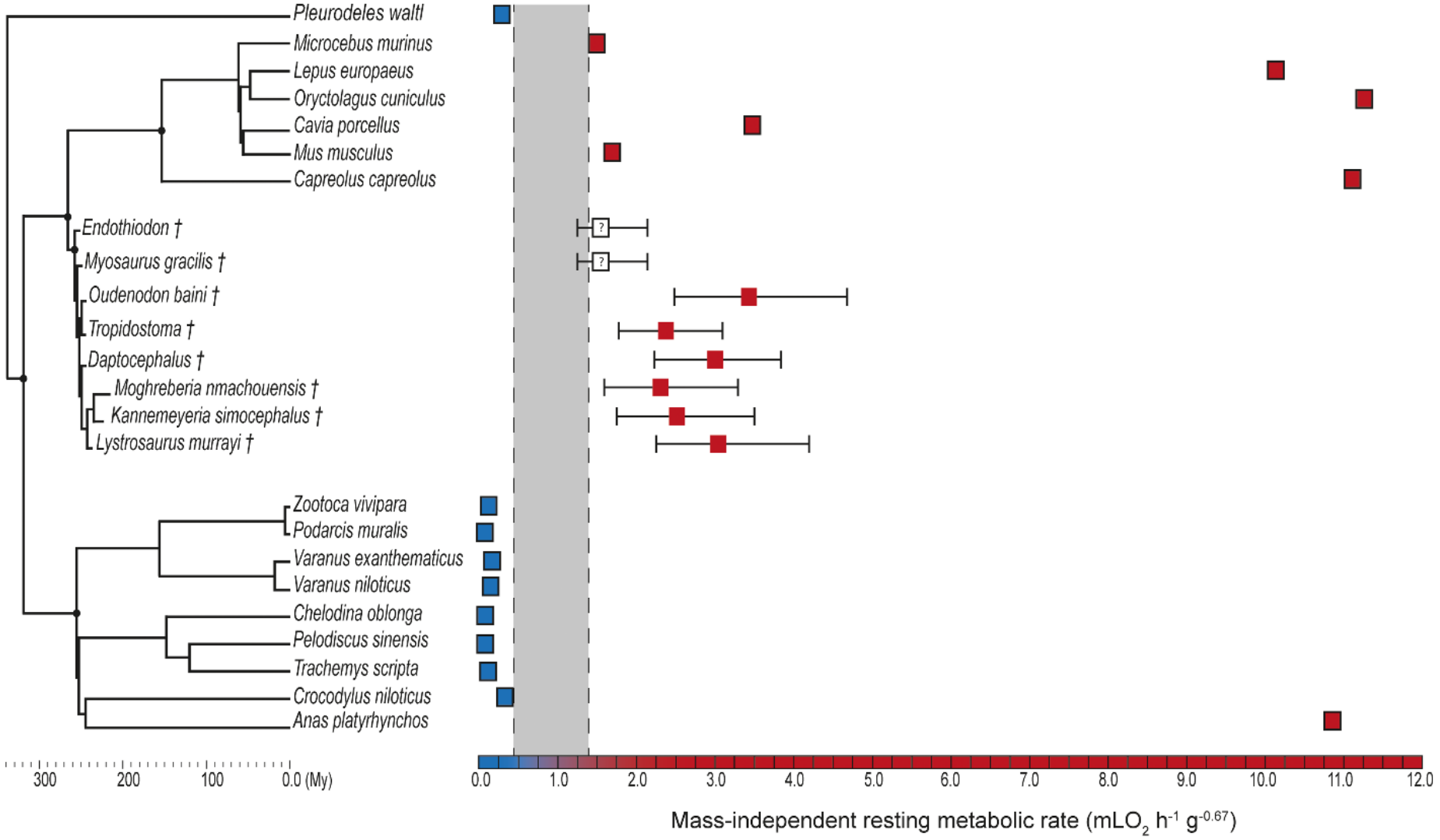
Pleurodeles waltl
Microcebus murinus
Lepus europaeus
Oryctolagus cuniculus
Cavia porcellus
Mus musculus
Capreolus capreolus
Endothiodon †
Myosaurus gracilis †
Oudenodon baini †
Tropidostoma †
Daptocephalus †
Moghreberia nmachouensis †
Kannemeyeria simocephalus †
Lystrosaurus murrayi †
Zootoca vivipara
Podarcis muralis
Varanus exanthematicus
Varanus niloticus
Chelodina oblonga
Pelodiscus sinensis
Trachemys scripta
Crocodylus niloticus
Anas platyrhynchos
?
?
300
200
100
0.0 (My)
0.0
1.0
2.0
3.0
4.0
5.0
6.0
7.0
8.0
9.0
10.0
11.0
12.0
Mass-independent resting metabolic rate (mLO2 h-1 g-0.67)

TABLE 1. RMR and histological measurements in the femur in the extant and extinct taxa of the study taken from the literature and newly added.

Species	RMR ($mLO_2\ h^{-1}\ g^{-0.67}$)	OstD (ost./μm^2)	OstA (μm^2)	OstS	VascD (vas. cav./mm^2)
Anas platyrhynchos	10.865[a]	0.002567298[b]	20.6440151[b]	0.496256631[b]	0.582682
Capreolus capreolus	11.111[d]	0.00503404[c]	66.3338[c]	0.682011681[c]	0.735128
Cavia porcellus	3.477[a]	0.0018753[b]	34.1550045[b]	0.497251828[b]	0.336093
Chelodina oblonga	0.085[a]	0.000972828[b]	28.1246416[b]	0.615366523[b]	0
Crocodylus niloticus	0.336[a]	0.000707445[b]	29.6935670[b]	0.474721005[b]	0.051708
Lepus europaeus	10.149[e]	0.00485708[b]	49.1568[c]	0.6433817[c]	0.809494
Microcebus murinus	1.526[a]	0.003900548[b]	30.0081130[b]	0.586549866[b]	0.241296
Mus musculus	1.696[a]	0.001222124[b]	29.4847303[b]	0.48045441[b]	0.076195
Oryctolagus cuniculus	11.263[f]	0.00403514[b]	73.277[c]	0.646803938[c]	0.42166
Pelodiscus sinensis	0.083[a]	0.000913358[b]	24.4859618[b]	0.52191737[b]	0
Pleurodeles waltl	0.297[a]	0.0005911427[b]	134.939471[b]	0.59478267[b]	0
Podarcis muralis	0.084[a]	0.001117739[b]	11.9915127[b]	0.438353062[b]	0
Trachemys scripta	0.117[a]	0.001403736[b]	28.9630975[b]	0.494580499[b]	0
Varanus exanthematicus	0.173[a]	0.001195398[b]	33.3619992[b]	0.462645883[b]	0.005003
Varanus niloticus	0.157[a]	0.001007931[b]	39.6995653[b]	0.478829164[b]	0.017692
Zootoca vivipara	0.124[a]	0.002442651[b]	13.6767645[b]	0.42653396[b]	0
Moghreberia nmachouensis	NA	0.00316485[c]	82.1627[c]	0.6130401[c]	0.31360095
Oudenodon baini	NA	0.00495632[c]	21.0048[c]	0.5732658[c]	0.369144
Kannemeyeria simocephala	NA	0.003461466	90.37377	0.660984	0.5792235
Lystrosaurus murrayi	NA	0.004316035	66.175304	0.619432	0.52530187
Daptocephalus	NA	0.0041463	52.9261	0.65018	0.48533496
Tropidostoma	NA	0.0032531	69.8459	0.63246	0.49969028

[a] from (Montes *et al.* 2007); [b] from (Legendre *et al.* 2016); [c] from (Olivier *et al.* 2017); [d] from (Mauget *et al.* 1999); [e] from (Hackländer *et al.* 2002); [f] from (Seltmann *et al.* 2009).

Abbreviations: **OstA**, osteocyte area; **OstD**, osteocyte density; **OstS**, osteocyte shape; **ost**, osteocyte; **RMR**, mass-specific resting metabolic rate; **vasc**. **cav**., vascular cavities; **VascD**, primary osteon density.

TABLE 2. RMR and histological measurements in the humerus in the extant and extinct taxa of the study taken from the literature and newly added.

Species	RMR ($mLO_2\ h^{-1}\ g^{-0.67}$)	OstD (ost./μm^2)	OstA (μm^2)	OstS	VascD (vas. cav./mm^2)
Anas platyrhynchos	10.865[a]	0.002283169[b]	24.2913684	0.509126729	0.22331333
Capreolus capreolus	11.111[d]	0.00469016[c]	64.6514[c]	0.701349738[c]	0.9137543
Cavia porcellus	3.477[a]	0.001966108[b]	34.98627114[c]	0.485471037[c]	0.29232459
Chelodina oblonga	0.085[a]	0.001208368[c]	24.27796702[c]	0.56336775[c]	0
Crocodylus niloticus	0.336[a]	0.000699242[b]	34.60152723[b]	0.485430779[b]	0.05218821
Lepus europaeus	10.149[e]	0.00517246[c]	49.7288[c]	0.668795497[c]	0.52979847
Microcebus murinus	1.526[a]	0.003801204[b]	28.5159804[b]	0.526748184[b]	0.24489796
Mus musculus	1.696[a]	0.001230761[b]	22.62412616[b]	0.526253882[b]	0.12684615
Oryctolagus cuniculus	11. 263[f]	0.00401476[c]	79.9143[c]	0.661216357[c]	0.28426461
Pelodiscus sinensis	0.083[a]	0.001185422[b]	20.92560266[b]	0.497140919[b]	0
Pleurodeles waltl	0.297[a]	0.000834283[b]	107.919445[b]	0.553076316[b]	0
Podarcis muralis	0.084[a]	0.000864162[b]	11.95338603[b]	0.404075493[b]	0
Trachemys scripta	0.117[a]	0.001196311[b]	27.13462106[b]	0.516404884[b]	0
Varanus exanthematicus	0.173[a]	0.001232928[b]	36.29314955[b]	0.43520731[b]	0.04525424
Varanus niloticus	0.157[a]	0.001394133[b]	38.16383708[b]	0.470869021[b]	0.03805003
Zootoca vivipara	0.124[a]	0.003264965[b]	10.45412684[b]	0.442348205[b]	0
Moghreberia nmachouensis	NA	0.00361166	72.9888	0.5619222	0.4812
Oudenodon baini	NA	0.00418836	92.5187	0.51583	0.15008925
Lystrosaurus murrayi	NA	0.00404318	71.06834	0.603978	0.54666341
Tropidostoma	NA	0.003743684	92.963724	0.614617	0.45762625
Myosaurus gracilis	NA	0.005984664	46.205507	0.593428	0.359545
Endothiodon	NA	0.0046199	53.9649	0.6408	0.60566135

[a] from (Montes *et al.* 2007); [b] from (Legendre *et al.* 2016); [c] from (Olivier *et al.* 2017); [d] from (Mauget *et al.* 1999); [e] from (Hackländer *et al.* 2002); [f] from (Seltmann *et al.* 2009).

Abbreviations: **OstA**, osteocyte area; **OstD**, osteocyte density; **OstS**, osteocyte shape; **ost**, osteocyte; **RMR**, mass-specific resting metabolic rate; **vasc**. **cav**., vascular cavities; **VascD**, primary osteon density.

TABLE 3. Predicted mass-independent resting metabolic rate (in $mLO_2\ h^{-1}\ g^{-0.67}$) in dicynodont fossils, based on a continuous multiple regression model using MCMC and PGLS methods, considering the consensus clade (((*Moghreberia*, *Kannemeyeria*), *Lystrosaurus*), *Daptocephalus*) (e.g. Cox and Angielczyk 2015; Boos *et al.* 2016; Angielczyk and Kammerer 2017; Kammerer and Smith 2017; Angielczyk *et al.* 2018).

Taxa	Femur			Humerus		
	$\bar{x}$**RMR$_{pred}$**	**Min limit of CI$_{95\%}$**	**Max limit of CI$_{95\%}$**	$\bar{x}$**RMR$_{pred}$**	**Min limit of CI$_{95\%}$**	**Max limit of CI$_{95\%}$**
Kannemeyeria simocephalus †	8.2487	8.1417	8.3570	NA	NA	NA
Moghreberia nmachouensis †	5.4165	5.3506	5.4832	4.2684	4.2194	4.3179
Myosaurus gracilis †	NA	NA	NA	4.3141	4.2650	4.3637
Lystrosaurus murrayi †	6.4263	6.3515	6.5020	5.3439	5.2847	5.4039
Oudenodon baini †	2.2269	2.1951	2.2592	3.5929	3.5443	3.6421
Tropidostoma †	5.9379	5.8704	6.0062	6.1707	6.0985	6.2437
Daptocephalus †	5.6081	5.5439	5.6730	NA	NA	NA
Endothiodon †	NA	NA	NA	5.4032	5.3417	5.4655

Abbreviations: CI, 95% confidence interval; $\bar{x}$**RMR$_{pred}$**, the predicted arithmetic mean of the mass-specific resting metabolic rate.

TABLE 4. Predicted mass-independent resting metabolic rate (in $mLO_2\ h^{-1}\ g^{-0.67}$) in dicynodont fossils using PEMs (following the method of Guénard *et al.* (2013) and Legendre *et al.* (2016)), considering the consensus clade (((*Moghreberia*, *Kannemeyeria*), *Lystrosaurus*), *Daptocephalus*) (e.g. Cox and Angielczyk 2015; Boos *et al.* 2016; Angielczyk and Kammerer 2017; Kammerer and Smith 2017; Angielczyk *et al.* 2018).

Taxa	Femur			Humerus		
	$\bar{x}$**RMR$_{pred}$**	**Min limit of CI$_{95\%}$**	**Max limit of CI$_{95\%}$**	$\bar{x}$**RMR$_{pred}$**	**Min limit of CI$_{95\%}$**	**Max limit of CI$_{95\%}$**
Kannemeyeria simocephalus †	2.5697	1.8787	3.5148	NA	NA	NA
Moghreberia nmachouensis †	2.3782	1.6934	3.3399	1.6464	1.2530	2.1633
Myosaurus gracilis †	NA	NA	NA	1.6464	1.2921	2.0979
Lystrosaurus murrayi †	3.1099	2.2891	4.2250	1.6464	1.2842	2.1108
Oudenodon baini †	3.5050	2.5597	4.7995	1.6464	1.2921	2.0979
Tropidostoma †	2.4354	1.9079	3.1088	1.6464	1.2921	2.0979
Daptocephalus †	3.0039	2.2679	3.9785	NA	NA	NA
Endothiodon †	NA	NA	NA	1.6464	1.2921	2.0979

Abbreviations: CI, 95% confidence interval; $\bar{x}$**RMR$_{pred}$**, the predicted arithmetic mean of the mass-specific resting metabolic rate.

TABLE 5. Highest values of the predicted mass-independent resting metabolic rate (in $mLO_2\ h^{-1}\ g^{-0.67}$) in femur of dicynodont fossils using PGLS (continuous multiple regression model using MCMC) and PEMs (following the method of Guénard *et al.* (2013) and Legendre *et al.* (2016)), considering the clade (((*Moghreberia*, *Kannemeyeria*), *Daptocephalus*), *Lystrosaurus*) (Olivier *et al.* 2019).

Taxa	PGLS			PEMs		
	$\bar{x}$**RMR$_{pred}$**	**Min limit of CI$_{95\%}$**	**Max limit of CI$_{95\%}$**	$\bar{x}$**RMR$_{pred}$**	**Min limit of CI$_{95\%}$**	**Max limit of CI$_{95\%}$**
Kannemeyeria simocephalus †	8.3491	8.2417	8.4578	2.5697	1.8787	3.5148
Moghreberia nmachouensis †	5.5618	5.4946	5.6299	2.3782	1.6934	3.3399
Lystrosaurus murrayi †	6.3870	6.3123	6.4626	3.1099	2.2891	4.2250
Oudenodon baini †	2.2423	2.2120	2.2740	3.5050	2.5597	4.7995
Tropidostoma †	5.8899	5.8223	5.9583	2.4354	1.9079	3.1088
Daptocephalus †	5.4353	5.3737	5.4977	3.0039	2.2679	3.9785

Abbreviations: CI, 95% confidence interval; **PEMs**, analysis using Phylogenetic Eigenvector Maps approach; **PGLS**, analysis using Phylogenetic Generalised Least Squares approach; $\bar{x}$**RMR$_{pred}$**, the predicted arithmetic mean of the mass-specific resting metabolic rate.

CHAPTER V

DISCUSSION

Reconstruction of dicynodonts *Lisowicia* in a Late Triassic paleoenvironment of Poland (figure modified from Romano and Manucci, 2019)

Phylogenetic position still unconsensual

As largely developed in PAPER I, the taxonomic attribution of the first dicynodont specimen discovered by Counillon (1896) in the Luang Prabang Basin (Laos) has been strongly debated. The Laotian dicynodont is supposed to belong to *Dicynodon* or *Lystrosaurus* (e.g., Das Gupta, 1922; Woodward, 1932; Yuan and Young, 1934; Piveteau, 1938; Battail, 2009; Kammerer et al., 2011). The different analyses conducted in this work (PAPER I, PAPER II), as well as recent phylogenetic study (J. Liu, submitted, 2019) demonstrated that no consensus can be reach to position the Laotian skulls of *Counillonia* and *Repelinosaurus*. The phylogenetic analysis performed in PAPER I placed the new Laotian species *Counillonia superoculis* in Dicynodontidae with *Daptocephalus*, *Peramodon*, *Dinanomodon*, *Turfanodon*, *Euptychognathus*, *Sintocephalus*, *Jimusaria*, *Gordonia*, *Delectosaurus*, *Vivaxosaurus*, and *Dicynodon*. In the same analysis, *Repelinosaurus robustus* is sister taxa of all Triassic kannemeyeriiforms and thus considered as such by the comprehensive definition of Kannemeyeriiformes by Kammerer et al. (2013). In PAPER II, the phylogenetic matrix has been modified from PAPER I by: (1) addition of three new discrete characters (discrete 172-174) from Kammerer (2018), (2) revision of the cranial and postcranial coding of *Moghreberia nmachouensis*, (3) deletion of the species *Dicynodon huenei* and addition of *Dicynodon angielczyki* and *Daptocephalus huenei*, according to the recent taxonomic revision of Kammerer (2019a), (4) addition of *Pentasaurus goggai* (Kammerer, 2018), *Ufudocyclops mukanelai* (Kammerer et al., 2019), and *Lisowicia bojani* (Sulej & Niedźwiedzki 2019), and (5) revision of the coding of *Compsodon* and *Sangusaurus* according to the suggestions of Kammerer et al. (2019). The phylogenetic analysis conducted with the modified matrix in PAPER II led to a position of *Counillonia* and *Repelinosaurus* within Lystrosauridae with *Syops* and *Lystrosaurus*. In a recent analysis, both Laotian dicynodonts are included in Dicynodontidae (J. Liu, submitted, 2019). *Repelinosaurus* and *Counillonia* are placed sister taxa in the two later analyses (PAPER II; J. Liu, submitted, 2019).

The matrices differed in PAPER I, PAPER II, and a recent phylogenetic study (J. Liu, submitted, 2019). They thus resulted in different phylogenetic analyses and thus potentially different phylogenetic relationships. The ambiguous phylogenetic position of the Laotian dicynodonts may also be explained by their varied combination of character-states, with particular features only defined in Kannemeyeriiformes,

Dicynodontidae, and/or *Lystrosaurus*. Indeed, *Counillonia* and *Repelinosaurus* present an interparietal that does not contribute to the intertemporal skull roof (80[0]; PAPER II) and an occipital condyle distinctly triradiate (133[1]; PAPER II) as in *Dicynodon*, *Vivaxosaurus*, *Delectosaurus*, *Daptocephalus*, *Peramodon*, *Syops*, and *Lystrosaurus*. The ectopterygoids do not extend further posteriorly than the palatines in the Laotian dicynodonts (107[1]; PAPER II) as in *Syops*, *Sintocephalus*, and *Jimusaria*, while the ectopterygoids are absent in the majority of Kannemeyeriiformes and *Lystrosaurus*. As well as the majority of Kannemeyeriifromes, no intertuberal ridge is present between the two parabasisphenoid-basioccipital tubera in the Laotian dicynodonts (126[0]; PAPER II). This is not the case for *Dicynodon*, *Vivaxosaurus*, *Delectosaurus*, *Daptocephalus*, *Peramodon*, *Turfanodon*, *Jimusaria*, and *Lystrosaurus*. The anterior tip of snout is rounded in *Counillonia* (35[0]; PAPER II) as it is in *Dicynodon*, *Vivaxosaurus*, *Dinanomodon*, *Delectosaurus*, *Daptocephalus*, *Peramodon*, *Turfanodon*, *Gordonia*, and *Sintocephalus*. The nasals of *Repelinosaurus* bear a distinct median swelling (57[1]; PAPER II) as in *Dicynodon*, *Vivaxosaurus*, *Dinanomodon*, *Delectosaurus*, *Daptocephalus*, *Peramodon*, *Turfanodon*, and *Jimusaria*, while clear paired swellings are present in the majority of species of *Lystrosaurus* and Kannemeyeriiformes. However, the postorbitals of *Repelinosaurus* bear well-developed rugosities (65[1]; PAPER II) as in *Lystrosaurus* and the majority of Kannemeyeriiformes. Finally, *Repelinosaurus* would be particularly related to Kannemeyeriiformes by the absence of postfrontal bone (64[1]; PAPER II).

In addition to the three skulls LPB 1993-2, 1993-3, and 1995-9, abundant dicynodont postcranial and fragmentary cranial remains have also been excavated from the Purple Claystone Fm. The study of this new material should help to determine more precisey the phylogenetic position of the Laotian dicynodonts and their more closely relatives (Kannemeyeriiformes, Dicynodontidae, or *Lystrosaurus*). For instance, the precoracoid participates to the glenoid in *Lystrosaurus* (discrete character 172; PAPER II) and not to Kannemeyeriiformes, *Gordonia*, and *Daptocephalus leoniceps*, the only '*Dicynodon*'-grade taxa coded for this character. Also, the ilium is notched on its dorsal edge in *Lystrosaurus murrayi*, *Vivaxosaurus*, and *Peramodon*, as not in Kannemeyeriiformes (discrete character 183; PAPER II).

Datation of the Laotian dicynodont debated: discussion about the interpretation of "ghost lineages"

As discussed in PAPER I, the Purple Claystone Fm (Laos) has been dated using U-Pb geochronology on detrital zircon, which concluded to an age encompassing the Permo-Triassic boundary (Rossignol et al., 2016). However, while a late Permian age can not be excluded, an Early Triassic age appears the most likely. This hypothesis is notably based on (1) zircon grains older than the real age of sedimentation of the deposits bearing the dicynodonts and (2) volcaniclasts (likely comprising the youngest zircon grains) extensively reworked (PAPER I; Bercovici et al., 2012; Blanchard et al., 2013; Rossignol et al., 2016). Battail (2009) supposed a late Permian age based on the attribution of the Laotian skulls LPB 1993-2, 1993-3, and 1995-9 to the Permian genus "*Dicynodon*". A similar age has also been suggested by a recent phylogenetic study including the Laotian dicynodonts (J. Liu, submitted, 2019). The author supported his hypothesis by the close relationships between *Counillonia*, *Repelinosaurus*, and Permian dicynodontids, and the interpretation of the implied "ghost lineage" by a stratigraphic bias. The shorter the ghost lineage, the more parsimonious is the hypothesis to date the Laotian taxa. However, this latter interpretation rests on only one of the multiple possible interpretations of the "ghost lineage".

According to Norell (1992), the ghost lineage is an unknown evolutionnary line resulting from the combination of the stratigraphy and phylogeny. It is respresented by the difference in age between the oldest occurences of two sister taxa. A clear disctinction was made between the "ghost lineages" meaning "the corrected extensions of groups", and the "ghost taxa" meaning "the kinds of ghost lineages that are embedded in the internal structure of trees" (Fig. V.1; Norell, 1993). In other words, the ghost lineage represents a stratigraphic gap in fossil records implied by the phylogenetic relationships. Following the Norell (1993)'s scheme, the "ghost taxa" are groups that filled the stratigraphic gap. However, Norell (1993) practically defined the "ghost taxa" as the ancestral group of the clade emerging from the ghost lineage (for instance, see E, the ancestral group of the clade A+B; Fig. V.1). This assumption is erroneous under the light of a pattern interpretation of the cladogram. As opposed to some authors (e.g., Sidor and Hopson, 1998), I thus assume that distinguishing the "ghost lineage" and "ghost taxa" is critical. Indeed, using the example given by Norell

(1993) (Fig. V.1), I consider the “ghost taxa” as all taxa more closely related to the clade A+B, or to A, or to B than to the clade C+D, with occurences included in the stratigraphic gap of the “ghost lineage”. According to the latter definition, the “ghost taxa” could either correspond to (1) the occurences of unknown stem-taxa of the clade A+B or (2) the unknown occurrence of the taxa A and/or B (Fig. V.1). In the first case, the age of the clade A+B remains unchanged whereas in the second case, its age can effectively be extended to the older occurrences of the “ghost taxa”. There is no reason

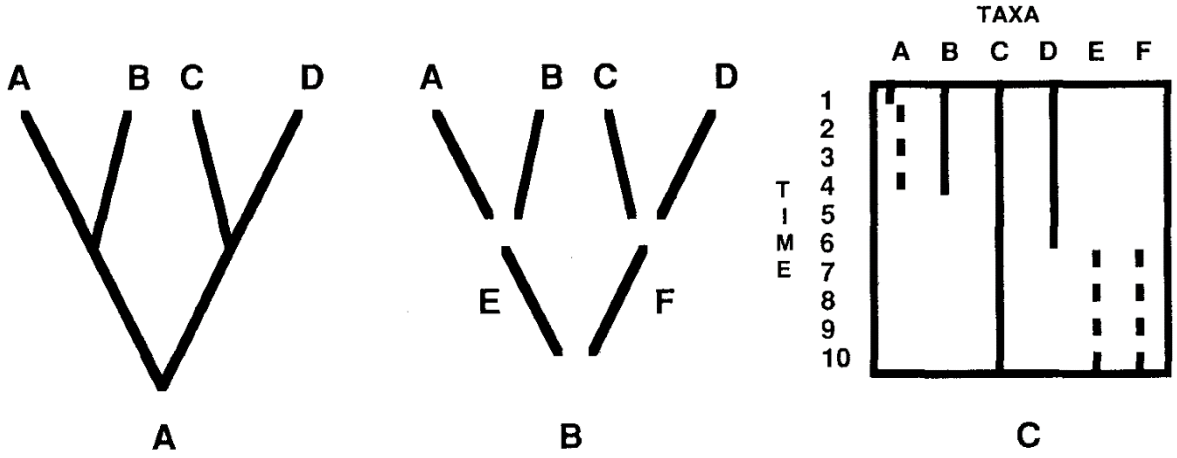

Fig. 2. A resolved phylogeny is shown in A, and fossil ranges for taxa A, B, C, and D are indicated by the solid lines in C. The phylogeny in A can be divided up into all of its separate component taxa. Taxa E and F are species that were ancestral to groups A-B and C-D respectively as predicted by the phylogeny in A. This tree can be calibrated using the fossil record in C. Therefore the minimum time of divergence of A and B is 4, and C and D is 10. The range of the lineage of taxon A has a corrected range of 4, 1 from the group plus 3 from the ghost lineage. Similarly the lineage origin for D is extended to 10, a group origin at 6 plus a ghost lineage duration of 4. Group A-B split from group C-D at 10. Because A or B do not appear until 4, a ghost taxon E is required. The minimum time of origin of this ghost taxon was at time 10, as calibrated by taxon C. Therefore the diagram in C can be used to indicate diversity. At time 9 the cladogram and the fossil record predict that a minimum of three taxa were present even though only one has been recovered in the fossil record.

Figure V.1. Distinction between the “ghost lineages” and “ghost taxa”, figure provided from Norell (1993)

to choose one hypothesis over the others.

As mentioned above, the interpretation of a late Permian age based on the phylogenetic relationships between the Laotian dicynodonts and Permian dicynodontoids thus did not contemplate all the possible hypotheses of the implied ghost lineage. Similarly, the hypothesis of unknown kannemeyeriiforms in late Permian only supported by Permian close relatives (Dicynodontidae and/or *Lystrosaurus*) (e.g., Fröbisch, 2007; Fröbisch et al., 2010; Kammerer et al., 2011), must be considered with caution. Considering the survivorship of multiple dicynodont lineages across the P-Tr boundary (discussed in PAPER I), it is risky to assume that Kannemeyeriiformes

survived the crisis. Based on their real stratigraphic occurences, it is more reasonable to suggest that the group comprising Kannemeyeriiformes and their sister-taxa has survived the crisis. Also, it is more accurate to assume that the emydopoids have survived the P-Tr crisis, than to suggest hypothetical occurences of the Triassic *Myosaurus* and *Kombuisia* in Permian.

To go even further, the relevance of the concept of the “ghost lineage” can also be discussed. This concept implicitly recognises the evolutionnary process of diversification as dichotomic implying a same age for two sister-taxa. In this case, the cladogram is a direct image of the evolutionnary history of the groups. Still, multiple evolutionnary scenarii can match a unique cladogram (Fig. V.2; e.g., Harper, 1976; Platnick, 1977). As shown by Platnick (1977) (Fig. V.2), the topology A1 can result either from a dichotomic evolutionnary process (“cladogenesis” according to Rensch, 1929, 1959; see A1 on Fig. V.2) or a linear and gradual evolutionnary process (“anagenesis” according to Rensch, 1929, 1959; see B1 on Fig. V.2). Also, a

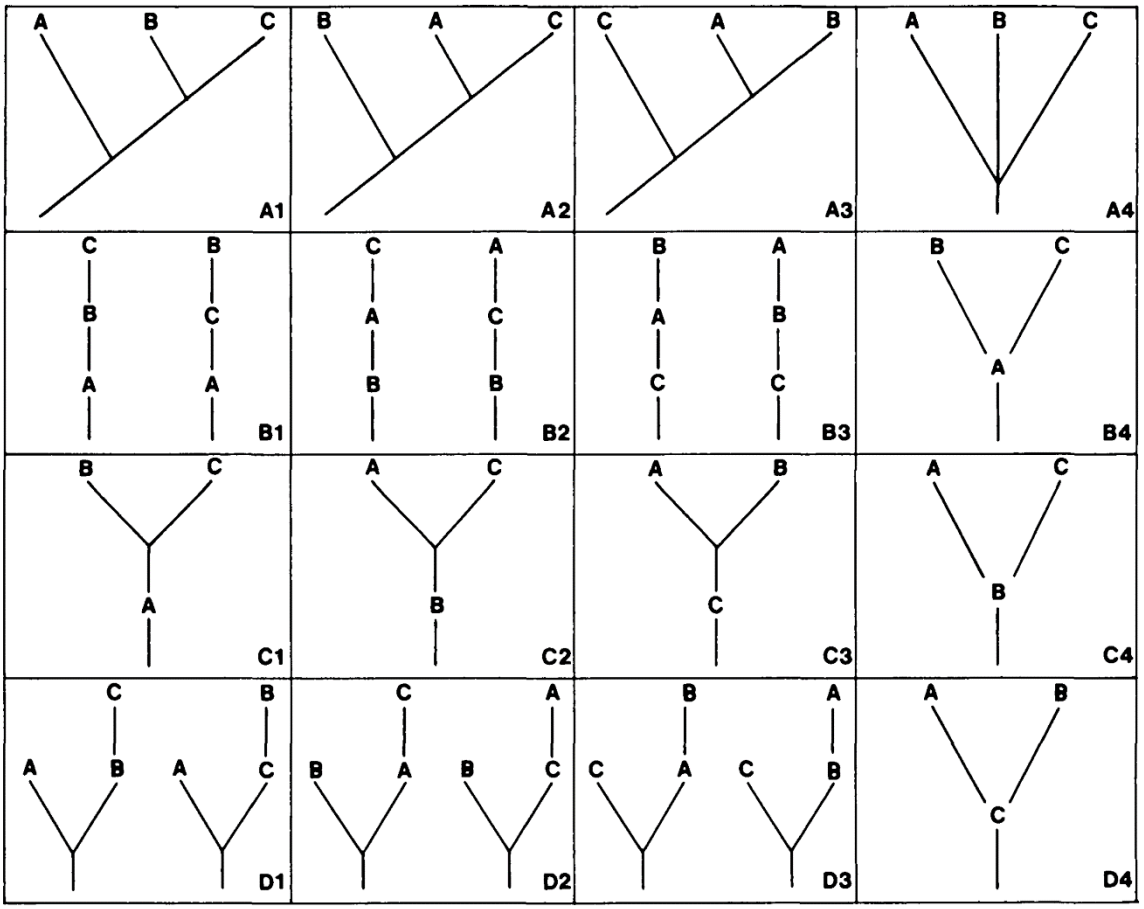

FIG. 2.—The four possible three-taxon cladograms (row A) and 22 possible three-taxon phylogenetic trees (rows A–D). The trees in each column are the set represented by the cladograms isomorphic with the

Figure V.2. Cladograms and their multiple possible evolutionnary scenarii associated, figure provided by Platnick (1977)

combination of both evolutionnary processes (see C1 and D1 on Fig. V.2) can be considered. Therefore, the evolutionnary history of the kannemeyeriiforms could be interpreted either as an ancestral group splitting into the kannemeyeriiforms and their sister-taxa representatives (“cladogenesis”, named ‘scenario 1’), or as an emergence of the kannemeyeriiforms within their sister-taxa representatives (“anagenesis”, named ‘scenario 2’). Theoritically, the kannemeyeriiforms may also be the ancestral population of their sister-taxa representatives. However, this last scenario is less likely considering the stratigraphic records. Returning to the “ghost lineage” concept, in scenario 1, the “ghost lineage” is an effective stratigraphic gap in the fossil record. The “ghost taxa” can thus be unknown Permian kannemeyeriiforms and/or unknown Permian stem-kannemeyeriiforms. In scenario 2, the “ghost lineage” may only be a topologic construction implied by the cladogram, and the “ghost taxa” do not exist. A stratigraphic extension of the fossil record of the kannemeyeriiforms and stem-kannemeyeriiforms until Permian is thus not required in scenario 2. Nevertheless, a stratigraphic overlap between the extensions of the two sister-taxa is necessary. In the case of a stratigraphic lacuna between the sister-taxa, scenario 2 involves a stratigraphic extension of one or both sister-taxa to reach the overlap. Only in this particular situation, there is an effective stratigraphic gap in fossil record in scenario 2. Nonetheless, filling this gap will always be more parsimonious than in the case of scenario 1.

As it is the case with Kannemeyeriiformes, the scenario 2 proposes an origin of the representatives of the Laotian dicynodonts *Counillonia* and *Repelinosaurus* within the Permian dicynodontids. However, considering this scenario, a Permian age of the Laotian dicynodonts is thus not required.

Dicynodonts: large dominant herbivores facing to the end Triassic crisis

After surviving the Permian-Triassic crisis, the dicynodonts greatly diversified during the Middle Triassic with the apparition of around twenty new genera (Fig. I.3). They constituted the dominant herbivores of their ecosystem, especially by their imposing size. Indeed, the body size of the dicynodonts noticeably increased during the Triassic. Among the few forms known in the Early Triassic, none of the skulls exceed thirty centimeters (basal lengths [BLS] measured in ventral view from the end of the premaxilla to the posterior border of the occipital condyle): *Lystrosaurus* (except the Permian *L. maccaigi*), *Kombuisia*, *Myosaurus*, and the Laotian dicynodonts

Counillonia and *Repelinosaurus* (see discussion about their age in PAPER I) (C. Olivier pers. observ.; e.g., Cluver, 1974; Hammer and Cosgriff, 1981; Botha and Smith, 2007; Fröbisch, 2007; Fröbisch et al., 2010; Ray et al., 2012). Except few big forms (BLS≈ 45 cm) such as *Kannemeyeria*, *Angonisaurus*, and *Dolichuranus* (C. Olivier pers. obs.), most of Middle Triassic dicynodonts such as *Rechnisaurus*, *Sangusaurus*, *Shaanbeikannemeyeria*, *Shansiodon*, *Tetragonias*, *Uralokannemeyeria*, and *Xiyukannemeyeria*, are middle-sized forms with a skull not exceeding 35 cm (C. Olivier pers. observ.; e.g., Cruickshank, 1967; Roy-Chowdhury, 1970; Bandyopadhyay, 1989; Angielczyk et al., 2018). The biggest dicynodonts mainly appeared during the Late Triassic with skulls ranging from 40 to 45 cm (*Dinodontosaurus*, *Jachaleria*, *Moghreberia*, *Parakannemeyeria*, *Placerias*, and *Stahleckeria*), and superior to 60 cm with *Ischigualastia* (C. Olivier pers. observ.; e.g., Camp and Welles, 1956; Vega-Dias et al., 2004; Abdala et al., 2013). While exceptional, small-sized dicynodont skulls around 20 cm, such as *Vinceria* and *Sinokannemeyeria* are also known in the Late Triassic (C. Olivier pers. observ.; e.g., Domnanovich and Marsicano, 2012). No firm conclusions resulted from the study of the dicynodont postcranial material discovered in the Argana Basin (Morocco) about the presence of multiple morphotypes and the taxonomic validity of the Moroccan genus *Azarifeneria* (PAPER II). However, a second big morphotype, distinct from *Moghreberia nmachouensis* by its clear robustness, can be highlighted (PAPER II). The femur MNHN.F.ALM 284 (maximum length [FL] of 47 cm) (Fig. 28F-H in PAPER II) is one of the biggest Late Triassic forms including *Ischigualastia* (FL= 47 cm), *Stahleckeria* (FL= 55 cm), and *Lisowicia* (FL= 80 cm) (C. Olivier pers. observ.; e.g., Sulej and Niedźwiedzki, 2019). In conclusion, both the skull and femora sizes of dicynodonts increase during the Triassic.

Predator-prey interactions could be a hypothesis explaining the increase of the body size in dicynodonts (Sinclair et al., 2003; Niedźwiedzki et al., 2011). Indeed, bite marks on dicynodont bones indicated that predatory dinosaurs hunted the dicynodonts in Late Triassic (Niedźwiedzki et al., 2011). An increase of the predator body size (i.e., dinosauromorphs and non-dinosaur archosauromorphs) might have lead to a bigger dicynodont body size (Niedźwiedzki et al., 2011). By selection pressure, a large size therefore constitutes a refuge from large predators. According to Sinclair et al. (2003), increase in body size implies a higher energetic need including the maintenance of a high metabolic rate in dicynodonts (PAPERS III and IV). The study of dicynodont coprolites by Bajdek et al. (2014) provided elements about their diet and suggested an

efficient digestive process, because of the high degree of decomposition of the ingested food. The retention time of the food bowl is related to the size of the digestive system (Fritz et al., 2009). With herbivory diet, selection favors long gastrointestinal tract and thus a large body size in mammals and reptiles to maximize the energetic gain (Fritz et al., 2010, 2011; Müller et al., 2013).

The abundance of dicynodont remains and their diversity, with 10 early Late Triassic genera including four newly appeared forms (*Dinodontosaurus*, *Stahleckeria*, *Sinokannemeyeria*, *Parakannemeyeria*, *Vinceria*, *Moghreberia*, *Eubrachiosaurus*, *Placerias*, *Ischigualastia*, and *Jachaleria*), suggest that they were well adapted to their ecosystems. Nonetheless, only *Jachaleria* survived the end of the Carnian (Fig. I.3). Newell (1963) indentified a mass extinction crisis in the end of Triassic (Tr-J crisis) that impacted more than a third of the fauna families. This crisis was considered as one of the big five major mass extinctions that include also: Late Ordovician, Late Devonian, Late Permian, and Late Cretaceous (e.g., McGhee et al., 2004; Twitchett, 2006). In the Eastern United States, catastrophic events in the Late Triassic have been suggested by Olsen et al. (2002) in the non dinosaurian vertebrate and plant assemblages. Nevertheless, a hard and abruptness decline of the biodiversity at the end of the Triassic has been questioned by some authors (e.g., Hallam, 2002; Lucas and Tanner, 2004; Tanner et al., 2004). Richoz et al. (2007) explained that the impact of the Tr-J crisis may be overestimated: it could have been multiple smaller crises taking place all Late Triassic long. During the Carnian and the early Norian, high changes in environment and biodiversity have been shown with a mean decreasing of 70% of the specific diversity of molluscs (McRoberts and Newton, 1995; Richoz et al., 2007). Benton (1991, 1994) supported that the environment perturbations in the late Carnian impacted more the diversity of European terrestrial tetrapods than the Tr-J crisis. High environmental changes have been noticed during the Carnian with negative excursions of the isotopic carbon, oceanic transgressions, climatic changes (“Carnian Humid Episode“). They have been correlated to perturbations in european plant assemblages (Richoz et al., 2007; Roghi et al., 2010; Ruffell et al., 2015; Sun et al., 2016). Lucas and Tanner (2004) and Tanner et al. (2004) explained the apparent abruptness of the Tr-J crisis by the stratigraphic imprecision (Teichert, 1988) deriving from the combination of multiple temporal distributions on a large scale (“Signor-Lipps effect”). Lucas (1994) called this inaccuracy the “Compiled Correlation Effect” (CCE). The CCE results in “artificial concentration of extinctions at stage/age boundaries; a complex

extinction of significant temporal duration during a stage/age is made to appear as a mass extinction at the end of the stage/age", as noted by Lucas and Tanner (2004). The CCE suggested that the ammonits became abruptly exinct at the end of the Rhaetian, while a more detailed study of the temporal distribution of the group demonstrated multiple small extinction events during the Rhaetian, suggesting a more gradual disappearance of the ammonits (Lucas and Tanner, 2004).

A significant faunal and floral turnover characterizes the Carnian (e.g., Behrensmeyer et al., 1992; Simms et al., 1994; Fraser and Sues, 2010). Fraser and Sues (2010) therefore designated this period as "the Dawn of the Modern World", with a major change from 'archaic' forms to 'modern'. Indeed, the terrestrial ecosystems was formerly dominated by the dicynodont therapsids and their comtemporaries: procolophonid parareptiles, chroniosuchian anthracosaurs, and some archosauromorphs such as the rhynchosaurs (e.g., Behrensmeyer et al., 1992; Simms et al., 1994; Fraser and Sues, 2010). The Late Triassic was marked by the appearance of the prosauropod dinosaurs and a Mesozoic ecosystem dominated by crocodiliforms, lepidosaurs, mammaliaforms, and dinosaurs. Behrensmeyer et al. (1992, p. 343) added that "the late Carnian and Norian produced a major turnover, not only in the groups of herbivorous tetrapods present but also in the nature of vertebrate herbivory". The domination of the 'herbivores' ecological niche by the dicynodont synapsids during the Triassic has been strongly impacted by the major floral changes during the Carnian, and then by the appearance of the larger and probably more competitive dinosaurs (prosauropods, sauropods, and ornithischians).

As it happened with the ammonits (Lucas and Tanner, 2004), the recent discovery of the kannemeyeriiforms *Pentasaurus* and *Lisowicia* dated to latest Norian–earlier Rhaetian would support a more gradual extinction of the dicynodonts during the Late Triassic (e.g., Knoll, 2004; Fraser and Sues, 2010; Kammerer, 2018; Sulej and Niedźwiedzki, 2019). In addition, Sulej and Niedźwiedzki (2019) confronted the classic picture of a Norian ecosystem dominated by dinosaurs by including the dicynodont *Lisowicia* as a potential challenger in the ecosystem. However, the volumic body mass of 9 tons of *Lisowicia* previously estimated (Sulej and Niedźwiedzki, 2019) was reassessed by Romano and Manucci (2019) and reduced to 6 tons. Nevertheless, Romano and Manucci (2019) confirmed the size of the big dicynodont reaching that of extant elephants.

CHAPTER VI

GENERAL CONCLUSIONS AND PERSPECTIVES

Artist's reconstruction of the dicynodont *Lisowicia* © Karolina Suchan-Okulska

Two new dicynodont species (*Counillonia superoculis* and *Repelinosaurus robustus*) were described in the Luang Prabang Basin (Laos), a poorly-studied geographic area. By the phylogenetic analysis, *Counillonia* and *Repelinosaurus* were first placed in Dicynodontidae and Kannemeyeriiformes, respectively. However, two more recent studies highlighted different phylogenetic position of these two taxa, both of them assigned to Lystrosauridae or Dicynodontidae. Their particular combination of character-states, specific of *Lystrosaurus*, dicynodontids, and/or kannemeyeriiforms, may likely explain their non-consensual phylogenetic relationships.

The age of the Purple Claystone Fm (bearing the two Laotian dicynodonts) ranging from the late Permian to Early Triassic shed new light on the paleogeography of the Indochina Block and its collision with the rest of the Pangea. Indeed, judging by the presence of the almost exclusively terrestrial Laotian dicynodonts on the Indochina Block, a terrestrial connection between this block and Pangea can thus be interpreted at least in late Permian-Early Triassic, most likely via the South and North China blocks.

An Early Triassic age for the Purple Claystone Fm being the most likely, the addition of two new dicynodont forms shortly after the P-Tr crisis supports, on one hand, the hypothesis of a more rapid recovery of the dicynodonts; and, on the other hand, the survivorship of multiple dicynodont lineages through the P-Tr boundary. However, the interpretation of the “ghost lineages” must be considered with caution. The current stratigraphic and phylogenetic results only allow to suppose the survivorship of Emydopoidae (with the Triassic *Kombuisia* and *Myosaurus*), of Lystrosauridae (with most of the *Lystrosaurus* species), and of the clade including Kannemeyeriiformes and their Permian sister taxa. The close affinities between the Laotian dicynodonts and Permian dicynodontids, resulted from some phylogenetic analyses, may also add Dicynodontidae to the list of the dicynodont lineages to have survived the crisis.

In parallel, the taxonomic validity of the three Moroccan dicynodont species *Mogherberia nmachouensis*, *Azarifeneria barrati*, and *A. robustus*, was reassessed. An abundant postcranial material found in the Argana Basin (Morocco) have been described and the major part was attributed to *M. nmachouensis*, the most abundantly represented by cranial remains. These new descriptions and the revised study of the cranial material clearly distinguished *Moghreberia* from the North American *Placerias*. In addition, the phylogenetic analysis showed that *Moghreberia* is more closely related

to *Lisowicia* than to *Placerias* in Stahleckeridae. The diagnosis of *M. nmachouensis* has thus been revised and completed.

The revised study of the cranial material of *Azarifeneria* did not emphasized significant differences between the genus and *Moghreberia* or other Triassic kannemeyeriiforms. However, while the current absence of diagnostic characters, a second morphotype is highlighted on the basis of the strong robustness of the postcranial material, which reminds the cranial specimens of *Azarifeneria*. The large size of *Moghreberia* and especially of the second big morphotype confirmed the increase of the body size in dicynodonts during the Triassic, with the largest forms in Late Triassic.

Integrated in a large comparative morphological study of the cranial and postcranial material of Triassic dicynodonts, the study of dicynodonts from Laos and Morocco highlighted a significant morphological variation and especially an intraspecific one (ontogeny, sexual dimorphism, and others). While most of this variation is known in dicynodonts and does not interfer in species distinction, it remains problematic when it concerns characters used in phylogeny. For instance, the preparietals depressed or flushed with the skull roof were both present in *Repelinosaurus*. Also, a distinct hemispherical and tab-like supinator process as well as reduced and more anteriorly-developped processes have been described in humeri of *Moghreberia*.

The paleophysiology of the dicynodonts has been investigated using statistical inference models. Paleohistological statistical models have indeed been built to infer the resting metabolic rate (RMR) of dicynodonts. A first statistical model using the Phylogenetic Eigenvector Maps approach was used following the method of Guénard et al. (2013) and Legendre et al. (2016). This first analysis dealed with three dicynodonts (*Moghreberia nmachouensis*, *Lystrosaurus* sp., and *Oudenodon baini*) and three histological variables (size, shape, and density of osteocyte lacunae). Later on, other paleohistological inference models have been performed including a larger dicynodont sample (*Daptocephalus*, *Endothiodon*, *Kannemeyeria simocephalus*, *Lystrosaurus murrayi*, *Moghreberia nmachouensis*, *Myosaurus gracilis*, *Oudenodon baini*, and *Tropidostoma*) and using two statistical approaches: PEMs and Phylogenetic Generalised Least Squares (PGLS) methods. As opposed to PEMs, the analyses using PGLS provided a more explicit evolutionnary model and the inclusion of a combination of histological variables (size, shape, and density of osteocyte lacunae, and primary osteon density). Except for *Endothiodon* and *Myosaurus*, a high

RMR was inferred in all Permian and Triassic studied dicynodonts by PEMs and PGLS methods.

The results first confirmed the previous qualitative histological studies highlighting fibrolamellar or 'incipient' fibrolamellar bone in dicynodonts. The inference of endothermy in all Permian and Triassic studied dicynodonts then confronted the hypothesis supposing the endothermy as the major explanatory factor of differential success across the P-Tr boundary. More broadly, the paleobiological inference models suggested a unique acquisition of the mammalian endothermy in Synapsida at least 260 Myr ago at the Neotherapsida node.

However, methodological limits have been observed in both statistical methods (PGLS and PEMs). The approach using PEMs proposed by Legendre et al (2016) implies the selection of the best model based on the phylogeny and eventually one of the histological predictive variables. Using the phylogeny only equal to a simple optimization of the RMR. The selection of the best model using PGLS with BayesTraits rests on the coefficient of determination R^2, which is unsufficient to attest to the predictive power of a statistical model. In addition, while a more explicit evolutionary model is useful to make inferences, it results in the choice of parameters without clear possible biological explanations (for instance, the distribution of the regression coefficients β of the histological predictive variable).

This work dealed with the evolution of the dicynodonts during the Triassic and especially highlighted the impact of the Laotian and Moroccan forms on paleobiogeographic, phylogenetic, and paleobiologic issues. However, most of these studies need to be completed and some problematics remain.

The non-consensual position of the Laotian dicynodonts could be more constrained by the study of their undescribed cranial and postcranial remains (present in MNHN collections). The use of field data (not possible for this sutdy) will enable to confidently associate cranial with postcranial remains and therefore to better understand the bone anatomy of the Laotian forms. Their study would also allow discussing on the presence of multiple morphotypes in the Laotian material and on possible morphological variation. If a clear taxonomic attribution of the Laotian postcrania is possible, the associated stylopods (femora and humeri) could be included in a qualitative and quantitative histological study to better understand the biology of dicynodonts living close to the P-Tr crisis.

Pending better preparation of the cranial remains of the Moroccan *Azarifeneria* and a probable highlight of diagnostic features, this genus is considered a *nomen dubium*. In addition, only the holotype (MNHN.F.AZA 366.1-.2-.3) of *A. barrati* has been discovered in the locality XII of the Argana Basin, a still poorly-studied region according to Dutuit (1976). Future field works in this region would provide supplementary carnial and/or postcranial material.

The big size of *Moghreberia* and the potential second form characterized by the robustness of its postcranium, confirmed the tendency to increase in size of the dicynodonts in Late Traissic. However, as opposed to the genera *Lisowicia*, and *Pentasaurus*, the Moroccan dicynodonts do not provide information about the features of the last dicynodont forms. A complete skeleton in connection of a Laotian form was discovered in the Red Claystone Fm, dated to Norian by U–Pb zircon geochronology, and attributed to an undetermined kannemeyeriiform (e.g., Blanchard et al., 2013; Rossignol et al., 2016). Its study would would lead to: (1) a description of the first complete dicynodont in Late Triassic, (2) the occurence of a new latest Triassic form or the stratigraphic extension of a known species, and (3) better understanding of the dicynodont biodiversity during Late Triassic and the conditions of the extinction of the dicynodonts.

Finally, despite the multiple methodological limits of PGLS, the most important perspective to improve the paleobiological inference models should be to add more extant synapsid taxa to later infer the RMR in a larger sample of extinct non-mammalian synapsid taxa.

BIBLIOGRAPHY

Dicynodont © tepuitrouble (www.deviantart.com)

Abdala, F., C. A. Marsicano, R. M. H. Smith, and R. Swart. 2013. Strengthening Western Gondwanan correlations: A Brazilian Dicynodont (Synapsida, Anomodontia) in the Middle Triassic of Namibia. Gondwana Research 23:1151–1162.

Angielczyk, K. D. 2001. Preliminary phylogenetic analysis and stratigraphic congruence of the dicynodont anomodonts (Synapsida: Therapsida). Palaeontologica Africana 37:53–79.

Angielczyk, K. D. 2007. New specimens of the tanzanian dicynodont "*Cryptocynodon*" *parringtoni* Von Huene, 1942 (Therapsida, Anomodontia), with an expanded analysis of Permian dicynodont phylogeny. Journal of Vertebrate Paleontology 27:116–131.

Angielczyk, K. D., and A. A. Kurkin. 2003. Phylogenetic analysis of Russian Permian dicynodonts (Therapsida: Anomodontia): implications for Permian biostratigraphy and Pangaean biogeography. Zoological Journal of the Linnean Society 139:157–212.

Angielczyk, K. D., and B. S. Rubidge. 2010. A new pylaecephalid dicynodont (Therapsida, Anomodontia) from the Tapinocephalus Assemblage Zone, Karoo Basin, Middle Permian of South Africa. Journal of Vertebrate Paleontology 30:1396–1409.

Angielczyk, K. D., and C. F. Kammerer. 2017. The cranial morphology, phylogenetic position and biogeography of the upper Permian dicynodont *Compsodon helmoedi* van Hoepen (Therapsida, Anomodontia). Papers in Palaeontology 3:513–545.

Angielczyk, K. D., P. J. Hancox, and A. Nabavizadeh. 2018. A redescription of the Triassic kannemeyeriiform dicynodont *Sangusaurus* (Therapsida, Anomodontia), with an analysis of its feeding system. Journal of Vertebrate Paleontology 37:189–227.

Arambourg, C. and Duffaud, F. 1960. Note sur la découverte d'un gisement de vertébrés continentaux dans le Trias du Haut Atlas. Bulletin de la Société Géologique de France, 2: 172–177.

Artabe, A. E., E. M. Morel, and L. A. Spalletti. 2003. Caracterización de las provincias fitogeográficas triásicas del Gondwana extratropical. Ameghiniana 40:387–405.

Bain, A. G. 1845. On the Discovery of the Fossil Remains of Bidental and other Reptiles in South Africa. Quarterly Journal of the Geological Society 1:317–318.

Bajdek, P., K. Owocki, and G. Niedźwiedzki. 2014. Putative dicynodont coprolites from the Upper Triassic of Poland. Palaeogeography, Palaeoclimatology, Palaeoecology 411:1–17.

Bandyopadhyay, S. 1988. A Kannemeyeriid Dicynodont from the Middle Triassic Yerrapalli Formation. Philosophical Transactions of the Royal Society of London B: Biological Sciences 320:185–233.

Bandyopadhyay, S. 1989. The mammals-like reptile *Rechnisaurus* from the Triassic of India. .

Barry, T. H. 1974. A new dicynodont ancestor from the Upper Ecca (lower Middle Permian) of South Africa. Annals of the South African Museum 64:7–136.

Battail, B. 1997. Les genres *Dicynodon* et *Lystrosaurus* (Therapsida, Dicynodontia) en Eurasie: Une mise au point. Geobios 30:39–48.

Battail, B. 2009. Late Permian dicynodont fauna from Laos. Geological Society, London, Special Publications 315:33–40.

Battail, B., J. Dejax, P. Richir, P. Taquet, and M. Véran. 1995. New data on the continental Upper Permian in the area of Luang-Prabang, Laos. Journal of Geology 11–15.

Behrensmeyer, A. K., J. D. Damuth, W. A. DiMichele, R. Potts, H.-D. Sues, and S. L. Wing. 1992. Terrestrial Ecosystems through Time: Evolutionnary Paleoecology of Terretrial Plants and Animals, The University of Chicago Press. Behrensmeyer, A. K., Damuth, J. D., DiMichele, W. A., Potts, R., Sues, H. -D., and Wing S. L., Chicago, 568 pp.

Benoit, J., P. Manger, V. Fernandez, and B. S. Rubidge. 2018. Evolution of facial innervation in anomodont therapsids (Synapsida): Insights from X-ray computerized microtomography. Journal of Morphology 1–29.

Benton, M. J. 1991. What really happened in the late Triassic? Historical Biology 5:263–278.

Benton, M. J. 1994. Late Triassic to Middle Jurassic extinctions among continental tetrapods: testing pattern; pp. 445 in In the shadow of the dinosaurs, University Press. N. C. Fraser & H. -D. Sues (eds), Cambridge, UK.

Benton, M. J. 2005. Vertebrate Palaeontology, 3rd ed. Blackwell Science, Malden, MA, 455 pp.

Bercovici, A., S. Bourquin, J. Broutin, J.-S. Steyer, B. Battail, M. Véran, R. Vacant, B. Khenthavong, and S. Vongphamany. 2012. Permian continental

paleoenvironments in Southeastern Asia: New insights from the Luang Prabang Basin (Laos). Journal of Asian Earth Sciences 60:197–211.

Bernardi, M., F. M. Petti, and M. J. Benton. 2018. Tetrapod distribution and temperature rise during the Permian–Triassic mass extinction. Proceedings of the Royal Society B: Biological Sciences 285:20172331.

Bernardi, M., F. M. Petti, E. Kustatscher, M. Franz, C. Hartkopf-Fröder, C. C. Labandeira, T. Wappler, J. H. A. van Konijnenburg-van Cittert, B. R. Peecook, and K. D. Angielczyk. 2017. Late Permian (Lopingian) terrestrial ecosystems: A global comparison with new data from the low-latitude Bletterbach Biota. Earth-Science Reviews 175:18–43.

Blanchard, S., C. Rossignol, S. Bourquin, M.-P. Dabard, E. Hallot, T. Nalpas, M. Poujol, B. Battail, N.-E. Jalil, J.-S. Steyer, R. Vacant, M. Véran, A. Bercovici, J. B. Diez, J.-L. Paquette, B. Khenthavong, and S. Vongphamany. 2013. Late Triassic volcanic activity in South-East Asia: New stratigraphical, geochronological and paleontological evidence from the Luang Prabang Basin (Laos). Journal of Asian Earth Sciences 70–71:8–26.

Bonaparte, J. F. 1969. Two new reptilian “faunas” of the Argentine Triassic. Gondwana Stratigraphy 2:283–306.

Bonaparte, J. F. 1970. Annotated list of the South American Triassic tetrapods. Proceedings and Papers 665–682.

Boos, A. D. S., C. F. Kammerer, C. L. Schultz, M. B. Soares, and A. L. R. Ilha. 2016. A New Dicynodont (Therapsida: Anomodontia) from the Permian of Southern Brazil and Its Implications for Bidentalian Origins. PLoS ONE 11.

Botha, J. 2003. Biological aspects of the Permian dicynodont *Oudenodon* (Therapsida: Dicynodontia) deduced from bone histology and cross-sectional geometry. Palaeontologica Africana 39:37–44.

Botha, J., and A. Chinsamy. 2000. Growth patterns deduced from the bone histology of the cynodonts *Diademodon* and *Cynognathus*. Journal of Vertebrate Paleontology 20:705–711.

Botha, J., and A. Chinsamy. 2004. Growth and life habits of the Triassic cynodont Trirachodon, inferred from bone histology. Acta Palaeontologica Polonica 49:619–627.

Botha, J., and R. M. H. Smith. 2006. Rapid vertebrate recuperation in the Karoo Basin of South Africa following the End-Permian extinction. Journal of African Earth Sciences 45:502–514.

Botha, J., and R. M. H. Smith. 2007. *Lystrosaurus* species composition across the Permo-Triassic boundary in the Karoo Basin of South Africa: Lystrosaurus across the PTB. Lethaia 40:125–137.

Botha-Brink, J., and K. D. Angielczyk. 2010. Do extraordinarily high growth rates in Permo-Triassic dicynodonts (Therapsida, Anomodontia) explain their success before and after the end-Permian extinction ? Zoological Journal of the Linnean Society 160:341–365.

Botha-Brink, J., F. Abdala, and A. Chinsamy-Turan. 2012. The radiation and osteohistology of Nonmammaliaform Cynodonts; pp. 223–248 in Forerunners of Mammals, Indiana Universiy Press. Chinsamy-Turan, A. (ed.).

Botha-Brink, J., D. Codron, A. K. Huttenlocker, K. D. Angielczyk, and M. Ruta. 2016. Breeding Young as a Survival Strategy during Earth's Greatest Mass Extinction. Scientific Reports 6:24053.

Broom, R. 1905. On the use of the term Anomodontia. Albany Museum Records 1:266–269.

Broom, R. 1911. On some new South African Permian reptiles. Proceedings of the Zoological Society of London 1911:1073–1082.

Bueno, A. de O. 2015. Descrição osteo-histológica de elementos fósseis de Dinodontosaurus turpior (Therapsida, Dicynodontia), Mesotriássico do Rio Grande do Sul, BrasilD. .

Camp, C. L. 1956. Triassic dicynodont reptiles. Part II. Triassic dicynodont compared. Memories of the University of California 13:305–337.

Camp, C. L., and S. P. Welles. 1956. Triassic dicynodont reptiles. Part I. The North American genus *Placerias*. Memories of the University of California 13:255–304.

Canoville, A., and M. Laurin. 2010. Evolution of humeral microanatomy and lifestyle in amniotes, and some comments on palaeobiological inferences. Biological Journal of the Linnean Society 100:384–406.

Cecca, F., and R. Zaragüeta i Bagils. 2015. Paléobiogéographie. Edp Sciences, Paris, France, 193 pp.

Chen, Z.-Q., and M. J. Benton. 2012. The timing and pattern of biotic recovery following the end-Permian mass extinction. Nature Geoscience 5:375–383.

Cheng, Z. 1980. Cheng, Z. (1980). Mesozoic stratigraphy and paleontology of the Shaanxi-Gansu-Ningxia basin. Vertebrate Fossils 2:115–188.

Cheng, Z. W. 1986. Vertebrate fossils; pp. 207–218 in Permian and Triassic Strata and Fossil Assemblages in the Dalongkou Area of Jimsar, Xinjiang, Geological Publishing House. Beijing.

Chinsamy, A., and B. S. Rubidge. 1993. Dicynodont (Therapsida) bone histology: phylogenetic and physiological implications. Palaeontologica Africana 30:97–102.

Chinsamy, A., and J. H. Hurum. 2006. Bone microstructure and growth patterns of early mammals. Acta Palaeontologica Polonica 51:325–338.

Chinsamy-Turan, A. 2005. The Microstructure of Dinosaur Bone: Deciphering Biology with Fine-Scale Techniques. Johns Hopkins University Press, Baltimore, 216 pp.

Chinsamy-Turan, A., and S. Ray. 2012. Bone histology of some Therocephalians and Gorgonopsians, and evidence of bone degradation by fungi; pp. 199–222 in Forerunners of Mammals, Indiana Universiy Press. Chinsamy-Turan, A. (ed.).

Clarke, A., and H.-O. Pörtner. 2010. Temperature, metabolic power and the evolution of endothermy. Biological Reviews 85:703–727.

Cluver, M. A. 1974. The Cranial Morphology of the Lower Triassic Dicynodont "*Myosaurus Gracilis*". Annals of The South African Museum 66:35–54.

Cluver, M. A., and N. Hotton III. 1981. The genera *Dicynodon* and *Diictodon* and their bearing of classification of the Dicynodontia (Reptilia, Therapsida). Annales of the South African Museum 83:99–146.

Cluver, M. A., and G. M. King. 1983. A reassessment of the relationships of Permian Dicynodontia (Reptilia, Therapsida) and a new classification of dicynodonts. Annals of South African Museum 91:195–273.

Colbert, E. H. 1982. The distribution of *Lystrosaurus* in pangaea and its implications. Geobios 15:375–383.

Cope, E. D. 1870. On the skull of dicynodont Reptilia. *Lystrosaurus frontosus* from Cape Colony. Proceedings of the American Philosophical Society 11:419.

Counillon, H. 1896. Documents pour servir à l'étude géologique des environs de Luang-Prabang (Cochinchine). Comptes Rendus de l'Académie Des Sciences, Paris 123:1330–1333.

Cox, C. B. 1962. Preliminary diagnosis of *Ischigualastia*, a new genus of Dicynodont from Argentina. Breviora 156:8–9.

Cox, C. B. 1965. New Triassic Dicynodonts from South America, Their Origins and Relationships. Philosophical Transactions of the Royal Society of London B 248:457–514.

Cox, C. B. 1969. Two new dicynodonts from the Triassic Ntawere Formation, Zambia. Bulletin of the British Museum (Natural History) Geology 17:257–294.

Cox, C. B. 1991. The Pangaea dicynodont *Rechnisaurus* and the comparative biostratigraphy of Triassic dicynodont faunas. Palaeontology 34:767–784.

Cox, C. B., and J. Li. 1983. A new genus of Triassic Dicynodont from East-Africa and its classification. Palaeontology 26:389–406.

Cox, C. B., and K. D. Angielczyk. 2015. A New Endothiodont Dicynodont (Therapsida, Anomodontia) from the Permian Ruhuhu Formation (Songea Group) of Tanzania and Its Feeding System. Journal of Vertebrate Paleontology 35:e935388.

Cracraft, J. 1974. Continental drift and vertebrate distribution. Annual Review of Ecology and Systematics 5:215–261.

Crompton, A. W., C. Musinsky, and T. Owerkowicz. 2015. Evolution of the mammalian nose; pp. 189–203 in The Great Transformations in Vertebrate Evolution, University of Chicago Press. E. L. Brainerd, Kenneth Dial, and N. H. Shubin, Chicago.

Crompton, A. W., T. Owerkowicz, B.-A. S. Bhullar, and C. Musinsky. 2017. Structure of the nasal region of non-mammalian cynodonts and mammaliaforms: Speculations on the evolution of mammalian endothermy. Journal of Vertebrate Paleontology 37:e1269116.

Cruickshank, A. R. I. 1967. A new dicynodont genus from the Manda Formation of Tanzania (Tanganyika). Journal of Zoology 153:163–208.

Cubo, J., and N.-E. Jalil. 2019. Bone histology of *Azendohsaurus laaroussii*: Implications for the evolution of thermometabolism in Archosauromorpha. Paleobiology 45:317–330.

Damiani, R., C. Vasconcelos, A. Renaut, J. Hancox, and A. Yates. 2007. *Dolichuranus primaevus* (Therapsida: Anomodontia) from the middle Triassic of Nambia and its phylogenetic relationships. Palaeontology 50:1531–1546.

Danilov, A. I. 1971. A new dicynodont from the Middle Triassic of southern Cisuralia. Paleontological Journal 5:265–268.

Das Gupta, H. C. 1922. Notes on the Panchet Reptile; pp. 237–241 in Sir Asutosh Mukherjee Silver Jubilee Volumes, University Press. vol. 2. Calcutta.

Domnanovich, N. S., and C. A. Marsicano. 2012. The Triassic dicynodont *Vinceria* (Therapsida, Anomodontia) from Argentina and a discussion on basal Kannemeyeriiformes. Geobios 45:173–186.

Dutuit, J. M. 1965. Découverte de dicynodontes (reptiles therapsides) dans le Trias du couloir d'Argana (Atlas occidental marocain). Comptes Rendus Hebdomadaires Des Séances de l'Académie Des Sciences 260:3447.

Dutuit, J. M. 1976. Introduction à l'étude paléontologique du Trias continental marocain. Description des premiers stégocéphales recueillis dans le couloir d'Argana (Atlas occidental). Mémoires Du Muséum National d'Histoire Naturelle 36:1–333.

Dutuit, J. M. 1980. Principaux caractères d'un genre de Dicynodonte du Trias marocain. Comptes Rendus de l'Académie Des Sciences, Paris 290:655–658.

Dutuit, J. M. 1988. Ostéologie crânienne et ses enseignements, apports géologique et paléoécologique, de *Moghreberia nmachouensis*, Dicynodonte (Reptilia, Therapsida) du Trias supérieur marocain. Bulletin Du Muséum National d'histoire Naturelle. Section C, Sciences de La Terre, Paléontologie, Géologie, Minéralogie 10:227–285.

Dutuit, J. M. 1989a. *Azarifeneria barrati*, un deuxieme genre de Dicynodonte du Trias supérieur marocain. Comptes Rendus de l'Académie Des Sciences. Série 2, Mécanique, Physique, Chimie, Sciences de l'univers, Sciences de La Terre 309:303–306.

Dutuit, J. M. 1989b. Confirmation des affinités entre Trias supérieurs marocain et sud-américain: découverte d'un troisième Dicynodonte (Reptilia, Therapsida), *Azarifeneria robustus*, n. sp., de la formation d'Argana (Atlas occidental). Comptes Rendus de l'Académie Des Sciences. Série 2, Mécanique, Physique, Chimie, Sciences de l'univers, Sciences de La Terre 309:1267–1270.

Efremov, J. A. 1951. On the structure of the knee joint in the higher Dicynodontidae. Doklady Akademii Nauk SSSR 7 77:483–485.

Elder, A. L. 2000. Late Triassic Dicynodonts: their anatomy, relationships, and paleobiogeography. the Graduate Faculty of Texas Tech University, 114 pp.

Ezcurra, M. D. 2010. Biogeography of Triassic tetrapods: evidence for provincialism and driven sympatric cladogenesis in the early evolution of modern tetrapod lineages. Proceedings of the Royal Society B: Biological Sciences 277:2547–2552.

Fleischle, C. V., T. Wintrich, and P. M. Sander. 2018. Quantitative histological models suggest endothermy in plesiosaurs. PeerJ 6:e4955.

Francillon Vieillot, H., V. de Buffrénil, J. Castanet, J. Géraudie, F. J. Meunier, J. Y. Sire, L. Zylberberg, and A. De Ricqlès. 1990. Microstructure and mineralization of vertebrate skeletal tissues; pp. 471–530 in Skeletal biomineralization : patterns, process and evolutionary trends. Carter, J. G. (ed.).

Fraser, N. C., and H.-D. Sues. 2010. The beginning of the ‘Age of Dinosaurs’: a brief overview of terrestrial biotic changes during the Triassic. Earth and Environmental Science Transactions of the Royal Society of Edinburgh 101:189–200.

Fritz, J., J. Hummel, E. Kienzle, W. J. Streich, and M. Clauss. 2010. To chew or not to chew: fecal particle size in herbivorous reptiles and mammals. Journal of Experimental Zoology Part A: Ecological Genetics and Physiology 313A:579–586.

Fritz, J., J. Hummel, E. Kienzle, C. Arnold, C. Nunn, and M. Clauss. 2009. Comparative chewing efficiency in mammalian herbivores. Oikos 118:1623–1632.

Fritz, J., J. Hummel, E. Kienzle, O. Wings, W. J. Streich, and M. Clauss. 2011. Gizzard vs. teeth, it’s a tie: food-processing efficiency in herbivorous birds and mammals and implications for dinosaur feeding strategies. Paleobiology 37:577–586.

Fröbisch, J. 2007. The cranial anatomy of *Kombuisia frerensis* Hotton (Synapsida, Dicynodontia) and a new phylogeny of anomodont therapsids. Zoological Journal of the Linnean Society 150:117–144.

Fröbisch, J. 2009. Composition and similarity of global anomodont-bearing tetrapod faunas. Earth-Science Reviews 95:119–157.

Fröbisch, J., and R. R. Reisz. 2008. A new species of Emydops (Synapsida, Anomodontia) and a discussion of dental variability and pathology in dicynodonts. Journal of Vertebrate Paleontology 28:770–787.

Fröbisch, J., K. D. Angielczyk, and C. A. Sidor. 2010. The Triassic dicynodont *Kombuisia* (Synapsida, Anomodontia) from Antarctica, a refuge from the terrestrial Permian-Triassic mass extinction. Naturwissenschaften 97:187–196.

Germain, D., and M. Laurin. 2005. Microanatomy of the radius and lifestyle in amniotes (Vertebrata, Tetrapoda). Zoologica Scripta 34:335–350.

Girondot, M., and M. Laurin. 2003. Bone profiler: a tool to quantify, model, and statistically compare bone-section compactness profiles. Journal of Vertebrate Paleontology 23:458–461.

Govender, R., and A. Yates. 2009. Dicynodont postcrania from the Triassic of Namibia and their implication for the systematics of Kannemeyeriiforme dicynodonts. Palaeontologica Africana 44:41–57.

Green, J. L. 2012. Bone and Dental Histology of Late Triassic Dicynodonts from North America; pp. 179–198 in Forerunners of Mammals, Indiana Universiy Press. Chinsamy-Turan, A. (ed.).

Green, J. L., M. H. Schweitzer, and E.-T. Lamm. 2010. Limb bone histology and growth in *Placerias hesternus* (Therapsida: Anomodontia) from the Upper Triassic of North America. Palaeontology 53:347–364.

Grine, F. E., C. A. Forster, M. A. Cluver, and J. A. Georgi. 2006. Cranial variability, ontogeny and taxonomy of Lystrosaurus from the Karoo Basin of South Africa; pp. 432–503 in Amniote Paleobiology: Perspectives on the Evolution of Mammals, Birds, and Reptiles, University of Chicago Press. Carrano M. T., Gaudin T. J., Blob R. W. & Wible J. R., Chicago.

Guénard, G., P. Legendre, and P. Peres-Neto. 2013. Phylogenetic eigenvector maps: a framework to model and predict species traits. Methods in Ecology and Evolution 4:1120–1131.

Hallam, A. 2002. How catastrophic was the end-Triassic mass extinction? Lethaia 35:147–157.

Hammer, W. R., and J. W. Cosgriff. 1981. *Myosaurus gracilis*, an anomodont reptile from the Lower Triassic of Antarctica and South Africa. Journal of Paleontology 55:410–424.

Hancox, P. J., K. D. Angielczyk, and B. S. Rubidge. 2013. *Angonisaurus* and *Shansiodon*, dicynodonts (Therapsida, Anomodontia) from subzone C of the Cynognathus Assemblage Zone (Middle Triassic) of South Africa. Journal of Vertebrate Paleontology 33:655–676.

Harper, C. W. J. 1976. Phylogenetic inference in paleontology. Journal of Vertebrate Paleontology 50:180–193.

Hillenius, W. J. 1992. The evolution of nasal turbinates and mammalian endothermy. Paleobiology 18:17–29.

Hillenius, W. J. 1994. Turbinates in Therapsids: Evidence for Late Permian Origins of Mammalian Endothermy. Evolution 48:207–229.

Huene, F. 1935. Die fossilen Reptilien des südamerikanischen Gondwanalandes; pp. 93–159 in Ergebnisse der Sauriergrabungen in Südbrasilien 1928–29. Lieferung 1, Verlag Franz F. Heine. Tübingen.

Huene, F. 1948. Short review of the lower tetrapods; pp. 65–106 in Robert Broom Commemorative Volume, Special Publications of theRoyal Society of South Africa. A. L. Du Toit (ed.), Cape Town.

Hunt, A. P., and S. G. Lucas. 1991. The *Paleorhinus* biochron and the correlation of the non-marine Upper Triassic of Pangaea. Palaeontology 34:487–501.

Huttenlocker, A. K., and J. Botha-Brink. 2014. Bone microstructure and the evolution of growth patterns in Permo-Triassic therocephalians (Amniota, Therapsida) of South Africa. PeerJ 2:e325.

Huxley, T. H. 1859. On a new species of dicynodont (*D. murrayi*) from near Colesburg, South Africa; and on the structure of the skull in dicynodonts. Quarterly Journal of the Geological Society of London 15:649–659.

Huxley, T. H. 1865. On a colle.ction of vertebrate fossils from the Panchet rocks, Raniganj Coalfield. Memoirs of the Geological Survey of India, Palaeontologia Indica 1:2–24.

Irmis, R. B., and J. H. Whiteside. 2012. Delayed recovery of non-marine tetrapods after the end-Permian mass extinction tracks global carbon cycle. Proceedings of the Royal Society of London B: Biological Sciences 279:1310–1318.

Irmis, R. B., S. J. Nesbitt, K. Padian, N. D. Smith, A. H. Turner, D. Woody, and A. Downs. 2007. A Late Triassic Dinosauromorph Assemblage from New Mexico and the Rise of Dinosaurs. Science 317:358–361.

Jasinoski, S. C., M. A. Cluver, A. Chinsamy, and B. D. Reddy. 2014. Anatomical Plasticity in the Snout of *Lystrosaurus*; pp. 139–149 in C. F. Kammerer, K. D. Angielczyk, and J. Fröbisch (eds.), Early Evolutionary History of the Synapsida. Springer Netherlands, Dordrecht.

Kalandadze, N. N. 1970. New Triassic kanemeyeriids from the South Ural region; pp. 51–57 in Materials on evolution of terrestrial vertebrates, K. K. Flerov (ed.). Nauka Press, Moscow.

Kalandadze, N. N., and A. G. Sennikov. 1985. New reptiles from the Middle Triassic in the southern Ural forelands. Paleontological Journal 19:73–80.

Kammerer, C. F. 2018. The first skeletal evidence of a dicynodont from the lower Elliot Formation of South Africa. Palaeontologia Africana 52:102–128.

Kammerer, C. F. 2019a. Revision of the Tanzanian dicynodont *Dicynodon huenei* (Therapsida: Anomodontia) from the Permian Usili Formation. PeerJ 33.

Kammerer, C. F. 2019b. A new dicynodont (Anomodontia: Emydopoidea) from the terminal Permian of KwaZulu-Natal, South Africa. Palaeontologia Africana.

Kammerer, C. F., and K. D. Angielczyk. 2009. A proposed higher taxonomy of anomodont therapsids. Zootaxa 2018:1–24.

Kammerer, C. F., and R. M. H. Smith. 2017. An early geikiid dicynodont from the Tropidostoma Assemblage Zone (late Permian) of South Africa. PeerJ 5:e2913.

Kammerer, C. F., K. D. Angielczyk, and J. Fröbisch. 2011. A comprehensive taxonomic revision of "*Dicynodon*" (Therapsida, Anomodontia) and its implications for dicynodont phylogeny, biogeography, and biostratigraphy. Journal of Vertebrate Paleontology 31:1–158.

Kammerer, C. F., J. Fröbisch, and K. D. Angielczyk. 2013. On the Validity and Phylogenetic Position of *Eubrachiosaurus browni*, a Kannemeyeriiform Dicynodont (Anomodontia) from Triassic North America. PLoS ONE 8:e64203.

Kammerer, C. F., P. A. Viglietti, P. J. Hancox, R. J. Butler, and J. N. Choiniere. 2019. A new kannemeyeriiform dicynodont (*Ufudocyclops mukanelai* , gen. et sp. nov.) from Subzone C of the *Cynognathus* Assemblage Zone, Triassic of South Africa, with implications for biostratigraphic correlation with other African Triassic Faunas. Journal of Vertebrate Paleontology e1596921.

Kemp, T. S. 1980. Origin of the mammal-like reptiles. Nature 283:378–380.

Kent, D. V., P. S. Malnis, C. E. Colombi, O. A. Alcober, and R. N. Martínez. 2014. Age constraints on the dispersal of dinosaurs in the Late Triassic from

magnetochronology of the Los Colorados Formation (Argentina). Proceedings of the National Academy of Sciences 111:7958–7963.

Keyser, A. W. 1973. A new Triassic vertebrate fauna from South West Africa. Paleontologica Africana 16:1–15.

Keyser, A. W., and A. R. I. Cruickshank. 1979. The origins and classification of Triassic dicynodonts. Transactions of the Geological Society of South Africa 82:81–108.

Khaldoune, F., N. E. Jalil, D. Germain, and J. S. Steyer. 2017. Les vertébrés du Permien et du Trias du Maroc (Bassin d'Argana, Haut Atlas occidental) : fenêtre ouverte sur l'évolution autour de la grande crise fin-paléozoïque. Mémoires de La Société Géologique de France 64p.

King, G. M., and M. A. Cluver. 1990. The aquatic *Lystrosaurus*: an alternative lifestyle. Historical Biology 4:323–341.

Knoll, F. 2004. Review of the tetrapod fauna of the "Lower Stormberg Group" of the main Karoo Basin (southern Africa): implication for the age of the Lower Elliot Formation. Bulletin de La Societe Geologique de France 175:73–83.

Knutsen, E. M., and E. Oerlemans. 2020. The last dicynodont? Re-assessing the taxonomic and temporal relationships of a contentious Australian fossil. Gondwana Research 77:184–203.

Kriloff, A., D. Germain, A. Canoville, P. Vincent, M. Sache, and M. Laurin. 2008. Evolution of bone microanatomy of the tetrapod tibia and its use in palaeobiological inference. Journal of Evolutionary Biology 21:807–826.

Legendre, L. J., G. Guénard, J. Botha-Brink, and J. Cubo. 2016. Palaeohistological Evidence for Ancestral High Metabolic Rate in Archosaurs. Systematic Biology 65:989–996.

Liu, J., and J. Li. 2003. A new material of kannemeyerid from Xinjiang and the restudy of Parakannemeyeria brevirostris. Vertebrata Palasiatica 41:147–156.

Lucas, S. 2015. Age and correlation of Late Triassic tetrapods from southern Poland. Annales Societatis Geologorum Poloniae.

Lucas, S. G. 1904. A new batrachian and a new reptile from the Triassic of Arizona. Proceeding of the U. S. National Museum 27:193–197.

Lucas, S. G. 1993. *Barysoma lenzii* (Synapsida: Dicynodontia) from the Middle Triassic of Brazil, a synonym of *Stahleckeria potens*. Journal of Paleontology 67:318–321.

Lucas, S. G. 1994. Triassic Tetrapod Extinctions and the Compiled Correlation Effect. 869–875.

Lucas, S. G. 1995. Triassic dicynodont biochronology. Albertiana 16:33–40.

Lucas, S. G. 2018. Late Triassic Terrestrial Tetrapods: Biostratigraphy, Biochronology and Biotic Events; pp. 351–405 in L. H. Tanner (ed.), The Late Triassic World. vol. 46. Springer International Publishing, Cham.

Lucas, S. G., and A. P. Hunt. 1993a. *Fukangolepis* Yang, 1978 from the Triassic of China is not an aetosaur. Journal of Vertebrate Paleontology 13:145–147.

Lucas, S. G., and A. P. Hunt. 1993b. A dicynodont from ther Upper Triassic of New Mexico and its biochronologic significance. New Mexico Museum Natural History and Science Bulletin 3:321–325.

Lucas, S. G., and R. Wild. 1995. A Middle Triassic dicynodont from Germany and the biochronology of Triassic dicynodonts. Stuttgarter Beiträge Zur Naturkunde B 220:1–16.

Lucas, S. G., and L. H. Tanner. 2004. Late Triassic extinction events. Albertiana 31:31–40.

Magwene, P. M. 1993. What's Bred in the Bone: Histology and Cross-Sectional Geometry of Mammal-like Reptile Long Bones: Evidence of Changing Physiological and Biomechanical Demands. Harvard University, Cambridge, Massacuhssetts, pp.

Maisch, M. W. 2001. Observations on Karoo and Gondwana vertebrates. Part 2: A new skull-reconstruction of *Stahleckeria potens* Von Huene, 1935 (Dicynodontia, Middle Triassic) and a reconsideration of kannemeyeriiform. Neues Jahrbuch Für Geologie Und Paläontologie - Abhandlungen 220:127–152.

Maisch, M. W., and A. T. Matzke. 2014. *Sungeodon kimkraemerae* n. gen. n. sp., the oldest kannemeyeriiform (Therapsida, Dicynodontia) and its implications for the early diversification of large herbivores after the P/T boundary. Neues Jahrbuch Für Geologie Und Paläontologie - Abhandlungen 272:1–12.

McGhee, G. R., P. M. Sheehan, D. J. Bottjer, and M. L. Droser. 2004. Ecological ranking of Phanerozoic biodiversity crises: ecological and taxonomic severities are decoupled. Palaeogeography, Palaeoclimatology, Palaeoecology 211:289–297.

McNab, B. K. 1997. On the Utility of Uniformity in the Definition of Basal Rate of Metabolism. Physiological Zoology 70:718–720.

McRoberts, C. A., and C. R. Newton. 1995. Selective extinction among end-Triassic European bivalves. Geology 23:102.

Montes, L., N. Le Roy, M. Perret, V. De Buffrenil, J. Castanet, and J. Cubo. 2007. Relationships between bone growth rate, body mass and resting metabolic rate in growing amniotes: a phylogenetic approach. Biological Journal of the Linnean Society 92:63–76.

Müller, D. W. H., D. Codron, C. Meloro, A. Munn, A. Schwarm, J. Hummel, and M. Clauss. 2013. Assessing the Jarman–Bell Principle: Scaling of intake, digestibility, retention time and gut fill with body mass in mammalian herbivores. Comparative Biochemistry and Physiology Part A: Molecular & Integrative Physiology 164:129–140.

Newell, A. J. 1963. Crises in the history of life. Scientific American 76–93.

Niedźwiedzki, G., P. Gorzelak, and T. Sulej. 2011. Bite traces on dicynodont bones and the early evolution of large terrestrial predators. Lethaia 44:87–92.

Norell, M. A. 1992. The Effect of Phylogeny, in Extinction and Phylogeny; pp. 89–118 in Taxic Origin and Temporal Diversity, Columbia University Press. Novacek, M.J. and Wheeler, Q.D. (eds.), New York.

Norell, M. A. 1993. Tree-based approaches to understanding history; comments on ranks, rules and the quality of the fossil record. American Journal of Science 293:407–407.

Nowack, J., S. Giroud, W. Arnold, and T. Ruf. 2017. Muscle Non-shivering Thermogenesis and Its Role in the Evolution of Endothermy. Frontiers in Physiology 8:889.

Olivier, C., B. Battail, S. Bourquin, C. Rossignol, J.-S. Steyer, and N.-E. Jalil. 2019. New dicynodonts (Therapsida, Anomodontia) from near the Permo-Triassic boundary of Laos: implications for dicynodont survivorship across the Permo-Triassic mass extinction and the paleobiogeography of Southeast Asian blocks. Journal of Vertebrate Paleontology 0:e1584745.

Olsen, P. E., D. V. Kent, H.-D. Sues, C. Koeberl, H. Huber, A. Montanari, E. C. Rainforth, S. J. Fowell, M. J. Szajna, and B. W. Hartline. 2002. Ascent of dinosaurs linked to an Iridium anomaly at the Triassic-Jurassic Boundary. Science 296:1305–1307.

Owen. 1860a. On some Reptilian Fossils from South Africa. Quarterly Journal of the Geological Society 16:49–63.

Owen, R. 1845. Report on the Reptilian Fossils of South Africa: PART I.-Description of certain Fossil Crania, discovered by AG Bain, Esq., in Sandstone Rocks at the South-eastern extremity of Africa, referable to different species of an Extinct genus of Reptilia (*Dicynodon*), and indicative of a new Tribe or Sub-order of Sauria. Proceedings of the Zoological Society of London 91:647–674.

Owen, R. 1860b. On the orders of fossil and recent Reptilia, and their distribution in time. Report of the British Association for the Advancement of Science 29:e166.

Owen, R. 1876. Descriptive and illustrated catalogue of the fossil Reptilia of South Africa in the collection of the British Museum. .

Owerkowicz, T., C. Musinsky, K. M. Middleton, and A. W. Crompton. 2015. Respiratory Turbinates and the Evolution of Endothermy in Mammals and Birds; pp. 143–165 in The Great Transformations in Vertebrate Evolution, University of Chicago Press. E. L. Brainerd, Kenneth Dial, and N. H. Shubin, Chicago.

Padian, K., J. R. Horner, and A. De Ricqlès. 2004. Growth in small dinosaurs and pterosaurs: the evolution of archosaurian growth strategies. Journal of Vertebrate Paleontology 24:555–571.

Pagel, M., and A. Meade. 2016. BayesTraits V3 Manual.

Piveteau, J. 1938. Un Therapside d'Indochine. Remarques sur la notion de continent de Gondwana. Annales de Paléontologie 27:137–152.

Platnick, N. I. 1977. Cladograms, Phylogenetic Trees, and Hypothesis Testing. Systematic Biology 26:438–442.

Ray, S. 2006. Functional and evolutionary aspects of the postcranial anatomy of dicynodonts (Synapsida, Therapsida). Palaeontology 49:1263–1286.

Ray, S., and A. Chinsamy. 2004. *Diictodon feliceps* (Therapsida, Dicynodontia): bone histology, growth, and biomechanics. Journal of Vertebrate Paleontology 24:180–194.

Ray, S., J. Botha, and A. Chinsamy. 2004. Bone histology and growth patterns of some nonmammalian therapsids. Journal of Vertebrate Paleontology 24:634–648.

Ray, S., A. Chinsamy, and S. Bandyopadhyay. 2005. *Lystrosaurus murrayi* (Therapsida, Dicynodontia): bone histology, growth and lifestyle adaptations. Palaeontology 48:1169–1185.

Ray, S., S. Bandyopadhyay, and R. Appana. 2010. Bone Histology of a Kannemeyeriid Dicynodont *Wadiasaurus*: Palaeobiological Implications; pp. 73–89 in New

Aspects of Mesozoic Biodiversity. vol. 132. Springer Berlin Heidelberg, Berlin, Heidelberg.

Ray, S., J. Botha-Brink, and A. Chinsamy-Turan. 2012. Dicynodont growth dynamics and lifestyle adaptations; pp. 121–148 in Forerunners of Mammals, Indiana University Press. Chinsamy-Turan, A. (ed.).

Rensch, B. 1929. Das Prinzip Geographischer Rassenkreise Und Das Problem Der Artbildung. Borntraeger, Berlin, pp.

Rensch, B. 1959. Evolution above the Species Level, Second edition. Columbia University Press, New York, 426 pp.

Répelin, J. 1923. Sur un fragment de crâne de *Dicynodon* recueilli par H. Counillon dans les environs de Luang- Prabang (Haut-Laos). , 12, 1–7. Bulletin Du Service Géologique de l'Indochine 12:1–7.

Richoz, S., L. Krystyn, and C. Spötl. 2007. Towards a carbon isotope reference curve of the Upper Triassic. New Mexico Museum of Natural History and Science Bulletin 41:366–367.

Ricqlès, A., F. J. Meunier, J. Castanet, and H. Francillon-Vieillot. 1991. Comparative microstructure of bone. Bone 3:1–78.

Ricqlès, A. D. 1969. L'histologie osseuse envisagée comme un indicateur de la physiologie thermique chez les tétrapodes fossiles. Comptes Rendus de l'Académie Des Sciences, Paris 268:782–785.

Roghi, G., P. Gianolla, L. Minarelli, C. Pilati, and N. Preto. 2010. Palynological correlation of Carnian humid pulses throughout western Tethys. Palaeogeography, Palaeoclimatology, Palaeoecology 290:89–106.

Romano, M., and F. Manucci. 2019. Resizing *Lisowicia bojani*: volumetric body mass estimate and 3D reconstruction of the giant Late Triassic dicynodont. Historical Biology 0:1–6.

Romer, A. S. 1943. Recent mounts of fossil reptiles and amphibians in the Museum of Comparative Zoölogy. Bulletin of the Museum of Comparative Zoölogy 92:331–338.

Romer, A. S. 1956. The Vertebrate Body, Second edition. W.B. Saunders Company, Philadelphia, USA, 644 pp.

Rossignol, C., S. Bourquin, M. Poujol, E. Hallot, M.-P. Dabard, and T. Nalpas. 2016. The volcaniclastic series from the Luang Prabang Basin, Laos: A witness of a Triassic magmatic arc? Journal of Asian Earth Sciences 120:159–183.

Rowland, L. A., N. C. Bal, and M. Periasamy. 2015. The role of skeletal-muscle-based thermogenic mechanisms in vertebrate endothermy. Biological Reviews of the Cambridge Philosophical Society 90:1279–1297.

Roy-Chowdhury, T. 1970. Two new dicynodonts from the Triassic Yerrapalli Formation of central India. Palaeontology 13:132–144.

Ruben, J. A., and T. D. Jones. 2000. Selective Factors Associated with the Origin of Fur and Feathers. Integrative and Comparative Biology 40:585–596.

Ruben, J. A., W. J. Hillenius, T. S. Kemp, and D. E. Quick. 2012. The evolution of mammalian endothermy; pp. 273–286 in Forerunners of Mammals, Indiana Universiy Press. Chinsamy-Turan, A. (ed.).

Ruben, J. A., W. J. Hillenius, N. R. Geist, A. Leitch, T. D. Jones, P. J. Currie, J. R. Horner, and G. Espe. 1996. The Metabolic Status of Some Late Cretaceous Dinosaurs. Science 273:1204–1207.

Rubidge, B. S. 1990. The cranial morphology of a new species of the genus *Eodicynodon* (Therapsida, Dicynodontia). Navorsinge van Die Nasionale Museum Bloemfontein 7:29–41.

Ruffell, A., M. J. Simms, and P. B. Wignall. 2015. The Carnian Humid Episode of the Late Triassic: a review. Geological Magazine 153:271–284.

Sahney, S., and M. J. Benton. 2008. Recovery from the most profound mass extinction of all time. Proceedings of the Royal Society of London B: Biological Sciences 275:759–765.

Saurin, E. 1962. Luang Prabang Est. Carte géologique du Vietnam, Cambodge, Laos. .

Seeley, H. G. 1898. On the skull of Mochlorhinus platyceps from Bethulie, Orange Free State, preserved in the Albany Museum, Grahamstown. Annals and Magazine of Natural History 1:164–176.

Seeley, H. G. 1904. On a new Type of Reptilian Tooth (Ptychocynodon) from the Upper Karroo Beds near Burghersdorp, Cape Colony. Journal of Natural History 14:290–293.

Seeley, H. G. 1908. On a fossil reptile with a trunk from the Upper Karroo rocks of Cape Colony. Report British Association 78:713.

Seymour, R. S., C. L. Bennett-Stamper, S. D. Johnston, D. R. Carrier, and G. C. Grigg. 2004. Evidence for Endothermic Ancestors of Crocodiles at the Stem of

Archosaur Evolution. Physiological and Biochemical Zoology: Ecological and Evolutionary Approaches 77:1051–1067.

Shelton, C. D., and P. M. Sander. 2017. Long bone histology of Ophiacodon reveals the geologically earliest occurrence of fibrolamellar bone in the mammalian stem lineage. Comptes Rendus Palevol.

Shelton, C. D., P. M. Sander, K. Stein, and H. Winkelhorst. 2013. Long bone histology indicates sympatric species of *Dimetrodon* (Lower Permian, Sphenacodontidae). Earth and Environmental Science Transactions of The Royal Society of Edinburgh 103:217–236.

Shubin, N. H., and H.-D. Sues. 1991. Biogeography of early Mesozoic continental tetrapods: patterns and implications. Paleobiology 17:214–230.

Sidor, C. A., and J. A. Hopson. 1998. Ghost lineages and “mammalness”: assessing the temporal pattern of character acquisition in the Synapsida. Paleobiology 24:254–273.

Simms, M. J., A. H. Ruffell, and A. L. A. Johnson. 1994. Biotic and climatic changes in the Carnian (Triassic) of Europe and adjacent areas; pp. 445 in In the shadow of the dinosaurs, University Press. N. C. Fraser & H. -D. Sues (eds), Cambridge, UK.

Sinclair, A. R. E., S. Mduma, and J. S. Brashares. 2003. Patterns of predation in a diverse predator–prey system. Nature 425:288–290.

Smith, R., B. S. Rubidge, and M. van der Walt. 2012. Therapsid biodiversity patterns and paleoenvironments of the Karoo Basin, South Africa; pp. 31–64 in Forerunners of Mammals, Indiana Universiy Press. Chinsamy-Turan, A. (ed.).

Smith, R. M., and P. D. Ward. 2001. Pattern of vertebrate extinctions across an event bed at the Permian-Triassic boundary in the Karoo Basin of South Africa. Geology 29:1147–1150.

Smith, R. M. H., and J. Botha-Brink. 2011. Morphology and composition of bone-bearing coprolites from the Late Permian Beaufort Group, Karoo Basin, South Africa. Palaeogeography, Palaeoclimatology, Palaeoecology 312:40–53.

Smith, R. M. H., and J. Botha-Brink. 2014. Anatomy of a mass extinction: Sedimentological and taphonomic evidence for drought-induced die-offs at the Permo-Triassic boundary in the main Karoo Basin, South Africa. Palaeogeography, Palaeoclimatology, Palaeoecology 396:99–118.

Sulej, T., and G. Niedźwiedzki. 2019. An elephant-sized Late Triassic synapsid with erect limbs. Science 363:78–80.

Sun, A. 1960. On a new genus of kannemeyerids from Ningwu, Shansi. Vertebrata Palasiatica 4:67–81.

Sun, A. 1964. Preliminary report of a new species of *Lystrosaurus* of Sinkiang. Vertebrata PalAsiatica 8:216–217.

Sun, A. 1973. Permo-Triassic dicynodonts from Turfan, Sinkiang. Memoirs of the Institute of Vertebrate Palaeontology and Paleoanthropology, Academia Sinica 10:53–68.

Sun, Y., M. M. Joachimski, P. B. Wignall, C. Yan, Y. Chen, H. Jiang, L. Wang, and X. Lai. 2012. Lethally Hot Temperatures During the Early Triassic Greenhouse. Science 338:366–370.

Sun, Y. D., P. B. Wignall, M. M. Joachimski, D. P. G. Bond, S. E. Grasby, X. L. Lai, L. N. Wang, Z. T. Zhang, and S. Sun. 2016. Climate warming, euxinia and carbon isotope perturbations during the Carnian (Triassic) Crisis in South China. Earth and Planetary Science Letters 444:88–100.

Surkov, M. V. 1999a. New data on Middle Triassic anomodonts from the southern Fore-Urals. Paleontological Journal 33:302–307.

Surkov, M. V. 1999b. A new middle Triassic Kannemeyeriin from the Pechora district. Paleontological Journal 33:420–421.

Surkov, M. V. 2005. The first dicynodont from the terminal Lower Triassic of European Russia, with special reference to the evolution of the masticatory apparatus of these therapsids. Paleontological Journal 39:72–78.

Tanner, L. H., S. G. Lucas, and M. G. Chapman. 2004. Assessing the record and causes of Late Triassic extinctions. Earth-Science Reviews 65:103–139.

Teichert, C. 1988. Crises in cephalopod evolution; pp. 7–64 in L'évolution dans sa Réalité et ses Diverses Modalités, Fondation Singer-Polignac. Marois M. (ed.), Paris, France.

Thackeray, J. F. 2018. Do specimens attributed to *Lystrosaurus murrayi* and *L*. *declivis* (Triassic Therapsida) represent one species? South African Journal of Science 114.

Thulborn, T., and S. Turner. 2003. The last dicynodont: an Australian Cretaceous relict. Proceedings of the Royal Society of London B: Biological Sciences 270:985–993.

Tripathi, C., and P. P. Satsangi. 1963. *Lystrosaurus* fauna of the Panchet series of the Raniganj coalfield. Memoirs of the Geological Survey of India, Palaeontologia Indica, New Series 37:1–65.

Tumarkin-Deratzian, A. R. 2007. Fibrolamellar Bone in Wild Adult Alligator Mississippiensis. Journal of Herpetology 41:341–345.

Twitchett, R. J. 2006. The palaeoclimatology, palaeoecology and palaeoenvironmental analysis of mass extinction events. Palaeogeography, Palaeoclimatology, Palaeoecology 232:190–213.

Vega-Dias, C., M. W. Maisch, and C. L. Schultz. 2004. A new phylogenetic analysis of Triassic dicynodonts (Therapsida) and the systematic position of *Jachaleria* candelariensis from the Upper Triassic of Brazil. Neues Jahrbuch Fur Geologie Und Palaontologie Abhandlungen 231:145–166.

Viglietti, P. A., R. M. H. Smith, and B. S. Rubidge. 2018. Changing palaeoenvironments and tetrapod populations in the *Daptocephalus* Assemblage Zone (Karoo Basin, South Africa) indicate early onset of the Permo-Triassic mass extinction. Journal of African Earth Sciences 138:102–111.

Vjuschkov, V. P. 1969. New dicynodonts from the Triassic of Southern Cisuralia. Paleontological Journal 3:237–242.

Wall, W. P. 1983. The correlation between high limb-bone density and aquatic habits in recent mammals. Journal of Paleontology 57:197–207.

Walter, I., and F. Seebacher. 2009. Endothermy in birds: underlying molecular mechanisms. Journal of Experimental Biology 212:2328–2336.

Ward, P. D., J. Botha, R. Buick, M. O. De Kock, D. H. Erwin, G. H. Garrison, J. L. Kirschvink, and R. Smith. 2005. Abrupt and Gradual Extinction Among Late Permian Land Vertebrates in the Karoo Basin, South Africa. Science 307:709–714.

Watson, D. M. S. 1917. A sketch classification of the pre-Jurassic tetrapod vertebrates. Proceedings of the Zoological Society of London 1917:167–186.

Weithofer, A. 1888. Ueber einen neuen Dicynodonten (*Dicynodon simocephalus*) aus der Karrooformation Südafrikas. Annalen Des Naturhistorischen Museums in Wien 3:1–6.

Williston, S. W. 1904. Notice of some new reptiles from the Upper Trias of Wyoming. The Journal of Geology 12:688–697.

Woodward, A. S. 1932. Dicynodontidae; pp. 257–260 in Textbook of Palaeontology. vol. 2. Von Zittel, K. A. (ed.).

Yeh, H. K. 1959. New dicynodont from *Sinokannemeyeria*-fauna from Shansi. Vertebrata Palasiatica 3:187–204.

Young, C. C. 1935. On Two Skeletons of Dicynodontia from Sinkiang*. Bulletin of the Geological Society of China 14:483–518.

Young, C. C. 1937. On the Triassic Dicynodonts from Shansi*. Bulletin of the Geological Society of China 17:393–412.

Young, C. C. 1939. Additional Dicynodontia remains from Sinkiang. Bulletin of the Geological Society of China 19:111–139.

Yuan, P. L., and C. C. Young. 1934. On the Occurrence of *Lystrosaurus* in Sinkiang. Bulletin of the Geological Society of China 12:575–580.

APPENDICES

Appendix I: Supplementary data of PAPER I

1. Discrete and continuous characters used in the phylogenetic analysis (modified from Angielczyk and Kammerer, 2017) (p. 285–295).
2. **Table 1S.** Phylogenetic matrix used in the analysis (p. 296–312).

Discrete and continuous characters used in the phylogenetic analysis (modified from Angielczyk and Kammerer, 2017).

Continuous Characters

(1) Length of preorbital region of skull relative to basal length of skull. (From Kammerer et al., 2011: 1)
(2) Relative length of premaxillary secondary palate. (From Angielczyk 2007: 63)
(3) Minimum width of interorbital skull roof relative to basal length of skull. (From Kammerer et al., 2011: 3)
(4) Relative width of temporal bar at level of postorbital bar versus the relative width at the junction of the intertemporal bar with the occipital plate. (From Kammerer et al., 2011: 4)
(5) Length of temporal fenestra relative to basal length of skull. (From Kammerer et al., 2011: 5)
(6) Relative position of pineal foramen, measured as the ratio of dorsal skull length posterior to the foramen versus dorsal skull length anterior to the foramen. (From Angielczyk and Kammerer, 2017: continuous 7)
(7) Height of anterior pterygoid keel in lateral view relative height of non-keel ramus. (From Angielczyk and Kammerer, 2017: continuous 8)
(8) Width of median pterygoid plate relative to basal skull length. (From Kammerer et al., 2011: 6)
(9) Angle formed by the posterior pterygoid rami. (From Kammerer et al., 2011: 7)
(10) Length of interpterygoid vacuity relative to basal length of skull. (From Kammerer et al., 2011: 8)
(11) Relative area of the internal nares. (From Angielczyk, 2007: 64)
(12) Angle between ascending and zygomatic processes of the squamosal. (From Kammerer et al., 2011: 10)
(13) Angulation of the occiput relative to the palate, expressed the ratio of dorsal and basal lengths of the skull. (From Kammerer et al., 2011: 11)
(14) Ratio of length to height of mandibular fenestra in lateral view. (From Kammerer et al., 2011: 12)
(15) Ratio of height of dentary ramus to height of dentary symphysis. (From Kammerer et al., 2011: 13)
(16) Ratio of maximum height of postdentary bones (excluding reflected lamina of angular) to the height of the dentary ramus. (From Kammerer et al., 2011: 14)
(17) Ratio of minimum width of the scapula to maximum width of dorsal end of scapula. (From Angielczyk, 2007: 72)
(18) Length of the deltopectoral crest relative to total length of the humerus. (From Angielczyk, 2007: 68)
(19) Maximum width of the distal end of the radius relative to the maximum length of the radius. (From Angielczyk, 2007: 69)
(20) Ratio of posterior iliac process length to acetabulum diameter. (From Sidor and Hopson, 1998: 157)
(21) Ratio of anterior iliac process length to acetabulum diameter. (From Sidor and Hopson, 1998: 158)
(22) Length of trochanteric crest on femur relative to length of femur. (From Kammerer et al., 2011: 20)

(23) Breadth of scapula measured as ration of maximal proximal width of scapula versus length of scapula (measured from dorsal edge of glenoid to proximal tip). (From Kammerer et al., 2013: 21)

Discrete Characters

(24) Premaxillae unfused (0) or fused (1). (From Angielczyk and Kurkin, 2003: 3)
(25) Paired anterior ridges on palatal surface of premaxilla absent (0), present and converge posteriorly (1), or present and do not converge (2). (From Angielczyk and Kurkin, 2003: 7)
(26) Lateral anterior palatal ridges absent (0) or present (1). (From Angielczyk, 2007: 60)
(27) Rounded depression on anterior palatal surface of premaxilla: absent (0), present (1). (From Angielczyk and Kammerer, 2017: discrete 4)
(28) Posterior median ridge on palatal surface of premaxilla absent (0), present with a flattened, expanded anterior area (1), or present without a flattened, expanded anterior area (2). (From Angielczyk and Kurkin, 2003: 8)
(29) Palatal surface of premaxilla with well-defined depressions with curved sides lateral to median ridge (if present) (0), with distinct accessory ridges lateral to medial ridge (1), or relatively flat with poorly defined or no depressions present (2). (From Angielczyk and Kammerer, 2017: discrete 6)
(30) Palatal surface of premaxilla with antero-posterior vascular groove lateral to median ridge (if present) absent (0), present (1). (From Angielczyk and Kammerer, 2017: discrete 7)
(31) Location of premaxillary teeth lateral (0), medial (1) or absent (2). (From Angielczyk and Kurkin, 2003: 2)
(32) Posterior exposure of the premaxilla on the palate: absent (0), present (1). (From Hopson and Barghusen, 1986: 6.8)
(33) Posterior process of the premaxilla with a non-bifurcated posterior tip (0) or with a bifurcated posterior tip (1). (From Kammerer et al., 2011: 153)
(34) Palatine shelf ventral to internal naris: absent (0), present (1). (From Hopson and Barghusen, 1986: 20.3 and 21.4)
(35) Anterior tip of snout rounded (0), squared off (1), or with a deep central invagination, giving the snout a “hare-lip” appearance in anterior view (2). (From Angielczyk and Kammerer, 2017: discrete 12)
(36) Marked anterior expansion of preorbital region absent (0) or present (1). (From Kammerer et al., 2011: 30)
(37) Snout roughly parallel to long axis of skull (0) or strongly angled ventrally (1). (From Kammerer et al., 2011: 31)
(38) Height of canine-bearing portion of maxilla: relatively short (0), extremely deep, with long caniniform process, but with equally long premaxilla resulting in an overall tall snout (1), extremely long caniniform process offset from rest of snout (2). (From Angielczyk and Kammerer, 2017: discrete 15)
(39) Snout open to back of the skull (0) or anterior margin of orbit extended posteromedially to partly close off the snout from the rest of the skull (1). (From Angielczyk and Kurkin, 2003: 25)
(40) Septomaxilla posterodorsal spur present and widely separates nasal and maxilla (0), spur present but does not separate maxilla and nasal (i.e., nasal-maxilla suture present and well defined in this region) (1), septomaxilla spur absent (2). (From Kammerer et al., 2011: 33)

(41) Notch on dorsal edge of narial opening absent (0) or present (1). (From Kammerer et al., 2011: 34)
(42) Postnarial excavation absent (0), present, relatively small, and rounded posteriorly (1), or present, very large, and elongate (2). (From Vega-Dias et al, 2004: 8)
(43) Maxillary alveolar region short, occupying less than 53% of the ventral length of the bone (0) or tooth bearing region long, occupying 72% or more of the ventral length of the bone (1). (From Modesto et al., 1999: 9)
(44) Palatal surface of premaxilla exposed in lateral view (1) or not exposed in lateral view (0). (From Kammerer et al., 2011: 37)
(45) Maxillary canine present as large member of tooth series (0), absent (1), or present as tusk (2). (From Modesto et al., 2003: 6)
(46) Maxillary non-caniniform teeth located near lateral margin of maxilla (0), located more medially, (1), or absent (2). (From Angielczyk and Kurkin, 2003: 4)
(47) Shelf-like area lateral to the maxillary non-caniniform teeth absent (0) or present (1). (From Angielczyk and Kurkin, 2003: 5)
(48) Fine serrations on maxillary teeth present (0), serrations absent (1), or coarse serrations present (2). (From Modesto et al., 1999: 3)
(49) Sutural contact of maxilla and prefrontal present (0) or absent (1). (From Modesto et al., 2003: 10)
(50) Caniniform process absent (0) or present (1). (From Kammerer et al., 2011: 43)
(51) Caniniform depression: has the form of an embayment bounded by a ridge medially of palatal rim anterior to caniniform process or tusk (1), has the form of a notch in palatal rim anterior to caninfiorm process (2), or absent (0). (From Angielczyk and Kammerer, 2017: discrete 28)
(52) Distinct lateral caniniform buttress absent (0), present (1), or present with posteroventral furrow (2). (From Damiani et al., 2007: 25)
(53) Keel-like extension of the palatal rim posterior to the caniniform process absent (0) or present (1). (From Angielczyk and Kurkin, 2003: 1)
(54) Postcaniniform crest absent (0) or present (1). (From Angielczyk and Kurkin, 2003: 28)
(55) Ventral edge of the caniniform process or dorsal edge of the erupted portion of the canine tusk anterior (0) to, or at the same level to slightly posterior to (1) the anterior orbital margin. (From Angielczyk and Kurkin, 2003: 44)
(56) Nasals with a long median suture that separates the premaxilla from the frontals (0) or with a short median suture and frontals and premaxilla in close proximity (1) (From Kammerer et al., 2011: 155)
(57) Nasal bosses absent (0), present as a median swelling with a continuous posterior margin (1), present as paired swellings near the dorsal or posterodorsal margin of external nares (2), present as paired swellings that meet in the midline to form a swollen anterodorsal surface on the snout (3). (From Kammerer et al., 2011: 48)
(58) Naso-frontal suture relatively straight, interdigitated, or gently bowed (0), with a distinct anterior process (1), or with a distinct posterior process (2). (From Kammerer et al., 2011: 154)
(59) Transverse crest approximately at level of naso-frontal suture absent (0); present and straightly transverse to curved with posterior convexity (1); present and strongly curved with posterior concavity (2). (From Angielczyk and Kammerer, 2017: discrete 36)

(60) Lacrimal does not contact septomaxilla (0) or does contact septomaxilla (1). (From Vega-Dias et al., 2004: 9)
(61) Prefrontal bosses absent (0), present but separate from nasals (1), or present and confluent with nasal bosses (2). (From Kammerer et al., 2011: 50)
(62) Raised, sometimes rugose, circumorbital rim absent (0) or present (1). (From Kammerer et al., 2011: 51)
(63) Frontal contribution to the dorsal rim of the orbit: broad, frontal forms a major part of the orbital rim (0); thin or absent, if present a thin frontal process extends laterally between the prefrontal and postorbital to reach the orbital margin (1). (From Kammerer et al., 2013: 38)
(64) Postfrontal bone present on dorsal surface of skull (0) or absent (1). (From Maisch, 2002: 8)
(65) Postorbital bar without (0) or with thickenings and rugosities (1). (From Maisch and Gebauer, 2005: 5)
(66) Mediolateral flattening and anteroposterior expansion of postorbital bar for most or all of its length absent (0) or present (1). (From Kammerer et al., 2011: 143)
(67) Temporal portion of skull roof relatively straight, without a strong break in slope (0), or temporal portion of skull roof angled dorsally with a strong break in slope near its anterior end (1). (From Kammerer et al., 2011: 54)
(68) Preparietal bone absent (0), present and flush with skull roof (1), present and depressed (2). (From Angielczyk and Kammerer, 2017: discrete 45)
(69) Lateral ridges bounding preparietal absent (0) or present (1). (From Angielczyk and Kammerer, 2017: discrete 46)
(70) Parietals' contribution to skull table transversely as broad as long (0), longer anteroposteriorly than broad (1), or shorter anteroposteriorly than broad (2). (From Modesto and Rybczynski, 2000: 16)
(71) Parietal posterolateral process slender and elongate (0), or short (1). (From Modesto and Rybczynski, 2000: 17)
(72) Parietals well exposed on the skull roof and relatively flat (0), parietals exposed in midline groove or channel (1), dorsal parietal exposure narrow and crest-like (2). (From Kammerer et al., 2013: 46)
(73) Parietals bulge outwards as ovoid swellings at posterior end of sagittal crest: no (0); yes (1). (From Kammerer et al., 2013: 47)
(74) Orientation of the temporal portion of the postorbital: relatively flat, so that most of the exterior surface of the bone faces dorsally (0), close to vertical, so that most of the exterior surface of the bone faces laterally (1), or bi-planar, with approximately equally-sized dorsal and lateral surfaces that are close to perpendicular (2). (From Kammerer et al., 2011: 59)
(75) Postorbitals extend the entire length of intertemporal bar (0) or do not extend the entire length of intertemporal bar, such that the posterior portion of the bar is formed only by the parietals (1). (From Kammerer et al., 2011: 146)
(76) Fossa on the ventral surface of the intertemporal bar formed by the postorbital and parietal large (0), reduced (1), or absent (2). (From Angielczyk and Kurkin, 2003: 53)
(77) Pineal foramen present (0); absent (1). (From Angielczyk and Kammerer, 2017: discrete 54)
(78) Circumpineal ornamentation: chimney-like boss (0); no boss, foramen flush with skull surface (1); dome- or collar-like boss, rugosity present (2); boss present with incomplete border, more strongly developed on lateral edges of pineal foramen (3). (From Angielczyk and Kammerer, 2017: discrete 55)

(79) Orientation of pineal foramen: exits perpendicular to long axis of intertemporal bar (0); angled anterior to perpendicular relative to long axis of intertemporal bar (1). (From Angielczyk and Kammerer, 2017: discrete 56)
(80) Interparietal does not contribute to intertemporal skull roof (0), makes a small contribution to intertemporal skull roof (1), or makes a large contribution to intertemporal skull roof (2). (From Kammerer et al., 2011: 62)
(81) Squamosal without (0) or with (1) a small or (2) large lateral fossa for the origin of the lateral branch of the M. adductor mandibulae externus. ORDERED (From Angielczyk and Kammerer, 2017: discrete 58)
(82) Distinct dorsolateral notch in squamosal below zygomatic arch in posterior view absent (0) or present (1). (From Kammerer et al., 2011: 64)
(83) Squamosal posteroventral process short such that there is relatively extensive exposure of quadrate and quadratojugal in posterior view and the quadrate foramen (if present) is visible in posterior view) (0) or long such that nearly all of the quadrate and quadratojugal are covered by the squamosal in posterior view and the quadrate foramen (if present) is not visible in posterior view (1). (From Kammerer et al., 2011: 65)
(84) Zygomatic portion of the squamosal without folded edge (0), out-turned to downturned (1) (*Oudenodon*, *Odontocylops*, etc.), or folded-over (2) (*Pelanomodon*, *Geikia*). ORDERED (From Angielczyk and Kammerer, 2017: discrete 61)
(85) Dorsoventral expansion of squamosal posterior to postorbital bar: (0) absent (1) present. (From Angielczyk and Kammerer, 2017: discrete 62)
(86) Zygomatic process of squamosal parasagittally deep (0), narrow and rod-like (1), or transversely expanded (2). (From Modesto et al., 1999: 12)
(87) Oblique ridge on lateral side of zygomatic arch giving triangular cross-section and overhanging a weak groove present (1) or absent (0). (From Kammerer et al., 2011: 157)
(88) Squamosal zygomatic process narrowly based and in line with occipital condyle (0) or widely based and flares posteriorly beyond occipital condyle (1). (From Modesto et al., 2003: 15)
(89) Sutural contact of squamosal and maxilla absent (0) or present (1). (From Angielczyk and Kurkin, 2003: 34)
(90) Squamosal separated by tabular bone from supraoccipital (0) or contacts supraoccipital (1). (From Modesto et al., 1999: 20)
(91) Suborbital boss on jugal absent (0) or present (1). (From Angielczyk and Kammerer, 2017: discrete 68)
(92) Quadratojugal narrow and rod-like (0) or plate-like distally (1). (From Modesto et al., 1999: 17)
(93) Quadrate with a dorsal lobe that has a convex, rounded anterior edge that rests against quadrate ramus of pterygoid (0) or with a dorsal lobe that is developed into a distinct process that extends anteriorly along the quadrate ramus of the pterygoid and is triangular to sub-triangular in shape (1). (From Kammerer et al., 2011: 72)
(94) Vomers unfused (0) or fused (1). (From Angielczyk and Kurkin, 2003: 11)
(95) Mid-ventral plate of vomers with an expanded, oval-shaped area posterior to junction with premaxilla (0) or without a notable expanded area posterior to junction with premaxilla (1). (From Angielczyk and Kurkin, 2003: 12)
(96) Mid-ventral plate of vomers relatively wide in ventral view (0), more narrow and blade-like in ventral view (1). (From Kammerer et al., 2011: 75)

(97) Trough on mid-ventral plate of vomers (i.e., ventral surface concave ventrally with raised edges): present (0) or absent (1). (From Kammerer et al., 2011: 76)
(98) Palatine dentition present (0) or absent (1). (From Modesto et al., 1999: 25)
(99) Bone texture of the palatine: primarily smooth, without evidence of keratinized covering (0), relatively smooth but with fine pitting and texturing suggestive of a keratinized covering (1), rugose and textured (2). (From Angielczyk and Kammerer, 2017: discrete 76)
(100) Position of palatine: raised, central palatine boss present (0); entire palatine flush with surrounding palatal elements (1), raised posterior section with anterior section that is flush with the secondary palate (2). (From Angielczyk and Kammerer, 2017: discrete 77)
(101) Paired fossae on palatine surface absent (0), present (1). (From Angielczyk and Kammerer, 2017: discrete 78)
(102) Palatine widest at its approximate midpoint of length (0), widens posteriorly (1), width relatively constant for entire length (2), widens anteriorly forming a palatine pad (3). ORDERED (from Angielczyk and Kammerer, 2017 : discrete character 79)
(103) Foramen on the palatal surface of the palatine absent (0) or present (1). (From Angielczyk and Kurkin, 2003: 24)
(104) Lateral palatal foramen absent (0), present at level of the anterior, expanded palatal exposure of the palatines (1), present posterior and dorsal to the level of the anterior, expanded palatal exposure of the palatines (2). (From Angielczyk and Kurkin, 2003: 35)
(105) Sutural contact of palatine and premaxilla absent (0) or present (1). (From Angielczyk and Kurkin, 2003: 27)
(106) Labial fossa surrounded by maxilla, jugal, and palatine absent (0) or present (1). (From Angielczyk, 2001: 19; Angielczyk and Kurkin 2003: 19)
(107) Ectopterygoid extends further posteriorly than palatine in palatal aspect (0), or does not extend further posteriorly than palatine in palatal aspect (1), or absent (2). (From Kammerer et al., 2011: 83)
(108) Ectopterygoid dentition absent (0) or present (1). (From Kammerer et al., 2013: 76)
(109) Pterygoids contact anteriorly (0) or separated by vomers (1). (From Kammerer et al., 2011: 84)
(110) Transverse flange of pterygoid projects laterally, free of posterior ramus (0), projects laterally, bound by posterior ramus (1) does not project laterally (2). (From Angielczyk and Kammerer, 2017: discrete 87)
(111) Anterior pterygoid keel: absent (0), present (1). (From Angielczyk and Kammerer, 2017: discrete 88)
(112) Anterior pterygoid keel extending for most of the length of anterior ramus of pterygoid (0), anterior pterygoid keel restricted to the anterior tip of the anterior ramus of the pterygoid (1). (From Angielczyk and Kammerer, 2017: discrete 89)
(113) Contact of pterygoid and maxilla absent (0) or present (1). (From Angielczyk and Kurkin, 2003: 46)
(114) Converging ventral keels on posterior portion of anterior pterygoid rami absent (0) or present (1). (From Kammerer et al., 2011: 150)
(115) Ventral surface of the median pterygoid plate depressed (0), smooth and flat (1), with a thin median ridge (2), with a wide, boss-like median ridge (3), or with a low rugose median swelling (4), or with a conical ventral projection (5), or with

thin paried ridges that are contiguous with the edges of the interpterygoid vacuity (6). (From Angielczyk and Kammerer, 2017: discrete 92)

(116) Pterygoid dentition present, conical (0); absent (1); present, bucco-lingually expanded. (From Kammerer et al., 2011: 88)

(117) Posterior edges of the interpterygoid vacuity located dorsal to the median pterygoid plate (0) or extended ventrally such that they are flush with the median pterygoid plate (1). (From Kammerer et al., 2011: 89)

(118) Development of the pila antotica as a rod-like process on the anterior edge of the periotic with a corresponding notch for the trigeminal never posterior to it (0), or pronounced pila antotica absent and trigeminal notch is a horizontal hollow in the anterior edge of the periotic (1). (From Surkov and Benton 2004: 12)

(119) Contact between periotic and parietal absent (0) or present (1). (From: Surkov and Benton 2004: 15)

(120) Parasphenoid excluded from (0) or reaches (1) interpterygoid vacuity. (From Modesto et al., 1999: 32)

(121) Basisphenoid contribution to the basisphenoid-basioccpital tubera slopes anterodorsally at a shallow angle, forming elongate ridges on the basicranium that are close to the same height as the tubera for most of their length (0), slopes anterodorsally at a steeper angle such that the parabasisphenoid conribution is still somewhat ridge-like but the portion of the ridge on the anterior surface of the tuber is more vertically-oriented (1), or is nearly vertical, forming very weak ridges if any (2). (From Angielczyk and Rubidge, 2013: 77)

(122) Stapedial facet of basisphenoid-basioccipital tuber exposed laterally (0), exposed ventrolaterally (1), or exposed ventrolaterally and open distally (2). (From Kammerer et al., 2011: 94)

(123) Exposure of internal carotid between mid-pterygoid plate and parasphenoid: directed laterally (0), directed medially (1). (From Angielczyk and Kammerer, 2017: discrete 100)

(124) Shape of basal tubera: bifurcating and posteriorly directed (0), laterally directed anteroposteriorly elongate with relatively narrow edges (1), strongly rounded, such that anterior and posterior tips of tuber curve towards each other, nearly enclosing the stapedial facet; tuber inflated (2), elongate, nearly quadrangular, with tubera extremely close together (3). (From Angielczyk and Kammerer, 2017: discrete 101)

(125) Margin of fenestra ovalis formed predominantly by parabasisphenoid, with little or no contribution from basioccipital (0), formed by approximately equal portions of parabasisphenoid and basioccipital (1), or formed predominantly by basioccipital, with little or no contribution by parabasisphenoid (2). (From Angielczyk, 2007: 54)

(126) Intertuberal ridge absent (0) or present (1). (From Angielczyk and Kurkin, 2003: 49)

(127) Dorsal process on anterior end of epipterygoid footplate absent (0) or present (1). (From Angielczyk and Rubidge 2010: 73)

(128) Stapedial foramen present (0) or absent (1). (From Angielczyk and Kurkin, 2003: 29)

(129) Dorsal process of the stapes present (0) or absent (1). (From Fröbisch, 2007: 72)

(130) Tabular contacts opisthotic (0) or separated from opisthotic by squamosal (1). (From Modesto et al., 1999: 21)

(131) Prootic bearing rectangular alar process that forms a plate raised above surface of temporal fenestra wall, in front of fossa: absent (0) present (1). (From Angielczyk and Kammerer, 2017: discrete 108)
(132) Exoccipital and basioccipital contributions to the occipital condyle distinct (0) or co-ossified into a single unit (1). (From Kammerer et al., 2011: 101)
(133) Occipital condyle round to subspherical in posterior view (0) or distinctly tri-radiate (1) in posterior view. (From Kammerer et al., 2011: 144)
(134) Circular central depression or fossa on the occipital condyle between the exoccipitals and basioccipital present (0) or absent (1). (From Kammerer et al., 2011: 147)
(135) Lateral edge of paroccipital process drawn into sharp posteriorly-directed process that is distinctly offset from the surface of the occipital plate: absent (0) present (1). (From Angielczyk and Kammerer, 2017: discrete 112)
(136) Floccular fossa present (0) or absent (1). (From Angielczyk and Kurkin, 2003: 41)
(137) Mandibular fenestra absent (0), present (1), or present but occluded by a thin sheet of the dentary (2). (From Kammerer et al., 2011: 103)
(138) Jaw ramus straight in dorsal view, without strong lateral bends (0), or bends strongly laterally (1) posterior to symphysis. (From Kammerer et al., 2011: 104)
(139) Dentaries sutured (0) or fused (1) at symphysis. (From Modesto et al., 1999: 33)
(140) Teeth present on dorsal surface of dentaries (0), medially displaced, sometimes on a swelling or shelf (1), or absent (2). (From Angielczyk and Kurkin, 2003: 10)
(141) Fine serrations on dentary teeth present (0), serrations absent (1), or coarse serrations present (2). (From Kammerer et al., 2011: 107)
(142) Denticulated cingulum on dentary teeth absent (0) or present (1). (From Kammerer et al., 2011: 108)
(143) Anteriormost dentary tooth: not distinct from rest of tooth row (0); massively enlarged and incisiform (1). (From Angielczyk and Kammerer, 2017: discrete 120)
(144) Jaw symphysis terminates in dorsal platform bearing the incisors and canine elevated above level of posterior dentary ramus (0); symphyseal region of lower jaw smoothly rounded and at same level as rest of dentary ramus in lateral view (1), with an upturned beak that is raised above the level of the dorsal surface of the jaw rami and has a scooped-out depression on its posterior surface (2), drawn into a sharp, spiky beak (3), or shovel-shaped beak with a rounded or squared-off edge and a weak depression on its posterior surface (4). (From Angielczyk and Kammerer, 2017: discrete 121)
(145) Curved ridge that follows the profile of the symphysis present on the edge between the anterior and lateral surfaces of the dentary absent (0) or present (1). (From Kammerer et al., 2011: 142)
(146) Boss present on ventral surface of anterior dentary ramus absent (0) present (1). (From Angielczyk and Kammerer, 2017: discrete 123)
(147) Dentary table absent (0) or present (1). (From Angielczyk and Rubidge, 2013: 15)
(148) Posterior dentary sulcus absent (0), present but does not extend past dentary teeth (if present) (1), present and extends past dentary teeth (if present), but is relatively wide and shallow (2), or present, extends past dentary teeth (if present) and is narrower and deeper (3). (From Angielczyk and Rubidge, 2013: 16)

(149) Tall, dorsally-convex cutting blade on medial edge of dorsal surface of dentary absent (0) or present (1). (From Angielczyk and Rubidge, 2013: 78)
(150) Lateral dentary shelf absent (0), present but relatively small (1), present and well developed (2). (From Kammerer et al., 2011: 113)
(151) Anterodorsal edge of lateral dentary shelf relatively flat (0), with a groove (1), or developed into a rounded swelling (2). (From Kammerer et al., 2011: 114)
(152) Lateral dentary shelf relatively thick, with distinct dorsal and ventral surfaces above the mandibular fenestra (0) or a thin ventrolaterally-directed sheet that forms the dorsal margin of the mandibular fenestra (1). (From Kammerer et al., 2011: 148)
(153) Splenial symphysis unfused (0) or fused (1). (From Sidor, 2001: 26)
(154) Spenial contribution to dentary symphysis: anterior process on splenial present in ventral view (0) or absent (1). (From Kammerer et al., 2011: 116)
(155) Exposed contribution of the angular to the symphysis: absent (0) present (1). (From Angielczyk and Kammerer, 2017: discrete 132)
(156) Coronoid bone present (0), or absent (1). (From Modesto et al., 1999: 38)
(157) Angular with anterolateral trough for the posterior process of the dentary absent (0) or present (1). (From Kammerer et al., 2011: 118)
(158) Reflected lamina: (0) reflected lamina large, rounded, unornamented; (1) with perpendicular ridges, (2) with reticulate ridges, (3) triradiate, with distinct groove-ridge-groove morphology dorsoventrally arrayed along lamina, (4) small, tab-like (more elongate than rounded), unornamented (5), large, rounded, but with only a central groove bisecting the lamina. (From Angielczyk and Kammerer, 2017: discrete 135)
(159) Reflected lamina of angular closely approaches or touches articular (0) or widely separated from articular (1). (From Maisch, 2001: 28)
(160) Prearticular with (0) or without (1) lateral exposure posteriorly. (From Modesto et al., 1999: 39)
(161) Articular distinct (0) or at least partially fused to prearticular (1). (From Sidor, 2001: 48)
(162) Surangular vertical lamina present and lateral to articular (0) or absent (1). (From Modesto et al., 1999: 37)
(163) Jaw joint allows strictly orthal closure (0); allows parasagittal movement with joint surfaces of quadrate and articular approximately equal (1), allows parasagittal movement with joint surfaces on articular large than that of quadrate (2). (From Angielczyk and Kammerer, 2017: discrete 135) ORDERED
(164) Enlarged dentary caniniform present (0) or absent (1). (From Kammerer et al., 2011: 123)
(165) Number of sacral vertebrae three (0), four (1), five (2), or six (3). (From Angielczyk and Kurkin, 2003: 36)
(166) Number of sternal bosses: 2 (0), 4(1). (From Vega-Dias et al., 2004: 32)
(167) Cleithrum absent (0) or present (1). (From Angielczyk and Kurkin, 2003: 39)
(168) Anterior edge of scapula extended laterally to form a strong crest (1) or not (0). (From Kammerer et al., 2011: 159)
(169) Origin of triceps on posterior surface of scapula relatively low (0) or developed into a prominent posterior projection (1). (From Kammerer et al., 2011: 160)
(170) Acromion process: absent or very small (0) or present and well defined (1). (From Kammerer et al., 2011: 126)

(171) Procoracoid foramen or notch entirely contained within the procoracoid (0) or formed by contributions of the procoracoid and scapula in lateral view (1). (From Angielczyk, 2007: 66)
(172) Procoracoid does not participate in formation of glenoid (0) or participates in formation of glenoid (1). (From Angielczyk, 2007: 67)
(173) Proximal articular surface of humerus formed by a slightly convex area on proximal surface of the bone without much expansion onto the dorsal surface (0), somewhat expanded with some encroachment onto the dorsal surface (1), or strongly developed and set off from rest of humerus by a weak neck (2). (From Angielczyk and Kurkin, 2003: 30) ORDERED Angielczyk and Kammerer, 2017
(174) Insertion of M. subcoracoscapularis on humerus a rounded, rugose area on proximal end of humerus (0), short, pinna-like process (1); large elongate process (2). (From Angielczyk and Kammerer, 2017: discrete 151) ORDERED
(175) Insertion of M. latissimus dorsi at rugose tuberosity on the posteroventral surface of humerus (0) or extended into a dorsoventrally flattened pinna-like process (1). (From Angielczyk and Kurkin, 2003: 50)
(176) Anterior and distal edges of deltopectoral crest close to perpendicular (0) or very obtuse (1). (From Kammerer et al., 2011: 149)
(177) Ectepicondylar foramen on humerus present (0) or absent (1). (From Angielczyk and Kurkin, 2003: 38)
(178) Radial and ulnar condyle continuous (0) or well ossified and separate (1) on ventral surface of humerus. (From Surkov et al., 2005: 12)
(179) Ulna with small olecranon process that does not extend far past the articular surface for the humerus (0), or with a large olecranon process that extends well past the articular surface for the humerus (1). (From Angielczyk, 2007: 61)
(180) Distal carpal 5: present as a distinct element (0), not present as a distinct element (1). (From Kammerer et al., 2011: 140)
(181) Manual digit III, shape of second phalanx: long (0), short (disc-like) (1), absent (2). (From Sidor and Hopson, 1998: 152)
(182) Manual digit IV, phalangeal number: 5 (0), or 3 (1). (From Angielczyk and Kammerer, 2017: discrete 159)
(183) Dorsal edge of ilium: unnotched (0) or notched (1). (From Kammerer et al., 2011: 134)
(184) Pubic plate is significantly expanded anteroposteriorly, such that its length is comparable to that of ischium (0) or anteroposteriorly short, so that it is much shorter than ischium (1). (From Kammerer et al., 2011: 136)
(185) Pubic plate is significantly expanded ventrally such that it is nearly the same height as ischium (0) or reduced ventrally such that it is shorter than ischium (1). (From Kammerer et al., 2011: 145)
(186) Distinct cranial process on anterior end of pubis absent (0) or present (1). (From Kammerer et al., 2011: 137)
(187) Femoral head continuous with the dorsal margin of femur (0) or offset dorsally from dorsal margin (1). (From Kammerer et al., 2011: 162)
(188) Proximal articular surface of the femur present as a weak swelling that is mostly limited to the proximal surface of the bone (0) or present as a more rounded, hemispherical swelling that has some encroachment on the anterior surface of the femur (1). (From Kammerer et al., 2011: 138)
(189) Insertion of M. iliofemoralis present as a low rugosity on the dorsolateral portion of the femur (0), developed into a distinct crest that extends down part of the

lateral surface of the femur (1) or a lateral crest that is split into a distinct first trochanter and third trochanter (2). (From Kammerer et al., 2011: 139) ORDERED Angielczyk and Kammerer, 2017

(190) Pedal digit III, shape of second phalanx: long (0), short (disc-like) (1), absent (2). (From Sidor and Hopson, 1998: 178)

(191) Pedal digit IV, phalangeal number: 5 (0), 4 (1), or 3 (2). (From Sidor and Hopson, 1998: 179)

(192) Pedal digit IV, shape of second and third phalanges: long (0), short (1). (From Sidor and Hopson, 1998: 180)

(193) Pedal digit V, shape of second phalanx: short (0), absent (1). (From Angielczyk and Kammerer, 2017: discrete 170)

(194) Greatly enlarged vascular channels present (1) or absent (0). (From Angielczyk, 2007: 74)

Table 1S. Phylogenetic matrix used in the analysis →

	1	2	3	4	5	6	7	8	9	10	11	12	13	14	15	16	17	18	19	20	21	22	23
Biarmosuchus	0.693	?	0.261	?	0.148	0.029	?	?	5.8	?	?	?	1.06	?	0.502	1.87	?	0.446	?	0.553	0.426	0.0	?
Hipposaurus boonstrai	0.606	?	0.263	0.842	0.19	0.046	?	?	3.5	?	?	?	1.07	?	0.539	2.63	0.667	0.367	0.125	?	?	0.0	0.222
Archaeosyodon praeventor	?	?	?	?	?	0.104	?	?	5.6	?	?	?	?	?	0.92	?	?	?	?	?	?	?	?
Titanophoneus potens	0.758	?	0.244	0.7	0.227	0.051	?	?	6.2	?	?	?	1.16	?	0.855	1.62	0.5	0.292	0.274	0.5	?	0.0	0.343
Gorgonops torvus	0.504	?	0.29	1.15	0.305	0.072	?	?	8.5	?	?	?	0.977	?	?	?	?	0.329	?	?	?	?	?
Lycosuchus vanderrieti	0.509	?	0.261	0.333	0.352	0.303	?	?	7.7	0.094	?	?	1.06	?	0.595	1.71	0.5	0.333	0.294	?	?	0.0	0.4
Glanosuchus macrops	0.547	?	0.145	0.25	0.367	0.218	?	?	5.3	0.05	?	?	1.02	?	0.718	2.12	0.545	0.309	0.2	0.833	?	0.0	0.342
Biseridens qilianicus	?	?	?	1.032	?	0.094	?	?	?	?	?	11.0	?	?	0.956	?	?	?	?	?	?	?	?
Anomocephalus africanus	?	?	?	?	?	?	?	?	?	?	?	?	?	?	?	?	?	?	?	?	?	?	?
Tiarajudens eccentricus	?	?	?	?	?	?	?	?	?	?	?	?	?	?	?	?	?	0.396	0.164	?	?	?	?
Otsheria netzvetajevi	0.381	5.425	0.231	?	0.512	0.108	?	0.181	5.3	0.108	10.95	15.5	0.86	?	?	?	?	?	?	?	?	?	?
Ulemica	0.47	5.364	0.125	1.06	0.407	0.102	?	0.216	4.9	?	10.91	15.4	1.098	0.294	0.698	1.135	?	?	?	?	?	?	?
Suminia getmanovi	0.336	4.879	0.205	?	0.23	0.105	?	0.198	5.0	0.09	10.46	11.6	0.902	0.395	0.698	1.136	0.558	0.299	0.133	0.709	0.966	0.0	0.186
Patranomodon nyaphulii	0.29	?	0.228	0.914	0.272	0.076	?	0.202	6.0	0.043	11.03	13.7	0.744	0.476	1.25	1.059	?	?	?	?	?	0.0	?
Galeops whaitsi	0.339	5.325	0.18	?	0.327	?	?	0.136	4.1	?	10.39	?	?	0.489	0.831	0.968	0.646	0.356	0.181	?	?	?	0.257
Galepus jouberti	?	?	?	0.855	?	?	?	?	?	?	?	?	?	?	?	?	?	0.351	0.149	?	?	0.0	?
Galechirus scholtzi	?	?	?	?	?	?	?	?	?	?	?	?	?	0.355	0.865	0.7	?	0.401	0.206	?	?	0.0	?
Eodicynodon oelofseni	0.351	?	?	0.968	0.435	?	2.47	?	?	?	?	12.0	?	0.259	0.708	?	?	?	?	?	?	?	?
Eodicynodon oosthuizeni	0.322	5.555	0.234	0.908	0.518	0.111	2.501	0.14	8.2	0.182	10.46	9.0	0.847	0.253	0.698	1.061	0.446	0.509	0.244	0.3	0.5	0.0	0.475
Colobodectes cluveri	0.203	5.714	0.195	?	0.52	0.269	2.07	0.142	6.6	0.206	10.18	?	0.948	?	?	?	?	?	?	?	?	?	?
Lanthanostegus mohoii	?	?	?	0.661	?	?	2.434	?	?	?	?	?	?	?	?	?	?	?	?	?	?	?	?
Eosimops newtoni	0.186	5.89	0.243	0.795	0.541	0.257	2.014	0.126	8.1	0.172	9.402	11.3	0.831	0.402	0.803	0.904	0.633	0.466	0.26	?	?	0.0	0.444
Prosictodon dubei	0.238	5.807	0.171	0.864	0.548	0.228	2.469	0.098	8.1	0.131	9.78	9.3	0.881	?	0.834	0.637	?	?	?	?	?	?	?
Diictodon feliceps	0.247	5.925	0.223	0.64	0.534	0.273	1.702	0.134	8.0	0.214	9.418	11.9	0.881	0.257	0.742	0.901	0.443	0.486	0.297	0.67	1.388	0.0	0.366
Robertia broomiana	0.237	5.863	0.197	0.721	0.555	0.259	1.681	0.105	8.6	0.199	9.417	9.8	0.85	0.132	0.711	0.868	0.487	0.502	0.227	?	?	0.0	0.309
Pristerodon mackayi	0.225	5.874	0.184	1.026	0.582	0.222	1.751	0.116	10.0	0.206	9.578	11.2	0.813	0.208	0.723	0.928	0.594	0.43	0.277	0.275	0.5	0.0	0.275
Brachyprosopus broomi	0.231	5.81	0.19	0.998	0.515	0.338	1.847	0.108	6.8	0.15	9.687	10.6	0.898	0.132	0.715	0.824	0.612	0.437	?	?	?	0.0	0.315
Endothiodon bathystoma	0.335	5.396	0.378	0.268	0.599	0.4	1.457	0.111	8.1	0.147	9.694	7.1	0.988	0.373	0.798	0.73	0.554	0.491	0.406	0.301	0.964	0.0	0.414
Endothiodon tolani	0.328	?	?	0.396	?	0.025	1.505	0.109	10.6	?	?	?	0.902	0.319	0.723	0.825	?	?	?	?	?	?	?
Niassodon mfumukasi	?	?	?	0.867	?	?	1.548	?	8.4	?	?	9.5	0.697	0.29	0.859	0.938	?	?	?	0.214	1.145	?	?
Digalodon rubidgei	0.354	6.155	0.294	0.899	0.473	0.139	1.565	0.134	?	0.173	?	?	0.871	0.293	?	?	?	?	?	?	?	?	?
Emydops	0.22	5.872	0.204	0.906	0.537	0.166	1.646	0.118	9.8	0.176	9.667	9.3	0.84	0.398	0.692	0.955	0.668	0.428	0.23	0.454	1.283	0.0	0.353
Dicynodontoides	0.269	5.95	0.24	0.764	0.539	0.211	1.492	0.085	8.823	0.181	9.814	11.9	0.887	?	0.726	0.924	0.304	0.497	?	0.167	2.5	0.406	0.359
Kombuisia frerensis	0.193	5.976	0.202	0.4	0.555	?	1.589	0.195	?	?	9.645	?	0.746	?	0.684	?	?	?	?	?	?	?	?
Myosaurus gracilis	0.26	5.902	0.275	1.032	0.483	0.108	1.59	0.085	9.6	0.208	9.775	9.6	0.853	0.348	0.958	0.942	0.586	?	?	?	?	?	0.208
Sauroscaptor tharavati	0.281	?	0.298	1.339	0.421	0.048	?	?	?	?	?	?	0.912	0.564	0.73	0.714	?	?	?	?	?	?	?
Cistecephalus microrhinus	0.279	6.056	0.289	1.139	0.509	0.088	1.49	0.117	9.55	0.0	9.965	10.2	0.872	0.38	0.687	0.789	0.485	0.403	0.317	0.754	1.857	0.0	0.324
Cistecephaloides boonstrai	0.311	6.047	0.425	1.319	0.372	0.04	?	0.194	?	?	10.31	12.5	0.632	0.346	0.796	0.914	?	?	?	?	?	?	?
Kawingasaurus fossilis	0.308	5.933	0.33	1.404	0.34	?	1.5	0.135	10.7	?	10.12	10.0	0.836	0.286	?	0.964	0.298	0.419	?	?	?	?	0.446
Rhachiocephalus magnus	0.329	6.094	0.271	0.738	0.598	0.606	1.48	0.094	8.8	0.143	9.17	12.8	1.011	0.167	0.838	0.777	0.501	0.506	?	?	?	?	0.372
Kitchinganomodon crassus	0.32	6.137	0.318	0.708	0.566	0.752	1.556	0.108	7.4	0.07	9.747	11.1	0.936	0.165	0.843	0.752	?	0.466	?	?	?	?	?
Oudenodon bainii	0.281	6.054	0.173	0.844	0.609	0.271	1.458	0.092	8.1	0.141	9.219	11.3	0.864	0.264	0.798	0.745	0.57	0.491	0.366	0.514	0.765	0.353	0.411
Tropidostoma dubium	0.284	5.989	0.197	0.899	0.565	0.277	1.436	0.098	8.8	0.14	9.106	12.4	0.875	0.237	0.758	0.766	0.531	0.503	?	0.474	1.368	0.345	0.378
Australobarbarus	0.333	6.058	0.183	0.697	0.561	0.298	1.324	0.101	6.1	0.16	9.822	13.35	0.882	0.193	0.624	0.694	0.466	0.485	?	0.848	1.033	0.333	0.391
Odontocyclops whaitsi	0.376	6.066	0.232	0.988	0.551	0.232	1.448	0.092	10.1	0.131	9.74	12.3	0.929	0.213	0.787	0.731	0.551	0.518	0.427	0.435	1.13	0.426	0.491
Idelesaurus tataricus	0.367	5.967	0.175	1.022	0.5	0.174	1.497	0.107	8.25	0.173	10.12	13.5	0.969	0.204	0.693	0.764	?	?	?	?	?	?	?

	1	2	3	4	5	6	7	8	9	10	11	12	13	14	15	16	17	18	19	20	21	22	23
Aulacephalodon bainii	0.3	6.089	0.323	0.892	0.583	0.204	1.425	0.117	6.8	0.122	9.48	13.5	0.822	0.172	0.76	0.785	0.55	0.532	0.348	0.714	1.067	0.395	0.491
Pelanomodon moschops	0.289	6.093	0.305	0.912	0.584	0.213	1.468	0.104	9.4	0.155	9.414	12.3	0.801	?	0.856	0.742	?	?	?	?	?	?	?
Geikia locusticeps	0.256	6.049	0.278	0.908	0.514	0.251	1.627	0.104	8.72	0.141	9.392	13.9	0.756	0.205	0.818	0.848	?	?	?	?	?	?	?
Geikia elginensis	0.366	?	0.521	0.846	0.529	?	1.429	?	?	?	?	13.1	0.829	0.212	0.9	0.987	?	?	?	?	?	?	?
Elph borealis	0.279	5.927	0.186	0.64	0.544	0.29	1.515	0.157	8.9	?	?	13.0	0.914	?	0.781	?	?	?	?	?	?	?	?
Interpresosaurus blomi	?	?	?	?	?	?	?	?	?	?	?	?	?	?	?	?	?	?	?	?	?	?	?
Katumbia parringtoni	0.196	5.868	0.22	0.527	0.541	0.347	1.489	0.112	9.3	0.132	9.928	14.4	?	?	0.833	0.822	?	?	?	?	?	?	?
Delectosaurus arefjevi	0.369	5.861	0.258	0.702	0.546	0.334	1.618	0.119	7.8	0.13	9.798	14.7	0.985	?	?	?	?	?	?	?	?	?	?
Dicynodon lacerticeps	0.324	5.982	0.253	0.607	0.546	0.359	1.485	0.117	7.7	0.121	9.869	11.9	0.926	0.241	0.749	0.766	?	?	?	?	?	?	?
Dicynodon huenei	0.317	5.952	0.243	0.526	0.566	0.353	1.317	0.111	8.2	0.115	9.889	11.8	0.961	0.206	0.756	0.818	0.538	0.554	0.317	0.625	1.313	0.374	0.522
Daptocephalus leoniceps	0.268	6.091	0.237	0.539	0.567	0.437	1.5	0.118	6.4	0.111	9.378	?	0.858	0.238	0.763	0.75	?	0.545	?	?	1.667	?	?
Daqingshanodon limbus	0.282	6.112	0.26	0.619	0.442	0.18	1.528	0.08	?	0.189	9.34	10.3	0.808	0.212	0.677	0.819	?	?	?	?	?	?	?
Dinanomodon gilli	0.337	6.17	0.205	0.48	0.577	0.522	1.347	0.116	7.8	0.107	9.751	9.9	1.047	0.186	?	0.724	?	?	?	?	?	?	?
Peramodon amalitzkii	0.272	?	0.224	0.563	0.553	0.369	?	?	?	?	?	9.5	0.839	0.167	0.676	0.68	0.463	?	?	?	?	?	0.494
Vivaxosaurus trautscholdi	0.38	6.019	0.23	0.685	0.481	0.285	1.824	0.116	7.9	0.121	10.20	13.9	1.041	0.203	0.702	0.731	0.317	0.544	?	?	?	?	0.641
Jimusaria sinkiangensis	0.307	?	0.278	0.672	0.767	0.464	1.443	0.089	7.2	0.098	?	8.9	0.992	0.251	?	0.699	?	?	?	?	?	?	?
Sintocephalus alticeps	0.354	5.969	0.244	0.516	0.522	0.294	1.338	0.124	6.5	0.132	9.399	9.6	1.022	?	?	?	?	?	?	?	?	?	?
Basilodon woodwardi	0.315	5.994	0.212	0.722	0.497	0.225	1.305	0.128	5.7	0.139	9.599	12.6	0.814	?	?	?	?	?	?	?	?	?	?
Turfanodon bogdaensis	?	?	?	0.588	?	0.405	1.327	?	?	?	?	10.3	0.895	?	?	?	?	?	?	?	?	?	?
Keyseria benjamini	0.244	6.155	0.159	1.034	0.605	0.203	1.6	0.083	6.3	?	?	9.0	0.831	?	?	?	?	?	?	?	?	?	?
Gordonia traquairi	0.252	?	0.139	0.65	0.604	0.309	?	?	?	?	?	?	0.924	0.188	?	0.773	0.543	0.49	0.144	?	?	?	0.476
Syops vanhoepeni	?	?	?	0.484	?	0.343	?	?	?	?	?	?	?	?	?	?	?	?	?	?	?	?	?
Euptychognathus bathyrhynchus	0.336	6.028	0.13	0.562	0.56	0.238	1.559	0.091	6.5	0.084	9.663	10.25	0.792	?	0.79	0.815	?	?	?	?	?	?	?
Lystrosaurus hedini	0.32	6.111	0.414	0.705	0.413	0.146	1.471	0.174	9.2	0.079	10.20	11.4	0.673	0.294	0.691	0.781	?	?	?	?	?	?	?
Lystrosaurus maccaigi	0.274	6.072	0.347	0.656	0.325	0.108	1.764	0.165	8.4	0.123	10.02	10.9	0.805	0.354	0.711	0.706	?	0.526	0.54	?	?	0.389	?
Lystrosaurus curvatus	0.315	6.005	0.383	0.689	0.417	0.119	1.664	0.162	7.4	0.086	10.15	8.6	0.906	0.289	0.767	0.643	0.473	0.485	0.465	0.787	1.484	0.313	0.489
Lystrosaurus declivis	0.347	5.954	0.424	0.705	0.415	0.112	2.141	0.157	8.8	0.097	10.31	9.7	0.874	0.315	0.757	0.711	0.418	0.458	0.478	0.75	1.3	0.347	0.545
Lystrosaurus murrayi	0.288	6.003	0.427	0.726	0.466	0.143	2.002	0.175	8.4	0.101	10.36	11.7	0.816	0.316	0.793	0.754	0.478	0.46	0.441	0.843	1.455	0.392	0.605
Angonisaurus cruickshanki	0.339	6.301	0.514	0.667	0.572	0.6	1.491	0.19	5.9	0.06	10.21	10.0	1.012	0.143	0.785	0.722	?	0.524	?	0.647	2.541	?	?
Tetragonias njalilus	0.378	5.912	0.354	0.201	0.574	0.446	?	0.125	6.8	0.088	10.01	10.4	1.004	0.205	0.858	0.796	0.447	0.481	0.3	0.675	1.825	0.304	0.596
Shansiodon	0.265	6.064	0.327	0.163	0.538	0.633	1.314	0.13	7.2	0.1	9.78	11.2	1.129	0.286	0.821	0.84	0.575	0.479	?	0.758	1.363	0.363	0.675
Vinceria andina	0.267	6.099	0.352	0.201	0.49	0.466	?	0.137	7.0	0.153	10.53	11.3	0.983	?	?	?	?	?	?	?	?	?	?
Rhinodicynodon gracile	0.304	6.213	0.253	0.5	0.523	0.435	1.568	0.1	?	?	9.174	10.1	0.879	0.24	0.875	0.734	0.49	0.354	0.361	?	?	0.352	0.383
Dinodontosaurus	0.398	6.104	0.347	0.24	0.461	0.328	1.414	0.135	7.3	0.074	10.16	10.9	0.926	0.202	0.814	0.653	0.398	0.507	0.423	0.652	1.896	0.31	0.752
Kannemeyeria simocephalus	0.421	6.121	0.409	0.289	0.531	0.479	1.461	0.147	9.8	0.074	10.48	12.1	1.147	0.179	0.8	0.686	0.551	0.558	0.338	?	1.381	0.372	0.411
Kannemeyeria lophorhinus	0.361	6.286	?	0.663	?	0.318	2.051	0.149	10.8	0.086	10.43	?	?	0.077	0.786	0.542	?	?	?	?	?	?	?
Dolichuranus primaevus	0.356	6.079	0.392	0.293	0.484	0.4	1.339	0.143	8.7	0.085	10.67	9.7	1.018	0.192	0.756	0.542	?	0.519	?	?	?	0.425	?
Wadiasaurus indicus	0.423	6.105	0.337	0.539	0.506	0.523	?	0.218	?	?	?	10.6	1.052	0.344	0.9	0.81	0.607	0.563	0.45	0.562	1.239	0.417	0.355
Rabidosaurus cristatus	0.464	?	?	0.268	0.607	?	?	?	?	?	?	?	?	?	?	?	?	?	?	?	?	?	?
Rhadiodromus	0.509	6.144	0.403	0.285	0.574	0.254	?	0.122	6.9	0.088	10.02	10.8	1.085	?	?	?	?	?	0.604	?	?	?	?
Rechnisaurus cristarhynchus	0.51	5.971	0.436	0.154	?	0.211	?	0.14	9.9	?	?	?	?	?	?	?	?	?	?	?	?	?	?
Uralokannemeyeria vjuschkovi	0.49	?	0.407	0.526	0.454	0.233	?	0.147	?	0.091	?	11.9	1.154	?	?	?	?	?	?	0.819	1.193	?	?
Shaanbeikannemeyeria	0.527	6.069	0.513	0.886	0.5	0.414	?	0.157	7.8	0.176	10.64	11.3	1.432	?	0.734	?	?	0.58	?	?	?	0.416	?
Xiyukannemeyeria brevirostris	0.286	6.203	0.413	0.46	0.433	0.23	?	0.169	8.5	0.086	10.03	8.9	0.795	0.32	?	0.668	?	?	?	?	?	?	?
Parakannemeyeria	0.455	6.28	0.377	0.359	0.354	0.195	1.468	0.122	7.5	0.102	9.688	12.3	0.92	0.166	0.79	0.515	0.467	0.52	0.478	0.443	1.465	0.411	0.294
Sinokannemeyeria	0.42	6.14	0.478	0.543	0.382	0.175	1.505	0.161	5.9	0.109	10.47	?	0.918	0.243	0.549	0.385	0.494	0.489	0.556	0.458	1.187	0.408	0.405

	1	2	3	4	5	6	7	8	9	10	11	12	13	14	15	16	17	18	19	20	21	22	23
Stahleckeria potens	0.438	5.992	0.445	0.726	0.491	0.288	?	0.183	11.1	0.052	10.28	8.7	0.953	0.237	0.856	0.897	0.442	0.53	?	0.391	2.217	0.434	0.565
Eubrachiosaurus browni	?	?	?	?	?	?	?	?	?	?	?	?	?	?	?	?	?	0.538	?	?	1.789	?	?
Sangusaurus parringtonii	0.411	6.177	0.461	0.618	?	0.368	1.129	0.144	?	0.091	?	9.2	1.061	?	0.832	?	?	?	?	0.592	1.944	0.433	?
Ischigualastia jenseni	0.482	6.139	0.423	0.331	0.479	0.528	1.39	0.151	5.7	0.064	10.02	?	1.032	?	0.912	0.841	0.419	0.577	0.561	?	0.818	0.412	0.526
Jachaleria	0.392	6.078	0.393	0.199	0.379	0.499	1.431	0.161	4.0	0.084	10.27	?	0.766	?	0.822	0.766	0.427	?	0.529	?	0.808	0.434	0.667
Zambiasaurus submersus	?	?	?	?	?	?	?	?	?	?	?	?	?	?	?	?	?	0.498	?	?	?	0.401	?
Placerias hesternus	?	?	?	?	?	?	?	?	?	?	?	?	?	?	?	?	?	0.49	0.499	?	?	?	?
Moghreberia nmachouensis	?	?	?	?	?	?	?	?	?	?	?	?	?	?	?	?	?	?	?	?	?	?	?
Rastodon procurvidens	0.221	?	0.209	0.444	0.57	0.258	?	0.128	6.3	0.105	?	12.0	0.907	0.1	0.824	0.786	?	?	?	?	?	?	?
Bulbasaurus phylloxyron	0.284	6.003	0.25	0.562	0.534	0.233	1.362	0.112	10.33	0.052	9.851	14.78	0.887	?	0.643	?	?	?	?	?	?	?	?
Compsodon helmoedi	0.196	5.874	0.207	1.066	0.431	0.187	1.71	0.082	10.3	0.22	9.858	11.0	0.817	?	?	?	?	?	?	?	?	?	?
LPB 1993 3	0.297	5.068	?	?	0.276	0.134	?	0.131	8.333	0.140	?	9.616	0.876	?	?	?	?	?	?	?	?	?	?
LPB 1993 2	0.200	?	0.295	?	0.408	0.281	?	?	?	?	?	14.70	0.829	?	?	?	?	?	?	?	?	?	?
LPB 1995 9	0.205	?	0.254	?	?	0.316	?	0.124	?	0.101	?	?	0.935	?	?	?	?	?	?	?	?	?	?

	24	25	26	27	28	29	30	31	32	33	34	35	36	37	38	39	40	41	42	43	44	45	46	47	48	49	50	51	52	53	54
Biarmosuchus	0	0	0	0	0	2	0	0	0	0	0	0	0	0	0	0	0	0	0	1	0	0	0	0	0	0	0	?	?	?	?
Hipposaurus boonstrai	0	0	0	0	0	2	0	0	0	0	0	0	0	0	0	0	0	0	0	1	0	0	0	0	0	0	0	?	?	?	?
Archaeosyodon praeventor	0	0	0	0	0	2	0	0	0	0	0	0	0	0	0	0	0	0	0	1	0	0	0	0	1	0	0	?	?	?	?
Titanophoneus potens	0	0	0	0	0	2	0	0	0	0	0	0	0	0	0	0	1	0	0	0	0	0	0	0	0	0	0	?	?	?	?
Gorgonops torvus	0	0	0	0	0	2	0	0	0	0	0	0	0	0	0	0	0	0	0	0	0	0	0	0	0	0	0	?	?	?	?
Lycosuchus vanderrieti	0	0	0	0	0	2	0	0	0	0	0	0	0	0	0	0	0	0	0	0	0	0	0	1	0	0	0	?	?	?	?
Glanosuchus macrops	0	0	0	0	0	2	0	0	0	0	0	0	0	0	0	0	0	0	0	1	0	0	0	0	0	0	0	?	?	?	?
Biseridens qilianicus	0	0	0	0	0	2	1	0	0	0	0	0	0	0	0	0	1	0	0	1	0	0	0	0	1	0	0	?	?	?	?
Anomocephalus africanus	?	?	?	?	?	?	?	0	?	?	?	?	?	0	0	?	?	0	?	0	?	1	0	0	?	?	0	?	?	?	?
Tiarajudens eccentricus	0	?	?	?	?	?	?	0	?	0	?	?	0	0	0	0	1	0	0	0	0	0	0	0	1	0	0	?	?	?	?
Otsheria netzvetajevi	0	0	0	0	0	2	1	0	1	0	0	0	0	0	0	?	1	0	0	1	?	1	0	0	?	0	0	?	?	?	?
Ulemica	0	0	0	0	0	2	1	0	1	0	1	0	0	0	0	?	1	0	0	1	?	0	0	0	1	0	0	?	?	?	?
Suminia getmanovi	0	0	0	0	0	2	?	0	1	0	1	0	0	0	0	0	1	0	0	1	?	1	0	0	2	0	0	?	?	?	?
Patranomodon nyaphulii	0	0	0	?	0	?	1	0	1	0	1	?	0	0	0	0	2	0	0	0	?	1	0	0	1	0	0	?	?	?	?
Galeops whaitsi	0	0	0	0	0	2	1	0	1	0	1	0	0	0	0	0	2	0	0	0	?	1	0	0	1	0	0	?	?	?	?
Galepus jouberti	?	0	0	?	0	2	?	?	1	?	?	?	?	0	0	?	?	0	?	?	?	?	?	?	?	?	0	?	?	?	?
Galechirus scholtzi	0	0	?	?	0	?	?	0	1	0	?	0	?	0	0	?	?	0	0	0	?	1	0	0	1	?	0	?	?	?	?
Eodicynodon oelofseni	?	?	?	?	?	?	?	0	1	?	1	0	0	0	0	0	2	0	0	0	0	1	0	0	1	?	0	?	?	?	?
Eodicynodon oosthuizeni	0	0	0	0	1	0	1	2	1	0	1	0	0	0	0	0	2	0	0	0	0	2	0	0	1	0	1	0	0	0	0
Colobodectes cluveri	0	1	0	0	1	0	1	2	1	0	1	0	0	0	0	0	2	0	0	0	0	2	0	0	1	0	1	0	0	0	0
Lanthanostegus mohoii	0	?	?	?	?	?	?	?	?	?	1	?	?	?	?	0	?	?	?	?	?	2	0	0	?	1	?	?	?	?	?
Eosimops newtoni	1	1	1	0	1	0	1	2	1	1	1	0	0	0	0	0	2	0	0	0	0	2	1	0	1	1	1	2	0	0	0
Prosictodon dubei	1	1	1	0	1	0	1	2	1	1	1	0	0	0	0	0	2	0	0	0	0	2	1	0	1	1	1	2	0	0	0
Diictodon feliceps	1	1	1	0	1	0	1	2	1	1	1	0	0	0	0	0	2	0	0	0	0	2	2	?	?	1	1	2	0	0	0
Robertia broomiana	1	1	1	0	1	0	1	2	1	1	1	0	0	0	0	0	2	0	0	0	0	2	1	0	1	1	1	2	0	0	0
Pristerodon mackayi	1	1	0	0	1	2	1	2	1	0	1	0	0	0	0	0	2	0	0	0	0	2	1	0	1	1	1	0	0	1	0
Brachyprosopus broomi	1	0	1	1	1	2	1	2	1	0	1	1	0	0	0	1	2	0	0	0	0	2	1	1	1	1	1	0	0	1	0
Endothiodon bathystoma	1	0	0	1	[01]	2	1	1	1	0	1	2	0	0	0	0	2	0	1	0	0	1	1	1	2	0	0	?	?	?	?
Endothiodon tolani	1	0	0	1	0	2	1	1	1	0	1	2	0	0	0	1	2	0	1	0	0	2	1	1	2	0	0	?	?	?	?
Niassodon mfumukasi	1	?	?	?	2	2	?	1	1	?	1	?	0	0	0	1	?	?	?	0	?	1	1	0	1	1	1	0	0	1	0
Digalodon rubidgei	1	2	1	0	2	0	1	2	1	0	1	0	0	0	0	1	2	0	0	0	0	2	2	?	?	0	1	1	0	1	0
Emydops	1	0	1	1	1	0	1	2	1	0	1	0	0	0	0	0	2	0	0	0	0	2	0	0	1	1	1	1	0	1	0
Dicynodontoides	1	0	1	1	2	0	1	2	1	0	1	0	0	0	0	1	2	0	0	0	0	2	2	?	?	1	1	1	0	1	0
Kombuisia frerensis	1	0	1	0	2	0	1	2	1	0	1	0	0	0	0	1	2	?	0	0	0	1	2	?	?	0	1	1	0	1	0
Myosaurus gracilis	1	0	0	0	2	1	1	2	1	0	1	0	0	0	0	1	2	0	0	0	0	1	2	?	?	1	1	1	0	1	0
Sauroscaptor tharavati	1	?	?	?	2	?	?	2	1	?	1	0	0	0	0	1	?	0	0	0	0	1	2	?	?	?	1	1	0	1	0
Cistecephalus microrhinus	1	0	1	0	2	0	1	2	1	0	1	0	0	0	0	1	2	0	1	0	0	1	2	?	?	1	1	1	0	1	0
Cistecephaloides boonstrai	1	0	0	0	2	0	1	2	1	0	1	0	0	0	0	1	2	0	1	0	0	1	2	?	?	0	1	1	0	1	0
Kawingasaurus fossilis	1	0	0	0	2	0	1	2	1	0	1	0	0	0	0	1	2	0	1	0	0	1	2	?	?	0	1	1	0	1	0
Rhachiocephalus magnus	1	2	0	0	2	2	1	2	1	0	1	1	0	0	0	0	2	0	0	0	0	1	2	?	?	1	1	0	0	0	1
Kitchinganomodon crassus	1	2	0	0	2	2	1	2	1	0	1	1	0	0	0	0	2	0	0	0	0	1	2	?	?	1	1	0	0	0	1
Oudenodon bainii	1	2	0	0	2	2	1	2	1	0	1	1	0	0	0	0	2	0	0	0	0	1	2	?	?	1	1	0	1	0	1
Tropidostoma dubium	1	2	0	0	2	2	1	2	1	0	1	1	0	0	0	0	2	0	0	0	0	2	1	0	1	1	1	0	1	0	1
Australobarbarus	1	2	0	0	2	2	1	2	1	0	1	1	0	0	0	0	2	0	0	0	0	2	1	0	?	1	1	0	1	0	1
Odontocyclops whaitsi	1	2	0	0	2	2	1	2	1	0	1	1	0	0	0	0	2	0	0	0	0	2	2	?	?	1	1	0	1	0	1
Idelesaurus tataricus	1	2	0	0	2	2	1	2	1	0	1	1	0	0	0	0	2	0	0	0	0	2	2	?	?	1	1	0	1	0	1

	55	56	57	58	59	60	61	62	63	64	65	66	67	68	69	70	71	72	73	74	75	76	77	78	79	80	81	82	83	84	85
Biarmosuchus	0	0	0	0	0	0	0	0	0	0	0	0	0	0	?	2	0	0	0	2	0	0	0	0	0	0	0	0	0	0	0
Hipposaurus boonstrai	0	0	0	0	0	0	0	0	0	0	0	0	0	1	0	2	0	0	0	0	0	0	0	0	0	0	0	0	0	0	0
Archaeosyodon praeventor	0	0	0	0	0	0	0	1	0	0	0	0	0	0	?	2	0	0	0	1	0	0	0	0	0	0	0	0	0	0	0
Titanophoneus potens	0	0	0	0	0	0	0	1	0	0	1	0	0	0	?	1	0	0	0	0	0	0	0	[02]	0	0	0	0	0	0	0
Gorgonops torvus	0	0	0	0	0	0	0	0	1	0	0	0	0	1	0	2	0	0	0	2	0	0	0	2	0	0	0	0	0	0	0
Lycosuchus vanderrieti	0	0	0	2	0	0	0	0	0	0	0	0	0	0	?	1	0	2	0	1	1	0	0	1	0	0	0	0	0	0	0
Glanosuchus macrops	0	0	0	0	0	0	0	0	0	0	0	0	1	0	?	1	0	2	0	1	1	0	0	1	0	0	0	0	0	0	0
Biseridens qilianicus	0	0	0	0	0	0	0	1	0	0	0	1	0	0	?	2	0	0	0	1	0	0	0	0	0	0	0	0	0	0	0
Anomocephalus africanus	?	?	0	?	?	?	0	?	?	?	0	0	?	?	?	?	?	?	?	?	?	?	?	?	?	?	0	?	?	0	0
Tiarajudens eccentricus	0	0	0	?	?	0	0	?	0	0	0	0	?	?	?	?	?	?	?	?	?	?	?	?	?	?	0	0	?	0	0
Otsheria netzvetajevi	?	0	0	0	0	0	0	0	0	0	0	0	0	0	?	2	?	0	0	1	0	?	0	0	0	0	0	0	0	0	0
Ulemica	0	0	0	0	0	0	0	1	0	0	0	0	0	0	?	2	0	0	0	1	0	?	0	0	0	0	1	0	0	0	0
Suminia getmanovi	?	0	0	1	0	0	0	0	0	0	0	0	0	0	?	2	1	0	0	1	0	?	0	0	0	0	2	0	0	0	0
Patranomodon nyaphulii	?	0	0	0	0	0	0	0	0	0	0	0	0	1	0	0	1	0	0	0	0	0	0	1	0	0	0	0	0	0	0
Galeops whaitsi	?	?	1	?	0	0	0	0	0	0	0	0	0	?	?	?	1	0	0	0	?	0	0	?	0	?	2	0	0	0	0
Galepus jouberti	?	?	?	?	?	?	?	?	?	?	0	0	?	?	?	?	?	?	?	?	?	?	?	?	?	?	?	?	?	?	0
Galechirus scholtzi	?	?	1	?	?	0	0	?	?	?	?	?	?	?	?	?	?	?	?	?	?	?	?	?	?	?	?	?	?	?	?
Eodicynodon oelofseni	?	?	?	?	0	?	0	0	0	0	0	0	0	1	0	?	?	0	0	1	0	0	0	1	0	0	2	0	1	0	?
Eodicynodon oosthuizeni	0	0	1	1	0	0	0	0	0	0	0	0	0	1	0	0	1	0	0	1	0	0	0	1	0	0	2	1	1	0	0
Colobodectes cluveri	0	0	1	1	0	0	0	0	0	1	0	0	0	1	0	1	1	0	0	0	0	0	0	1	0	?	2	1	1	0	0
Lanthanostegus mohoii	0	?	?	?	0	?	0	1	0	0	0	1	0	1	0	1	?	0	0	1	0	0	0	2	0	0	?	?	?	0	0
Eosimops newtoni	1	0	1	0	0	0	0	1	0	0	0	1	0	1	0	1	1	0	0	1	0	0	0	2	0	0	2	1	1	0	0
Prosictodon dubei	1	0	1	1	0	0	0	1	0	0	0	0	0	1	0	1	1	2	0	0	0	0	0	1	0	?	2	1	1	0	0
Diictodon feliceps	1	[01]	1	[01]	0	0	0	1	0	0	0	0	0	1	0	1	1	2	0	0	0	0	0	[12]	0	0	2	1	1	0	0
Robertia broomiana	1	0	1	0	0	0	0	1	0	0	0	0	0	1	0	1	1	0	0	1	0	0	0	2	0	0	2	1	1	0	0
Pristerodon mackayi	0	0	1	0	0	0	0	1	0	0	0	?	0	1	0	1	1	0	0	1	0	0	0	1	0	1	2	1	1	0	0
Brachyprosopus broomi	0	0	1	0	0	0	0	1	0	0	0	0	0	1	0	1	1	0	0	1	0	0	0	2	0	0	2	1	1	0	0
Endothiodon bathystoma	?	0	[12]	?	0	0	1	0	0	[01]	1	0	1	1	1	1	1	1	0	1	0	1	0	2	0	0	2	1	1	0	0
Endothiodon tolani	?	?	[01]	0	0	0	0	0	0	1	?	?	0	1	0	1	1	1	0	1	0	1	0	1	0	0	2	?	1	?	?
Niassodon mfumukasi	1	0	1	0	0	0	0	0	0	0	0	0	0	2	1	2	1	0	0	2	0	0	0	1	0	0	2	0	1	0	0
Digalodon rubidgei	0	0	1	0	0	0	0	0	0	1	0	0	0	1	0	1	1	0	0	2	0	0	0	3	0	1	2	1	1	0	0
Emydops	1	0	1	0	0	0	0	0	0	0	0	0	0	1	0	1	1	0	0	1	0	0	0	1	0	0	2	0	1	0	0
Dicynodontoides	0	0	1	0	0	0	0	0	0	1	0	0	0	2	0	1	1	2	0	0	0	0	0	1	0	0	2	1	1	0	0
Kombuisia frerensis	1	0	1	0	0	0	0	0	0	1	0	0	0	2	0	1	0	2	0	1	1	?	1	?	?	0	2	?	1	0	0
Myosaurus gracilis	1	0	1	2	0	0	0	0	0	1	0	0	0	1	0	2	0	0	0	2	0	0	0	1	0	0	2	0	1	0	0
Sauroscaptor tharavati	0	?	1	?	0	?	0	0	?	1	0	0	0	0	?	?	?	0	0	2	0	?	0	1	0	0	2	0	1	0	0
Cistecephalus microrhinus	1	0	1	0	0	0	[01]	1	0	1	[01]	0	0	0	?	2	1	0	0	2	0	0	0	1	0	1	2	0	1	0	0
Cistecephaloides boonstrai	0	0	1	0	0	0	0	0	1	1	0	0	0	0	?	2	1	0	0	2	0	0	0	1	0	1	2	0	1	0	0
Kawingasaurus fossilis	0	0	0	2	0	0	0	0	0	1	0	0	0	0	?	2	1	0	0	2	0	0	1	?	?	?	2	0	1	0	0
Rhachiocephalus magnus	0	0	2	0	0	1	1	0	0	0	1	0	0	1	0	1	1	2	0	0	0	0	0	2	1	0	2	1	1	0	0
Kitchinganomodon crassus	0	0	2	0	0	1	1	0	0	0	1	0	0	1	0	1	1	2	0	0	0	0	0	2	1	1	2	1	1	1	0
Oudenodon bainii	0	0	2	1	0	[01]	0	1	0	0	0	0	0	1	0	1	1	1	0	0	0	0	0	1	0	1	2	1	1	1	0
Tropidostoma dubium	0	0	2	1	0	1	0	1	0	0	0	0	0	1	0	1	1	1	0	0	0	0	0	1	0	1	2	1	1	1	0
Australobarbarus	0	0	2	?	0	?	0	1	0	0	0	0	0	1	0	1	1	1	0	0	0	0	0	1	0	1	2	1	1	1	0
Odontocyclops whaitsi	0	0	2	0	0	1	2	0	0	0	0	0	0	2	1	1	1	1	0	0	0	0	0	2	0	1	2	1	1	1	0
Idelesaurus tataricus	0	0	2	1	0	1	1	0	0	0	0	0	0	2	1	1	1	1	0	0	0	0	0	1	0	0	2	1	1	1	0

	86	87	88	89	90	91	92	93	94	95	96	97	98	99	100	101	102	103	104	105	106	107	108	109	110	111	112	113	114	115	116
Biarmosuchus	0	0	1	0	0	0	0	0	1	0	0	1	0	0	0	0	0	0	0	0	0	0	0	0	0	0	?	0	1	2	0
Hipposaurus boonstrai	0	0	1	0	0	0	0	0	1	0	1	1	0	0	0	0	0	0	0	0	0	0	0	0	0	0	?	0	1	0	0
Archaeosyodon praeventor	0	0	1	0	0	0	?	?	0	1	0	0	0	0	0	0	1	0	0	0	0	0	0	0	0	0	?	0	1	2	0
Titanophoneus potens	0	0	1	0	0	0	0	0	0	1	0	0	0	0	0	0	1	0	0	0	0	0	0	0	0	0	?	0	1	2	0
Gorgonops torvus	0	0	1	0	0	0	0	0	1	0	0	0	0	0	0	0	0	0	0	0	0	0	0	0	0	0	?	0	1	2	0
Lycosuchus vanderrieti	0	0	1	0	0	0	0	0	0	1	0	0	1	0	0	0	1	1	0	0	0	0	0	0	0	0	?	0	1	2	0
Glanosuchus macrops	0	0	1	0	0	0	0	0	0	1	0	0	1	0	0	0	1	1	0	0	0	0	0	0	0	0	?	0	1	2	0
Biseridens qilianicus	0	0	1	0	0	1	?	?	0	0	0	0	0	0	0	0	1	0	0	0	0	0	0	0	0	0	?	0	0	?	0
Anomocephalus africanus	0	0	?	0	?	0	1	?	?	?	?	?	?	?	?	?	?	?	?	?	?	?	1	?	?	?	?	?	?	?	2
Tiarajudens eccentricus	0	0	?	0	?	0	1	?	?	?	?	?	?	?	?	?	?	?	?	?	0	1	1	?	?	?	?	0	?	?	2
Otsheria netzvetajevi	1	0	1	0	1	0	?	?	1	1	?	?	1	0	1	0	0	0	0	1	0	1	0	0	0	0	?	0	0	0	1
Ulemica	1	0	1	0	?	0	0	0	1	1	0	0	1	1	1	0	2	0	0	1	0	1	0	0	1	0	?	0	0	0	1
Suminia getmanovi	1	0	?	0	1	0	0	0	1	1	0	0	?	1	1	0	2	0	2	1	0	1	0	0	1	0	?	0	1	0	1
Patranomodon nyaphulii	1	0	0	0	0	0	0	0	0	0	0	0	1	0	0	0	1	0	?	0	1	1	0	0	0	0	?	0	1	0	1
Galeops whaitsi	1	0	1	0	?	0	0	1	0	0	0	0	1	?	0	0	1	0	?	0	?	1	0	0	0	0	?	0	?	0	1
Galepus jouberti	?	?	?	?	?	0	?	?	?	?	?	?	?	?	?	?	?	?	?	?	?	?	?	?	?	?	?	?	?	?	?
Galechirus scholtzi	?	?	?	0	?	0	?	?	?	?	?	?	?	?	?	?	?	?	?	?	?	?	?	?	?	?	?	?	?	?	?
Eodicynodon oelofseni	2	0	0	?	?	0	?	?	0	0	0	0	1	1	1	0	3	0	?	?	?	?	0	1	2	?	?	?	1	3	1
Eodicynodon oosthuizeni	2	0	1	0	1	0	1	0	0	0	0	0	1	1	1	0	3	0	1	0	0	1	0	1	2	1	0	0	1	3	1
Colobodectes cluveri	2	0	1	0	1	0	?	?	0	0	0	1	1	1	1	0	3	0	1	0	0	1	0	1	2	1	0	0	1	3	1
Lanthanostegus mohoii	0	0	?	0	?	0	?	?	0	?	?	?	1	1	1	0	3	0	1	?	0	1	0	1	2	1	1	0	?	3	1
Eosimops newtoni	2	0	1	1	1	0	1	0	1	0	[01]	[01]	1	1	1	0	3	0	1	0	0	1	0	1	2	1	0	0	1	3	1
Prosictodon dubei	2	0	1	1	1	0	1	0	1	0	0	0	1	1	1	0	3	0	1	0	0	1	0	1	2	1	0	0	1	2	1
Diictodon feliceps	2	0	1	1	1	0	1	0	1	1	1	1	1	1	1	0	3	0	1	0	0	1	0	1	2	1	0	0	1	2	1
Robertia broomiana	2	0	1	1	1	0	1	0	1	0	0	0	1	1	1	0	3	0	1	0	0	1	0	1	2	1	0	0	1	2	1
Pristerodon mackayi	2	0	1	1	1	0	1	0	1	0	0	0	1	1	1	0	3	0	2	1	0	1	0	1	2	1	0	0	1	2	1
Brachyprosopus broomi	2	0	1	0	1	0	1	0	0	0	0	0	1	1	1	0	3	0	2	0	0	1	0	1	2	1	0	0	1	2	1
Endothiodon bathystoma	2	0	1	0	1	1	1	0	1	0	0	0	1	1	1	1	3	0	2	1	0	1	0	1	2	0	?	0	1	3	1
Endothiodon tolani	2	?	?	0	?	1	1	0	1	1	0	0	1	1	1	1	3	0	2	1	0	1	0	1	2	1	0	0	1	3	1
Niassodon mfumukasi	2	0	1	0	1	0	1	0	1	0	0	0	1	1	1	1	3	1	1	1	0	?	0	1	2	1	1	0	1	2	1
Digalodon rubidgei	2	0	1	1	1	0	1	0	1	1	1	1	1	1	1	0	3	0	1	1	0	1	0	1	2	1	0	0	1	2	1
Emydops	2	0	1	1	1	0	1	0	1	1	1	1	1	1	1	0	3	0	1	1	0	1	0	1	2	1	1	0	0	2	1
Dicynodontoides	2	0	1	0	1	0	1	0	1	0	0	0	1	1	1	0	3	0	1	1	0	1	0	1	2	1	1	0	0	2	1
Kombuisia frerensis	2	0	?	0	1	0	1	?	1	?	?	?	1	1	1	0	3	0	1	1	0	1	0	?	2	1	1	0	0	?	1
Myosaurus gracilis	2	0	1	0	1	0	1	0	1	1	1	1	1	0	1	0	3	1	1	1	0	1	0	1	2	1	1	0	1	2	1
Sauroscaptor tharavati	2	0	0	1	1	0	1	0	1	1	?	?	1	1	1	0	3	?	?	1	0	?	0	1	2	1	1	?	1	3	1
Cistecephalus microrhinus	2	0	0	1	1	0	1	0	1	1	0	1	1	1	1	0	3	1	1	1	0	1	0	1	2	1	1	0	0	2	1
Cistecephaloides boonstrai	2	0	0	0	1	0	1	0	1	1	0	1	1	1	1	0	3	?	1	1	0	1	0	1	2	0	?	?	0	?	1
Kawingasaurus fossilis	2	0	0	1	?	0	1	0	1	1	0	1	1	1	1	0	3	1	1	1	0	1	0	1	2	0	?	0	0	1	1
Rhachiocephalus magnus	2	0	1	1	1	0	1	1	1	1	1	1	1	2	2	0	3	0	1	1	0	1	0	1	2	1	0	0	1	2	1
Kitchinganomodon crassus	2	0	1	1	1	0	1	1	1	1	0	1	1	2	2	0	3	0	1	1	0	1	0	1	2	1	0	0	1	3	1
Oudenodon bainii	2	0	1	1	1	0	1	0	1	1	1	1	1	2	2	0	3	0	1	1	0	1	0	1	2	1	0	0	1	2	1
Tropidostoma dubium	2	0	1	1	1	0	1	0	1	1	0	0	1	2	2	0	3	0	1	1	0	1	0	1	2	1	0	0	1	2	1
Australobarbarus	2	0	1	1	1	0	1	0	1	1	1	1	1	2	2	0	3	0	1	0	0	1	0	1	2	1	0	1	1	2	1
Odontocyclops whaitsi	2	0	1	1	1	0	1	0	1	1	1	1	1	2	2	0	3	0	1	1	0	1	0	1	2	1	0	0	1	2	1
Idelesaurus tataricus	2	0	1	1	1	0	1	0	1	1	0	0	1	2	2	0	3	0	1	1	1	1	0	1	2	1	0	0	1	2	1

	117	118	119	120	121	122	123	124	125	126	127	128	129	130	131	132	133	134	135	136	137	138	139	140	141	142	143	144	145	146	147
Biarmosuchus	1	?	?	0	?	?	0	0	?	0	?	?	0	0	0	0	?	?	0	0	0	0	0	0	0	0	0	0	0	0	0
Hipposaurus boonstrai	1	?	?	0	?	0	0	0	?	0	?	?	?	0	0	0	0	0	0	?	0	0	0	0	0	0	0	0	0	0	0
Archaeosyodon praeventor	1	?	?	0	?	?	?	0	?	?	?	?	?	?	?	?	?	?	?	?	0	0	0	0	1	1	0	0	0	0	0
Titanophoneus potens	1	0	0	0	0	0	0	0	?	0	0	1	0	0	0	0	1	0	0	0	0	0	0	0	0	0	0	0	0	0	0
Gorgonops torvus	1	0	0	0	0	0	0	0	?	0	0	0	0	0	0	0	0	0	0	0	0	0	0	0	0	0	0	0	0	0	0
Lycosuchus vanderrieti	1	0	0	1	0	0	0	0	1	0	0	1	?	0	0	0	0	0	0	0	0	0	0	0	0	0	0	0	0	0	0
Glanosuchus macrops	1	0	0	0	0	0	0	0	1	0	0	1	0	0	0	0	0	0	0	0	0	0	0	0	0	0	0	0	0	0	0
Biseridens qilianicus	1	?	?	?	?	?	?	0	?	0	?	?	?	0	0	0	1	0	0	?	0	0	1	0	1	0	0	1	0	0	0
Anomocephalus africanus	?	?	?	?	?	?	?	?	?	?	?	?	?	?	?	?	?	?	?	?	1	?	?	0	1	0	?	?	?	?	?
Tiarajudens eccentricus	?	?	?	?	?	?	?	?	?	?	?	?	?	?	?	?	?	?	?	?	?	?	?	?	?	?	?	?	?	?	?
Otsheria netzvetajevi	1	?	?	?	0	0	?	0	0	0	?	?	?	1	?	1	?	?	0	?	?	?	?	?	?	?	?	?	?	?	?
Ulemica	1	?	?	1	0	0	0	0	1	0	?	1	0	?	?	1	?	0	0	0	1	0	1	0	1	1	1	1	0	1	0
Suminia getmanovi	1	0	?	1	0	0	?	0	0	0	0	1	0	1	0	0	1	?	0	?	1	0	0	0	2	1	1	1	0	0	0
Patranomodon nyaphulii	1	?	?	0	0	0	1	1	0	0	?	1	0	1	0	0	1	0	0	?	1	0	?	0	1	0	0	1	0	0	0
Galeops whaitsi	1	0	?	1	?	1	?	1	?	?	?	?	?	?	?	?	?	?	?	?	1	0	0	0	?	?	0	1	0	0	0
Galepus jouberti	?	?	?	?	?	?	?	?	?	?	?	?	?	?	?	?	?	?	?	?	?	0	?	0	1	0	0	1	?	0	0
Galechirus scholtzi	?	?	?	?	?	?	?	?	?	?	?	?	?	?	?	?	?	?	?	?	1	0	?	0	1	0	0	1	0	0	?
Eodicynodon oelofseni	0	?	?	0	0	0	?	?	?	0	?	?	?	?	0	?	1	0	?	0	1	0	1	1	1	0	0	2	0	0	0
Eodicynodon oosthuizeni	0	0	1	0	0	0	0	1	0	0	0	0	1	1	0	1	1	0	0	0	1	0	1	0	1	0	0	2	0	0	1
Colobodectes cluveri	0	0	1	0	0	0	0	1	1	0	0	?	?	1	0	?	?	?	0	?	?	?	?	?	?	?	?	?	?	?	?
Lanthanostegus mohoii	0	?	1	0	0	?	0	1	1	0	?	?	?	?	?	?	?	?	?	?	?	?	?	?	?	?	?	?	?	?	?
Eosimops newtoni	0	0	?	0	0	0	0	1	1	0	0	1	?	1	?	1	1	0	0	?	1	0	1	1	?	?	?	4	0	0	0
Prosictodon dubei	0	?	?	0	0	0	1	1	1	0	0	1	1	1	?	1	1	0	0	?	1	0	1	1	?	?	?	2	0	?	1
Diictodon feliceps	0	0	0	0	0	0	1	1	2	0	0	1	1	1	0	1	1	0	0	0	1	0	1	2	?	?	?	2	0	0	1
Robertia broomiana	0	0	?	0	0	0	1	1	1	0	0	1	?	1	0	1	1	0	0	0	1	0	1	1	1	0	?	2	0	0	1
Pristerodon mackayi	0	0	1	0	0	0	1	1	2	0	0	1	1	1	0	1	1	0	0	0	1	0	1	1	2	0	0	2	?	0	1
Brachyprosopus broomi	1	0	1	0	0	0	1	1	2	0	0	1	?	1	1	1	1	0	0	0	1	0	1	1	2	0	0	2	0	0	1
Endothiodon bathystoma	0	0	0	0	0	0	1	1	2	0	0	1	?	1	?	1	1	0	0	0	1	0	1	1	2	0	0	3	0	1	1
Endothiodon tolani	0	0	0	0	0	0	?	1	2	0	0	?	?	1	1	1	1	0	0	0	1	0	1	1	2	0	0	3	0	1	1
Niassodon mfumukasi	0	0	0	0	0	0	1	1	1	0	0	1	1	1	1	1	1	0	0	0	1	0	1	1	?	?	0	4	0	0	?
Digalodon rubidgei	0	0	0	0	0	1	1	1	?	0	0	1	?	1	1	1	1	0	0	?	1	0	1	2	?	?	?	4	0	0	0
Emydops	0	0	0	0	0	1	1	1	2	0	0	1	0	1	1	1	1	0	1	0	1	0	1	1	[12]	0	0	4	0	0	0
Dicynodontoides	0	0	0	0	0	1	1	1	2	0	0	1	0	1	1	1	1	0	0	0	2	0	1	2	?	?	?	4	1	0	0
Kombuisia frerensis	?	?	1	0	0	1	1	1	2	0	0	1	0	1	1	0	1	0	0	?	2	0	1	2	?	?	?	4	1	0	1
Myosaurus gracilis	0	0	1	0	0	1	1	1	2	0	0	1	1	1	1	1	1	0	0	0	1	0	1	2	?	?	?	4	1	0	0
Sauroscaptor tharavati	?	?	?	?	0	1	?	1	?	0	0	?	?	?	?	1	1	0	0	?	1	1	1	?	?	?	?	4	0	0	0
Cistecephalus microrhinus	?	0	0	?	0	1	1	1	2	0	0	0	1	?	1	1	1	0	0	?	1	1	1	2	?	?	?	4	0	0	0
Cistecephaloides boonstrai	?	?	?	?	0	1	1	1	1	0	?	1	?	?	1	1	1	0	0	?	1	1	1	2	?	?	?	4	0	0	0
Kawingasaurus fossilis	?	?	?	?	0	1	1	1	1	0	?	0	?	?	0	1	1	0	0	0	1	0	1	2	?	?	?	?	?	0	0
Rhachiocephalus magnus	0	0	0	0	1	2	1	1	2	0	0	1	1	1	0	1	1	0	0	0	1	1	1	2	?	?	?	2	0	0	1
Kitchinganomodon crassus	?	0	?	0	1	2	1	1	2	0	1	1	?	1	0	1	1	0	0	?	1	1	1	2	?	?	?	2	0	0	1
Oudenodon bainii	0	0	0	0	1	2	1	1	2	0	0	1	1	1	0	1	1	0	0	0	1	1	1	2	?	?	?	2	0	0	1
Tropidostoma dubium	0	0	?	0	1	2	1	1	2	0	0	1	1	1	0	1	1	0	0	0	1	1	1	1	?	?	?	2	0	0	1
Australobarbarus	0	?	?	0	1	2	1	1	2	0	1	1	1	1	0	1	1	0	0	?	1	1	1	1	2	0	?	2	0	0	1
Odontocyclops whaitsi	0	0	?	0	1	2	1	1	2	0	1	1	?	1	0	1	1	0	0	?	1	1	1	2	?	?	?	2	0	0	1
Idelesaurus tataricus	0	0	0	0	0	2	1	1	2	0	1	?	?	1	0	0	1	0	0	?	1	1	1	2	?	?	?	2	1	0	1

	148	149	150	151	152	153	154	155	156	157	158	159	160	161	162	163	164	165	166	167	168	169	170	171	172	173	174	175	176	177	178
Biarmosuchus	0	0	0	?	?	0	0	0	0	0	0	0	0	0	0	0	0	0	?	0	0	0	0	?	1	0	0	0	0	1	1
Hipposaurus boonstrai	0	0	0	?	?	0	0	0	0	0	1	0	0	0	0	0	0	0	?	1	0	0	0	0	1	0	0	0	1	1	1
Archaeosyodon praeventor	0	0	0	?	?	0	0	0	?	?	?	?	?	?	?	?	0	?	?	?	?	?	?	?	?	?	?	?	?	?	?
Titanophoneus potens	0	0	0	?	?	0	0	0	1	0	0	0	0	0	0	0	0	0	?	0	0	0	0	0	?	0	0	0	0	0	0
Gorgonops torvus	0	0	0	?	?	0	0	0	0	0	1	1	0	0	0	0	0	0	?	0	0	0	0	0	1	0	0	0	1	0	0
Lycosuchus vanderrieti	0	0	0	?	?	0	1	0	0	0	2	0	1	0	0	0	0	0	?	0	0	0	0	0	1	0	0	0	1	0	0
Glanosuchus macrops	0	0	0	?	?	0	1	0	0	0	2	0	1	0	0	0	0	0	?	0	0	0	0	0	1	0	0	0	1	0	0
Biseridens qilianicus	0	0	0	?	?	0	0	0	0	0	0	?	1	?	?	?	0	?	?	?	?	?	?	?	?	?	?	?	?	?	?
Anomocephalus africanus	?	?	0	?	?	?	?	?	?	?	?	?	?	?	?	?	?	?	?	?	?	?	?	?	?	?	?	?	?	?	?
Tiarajudens eccentricus	?	?	?	?	?	?	?	?	?	?	?	?	?	?	?	?	?	?	?	?	0	0	?	?	?	0	0	0	1	0	1
Otsheria netzvetajevi	?	?	?	?	?	?	?	?	?	?	?	?	?	?	?	?	?	?	?	?	?	?	?	?	?	?	?	?	?	?	?
Ulemica	0	0	1	0	0	[01]	0	0	0	0	0	0	1	0	0	1	1	?	?	?	?	?	?	?	?	?	?	?	?	?	?
Suminia getmanovi	0	0	1	0	0	0	0	0	0	0	0	0	0	0	0	2	1	0	?	0	0	0	0	0	0	0	0	0	0	0	0
Patranomodon nyaphulii	0	0	0	?	?	?	?	0	0	0	3	1	0	0	0	0	1	0	?	?	?	?	?	?	?	?	?	?	?	?	?
Galeops whaitsi	0	0	1	0	0	?	1	0	1	1	3	1	0	0	0	1	1	?	?	0	0	1	0	0	0	0	0	0	0	1	0
Galepus jouberti	0	0	?	?	?	?	?	?	?	?	?	?	?	?	?	?	1	?	?	?	?	?	?	1	?	0	0	0	1	0	?
Galechirus scholtzi	?	0	?	?	?	?	?	?	?	0	3	1	?	?	?	?	1	?	?	?	0	0	0	0	?	?	0	?	1	0	0
Eodicynodon oelofseni	0	0	1	0	0	1	?	0	1	?	?	1	?	?	1	2	1	?	?	?	?	?	?	?	?	?	?	?	?	?	?
Eodicynodon oosthuizeni	0	0	2	0	0	1	0	0	1	1	3	1	1	1	1	2	1	0	?	0	0	0	1	0	0	0	0	0	0	1	1
Colobodectes cluveri	?	?	?	?	?	?	?	?	?	?	?	?	?	?	?	?	?	?	?	?	?	?	?	?	?	?	?	?	?	?	?
Lanthanostegus mohoii	?	?	?	?	?	?	?	?	?	?	?	?	?	?	?	?	?	?	?	?	?	?	?	?	?	?	?	?	?	?	?
Eosimops newtoni	1	1	1	0	0	0	0	0	1	1	3	1	?	1	1	2	1	0	?	1	0	0	1	1	?	0	0	0	0	0	1
Prosictodon dubei	1	1	1	0	0	?	0	?	1	?	?	1	?	?	1	2	1	?	?	?	?	?	?	?	?	?	?	?	?	?	?
Diictodon feliceps	1	1	1	0	0	1	0	0	1	1	3	1	1	1	1	2	1	1	?	1	0	0	1	1	0	0	0	0	0	0	0
Robertia broomiana	1	1	1	0	0	?	0	0	1	1	3	1	1	1	1	2	1	0	?	1	0	0	1	?	0	0	0	0	0	0	0
Pristerodon mackayi	2	0	2	0	0	1	0	0	1	1	3	1	1	1	1	2	1	2	?	1	1	0	1	0	0	0	0	0	0	1	0
Brachyprosopus broomi	2	0	1	0	0	1	0	0	1	1	3	1	1	1	1	2	1	?	?	0	0	0	1	?	?	0	0	0	0	1	0
Endothiodon bathystoma	2	0	2	0	0	1	0	0	1	1	4	1	1	1	1	2	1	2	?	0	0	0	1	0	?	0	0	0	0	1	0
Endothiodon tolani	2	0	2	0	0	1	0	0	1	1	4	1	1	1	1	2	1	?	?	?	?	?	?	?	?	?	?	?	?	?	?
Niassodon mfumukasi	2	0	2	0	0	1	0	0	1	1	4	?	1	1	1	2	1	1	?	?	?	?	?	?	?	?	?	?	?	?	?
Digalodon rubidgei	2	?	?	?	?	1	0	0	?	?	?	?	?	?	?	?	?	?	?	?	?	?	?	?	?	?	?	?	?	?	?
Emydops	2	0	2	1	0	1	0	0	1	1	3	1	1	1	1	2	1	0	?	1	?	0	1	0	?	0	0	0	0	0	0
Dicynodontoides	0	0	2	1	0	1	0	0	1	1	3	1	1	1	1	2	1	1	0	0	1	0	1	1	0	1	1	0	0	0	1
Kombuisia frerensis	0	0	2	0	0	1	?	0	1	1	?	1	1	0	1	2	1	?	?	?	?	?	?	?	?	?	?	?	?	?	?
Myosaurus gracilis	0	0	2	1	0	?	?	0	1	1	3	1	?	?	1	2	1	0	?	1	1	0	1	1	0	1	0	1	1	0	?
Sauroscaptor tharavati	?	0	2	1	0	1	0	?	?	1	?	1	?	?	?	?	1	?	?	?	?	?	?	?	?	?	?	?	?	?	?
Cistecephalus microrhinus	2	0	2	1	0	1	0	1	1	1	3	1	1	1	1	2	1	0	?	1	1	0	0	0	1	2	2	1	0	0	1
Cistecephaloides boonstrai	2	0	2	1	0	1	?	1	1	1	?	1	1	1	1	2	1	?	?	?	?	?	?	?	?	?	?	?	?	?	?
Kawingasaurus fossilis	0	0	1	0	0	1	1	1	1	?	?	?	1	1	1	2	1	?	?	1	1	0	0	0	?	2	2	0	0	0	1
Rhachiocephalus magnus	3	0	1	0	0	1	0	0	1	1	4	1	1	1	1	2	1	?	?	0	0	1	1	[01]	1	1	0	1	0	1	0
Kitchinganomodon crassus	?	0	1	2	1	?	?	0	?	1	4	1	1	?	1	2	1	?	?	?	0	0	?	?	?	1	0	?	0	1	0
Oudenodon bainii	3	0	1	2	1	1	0	0	1	1	4	1	1	1	1	2	1	2	0	0	0	0	1	0	0	1	0	1	0	1	0
Tropidostoma dubium	3	0	1	2	1	1	?	0	1	1	4	1	1	1	1	2	1	2	?	0	0	0	1	0	0	1	0	1	0	1	0
Australobarbarus	3	0	1	2	1	1	?	0	1	1	4	1	?	?	1	2	1	?	?	?	?	?	?	?	?	?	?	?	?	?	?
Odontocyclops whaitsi	3	0	1	2	1	?	?	0	1	1	4	1	1	?	1	2	1	2	0	0	0	0	1	?	?	1	0	1	0	1	0
Idelesaurus tataricus	3	0	1	2	1	1	?	0	1	1	4	1	1	1	1	2	1	?	?	?	?	?	?	?	?	?	?	?	?	?	?

	179	180	181	182	183	184	185	186	187	188	189	190	191	192	193	194
Biarmosuchus	0	1	?	0	0	0	1	1	0	0	0	0	1	1	0	?
Hipposaurus boonstrai	0	1	?	?	?	?	0	?	0	0	0	0	1	0	?	?
Archaeosyodon praeventor	?	?	?	?	?	?	?	?	?	?	?	?	?	?	?	?
Titanophoneus potens	0	0	1	1	0	0	1	1	0	0	0	1	2	?	1	?
Gorgonops torvus	0	1	0	0	0	1	1	0	1	1	1	0	0	1	1	?
Lycosuchus vanderrieti	0	1	1	1	0	?	?	?	0	0	0	?	?	?	?	?
Glanosuchus macrops	0	1	1	1	0	0	1	0	0	0	0	1	2	1	1	?
Biseridens qilianicus	?	?	?	?	?	?	?	?	?	?	?	?	?	?	?	?
Anomocephalus africanus	?	?	?	?	?	?	?	?	?	?	?	?	?	?	?	?
Tiarajudens eccentricus	0	?	?	?	?	?	?	?	?	?	?	1	2	?	1	?
Otsheria netzvetajevi	?	?	?	?	?	?	?	?	?	?	?	?	?	?	?	?
Ulemica	?	?	?	?	?	?	?	?	?	?	?	?	?	?	?	?
Suminia getmanovi	0	1	0	0	0	0	0	0	0	0	0	0	0	1	0	?
Patranomodon nyaphulii	?	0	1	1	0	?	?	?	0	0	0	?	?	?	?	?
Galeops whaitsi	0	?	?	?	?	?	?	?	?	?	?	?	?	?	?	0
Galepus jouberti	0	?	1	1	?	0	0	?	0	0	0	?	2	?	1	?
Galechirus scholtzi	0	0	1	1	?	0	0	?	0	0	0	1	2	1	1	?
Eodicynodon oelofseni	?	?	?	?	?	?	?	?	?	?	?	?	?	?	?	?
Eodicynodon oosthuizeni	0	?	1	1	0	1	0	0	0	0	0	1	?	?	?	1
Colobodectes cluveri	?	?	?	?	?	?	?	?	?	?	?	?	?	?	?	?
Lanthanostegus mohoii	?	?	?	?	?	?	?	?	?	?	?	?	?	?	?	?
Eosimops newtoni	0	?	1	1	0	1	0	0	0	0	0	1	?	?	?	?
Prosictodon dubei	?	?	?	?	?	?	?	?	?	?	?	?	?	?	?	?
Diictodon feliceps	0	?	1	1	0	1	0	0	0	0	0	1	2	1	1	0
Robertia broomiana	0	?	1	1	?	?	?	0	0	0	0	1	2	1	1	?
Pristerodon mackayi	0	?	1	1	0	1	?	0	0	0	0	1	2	1	1	?
Brachyprosopus broomi	?	?	?	?	?	?	?	?	0	1	?	?	?	?	?	?
Endothiodon bathystoma	0	?	1	1	0	1	1	?	0	0	0	1	2	1	1	0
Endothiodon tolani	?	?	?	?	?	?	?	?	?	?	?	?	?	?	?	?
Niassodon mfumukasi	?	?	?	?	0	1	?	?	?	1	?	?	?	?	?	?
Digalodon rubidgei	?	?	?	?	?	?	?	?	?	?	?	?	?	?	?	?
Emydops	0	1	1	1	0	?	?	?	0	0	0	1	2	1	1	?
Dicynodontoides	?	1	?	?	0	1	1	0	0	1	1	1	2	1	1	0
Kombuisia frerensis	?	?	?	?	?	?	?	?	?	?	?	?	?	?	?	?
Myosaurus gracilis	?	?	?	?	0	?	?	?	?	?	?	?	?	?	?	0
Sauroscaptor tharavati	?	?	?	?	?	?	?	?	?	?	?	?	?	?	?	?
Cistecephalus microrhinus	1	1	1	1	0	1	0	0	1	1	0	1	2	1	1	0
Cistecephaloides boonstrai	?	?	?	?	?	?	?	?	?	?	?	?	?	?	?	?
Kawingasaurus fossilis	1	?	1	1	?	?	?	?	?	?	?	1	2	1	1	?
Rhachiocephalus magnus	0	?	?	?	?	?	?	?	0	1	1	?	?	?	?	1
Kitchinganomodon crassus	?	?	?	?	?	?	?	?	?	?	?	?	?	?	?	?
Oudenodon bainii	0	?	1	1	0	1	1	1	0	1	1	1	2	1	1	0
Tropidostoma dubium	0	?	?	?	0	?	?	?	0	1	1	?	?	?	?	0
Australobarbarus	?	?	?	?	?	?	?	?	?	?	?	?	?	?	?	?
Odontocyclops whaitsi	0	?	?	?	0	1	1	1	0	1	1	?	?	?	?	?
Idelesaurus tataricus	?	?	?	?	?	?	?	?	?	?	?	?	?	?	?	?

	24	25	26	27	28	29	30	31	32	33	34	35	36	37	38	39	40	41	42	43	44	45	46	47	48	49	50	51	52	53	54
Aulacephalodon bainii	1	2	0	0	2	2	1	2	1	0	1	1	1	0	0	0	2	0	0	0	0	2	2	?	?	1	1	0	1	0	[01]
Pelanomodon moschops	1	2	0	0	2	2	1	2	1	0	1	1	1	0	0	0	2	0	0	0	0	1	2	?	?	1	1	0	1	0	1
Geikia locusticeps	1	2	0	0	2	2	1	2	1	0	1	1	1	0	0	0	2	0	0	0	0	1	2	?	?	1	1	0	1	0	1
Geikia elginensis	1	2	0	0	2	2	?	2	1	0	1	1	1	0	0	0	2	0	0	0	0	1	2	?	?	1	1	0	1	0	1
Elph borealis	1	?	?	0	2	?	?	2	1	0	1	0	0	0	0	0	2	0	1	0	0	2	2	?	?	1	1	0	1	0	0
Interpresosaurus blomi	1	2	0	0	?	?	1	2	1	0	1	0	0	0	0	0	2	0	1	0	0	2	2	?	?	1	1	0	1	0	0
Katumbia parringtoni	1	2	0	0	2	2	1	2	1	0	1	?	0	0	0	0	?	?	1	0	0	2	2	?	?	1	1	0	0	0	0
Delectosaurus arefjevi	1	2	0	0	2	2	1	2	1	0	1	0	0	0	0	0	2	1	0	0	0	2	2	?	?	1	1	0	1	0	0
Dicynodon lacerticeps	1	2	0	0	2	2	1	2	1	0	1	0	0	0	0	0	2	0	0	0	0	2	2	?	?	1	1	0	1	0	0
Dicynodon huenei	1	2	0	0	2	2	?	2	1	0	1	0	0	0	0	0	2	0	0	0	0	2	2	?	?	1	1	0	1	0	0
Daptocephalus leoniceps	1	2	0	0	2	2	?	2	1	0	1	0	0	0	0	0	2	0	0	0	0	2	2	?	?	1	1	0	1	0	0
Daqingshanodon limbus	1	2	0	0	2	2	1	2	1	0	1	0	0	0	0	0	2	0	0	0	0	2	2	?	?	1	1	0	1	0	1
Dinanomodon gilli	1	2	0	0	2	2	1	2	1	0	1	0	0	0	0	0	2	1	1	0	1	2	2	?	?	1	1	0	1	0	0
Peramodon amalitzkii	1	?	?	0	?	?	?	?	?	0	?	0	0	0	0	0	2	0	1	0	0	2	?	?	?	1	1	?	1	0	0
Vivaxosaurus trautscholdi	1	2	0	0	2	2	?	2	1	0	1	0	0	0	0	0	2	0	1	0	0	2	2	?	?	1	1	0	1	0	0
Jimusaria sinkiangensis	1	2	0	0	?	?	?	2	1	0	1	1	0	0	0	0	2	0	0	0	0	2	?	?	?	1	1	0	2	0	0
Sintocephalus alticeps	1	2	0	0	2	2	?	2	1	0	1	0	0	0	0	?	2	0	0	0	0	2	2	?	?	1	1	0	0	0	0
Basilodon woodwardi	1	2	0	0	2	2	?	2	1	0	1	1	0	0	0	0	2	0	0	0	0	2	2	?	?	1	1	0	0	0	0
Turfanodon bogdaensis	1	2	?	0	?	?	?	2	1	0	1	?	0	0	0	0	?	?	?	0	?	2	2	?	?	1	1	0	1	0	0
Keyseria benjamini	1	2	0	0	2	2	?	2	1	0	1	0	0	0	0	?	2	0	0	0	0	2	2	?	?	1	1	0	1	0	1
Gordonia traquairi	1	2	0	0	2	2	?	2	1	?	1	0	0	0	0	?	?	0	0	0	0	2	2	?	?	1	1	0	1	0	0
Syops vanhoepeni	1	?	?	0	1	2	?	2	1	0	1	1	0	0	0	?	2	0	0	0	0	2	2	?	?	1	1	0	1	0	1
Euptychognathus bathyrhynchus	1	2	0	0	2	2	?	2	1	0	1	1	0	1	1	0	2	0	0	0	0	2	2	?	?	1	1	0	1	0	0
Lystrosaurus hedini	1	2	0	0	2	2	1	2	1	0	1	1	1	1	1	0	2	0	0	0	0	2	2	?	?	1	1	0	1	0	0
Lystrosaurus maccaigi	1	2	0	0	2	2	?	2	1	0	1	1	1	1	1	?	2	0	0	0	0	2	2	?	?	1	1	0	1	0	0
Lystrosaurus curvatus	1	2	0	0	2	2	?	2	1	0	1	1	1	1	1	0	2	0	0	0	0	2	2	?	?	1	1	0	1	0	0
Lystrosaurus declivis	1	2	0	0	2	2	1	2	1	0	1	1	1	1	1	0	2	0	0	0	0	2	2	?	?	1	1	0	1	0	0
Lystrosaurus murrayi	1	2	0	0	2	2	1	2	1	0	1	1	1	1	1	0	2	0	0	0	0	2	2	?	?	1	1	0	1	0	0
Angonisaurus cruickshanki	1	2	0	0	2	2	?	2	1	?	1	1	0	0	0	0	2	?	0	0	1	1	2	?	?	1	1	0	1	0	0
Tetragonias njalilus	1	2	0	0	2	2	1	2	1	0	1	1	0	0	0	0	2	0	0	0	0	2	2	?	?	1	1	0	[12]	0	0
Shansiodon	1	2	0	0	2	2	1	2	1	0	1	1	0	0	0	0	2	0	0	0	0	2	2	?	?	1	1	0	1	0	0
Vinceria andina	1	2	0	0	2	2	?	2	1	0	1	1	0	0	0	?	2	0	0	0	0	2	2	?	?	1	1	0	2	0	0
Rhinodicynodon gracile	1	2	0	0	2	2	?	2	1	0	1	1	0	0	0	0	2	0	0	0	0	2	2	?	?	1	1	0	1	0	0
Dinodontosaurus	1	2	0	0	2	2	?	2	1	0	1	1	0	0	0	0	2	0	1	0	0	2	2	?	?	1	1	0	1	0	0
Kannemeyeria simocephalus	1	2	0	0	2	2	?	2	1	0	1	0	0	0	0	0	2	1	1	0	0	2	2	?	?	0	1	0	2	0	0
Kannemeyeria lophorhinus	1	2	0	0	2	2	?	2	1	0	1	0	0	0	2	0	2	1	1	0	1	2	2	?	?	0	1	0	1	0	0
Dolichuranus primaevus	1	2	0	0	2	2	?	2	1	0	1	1	0	0	0	0	2	1	1	0	0	2	2	?	?	1	1	0	2	0	0
Wadiasaurus indicus	1	2	0	0	2	2	?	2	1	0	1	0	0	0	0	?	2	1	1	0	0	[12]	2	?	?	1	1	0	?	0	0
Rabidosaurus cristatus	1	2	0	?	2	2	?	2	1	0	1	0	0	0	0	0	2	1	1	0	0	2	2	?	?	1	1	0	?	0	0
Rhadiodromus	1	2	0	0	2	2	?	2	1	0	1	1	0	0	0	0	2	0	1	0	0	2	2	?	?	1	1	0	2	0	0
Rechnisaurus cristarhynchus	1	2	0	0	2	2	?	2	1	0	1	1	0	0	2	?	2	0	1	0	1	2	2	?	?	1	1	0	?	0	0
Uralokannemeyeria vjuschkovi	1	2	0	0	2	2	?	2	1	?	1	1	0	0	2	?	2	?	?	0	1	2	2	?	?	?	1	0	?	0	0
Shaanbeikannemeyeria	1	2	0	0	2	2	?	2	1	0	1	1	0	0	0	0	2	0	1	0	0	2	2	?	?	1	1	0	1	0	0
Xiyukannemeyeria brevirostris	1	2	0	?	?	?	?	2	1	0	1	1	0	0	2	?	2	0	2	0	0	2	2	?	?	1	1	0	2	0	0
Parakannemeyeria	1	2	0	0	2	2	?	2	1	0	1	1	0	0	2	0	2	0	2	0	1	2	2	?	?	1	1	0	2	0	0
Sinokannemeyeria	1	2	0	0	2	2	?	2	1	0	1	0	0	0	2	0	2	1	2	0	0	2	2	?	?	1	1	0	1	0	0

	55	56	57	58	59	60	61	62	63	64	65	66	67	68	69	70	71	72	73	74	75	76	77	78	79	80	81	82	83	84	85
Aulacephalodon bainii	0	0	2	0	1	1	2	0	0	[01]	1	0	0	[12]	0	0	1	0	0	1	0	0	0	[12]	0	0	2	1	1	1	0
Pelanomodon moschops	0	0	2	0	1	1	2	0	0	1	1	0	0	2	1	0	1	0	0	1	0	0	0	2	0	0	2	1	1	2	0
Geikia locusticeps	0	0	2	0	1	1	2	1	0	1	1	0	0	2	1	1	1	1	0	0	0	0	0	2	?	0	2	0	1	2	0
Geikia elginensis	1	1	2	0	?	?	2	1	?	?	1	0	0	?	?	?	?	1	0	0	0	0	?	?	?	0	2	1	1	2	0
Elph borealis	1	0	0	0	0	0	0	1	0	0	0	0	0	1	0	1	1	2	0	0	0	0	0	1	0	0	2	1	1	0	0
Interpresosaurus blomi	1	?	0	?	0	0	0	1	0	0	?	?	?	1	0	?	?	2	?	1	?	?	?	?	?	?	?	?	?	?	?
Katumbia parringtoni	1	0	1	0	0	0	0	1	0	0	0	0	0	1	1	1	1	2	0	0	0	0	0	1	0	0	2	1	1	?	0
Delectosaurus arefjevi	0	0	1	1	0	0	0	1	0	0	0	0	0	2	0	1	1	2	0	1	0	1	0	1	0	0	2	1	1	0	0
Dicynodon lacerticeps	0	0	1	[01]	0	0	1	1	0	0	0	0	0	2	0	1	1	2	0	1	0	1	0	1	0	0	2	1	1	0	0
Dicynodon huenei	0	0	1	0	0	0	1	1	0	[01]	0	0	0	2	0	1	1	2	0	1	0	1	0	1	0	0	2	1	1	0	0
Daptocephalus leoniceps	1	0	1	1	0	0	1	1	0	0	0	0	0	2	0	1	1	2	0	1	0	1	0	1	0	0	2	1	1	0	0
Daqingshanodon limbus	0	0	2	0	0	?	0	0	0	1	0	0	0	1	0	1	1	1	0	0	0	0	0	0	0	0	2	1	1	?	0
Dinanomodon gilli	0	1	1	1	0	0	1	1	0	0	0	0	0	2	0	1	1	2	0	1	0	1	0	1	0	0	2	1	1	0	0
Peramodon amalitzkii	1	0	1	1	0	0	0	1	0	0	0	0	0	2	0	1	1	2	0	1	0	?	0	1	0	0	2	1	1	0	0
Vivaxosaurus trautscholdi	0	1	1	1	0	0	0	0	0	0	0	0	0	2	0	1	1	1	0	1	0	1	0	1	0	0	2	1	1	0	0
Jimusaria sinkiangensis	0	0	1	0	0	0	0	1	0	0	0	0	0	1	0	1	1	2	0	1	0	1	0	1	0	1	2	1	1	0	0
Sintocephalus alticeps	0	0	0	1	0	1	1	0	0	0	0	0	0	1	0	1	1	1	0	1	0	?	0	1	0	1	2	1	?	0	0
Basilodon woodwardi	0	0	2	0	0	1	1	1	0	0	0	0	0	2	0	1	1	1	0	1	0	0	0	1	0	1	2	1	1	0	0
Turfanodon bogdaensis	1	1	1	1	0	0	1	0	0	0	?	?	0	2	0	1	1	2	0	1	0	1	0	1	0	1	2	1	1	0	0
Keyseria benjamini	1	0	2	0	0	0	0	0	0	0	0	0	0	1	0	1	1	0	0	0	0	?	0	0	0	0	2	1	1	0	0
Gordonia traquairi	1	?	2	?	0	?	0	1	0	?	0	0	0	1	0	1	1	2	0	1	0	?	0	1	0	?	2	1	1	0	0
Syops vanhoepeni	1	0	2	0	0	1	1	?	0	0	?	?	0	2	0	1	1	2	0	1	0	1	0	1	0	0	?	?	1	?	?
Euptychognathus bathyrhynchus	1	?	0	?	1	?	1	0	0	0	0	0	0	1	0	1	1	2	0	1	0	1	0	1	0	?	2	1	1	0	0
Lystrosaurus hedini	0	0	2	0	0	1	1	0	0	0	1	0	0	1	0	1	1	0	0	1	0	1	0	1	0	0	2	1	1	0	0
Lystrosaurus maccaigi	1	1	0	1	0	1	1	1	0	?	1	0	0	2	0	?	1	0	0	1	0	?	0	1	0	0	2	1	1	0	0
Lystrosaurus curvatus	1	0	2	1	0	1	1	1	0	0	1	0	0	2	0	1	1	0	0	1	0	1	0	1	0	0	2	1	1	0	0
Lystrosaurus declivis	1	0	2	1	2	1	1	1	0	0	1	0	0	2	0	1	1	0	0	1	0	1	0	1	0	0	2	1	1	0	0
Lystrosaurus murrayi	1	0	2	0	2	1	1	0	0	0	1	0	0	2	0	1	1	0	0	1	0	1	0	1	0	0	2	1	1	0	0
Angonisaurus cruickshanki	1	?	?	?	0	0	1	0	0	1	1	0	0	2	0	1	1	0	0	1	1	1	0	1	0	1	2	0	1	0	0
Tetragonias njalilus	1	0	2	0	0	0	1	0	0	1	0	0	0	1	0	1	1	2	0	1	1	2	0	1	0	1	2	0	1	0	0
Shansiodon	1	?	2	?	0	0	1	1	0	1	0	0	0	2	0	1	1	2	0	1	1	2	0	1	0	1	2	0	1	0	0
Vinceria andina	1	0	2	0	0	?	1	0	0	1	0	0	0	1	0	1	1	2	0	1	1	2	0	1	0	1	2	0	1	0	0
Rhinodicynodon gracile	1	0	2	1	0	0	1	1	0	1	0	0	0	1	0	1	1	2	0	1	1	2	0	1	0	0	2	0	1	0	0
Dinodontosaurus	1	0	3	1	0	0	1	0	0	1	0	0	0	2	0	1	1	2	0	1	1	2	0	1	0	1	2	0	1	0	0
Kannemeyeria simocephalus	0	0	3	2	0	0	0	0	0	1	1	0	1	2	0	1	1	2	1	1	0	2	0	1	0	1	2	1	1	0	0
Kannemeyeria lophorhinus	0	0	3	2	0	0	2	0	0	1	0	0	1	1	0	1	1	2	1	1	0	2	0	1	0	1	2	1	1	0	?
Dolichuranus primaevus	0	0	3	0	0	0	1	0	0	1	1	0	0	1	0	1	1	2	1	1	0	2	0	1	0	1	2	0	1	0	0
Wadiasaurus indicus	0	?	?	?	0	0	1	0	?	?	0	0	1	?	?	1	1	0	1	1	?	?	0	?	?	1	2	0	1	0	0
Rabidosaurus cristatus	0	?	3	?	0	0	1	0	0	1	1	?	1	2	0	1	?	0	?	1	?	?	0	1	0	?	2	1	1	?	?
Rhadiodromus	0	0	3	1	0	[01]	1	0	0	1	1	0	1	1	1	1	1	2	0	1	0	2	0	1	0	?	2	0	1	0	0
Rechnisaurus cristarhynchus	0	0	3	0	0	0	1	0	0	1	0	0	1	?	?	1	?	1	0	1	0	2	0	1	0	?	2	?	?	0	?
Uralokannemeyeria vjuschkovi	0	?	?	?	?	0	1	?	0	1	1	0	1	2	0	1	1	1	0	1	0	?	0	1	0	?	2	0	1	?	0
Shaanbeikannemeyeria	0	0	3	1	0	0	1	0	0	1	1	0	1	1	0	1	1	2	0	1	0	?	0	1	0	1	2	1	1	0	0
Xiyukannemeyeria brevirostris	1	0	3	?	0	1	1	0	0	1	1	0	1	2	0	1	1	2	0	1	0	1	0	1	0	?	2	0	1	0	0
Parakannemeyeria	0	0	3	?	0	1	1	0	0	1	1	0	1	2	0	1	1	2	0	1	0	1	0	1	0	1	2	0	1	0	0
Sinokannemeyeria	0	0	3	1	0	?	1	0	0	1	1	0	1	2	0	1	1	2	0	1	0	1	0	1	0	1	2	0	1	0	0

	86	87	88	89	90	91	92	93	94	95	96	97	98	99	100	101	102	103	104	105	106	107	108	109	110	111	112	113	114	115	116
Aulacephalodon bainii	2	0	1	1	1	0	1	0	1	1	0	1	1	2	2	0	3	0	1	1	1	1	0	1	2	1	0	0	1	2	1
Pelanomodon moschops	2	0	1	1	1	0	1	0	1	1	1	1	1	2	2	0	3	0	1	1	1	1	0	1	2	1	0	[01]	1	2	1
Geikia locusticeps	2	0	1	1	1	0	1	0	1	1	1	1	1	2	2	0	3	0	1	1	1	1	0	1	2	1	0	1	1	2	1
Geikia elginensis	2	0	1	?	?	0	1	?	1	1	1	1	1	?	2	0	3	0	?	1	?	?	0	1	2	1	0	?	?	2	1
Elph borealis	2	0	1	1	1	0	1	0	?	?	?	?	1	2	2	0	3	0	1	1	0	1	0	?	2	1	0	0	?	1	1
Interpresosaurus blomi	?	?	?	?	?	?	?	?	1	?	?	?	1	?	?	?	3	0	?	?	0	?	?	?	?	?	?	?	?	?	?
Katumbia parringtoni	2	0	1	1	?	0	1	0	1	1	1	1	1	2	2	0	3	0	1	1	0	1	0	1	2	1	0	1	0	2	1
Delectosaurus arefjevi	2	0	1	1	1	0	1	0	1	1	1	1	1	2	1	0	3	0	1	1	1	[12]	0	1	2	1	0	1	1	2	1
Dicynodon lacerticeps	2	0	1	1	1	0	1	0	1	1	1	1	1	2	1	0	3	0	1	1	1	1	0	1	2	1	0	0	1	2	1
Dicynodon huenei	2	0	1	1	1	0	1	0	1	1	1	1	1	2	1	0	3	0	1	1	1	1	0	1	2	1	0	1	1	2	1
Daptocephalus leoniceps	2	0	1	1	1	0	1	0	1	1	1	1	1	2	1	0	3	0	1	1	1	1	0	1	2	1	0	1	0	1	1
Daqingshanodon limbus	2	0	1	1	1	0	1	0	1	1	?	?	1	2	2	0	3	0	1	1	0	1	0	1	2	1	0	0	1	2	1
Dinanomodon gilli	2	0	1	1	1	0	1	0	1	1	1	1	1	2	1	0	3	0	1	1	1	1	0	1	2	1	1	1	0	2	1
Peramodon amalitzkii	2	0	1	1	?	0	1	0	?	?	?	?	?	?	?	?	?	?	?	?	?	?	?	1	2	?	?	?	?	2	1
Vivaxosaurus trautscholdi	2	0	1	1	1	0	1	0	1	1	0	0	1	2	1	0	3	0	1	1	1	[12]	0	1	2	1	0	1	1	2	1
Jimusaria sinkiangensis	2	0	1	1	1	0	1	0	?	?	?	?	1	2	1	0	3	0	1	?	1	1	0	1	2	1	0	0	?	2	1
Sintocephalus alticeps	2	0	?	1	?	0	?	?	?	?	?	?	1	2	1	0	3	0	1	1	?	1	0	1	2	1	0	1	?	2	1
Basilodon woodwardi	2	0	1	1	1	0	1	0	1	1	1	1	1	2	2	0	3	0	1	1	1	1	0	1	2	1	0	1	?	2	1
Turfanodon bogdaensis	2	0	1	?	1	0	?	?	?	?	?	?	1	2	1	0	3	0	1	?	?	2	0	1	2	1	1	1	1	2	1
Keyseria benjamini	2	0	1	1	1	0	1	0	1	1	?	?	1	2	2	0	3	0	?	1	?	1	0	1	2	1	0	0	0	2	1
Gordonia traquairi	2	0	1	1	?	0	1	0	?	1	?	?	1	?	1	0	3	?	?	?	?	?	?	1	2	1	0	1	?	?	1
Syops vanhoepeni	?	?	?	1	1	?	?	0	1	1	1	1	1	2	2	0	3	0	1	1	1	1	?	1	2	1	?	1	?	?	1
Euptychognathus bathyrhynchus	2	0	1	1	1	0	1	0	1	1	1	1	1	2	1	0	3	0	?	1	?	?	?	1	2	1	0	?	1	2	1
Lystrosaurus hedini	2	0	1	1	1	0	1	0	1	1	1	1	1	2	1	0	3	0	1	1	1	2	?	1	2	1	0	1	0	4	1
Lystrosaurus maccaigi	2	0	1	1	1	0	1	?	1	1	1	1	1	2	1	0	3	0	1	0	1	2	?	1	2	1	0	1	0	4	1
Lystrosaurus curvatus	2	0	1	1	1	0	1	0	1	1	1	1	1	2	1	0	3	0	1	0	1	2	?	1	2	1	0	1	1	2	1
Lystrosaurus declivis	2	0	1	1	1	0	1	0	1	1	1	1	1	2	1	0	3	0	1	0	1	2	?	1	2	1	0	1	1	2	1
Lystrosaurus murrayi	2	0	1	1	1	0	1	0	1	1	1	1	1	2	1	0	3	0	1	0	1	2	?	1	2	1	0	1	1	2	1
Angonisaurus cruickshanki	2	0	1	1	1	0	?	?	1	1	1	1	1	?	?	?	3	0	?	1	?	?	?	1	2	1	0	1	?	?	1
Tetragonias njalilus	2	1	1	1	1	0	1	0	1	1	1	1	1	2	1	0	3	0	1	0	1	2	?	1	2	1	0	1	0	2	1
Shansiodon	2	1	1	1	1	0	1	?	?	?	?	?	1	2	1	0	3	0	1	?	1	2	?	1	2	1	0	1	?	?	1
Vinceria andina	2	0	1	1	1	0	?	?	1	1	1	1	1	?	?	?	3	0	?	?	1	2	?	1	2	1	0	1	0	2	1
Rhinodicynodon gracile	2	1	1	1	1	0	1	0	?	?	?	?	1	2	1	0	3	0	?	1	1	2	?	1	2	1	0	1	?	?	1
Dinodontosaurus	2	1	1	1	1	0	1	0	1	1	1	1	1	2	1	0	3	0	0	0	1	1	0	1	2	1	0	1	0	1	1
Kannemeyeria simocephalus	2	0	1	1	1	0	1	0	1	1	1	1	1	2	1	0	3	0	1	1	1	2	?	1	2	1	0	1	0	1	1
Kannemeyeria lophorhinus	2	0	1	1	1	0	1	?	1	1	1	1	1	2	1	0	3	0	1	?	1	2	?	1	2	1	0	1	1	1	1
Dolichuranus primaevus	2	0	1	1	1	0	1	0	1	1	1	1	1	2	1	0	3	0	1	0	1	1	0	1	2	1	0	1	1	6	1
Wadiasaurus indicus	2	0	1	?	1	0	1	0	?	?	?	?	1	?	?	?	3	0	?	?	1	2	?	1	2	1	0	1	?	?	1
Rabidosaurus cristatus	2	?	1	1	1	0	?	?	?	?	?	?	1	2	?	?	3	0	1	0	1	?	?	1	2	1	?	1	?	1	1
Rhadiodromus	2	0	1	1	1	0	?	?	1	1	1	1	1	2	1	0	3	0	?	1	?	1	0	1	2	?	?	1	?	?	1
Rechnisaurus cristarhynchus	2	?	?	?	?	?	?	?	?	?	?	?	1	2	1	0	3	0	?	0	1	1	0	1	2	1	0	1	?	?	1
Uralokannemeyeria vjuschkovi	2	0	1	1	1	0	1	0	1	1	1	1	1	?	?	?	3	0	?	?	?	?	?	1	2	?	?	?	1	2	1
Shaanbeikannemeyeria	2	1	1	1	1	0	1	?	1	1	1	1	1	2	1	0	3	0	1	1	1	?	0	1	2	1	0	1	?	2	1
Xiyukannemeyeria brevirostris	2	1	1	1	1	0	1	0	1	1	1	1	1	2	?	?	3	0	1	?	1	2	?	1	2	?	?	1	0	2	1
Parakannemeyeria	2	1	1	1	1	0	1	0	1	1	1	1	1	2	1	0	3	0	1	?	1	2	?	1	2	1	0	1	0	1	1
Sinokannemeyeria	2	1	1	1	1	0	1	1	1	1	1	1	1	2	1	0	3	0	1	?	?	2	?	1	2	1	0	1	?	2	1

	117	118	119	120	121	122	123	124	125	126	127	128	129	130	131	132	133	134	135	136	137	138	139	140	141	142	143	144	145	146	147
Aulacephalodon bainii	0	0	0	0	1	2	1	1	2	[01]	0	1	1	1	0	1	1	0	0	0	1	1	1	2	?	?	?	2	0	0	1
Pelanomodon moschops	0	0	?	0	1	2	1	1	2	1	0	1	1	1	0	1	1	0	0	?	?	?	?	?	?	?	?	?	?	?	?
Geikia locusticeps	0	0	0	0	2	2	1	1	2	1	0	1	1	1	0	1	1	0	0	?	1	1	1	2	?	?	?	2	1	0	1
Geikia elginensis	0	?	1	0	?	?	?	?	?	?	?	?	?	?	?	?	?	?	0	?	1	0	1	2	?	?	?	2	1	0	1
Elph borealis	?	0	0	0	1	2	1	1	2	0	?	?	?	1	0	1	1	0	0	?	1	1	1	2	?	?	?	2	0	?	1
Interpresosaurus blomi	?	?	?	?	?	?	?	?	?	?	?	?	?	?	?	?	?	?	?	?	?	?	?	?	?	?	?	?	?	?	?
Katumbia parringtoni	0	?	?	0	1	2	1	1	2	1	1	1	1	?	0	0	1	0	0	?	1	1	1	2	?	?	?	2	1	0	1
Delectosaurus arefjevi	1	0	?	0	1	2	1	1	2	1	?	?	?	1	0	0	1	0	0	0	?	?	?	?	?	?	?	?	?	?	?
Dicynodon lacerticeps	0	0	0	0	2	2	1	1	2	1	1	1	1	1	0	1	1	0	0	1	1	1	1	2	?	?	?	2	1	0	1
Dicynodon huenei	0	0	0	0	2	2	1	1	2	1	1	1	1	1	0	1	1	0	0	1	1	1	1	2	?	?	?	2	?	0	1
Daptocephalus leoniceps	1	0	1	0	1	2	1	1	2	1	1	1	1	1	0	1	1	1	0	1	1	1	1	2	?	?	?	2	1	0	1
Daqingshanodon limbus	0	?	0	0	?	?	1	1	?	?	?	?	?	1	0	1	1	?	0	?	1	1	1	2	?	?	?	2	1	0	1
Dinanomodon gilli	1	?	?	0	1	2	1	1	2	1	1	1	1	1	0	1	1	?	0	1	1	?	1	?	?	?	?	?	1	0	?
Peramodon amalitzkii	?	0	?	0	?	2	?	1	2	1	?	1	1	?	0	?	1	?	?	?	1	1	1	?	?	?	?	2	1	0	?
Vivaxosaurus trautscholdi	1	0	?	0	2	2	1	1	2	[01]	?	1	?	1	0	1	1	0	0	1	1	1	1	2	?	?	?	2	1	0	1
Jimusaria sinkiangensis	1	0	1	0	2	2	1	1	2	1	1	1	?	1	0	?	?	?	0	?	1	1	1	2	?	?	?	2	1	0	1
Sintocephalus alticeps	0	?	?	0	?	?	?	?	?	?	?	?	?	?	?	?	?	?	?	?	?	?	?	?	?	?	?	?	?	?	?
Basilodon woodwardi	0	?	?	0	1	2	1	1	2	1	?	1	?	1	?	1	1	0	1	?	1	?	1	?	?	?	?	?	1	?	?
Turfanodon bogdaensis	1	?	?	0	1	2	1	1	2	1	?	?	?	1	0	1	1	0	0	1	?	?	?	?	?	?	?	?	?	?	?
Keyseria benjamini	0	?	?	0	1	?	1	1	2	1	0	1	1	1	?	1	1	0	0	?	?	?	?	?	?	?	?	?	?	?	?
Gordonia traquairi	?	?	?	0	?	?	?	1	2	?	?	1	1	?	?	?	1	?	0	?	1	1	1	2	?	?	?	2	?	0	?
Syops vanhoepeni	?	?	?	?	?	2	?	?	?	?	0	?	?	1	?	0	1	0	?	?	1	?	1	?	?	?	?	2	0	0	?
Euptychognathus bathyrhynchus	0	?	?	0	2	2	1	1	?	1	1	?	?	1	0	1	1	0	0	?	1	1	1	2	?	?	?	2	1	0	1
Lystrosaurus hedini	1	?	?	0	2	2	1	1	2	1	0	?	?	1	0	1	1	0	0	1	1	1	1	2	?	?	?	2	1	0	1
Lystrosaurus maccaigi	1	?	?	0	2	2	1	1	2	1	0	?	?	1	?	1	1	0	0	?	1	1	1	2	?	?	?	2	1	0	1
Lystrosaurus curvatus	1	0	0	0	2	2	1	1	2	1	?	?	?	1	0	0	1	0	0	1	1	1	1	?	?	?	?	1	0	?
Lystrosaurus declivis	1	0	0	0	2	2	1	1	2	1	0	1	1	1	0	0	1	0	0	1	1	1	1	2	?	?	?	2	1	0	1
Lystrosaurus murrayi	1	?	0	0	2	2	1	1	2	1	1	1	1	1	0	1	1	0	0	0	1	1	1	2	?	?	?	2	1	0	1
Angonisaurus cruickshanki	1	0	?	0	2	2	1	1	2	0	?	?	?	1	?	1	1	0	?	1	1	1	1	2	?	?	?	2	1	0	1
Tetragonias njalilus	1	0	1	0	?	2	1	1	2	1	1	1	1	1	0	1	1	0	0	1	1	1	1	2	?	?	?	2	1	0	1
Shansiodon	?	0	?	0	2	2	1	1	2	0	?	1	1	1	?	1	1	0	0	1	1	1	1	2	?	?	?	2	0	0	1
Vinceria andina	1	?	?	0	2	2	?	1	?	0	?	1	1	1	?	1	1	?	?	?	1	?	?	2	?	?	?	?	?	?	?
Rhinodicynodon gracile	?	0	?	0	2	2	?	1	?	?	?	?	?	1	?	0	1	0	0	?	1	1	1	2	?	?	?	2	1	0	1
Dinodontosaurus	1	?	1	0	2	2	?	1	2	1	1	?	?	?	0	1	0	0	0	1	1	1	1	2	?	?	?	2	1	0	1
Kannemeyeria simocephalus	1	1	1	0	2	2	1	2	2	0	1	?	?	1	0	1	0	0	1	1	1	1	1	2	?	?	?	2	1	0	1
Kannemeyeria lophorhinus	1	0	1	0	2	2	?	?	2	0	1	?	?	1	?	0	0	0	?	?	1	1	1	2	?	?	?	2	1	0	1
Dolichuranus primaevus	1	0	?	0	2	2	1	2	2	0	0	?	?	1	?	1	0	0	1	?	1	1	1	2	?	?	?	2	1	0	1
Wadiasaurus indicus	?	?	?	0	2	2	?	?	2	0	?	?	?	1	?	1	1	?	1	?	1	1	1	2	?	?	?	2	?	?	1
Rabidosaurus cristatus	?	?	?	0	?	2	?	?	?	?	1	?	?	1	?	?	0	0	?	1	?	?	?	?	?	?	?	?	?	?	?
Rhadiodromus	?	1	1	0	2	2	?	2	2	0	?	?	?	1	0	1	1	0	?	?	?	?	?	?	?	?	?	?	?	?	?
Rechnisaurus cristarhynchus	?	?	?	0	2	2	1	2	2	0	?	?	?	?	?	?	?	0	?	?	?	?	?	?	?	?	?	?	?	?	?
Uralokannemeyeria vjuschkovi	1	?	?	0	2	2	?	2	2	0	?	?	?	1	?	1	0	0	?	?	?	?	?	?	?	?	?	?	?	?	?
Shaanbeikannemeyeria	1	?	?	0	2	2	1	2	2	0	?	?	?	?	?	1	0	0	?	?	1	1	1	2	?	?	?	2	0	?	1
Xiyukannemeyeria brevirostris	1	?	?	0	2	2	?	?	2	0	?	1	1	1	?	0	0	0	?	?	1	1	1	2	?	?	?	2	1	0	?
Parakannemeyeria	1	0	?	0	2	2	?	?	2	0	1	1	1	1	0	1	0	0	1	1	1	1	1	2	?	?	?	2	1	0	1
Sinokannemeyeria	1	?	?	0	2	2	1	?	2	0	?	1	1	1	0	1	0	0	1	1	1	1	1	2	?	?	?	2	1	0	1

	148	149	150	151	152	153	154	155	156	157	158	159	160	161	162	163	164	165	166	167	168	169	170	171	172	173	174	175	176	177	178
Aulacephalodon bainii	3	0	1	2	1	1	1	0	1	1	4	1	1	1	1	2	1	2	1	0	0	0	1	0	0	1	0	1	0	1	0
Pelanomodon moschops	?	?	?	?	?	?	?	?	?	?	?	?	?	?	?	2	?	?	?	?	?	?	?	?	?	?	?	?	?	?	?
Geikia locusticeps	3	0	1	0	1	1	0	0	1	1	4	1	1	1	1	2	1	?	?	0	0	?	1	0	?	?	?	?	?	?	?
Geikia elginensis	3	0	1	2	1	?	?	?	?	?	4	1	?	?	1	2	1	?	?	?	?	?	?	?	?	?	0	1	0	1	?
Elph borealis	3	0	1	2	1	1	1	0	?	?	?	?	?	?	?	2	1	?	?	?	?	?	?	?	?	?	?	?	?	?	?
Interpresosaurus blomi	?	?	?	?	?	?	?	?	?	?	?	?	?	?	?	?	?	?	?	?	?	?	?	?	?	?	?	?	?	?	?
Katumbia parringtoni	3	0	1	2	1	1	1	0	?	?	?	?	?	?	?	2	1	?	?	?	?	?	?	?	?	?	?	?	?	?	?
Delectosaurus arefjevi	?	?	?	?	?	?	?	?	?	?	?	?	?	?	?	?	?	?	?	?	?	?	?	?	?	?	?	?	?	?	?
Dicynodon lacerticeps	3	0	2	2	1	1	1	1	1	1	5	1	1	1	1	2	1	?	?	?	?	?	?	?	?	?	?	?	?	?	?
Dicynodon huenei	3	0	2	2	1	1	1	?	1	1	5	1	1	1	1	2	1	2	?	0	0	0	1	0	1	1	0	1	0	1	0
Daptocephalus leoniceps	3	0	2	2	1	1	1	1	1	1	5	1	1	1	1	2	1	?	?	?	?	?	?	?	?	1	0	1	1	1	0
Daqingshanodon limbus	3	0	1	2	1	1	?	0	1	1	4	1	1	1	1	2	1	?	?	?	?	?	?	?	?	?	?	?	?	?	?
Dinanomodon gilli	3	?	1	2	1	?	?	1	?	1	5	1	1	?	1	2	?	?	?	?	?	?	?	?	?	?	?	?	?	?	?
Peramodon amalitzkii	?	?	2	2	1	1	1	1	?	1	5	1	1	?	1	2	?	3	?	1	0	0	1	0	1	?	?	?	?	?	?
Vivaxosaurus trautscholdi	3	0	2	2	1	?	?	1	1	1	5	1	1	0	1	2	1	?	?	0	0	0	?	?	1	1	0	1	1	1	0
Jimusaria sinkiangensis	3	0	2	2	1	1	0	1	1	1	5	1	1	?	1	2	1	?	?	?	?	?	?	?	?	?	?	?	?	?	?
Sintocephalus alticeps	?	?	?	?	?	?	?	?	?	?	?	?	?	?	?	2	?	?	?	?	?	?	?	?	?	?	?	?	?	?	?
Basilodon woodwardi	?	?	2	2	1	?	?	?	?	?	?	1	?	?	?	2	?	?	?	?	?	?	?	?	?	?	?	?	?	?	?
Turfanodon bogdaensis	?	?	?	?	?	?	?	?	?	?	?	?	?	?	?	?	?	?	?	?	?	?	?	?	?	?	?	?	?	?	?
Keyseria benjamini	?	?	?	?	?	?	?	?	?	?	?	?	?	?	?	2	?	?	?	?	?	?	?	?	?	?	?	?	?	?	?
Gordonia traquairi	3	0	2	2	1	?	?	?	?	1	?	1	?	?	1	2	1	?	?	?	0	0	1	?	?	1	0	?	0	1	0
Syops vanhoepeni	?	?	?	?	?	?	?	0	?	?	?	1	1	?	1	2	?	?	?	?	?	?	?	?	?	?	?	?	?	?	?
Euptychognathus bathyrhynchus	3	0	2	2	1	1	?	1	?	?	?	1	?	?	?	2	1	?	?	?	?	?	?	?	?	?	?	?	?	?	?
Lystrosaurus hedini	3	0	2	2	1	1	0	1	1	1	5	1	1	0	1	2	1	?	?	?	?	?	1	?	?	?	?	?	?	?	?
Lystrosaurus maccaigi	3	0	2	2	1	?	?	1	1	1	5	1	?	?	1	2	1	3	?	?	?	?	?	?	?	?	0	1	0	1	0
Lystrosaurus curvatus	?	?	2	2	1	1	0	1	?	1	5	1	1	?	1	2	?	?	?	0	0	0	1	?	?	1	0	1	0	1	?
Lystrosaurus declivis	3	0	2	2	1	1	0	1	1	1	5	1	1	0	1	2	1	3	?	0	0	?	?	1	?	?	1	0	1	1	0
Lystrosaurus murrayi	3	0	2	2	1	1	0	1	1	1	5	1	1	0	1	2	1	?	?	0	0	0	1	1	1	1	0	1	1	1	0
Angonisaurus cruickshanki	3	0	1	2	1	1	0	1	1	0	0	1	1	?	1	2	1	3	?	?	0	0	1	0	0	?	1	0	?	1	0
Tetragonias njalilus	3	0	1	2	1	1	0	1	1	0	5	1	1	1	1	2	1	2	0	0	0	0	1	0	0	1	1	1	0	1	0
Shansiodon	3	0	2	2	1	1	0	?	?	0	?	1	?	?	1	2	1	2	?	0	0	0	1	?	?	1	1	1	0	1	1
Vinceria andina	?	?	?	?	?	?	?	?	?	?	?	?	?	?	1	2	1	?	?	?	?	?	?	?	?	?	?	?	?	?	?
Rhinodicynodon gracile	3	0	2	2	1	?	?	1	1	?	?	1	?	?	1	2	1	?	?	0	0	0	1	0	0	1	0	1	?	1	0
Dinodontosaurus	3	0	1	2	1	1	0	0	1	0	?	1	1	?	1	2	1	3	0	0	0	0	1	0	0	1	1	0	0	1	0
Kannemeyeria simocephalus	3	0	2	2	1	1	0	1	1	1	5	1	1	1	1	2	1	3	0	0	0	1	1	0	0	1	0	1	0	1	0
Kannemeyeria lophorhinus	3	0	1	2	1	?	?	1	1	0	?	0	1	0	1	2	1	?	?	?	0	0	?	?	?	1	1	?	1	1	0
Dolichuranus primaevus	3	0	1	2	1	1	?	1	1	0	?	1	1	?	1	2	1	?	?	0	0	0	0	?	?	1	1	0	0	1	0
Wadiasaurus indicus	3	0	?	?	?	?	?	?	?	?	?	1	1	?	1	2	1	2	0	0	1	0	1	?	0	1	1	1	1	1	0
Rabidosaurus cristatus	?	?	?	?	?	?	?	?	?	?	?	?	?	?	?	?	?	?	?	?	?	?	?	?	?	?	1	?	?	?	?
Rhadiodromus	?	?	?	?	?	?	?	?	?	?	?	?	?	?	?	?	?	?	?	?	?	?	?	?	?	?	?	?	?	?	?
Rechnisaurus cristarhynchus	?	?	?	?	?	?	?	?	?	?	?	?	?	?	?	?	?	?	?	?	?	?	?	?	?	?	?	?	?	?	?
Uralokannemeyeria vjuschkovi	?	?	?	?	?	?	?	?	?	?	?	?	?	?	?	2	?	2	?	?	?	?	?	?	?	?	?	?	?	?	?
Shaanbeikannemeyeria	?	?	1	2	1	?	?	?	?	?	?	?	?	1	?	2	1	?	?	?	0	0	1	?	?	1	?	?	1	1	0
Xiyukannemeyeria brevirostris	?	?	1	2	1	1	?	?	1	?	?	1	1	?	1	2	1	?	?	?	0	?	1	?	?	1	1	1	0	?	0
Parakannemeyeria	?	0	1	2	1	?	?	?	1	?	?	1	1	?	1	2	1	3	?	0	0	0	1	0	0	1	0	1	0	1	0
Sinokannemeyeria	3	0	1	2	1	1	?	?	?	0	?	1	1	?	1	2	1	2	0	0	0	0	1	0	?	1	1	1	0	1	0

	179	180	181	182	183	184	185	186	187	188	189	190	191	192	193	194
Aulacephalodon bainii	0	?	1	1	0	1	0	1	0	1	1	1	2	1	1	1
Pelanomodon moschops	?	?	?	?	?	?	?	?	?	?	?	?	?	?	?	?
Geikia locusticeps	?	?	?	?	?	?	?	?	?	?	?	?	?	?	?	?
Geikia elginensis	?	?	?	?	?	?	?	?	?	?	?	?	?	?	?	?
Elph borealis	?	?	?	?	?	?	?	?	?	?	?	?	?	?	?	?
Interpresosaurus blomi	?	?	?	?	?	?	?	?	?	?	?	?	?	?	?	?
Katumbia parringtoni	?	?	?	?	?	?	?	?	?	?	?	?	?	?	?	?
Delectosaurus arefjevi	?	?	?	?	?	?	?	?	?	?	?	?	?	?	?	?
Dicynodon lacerticeps	?	?	?	?	?	?	?	?	?	?	?	?	?	?	?	?
Dicynodon huenei	0	?	1	1	0	1	1	1	0	1	1	?	?	?	?	?
Daptocephalus leoniceps	?	?	?	?	0	1	1	1	?	?	?	?	?	?	?	?
Daqingshanodon limbus	?	?	?	?	?	?	?	?	?	?	?	?	?	?	?	?
Dinanomodon gilli	?	?	?	?	?	?	?	?	?	?	?	?	?	?	?	?
Peramodon amalitzkii	?	?	?	?	?	?	?	?	?	?	?	?	?	?	?	?
Vivaxosaurus trautscholdi	?	?	?	?	?	?	?	?	?	?	?	?	?	?	?	?
Jimusaria sinkiangensis	?	?	?	?	?	?	?	?	?	?	?	?	?	?	?	?
Sintocephalus alticeps	?	?	?	?	?	?	?	?	?	?	?	?	?	?	?	?
Basilodon woodwardi	?	?	?	?	?	?	?	?	?	?	?	?	?	?	?	?
Turfanodon bogdaensis	?	?	?	?	?	?	?	?	?	?	?	?	?	?	?	?
Keyseria benjamini	?	?	?	?	?	?	?	?	?	?	?	?	?	?	?	?
Gordonia traquairi	0	?	?	?	0	?	?	?	?	?	?	?	?	?	?	?
Syops vanhoepeni	?	?	?	?	?	?	?	?	?	?	?	?	?	?	?	?
Euptychognathus bathyrhynchus	?	?	?	?	?	?	?	?	?	?	?	?	?	?	?	?
Lystrosaurus hedini	?	?	?	?	?	?	?	?	?	?	?	?	?	?	?	?
Lystrosaurus maccaigi	0	?	1	1	?	1	1	?	0	0	1	1	2	1	1	1
Lystrosaurus curvatus	0	?	?	?	1	?	?	?	0	0	1	?	?	?	?	1
Lystrosaurus declivis	0	?	1	1	1	1	1	1	0	1	1	1	2	1	1	1
Lystrosaurus murrayi	0	?	1	1	1	?	?	1	0	1	1	1	2	1	1	1
Angonisaurus cruickshanki	?	?	?	?	0	1	1	1	?	?	?	?	?	?	?	?
Tetragonias njalilus	0	?	1	1	0	1	1	1	1	1	2	1	2	1	1	?
Shansiodon	1	?	1	1	0	?	?	?	1	1	1	1	2	1	1	?
Vinceria andina	?	?	?	?	?	?	?	?	?	?	?	?	?	?	?	?
Rhinodicynodon gracile	0	?	?	?	0	1	1	1	1	1	2	?	?	?	?	?
Dinodontosaurus	1	?	1	1	0	1	1	1	0	1	2	1	2	1	1	?
Kannemeyeria simocephalus	0	?	1	1	0	1	1	1	0	1	1	1	2	1	1	1
Kannemeyeria lophorhinus	?	?	?	?	0	?	?	?	?	?	?	?	?	?	?	?
Dolichuranus primaevus	1	?	?	?	?	?	?	?	0	1	2	?	?	?	?	?
Wadiasaurus indicus	1	?	?	?	0	1	1	1	1	1	1	?	?	?	?	?
Rabidosaurus cristatus	?	?	?	?	?	?	?	?	?	?	?	?	?	?	?	?
Rhadiodromus	?	?	?	?	?	?	?	?	?	?	?	?	?	?	?	?
Rechnisaurus cristarhynchus	?	?	?	?	?	?	?	?	?	?	?	?	?	?	?	?
Uralokannemeyeria vjuschkovi	?	?	?	?	0	?	?	?	?	?	?	?	?	?	?	?
Shaanbeikannemeyeria	0	?	?	?	?	?	?	?	0	1	1	?	?	?	?	?
Xiyukannemeyeria brevirostris	0	?	1	1	0	?	?	?	0	1	1	1	2	1	1	?
Parakannemeyeria	0	?	1	1	0	1	1	1	[01]	1	1	1	2	1	1	?
Sinokannemeyeria	1	?	1	1	0	?	?	?	0	1	1	1	2	1	1	?

	24	25	26	27	28	29	30	31	32	33	34	35	36	37	38	39	40	41	42	43	44	45	46	47	48	49	50	51	52	53	54
Stahleckeria potens	1	2	0	0	2	0	?	2	1	0	1	1	0	0	0	0	2	1	2	0	1	1	2	?	?	1	1	0	1	0	0
Eubrachiosaurus browni	?	?	?	?	?	?	?	?	?	?	?	?	?	?	?	?	?	?	?	?	?	?	?	?	?	?	?	?	?	?	?
Sangusaurus parringtonii	1	2	0	0	2	2	?	2	1	0	1	1	0	0	0	0	0	0	1	0	1	1	2	?	?	0	1	0	1	0	0
Ischigualastia jenseni	1	2	0	0	2	2	?	2	1	0	1	1	0	0	0	0	2	1	2	0	1	1	2	?	?	1	1	0	1	0	0
Jachaleria	1	2	0	0	2	2	1	2	1	0	1	1	0	0	0	0	2	1	1	0	1	1	2	?	?	1	1	0	1	0	0
Zambiasaurus submersus	1	2	0	0	2	2	?	2	1	?	?	1	?	?	?	?	?	?	?	0	0	1	2	?	?	?	1	?	0	?	?
Placerias hesternus	1	2	0	0	0	2	?	2	1	?	?	0	0	0	2	0	2	0	0	0	0	2	2	?	?	1	1	1	0	0	0
Moghreberia nmachouensis	1	?	0	0	0	2	?	2	1	0	1	0	0	0	2	?	?	0	2	0	0	2	2	?	?	?	1	0	2	0	0
Rastodon procurvidens	1	?	?	?	?	?	?	2	1	0	1	0	0	0	0	0	2	0	0	0	0	2	?	?	?	1	1	0	0	0	0
Bulbasaurus phylloxyron	1	2	0	0	2	2	1	2	1	0	1	1	0	0	0	0	2	0	0	0	0	2	2	?	?	1	1	0	1	0	0
Compsodon helmoedi	1	0	1	1	1	0	1	2	1	0	1	0	0	0	0	1	2	0	1	0	0	2	0	0	1	1	1	1	0	1	0
LPB 1993 3	1	2	0	0	2	2	1	2	1	0	1	0	0	0	0	?	?	?	0	0	0	2	2	?	?	1	1	0	1	0	0
LPB 1993 2	1	2	0	0	2	2	1	2	1	0	?	1	0	0	0	0	?	1	0	0	?	2	2	?	?	1	1	0	1	0	0
LPB 1995 9	1	2	0	0	2	0	1	2	1	0	1	?	0	0	0	?	?	1	0	0	0	2	2	?	?	0	1	0	1	0	0

	55	56	57	58	59	60	61	62	63	64	65	66	67	68	69	70	71	72	73	74	75	76	77	78	79	80	81	82	83	84	85
Stahleckeria potens	0	0	3	1	0	0	1	0	1	1	1	0	1	0	?	1	1	0	0	1	0	1	0	1	0	2	2	0	1	0	0
Eubrachiosaurus browni	?	?	?	?	?	?	?	?	?	?	?	?	?	?	?	?	?	?	?	?	?	?	?	?	?	?	?	?	?	?	?
Sangusaurus parringtonii	0	0	3	1	0	0	2	0	1	1	1	0	0	1	0	1	1	1	0	1	0	2	0	1	0	2	2	0	1	0	0
Ischigualastia jenseni	0	0	3	1	0	0	1	0	1	1	1	0	1	1	0	1	1	2	0	1	1	2	0	1	0	2	2	0	1	0	0
Jachaleria	1	0	3	1	0	1	1	0	1	1	1	0	0	2	0	1	1	2	0	1	1	2	0	1	0	2	2	0	1	0	0
Zambiasaurus submersus	?	?	?	?	?	?	?	0	0	?	?	?	1	0	?	1	1	0	0	?	?	?	0	1	0	2	2	0	?	?	?
Placerias hesternus	0	0	3	1	0	?	1	0	0	1	1	0	1	1	0	1	0	0	0	1	1	1	0	1	0	2	2	0	1	0	1
Moghreberia nmachouensis	0	?	3	?	0	?	?	0	0	1	1	?	1	2	0	1	0	0	0	1	1	1	0	1	0	2	2	0	?	0	1
Rastodon procurvidens	0	0	1	0	0	0	0	0	0	0	0	0	0	1	0	1	1	1	0	0	0	0	0	0	0	0	2	1	1	0	0
Bulbasaurus phylloxyron	0	[01]	2	[01]	1	0	0	0	0	1	1	0	0	2	0	1	1	[12]	0	1	0	0	0	[12]	0	0	2	1	1	1	0
Compsodon helmoedi	1	0	1	0	0	0	0	1	0	0	0	0	0	2	1	1	0	1	0	0	0	0	0	3	0	0	2	1	1	0	0
LPB 1993 3	0	?	?	2	?	?	?	?	?	?	?	?	0	?	?	?	?	?	?	?	0	?	0	1	0	0	2	1	1	0	0
LPB 1993 2	1	?	1	0	0	?	1	0	?	?	1	0	0	2	0	1	1	1	0	0	0	0	0	1	0	0	2	1	1	0	0
LPB 1995 9	1	?	1	0	0	0	1	0	0	1	?	0	0	1	0	?	1	1	0	0	0	0	0	1	0	0	2	1	1	?	0

	86	87	88	89	90	91	92	93	94	95	96	97	98	99	100	101	102	103	104	105	106	107	108	109	110	111	112	113	114	115	116
Stahleckeria potens	2	0	1	1	1	0	1	0	1	1	1	1	1	2	1	0	3	0	1	1	1	1	0	1	2	1	1	1	0	1	1
Eubrachiosaurus browni	?	?	?	?	?	?	?	?	?	?	?	?	?	?	?	?	?	?	?	?	?	?	?	?	?	?	?	?	?	?	?
Sangusaurus parringtonii	2	0	0	1	1	0	1	0	1	?	?	?	1	2	1	0	3	0	1	1	1	2	?	1	2	1	0	1	0	1	1
Ischigualastia jenseni	2	0	0	1	1	0	1	1	1	1	1	1	1	2	1	0	3	0	?	?	1	2	?	1	2	1	0	1	0	5	1
Jachaleria	2	0	0	1	1	0	1	1	1	1	1	1	1	2	1	0	3	0	1	0	?	2	?	1	2	1	0	1	0	1	1
Zambiasaurus submersus	2	?	1	?	?	?	?	0	?	?	?	?	?	?	?	?	?	?	?	?	?	?	?	?	?	?	?	?	?	?	?
Placerias hesternus	2	0	1	1	1	0	1	0	?	?	?	?	?	?	?	?	?	?	?	?	?	?	?	1	?	?	?	?	0	5	1
Moghreberia nmachouensis	2	0	1	?	?	0	?	0	1	1	1	1	1	2	1	0	3	0	1	1	?	?	?	?	2	1	0	?	?	?	1
Rastodon procurvidens	2	0	1	1	1	0	1	0	?	1	1	0	?	?	?	?	?	?	?	?	0	?	?	1	2	1	0	?	1	2	1
Bulbasaurus phylloxyron	2	0	1	1	1	0	1	0	1	1	0	1	1	2	2	0	3	0	1	1	0	1	0	1	2	1	0	0	1	2	1
Compsodon helmoedi	2	0	1	1	?	0	1	0	1	1	1	0	1	1	1	0	3	1	1	1	0	1	0	1	2	1	1	0	0	2	0
LPB 1993 3	2	0	1	1	?	0	?	?	1	1	1	1	1	2	1	0	3	0	1	?	?	1	0	1	2	1	0	1	0	2	1
LPB 1993 2	2	0	1	?	?	0	?	?	?	?	?	?	1	?	?	?	?	?	?	?	?	1	0	1	2	?	?	1	0	?	1
LPB 1995 9	2	?	?	1	?	0	?	?	1	1	1	1	1	2	1	0	3	0	?	?	?	1	0	1	2	1	0	1	?	2	1

	117	118	119	120	121	122	123	124	125	126	127	128	129	130	131	132	133	134	135	136	137	138	139	140	141	142	143	144	145	146	147
Stahleckeria potens	1	1	1	0	2	2	1	1	2	1	1	1	?	1	0	1	0	0	0	1	1	1	1	2	?	?	?	2	1	0	1
Eubrachiosaurus browni	?	?	?	?	?	?	?	?	?	?	?	?	?	?	?	?	?	?	?	?	?	?	?	?	?	?	?	?	?	?	?
Sangusaurus parringtonii	1	1	1	0	2	2	1	1	2	1	?	?	?	1	1	1	0	0	0	1	1	1	1	2	?	?	?	?	1	0	1
Ischigualastia jenseni	1	?	1	0	2	2	1	3	2	0	?	1	1	1	0	1	0	0	0	?	1	1	1	2	?	?	?	2	1	0	1
Jachaleria	1	?	1	0	2	2	1	3	2	0	0	?	?	1	0	1	0	0	0	?	?	1	1	2	?	?	?	2	?	0	1
Zambiasaurus submersus	?	?	?	?	?	?	?	?	?	?	?	?	?	?	?	1	1	0	?	?	?	?	1	2	?	?	?	2	?	?	1
Placerias hesternus	1	1	0	0	2	2	?	?	2	0	?	1	1	1	?	1	0	1	?	1	1	1	1	2	?	?	?	2	0	0	1
Moghreberia nmachouensis	?	?	0	?	2	2	1	?	2	0	?	?	?	?	?	1	0	1	?	?	1	1	1	2	?	?	?	2	?	0	1
Rastodon procurvidens	0	0	?	0	0	?	?	1	?	0	0	?	?	1	0	1	1	0	0	?	1	0	1	?	?	?	?	2	0	0	?
Bulbasaurus phylloxyron	0	0	0	0	1	2	1	1	2	0	?	?	?	1	0	1	1	0	0	?	1	1	1	?	?	?	?	2	1	0	1
Compsodon helmoedi	0	0	?	0	1	1	1	1	2	0	0	1	1	1	1	0	1	0	1	?	1	?	?	?	?	?	?	?	?	?	?
LPB 1993 3	1	0	?	0	2	2	?	1	2	0	?	?	?	?	?	0	1	0	1	1	?	?	?	?	?	?	?	?	?	?	?
LPB 1993 2	1	?	?	0	2	2	?	1	2	0	?	?	?	?	?	0	1	?	?	1	?	?	?	?	?	?	?	?	?	?	?
LPB 1995 9	1	0	?	0	2	?	?	?	2	0	?	?	?	?	?	?	?	?	1	?	?	?	?	?	?	?	?	?	?	?	?

	148	149	150	151	152	153	154	155	156	157	158	159	160	161	162	163	164	165	166	167	168	169	170	171	172	173	174	175	176	177	178
Stahleckeria potens	3	0	1	2	1	1	0	1	1	1	0	0	1	1	1	2	1	3	1	0	1	0	1	0	0	1	1	1	0	1	0
Eubrachiosaurus browni	?	?	?	?	?	?	?	?	?	?	?	?	?	?	?	?	?	?	?	?	1	0	1	?	?	1	?	0	0	1	0
Sangusaurus parringtonii	3	0	1	2	1	1	1	1	?	1	0	0	1	1	1	2	1	3	?	?	?	?	?	?	?	?	?	?	?	?	?
Ischigualastia jenseni	3	0	1	?	?	?	?	1	?	?	0	0	1	?	1	2	1	2	1	0	1	0	0	1	0	1	1	0	0	1	0
Jachaleria	?	0	?	?	?	?	?	?	?	?	?	?	?	?	1	2	1	2	1	0	0	1	0	?	?	?	1	?	?	?	?
Zambiasaurus submersus	?	?	?	?	?	?	0	?	?	?	?	?	?	?	?	?	1	?	0	?	1	1	1	0	0	1	?	0	1	1	0
Placerias hesternus	3	0	?	?	?	1	0	?	?	1	?	1	?	?	1	2	1	?	0	0	1	1	1	0	0	1	?	0	0	1	0
Moghreberia nmachouensis	3	0	1	2	1	1	0	?	?	?	?	0	?	?	1	2	1	?	?	?	?	?	?	?	?	?	?	?	?	?	?
Rastodon procurvidens	?	0	2	0	0	1	0	0	?	1	?	1	?	?	?	?	1	?	?	?	?	?	?	?	?	?	?	?	?	?	?
Bulbasaurus phylloxyron	?	0	1	2	1	1	?	?	?	?	?	?	?	?	?	?	1	?	?	?	?	?	?	?	?	?	?	?	0	?	?
Compsodon helmoedi	?	?	?	?	?	?	?	?	?	?	?	?	?	?	?	?	?	?	?	?	?	?	?	?	?	?	?	?	?	?	?
LPB 1993 3	?	?	?	?	?	?	?	?	?	?	?	?	?	?	?	?	?	?	?	?	?	?	?	?	?	?	?	?	?	?	?
LPB 1993 2	?	?	?	?	?	?	?	?	?	?	?	?	?	?	?	?	?	?	?	?	?	?	?	?	?	?	?	?	?	?	?
LPB 1995 9	?	?	?	?	?	?	?	?	?	?	?	?	?	?	?	?	?	?	?	?	?	?	?	?	?	?	?	?	?	?	?

	179	180	181	182	183	184	185	186	187	188	189	190	191	192	193	194
Stahleckeria potens	1	?	1	1	0	1	1	1	1	1	1	1	2	1	1	?
Eubrachiosaurus browni	?	?	?	?	0	?	?	?	?	?	?	?	?	?	?	?
Sangusaurus parringtonii	?	?	?	?	0	1	1	1	1	1	1	?	?	?	?	?
Ischigualastia jenseni	1	?	1	1	0	1	1	1	1	1	1	1	2	1	1	?
Jachaleria	1	?	?	?	0	1	1	1	1	1	1	?	?	?	?	?
Zambiasaurus submersus	0	?	?	?	0	1	1	1	1	1	1	?	?	?	?	?
Placerias hesternus	?	?	?	?	0	1	1	1	1	1	1	?	?	?	?	1
Moghreberia nmachouensis	?	?	?	?	?	?	?	?	?	?	?	?	?	?	?	?
Rastodon procurvidens	?	?	?	?	?	?	?	?	?	?	?	?	?	?	?	?
Bulbasaurus phylloxyron	?	?	?	?	?	?	?	?	?	?	?	?	?	?	?	?
Compsodon helmoedi	?	?	?	?	?	?	?	?	?	?	?	?	?	?	?	?
LPB 1993 3	?	?	?	?	?	?	?	?	?	?	?	?	?	?	?	?
LPB 1993 2	?	?	?	?	?	?	?	?	?	?	?	?	?	?	?	?
LPB 1995 9	?	?	?	?	?	?	?	?	?	?	?	?	?	?	?	?

Bibliography

Angielczyk, K. D. 2001. Preliminary phylogenetic analysis and stratigraphic congruence of the dicynodont anomodonts (Synapsida: Therapsida). Palaeontologica Africana 37:53–79.

Angielczyk, K. D. 2004. Phylogenetic evidence for and implications of a dual origin of propaliny in anomodont therapsids. Paleobiology 30:268–296.

Angielczyk, K. D. 2007. New specimens of the Tanzanian dicynodont "*Cryptocynodon*" *parringtoni* von Huene, 1943 (Therapsida, Anomodontia), with an expanded analysis of Permian dicynodont phylogeny. Journal of Vertebrate Paleontology 27: 116–131.

Angielczyk, K. D., and C. F. Kammerer. 2017. The cranial morphology, phylogenetic position and biogeography of the upper Permian dicynodont *Compsodon helmoedi* van Hoepen (Therapsida, Anomodontia). Papers in Palaeontology 1–33.

Angielczyk, K. D., and A. A. Kurkin. 2003. Phylogenetic analysis of Russian Permian dicynodonts (Therapsida: Anomodontia): implications for Permian biostratigraphy and Pangaean biogeography. Zoological Journal of the Linnean Society 139:157–212.

Angielczyk, K. D., and B. S. Rubidge. 2010. A new pylaecephalid dicynodont (Therapsida, Anomodontia) from the *Tapinocephalus* Assemblage Zone, Karoo Basin, Middle Permian of South Africa. Journal of Vertebrate Paleontology 30:1396–1409.

Angielczyk, K. D., and B. S. Rubidge. 2013. Skeletal morphology, phylogenetic relationships, and stratigraphic range of *Eosimops newtoni* Broom, 1921, a pylaecephalid dicynodont (Therapsida, Anomodontia) from the Middle Permian of South Africa. Journal of Systematic Palaeontology 11:191–231.

Damiani, R., C. Vasconcelos, A. Renaut, J. Hancox, and A. Yates. 2007. *Dolichuranus primaevus* (Therapsida: Anomodontia) from the Middle Triassic of Namibia and its phylogenetic relationships. Palaeontology 50:1531–1546.

Fröbisch, J. 2007. The cranial anatomy of *Kombuisia frerensis* Hotton (Synapsida, Dicynodontia) and a new phylogeny of anomodont therapsids. Zoological Journal of the Linnean Society 150:117–144.

Kammerer, C. F., K. D. Angielczyk, and J. Fröbisch. 2011. A comprehensive taxonomic revision of "*Dicynodon*" (Therapsida, Anomodontia) and its implications for dicynodont phylogeny, biogeography, and biostratigraphy. Journal of Vertebrate Paleontology 31:1–158.

Kammerer, C. F., J. Fröbisch, and K. D. Angielczyk. 2013. On the Validity and Phylogenetic Position of *Eubrachiosaurus browni*, a Kannemeyeriiform Dicynodont (Anomodontia) from Triassic North America. PLoS ONE 8:e64203.

Maisch, M. W. 2001. Observations on Karoo and Gondwana vertebrates. Part 2: A new skull-reconstruction of *Stahleckeria potens* von Huene, 1935 (Dicynodontia, Middle Triassic) and a reconsideration of kannemeyeriiform phylogeny. Neues Jahrbuch für Geologie und Paläontologie – Abhandlungen 220:127–152.

Maisch, M. W. 2002. A new basal lystrosaurid dicynodont from the Upper Permian of South Africa. Palaeontology 45:343–359.

Maisch, M. W., and E.V.I. Gebauer. 2005. Reappraisal of *Geikia locusticeps* (Therapsida: Dicynodontia) from the Upper Permian of Tanzania. Palaeontology 48:309–324.

Modesto, S. P., and N. Rybczynski. 2000. The amniote faunas of the Russian Permian: implications for Late Permian terrestrial vertebrate biogeography; pp. 17–34 in M.J.

Benton, M.A. Shishkin, D.M. Unwin, and E.N. Kurochkin (eds.), The age of dinosaurs in Russia and Mongolia. Cambridge University Press, Cambridge.

Modesto, S. P., B. Rubidge, and J. Welman. 1999. The most basal anomodont therapsid and the primacy of Gondwana in the evolution of the anomodonts. Proceedings of the Royal Society of London B: Biological Sciences 266:331–337.

Modesto, S. P., B. Rubidge, I. Visser, and J. Welman. 2003. A new basal dicynodont from the Upper Permian of South Africa. Palaeontology 46:211–223.

Sidor, C. A. 2001. Simplification as a trend in synapsid cranial evolution. Evolution 55:1419–1442.

Sidor, C. A., and J. A. Hopson. 1998. Ghost lineages and 'mammal-ness': assessing the temporal pattern of character acquisition in the Synapsida. Paleobiology 24:254–273.

Surkov, M. V., and M. J. Benton. 2004. The basicranium of dicynodonts (Synapsida) and its use in phylogenetic analysis. Palaeontology 47:619–638.

Surkov, M. V., N. N. Kalandadze, and M. J. Benton. 2005. *Lystrosaurus georgi*, a dicynodont from the Lower Triassic of Russia. Journal of Vertebrate Paleontology 25:402–413.

Vega-Dias, C., M. W. Maisch, and C. L. Schultz. 2004. A new phylogenetic analysis of Triassic dicynodonts (Therapsida) and the systematic position of *Jachaleria candelariensis* from the Upper Triassic of Brazil. Neues Jahrbuch für Geologie und Paläontologie – Abhandlungen 231:145–166.

Appendix II: Supplementary data of PAPER II (unpublished)

Table 1S. Postcranial remains found in the Argana Basin and attributed to Dicynodontia.

Specimen number	Original bone identification	Current bone identification	Preservation	Original attribution	Current attribution[c]	Locality
MNHN.F.ALM 120	Four connected vertebrae[b]	Three connected dorsal vertebrae ('MNHN.F.ALM 120-1, -2, and -3' following the anteroposterior axis) and a fourth dorsal vertebra ('MNHN.F.ALM 120-4') associated with MNHN.F.ALM 120-3[c]	Vertebrae connected, except MNHN.F.ALM 120-4 originally associated with MNHN.F.ALM 120-3. Bones slightly compressed. Details of connections and bone structures hidden by remaining sediment. Anterior surface of MNHN.F.ALM 120-1 partly eroded with left processes (transverse and prezygapophysis) and the right border of the centrum missing. MNHN.F.ALM 120-3 partially disconnected from MNHN.F.ALM 120-2 and shifting to the right. Left prezygapophysis of MNHN.F.ALM 120-3 eroded. Neural spine partially or completely missing in MNHN.F.ALM 120-3 and -4, respectively. Postzygapophyses and distal end of the left transverse process missing in MNHN.F.ALM 120-4.	*M. nmachouensis*[b]	Unchanged	Locality XIb in Argana Basin (Morocco)[a]
MNHN.F.ALM 136	Sacral vertebrae[a]	Five sacral vertebrae ('MNHN.F.ALM 136-1, -2, -3, -4, and -5')[c]	Ventral and dorsal sides of the vertebrae only observable, all the rest included in sediment. Part of the neural spine and fragment of the left associated ribs only preserved in MHNH.F.ALM 136-1. MNHN.F.ALM 136-5 only preserved by its left associated sacral rib and the small anterior part of its centrum highly eroded. Neural spine and associated right sacral ribs of the other vertebrae missing. External ventral surface of MNHN.F.ALM 136-2 eroded.	Dicynodontia[a]	*M. nmachouensis*	Locality XIb in Argana Basin (Morocco)[a]
MNHN.F.ALM 159	Two vertebrae[a]	Two connected dorsal vertebrae ('MNHN.F.ALM 159-1 and 2')[c]	Connections (posterior side of MNHN.F.ALM 159-1 and anterior side of MNHN.F.ALM 159-2) and bone structures hidden by remaining sediment. MNHN.F.ALM 159-2 transversely crushed. Neural canals of both vertebrae filled by sediment. Neural spine of both vertebrae and left transverse process	Dicynodontia[a]	*M. nmachouensis*	Locality XIb in Argana Basin (Morocco)[a]

			of MNHN.F.ALM 159-1 broken. Transverse processes and prezygapophyses of MNHN.F.ALM 159-1, as well as postzygapophyses of MNHN.F.ALM 159-2 highly eroded.			
MNHN.F.ALM 198	Vertebra[a]	Posterior part of neural arch of a last cervical or first dorsal vertebra[c]	Posterior part of the neural arch of the vertebra only preserved. Neural spine missing. Pre- and postzygapophyses highly eroded. Right transverse process broken.	Unattributed[a]	*M. nmachouensis*	Argana Basin (Morocco)[a]
MNHN.F.ALM 265	Dorsal vertebra[b]	Unchanged	Vertebra with distorted neural canal due to a post-mortem compression. Left anterior margin of the centrum, left transverse process, and prezygapophyses broken. Anterior surface highly eroded.	Dicynodontia[a]	*M. nmachouensis*	Locality XIb in Argana Basin (Morocco)[a]
MNHN.F.ALM 288	Vertebra[a]	Vertebra (last cervical or first dorsal)[c]	Highly anteroposteriorly compressed vertebrae with transverse processes flattened. Sediment layers covering the bone surface, and especially the lateral surface of the centrum, in the neural canal, and around the neural spine.	? *M. nmachouensis*[b]	*M. nmachouensis*	Locality XIb in Argana Basin (Morocco)[a]
Unnumbered	Two connected vertebrae[b]	Two connected vertebrae ('Vunknb 1 and 2') identified as last cervical vertebrae and/or first dorsals[c]	Sediment covering some connections and bone structures. Transverse processes, pre- and postzygapophyses of vertebrae highly eroded. Neural spine completely and partly missing in Vunknb 1 and 2, respectively. Neural canal completely or partly filled by sediment in Vunknb 1 and 2, respectively.	Unattributed[b]	*M. nmachouensis*	Unknown[b]
MNHN.F.ALM 86	Rib[a]	Right dorsal rib in middle or posterior position[c]	Well-preserved but fractured bone with a distal part broken and highly eroded.	*M. nmachouensis*[b]	Unchanged	Locality XIb in Argana Basin (Morocco)[a]
MNHN.F.ALM 90	Limb bone[a]	Left rib (associated with last cervical or first dorsal vertebrae?)[c]	Proximal and distal ends of rib missing. Sediment covering the posterior side of the head and distal part of the rib. Posterior side of rib highly eroded.	Unattributed[a]	*M. nmachouensis*	Locality XIb in Argana Basin (Morocco)[a]

MNHN.F.ALM 91	Rib[b]	Left rib associated with last cervical or first dorsal vertebrae[c]	Well-preserved bone but fractured, with a distal part broken and highly eroded. Sediment covering the posterior side of the distal end.	Dicynodontia[b]	*M. nmachouensis*	Locality XIb in Argana Basin (Morocco)[a]
MNHN.F.ALM 95	Rib[a]	Left dorsal rib in middle or posterior position[c]	Well-preserved but fractured with a distal part broken and highly eroded.	Dicynodontia[b]	*M. nmachouensis*	Locality XIb in Argana Basin (Morocco)[a]
MNHN.F.ALM 96	Rib[a]	Right anterior dorsal rib (with a single head)[c]	Fractured rib entirely preserved.	Dicynodontia[b]	Dicynodontoidae indet.	Locality XIb in Argana Basin (Morocco)[a]
MNHN.F.ALM 97	Rib[a]	Right dorsal rib in middle or posterior position[c]	Well-preserved but fractured with a distal part broken and highly eroded. Sediment covering the posterior side of the proximal head highly eroded.	Dicynodontia[b]	*M. nmachouensis*	Locality XIb in Argana Basin (Morocco)[a]
MNHN.F.ALM 163	Distal part of a rib[a]	Proximal head of a right rib, probably anterior dorsal[c]	Articular surfaces highly eroded with sediment remaining.	? *M. nmachouensis*[b]	*M. nmachouensis*	Locality XIb in Argana Basin (Morocco)[a]
MNHN.F.ALM 272	Fragmentary rib[a]	Proximal head of a right rib[c]	Sediment covering the dorsal side of the costal head of rib. Proximal part highly eroded and broken.	Dicynodontia[b]	*M. nmachouensis*	Locality XIb in Argana Basin (Morocco)[a]
MNHN.F.ALM 296	Rib[a]	Left rib[c]	Well-preserved bone but fractured rib with proximal end missing. Distal part broken and highly eroded.	Dicynodontia[b]	*M. nmachouensis*	Locality XIb in Argana Basin (Morocco)[a]
Unnumbered	Unidentified[b]	Proximal head of a left rib (associated with last cervical or first dorsal vertebrae?)[c]	Relatively well-preserved proximal costal head with eroded articular surfaces.	Unattributed[b]	*M. nmachouensis*	? Argana Basin (Morocco)[b]
MNHN.F.ALM 17	Scapula[b]	Left scapula[c]	Dorsal expansion and anterior blade of the ventral part broken. Lateral surface of the ventral part crushed with a lack of bone. Sediment covering the medial part of the dorsal and ventral ends.	*M. nmachouensis*[b]	Unchanged	Locality XIa in Argana Basin (Morocco)[a]

MNHN.F.ALM 19	Left scapula[b]	Unchanged	Nearly complete scapula. Glenoid process missing. Dorsal part poorly preserved with sediment remaining.	Dicynodontia[b]	*M. nmachouensis*	Locality XIb in Argana Basin (Morocco)[a]
MNHN.F.ALM 29	Scapula[b]	Right scapula[c]	Complete scapula crushed at the ventral region. Sediment covering the medial surface of the anterior blade of the ventral part.	Dicynodontia[b]	*M. nmachouensis*	Locality XIb in Argana Basin (Morocco)[a]
MNHN.F.ALM 30	Left scapula[b]	Unchanged	Nearly complete scapula. Glenoid facet and dorsal end poorly preserved. Sediment covering the lateral surface of the dorsal part and slightly the medial side of most bone surface.	*M. nmachouensis*[b]	Unchanged	Locality XIb in Argana Basin (Morocco)[a]
MNHN.F.ALM 83	Scapula[a]	Left scapula[b]	Well-preserved bone without any particular taphonomic tampering.	Dicynodontia[b]	*M. nmachouensis*	Locality XIb in Argana Basin (Morocco)[a]
MNHN.F.ALM 92	Scapula[a]	Left scapula in connection with precoracoid and coracoid[c]	Dorsal expansion and anterior blade of the ventral part not preserved. External surface of the precoracoid and coracoid eroded with fractured outlines.	Dicynodontia ? *M. nmachouensis*[b]	*M. nmachouensis*	Locality XIb in Argana Basin (Morocco)[a]
MNHN.F.ALM 98	Right scapula[b]	Left scapula[c]	Complete scapula highly fragmented. Anteroventral corner of the anterior blade missing	*M. nmachouensis*[b]	Unchanged	Locality XIb in Argana Basin (Morocco)[a]
MNHN.F.ALM 113	Left scapula[b]	Unchanged	Well-preserved bone, but dorsal region missing.	*M. nmachouensis*[b]	Unchanged	Locality XIa in Argana Basin (Morocco)[a]
MNHN.F.ALM 114	Fragment of scapula[a]	Left scapula[c]	Dorsal part missing and ventral part crushed. Anterior blade of the ventral part missing. Lateral side of the ventral part highly eroded. Sediment covering the bone external surface.	*M. nmachouensis*[b]	Unchanged	Locality XIa in Argana Basin (Morocco)[a]
MNHN.F.ALM 132	Scapula[a]	Left scapula[c]	Well-preserved bone, but dorsal region missing.	Dicynodontia[a]	*M. nmachouensis*	Locality XIb in Argana Basin (Morocco)[a]
MNHN.F.ALM 153	Scapula[a]	Right scapula[c]	Nearly complete scapula preserved in three parts. Sediment covering the medial side of the middle and ventral fragments, and at the glenoid facet. Anterior blade of the ventral part and posterior margin of the dorsal expansion missing.	*M. nmachouensis*[b]	Unchanged	Locality XIb in Argana Basin (Morocco)[a]
MNHN.F.ALM 155	Scapula[a]	Left scapula[c]	Nearly complete scapula. Ventral sutural zone poorly preserved and anterior blade of the ventral	Dicynodontia[a]	*M. nmachouensis*	Locality XIb in Argana Basin (Morocco)[a]

			part broken. Sediment covering the whole medial region.			
MNHN.F.ALM 259	Scapula[a]	Left scapula[c]	Nearly complete scapula. Dorsal part and anterior blade of the ventral region missing. Sediment covering the medial side, above the sutural zone with the coracoid.	*M. nmachouensis*[b]	Unchanged	Locality XIb in Argana Basin (Morocco)[a]
MNHN.F.ALM 263	Fragmentary scapula[a]	Right scapula[c]	Fractured and crushed bone. Dorsal expansion without the anterior crest only preserved.	? M. nmachouensis[b]	*M. nmachouensis*	Locality XIb in Argana Basin (Morocco)[a]
MNHN.F.ALM 283	Scapula[a]	Right scapula[c]	Well-preserved and nearly complete scapula. Proximal end missing. Part of the anterior blade of the ventral region broken.	Dicynodontia[a]	*M. nmachouensis*	Locality XIb in Argana Basin (Morocco)[a]
MNHN.F.ALM 292	Scapula[a]	Right scapula[c]	Highly curved scapula in anterior view. Glenoid and sutural facets, and anterior blade of the ventral region poorly preserved.	Dicynodontia[a]	*M. nmachouensis*	Locality XIb in Argana Basin (Morocco)[a]
MNHN.F.ALM 298	Scapula[a]	Left scapula in connection with precoracoid and coracoid[c]	Well-preserved scapulocoracoid complex. Posterior margin of the dorsal expansion and anterior margin of the ventral region eroded. Sediment covering the lateral side of the dorsal region, anterior expansion of the ventral part, precoracoid, and coracoid. Glenoid facet, acromion and *triceps* muscle processes poorly preserved.	Dicynodontia ? *M. nmachouensis*[b]	*M. nmachouensis*	Locality XIb in Argana Basin (Morocco)[a]
MNHN.F.ALM 299	Scapula[a]	Right scapula[c]	Highly fragmented but complete scapula. Glenoid and coracoid facets poorly preserved.	Dicynodontia[a]	Dicynodontoidae indet.	Locality XIa in Argana Basin (Morocco)[a]
MNHN.F.AZA 365	Scapula[a]	Right scapula[c]	The more robust scapula of the collection. Middle and ventral regions preserved. Anterior blade of the ventral part missing.	Dicynodontia[a]	Dicynodontoidae indet.	Locality XIII in Argana Basin (Morocco)[a] (the only dicynodont bone found associated to remains mainly attributed to Metoposaurus ouazzaoui)

Unnumbered	Right scapula[b]	Unchanged (‘Sunknb 1’)	Poorly-preserved and fragmented scapula. Almost the whole ventral region and anterior margin of the dorsal part missing.	? *M. nmachouensis*[b]	*M. nmachouensis*	Locality XI in Argana Basin (Morocco)[b]
Unnumbered	Scapula[b]	Left scapula (‘Sunknb 2’)[c]	Poorly-preserved bone with highly eroded lateral external bone surface. Sediment covering the medial side of the dorsal and ventral regions.	Unattributed[b]	*M. nmachouensis*	Locality XI in Argana Basin (Morocco)[b]
Unnumbered	Unidentified[b]	Right scapula (‘Sunknb 3’)[a]	Nearly complete but crushed bone. Sutural facet with the coracoid, anterior blade of the dorsal and ventral regions highly altered.	Unattributed[b]	*M. nmachouensis*	? Argana Basin (Morocco)[b]
MNHN.F.ALM 93	Interclavicle[b]	Unchanged	Highly fractured bone. Bone missing particularly in the anterior part. Sediment covering the external surface of bone.	Dicynodontia[b]	*M. nmachouensis*	Locality XIb in Argana Basin (Morocco)[a]
MNHN.F.ALM 94	Interclavicle[b]	Unchanged	Interclavicle fractured in two parts. External bone surface eroded. Anterior and posterior ends broken. Sediment covering the whole dorsal side.	? Dicynodontia[b]	*M. nmachouensis*	Locality XIb in Argana Basin (Morocco)[a]
MNHN.F.ALM 158	? Interclavicle[b]	Interclavicle[c]	Relatively well-preserved interclavicle with anterior and posterior regions broken. Sediment covering on the whole dorsal side.	*M. nmachouensis*[b]	Unchanged	Locality XIb in Argana Basin (Morocco)[a]
MNHN.F.ALM 260	Interclavicle[b]	Unchanged	Relatively well-preserved posterior region, as opposed to the anterior one where bone missing. Sediment covering the whole dorsal side.	*M. nmachouensis*[b]	Dicynodontoidae indet.	Locality XIb in Argana Basin (Morocco)[a]
MNHN.F.ALM 278	Bone from pectoral girdle[a]	Interclavicle[c]	Anterior part missing and lateral margins eroded. Sediment covering the whole dorsal side.	Dicynodontia[a]	*M. nmachouensis*	Locality XIb in Argana Basin (Morocco)[a]
MNHN.F.ALM 295	Interclavicle[b]	Unchanged	Well-preserved external bone surface. Anterior and posterior ends missing.	*M. nmachouensis*[b]	Unchanged	Locality XI in Argana Basin (Morocco)[b]
Unnumbered	Incompleted interclavicle[b]	Anterior part of interclavicle (‘Intunknb 1’)[c]	Anterior part of the bone only preserved, with eroded anterior margin. Anterior end missing.	Dicynodontia[b]	*M. nmachouensis*	Locality XI in Argana Basin (Morocco)[b]
Unnumbered	? Interclavicle[b]	Interclavicle (‘Intunknb 2’)[c]	Highly eroded and fragmented interclavicle. Distorted bone with poorly-preserved posterior and anterior parts not aligned and slightly twisted	*M. nmachouensis*[b]	Unchanged	Locality XI in Argana Basin (Morocco)[b]

			at the middle constriction. Anterior part laterally compressed.			
MNHN.F.ALM 134	Bone from girdle?[a]	Sternum[c]	Posterior region poorly preserved. Ventral side entirely covered by sediment	Dicynodontia[a]	*M. nmachouensis*	Locality XIb in Argana Basin (Morocco)[a]
MNHN.F.ALM 24	Left humerus[b]	Unchanged	Well-preserved complete humerus. Proximal end missing. Dorsal surface of distal part highly eroded.	*M. nmachouensis*[b]	Unchanged	Locality XIb in Argana Basin (Morocco)[a]
MNHN.F.ALM 25	Left humerus[b]	Unchanged	Well-preserved complete humerus. Proximal end missing. Dorsal surface of the distal part highly eroded.	*M. nmachouensis*[b]	Unchanged	Locality XIb in Argana Basin (Morocco)[a]
MNHN.F.ALM 101	Humerus[a]	Right humerus[c]	Relatively well-preserved complete humerus. Sediment covering the posterior part of the proximal expansion. Distal epiphysis eroded.	Dicynodontia[b]	*M. nmachouensis*	Locality XIb in Argana Basin (Morocco)[a]
MNHN.F.ALM 102	Left humerus[b]	Unchanged	Well-preserved complete humerus. Sediment covering the dorsal side of the distal expansion.	*M. nmachouensis*[b]	Unchanged	Locality XIb in Argana Basin (Morocco)[a]
MNHN.F.ALM 105	Partial humerus[a]	Left humerus[c]	Highly fractured humerus with epiphyses and part of metaphyses of the proximal and distal expansions missing. Sediment covering the ventral margin of the deltopectoral crest and most of the distal expansion.	Unattributed[a]	*M. nmachouensis*	Locality XIb in Argana Basin (Morocco)[a]
MNHN.F.ALM 115	Humerus[a]	Right humerus[c]	Fractured humerus with epiphyses and part of metaphyses of the proximal and distal expansion missing. Sediment covering the proximal and distal expansions. Two third of the distal part of the deltopectoral crest well preserved.	Unattributed[a]	*M. nmachouensis*	Locality XIa in Argana Basin (Morocco)[a]
MNHN.F.ALM 121-1-2-3	Humerus[a]	Fragmentary parts of a left humerus[c]	Highly fractured and eroded bone preserved in three parts: the shaft and the distal expansion (MNHN.F.ALM 121-1), the posterior corner of the proximal end with the humeral head (MNHN.F.ALM 121-2), and a fragmentary part of the deltopectoral crest (MNHN.F.ALM 121-3). Humeral head, external surface of the shaft, and entepicondyle foramen well preserved.	Dicynodontia[a]	*M. nmachouensis*	Locality XIb in Argana Basin (Morocco)[a]

MNHN.F.ALM 133	Framentary part of humerus[a]	Fragmentary part of a left humerus[c]	Shaft and proximal part of the distal expansion (with visible entepicondyle foramen) only preserved. Sediment covering most of bone.	Dicynodontia[a]	*M. nmachouensis*	Locality XIb in Argana Basin (Morocco)[a]
MNHN.F.ALM 147	Limb bone[a]	Distal part of a right humerus[c]	Highly eroded distal part of humerus with preserved ventral surface of the trochlea and capitelum.	Dicynodontia[a]	*M. nmachouensis*	Locality XIb in Argana Basin (Morocco)[a]
MNHN.F.ALM 275	Humerus[a]	Left humerus[c]	The biggest humerus of the collection, but highly fractured. Proximal end and entepicondyle missing. Deltopectoral crest highly altered.	Dicynodontia[a]	Dicynodontoidae indet.	Locality XIa in Argana Basin (Morocco)[a]
MNHN.F.ALM 297	Humerus[a]	Left humerus[c]	Highly eroded complete humerus. Proximal corner of deltopectoral crest missing.	Dicynodontia[b]	*M. nmachouensis*	Locality XIb in Argana Basin (Morocco)[a]
Unnumbered	Distal part of humerus[b]	Proximal part of a right humerus ('Humunknb 1')[c]	Posterior part of the proximal expansion of humerus only preserved. Sediment covering the humeral head and posterior surface of bone. Deltopectoral crest not preserved.	Dicynodontia[b]	*M. nmachouensis*	Locality XI in Argana Basin (Morocco)[b]
Unnumbered	Distal part of humerus[b]	Distal part of a right humerus ('Humunknb 2')[c]	Shaft and ectepicondyle well preserved. Distal part of the entepicondyle missing. Sediment covering most of bone.	Dicynodontia[b]	*M. nmachouensis*	Locality X, XI or XVI? in Argana Basin (Morocco)[b]
MNHN.F.ALM 84	Radius[b]	Left radius[c]	Complete radius with eroded proximal and distal ends. Sediment covering its posterior side.	*M. nmachouensis*[b]	Unchanged	Locality XIb in Argana Basin (Morocco)[a]
MNHN.F.ALM 131	Limb bone[a]	Left radius[c]	Broken at the middle of the shaft. Distal expansion crushed and poorly preserved. Fractured and eroded proximal end.	Dicynodontia[a]	*M. nmachouensis*	Locality XIb in Argana Basin (Morocco)[a]
MNHN.F.ALM 287	Radius[b]	Right radius[c]	Well-preserved complete radius with eroded proximal and distal ends	*M. nmachouensis*[b]	Unchanged	Locality XIb in Argana Basin (Morocco)[a]
MNHN.F.ALM 289	Radius[b]	Left radius[c]	Highly crushed with some cracks. Sediment covering its proximal and distal ends.	*M. nmachouensis*[b]	Unchanged	Locality XIb in Argana Basin (Morocco)[a]
Unnumbered	Distal parts of a radius and an ulna[b]	Distal parts of left radius and ulna[c]	Radius highly fractured and compressed, with distal end eroded. No diagnostic features present on the ulnar fragment except the anterior crest bordering the radial facet anteriorly.	*M. nmachouensis*[b]	Unchanged	Unknown[b]

MNHN.F.ALM 18	Ulna[b]	Right ulna[c]	Lack of bone and medial part of the olecranon process crushed.	*M. nmachouensis*[b]	Unchanged	Locality XIb in Argana Basin (Morocco)[a]
MNHN.F.ALM 27	Dorsal part of ulna[b]	Dorsal part of the olecranon process of a right ulna[c]	Dorsal part of the olecranon process only preserved. Highly eroded and fractured bone. One of the two biggest ulnae.	Dicynodontia[b]	Dicynodontoidae indet.	Locality XIb in Argana Basin (Morocco)[a]
MNHN.F.ALM 28	Ulna[b]	Left ulna[c]	Fractured ulna with lack of bone at the olecranon process and ventral epiphysis.	Dicynodontia[b]	*M. nmachouensis*	Locality XIb in Argana Basin (Morocco)[a]
MNHN.F.ALM 35	Ulna[b]	Right ulna[c]	Sediment covering the olecranon process. Ventral epiphysis missing.	*M. nmachouensis*[b]	Unchanged	Locality XI in Argana Basin (Morocco)[b]
MNHN.F.ALM 87	Ulna and the proximal part of a rib[b]	Right ulna and the proximal part of a right rib[c]	Ulna fragmented in two parts. Highly eroded and fractured proximal part. Lack of bone and sediment covering the medial side of the ventral region. Ventral epiphysis and external bone surface highly eroded.	*M. nmachouensis*[b]	Unchanged	Locality XIb in Argana Basin (Morocco)[a]
MNHN.F.ALM 126-1, -2	Fragmentary ulna[a]	Left ulna[c]	Fragmented and highly eroded bone. One of the two biggest ulnae.	*M. nmachouensis*[b]	Unchanged	Locality XIb in Argana Basin (Morocco)[a]
MNHN.F.ALM 154	Ulna[a]	Left ulna[c]	Well-preserved ulna. Dorsal end of the olecranon process missing. Lack of bone at the ventral epiphysis.	Dicynodontia[a]	Dicynodontoidae indet.	Locality XIa in Argana Basin (Morocco)[a]
MNHN.F.ALM 261	Ulna[a]	Left ulna[c]	Lack of bone and medial part of the olecranon process crushed.	? *M. nmachouensis*[b]	*M. nmachouensis*	Locality XIb in Argana Basin (Morocco)[a]
MNHN.F.ALM 274	? Vertebrae and pelvis[a]	Pelvic girdle connected to sacral and caudal vertebrae, and two associated disconnected vertebrae ('MNHN.F.ALM 274-1 and -2') that are interpreted as posterior dorsal vertebrae[c]	Pelvis laterally compressed. Two puboischiatic plates not in natural position, with posterior margins of the ischia very closely spaced. Pubes connected by their ventral margins most likely due to the lateral compression. Left ilium almost entirely preserved, while distorted, as opposed to the right one (iliac blade highly altered). Left puboischiatic plate entirely preserved, while ischium particularly crushed. Posterior flattened expansion of this latter highly fractured. Right puboischiatic plate more altered, with posterior part of the right ischium missing. Obturator foramens filled by sediment.	Unattributed[a]	*M. nmachouensis*	Unknown[a]

			Vertebrae MNHN.F.ALM 274-1 and -2 relatively well preserved, except some cracks and a lack of bone structures. Neural spine, distal part of the right transverse process, and postzygapophyses of MNHN.F.ALM 274-2 missing. Centra of both MNHN.F.ALM 274-1 and -2 altered, while a well preservation of the rest of MNHN.F.ALM 274-1. Ventral side of sacral vertebrae well visible as opposed to the dorsal side, mainly included in sediment. Left rib of the first sacral vertebra cracked and almost entirely missing. Caudal vertebrae connected to the last sacral vertebra, but most entirely included in sediment. Neural spines only observable, as well as most of the first and last centra. Neural spine of the most posterior caudal vertebrae missing.			
MNHN.F.ALM 104	Left ilium[b]	Unchanged	Well-preserved ilium. Posterodorsal margin of its iliac blade missing. Right expanded transverse process of the first sacral vertebra connected to the medial part of the iliac blade dorsally. Sediment covering the acetabulum fossa and the medial side of the anterior tubercle of the ilium.	? *M. nmachouensis*[b]	*M. nmachouensis*	Locality XIb in Argana Basin (Morocco)[a]
MNHN.F.ALM 123	Bone from pelvic girdle ?[a]	Right ischium[c]	Relatively well-preserved ischium with sligh break on anterior and posterior margins of the ventral expansion.	Dicynodontia[a]	*M. nmachouensis*	Locality XIb in Argana Basin (Morocco)[a]
MNHN.F.ALM 125	Bone from girdle ?[a]	Left ischium[c]	Whole lateral side and acetabular region hidden by sediment. Posteroventral margin of the obturator foramen broken, as well as most of its posterior flattened expansion.	Dicynodontia[a]	*M. nmachouensis*	Locality XIb in Argana Basin (Morocco)[a]
MNHN.F.ALM 138	Scapula[a]	Right ischium[c]	Relatively well-preserved ischium with sligh break on anterior and posterior margins of the ventral expansion. Whole medial side covered by sediment.	Dicynodontia[a]	*M. nmachouensis*	Locality XIb in Argana Basin (Morocco)[a]
MNHN.F.ALM 122	Humerus[a]	Left pubis[c]	Well-preserved bone with ventral and posterior margins slightly eroded and fractured.	Dicynodontia[a]	*M. nmachouensis*	Locality XIb in Argana Basin (Morocco)[a]

MNHN.F.ALM 21	Left femur[b]	Unchanged	Well-preserved complete femur with sediment covering the femoral head and ventral condyles. Lateral margin of trochanteric crest and proximal part of shaft partially altered.	*M. nmachouensis*[b]	Unchanged	Locality XIb in Argana Basin (Morocco)[a]
MNHN.F.ALM 22	? femur[b]	Right femur[c]	Complete femur with taphonomic compression. Epiphyses appearing missing.	Dicynodontia[b]	Dicynodontoidae indet.	Locality XIb in Argana Basin (Morocco)[a]
MHN.F.ALM 23	Femur[b]	Right femur[c]	Well-preserved complete femur with sediment covering the whole bone. Slight taphonomic distortion along the long axis of bone.	*M. nmachouensis*[b]	Unchanged	Locality XIb in Argana Basin (Morocco)[a]
MNHN.F.ALM 26	Femur[b]	Left femur[c]	Well-preserved complete femur with sediment covering the femoral head and ventral condyles. Lateral margin of trochanteric crest slightly altered.	Dicynodontia[b]	*M. nmachouensis*	Locality XIb in Argana Basin (Morocco)[a]
MNHN.F.ALM 34	Unidentified[a]	Right femur[c]	Fragmentary femur, with shaft and part of the ventral expansion only preserved.	Dicynodontia[b]	*M. nmachouensis*	Unknown[a]
MNHN.F.ALM 85	Femur[b]	Right femur[c]	Complete but fractured femur, with highly eroded surface especially at epiphyses.	Dicynodontia[b]	*M. nmachouensis*	Locality XIb in Argana Basin (Morocco)[a]
MNHN.F.ALM 100	Femur[b]	Left femur[c]	Complete femur with highly eroded surface especially at epiphyses. Lateral margin of trochanteric crest altered.	Dicynodontia[b]	*M. nmachouensis*	Locality XIb in Argana Basin (Morocco)[a]
MNHN.F.ALM 290	Femur[b]	Left femur[c]	Highly eroded and fractured femur. Proximal end missing. Distal condyles highly eroded.	Dicynodontia[a]	*M. nmachouensis*	Locality XIb in Argana Basin (Morocco)[a]
MNHN.F.ALM 284	Femur[a]	Left femur[c]	The biggest complete femur of the collection. Proximal part and distal condyles eroded. Femoral head and lateral margin of trochanteric crest slightly altered.	Dicynodontia[a]	Dicynodontoidae indet.	Locality XIa in Argana Basin (Morocco)[a]
MNHN.F.ALM 33	Unidentified[a]	Right tibia[c]	Poorly preserved bone with metaphyses and epiphyses highly eroded.	Dicynodontia[b]	*M. nmachouensis*	Locality XI in Argana Basin (Morocco)[b]
MNHN.F.ALM 291	Limb bone[a]	Left tibia[c]	The biggest tibia of the collection. Reliefs smoothed and most likely eroded.	? Dicynodontia[a]	Dicynodontoidae indet.	Locality XIa in Argana Basin (Morocco)[a]
Unnumbered	Limb bone[b]	Right tibia[c]	Complete tibia with eroded proximal and distal ends. Lack of bone at the cnemial crest. Sediment covering the epiphyses.	Dicynodontia[b]	*M. nmachouensis*	Locality XI in Argana Basin (Morocco)[b]

MNHN.F.ALM 32	Unidentified[a]	Left fibula[c]	Complete fibula with lack of bone at proximal and distal ends.	Unattributed[a]	*M. nmachouensis*	Argana Basin (Morocco)[b]

[a]from the collection catalogue edited by J.M. Dutuit
[b]additional information or modifications by the research curator N.-E. Jalil
[c]additional information or modifications by C. Olivier

Discrete and continuous characters used in the phylogenetic analysis (modified from Kamerer, 2018)

The characters from 1 to 194 were provided by the phylogenetic matrix of PAPER I (Olivier et al., 2019, modified from Angielczyk and Kammerer, 2017). The following characters are provided by Kammerer (2018):

(195) Anterior face of dentary symphysis: 0, unornamented; 1, with median ridge. (From Kammerer 2018: discrete 172)

(196) Supinator process above ectepicondyle of humerus: 0, absent; 1, present. (From Kammerer 2018: discrete 173)

(197) Morphology of supinator process: 0, low, broadly separated from the shaft; 1, tall and subvertical, with dorsal margin close to base of shaft; 2, discrete, tab-like process occupying restricted portion of anterior face of distal humerus. (From Kammerer 2018: discrete 174)

Table 2S. Measurements of the continuous characters in *Moghreberia nmachouensis*

Phylogenetic characters	Specimens	Ratio
continuous 4	MNHN.F.ALM 280	0.863
continuous 17	MNHN.F.ALM 29	0.476
	MNHN.F.ALM 298	0.493
continuous 18	MNHN.F.ALM 25	0.517
	MNHN.F.ALM 101	0.588
	MNHN.F.ALM 102	0.572
continuous 19	MNHN.F.ALM 287	0.402
	MNHN.F.ALM 289	0.429
continuous 22	MNHN.F.ALM 21	0.359
	MNHN.F.ALM 26	0.369
continuous 23	MNHN.F.ALM 29	0.280
	MNHN.F.ALM 298	0.299

New or changed coding from the phylogenetic matrix of Kammerer (2018)

[a]*The poor preservation of the premaxilla in MNHN.F.ALM 37, 280, and 281 does not permit concluding about their bone contacts and the form of the snout.*

[b]*The pterygoids are not preserved in MNHN.F.ALM 37 and 281, and almost entirely missing in MNHN.F.ALM 280. Interpretations about their forms and bone contacts are impossible.*

Cranial characters

- Character 32: *Moghreberia* changed from 1→?[a]
- Character 33: *Moghreberia* changed from 0→?[a]
- Character 35: *Moghreberia* changed from 0→?[a]
- Character 38: *Moghreberia* changed from 2→0 (height of canine-bearing portion of maxilla relatively short). As opposed to the previous coding, the study of the caniniform of MNHN.F.ALM 280 revealed low ventral expansions of the maxilla as in *Angonisaurus cruickshanki* (NHMUK R9732, C. Olivier pers. observ.), *Dinodontosaurus* (MCZ 1679 and 3453, C. Olivier pers. observ.), *Ischigualastia* (MCZ 3118, C. Olivier pers. observ.), or *Kannemeyeria simocephalus* (BP/1/1168, C. Olivier pers. observ.).
- Character 44: *Moghreberia* changed from 0→?[a]
- Character 56: *Moghreberia* changed from ?→1 (nasals with a short median suture and frontals and premaxilla in close proximity). As opposed to the interpretation of the bone contacts figured by (Dutuit 1988) in MNHN.F.ALM 37, we suggested a marked and triangular posterior process of the premaxilla that contact the nasals posteriorly. The median suture between the nasals is short. They posteriorly contact the frontals with a suture mainly straight, however the preservation of the external bone surface does not permit to conclude about a potential anterior or posterior process of the suture.
- Character 62: *Moghreberia* changed from 0→?. None orbital margin is sufficiently well preserved to conclude about a potential circumorbital rim in *Moghreberia*.
- Character 63: *Moghreberia* changed from 0→?. The frontals of MNHN.F.ALM 280 are the best preserved in *Moghreberia*, however, their lateral expansion are missing, the interpretation about the contributions of these bones in the orbital margin is thus impossible.
- Character 64: *Moghreberia* changed from 1→?. In MNHN.F.ALM 280, the erosion of the bone surface around the postorbito-frontal contact does not permit to firmly conclude about a potential postfrontal.
- Character 80: *Moghreberia* changed from 2→1 (interparietal makes a small contribution to intertemporal skull roof). The interpretation of the contribution of the interparietal to the skull roof depending on the definition of the skull roof.

MNHN.F.ALM 280, the holotype of *Moghreberia* shows an occipital crests highly developed, as also described by (Dutuit, 1988), with an obtuse angle between the occipital plate and the palate. If we define the skull roof of MNHN.F.ALM 280 until the occipital crest, we could conclude to a large contribution of the interparietal to the skull roof. We choose to define posterior margin of the skull roof of MNHN.F.ALM 280 at the origin of the lateral expansion of the squamosals, the contribution of the interparietal can thus be considered as short. In addition, the occipital crest of MNHN.F.ALM 281 is not as developed as in MNHN.F.ALM 280 and not forms a high angulation between the interparietal and the rest of the occipital plate. A small contribution of the interparietal to the skull roof of MNHN.F.ALM 281 can also be interpreted.

- Character 105: *Moghreberia* changed from 1→?[a]
- Character 109: *Moghreberia* changed from ?→1. While the pterygoid are poorly preserved in MNHN.F.ALM 280, the developed anterior expansion of the fused vomer most likely suggests pterygoids separated by the vomer.
- Character 110: *Moghreberia* changed from 2→?[b]
- Character 111: *Moghreberia* changed from 1→?[b]
- Character 112: *Moghreberia* changed from 0→?[b]
- Character 119: *Moghreberia* changed from 0→?. The poor preservation of the medial side of the temporal fossa does not allow distinguishing the periotic.
- Character 123: *Moghreberia* changed from 1→?. A connection between the parasphenoid and the median pterygoid plate is only preserved in MNHN.F.ALM 280. A clear exposure of the internal carotid cannot be observed due to the highly eroded bone surface.
- Character 124: *Moghreberia* changed from ?→1 (basal tubera laterally directed and anteroposteriorly elongate with relatively narrow edges). The basal tubera have been well preserved in MNHN.F.ALM 268 and 280. They appear relatively narrow and anteroposteriorly straight as in *Stahleckeria potens* (AMNH 3857, C. Olivier pers. observ.) or *Dinodontosaurus turpior* (MCZ 1628, C. Olivier pers. observ.), as opposed to *Shaanbeikannemeyeria xilougouensis* (IVPP V11674 and V11677, C. Olivier pers. observ.), *Dolichuranus* (BP/1/4569 and BP/1/4573, C. Olivier pers. observ.), and *Kannemeyeria simocephalus* (BP/1/4523, C. Olivier pers. observ.) in which the basal tubera are thicker and crescent-shaped.
- Character 134: *Moghreberia* changed from 1→?. The preservation of the external bone surface of the occipital condyle in MNHN.F.ALM 268, 280, and 281 does not allow firm conclusion about the presence of a central depression on the condyle between the exoccipitals and basioccipital.

<u>Mandibular characters</u>

- Character 145: *Moghreberia* changed from ?→1 (curved ridge that follows the profile of the symphysis present on the edge between the anterior and lateral

surfaces of the dentary present). A lateral ridge have been observed on each lateral side of MNHN.F.ALM 38 around the posterior margin of the dentary symphysis.

- Character 159: *Moghreberia* changed from 0→?. The attribution of the specimen MNHN.F.ALM 80 to *Moghreberia* is doubtful due to the particular form of the tip of the dentary compared to MNHN.F.ALM 38. The posterior part of the mandibular rim and especially the articulars are not preserved in MNHN.F.ALM 38.
- Character 162: *Moghreberia* changed from 1→?. The surangulars are poorly preserved even missing in MNHN.F.ALM 38 that we considered the only mandible firmly attributed to *Moghreberia*.
- Character 163: *Moghreberia* changed from 2→?. None cranial remain have quadrate in original position and the articulars are not preserved in MNHN.F.ALM 38.

Postcranial characters

Concerning Moghreberia, the description of the new postcranial material permitted to code some phylogenetic associated characters.

- Character 166: *Moghreberia* changed from ?→0 (2 sternal bosses)
- Character 168: *Moghreberia* changed from ?→1 (anterior edge of scapula extended laterally to form a strong crest)
- Character 169: *Moghreberia* changed from ?→1 (origin of triceps on posterior surface of scapula developed into a prominent posterior projection)
- Character 170: *Moghreberia* changed from ?→0 (acromion process absent or very small)
- Character 171: *Moghreberia* changed from ?→0 (procoracoid foramen entirely contained within the procoracoid)
- Character 173: *Moghreberia* changed from ?→1 (proximal articular surface of humerus somewhat expanded with some encroachment onto the dorsal surface)
- Character 174: *Moghreberia* changed from ?→1 (insertion of M. *subcoracoscapularis* on humerus as a pinna-like process)
- Character 175: *Moghreberia* changed from ?→1, (insertion of M. *latissimus dorsi* extended into a dorsoventrally flattened pinna-like process)
- Character 176: *Moghreberia* changed from ?→1 (anterior and distal edges of deltopectoral crest very obtuse)
- Character 177: *Moghreberia* changed from ?→1 (ectepicondylar foramen on humerus absent)
- Character 178: *Moghreberia* changed from ?→0 (radial and ulnar condyle continuous on ventral surface of humerus)

- Character 179: *Moghreberia* changed from ?→1 (ulna with a large olecranon process that extends well past the articular surface for the humerus)
- Character 183: *Moghreberia* changed from ?→0 (dorsal edge of ilium unnotched)
- Character 184: *Moghreberia* changed from ?→1 (pubic plate significantly expanded anteroposteriorly so that it is much shorter than ischium)
- Character 185: *Moghreberia* changed from ?→1 (pubic plate is significantly expanded ventrally such that it is shorter than ischium)
- Character 186: *Moghreberia* changed from ?→1 (distinct cranial process present on anterior end of pubis)
- Character 187: *Moghreberia* changed from ?→1 (femoral head offset dorsally from dorsal margin)
- Character 188: *Moghreberia* changed from ?→1 (proximal articular surface of the femur present as a more rounded, hemispherical swelling that has some encroachment on the anterior surface of the femur)
- Character 189: *Moghreberia* changed from ?→1 (insertion of M. *iliofemoralis* developed into a distinct crest that extends down part of the lateral surface of the femur)
- Character 194: *Moghreberia* changed from ?→1 (greatly enlarged vascular channels present). This histological characters has been coded according the histological study of (Olivier et al., 2017)
- Character 195: *Lisowicia* coded "?" because only the right posterior part of a mandible is known for the mandible.
- Character 196: *Moghreberia* changed from ?→1 (presence of a supinator process above ectepicondyle of humerus) based on condition in MNHN.F.ALM 24, 25, 101, 102, and 121. *Lisowicia* coded "1" based on condition in ZPAL V.33/96, in which distinct process is also clearly present above the ectepicondyle.
- Character 197: *Lisowicia* coded "1" (tall and subvertical supinator process, with dorsal margin close to base of shaft) based on condition in ZPAL V.33/96.

Table 3S. Phylogenetic matrix used in the analysis →

	1	2	3	4	5	6	7	8	9	10	11	12	13	14	15	16	17	18	19	20	21	22	23
Biarmosuchus	0.693	?	0.261	?	0.148	0.029	?	?	5.8	?	?	?	1.06	?	0.502	1.87	?	0.446	?	0.553	0.426	0.0	?
Hipposaurus boonstrai	0.606	?	0.263	0.842	0.19	0.046	?	?	3.5	?	?	?	1.07	?	0.539	2.63	0.667	0.367	0.125	?	?	0.0	0.222
Archaeosyodon praeventor	?	?	?	?	?	0.104	?	?	5.6	?	?	?	?	?	0.92	?	?	?	?	?	?	?	?
Titanophoneus potens	0.758	?	0.244	0.7	0.227	0.051	?	?	6.2	?	?	?	1.16	?	0.855	1.62	0.5	0.292	0.274	0.5	?	0.0	0.343
Gorgonops torvus	0.504	?	0.29	1.15	0.305	0.072	?	?	8.5	?	?	?	0.977	?	?	?	?	0.329	?	?	?	?	?
Lycosuchus vanderrieti	0.509	?	0.261	0.333	0.352	0.303	?	?	7.7	0.094	?	?	1.06	?	0.595	1.71	0.5	0.333	0.294	?	?	0.0	0.4
Glanosuchus macrops	0.547	?	0.145	0.25	0.367	0.218	?	?	5.3	0.05	?	?	1.02	?	0.718	2.12	0.545	0.309	0.2	0.833	?	0.0	0.342
Biseridens qilianicus	?	?	?	1.032	?	0.094	?	?	?	?	?	11.0	?	?	0.956	?	?	?	?	?	?	?	?
Anomocephalus africanus	?	?	?	?	?	?	?	?	?	?	?	?	?	?	?	?	?	?	?	?	?	?	?
Tiarajudens eccentricus	?	?	?	?	?	?	?	?	?	?	?	?	?	?	?	?	?	0.396	0.164	?	?	?	?
Otsheria netzvetajevi	0.381	5.425	0.231	?	0.512	0.108	?	0.181	5.3	0.108	10.95	15.5	0.86	?	?	?	?	?	?	?	?	?	?
Ulemica	0.47	5.364	0.125	1.06	0.407	0.102	?	0.216	4.9	?	10.91	15.4	1.098	0.294	0.698	1.135	?	?	?	?	?	?	?
Suminia getmanovi	0.336	4.879	0.205	?	0.23	0.105	?	0.198	5.0	0.09	10.46	11.6	0.902	0.395	0.698	1.136	0.558	0.299	0.133	0.709	0.966	0.0	0.186
Patranomodon nyaphulii	0.29	?	0.228	0.914	0.272	0.076	?	0.202	6.0	0.043	11.03	13.7	0.744	0.476	1.25	1.059	?	?	?	?	?	0.0	?
Galeops whaitsi	0.339	5.325	0.18	?	0.327	?	?	0.136	4.1	?	10.39	?	?	0.489	0.831	0.968	0.646	0.356	0.181	?	?	?	0.257
Galepus jouberti	?	?	?	0.855	?	?	?	?	?	?	?	?	?	?	?	?	?	0.351	0.149	?	?	0.0	?
Galechirus scholtzi	?	?	?	?	?	?	?	?	?	?	?	?	?	0.355	0.865	0.7	?	0.401	0.206	?	?	0.0	?
Eodicynodon oelofseni	0.351	?	?	0.968	0.435	?	2.47	?	?	?	?	12.0	?	0.259	0.708	?	?	?	?	?	?	?	?
Eodicynodon oosthuizeni	0.322	5.555	0.234	0.908	0.518	0.111	2.501	0.14	8.2	0.182	10.46	9.0	0.847	0.253	0.698	1.061	0.446	0.509	0.244	0.3	0.5	0.0	0.475
Colobodectes cluveri	0.203	5.714	0.195	?	0.52	0.269	2.07	0.142	6.6	0.206	10.18	?	0.948	?	?	?	?	?	?	?	?	?	?
Lanthanostegus mohoii	?	?	?	0.661	?	?	2.434	?	?	?	?	?	?	?	?	?	?	?	?	?	?	?	?
Eosimops newtoni	0.186	5.89	0.243	0.795	0.541	0.257	2.014	0.126	8.1	0.172	9.402	11.3	0.831	0.402	0.803	0.904	0.633	0.466	0.26	?	?	0.0	0.444
Prosictodon dubei	0.238	5.807	0.171	0.864	0.548	0.228	2.469	0.098	8.1	0.131	9.78	9.3	0.881	?	0.834	0.637	?	?	?	?	?	?	?
Diictodon feliceps	0.247	5.925	0.223	0.64	0.534	0.273	1.702	0.134	8.0	0.214	9.418	11.9	0.881	0.257	0.742	0.901	0.443	0.486	0.297	0.67	1.388	0.0	0.366
Robertia broomiana	0.237	5.863	0.197	0.721	0.555	0.259	1.681	0.105	8.6	0.199	9.417	9.8	0.85	0.132	0.711	0.868	0.487	0.502	0.227	?	?	0.0	0.309
Pristerodon mackayi	0.225	5.874	0.184	1.026	0.582	0.222	1.751	0.116	10.0	0.206	9.578	11.2	0.813	0.208	0.723	0.928	0.594	0.43	0.277	0.275	0.5	0.0	0.275
Brachyprosopus broomi	0.231	5.81	0.19	0.998	0.515	0.338	1.847	0.108	6.8	0.15	9.687	10.6	0.898	0.132	0.715	0.824	0.612	0.437	?	?	?	0.0	0.315
Endothiodon bathystoma	0.335	5.396	0.378	0.268	0.599	0.4	1.457	0.111	8.1	0.147	9.694	7.1	0.988	0.373	0.798	0.73	0.554	0.491	0.406	0.301	0.964	0.0	0.414
Endothiodon tolani	0.328	?	?	0.396	?	0.025	1.505	0.109	10.6	?	?	?	0.902	0.319	0.723	0.825	?	?	?	?	?	?	?
Niassodon mfumukasi	?	?	?	0.867	?	?	1.548	?	8.4	?	?	9.5	0.697	0.29	0.859	0.938	?	?	?	0.214	1.145	?	?
Digalodon rubidgei	0.354	6.155	0.294	0.899	0.473	0.139	1.565	0.134	?	0.173	?	?	0.871	0.293	?	?	?	?	?	?	?	?	?
Emydops	0.22	5.872	0.204	0.906	0.537	0.166	1.646	0.118	9.8	0.176	9.667	9.3	0.84	0.398	0.692	0.955	0.668	0.428	0.23	0.454	1.283	0.0	0.353
Dicynodontoides	0.269	5.95	0.24	0.764	0.539	0.211	1.492	0.085	8.823	0.181	9.814	11.9	0.887	?	0.726	0.924	0.304	0.497	?	0.167	2.5	0.406	0.359
Kombuisia frerensis	0.193	5.976	0.202	0.4	0.555	?	1.589	0.195	?	?	9.645	?	0.746	?	0.684	?	?	?	?	?	?	?	?
Myosaurus gracilis	0.26	5.902	0.275	1.032	0.483	0.108	1.59	0.085	9.6	0.208	9.775	9.6	0.853	0.348	0.958	0.942	0.586	?	?	?	?	?	0.208
Sauroscaptor tharavati	0.281	?	0.298	1.339	0.421	0.048	?	?	?	?	?	?	0.912	0.564	0.73	0.714	?	?	?	?	?	?	?
Cistecephalus microrhinus	0.279	6.056	0.289	1.139	0.509	0.088	1.49	0.117	9.55	0.0	9.965	10.2	0.872	0.38	0.687	0.789	0.485	0.403	0.317	0.754	1.857	0.0	0.324
Cistecephaloides boonstrai	0.311	6.047	0.425	1.319	0.372	0.04	?	0.194	?	?	10.31	12.5	0.632	0.346	0.796	0.914	?	?	?	?	?	?	?
Kawingasaurus fossilis	0.308	5.933	0.33	1.404	0.34	?	1.5	0.135	10.7	?	10.12	10.0	0.836	0.286	?	0.964	0.298	0.419	?	?	?	?	0.446
Rhachiocephalus magnus	0.329	6.094	0.271	0.738	0.598	0.606	1.48	0.094	8.8	0.143	9.17	12.8	1.011	0.167	0.838	0.777	0.501	0.506	?	?	?	?	0.372
Kitchinganomodon crassus	0.32	6.137	0.318	0.708	0.566	0.752	1.556	0.108	7.4	0.07	9.747	11.1	0.936	0.165	0.843	0.752	?	0.466	?	?	?	?	?
Oudenodon bainii	0.281	6.054	0.173	0.844	0.609	0.271	1.458	0.092	8.1	0.141	9.219	11.3	0.864	0.264	0.798	0.745	0.57	0.491	0.366	0.514	0.765	0.353	0.411
Tropidostoma dubium	0.284	5.989	0.197	0.899	0.565	0.277	1.436	0.098	8.8	0.14	9.106	12.4	0.875	0.237	0.758	0.766	0.531	0.503	?	0.474	1.368	0.345	0.378
Australobarbarus	0.333	6.058	0.183	0.697	0.561	0.298	1.324	0.101	6.1	0.16	9.822	13.35	0.882	0.193	0.624	0.694	0.466	0.485	?	0.848	1.033	0.333	0.391
Odontocyclops whaitsi	0.376	6.066	0.232	0.988	0.551	0.232	1.448	0.092	10.1	0.131	9.74	12.3	0.929	0.213	0.787	0.731	0.551	0.518	0.427	0.435	1.13	0.426	0.491
Idelesaurus tataricus	0.367	5.967	0.175	1.022	0.5	0.174	1.497	0.107	8.25	0.173	10.12	13.5	0.969	0.204	0.693	0.764	?	?	?	?	?	?	?

	1	2	3	4	5	6	7	8	9	10	11	12	13	14	15	16	17	18	19	20	21	22	23
Aulacephalodon bainii	0.3	6.089	0.323	0.892	0.583	0.204	1.425	0.117	6.8	0.122	9.48	13.5	0.822	0.172	0.76	0.785	0.55	0.532	0.348	0.714	1.067	0.395	0.491
Pelanomodon moschops	0.289	6.093	0.305	0.912	0.584	0.213	1.468	0.104	9.4	0.155	9.414	12.3	0.801	?	0.856	0.742	?	?	?	?	?	?	?
Geikia locusticeps	0.256	6.049	0.278	0.908	0.514	0.251	1.627	0.104	8.72	0.141	9.392	13.9	0.756	0.205	0.818	0.848	?	?	?	?	?	?	?
Geikia elginensis	0.366	?	0.521	0.846	0.529	?	1.429	?	?	?	?	13.1	0.829	0.212	0.9	0.987	?	?	?	?	?	?	?
Elph borealis	0.279	5.927	0.186	0.64	0.544	0.29	1.515	0.157	8.9	?	?	13.0	0.914	?	0.781	?	?	?	?	?	?	?	?
Interpresosaurus blomi	?	?	?	?	?	?	?	?	?	?	?	?	?	?	?	?	?	?	?	?	?	?	?
Katumbia parringtoni	0.196	5.868	0.22	0.527	0.541	0.347	1.489	0.112	9.3	0.132	9.928	14.4	?	?	0.833	0.822	?	?	?	?	?	?	?
Delectosaurus arefjevi	0.369	5.861	0.258	0.702	0.546	0.334	1.618	0.119	7.8	0.13	9.798	14.7	0.985	?	?	?	?	?	?	?	?	?	?
Dicynodon lacerticeps	0.324	5.982	0.253	0.607	0.546	0.359	1.485	0.117	7.7	0.121	9.869	11.9	0.926	0.241	0.749	0.766	?	?	?	?	?	?	?
Dicynodon angielczyki	0.308	5.937	0.253	0.524	0.569	0.359	1.351	0.105	7.56	0.114	9.95	12.0	0.965	0.219	0.808	?	0.476	?	?	?	?	?	?
Daptocephalus leoniceps	0.268	6.091	0.237	0.539	0.567	0.437	1.5	0.118	6.4	0.111	9.378	?	0.858	0.238	0.763	0.75	?	0.545	?	?	1.667	?	?
Daptocephalus huenei	0.292	6.091	0.249	0.450	0.574	?	1.25	0.123	?	0.117	9.68	?	1.024	?	?	?	?	0.573	?	?	?	?	?
Daqingshanodon limbus	0.282	6.112	0.26	0.619	0.442	0.18	1.528	0.08	?	0.189	9.34	10.3	0.808	0.212	0.677	0.819	?	?	?	?	?	?	?
Dinanomodon gilli	0.337	6.17	0.205	0.48	0.577	0.522	1.347	0.116	7.8	0.107	9.751	9.9	1.047	0.186	?	0.724	?	?	?	?	?	?	?
Peramodon amalitzkii	0.272	?	0.224	0.563	0.553	0.369	?	?	?	?	?	9.5	0.839	0.167	0.676	0.68	0.463	?	?	?	?	?	0.494
Vivaxosaurus trautscholdi	0.38	6.019	0.23	0.685	0.481	0.285	1.824	0.116	7.9	0.121	10.20	13.9	1.041	0.203	0.702	0.731	0.317	0.544	?	?	?	?	0.641
Jimusaria sinkiangensis	0.307	?	0.278	0.672	0.767	0.464	1.443	0.089	7.2	0.098	?	8.9	0.992	0.251	?	0.699	?	?	?	?	?	?	?
Sintocephalus alticeps	0.354	5.969	0.244	0.516	0.522	0.294	1.338	0.124	6.5	0.132	9.399	9.6	1.022	?	?	?	?	?	?	?	?	?	?
Basilodon woodwardi	0.315	5.994	0.212	0.722	0.497	0.225	1.305	0.128	5.7	0.139	9.599	12.6	0.814	?	?	?	?	?	?	?	?	?	?
Turfanodon bogdaensis	?	?	?	0.588	?	0.405	1.327	?	?	?	?	10.3	0.895	?	?	?	?	?	?	?	?	?	?
Keyseria benjamini	0.244	6.155	0.159	1.034	0.605	0.203	1.6	0.083	6.3	?	?	9.0	0.831	?	?	?	?	?	?	?	?	?	?
Gordonia traquairi	0.252	?	0.139	0.65	0.604	0.309	?	?	?	?	?	?	0.924	0.188	?	0.773	0.543	0.49	0.144	?	?	?	0.476
Syops vanhoepeni	?	?	?	0.484	?	0.343	?	?	?	?	?	?	?	?	?	?	?	?	?	?	?	?	?
Euptychognathus bathyrhynchus	0.336	6.028	0.13	0.562	0.56	0.238	1.559	0.091	6.5	0.084	9.663	10.25	0.792	?	0.79	0.815	?	?	?	?	?	?	?
Lystrosaurus hedini	0.32	6.111	0.414	0.705	0.413	0.146	1.471	0.174	9.2	0.079	10.20	11.4	0.673	0.294	0.691	0.781	?	?	?	?	?	?	?
Lystrosaurus maccaigi	0.274	6.072	0.347	0.656	0.325	0.108	1.764	0.165	8.4	0.123	10.02	10.9	0.805	0.354	0.711	0.706	?	0.526	0.54	?	?	0.389	?
Lystrosaurus curvatus	0.315	6.005	0.383	0.689	0.417	0.119	1.664	0.162	7.4	0.086	10.15	8.6	0.906	0.289	0.767	0.643	0.473	0.485	0.465	0.787	1.484	0.313	0.489
Lystrosaurus declivis	0.347	5.954	0.424	0.705	0.415	0.112	2.141	0.157	8.8	0.097	10.31	9.7	0.874	0.315	0.757	0.711	0.418	0.458	0.478	0.75	1.3	0.347	0.545
Lystrosaurus murrayi	0.288	6.003	0.427	0.726	0.466	0.143	2.002	0.175	8.4	0.101	10.36	11.7	0.816	0.316	0.793	0.754	0.478	0.46	0.441	0.843	1.455	0.392	0.605
Angonisaurus cruickshanki	0.339	6.301	0.514	0.667	0.572	0.6	1.491	0.19	5.9	0.06	10.21	10.0	1.012	0.143	0.785	0.722	?	0.524	?	0.647	2.541	?	?
Tetragonias njalilus	0.378	5.912	0.354	0.201	0.574	0.446	?	0.125	6.8	0.088	10.01	10.4	1.004	0.205	0.858	0.796	0.447	0.481	0.3	0.675	1.825	0.304	0.596
Shansiodon	0.265	6.064	0.327	0.163	0.538	0.633	1.314	0.13	7.2	0.1	9.78	11.2	1.129	0.286	0.821	0.84	0.575	0.479	?	0.758	1.363	0.363	0.675
Vinceria andina	0.267	6.099	0.352	0.201	0.49	0.466	?	0.137	7.0	0.153	10.53	11.3	0.983	?	?	?	?	?	?	?	?	?	?
Rhinodicynodon gracile	0.304	6.213	0.253	0.5	0.523	0.435	1.568	0.1	?	?	9.174	10.1	0.879	0.24	0.875	0.734	0.49	0.354	0.361	?	?	0.352	0.383
Dinodontosaurus	0.398	6.104	0.347	0.24	0.461	0.328	1.414	0.135	7.3	0.074	10.16	10.9	0.926	0.202	0.814	0.653	0.398	0.507	0.423	0.652	1.896	0.31	0.752
Kannemeyeria simocephalus	0.421	6.121	0.409	0.289	0.531	0.479	1.461	0.147	9.8	0.074	10.48	12.1	1.147	0.179	0.8	0.686	0.551	0.558	0.338	?	1.381	0.372	0.411
Kannemeyeria lophorhinus	0.361	6.286	?	0.663	?	0.318	2.051	0.149	10.8	0.086	10.43	?	?	0.077	0.786	0.542	?	?	?	?	?	?	?
Dolichuranus primaevus	0.356	6.079	0.392	0.293	0.484	0.4	1.339	0.143	8.7	0.085	10.67	9.7	1.018	0.192	0.756	0.542	?	0.519	?	?	?	0.425	?
Wadiasaurus indicus	0.423	6.105	0.337	0.539	0.506	0.523	?	0.218	?	?	?	10.6	1.052	0.344	0.9	0.81	0.607	0.563	0.45	0.562	1.239	0.417	0.355
Rabidosaurus cristatus	0.464	?	?	0.268	0.607	?	?	?	?	?	?	?	?	?	?	?	?	?	?	?	?	?	?
Rhadiodromus	0.509	6.144	0.403	0.285	0.574	0.254	?	0.122	6.9	0.088	10.02	10.8	1.085	?	?	?	?	?	0.604	?	?	?	?
Rechnisaurus cristarhynchus	0.51	5.971	0.436	0.154	?	0.211	?	0.14	9.9	?	?	?	?	?	?	?	?	?	?	?	?	?	?
Uralokannemeyeria vjuschkovi	0.49	?	0.407	0.526	0.454	0.233	?	0.147	?	0.091	?	11.9	1.154	?	?	?	?	?	?	0.819	1.193	?	?
Shaanbeikannemeyeria	0.527	6.069	0.513	0.886	0.5	0.414	?	0.157	7.8	0.176	10.64	11.3	1.432	?	0.734	?	?	0.58	?	?	?	0.416	?
Xiyukannemeyeria brevirostris	0.286	6.203	0.413	0.46	0.433	0.23	?	0.169	8.5	0.086	10.03	8.9	0.795	0.32	?	0.668	?	?	?	?	?	?	?
Parakannemeyeria	0.455	6.28	0.377	0.359	0.354	0.195	1.468	0.122	7.5	0.102	9.688	12.3	0.92	0.166	0.79	0.515	0.467	0.52	0.478	0.443	1.465	0.411	0.294

	1	2	3	4	5	6	7	8	9	10	11	12	13	14	15	16	17	18	19	20	21	22	23
Sinokannemeyeria	0.42	6.14	0.478	0.543	0.382	0.175	1.505	0.161	5.9	0.109	10.47	?	0.918	0.243	0.549	0.385	0.494	0.489	0.556	0.458	1.187	0.408	0.405
Stahleckeria potens	0.438	5.992	0.445	0.726	0.491	0.288	?	0.183	11.1	0.052	10.28	8.7	0.953	0.237	0.856	0.897	0.442	0.53	?	0.391	2.217	0.434	0.565
Eubrachiosaurus browni	?	?	?	?	?	?	?	?	?	?	?	?	?	?	?	?	?	0.538	?	?	1.789	?	?
Sangusaurus parringtonii	0.411	6.177	0.461	0.618	?	0.368	1.129	0.144	?	0.091	?	9.2	1.061	?	0.832	?	?	?	?	0.592	1.944	0.433	?
Ischigualastia jenseni	0.482	6.139	0.423	0.331	0.479	0.528	1.39	0.151	5.7	0.064	10.02	?	1.032	?	0.912	0.841	0.419	0.577	0.561	?	0.818	0.412	0.526
Jachaleria	0.392	6.078	0.393	0.199	0.379	0.499	1.431	0.161	4.0	0.084	10.27	?	0.766	?	0.822	0.766	0.427	?	0.529	?	0.808	0.434	0.667
Zambiasaurus submersus	?	?	?	?	?	?	?	?	?	?	?	?	?	?	?	?	?	0.498	?	?	?	0.401	?
Placerias hesternus	?	?	?	?	?	?	?	?	?	?	?	?	?	?	?	?	?	0.49	0.499	?	?	?	?
Moghreberia nmachouensis	?	?	?	0.863	?	?	?	?	?	?	?	?	?	?	?	?	0.486	0.559	0.416	?	?	0.364	0.290
Rastodon procurvidens	0.221	?	0.209	0.444	0.57	0.258	?	0.128	6.3	0.105	?	12.0	0.907	0.1	0.824	0.786	?	?	?	?	?	?	?
Bulbasaurus phylloxyron	0.284	6.003	0.25	0.562	0.534	0.233	1.362	0.112	10.33	0.052	9.851	14.78	0.887	?	0.643	?	?	?	?	?	?	?	?
Compsodon helmoedi	0.196	5.874	0.207	1.066	0.431	0.187	1.71	0.082	10.3	0.22	9.858	11.0	0.817	?	?	?	?	?	?	?	?	?	?
LPB 1993 3	0.297	5.068	?	?	0.276	0.134	?	0.131	8.333	0.140	?	9.616	0.876	?	?	?	?	?	?	?	?	?	?
LPB 1993 2	0.200	?	0.295	?	0.408	0.281	?	?	?	?	?	14.70	0.829	?	?	?	?	?	?	?	?	?	?
LPB 1995 9	0.205	?	0.254	?	?	0.316	?	0.124	?	0.101	?	?	0.935	?	?	?	?	?	?	?	?	?	?
Pentasaurus goggai	?	?	?	?	?	?	?	?	?	?	?	?	?	?	?	?	?	?	?	?	?	?	?
Ufudocyclops mukanelai	0.376	?	0.468	0.45	0.515	0.363	1.409	0.156	9.31	?	?	10.9	0.983	?	?	?	?	?	?	?	?	?	?
Lisowicia bojani	?	?	?	?	?	?	?	?	?	?	?	?	?	?	?	?	0.517	0.576	0.522	0.764	0.963	0.438	0.457

	24	25	26	27	28	29	30	31	32	33	34	35	36	37	38	39	40	41	42	43	44	45	46	47	48	49	50	51	52	53	54
Biarmosuchus	0	0	0	0	0	2	0	0	0	0	0	0	0	0	0	0	0	0	0	1	0	0	0	0	0	0	0	?	?	?	?
Hipposaurus boonstrai	0	0	0	0	0	2	0	0	0	0	0	0	0	0	0	0	0	0	0	1	0	0	0	0	0	0	0	?	?	?	?
Archaeosyodon praeventor	0	0	0	0	0	2	0	0	0	0	0	0	0	0	0	0	0	0	0	1	0	0	0	0	1	0	0	?	?	?	?
Titanophoneus potens	0	0	0	0	0	2	0	0	0	0	0	0	0	0	0	0	1	0	0	0	0	0	0	0	0	0	0	?	?	?	?
Gorgonops torvus	0	0	0	0	0	2	0	0	0	0	0	0	0	0	0	0	0	0	0	0	0	0	0	0	0	0	0	?	?	?	?
Lycosuchus vanderrieti	0	0	0	0	0	2	0	0	0	0	0	0	0	0	0	0	0	0	0	0	0	0	0	1	0	0	0	?	?	?	?
Glanosuchus macrops	0	0	0	0	0	2	0	0	0	0	0	0	0	0	0	0	0	0	0	1	0	0	0	0	0	0	0	?	?	?	?
Biseridens qilianicus	0	0	0	0	0	2	1	0	0	0	0	0	0	0	0	0	1	0	0	1	0	0	0	0	1	0	0	?	?	?	?
Anomocephalus africanus	?	?	?	?	?	?	?	0	?	?	?	?	?	0	0	?	?	0	?	0	?	1	0	0	?	?	0	?	?	?	?
Tiarajudens eccentricus	0	?	?	?	?	?	?	0	?	0	?	?	0	0	0	0	1	0	0	0	0	0	0	0	1	0	0	?	?	?	?
Otsheria netzvetajevi	0	0	0	0	0	2	1	0	1	0	0	0	0	0	0	?	1	0	0	1	?	1	0	0	?	0	0	?	?	?	?
Ulemica	0	0	0	0	0	2	1	0	1	0	1	0	0	0	0	?	1	0	0	1	?	0	0	0	1	0	0	?	?	?	?
Suminia getmanovi	0	0	0	0	0	2	?	0	1	0	1	0	0	0	0	0	1	0	0	1	?	1	0	0	2	0	0	?	?	?	?
Patranomodon nyaphulii	0	0	0	?	0	?	1	0	1	0	1	?	0	0	0	0	2	0	0	0	?	1	0	0	1	0	0	?	?	?	?
Galeops whaitsi	0	0	0	0	0	2	1	0	1	0	1	0	0	0	0	0	2	0	0	0	?	1	0	0	1	0	0	?	?	?	?
Galepus jouberti	?	0	0	?	0	2	?	?	1	?	?	?	?	0	0	?	?	0	?	?	?	?	?	?	?	?	0	?	?	?	?
Galechirus scholtzi	0	0	?	?	0	?	?	0	1	0	?	0	?	0	0	?	?	0	0	0	?	1	0	0	1	?	0	?	?	?	?
Eodicynodon oelofseni	?	?	?	?	?	?	?	0	1	?	1	0	0	0	0	0	2	0	0	0	0	1	0	0	1	?	0	?	?	?	?
Eodicynodon oosthuizeni	0	0	0	0	1	0	1	2	1	0	1	0	0	0	0	0	2	0	0	0	0	2	0	0	1	0	1	0	0	0	0
Colobodectes cluveri	0	1	0	0	1	0	1	2	1	0	1	0	0	0	0	0	2	0	0	0	0	2	0	0	1	0	1	0	0	0	0
Lanthanostegus mohoii	0	?	?	?	?	?	?	?	?	?	1	?	?	?	?	0	?	?	?	?	?	2	0	0	?	1	?	?	?	?	?
Eosimops newtoni	1	1	1	0	1	0	1	2	1	1	1	0	0	0	0	0	2	0	0	0	0	2	1	0	1	1	1	2	0	0	0
Prosictodon dubei	1	1	1	0	1	0	1	2	1	1	1	0	0	0	0	0	2	0	0	0	0	2	1	0	1	1	1	2	0	0	0
Diictodon feliceps	1	1	1	0	1	0	1	2	1	1	1	0	0	0	0	0	2	0	0	0	0	2	2	?	?	1	1	2	0	0	0
Robertia broomiana	1	1	1	0	1	0	1	2	1	1	1	0	0	0	0	0	2	0	0	0	0	2	1	0	1	1	1	2	0	0	0
Pristerodon mackayi	1	1	0	0	1	2	1	2	1	0	1	0	0	0	0	0	2	0	0	0	0	2	1	0	1	1	1	0	0	1	0
Brachyprosopus broomi	1	0	1	1	1	2	1	2	1	0	1	1	0	0	0	1	2	0	0	0	0	2	1	1	1	1	1	0	0	1	0
Endothiodon bathystoma	1	0	0	1	[01]	2	1	1	1	0	1	2	0	0	0	0	2	0	1	0	0	1	1	1	2	0	0	?	?	?	?
Endothiodon tolani	1	0	0	1	0	2	1	1	1	0	1	2	0	0	0	1	2	0	1	0	0	2	1	1	2	0	0	?	?	?	?
Niassodon mfumukasi	1	?	?	?	2	2	?	1	1	?	1	?	0	0	0	1	?	?	?	0	?	1	1	0	1	1	1	0	0	1	0
Digalodon rubidgei	1	2	1	0	2	0	1	2	1	0	1	0	0	0	0	1	2	0	0	0	0	2	2	?	?	0	1	1	0	1	0
Emydops	1	0	1	1	1	0	1	2	1	0	1	0	0	0	0	0	2	0	0	0	0	2	0	0	1	1	1	1	0	1	0
Dicynodontoides	1	0	1	1	2	0	1	2	1	0	1	0	0	0	0	1	2	0	0	0	0	2	2	?	?	1	1	1	0	1	0
Kombuisia frerensis	1	0	1	0	2	0	1	2	1	0	1	0	0	0	0	1	2	?	0	0	0	1	2	?	?	0	1	1	0	1	0
Myosaurus gracilis	1	0	0	0	2	1	1	2	1	0	1	0	0	0	0	1	2	0	0	0	0	1	2	?	?	1	1	1	0	1	0
Sauroscaptor tharavati	1	?	?	?	2	?	?	2	1	?	1	0	0	0	0	1	?	0	0	0	0	1	2	?	?	?	1	1	0	1	0
Cistecephalus microrhinus	1	0	1	0	2	0	1	2	1	0	1	0	0	0	0	1	2	0	1	0	0	1	2	?	?	1	1	1	0	1	0
Cistecephaloides boonstrai	1	0	0	0	2	0	1	2	1	0	1	0	0	0	0	1	2	0	1	0	0	1	2	?	?	0	1	1	0	1	0
Kawingasaurus fossilis	1	0	0	0	2	0	1	2	1	0	1	0	0	0	0	1	2	0	1	0	0	1	2	?	?	0	1	1	0	1	0
Rhachiocephalus magnus	1	2	0	0	2	2	1	2	1	0	1	1	0	0	0	0	2	0	0	0	0	1	2	?	?	1	1	0	0	0	1
Kitchinganomodon crassus	1	2	0	0	2	2	1	2	1	0	1	1	0	0	0	0	2	0	0	0	0	1	2	?	?	1	1	0	0	0	1
Oudenodon bainii	1	2	0	0	2	2	1	2	1	0	1	1	0	0	0	0	2	0	0	0	0	1	2	?	?	1	1	0	1	0	1
Tropidostoma dubium	1	2	0	0	2	2	1	2	1	0	1	1	0	0	0	0	2	0	0	0	0	2	1	0	1	1	1	0	1	0	1
Australobarbarus	1	2	0	0	2	2	1	2	1	0	1	1	0	0	0	0	2	0	0	0	0	2	1	0	?	1	1	0	1	0	1
Odontocyclops whaitsi	1	2	0	0	2	2	1	2	1	0	1	1	0	0	0	0	2	0	0	0	0	2	2	?	?	1	1	0	1	0	1
Idelesaurus tataricus	1	2	0	0	2	2	1	2	1	0	1	1	0	0	0	0	2	0	0	0	0	2	2	?	?	1	1	0	1	0	1

	55	56	57	58	59	60	61	62	63	64	65	66	67	68	69	70	71	72	73	74	75	76	77	78	79	80	81	82	83	84	85
Biarmosuchus	0	0	0	0	0	0	0	0	0	0	0	0	0	0	?	2	0	0	0	2	0	0	0	0	0	0	0	0	0	0	0
Hipposaurus boonstrai	0	0	0	0	0	0	0	0	0	0	0	0	0	1	0	2	0	0	0	0	0	0	0	0	0	0	0	0	0	0	0
Archaeosyodon praeventor	0	0	0	0	0	0	0	1	0	0	0	0	0	0	?	2	0	0	0	1	0	0	0	0	0	0	0	0	0	0	0
Titanophoneus potens	0	0	0	0	0	0	0	1	0	0	1	0	0	0	?	1	0	0	0	0	0	0	0	[02]	0	0	0	0	0	0	0
Gorgonops torvus	0	0	0	0	0	0	0	0	1	0	0	0	0	1	0	2	0	0	0	2	0	0	0	2	0	0	0	0	0	0	0
Lycosuchus vanderrieti	0	0	0	2	0	0	0	0	0	0	0	0	0	0	?	1	0	2	0	1	1	0	0	1	0	0	0	0	0	0	0
Glanosuchus macrops	0	0	0	0	0	0	0	0	0	0	0	0	1	0	?	1	0	2	0	1	1	0	0	1	0	0	0	0	0	0	0
Biseridens qilianicus	0	0	0	0	0	0	0	1	0	0	0	1	0	0	?	2	0	0	0	1	0	0	0	0	0	0	0	0	0	0	0
Anomocephalus africanus	?	?	0	?	?	?	0	?	?	?	0	0	?	?	?	?	?	?	?	?	?	?	?	?	?	?	0	?	?	0	0
Tiarajudens eccentricus	0	0	0	?	?	0	0	?	0	0	0	0	?	?	?	?	?	?	?	?	?	?	?	?	?	?	0	0	?	0	0
Otsheria netzvetajevi	?	0	0	0	0	0	0	0	0	0	0	0	0	0	?	2	?	0	0	1	0	?	0	0	0	0	0	0	0	0	0
Ulemica	0	0	0	0	0	0	0	1	0	0	0	0	0	0	?	2	0	0	0	1	0	?	0	0	0	0	1	0	0	0	0
Suminia getmanovi	?	0	0	1	0	0	0	0	0	0	0	0	0	0	?	2	1	0	0	1	0	?	0	0	0	0	2	0	0	0	0
Patranomodon nyaphulii	?	0	0	0	0	0	0	0	0	0	0	0	0	1	0	0	1	0	0	0	0	0	0	1	0	0	0	0	0	0	0
Galeops whaitsi	?	?	1	?	0	0	0	0	0	0	0	0	0	?	?	?	1	0	0	0	?	0	0	?	0	?	2	0	0	0	0
Galepus jouberti	?	?	?	?	?	?	?	?	?	?	0	0	?	?	?	?	?	?	?	?	?	?	?	?	?	?	?	?	?	?	0
Galechirus scholtzi	?	?	1	?	?	0	0	?	?	?	?	?	?	?	?	?	?	?	?	?	?	?	?	?	?	?	?	?	?	?	?
Eodicynodon oelofseni	?	?	?	?	0	?	0	0	0	0	0	0	0	1	0	?	?	0	0	1	0	0	0	1	0	0	2	0	1	0	?
Eodicynodon oosthuizeni	0	0	1	1	0	0	0	0	0	0	0	0	0	1	0	0	1	0	0	1	0	0	0	1	0	0	2	1	1	0	0
Colobodectes cluveri	0	0	1	1	0	0	0	0	0	1	0	0	0	1	0	1	1	0	0	0	0	0	0	1	0	?	2	1	1	0	0
Lanthanostegus mohoii	0	?	?	?	0	?	0	1	0	0	0	1	0	1	0	1	?	0	0	1	0	0	0	2	0	0	?	?	?	0	0
Eosimops newtoni	1	0	1	0	0	0	0	1	0	0	0	1	0	1	0	1	1	0	0	1	0	0	0	2	0	0	2	1	1	0	0
Prosictodon dubei	1	0	1	1	0	0	0	1	0	0	0	0	0	1	0	1	1	2	0	0	0	0	0	1	0	?	2	1	1	0	0
Diictodon feliceps	1	[01]	1	[01]	0	0	0	1	0	0	0	0	0	1	0	1	1	2	0	0	0	0	0	[12]	0	0	2	1	1	0	0
Robertia broomiana	1	0	1	0	0	0	0	1	0	0	0	0	0	1	0	1	1	0	0	1	0	0	0	2	0	0	2	1	1	0	0
Pristerodon mackayi	0	0	1	0	0	0	0	1	0	0	0	?	0	1	0	1	1	0	0	1	0	0	0	1	0	1	2	1	1	0	0
Brachyprosopus broomi	0	0	1	0	0	0	0	1	0	0	0	0	0	1	0	1	1	0	0	1	0	0	0	2	0	0	2	1	1	0	0
Endothiodon bathystoma	?	0	[12]	?	0	0	1	0	0	[01]	1	0	1	1	1	1	1	1	0	1	0	1	0	2	0	0	2	1	1	0	0
Endothiodon tolani	?	?	[01]	0	0	0	0	0	0	1	?	?	0	1	0	1	1	1	0	1	0	1	0	1	0	0	2	?	1	?	?
Niassodon mfumukasi	1	0	1	0	0	0	0	0	0	0	0	0	0	2	1	2	1	0	0	2	0	0	0	1	0	0	2	0	1	0	0
Digalodon rubidgei	0	0	1	0	0	0	0	0	0	1	0	0	0	1	0	1	1	0	0	2	0	0	0	3	0	1	2	1	1	0	0
Emydops	1	0	1	0	0	0	0	0	0	0	0	0	0	1	0	1	1	0	0	1	0	0	0	1	0	0	2	0	1	0	0
Dicynodontoides	0	0	1	0	0	0	0	0	0	1	0	0	0	2	0	1	1	2	0	0	0	0	0	1	0	0	2	1	1	0	0
Kombuisia frerensis	1	0	1	0	0	0	0	0	0	1	0	0	0	2	0	1	0	2	0	1	1	?	1	?	?	0	2	?	1	0	0
Myosaurus gracilis	1	0	1	2	0	0	0	0	0	1	0	0	0	1	0	2	0	0	0	2	0	0	0	1	0	0	2	0	1	0	0
Sauroscaptor tharavati	0	?	1	?	0	?	0	0	?	1	0	0	0	0	?	?	?	0	0	2	0	?	0	1	0	0	2	0	1	0	0
Cistecephalus microrhinus	1	0	1	0	0	0	[01]	1	0	1	[01]	0	0	0	?	2	1	0	0	2	0	0	0	1	0	1	2	0	1	0	0
Cistecephaloides boonstrai	0	0	1	0	0	0	0	0	1	1	0	0	0	0	?	2	1	0	0	2	0	0	0	1	0	1	2	0	1	0	0
Kawingasaurus fossilis	0	0	0	2	0	0	0	0	0	1	0	0	0	0	?	2	1	0	0	2	0	0	1	?	?	?	2	0	1	0	0
Rhachiocephalus magnus	0	0	2	0	0	1	1	0	0	0	1	0	0	1	0	1	1	2	0	0	0	0	0	2	1	0	2	1	1	0	0
Kitchinganomodon crassus	0	0	2	0	0	1	1	0	0	0	1	0	0	1	0	1	1	2	0	0	0	0	0	2	1	1	2	1	1	1	0
Oudenodon bainii	0	0	2	1	0	[01]	0	1	0	0	0	0	0	1	0	1	1	1	0	0	0	0	0	1	0	1	2	1	1	1	0
Tropidostoma dubium	0	0	2	1	0	1	0	1	0	0	0	0	0	1	0	1	1	1	0	0	0	0	0	1	0	1	2	1	1	1	0
Australobarbarus	0	0	2	?	0	?	0	1	0	0	0	0	0	1	0	1	1	1	0	0	0	0	0	1	0	1	2	1	1	1	0
Odontocyclops whaitsi	0	0	2	0	0	1	2	0	0	0	0	0	0	2	1	1	1	1	0	0	0	0	0	2	0	1	2	1	1	1	0
Idelesaurus tataricus	0	0	2	1	0	1	1	0	0	0	0	0	0	2	1	1	1	1	0	0	0	0	0	1	0	0	2	1	1	1	0

	86	87	88	89	90	91	92	93	94	95	96	97	98	99	100	101	102	103	104	105	106	107	108	109	110	111	112	113	114	115	116
Biarmosuchus	0	0	1	0	0	0	0	0	1	0	0	1	0	0	0	0	0	0	0	0	0	0	0	0	0	0	?	0	1	2	0
Hipposaurus boonstrai	0	0	1	0	0	0	0	0	1	0	1	1	0	0	0	0	0	0	0	0	0	0	0	0	0	0	?	0	1	0	0
Archaeosyodon praeventor	0	0	1	0	0	0	?	?	0	1	0	0	0	0	0	0	1	0	0	0	0	0	0	0	0	0	?	0	1	2	0
Titanophoneus potens	0	0	1	0	0	0	0	0	0	1	0	0	0	0	0	0	1	0	0	0	0	0	0	0	0	0	?	0	1	2	0
Gorgonops torvus	0	0	1	0	0	0	0	0	1	0	0	0	0	0	0	0	0	0	0	0	0	0	0	0	0	0	?	0	1	2	0
Lycosuchus vanderrieti	0	0	1	0	0	0	0	0	0	1	0	0	1	0	0	0	1	1	0	0	0	0	0	0	0	0	?	0	1	2	0
Glanosuchus macrops	0	0	1	0	0	0	0	0	0	1	0	0	1	0	0	0	1	1	0	0	0	0	0	0	0	0	?	0	1	2	0
Biseridens qilianicus	0	0	1	0	0	1	?	?	0	0	0	0	0	0	0	0	1	0	0	0	0	0	0	0	0	0	?	0	0	?	0
Anomocephalus africanus	0	0	?	0	?	0	1	?	?	?	?	?	?	?	?	?	?	?	?	?	?	?	1	?	?	?	?	?	?	?	2
Tiarajudens eccentricus	0	0	?	0	?	0	1	?	?	?	?	?	?	?	?	?	?	?	?	?	0	1	1	?	?	?	?	0	?	?	2
Otsheria netzvetajevi	1	0	1	0	1	0	?	?	1	1	?	?	1	0	1	0	0	0	0	1	0	1	0	0	0	0	?	0	0	0	1
Ulemica	1	0	1	0	?	0	0	0	1	1	0	0	1	1	1	0	2	0	0	1	0	1	0	0	1	0	?	0	0	0	1
Suminia getmanovi	1	0	?	0	1	0	0	0	1	1	0	0	?	1	1	0	2	0	2	1	0	1	0	0	1	0	?	0	1	0	1
Patranomodon nyaphulii	1	0	0	0	0	0	0	0	0	0	0	0	1	0	0	0	1	0	?	0	1	1	0	0	0	0	?	0	1	0	1
Galeops whaitsi	1	0	1	0	?	0	0	1	0	0	0	0	1	?	0	0	1	0	?	0	?	1	0	0	0	0	?	0	?	0	1
Galepus jouberti	?	?	?	?	?	0	?	?	?	?	?	?	?	?	?	?	?	?	?	?	?	?	?	?	?	?	?	?	?	?	?
Galechirus scholtzi	?	?	?	0	?	0	?	?	?	?	?	?	?	?	?	?	?	?	?	?	?	?	?	?	?	?	?	?	?	?	?
Eodicynodon oelofseni	2	0	0	?	?	0	?	?	0	0	0	0	1	1	1	0	3	0	?	?	?	?	0	1	2	?	?	?	1	3	1
Eodicynodon oosthuizeni	2	0	1	0	1	0	1	0	0	0	0	0	1	1	1	0	3	0	1	0	0	1	0	1	2	1	0	0	1	3	1
Colobodectes cluveri	2	0	1	0	1	0	?	?	0	0	0	1	1	1	1	0	3	0	1	0	0	1	0	1	2	1	0	0	1	3	1
Lanthanostegus mohoii	0	0	?	0	?	0	?	?	0	?	?	?	1	1	1	0	3	0	1	?	0	1	0	1	2	1	1	0	?	3	1
Eosimops newtoni	2	0	1	1	1	0	1	0	1	0	[01]	[01]	1	1	1	0	3	0	1	0	0	1	0	1	2	1	0	0	1	3	1
Prosictodon dubei	2	0	1	1	1	0	1	0	1	0	0	0	1	1	1	0	3	0	1	0	0	1	0	1	2	1	0	0	1	2	1
Diictodon feliceps	2	0	1	1	1	0	1	0	1	1	1	1	1	1	1	0	3	0	1	0	0	1	0	1	2	1	0	0	1	2	1
Robertia broomiana	2	0	1	1	1	0	1	0	1	0	0	0	1	1	1	0	3	0	1	0	0	1	0	1	2	1	0	0	1	2	1
Pristerodon mackayi	2	0	1	1	1	0	1	0	1	0	0	0	1	1	1	0	3	0	2	1	0	1	0	1	2	1	0	0	1	2	1
Brachyprosopus broomi	2	0	1	0	1	0	1	0	0	0	0	0	1	1	1	0	3	0	2	0	0	1	0	1	2	1	0	0	1	2	1
Endothiodon bathystoma	2	0	1	0	1	1	1	0	1	0	0	0	1	1	1	1	3	0	2	1	0	1	0	1	2	0	?	0	1	3	1
Endothiodon tolani	2	?	?	0	?	1	1	0	1	1	0	0	1	1	1	1	3	0	2	1	0	1	0	1	2	1	0	0	1	3	1
Niassodon mfumukasi	2	0	1	0	1	0	1	0	1	0	0	0	1	1	1	1	3	1	1	1	0	?	0	1	2	1	1	0	1	2	1
Digalodon rubidgei	2	0	1	1	1	0	1	0	1	1	1	1	1	1	1	0	3	0	1	1	0	1	0	1	2	1	0	0	1	2	1
Emydops	2	0	1	1	1	0	1	0	1	1	1	1	1	1	1	0	3	0	1	1	0	1	0	1	2	1	1	0	0	2	1
Dicynodontoides	2	0	1	0	1	0	1	0	1	0	0	0	1	1	1	0	3	0	1	1	0	1	0	1	2	1	1	0	0	2	1
Kombuisia frerensis	2	0	?	0	1	0	1	?	1	?	?	?	1	1	1	0	3	0	1	1	0	1	0	?	2	1	1	0	0	?	1
Myosaurus gracilis	2	0	1	0	1	0	1	0	1	1	1	1	1	0	1	0	3	1	1	1	0	1	0	1	2	1	1	0	1	2	1
Sauroscaptor tharavati	2	0	0	1	1	0	1	0	1	1	?	?	1	1	1	0	3	?	?	1	0	?	0	1	2	1	1	?	1	3	1
Cistecephalus microrhinus	2	0	0	1	1	0	1	0	1	1	0	1	1	1	1	0	3	1	1	1	0	1	0	1	2	1	1	0	0	2	1
Cistecephaloides boonstrai	2	0	0	0	1	0	1	0	1	1	0	1	1	1	1	0	3	?	1	1	0	1	0	1	2	0	?	?	0	?	1
Kawingasaurus fossilis	2	0	0	1	?	0	1	0	1	1	0	1	1	1	1	0	3	1	1	1	0	1	0	1	2	0	?	0	0	1	1
Rhachiocephalus magnus	2	0	1	1	1	0	1	1	1	1	1	1	1	2	2	0	3	0	1	1	0	1	0	1	2	1	0	0	1	2	1
Kitchinganomodon crassus	2	0	1	1	1	0	1	1	1	1	0	1	1	2	2	0	3	0	1	1	0	1	0	1	2	1	0	0	1	3	1
Oudenodon bainii	2	0	1	1	1	0	1	0	1	1	1	1	1	2	2	0	3	0	1	1	0	1	0	1	2	1	0	0	1	2	1
Tropidostoma dubium	2	0	1	1	1	0	1	0	1	1	0	0	1	2	2	0	3	0	1	1	0	1	0	1	2	1	0	0	1	2	1
Australobarbarus	2	0	1	1	1	0	1	0	1	1	1	1	1	2	2	0	3	0	1	0	0	1	0	1	2	1	0	1	1	2	1
Odontocyclops whaitsi	2	0	1	1	1	0	1	0	1	1	1	1	1	2	2	0	3	0	1	1	0	1	0	1	2	1	0	0	1	2	1
Idelesaurus tataricus	2	0	1	1	1	0	1	0	1	1	0	0	1	2	2	0	3	0	1	1	1	1	0	1	2	1	0	0	1	2	1

	117	118	119	120	121	122	123	124	125	126	127	128	129	130	131	132	133	134	135	136	137	138	139	140	141	142	143	144	145	146	147
Biarmosuchus	1	?	?	0	?	?	0	0	?	0	?	?	0	0	0	0	?	?	0	0	0	0	0	0	0	0	0	0	0	0	0
Hipposaurus boonstrai	1	?	?	0	?	0	0	0	?	0	?	?	?	0	0	0	0	0	0	?	0	0	0	0	0	0	0	0	0	0	0
Archaeosyodon praeventor	1	?	?	0	?	?	?	0	?	?	?	?	?	?	?	?	?	?	?	?	0	0	0	0	1	1	0	0	0	0	0
Titanophoneus potens	1	0	0	0	0	0	0	0	?	0	0	1	0	0	0	0	1	0	0	0	0	0	0	0	0	0	0	0	0	0	0
Gorgonops torvus	1	0	0	0	0	0	0	0	?	0	0	0	0	0	0	0	0	0	0	0	0	0	0	0	0	0	0	0	0	0	0
Lycosuchus vanderrieti	1	0	0	1	0	0	0	0	1	0	0	1	?	0	0	0	0	0	0	0	0	0	0	0	0	0	0	0	0	0	0
Glanosuchus macrops	1	0	0	0	0	0	0	0	1	0	0	1	0	0	0	0	0	0	0	0	0	0	0	0	0	0	0	0	0	0	0
Biseridens qilianicus	1	?	?	?	?	?	?	0	?	0	?	?	?	0	0	0	1	0	0	?	0	0	1	0	1	0	0	1	0	0	0
Anomocephalus africanus	?	?	?	?	?	?	?	?	?	?	?	?	?	?	?	?	?	?	?	?	1	?	?	0	1	0	?	?	?	?	?
Tiarajudens eccentricus	?	?	?	?	?	?	?	?	?	?	?	?	?	?	?	?	?	?	?	?	?	?	?	?	?	?	?	?	?	?	?
Otsheria netzvetajevi	1	?	?	?	0	0	?	0	0	0	?	?	?	1	?	1	?	?	0	?	?	?	?	?	?	?	?	?	?	?	?
Ulemica	1	?	?	1	0	0	0	0	1	0	?	1	0	?	?	1	?	0	0	0	1	0	1	0	1	1	1	1	0	1	0
Suminia getmanovi	1	0	?	1	0	0	?	0	0	0	0	1	0	1	0	0	1	?	0	?	1	0	0	0	2	1	1	1	0	0	0
Patranomodon nyaphulii	1	?	?	0	0	0	1	1	0	0	?	1	0	1	0	0	1	0	0	?	1	0	?	0	1	0	0	1	0	0	0
Galeops whaitsi	1	0	?	1	?	1	?	1	?	?	?	?	?	?	?	?	?	?	?	?	1	0	0	0	?	?	0	1	0	0	0
Galepus jouberti	?	?	?	?	?	?	?	?	?	?	?	?	?	?	?	?	?	?	?	?	?	0	?	0	1	0	0	1	?	0	0
Galechirus scholtzi	?	?	?	?	?	?	?	?	?	?	?	?	?	?	?	?	?	?	?	?	1	0	?	0	1	0	0	1	0	0	?
Eodicynodon oelofseni	0	?	?	0	0	0	?	?	?	0	?	?	?	?	0	?	1	0	?	0	1	0	1	1	1	0	0	2	0	0	0
Eodicynodon oosthuizeni	0	0	1	0	0	0	0	1	0	0	0	0	1	1	0	1	1	0	0	0	1	0	1	0	1	0	0	2	0	0	1
Colobodectes cluveri	0	0	1	0	0	0	0	1	1	0	0	?	?	1	0	?	?	?	0	?	?	?	?	?	?	?	?	?	?	?	?
Lanthanostegus mohoii	0	?	1	0	0	?	0	1	1	0	?	?	?	?	?	?	?	?	?	?	?	?	?	?	?	?	?	?	?	?	?
Eosimops newtoni	0	0	?	0	0	0	0	1	1	0	0	1	?	1	?	1	1	0	0	?	1	0	1	1	?	?	?	4	0	0	0
Prosictodon dubei	0	?	?	0	0	0	1	1	1	0	0	1	1	1	?	1	1	0	0	?	1	0	1	1	?	?	?	2	0	?	1
Diictodon feliceps	0	0	0	0	0	0	1	1	2	0	0	1	1	1	0	1	1	0	0	0	1	0	1	2	?	?	?	2	0	0	1
Robertia broomiana	0	0	?	0	0	0	1	1	1	0	0	1	?	1	0	1	1	0	0	0	1	0	1	1	1	0	?	2	0	0	1
Pristerodon mackayi	0	0	1	0	0	0	1	1	2	0	0	1	1	1	0	1	1	0	0	0	1	0	1	1	2	0	0	2	?	0	1
Brachyprosopus broomi	1	0	1	0	0	0	1	1	2	0	0	1	?	1	1	1	1	0	0	0	1	0	1	1	2	0	0	2	0	0	1
Endothiodon bathystoma	0	0	0	0	0	0	1	1	2	0	0	1	?	1	?	1	1	0	0	0	1	0	1	1	2	0	0	3	0	1	1
Endothiodon tolani	0	0	0	0	0	0	?	1	2	0	0	?	?	1	1	1	1	0	0	0	1	0	1	1	2	0	0	3	0	1	1
Niassodon mfumukasi	0	0	0	0	0	0	1	1	1	0	0	1	1	1	1	1	1	0	0	0	1	0	1	1	?	?	0	4	0	0	?
Digalodon rubidgei	0	0	0	0	0	1	1	1	?	0	0	1	?	1	1	1	1	0	0	?	1	0	1	2	?	?	?	4	0	0	0
Emydops	0	0	0	0	0	1	1	1	2	0	0	1	0	1	1	1	1	0	1	0	1	0	1	1	[12]	0	0	4	0	0	0
Dicynodontoides	0	0	0	0	0	1	1	1	2	0	0	1	0	1	1	1	1	0	0	0	2	0	1	2	?	?	?	4	1	0	0
Kombuisia frerensis	?	?	1	0	0	1	1	1	2	0	0	1	0	1	1	0	1	0	0	?	2	0	1	2	?	?	?	4	1	0	1
Myosaurus gracilis	0	0	1	0	0	1	1	1	2	0	0	1	1	1	1	1	1	0	0	0	1	0	1	2	?	?	?	4	1	0	0
Sauroscaptor tharavati	?	?	?	?	0	1	?	1	?	0	0	?	?	?	?	1	1	0	0	?	1	1	1	?	?	?	?	4	0	0	0
Cistecephalus microrhinus	?	0	0	?	0	1	1	1	2	0	0	0	1	?	1	1	1	0	0	?	1	1	1	2	?	?	?	4	0	0	0
Cistecephaloides boonstrai	?	?	?	?	0	1	1	1	1	0	?	1	?	?	1	1	1	0	0	?	1	1	1	2	?	?	?	4	0	0	0
Kawingasaurus fossilis	?	?	?	?	0	1	1	1	1	0	?	0	?	?	0	1	1	0	0	0	1	0	1	2	?	?	?	?	?	0	0
Rhachiocephalus magnus	0	0	0	0	1	2	1	1	2	0	0	1	1	1	0	1	1	0	0	0	1	1	1	2	?	?	?	2	0	0	1
Kitchinganomodon crassus	?	0	?	0	1	2	1	1	2	0	1	1	?	1	0	1	1	0	0	?	1	1	1	2	?	?	?	2	0	0	1
Oudenodon bainii	0	0	0	0	1	2	1	1	2	0	0	1	1	1	0	1	1	0	0	0	1	1	1	2	?	?	?	2	0	0	1
Tropidostoma dubium	0	0	?	0	1	2	1	1	2	0	0	1	1	1	0	1	1	0	0	0	1	1	1	1	?	?	?	2	0	0	1
Australobarbarus	0	?	?	0	1	2	1	1	2	0	1	1	1	1	0	1	1	0	0	?	1	1	1	1	2	0	?	2	0	0	1
Odontocyclops whaitsi	0	0	?	0	1	2	1	1	2	0	1	1	?	1	0	1	1	0	0	?	1	1	1	2	?	?	?	2	0	0	1
Idelesaurus tataricus	0	0	0	0	0	2	1	1	2	0	1	?	?	1	0	0	1	0	0	?	1	1	1	2	?	?	?	2	1	0	1

	148	149	150	151	152	153	154	155	156	157	158	159	160	161	162	163	164	165	166	167	168	169	170	171	172	173	174	175	176	177	178
Biarmosuchus	0	0	0	?	?	0	0	0	0	0	0	0	0	0	0	0	0	0	?	0	0	0	0	?	1	0	0	0	0	1	1
Hipposaurus boonstrai	0	0	0	?	?	0	0	0	0	0	1	0	0	0	0	0	0	0	?	1	0	0	0	0	1	0	0	0	1	1	1
Archaeosyodon praeventor	0	0	0	?	?	0	0	0	?	?	?	?	?	?	?	?	0	?	?	?	?	?	?	?	?	?	?	?	?	?	?
Titanophoneus potens	0	0	0	?	?	0	0	0	1	0	0	0	0	0	0	0	0	0	?	0	0	0	0	0	?	0	0	0	0	0	0
Gorgonops torvus	0	0	0	?	?	0	0	0	0	0	1	1	0	0	0	0	0	0	?	0	0	0	0	0	1	0	0	0	1	0	0
Lycosuchus vanderrieti	0	0	0	?	?	0	1	0	0	0	2	0	1	0	0	0	0	0	?	0	0	0	0	0	1	0	0	0	1	0	0
Glanosuchus macrops	0	0	0	?	?	0	1	0	0	0	2	0	1	0	0	0	0	0	?	0	0	0	0	0	1	0	0	0	1	0	0
Biseridens qilianicus	0	0	0	?	?	0	0	0	0	0	0	?	1	?	?	?	0	?	?	?	?	?	?	?	?	?	?	?	?	?	?
Anomocephalus africanus	?	?	0	?	?	?	?	?	?	?	?	?	?	?	?	?	?	?	?	?	?	?	?	?	?	?	?	?	?	?	?
Tiarajudens eccentricus	?	?	?	?	?	?	?	?	?	?	?	?	?	?	?	?	?	?	?	?	0	0	?	?	?	0	0	0	1	0	1
Otsheria netzvetajevi	?	?	?	?	?	?	?	?	?	?	?	?	?	?	?	?	?	?	?	?	?	?	?	?	?	?	?	?	?	?	?
Ulemica	0	0	1	0	0	[01]	0	0	0	0	0	0	1	0	0	1	1	?	?	?	?	?	?	?	?	?	?	?	?	?	?
Suminia getmanovi	0	0	1	0	0	0	0	0	0	0	0	0	0	0	0	2	1	0	?	0	0	0	0	0	0	0	0	0	0	0	0
Patranomodon nyaphulii	0	0	0	?	?	?	?	0	0	0	3	1	0	0	0	0	1	0	?	?	?	?	?	?	?	?	?	?	?	?	?
Galeops whaitsi	0	0	1	0	0	?	1	0	1	1	3	1	0	0	0	1	1	?	?	0	0	1	0	0	0	0	0	0	0	1	0
Galepus jouberti	0	0	?	?	?	?	?	?	?	?	?	?	?	?	?	?	1	?	?	?	?	?	?	1	?	0	0	0	1	0	?
Galechirus scholtzi	?	0	?	?	?	?	?	?	?	0	3	1	?	?	?	?	1	?	?	?	0	0	0	0	?	?	0	?	1	0	0
Eodicynodon oelofseni	0	0	1	0	0	1	?	0	1	?	?	1	?	?	1	2	1	?	?	?	?	?	?	?	?	?	?	?	?	?	?
Eodicynodon oosthuizeni	0	0	2	0	0	1	0	0	1	1	3	1	1	1	1	2	1	0	?	0	0	0	1	0	0	0	0	0	0	1	1
Colobodectes cluveri	?	?	?	?	?	?	?	?	?	?	?	?	?	?	?	?	?	?	?	?	?	?	?	?	?	?	?	?	?	?	?
Lanthanostegus mohoii	?	?	?	?	?	?	?	?	?	?	?	?	?	?	?	?	?	?	?	?	?	?	?	?	?	?	?	?	?	?	?
Eosimops newtoni	1	1	1	0	0	0	0	0	1	1	3	1	?	1	1	2	1	0	?	1	0	0	1	1	?	0	0	0	0	0	1
Prosictodon dubei	1	1	1	0	0	?	0	?	1	?	?	1	?	?	1	2	1	?	?	?	?	?	?	?	?	?	?	?	?	?	?
Diictodon feliceps	1	1	1	0	0	1	0	0	1	1	3	1	1	1	1	2	1	1	?	1	0	0	1	1	0	0	0	0	0	0	0
Robertia broomiana	1	1	1	0	0	?	0	0	1	1	3	1	1	1	1	2	1	0	?	1	0	0	1	?	0	0	0	0	0	0	0
Pristerodon mackayi	2	0	2	0	0	1	0	0	1	1	3	1	1	1	1	2	1	2	?	1	1	0	1	0	0	0	0	0	0	1	0
Brachyprosopus broomi	2	0	1	0	0	1	0	0	1	1	3	1	1	1	1	2	1	?	?	0	0	0	1	?	?	0	0	0	0	1	0
Endothiodon bathystoma	2	0	2	0	0	1	0	0	1	1	4	1	1	1	1	2	1	2	?	0	0	0	1	0	?	0	0	0	0	1	0
Endothiodon tolani	2	0	2	0	0	1	0	0	1	1	4	1	1	1	1	2	1	?	?	?	?	?	?	?	?	?	?	?	?	?	?
Niassodon mfumukasi	2	0	2	0	0	1	0	0	1	1	4	?	1	1	1	2	1	1	?	?	?	?	?	?	?	?	?	?	?	?	?
Digalodon rubidgei	2	?	?	?	?	1	0	0	?	?	?	?	?	?	?	?	?	?	?	?	?	?	?	?	?	?	?	?	?	?	?
Emydops	2	0	2	1	0	1	0	0	1	1	3	1	1	1	1	2	1	0	?	1	?	0	1	0	?	0	0	0	0	0	0
Dicynodontoides	0	0	2	1	0	1	0	0	1	1	3	1	1	1	1	2	1	1	0	0	1	0	1	1	0	1	1	0	0	0	1
Kombuisia frerensis	0	0	2	0	0	1	?	0	1	1	?	1	1	0	1	2	1	?	?	?	?	?	?	?	?	?	?	?	?	?	?
Myosaurus gracilis	0	0	2	1	0	?	?	0	1	1	3	1	?	?	1	2	1	0	?	1	1	0	1	1	0	1	0	1	1	0	?
Sauroscaptor tharavati	?	0	2	1	0	1	0	?	?	1	?	1	?	?	?	?	1	?	?	?	?	?	?	?	?	?	?	?	?	?	?
Cistecephalus microrhinus	2	0	2	1	0	1	0	1	1	1	3	1	1	1	1	2	1	0	?	1	1	0	0	0	1	2	2	1	0	0	1
Cistecephaloides boonstrai	2	0	2	1	0	1	?	1	1	1	?	1	1	1	1	2	1	?	?	?	?	?	?	?	?	?	?	?	?	?	?
Kawingasaurus fossilis	0	0	1	0	0	1	1	1	1	?	?	?	1	1	1	2	1	?	?	1	1	0	0	0	?	2	2	0	0	0	1
Rhachiocephalus magnus	3	0	1	0	0	1	0	0	1	1	4	1	1	1	1	2	1	?	?	0	0	1	1	[01]	1	1	0	1	0	1	0
Kitchinganomodon crassus	?	0	1	2	1	?	?	0	?	1	4	1	1	?	1	2	1	?	?	?	?	0	0	?	?	?	1	0	?	0	1	0
Oudenodon bainii	3	0	1	2	1	1	0	0	1	1	4	1	1	1	1	2	1	2	0	0	0	0	1	0	0	1	0	1	0	1	0
Tropidostoma dubium	3	0	1	2	1	1	?	0	1	1	4	1	1	1	1	2	1	2	?	0	0	0	1	0	0	1	0	1	0	1	0
Australobarbarus	3	0	1	2	1	1	?	0	1	1	4	1	?	?	1	2	1	?	?	?	?	?	?	?	?	?	?	?	?	?	?
Odontocyclops whaitsi	3	0	1	2	1	?	?	0	1	1	4	1	1	?	1	2	1	2	0	0	0	0	1	?	?	1	0	1	0	1	0
Idelesaurus tataricus	3	0	1	2	1	1	?	0	1	1	4	1	1	1	1	2	1	?	?	?	?	?	?	?	?	?	?	?	?	?	?

	179	180	181	182	183	184	185	186	187	188	189	190	191	192	193	194	195	196	197
Biarmosuchus	0	1	?	0	0	0	1	1	0	0	0	0	1	1	0	?	0	0	?
Hipposaurus boonstrai	0	1	?	?	?	?	0	?	0	0	0	0	1	0	?	?	0	0	?
Archaeosyodon praeventor	?	?	?	?	?	?	?	?	?	?	?	?	?	?	?	?	0	?	?
Titanophoneus potens	0	0	1	1	0	0	1	1	0	0	0	1	2	?	1	?	0	0	?
Gorgonops torvus	0	1	0	0	0	1	1	0	1	1	1	0	0	1	1	?	0	0	?
Lycosuchus vanderrieti	0	1	1	1	0	?	?	?	0	0	0	?	?	?	?	?	0	0	?
Glanosuchus macrops	0	1	1	1	0	0	1	0	0	0	0	1	2	1	1	?	0	0	?
Biseridens qilianicus	?	?	?	?	?	?	?	?	?	?	?	?	?	?	?	?	?	?	?
Anomocephalus africanus	?	?	?	?	?	?	?	?	?	?	?	?	?	?	?	?	?	?	?
Tiarajudens eccentricus	0	?	?	?	?	?	?	?	?	?	?	1	2	?	1	?	?	0	?
Otsheria netzvetajevi	?	?	?	?	?	?	?	?	?	?	?	?	?	?	?	?	?	?	?
Ulemica	?	?	?	?	?	?	?	?	?	?	?	?	?	?	?	?	0	?	?
Suminia getmanovi	0	1	0	0	0	0	0	0	0	0	0	0	0	1	0	?	0	0	?
Patranomodon nyaphulii	?	0	1	1	0	?	?	?	0	0	0	?	?	?	?	?	0	?	?
Galeops whaitsi	0	?	?	?	?	?	?	?	?	?	?	?	?	?	?	0	0	?	?
Galepus jouberti	0	?	1	1	?	0	0	?	0	0	0	?	2	?	1	?	?	?	?
Galechirus scholtzi	0	0	1	1	?	0	0	?	0	0	0	1	2	1	1	?	?	?	?
Eodicynodon oelofseni	?	?	?	?	?	?	?	?	?	?	?	?	?	?	?	?	0	?	?
Eodicynodon oosthuizeni	0	?	1	1	0	1	0	0	0	0	0	1	?	?	?	1	0	0	?
Colobodectes cluveri	?	?	?	?	?	?	?	?	?	?	?	?	?	?	?	?	?	?	?
Lanthanostegus mohoii	?	?	?	?	?	?	?	?	?	?	?	?	?	?	?	?	?	?	?
Eosimops newtoni	0	?	1	1	0	1	0	0	0	0	0	1	?	?	?	?	0	0	?
Prosictodon dubei	?	?	?	?	?	?	?	?	?	?	?	?	?	?	?	?	0	0	?
Diictodon feliceps	0	?	1	1	0	1	0	0	0	0	0	1	2	1	1	0	0	0	?
Robertia broomiana	0	?	1	1	?	?	?	0	0	0	0	1	2	1	1	?	?	?	?
Pristerodon mackayi	0	?	1	1	0	1	?	0	0	0	0	1	2	1	1	?	0	0	?
Brachyprosopus broomi	?	?	?	?	?	?	?	?	0	1	?	?	?	?	?	?	0	?	?
Endothiodon bathystoma	0	?	1	1	0	1	1	?	0	0	0	1	2	1	1	0	0	?	?
Endothiodon tolani	?	?	?	?	?	?	?	?	?	?	?	?	?	?	?	?	0	?	?
Niassodon mfumukasi	?	?	?	?	0	1	?	?	?	1	?	?	?	?	?	?	0	0	?
Digalodon rubidgei	?	?	?	?	?	?	?	?	?	?	?	?	?	?	?	?	0	0	?
Emydops	0	1	1	1	0	?	?	?	0	0	0	1	2	1	1	?	0	?	?
Dicynodontoides	?	1	?	?	0	1	1	0	0	1	1	1	2	1	1	0	0	1	1
Kombuisia frerensis	?	?	?	?	?	?	?	?	?	?	?	?	?	?	?	?	0	?	?
Myosaurus gracilis	?	?	?	?	0	?	?	?	?	?	?	?	?	?	?	0	0	?	?
Sauroscaptor tharavati	?	?	?	?	?	?	?	?	?	?	?	?	?	?	?	?	0	1	1
Cistecephalus microrhinus	1	1	1	1	0	1	0	0	1	1	0	1	2	1	1	0	0	?	?
Cistecephaloides boonstrai	?	?	?	?	?	?	?	?	?	?	?	?	?	?	?	?	0	1	1
Kawingasaurus fossilis	1	?	1	1	?	?	?	?	?	?	?	1	2	1	1	?	0	1	0
Rhachiocephalus magnus	0	?	?	?	?	?	?	?	0	1	1	?	?	?	?	1	0	?	?
Kitchinganomodon crassus	?	?	?	?	?	?	?	?	?	?	?	?	?	?	?	?	1	1	0
Oudenodon bainii	0	?	1	1	0	1	1	1	0	1	1	1	2	1	1	0	0	0	?
Tropidostoma dubium	0	?	?	?	0	?	?	?	0	1	1	?	?	?	?	0	0	0	?
Australobarbarus	?	?	?	?	?	?	?	?	?	?	?	?	?	?	?	?	0	1	0
Odontocyclops whaitsi	0	?	?	?	0	1	1	1	0	1	1	?	?	?	?	?	0	?	?
Idelesaurus tataricus	?	?	?	?	?	?	?	?	?	?	?	?	?	?	?	?	?	?	?

	24	25	26	27	28	29	30	31	32	33	34	35	36	37	38	39	40	41	42	43	44	45	46	47	48	49	50	51	52	53	54
Aulacephalodon bainii	1	2	0	0	2	2	1	2	1	0	1	1	1	0	0	0	2	0	0	0	0	2	2	?	?	1	1	0	1	0	[01]
Pelanomodon moschops	1	2	0	0	2	2	1	2	1	0	1	1	1	0	0	0	2	0	0	0	0	1	2	?	?	1	1	0	1	0	1
Geikia locusticeps	1	2	0	0	2	2	1	2	1	0	1	1	1	0	0	0	2	0	0	0	0	1	2	?	?	1	1	0	1	0	1
Geikia elginensis	1	2	0	0	2	2	?	2	1	0	1	1	1	0	0	0	2	0	0	0	0	1	2	?	?	1	1	0	1	0	1
Elph borealis	1	?	?	0	2	?	?	2	1	0	1	0	0	0	0	0	2	0	1	0	0	2	2	?	?	1	1	0	1	0	0
Interpresosaurus blomi	1	2	0	0	?	?	1	2	1	0	1	0	0	0	0	0	2	0	1	0	0	2	2	?	?	1	1	0	1	0	0
Katumbia parringtoni	1	2	0	0	2	2	1	2	1	0	1	?	0	0	0	0	?	?	1	0	0	2	2	?	?	1	1	0	0	0	0
Delectosaurus arefjevi	1	2	0	0	2	2	1	2	1	0	1	0	0	0	0	0	2	1	0	0	0	2	2	?	?	1	1	0	1	0	0
Dicynodon lacerticeps	1	2	0	0	2	2	1	2	1	0	1	0	0	0	0	0	2	0	0	0	0	2	2	?	?	1	1	0	1	0	0
Dicynodon angielczyki	1	2	0	0	2	2	1	2	1	0	1	0	0	0	0	0	2	0	0	0	0	2	2	?	?	1	1	0	1	0	0
Daptocephalus leoniceps	1	2	0	0	2	2	?	2	1	0	1	0	0	0	0	0	2	0	0	0	0	2	2	?	?	1	1	0	1	0	0
Daptocephalus huenei	1	2	0	0	2	2	?	2	1	0	1	0	0	0	0	0	2	1	1	0	0	2	2	?	?	1	1	0	1	0	0
Daqingshanodon limbus	1	2	0	0	2	2	1	2	1	0	1	0	0	0	0	0	2	0	0	0	0	2	2	?	?	1	1	0	1	0	1
Dinanomodon gilli	1	2	0	0	2	2	1	2	1	0	1	0	0	0	0	0	2	1	1	0	1	2	2	?	?	1	1	0	1	0	0
Peramodon amalitzkii	1	?	?	0	?	?	?	?	?	0	?	0	0	0	0	0	2	0	1	0	0	2	?	?	?	1	1	?	1	0	0
Vivaxosaurus trautscholdi	1	2	0	0	2	2	?	2	1	0	1	0	0	0	0	0	2	0	1	0	0	2	2	?	?	1	1	0	1	0	0
Jimusaria sinkiangensis	1	2	0	0	?	?	?	2	1	0	1	1	0	0	0	0	2	0	0	0	0	2	?	?	?	1	1	0	2	0	0
Sintocephalus alticeps	1	2	0	0	2	2	?	2	1	0	1	0	0	0	0	?	2	0	0	0	0	2	2	?	?	1	1	0	0	0	0
Basilodon woodwardi	1	2	0	0	2	2	?	2	1	0	1	1	0	0	0	0	2	0	0	0	0	2	2	?	?	1	1	0	0	0	0
Turfanodon bogdaensis	1	2	?	0	?	?	?	2	1	0	1	?	0	0	0	0	?	?	?	0	?	2	2	?	?	1	1	0	1	0	0
Keyseria benjamini	1	2	0	0	2	2	?	2	1	0	1	0	0	0	0	?	2	0	0	0	0	2	2	?	?	1	1	0	1	0	1
Gordonia traquairi	1	2	0	0	2	2	?	2	1	?	1	0	0	0	0	?	?	0	0	0	0	2	2	?	?	1	1	0	1	0	0
Syops vanhoepeni	1	?	?	0	1	2	?	2	1	0	1	1	0	0	0	?	2	0	0	0	0	2	2	?	?	1	1	0	1	0	1
Euptychognathus bathyrhynchus	1	2	0	0	2	2	?	2	1	0	1	1	0	1	1	0	2	0	0	0	0	2	2	?	?	1	1	0	1	0	0
Lystrosaurus hedini	1	2	0	0	2	2	1	2	1	0	1	1	1	1	1	0	2	0	0	0	0	2	2	?	?	1	1	0	1	0	0
Lystrosaurus maccaigi	1	2	0	0	2	2	?	2	1	0	1	1	1	1	1	?	2	0	0	0	0	2	2	?	?	1	1	0	1	0	0
Lystrosaurus curvatus	1	2	0	0	2	2	?	2	1	0	1	1	1	1	1	0	2	0	0	0	0	2	2	?	?	1	1	0	1	0	0
Lystrosaurus declivis	1	2	0	0	2	2	1	2	1	0	1	1	1	1	1	0	2	0	0	0	0	2	2	?	?	1	1	0	1	0	0
Lystrosaurus murrayi	1	2	0	0	2	2	1	2	1	0	1	1	1	1	1	0	2	0	0	0	0	2	2	?	?	1	1	0	1	0	0
Angonisaurus cruickshanki	1	2	0	0	2	2	?	2	1	?	1	1	0	0	0	0	2	?	0	0	1	1	2	?	?	1	1	0	1	0	0
Tetragonias njalilus	1	2	0	0	2	2	1	2	1	0	1	1	0	0	0	0	2	0	0	0	0	2	2	?	?	1	1	0	[12]	0	0
Shansiodon	1	2	0	0	2	2	1	2	1	0	1	1	0	0	0	0	2	0	0	0	0	2	2	?	?	1	1	0	1	0	0
Vinceria andina	1	2	0	0	2	2	?	2	1	0	1	1	0	0	0	?	2	0	0	0	0	2	2	?	?	1	1	0	2	0	0
Rhinodicynodon gracile	1	2	0	0	2	2	?	2	1	0	1	1	0	0	0	0	2	0	0	0	0	2	2	?	?	1	1	0	1	0	0
Dinodontosaurus	1	2	0	0	2	2	?	2	1	0	1	1	0	0	0	0	2	0	1	0	0	2	2	?	?	1	1	0	1	0	0
Kannemeyeria simocephalus	1	2	0	0	2	2	?	2	1	0	1	0	0	0	0	0	2	1	1	0	0	2	2	?	?	0	1	0	2	0	0
Kannemeyeria lophorhinus	1	2	0	0	2	2	?	2	1	0	1	0	0	0	2	0	2	1	1	0	1	2	2	?	?	0	1	0	1	0	0
Dolichuranus primaevus	1	2	0	0	2	2	?	2	1	0	1	1	0	0	0	0	2	1	1	0	0	2	2	?	?	1	1	0	2	0	0
Wadiasaurus indicus	1	2	0	0	2	2	?	2	1	0	1	0	0	0	0	?	2	1	1	0	0	[12]	2	?	?	1	1	0	?	0	0
Rabidosaurus cristatus	1	2	0	?	2	2	?	2	1	0	1	0	0	0	0	0	2	1	1	0	0	2	2	?	?	1	1	0	?	0	0
Rhadiodromus	1	2	0	0	2	2	?	2	1	0	1	1	0	0	0	0	2	0	1	0	0	2	2	?	?	1	1	0	2	0	0
Rechnisaurus cristarhynchus	1	2	0	0	2	2	?	2	1	0	1	1	0	0	2	?	2	0	1	0	1	2	2	?	?	1	1	0	?	0	0
Uralokannemeyeria vjuschkovi	1	2	0	0	2	2	?	2	1	?	1	1	0	0	2	?	2	?	?	0	1	2	2	?	?	?	1	0	?	0	0
Shaanbeikannemeyeria	1	2	0	0	2	2	?	2	1	0	1	1	0	0	0	0	2	0	1	0	0	2	2	?	?	1	1	0	1	0	0
Xiyukannemeyeria brevirostris	1	2	0	?	?	?	?	2	1	0	1	1	0	0	2	?	2	0	2	0	0	2	2	?	?	1	1	0	2	0	0
Parakannemeyeria	1	2	0	0	2	2	?	2	1	0	1	1	0	0	2	0	2	0	2	0	1	2	2	?	?	1	1	0	2	0	0

	55	56	57	58	59	60	61	62	63	64	65	66	67	68	69	70	71	72	73	74	75	76	77	78	79	80	81	82	83	84	85
Aulacephalodon bainii	0	0	2	0	1	1	2	0	0	[01]	1	0	0	[12]	0	0	1	0	0	1	0	0	0	[12]	0	0	2	1	1	1	0
Pelanomodon moschops	0	0	2	0	1	1	2	0	0	1	1	0	0	2	1	0	1	0	0	1	0	0	0	2	0	0	2	1	1	2	0
Geikia locusticeps	0	0	2	0	1	1	2	1	0	1	1	0	0	2	1	1	1	1	0	0	0	0	0	2	?	0	2	0	1	2	0
Geikia elginensis	1	1	2	0	?	?	2	1	?	?	1	0	0	?	?	?	?	1	0	0	0	0	?	?	?	0	2	1	1	2	0
Elph borealis	1	0	0	0	0	0	0	1	0	0	0	0	0	1	0	1	1	2	0	0	0	0	0	1	0	0	2	1	1	0	0
Interpresosaurus blomi	1	?	0	?	0	0	0	1	0	0	?	?	?	1	0	?	?	2	?	1	?	?	?	?	?	?	?	?	?	?	?
Katumbia parringtoni	1	0	1	0	0	0	0	1	0	0	0	0	0	1	1	1	1	2	0	0	0	0	0	1	0	0	2	1	1	?	0
Delectosaurus arefjevi	0	0	1	1	0	0	0	1	0	0	0	0	0	2	0	1	1	2	0	1	0	1	0	1	0	0	2	1	1	0	0
Dicynodon lacerticeps	0	0	1	[01]	0	0	1	1	0	0	0	0	0	2	0	1	1	2	0	1	0	1	0	1	0	0	2	1	1	0	0
Dicynodon angielczyki	0	0	1	0	0	0	1	1	0	0	0	0	0	2	0	1	1	2	0	0	0	1	0	1	0	0	2	1	1	0	0
Daptocephalus leoniceps	1	0	1	1	0	0	1	1	0	0	0	0	0	2	0	1	1	2	0	1	0	1	0	1	0	0	2	1	1	0	0
Daptocephalus huenei	1	0	1	1	0	0	1	1	0	0	0	0	0	2	0	1	1	2	0	1	0	1	0	1	0	0	2	1	1	0	0
Daqingshanodon limbus	0	0	2	0	0	?	0	0	0	1	0	0	0	1	0	1	1	1	0	0	0	0	0	0	0	0	2	1	1	?	0
Dinanomodon gilli	0	1	1	1	0	0	1	1	0	0	0	0	0	2	0	1	1	2	0	1	0	1	0	1	0	0	2	1	1	0	0
Peramodon amalitzkii	1	0	1	1	0	0	0	1	0	0	0	0	0	2	0	1	1	2	0	1	0	?	0	1	0	0	2	1	1	0	0
Vivaxosaurus trautscholdi	0	1	1	1	0	0	0	0	0	0	0	0	0	2	0	1	1	1	0	1	0	1	0	1	0	0	2	1	1	0	0
Jimusaria sinkiangensis	0	0	1	0	0	0	0	1	0	0	0	0	0	1	0	1	1	2	0	1	0	1	0	1	0	1	2	1	1	0	0
Sintocephalus alticeps	0	0	0	1	0	1	1	0	0	0	0	0	0	1	0	1	1	1	0	1	0	?	0	1	0	1	2	1	?	0	0
Basilodon woodwardi	0	0	2	0	0	1	1	1	0	0	0	0	0	2	0	1	1	1	0	1	0	0	0	1	0	1	2	1	1	0	0
Turfanodon bogdaensis	1	1	1	1	0	0	1	0	0	0	?	?	0	2	0	1	1	2	0	1	0	1	0	1	0	1	2	1	1	0	0
Keyseria benjamini	1	0	2	0	0	0	0	0	0	0	0	0	0	1	0	1	1	0	0	0	0	?	0	0	0	0	2	1	1	0	0
Gordonia traquairi	1	?	2	?	0	?	0	1	0	?	0	0	0	1	0	1	1	2	0	1	0	?	0	1	0	?	2	1	1	0	0
Syops vanhoepeni	1	0	2	0	0	1	1	?	0	0	?	?	0	2	0	1	1	2	0	1	0	1	0	1	0	0	?	?	1	?	?
Euptychognathus bathyrhynchus	1	?	0	?	1	?	1	0	0	0	0	0	0	1	0	1	1	2	0	1	0	1	0	1	0	?	2	1	1	0	0
Lystrosaurus hedini	0	0	2	0	0	1	1	0	0	0	1	0	0	1	0	1	1	0	0	1	0	1	0	1	0	0	2	1	1	0	0
Lystrosaurus maccaigi	1	1	0	1	0	1	1	1	0	?	1	0	0	2	0	?	1	0	0	1	0	?	0	1	0	0	2	1	1	0	0
Lystrosaurus curvatus	1	0	2	1	0	1	1	1	0	0	1	0	0	2	0	1	1	0	0	1	0	1	0	1	0	0	2	1	1	0	0
Lystrosaurus declivis	1	0	2	1	2	1	1	1	0	0	1	0	0	2	0	1	1	0	0	1	0	1	0	1	0	0	2	1	1	0	0
Lystrosaurus murrayi	1	0	2	0	2	1	1	0	0	0	1	0	0	2	0	1	1	0	0	1	0	1	0	1	0	0	2	1	1	0	0
Angonisaurus cruickshanki	1	?	?	?	0	0	1	0	0	1	1	0	0	2	0	1	1	0	0	1	1	1	0	1	0	1	2	0	1	0	0
Tetragonias njalilus	1	0	2	0	0	0	1	0	0	1	0	0	0	1	0	1	1	2	0	1	1	2	0	1	0	1	2	0	1	0	0
Shansiodon	1	?	2	?	0	0	1	1	0	1	0	0	0	2	0	1	1	2	0	1	1	2	0	1	0	1	2	0	1	0	0
Vinceria andina	1	0	2	0	0	?	1	0	0	1	0	0	0	1	0	1	1	2	0	1	1	2	0	1	0	1	2	0	1	0	0
Rhinodicynodon gracile	1	0	2	1	0	0	1	1	0	1	0	0	0	1	0	1	1	2	0	1	1	2	0	1	0	0	2	0	1	0	0
Dinodontosaurus	1	0	3	1	0	0	1	0	0	1	0	0	0	2	0	1	1	2	0	1	1	2	0	1	0	1	2	0	1	0	0
Kannemeyeria simocephalus	0	0	3	2	0	0	0	0	0	1	1	0	1	2	0	1	1	2	1	1	0	2	0	1	0	1	2	1	1	0	0
Kannemeyeria lophorhinus	0	0	3	2	0	0	2	0	0	1	0	0	1	1	0	1	1	2	1	1	0	2	0	1	0	1	2	1	1	0	?
Dolichuranus primaevus	0	0	3	0	0	0	1	0	0	1	1	0	0	1	0	1	1	2	1	1	0	2	0	1	0	1	2	0	1	0	0
Wadiasaurus indicus	0	?	?	?	0	0	1	0	?	?	0	0	1	?	?	1	1	0	1	1	?	?	0	?	?	1	2	0	1	0	0
Rabidosaurus cristatus	0	?	3	?	0	0	1	0	0	1	1	?	1	2	0	1	?	0	?	1	?	?	0	1	0	?	2	1	1	?	?
Rhadiodromus	0	0	3	1	0	[01]	1	0	0	1	1	0	1	1	1	1	1	2	0	1	0	2	0	1	0	?	2	0	1	0	0
Rechnisaurus cristarhynchus	0	0	3	0	0	0	1	0	0	1	0	0	1	?	?	1	?	1	0	1	0	2	0	1	0	?	2	?	?	0	?
Uralokannemeyeria vjuschkovi	0	?	?	?	?	0	1	?	0	1	1	0	1	2	0	1	1	1	0	1	0	?	0	1	0	?	2	0	1	?	0
Shaanbeikannemeyeria	0	0	3	1	0	0	1	0	0	1	1	0	1	1	0	1	1	2	0	1	0	?	0	1	0	1	2	1	1	0	0
Xiyukannemeyeria brevirostris	1	0	3	?	0	1	1	0	0	1	1	0	1	2	0	1	1	2	0	1	0	1	0	1	0	?	2	0	1	0	0
Parakannemeyeria	0	0	3	?	0	1	1	0	0	1	1	0	1	2	0	1	1	2	0	1	0	1	0	1	0	1	2	0	1	0	0

	86	87	88	89	90	91	92	93	94	95	96	97	98	99	100	101	102	103	104	105	106	107	108	109	110	111	112	113	114	115	116
Aulacephalodon bainii	2	0	1	1	1	0	1	0	1	1	0	1	1	2	2	0	3	0	1	1	1	1	0	1	2	1	0	0	1	2	1
Pelanomodon moschops	2	0	1	1	1	0	1	0	1	1	1	1	1	2	2	0	3	0	1	1	1	1	0	1	2	1	0	[01]	1	2	1
Geikia locusticeps	2	0	1	1	1	0	1	0	1	1	1	1	1	2	2	0	3	0	1	1	1	1	0	1	2	1	0	1	1	2	1
Geikia elginensis	2	0	1	?	?	0	1	?	1	1	1	1	1	?	2	0	3	0	?	1	?	?	0	1	2	1	0	?	?	2	1
Elph borealis	2	0	1	1	1	0	1	0	?	?	?	?	1	2	2	0	3	0	1	1	0	1	0	?	2	1	0	0	?	1	1
Interpresosaurus blomi	?	?	?	?	?	?	?	?	1	?	?	?	1	?	?	?	3	0	?	?	0	?	?	?	?	?	?	?	?	?	?
Katumbia parringtoni	2	0	1	1	?	0	1	0	1	1	1	1	1	2	2	0	3	0	1	1	0	1	0	1	2	1	0	1	0	2	1
Delectosaurus arefjevi	2	0	1	1	1	0	1	0	1	1	1	1	1	2	1	0	3	0	1	1	1	[12]	0	1	2	1	0	1	1	2	1
Dicynodon lacerticeps	2	0	1	1	1	0	1	0	1	1	1	1	1	2	1	0	3	0	1	1	1	1	0	1	2	1	0	0	1	2	1
Dicynodon angielczyki	2	0	1	1	1	0	1	0	1	1	1	1	1	2	1	0	3	0	1	1	1	1	0	1	2	1	0	1	1	2	1
Daptocephalus leoniceps	2	0	1	1	1	0	1	0	1	1	1	1	1	2	1	0	3	0	1	1	1	1	0	1	2	1	0	1	0	1	1
Daptocephalus huenei	2	0	1	1	1	0	1	0	1	1	1	1	1	2	1	0	3	0	1	1	1	1	0	1	2	1	0	1	0	1	1
Daqingshanodon limbus	2	0	1	1	1	0	1	0	1	1	?	?	1	2	2	0	3	0	1	1	0	1	0	1	2	1	0	0	1	2	1
Dinanomodon gilli	2	0	1	1	1	0	1	0	1	1	1	1	1	2	1	0	3	0	1	1	1	1	0	1	2	1	1	1	0	2	1
Peramodon amalitzkii	2	0	1	1	?	0	1	0	?	?	?	?	?	?	?	?	?	?	?	?	?	?	?	1	2	?	?	?	?	2	1
Vivaxosaurus trautscholdi	2	0	1	1	1	0	1	0	1	1	0	0	1	2	1	0	3	0	1	1	1	[12]	0	1	2	1	0	1	1	2	1
Jimusaria sinkiangensis	2	0	1	1	1	0	1	0	?	?	?	?	1	2	1	0	3	0	1	?	1	1	0	1	2	1	0	0	?	2	1
Sintocephalus alticeps	2	0	?	1	?	0	?	?	?	?	?	?	1	2	1	0	3	0	1	1	?	1	0	1	2	1	0	1	?	2	1
Basilodon woodwardi	2	0	1	1	1	0	1	0	1	1	1	1	1	2	2	0	3	0	1	1	1	1	0	1	2	1	0	1	?	2	1
Turfanodon bogdaensis	2	0	1	?	1	0	?	?	?	?	?	?	1	2	1	0	3	0	1	?	?	2	0	1	2	1	1	1	1	2	1
Keyseria benjamini	2	0	1	1	1	0	1	0	1	1	?	?	1	2	2	0	3	0	?	1	?	1	0	1	2	1	0	0	0	2	1
Gordonia traquairi	2	0	1	1	?	0	1	0	?	1	?	?	1	?	1	0	3	?	?	?	?	?	?	1	2	1	0	1	?	?	1
Syops vanhoepeni	?	?	?	1	1	?	?	0	1	1	1	1	1	2	2	0	3	0	1	1	1	1	?	1	2	1	?	1	?	?	1
Euptychognathus bathyrhynchus	2	0	1	1	1	0	1	0	1	1	1	1	1	2	1	0	3	0	?	1	?	?	?	1	2	1	0	?	1	2	1
Lystrosaurus hedini	2	0	1	1	1	0	1	0	1	1	1	1	1	2	1	0	3	0	1	1	1	2	?	1	2	1	0	1	0	4	1
Lystrosaurus maccaigi	2	0	1	1	1	0	1	?	1	1	1	1	1	2	1	0	3	0	1	0	1	2	?	1	2	1	0	1	0	4	1
Lystrosaurus curvatus	2	0	1	1	1	0	1	0	1	1	1	1	1	2	1	0	3	0	1	0	1	2	?	1	2	1	0	1	1	2	1
Lystrosaurus declivis	2	0	1	1	1	0	1	0	1	1	1	1	1	2	1	0	3	0	1	0	1	2	?	1	2	1	0	1	1	2	1
Lystrosaurus murrayi	2	0	1	1	1	0	1	0	1	1	1	1	1	2	1	0	3	0	1	0	1	2	?	1	2	1	0	1	1	2	1
Angonisaurus cruickshanki	2	0	1	1	1	0	?	?	1	1	1	1	1	?	?	?	3	0	?	1	?	?	?	1	2	1	0	1	?	?	1
Tetragonias njalilus	2	1	1	1	1	0	1	0	1	1	1	1	1	2	1	0	3	0	1	0	1	2	?	1	2	1	0	1	0	2	1
Shansiodon	2	1	1	1	1	0	1	?	?	?	?	?	1	2	1	0	3	0	1	?	1	2	?	1	2	1	0	1	?	?	1
Vinceria andina	2	0	1	1	1	0	?	?	1	1	1	1	1	?	?	?	3	0	?	?	1	2	?	1	2	1	0	1	0	2	1
Rhinodicynodon gracile	2	1	1	1	1	0	1	0	?	?	?	?	1	2	1	0	3	0	?	1	1	2	?	1	2	1	0	1	?	?	1
Dinodontosaurus	2	1	1	1	1	0	1	0	1	1	1	1	1	2	1	0	3	0	0	0	1	1	0	1	2	1	0	1	0	1	1
Kannemeyeria simocephalus	2	0	1	1	1	0	1	0	1	1	1	1	1	2	1	0	3	0	1	1	1	2	?	1	2	1	0	1	0	1	1
Kannemeyeria lophorhinus	2	0	1	1	1	0	1	?	1	1	1	1	1	2	1	0	3	0	1	?	1	2	?	1	2	1	0	1	1	1	1
Dolichuranus primaevus	2	0	1	1	1	0	1	0	1	1	1	1	1	2	1	0	3	0	1	0	1	1	0	1	2	1	0	1	1	6	1
Wadiasaurus indicus	2	0	1	?	1	0	1	0	?	?	?	?	1	?	?	?	3	0	?	?	1	2	?	1	2	1	0	1	?	?	1
Rabidosaurus cristatus	2	?	1	1	1	0	?	?	?	?	?	?	1	2	?	?	3	0	1	0	1	?	?	1	2	1	?	1	?	1	1
Rhadiodromus	2	0	1	1	1	0	?	?	1	1	1	1	1	2	1	0	3	0	?	1	?	1	0	1	2	?	?	1	?	?	1
Rechnisaurus cristarhynchus	2	?	?	?	?	?	?	?	?	?	?	?	1	2	1	0	3	0	?	0	1	1	0	1	2	1	0	1	?	?	1
Uralokannemeyeria vjuschkovi	2	0	1	1	1	0	1	0	1	1	1	1	1	?	?	?	3	0	?	?	?	?	?	1	2	?	?	?	1	2	1
Shaanbeikannemeyeria	2	1	1	1	1	0	1	?	1	1	1	1	1	2	1	0	3	0	1	1	1	?	0	1	2	1	0	1	?	2	1
Xiyukannemeyeria brevirostris	2	1	1	1	1	0	1	0	1	1	1	1	1	2	?	?	3	0	1	?	1	2	?	1	2	?	?	1	0	2	1
Parakannemeyeria	2	1	1	1	1	0	1	0	1	1	1	1	1	2	1	0	3	0	1	?	1	2	?	1	2	1	0	1	0	1	1

	117	118	119	120	121	122	123	124	125	126	127	128	129	130	131	132	133	134	135	136	137	138	139	140	141	142	143	144	145	146	147
Aulacephalodon bainii	0	0	0	0	1	2	1	1	2	[01]	0	1	1	1	0	1	1	0	0	0	1	1	1	2	?	?	?	2	0	0	1
Pelanomodon moschops	0	0	?	0	1	2	1	1	2	1	0	1	1	1	0	1	1	0	0	?	?	?	?	?	?	?	?	?	?	?	?
Geikia locusticeps	0	0	0	0	2	2	1	1	2	1	0	1	1	1	0	1	1	0	0	?	1	1	1	2	?	?	?	2	1	0	1
Geikia elginensis	0	?	1	0	?	?	?	?	?	?	?	?	?	?	?	?	?	?	0	?	1	0	1	2	?	?	?	2	1	0	1
Elph borealis	?	0	0	0	1	2	1	1	2	0	?	?	?	1	0	1	1	0	0	?	1	1	1	2	?	?	?	2	0	?	1
Interpresosaurus blomi	?	?	?	?	?	?	?	?	?	?	?	?	?	?	?	?	?	?	?	?	?	?	?	?	?	?	?	?	?	?	?
Katumbia parringtoni	0	?	?	0	1	2	1	1	2	1	1	1	1	?	0	0	1	0	0	?	1	1	1	2	?	?	?	2	1	0	1
Delectosaurus arefjevi	1	0	?	0	1	2	1	1	2	1	?	?	?	1	0	0	1	0	0	0	?	?	?	?	?	?	?	?	?	?	?
Dicynodon lacerticeps	0	0	0	0	2	2	1	1	2	1	1	1	1	1	0	1	1	0	0	1	1	1	1	2	?	?	?	2	1	0	1
Dicynodon angielczyki	0	0	0	0	2	2	1	1	2	1	1	1	1	1	0	1	1	0	0	1	1	1	1	2	?	?	?	2	1	0	1
Daptocephalus leoniceps	1	0	1	0	1	2	1	1	2	1	1	1	1	1	0	1	1	1	0	1	1	1	1	2	?	?	?	2	1	0	1
Daptocephalus huenei	1	0	1	0	1	2	1	1	2	1	1	1	1	1	0	1	1	1	0	1	?	?	?	?	?	?	?	?	?	?	?
Daqingshanodon limbus	0	?	0	0	?	?	1	1	?	?	?	?	?	1	0	1	1	?	0	?	1	1	1	2	?	?	?	2	1	0	1
Dinanomodon gilli	1	?	?	0	1	2	1	1	2	1	1	1	1	1	0	1	1	?	0	1	1	?	1	?	?	?	?	?	1	0	?
Peramodon amalitzkii	?	0	?	0	?	2	?	1	2	1	?	1	1	?	0	?	1	?	?	?	1	1	1	?	?	?	?	2	1	0	?
Vivaxosaurus trautscholdi	1	0	?	0	2	2	1	1	2	[01]	?	1	?	1	0	1	1	0	0	1	1	1	1	2	?	?	?	2	1	0	1
Jimusaria sinkiangensis	1	0	1	0	2	2	1	1	2	1	1	1	?	1	0	?	?	?	0	?	1	1	1	2	?	?	?	2	1	0	1
Sintocephalus alticeps	0	?	?	0	?	?	?	?	?	?	?	?	?	?	?	?	?	?	?	?	?	?	?	?	?	?	?	?	?	?	?
Basilodon woodwardi	0	?	?	0	1	2	1	1	2	1	?	1	?	1	?	1	1	0	1	?	1	?	1	?	?	?	?	?	1	?	?
Turfanodon bogdaensis	1	?	?	0	1	2	1	1	2	1	?	?	?	1	0	1	1	0	0	1	?	?	?	?	?	?	?	?	?	?	?
Keyseria benjamini	0	?	?	0	1	?	1	1	2	1	0	1	1	1	?	1	1	0	0	?	?	?	?	?	?	?	?	?	?	?	?
Gordonia traquairi	?	?	?	0	?	?	?	1	2	?	?	1	1	?	?	?	1	?	0	?	1	1	1	2	?	?	?	2	?	0	?
Syops vanhoepeni	?	?	?	?	?	2	?	?	?	?	0	?	?	1	?	0	1	0	?	?	1	?	1	?	?	?	?	2	0	0	?
Euptychognathus bathyrhynchus	0	?	?	0	2	2	1	1	?	1	1	?	?	1	0	1	1	0	0	?	1	1	1	2	?	?	?	2	1	0	1
Lystrosaurus hedini	1	?	?	0	2	2	1	1	2	1	0	?	?	1	0	1	1	0	0	1	1	1	1	2	?	?	?	2	1	0	1
Lystrosaurus maccaigi	1	?	?	0	2	2	1	1	2	1	0	?	?	1	?	1	1	0	0	?	1	1	1	2	?	?	?	2	1	0	1
Lystrosaurus curvatus	1	0	0	0	2	2	1	1	2	1	?	?	?	1	0	0	1	0	0	1	1	1	1	?	?	?	?	?	1	0	?
Lystrosaurus declivis	1	0	0	0	2	2	1	1	2	1	0	1	1	1	0	0	1	0	0	1	1	1	1	2	?	?	?	2	1	0	1
Lystrosaurus murrayi	1	?	0	0	2	2	1	1	2	1	1	1	1	1	0	1	1	0	0	0	1	1	1	2	?	?	?	2	1	0	1
Angonisaurus cruickshanki	1	0	?	0	2	2	1	1	2	0	?	?	?	1	?	1	1	0	?	1	1	1	1	2	?	?	?	2	1	0	1
Tetragonias njalilus	1	0	1	0	?	2	1	1	2	1	1	1	1	1	0	1	1	0	0	1	1	1	1	2	?	?	?	2	1	0	1
Shansiodon	?	0	?	0	2	2	1	1	2	0	?	1	1	1	?	1	1	0	0	1	1	1	1	2	?	?	?	2	0	0	1
Vinceria andina	1	?	?	0	2	2	?	1	?	0	?	1	1	1	?	1	1	?	?	?	1	?	?	2	?	?	?	?	?	?	?
Rhinodicynodon gracile	?	0	?	0	2	2	?	1	?	?	?	?	?	1	?	0	1	0	0	?	1	1	1	2	?	?	?	2	1	0	1
Dinodontosaurus	1	?	1	0	2	2	?	1	2	1	1	?	?	?	0	1	0	0	0	1	1	1	1	2	?	?	?	2	1	0	1
Kannemeyeria simocephalus	1	1	1	0	2	2	1	2	2	0	1	?	?	1	0	1	0	0	1	1	1	1	1	2	?	?	?	2	1	0	1
Kannemeyeria lophorhinus	1	0	1	0	2	2	?	?	2	0	1	?	?	1	?	0	0	0	?	?	1	1	1	2	?	?	?	2	1	0	1
Dolichuranus primaevus	1	0	?	0	2	2	1	2	2	0	0	?	?	1	?	1	0	0	1	?	1	1	1	2	?	?	?	2	1	0	1
Wadiasaurus indicus	?	?	?	0	2	2	?	?	2	0	?	?	?	1	?	1	1	?	1	?	1	1	1	2	?	?	?	2	?	?	1
Rabidosaurus cristatus	?	?	?	0	?	2	?	?	?	?	1	?	?	1	?	?	0	0	?	1	?	?	?	?	?	?	?	?	?	?	?
Rhadiodromus	?	1	1	0	2	2	?	2	2	0	?	?	?	1	0	1	1	0	?	?	?	?	?	?	?	?	?	?	?	?	?
Rechnisaurus cristarhynchus	?	?	?	0	2	2	1	2	2	0	?	?	?	?	?	?	?	0	?	?	?	?	?	?	?	?	?	?	?	?	?
Uralokannemeyeria vjuschkovi	1	?	?	0	2	2	?	2	2	0	?	?	?	1	?	1	0	0	?	?	?	?	?	?	?	?	?	?	?	?	?
Shaanbeikannemeyeria	1	?	?	0	2	2	1	2	2	0	?	?	?	?	?	1	0	0	?	?	1	1	1	2	?	?	?	2	0	?	1
Xiyukannemeyeria brevirostris	1	?	?	0	2	2	?	?	2	0	?	1	1	1	?	0	0	0	?	?	1	1	1	2	?	?	?	2	1	0	?
Parakannemeyeria	1	0	?	0	2	2	?	?	2	0	1	1	1	1	0	1	0	0	1	1	1	1	1	2	?	?	?	2	1	0	1

	148	149	150	151	152	153	154	155	156	157	158	159	160	161	162	163	164	165	166	167	168	169	170	171	172	173	174	175	176	177	178
Aulacephalodon bainii	3	0	1	2	1	1	1	0	1	1	4	1	1	1	1	2	1	2	1	0	0	0	1	0	0	1	0	1	0	1	0
Pelanomodon moschops	?	?	?	?	?	?	?	?	?	?	?	?	?	?	?	2	?	?	?	?	?	?	?	?	?	?	?	?	?	?	?
Geikia locusticeps	3	0	1	0	1	1	0	0	1	1	4	1	1	1	1	2	1	?	?	0	0	?	1	0	?	?	?	?	?	?	?
Geikia elginensis	3	0	1	2	1	?	?	?	?	?	4	1	?	?	1	2	1	?	?	?	?	?	?	?	?	?	0	1	0	1	?
Elph borealis	3	0	1	2	1	1	1	0	?	?	?	?	?	?	?	2	1	?	?	?	?	?	?	?	?	?	?	?	?	?	?
Interpresosaurus blomi	?	?	?	?	?	?	?	?	?	?	?	?	?	?	?	?	?	?	?	?	?	?	?	?	?	?	?	?	?	?	?
Katumbia parringtoni	3	0	1	2	1	1	1	0	?	?	?	?	?	?	?	2	1	?	?	?	?	?	?	?	?	?	?	?	?	?	?
Delectosaurus arefjevi	?	?	?	?	?	?	?	?	?	?	?	?	?	?	?	?	?	?	?	?	?	?	?	?	?	?	?	?	?	?	?
Dicynodon lacerticeps	3	0	2	2	1	1	1	1	1	1	5	1	1	1	1	2	1	?	?	?	?	?	?	?	?	?	?	?	?	?	?
Dicynodon angielczyki	3	0	2	0	1	1	1	1	1	1	5	1	1	1	1	2	1	?	?	?	?	?	?	?	?	?	?	?	?	?	?
Daptocephalus leoniceps	3	0	2	2	1	1	1	1	1	1	5	1	1	1	1	2	1	?	?	?	?	?	?	?	?	1	0	1	1	1	0
Daptocephalus huenei	?	?	?	?	?	?	?	?	?	?	?	?	?	?	?	?	?	?	?	?	?	?	?	?	?	?	?	?	?	?	?
Daqingshanodon limbus	3	0	1	2	1	1	?	0	1	1	4	1	1	1	1	2	1	?	?	?	?	?	?	?	?	?	?	?	?	?	?
Dinanomodon gilli	3	?	1	2	1	?	?	1	?	1	5	1	1	?	1	2	?	?	?	?	?	?	?	?	?	?	?	?	?	?	?
Peramodon amalitzkii	?	?	2	2	1	1	1	1	?	1	5	1	1	?	1	2	?	3	?	1	0	0	1	0	1	?	?	?	?	?	?
Vivaxosaurus trautscholdi	3	0	2	2	1	?	?	1	1	1	5	1	1	0	1	2	1	?	?	0	0	0	?	?	1	1	0	1	1	1	0
Jimusaria sinkiangensis	3	0	2	2	1	1	0	1	1	1	5	1	1	?	1	2	1	?	?	?	?	?	?	?	?	?	?	?	?	?	?
Sintocephalus alticeps	?	?	?	?	?	?	?	?	?	?	?	?	?	?	?	2	?	?	?	?	?	?	?	?	?	?	?	?	?	?	?
Basilodon woodwardi	?	?	2	2	1	?	?	?	?	?	?	1	?	?	?	2	?	?	?	?	?	?	?	?	?	?	?	?	?	?	?
Turfanodon bogdaensis	?	?	?	?	?	?	?	?	?	?	?	?	?	?	?	?	?	?	?	?	?	?	?	?	?	?	?	?	?	?	?
Keyseria benjamini	?	?	?	?	?	?	?	?	?	?	?	?	?	?	?	2	?	?	?	?	?	?	?	?	?	?	?	?	?	?	?
Gordonia traquairi	3	0	2	2	1	?	?	?	?	1	?	1	?	?	1	2	1	?	?	?	0	0	1	?	?	1	0	?	0	1	0
Syops vanhoepeni	?	?	?	?	?	?	?	0	?	?	?	1	1	?	1	2	?	?	?	?	?	?	?	?	?	?	?	?	?	?	?
Euptychognathus bathyrhynchus	3	0	2	2	1	1	?	1	?	?	?	1	?	?	?	2	1	?	?	?	?	?	?	?	?	?	?	?	?	?	?
Lystrosaurus hedini	3	0	2	2	1	1	0	1	1	1	5	1	1	0	1	2	1	?	?	?	?	?	1	?	?	?	?	?	?	?	?
Lystrosaurus maccaigi	3	0	2	2	1	?	?	1	1	1	5	1	?	?	1	2	1	3	?	?	?	?	?	?	?	?	0	1	0	1	0
Lystrosaurus curvatus	?	?	2	2	1	1	0	1	?	1	5	1	1	?	1	2	?	?	?	0	0	0	1	?	?	1	0	1	0	1	?
Lystrosaurus declivis	3	0	2	2	1	1	0	1	1	1	5	1	1	0	1	2	1	3	?	0	?	?	1	?	?	1	0	1	1	1	0
Lystrosaurus murrayi	3	0	2	2	1	1	0	1	1	1	5	1	1	0	1	2	1	?	?	0	0	0	1	1	1	1	0	1	1	1	0
Angonisaurus cruickshanki	3	0	1	2	1	1	0	1	1	0	0	1	1	?	1	2	1	3	?	?	0	0	1	0	0	?	1	0	?	1	0
Tetragonias njalilus	3	0	1	2	1	1	0	1	1	0	5	1	1	1	1	2	1	2	0	0	0	0	1	0	0	1	1	1	0	1	0
Shansiodon	3	0	2	2	1	1	0	?	?	0	?	1	?	?	1	2	1	2	?	0	0	0	1	?	?	1	1	1	0	1	1
Vinceria andina	?	?	?	?	?	?	?	?	?	?	?	?	?	?	1	2	1	?	?	?	?	?	?	?	?	?	?	?	?	?	?
Rhinodicynodon gracile	3	0	2	2	1	?	?	1	1	?	?	1	?	?	1	2	1	?	?	0	0	0	1	0	0	1	0	1	?	1	0
Dinodontosaurus	3	0	1	2	1	1	0	0	1	0	?	1	1	?	1	2	1	3	0	0	0	0	1	0	0	1	1	0	0	1	0
Kannemeyeria simocephalus	3	0	2	2	1	1	0	1	1	1	5	1	1	1	1	2	1	3	0	0	0	1	1	0	0	1	0	1	0	1	0
Kannemeyeria lophorhinus	3	0	1	2	1	?	?	1	1	0	?	0	1	0	1	2	1	?	?	?	0	0	?	?	?	1	1	?	1	1	0
Dolichuranus primaevus	3	0	1	2	1	1	?	1	1	0	?	1	1	?	1	2	1	?	?	0	0	0	0	?	?	1	1	0	0	1	0
Wadiasaurus indicus	3	0	?	?	?	?	?	?	?	?	?	1	1	?	1	2	1	2	0	0	1	0	1	?	0	1	1	1	1	1	0
Rabidosaurus cristatus	?	?	?	?	?	?	?	?	?	?	?	?	?	?	?	?	?	?	?	?	?	?	?	?	?	?	1	?	?	?	?
Rhadiodromus	?	?	?	?	?	?	?	?	?	?	?	?	?	?	?	?	?	?	?	?	?	?	?	?	?	?	?	?	?	?	?
Rechnisaurus cristarhynchus	?	?	?	?	?	?	?	?	?	?	?	?	?	?	?	?	?	?	?	?	?	?	?	?	?	?	?	?	?	?	?
Uralokannemeyeria vjuschkovi	?	?	?	?	?	?	?	?	?	?	?	?	?	?	?	2	?	2	?	?	?	?	?	?	?	?	?	?	?	?	?
Shaanbeikannemeyeria	?	?	1	2	1	?	?	?	?	?	?	?	?	1	?	2	1	?	?	?	0	0	1	?	?	1	?	?	1	1	0
Xiyukannemeyeria brevirostris	?	?	1	2	1	1	?	?	1	?	?	1	1	?	1	2	1	?	?	?	0	?	1	?	?	1	1	1	0	?	0
Parakannemeyeria	?	0	1	2	1	?	?	?	1	?	?	1	1	?	1	2	1	3	?	0	0	0	1	0	0	1	0	1	0	1	0

	179	180	181	182	183	184	185	186	187	188	189	190	191	192	193	194	195	196	197
Aulacephalodon bainii	0	?	1	1	0	1	0	1	0	1	1	1	2	1	1	1	1	1	0
Pelanomodon moschops	?	?	?	?	?	?	?	?	?	?	?	?	?	?	?	?	1	?	?
Geikia locusticeps	?	?	?	?	?	?	?	?	?	?	?	?	?	?	?	?	1	?	?
Geikia elginensis	?	?	?	?	?	?	?	?	?	?	?	?	?	?	?	?	?	?	?
Elph borealis	?	?	?	?	?	?	?	?	?	?	?	?	?	?	?	?	0	?	?
Interpresosaurus blomi	?	?	?	?	?	?	?	?	?	?	?	?	?	?	?	?	?	?	?
Katumbia parringtoni	?	?	?	?	?	?	?	?	?	?	?	?	?	?	?	?	0	?	?
Delectosaurus arefjevi	?	?	?	?	?	?	?	?	?	?	?	?	?	?	?	?	?	?	?
Dicynodon lacerticeps	?	?	?	?	?	?	?	?	?	?	?	?	?	?	?	?	0	0	?
Dicynodon angielczyki	?	?	?	?	?	?	?	?	?	?	?	?	?	?	?	?	?	?	?
Daptocephalus leoniceps	?	?	?	?	0	1	1	1	?	?	?	?	?	?	?	?	1	0	?
Daptocephalus huenei	?	?	?	?	?	?	?	?	?	?	?	?	?	?	?	?	?	?	?
Daqingshanodon limbus	?	?	?	?	?	?	?	?	?	?	?	?	?	?	?	?	0	?	?
Dinanomodon gilli	?	?	?	?	?	?	?	?	?	?	?	?	?	?	?	?	1	?	?
Peramodon amalitzkii	?	?	?	?	?	?	?	?	?	?	?	?	?	?	?	?	1	?	?
Vivaxosaurus trautscholdi	?	?	?	?	?	?	?	?	?	?	?	?	?	?	?	?	0	?	?
Jimusaria sinkiangensis	?	?	?	?	?	?	?	?	?	?	?	?	?	?	?	?	0	?	?
Sintocephalus alticeps	?	?	?	?	?	?	?	?	?	?	?	?	?	?	?	?	?	?	?
Basilodon woodwardi	?	?	?	?	?	?	?	?	?	?	?	?	?	?	?	?	?	?	?
Turfanodon bogdaensis	?	?	?	?	?	?	?	?	?	?	?	?	?	?	?	?	?	?	?
Keyseria benjamini	?	?	?	?	?	?	?	?	?	?	?	?	?	?	?	?	?	?	?
Gordonia traquairi	0	?	?	?	0	?	?	?	?	?	?	?	?	?	?	?	0	0	?
Syops vanhoepeni	?	?	?	?	?	?	?	?	?	?	?	?	?	?	?	?	1	?	?
Euptychognathus bathyrhynchus	?	?	?	?	?	?	?	?	?	?	?	?	?	?	?	?	1	?	?
Lystrosaurus hedini	?	?	?	?	?	?	?	?	?	?	?	?	?	?	?	?	1	?	?
Lystrosaurus maccaigi	0	?	1	1	?	1	1	?	0	0	1	1	2	1	1	1	1	0	?
Lystrosaurus curvatus	0	?	?	?	1	?	?	?	0	0	1	?	?	?	?	1	1	0	?
Lystrosaurus declivis	0	?	1	1	1	1	1	1	0	1	1	1	2	1	1	1	1	0	?
Lystrosaurus murrayi	0	?	1	1	1	?	?	1	0	1	1	1	2	1	1	1	1	0	?
Angonisaurus cruickshanki	?	?	?	?	0	1	1	1	?	?	?	?	?	?	?	?	1	1	1
Tetragonias njalilus	0	?	1	1	0	1	1	1	1	1	2	1	2	1	1	?	1	1	0
Shansiodon	1	?	1	1	0	?	?	?	1	1	1	1	2	1	1	?	1	1	0
Vinceria andina	?	?	?	?	?	?	?	?	?	?	?	?	?	?	?	?	?	?	?
Rhinodicynodon gracile	0	?	?	?	0	1	1	1	1	1	2	?	?	?	?	?	1	1	0
Dinodontosaurus	1	?	1	1	0	1	1	1	0	1	2	1	2	1	1	?	1	0	?
Kannemeyeria simocephalus	0	?	1	1	0	1	1	1	0	1	1	1	2	1	1	1	1	1	0
Kannemeyeria lophorhinus	?	?	?	?	0	?	?	?	?	?	?	?	?	?	?	?	?	?	?
Dolichuranus primaevus	1	?	?	?	?	?	?	?	0	1	2	?	?	?	?	?	1	1	0
Wadiasaurus indicus	1	?	?	?	0	1	1	1	1	1	1	?	?	?	?	?	1	1	0
Rabidosaurus cristatus	?	?	?	?	?	?	?	?	?	?	?	?	?	?	?	?	?	?	?
Rhadiodromus	?	?	?	?	?	?	?	?	?	?	?	?	?	?	?	?	?	?	?
Rechnisaurus cristarhynchus	?	?	?	?	?	?	?	?	?	?	?	?	?	?	?	?	?	?	?
Uralokannemeyeria vjuschkovi	?	?	?	?	0	?	?	?	?	?	?	?	?	?	?	?	?	?	?
Shaanbeikannemeyeria	0	?	?	?	?	?	?	?	0	1	1	?	?	?	?	?	?	?	?
Xiyukannemeyeria brevirostris	0	?	1	1	0	?	?	?	0	1	1	1	2	1	1	?	1	1	0
Parakannemeyeria	0	?	1	1	0	1	1	1	[01]	1	1	1	2	1	1	?	?	1	0

	24	25	26	27	28	29	30	31	32	33	34	35	36	37	38	39	40	41	42	43	44	45	46	47	48	49	50	51	52	53	54
Sinokannemeyeria	1	2	0	0	2	2	?	2	1	0	1	0	0	0	2	0	2	1	2	0	0	2	2	?	?	1	1	0	1	0	0
Stahleckeria potens	1	2	0	0	2	0	?	2	1	0	1	1	0	0	0	0	2	1	2	0	1	1	2	?	?	1	1	0	1	0	0
Eubrachiosaurus browni	?	?	?	?	?	?	?	?	?	?	?	?	?	?	?	?	?	?	?	?	?	?	?	?	?	?	?	?	?	?	?
Sangusaurus parringtonii	1	2	0	0	2	2	?	2	1	0	1	1	0	0	0	0	0	0	1	0	1	1	2	?	?	0	1	0	1	0	0
Ischigualastia jenseni	1	2	0	0	2	2	?	2	1	0	1	1	0	0	0	0	2	1	2	0	1	1	2	?	?	1	1	0	1	0	0
Jachaleria	1	2	0	0	2	2	1	2	1	0	1	1	0	0	0	0	2	1	1	0	1	1	2	?	?	1	1	0	1	0	0
Zambiasaurus submersus	1	2	0	0	2	2	?	2	1	?	?	1	?	?	?	?	?	?	?	0	0	1	2	?	?	?	1	?	0	?	?
Placerias hesternus	1	2	0	0	0	2	?	2	1	?	?	0	0	0	2	0	2	0	0	0	0	2	2	?	?	1	1	1	0	0	0
Moghreberia nmachouensis	1	?	0	0	0	2	?	2	?	?	1	?	0	0	0	?	?	0	2	0	?	2	2	?	?	?	1	0	2	0	0
Rastodon procurvidens	1	?	?	?	?	?	?	2	1	0	1	0	0	0	0	0	2	0	0	0	0	2	?	?	?	1	1	0	0	0	0
Bulbasaurus phylloxyron	1	2	0	0	2	2	1	2	1	0	1	1	0	0	0	0	2	0	0	0	0	2	2	?	?	1	1	0	1	0	0
Compsodon helmoedi	1	0	1	1	1	0	1	2	1	0	1	0	0	0	0	1	2	0	1	0	0	2	0	0	1	1	1	1	0	1	0
LPB 1993 3	1	2	0	0	2	2	1	2	1	0	1	0	0	0	0	?	?	?	0	0	0	2	2	?	?	1	1	0	1	0	0
LPB 1993 2	1	2	0	0	2	2	1	2	1	0	?	1	0	0	0	0	?	1	0	0	?	2	2	?	?	1	1	0	1	0	0
LPB 1995 9	1	2	0	0	2	0	1	2	1	0	1	?	0	0	0	?	?	1	0	0	0	2	2	?	?	0	1	0	1	0	0
Pentasaurus goggai	?	?	?	?	?	?	?	?	?	?	?	?	?	?	?	?	?	?	?	?	?	?	?	?	?	?	?	?	?	?	?
Ufudocyclops mukanelai	1	2	0	?	2	2	?	2	1	0	1	?	0	0	0	0	2	0	1	0	?	1	2	?	?	1	1	0	1	0	0
Lisowicia bojani	?	?	?	?	?	?	?	?	?	?	?	?	0	?	2	0	?	?	?	?	?	2	2	1	?	?	1	?	0	?	0

	55	56	57	58	59	60	61	62	63	64	65	66	67	68	69	70	71	72	73	74	75	76	77	78	79	80	81	82	83	84	85
Sinokannemeyeria	0	0	3	1	0	?	1	0	0	1	1	0	1	2	0	1	1	2	0	1	0	1	0	1	0	1	2	0	1	0	0
Stahleckeria potens	0	0	3	1	0	0	1	0	1	1	1	0	1	0	?	1	1	0	0	1	0	1	0	1	0	2	2	0	1	0	0
Eubrachiosaurus browni	?	?	?	?	?	?	?	?	?	?	?	?	?	?	?	?	?	?	?	?	?	?	?	?	?	?	?	?	?	?	?
Sangusaurus parringtonii	0	0	3	1	0	0	2	0	1	1	1	0	0	1	0	1	1	1	0	1	0	2	0	1	0	2	2	0	1	0	0
Ischigualastia jenseni	0	0	3	1	0	0	1	0	1	1	1	0	1	1	0	1	1	2	0	1	1	2	0	1	0	2	2	0	1	0	0
Jachaleria	1	0	3	1	0	1	1	0	1	1	1	0	0	2	0	1	1	2	0	1	1	2	0	1	0	2	2	0	1	0	0
Zambiasaurus submersus	?	?	?	?	?	?	?	0	0	?	?	?	1	0	?	1	1	0	0	?	?	?	0	1	0	2	2	0	?	?	?
Placerias hesternus	0	0	3	1	0	?	1	0	0	1	1	0	1	1	0	1	0	0	0	1	1	1	0	1	0	2	2	0	1	0	1
Moghreberia nmachouensis	0	1	3	?	0	?	?	?	?	?	1	?	1	2	0	1	0	0	0	1	1	1	0	1	0	1	2	0	?	0	1
Rastodon procurvidens	0	0	1	0	0	0	0	0	0	0	0	0	0	1	0	1	1	1	0	0	0	0	0	0	0	0	2	1	1	0	0
Bulbasaurus phylloxyron	0	[01]	2	[01]	1	0	0	0	0	1	1	0	0	2	0	1	1	[12]	0	1	0	0	0	[12]	0	0	2	1	1	1	0
Compsodon helmoedi	1	0	1	0	0	0	0	1	0	0	0	0	0	2	1	1	0	1	0	0	0	0	0	3	0	0	2	1	1	0	0
LPB 1993 3	0	?	?	2	?	?	?	?	?	?	?	?	0	?	?	?	?	?	?	?	0	?	0	1	0	0	2	1	1	0	0
LPB 1993 2	1	?	1	0	0	?	1	0	?	?	1	0	0	2	0	1	1	1	0	0	0	0	0	1	0	0	2	1	1	0	0
LPB 1995 9	1	?	1	0	0	0	1	0	0	1	?	0	0	1	0	?	1	1	0	0	0	0	0	1	0	0	2	1	1	?	0
Pentasaurus goggai	?	?	?	?	?	?	?	?	?	?	?	?	?	2	0	?	?	?	?	?	?	1	0	1	0	?	?	?	?	?	?
Ufudocyclops mukanelai	0	?	2	?	0	0	1	0	0	1	1	0	0	0	?	1	1	0	1	1	1	1	0	1	0	2	2	0	1	0	0
Lisowicia bojani	?	?	?	?	?	?	1	?	1	1	1	1	1	2	0	1	?	0	?	?	1	2	0	?	0	1	?	?	1	?	1

	86	87	88	89	90	91	92	93	94	95	96	97	98	99	100	101	102	103	104	105	106	107	108	109	110	111	112	113	114	115	116
Sinokannemeyeria	2	1	1	1	1	0	1	1	1	1	1	1	1	2	1	0	3	0	1	?	?	2	?	1	2	1	0	1	?	2	1
Stahleckeria potens	2	0	1	1	1	0	1	0	1	1	1	1	1	2	1	0	3	0	1	1	1	1	0	1	2	1	1	1	0	1	1
Eubrachiosaurus browni	?	?	?	?	?	?	?	?	?	?	?	?	?	?	?	?	?	?	?	?	?	?	?	?	?	?	?	?	?	?	?
Sangusaurus parringtonii	2	0	0	1	1	0	1	?	1	?	?	?	1	2	1	0	3	0	1	1	1	2	?	1	2	1	0	1	0	1	1
Ischigualastia jenseni	2	0	0	1	1	0	1	1	1	1	1	1	1	2	1	0	3	0	?	?	1	2	?	1	2	1	0	1	0	5	1
Jachaleria	2	0	0	1	1	0	1	1	1	1	1	1	1	2	1	0	3	0	1	0	?	2	?	1	2	1	0	1	0	1	1
Zambiasaurus submersus	2	?	1	?	?	?	?	0	?	?	?	?	?	?	?	?	?	?	?	?	?	?	?	?	?	?	?	?	?	?	?
Placerias hesternus	2	0	1	1	1	0	1	0	?	?	?	?	?	?	?	?	?	?	?	?	?	?	?	1	?	?	?	?	0	5	1
Moghreberia nmachouensis	2	0	1	?	?	0	?	0	1	1	1	1	1	2	1	0	3	0	1	?	?	?	?	1	?	?	?	?	?	?	1
Rastodon procurvidens	2	0	1	1	1	0	1	0	?	1	1	0	?	?	?	?	?	?	?	?	0	?	?	1	2	1	0	?	1	2	1
Bulbasaurus phylloxyron	2	0	1	1	1	0	1	0	1	1	0	1	1	2	2	0	3	0	1	1	0	1	0	1	2	1	0	0	1	2	1
Compsodon helmoedi	2	0	1	1	?	0	1	0	1	1	1	0	1	1	1	0	3	1	1	1	0	1	0	1	2	1	1	0	0	2	0
LPB 1993 3	2	0	1	1	?	0	?	?	1	1	1	1	1	2	1	0	3	0	1	?	?	1	0	1	2	1	0	1	0	2	1
LPB 1993 2	2	0	1	?	?	0	?	?	?	?	?	?	1	?	?	?	?	?	?	?	?	1	0	1	2	?	?	1	0	?	1
LPB 1995 9	2	?	?	1	?	0	?	?	1	1	1	1	1	2	1	0	3	0	?	?	?	1	0	1	2	1	0	1	?	2	1
Pentasaurus goggai	?	?	?	?	?	?	?	?	?	?	?	?	?	?	?	?	?	?	?	?	?	?	?	?	?	?	?	?	?	?	?
Ufudocyclops mukanelai	2	0	1	1	1	0	1	0	1	1	1	1	1	2	1	0	3	0	2	1	1	2	?	1	2	1	1	1	0	1	1
Lisowicia bojani	?	?	?	?	?	?	1	?	?	?	?	?	?	?	?	?	?	?	?	?	?	?	?	?	?	?	?	?	?	?	1

	117	118	119	120	121	122	123	124	125	126	127	128	129	130	131	132	133	134	135	136	137	138	139	140	141	142	143	144	145	146	147
Sinokannemeyeria	1	?	?	0	2	2	1	?	2	0	?	1	1	1	0	1	0	0	1	1	1	1	1	2	?	?	?	2	1	0	1
Stahleckeria potens	1	1	1	0	2	2	1	1	2	1	1	1	?	1	0	1	0	0	0	1	1	1	1	2	?	?	?	2	1	0	1
Eubrachiosaurus browni	?	?	?	?	?	?	?	?	?	?	?	?	?	?	?	?	?	?	?	?	?	?	?	?	?	?	?	?	?	?	?
Sangusaurus parringtonii	1	1	1	0	2	2	1	1	2	1	?	?	?	1	1	1	0	0	0	1	1	1	1	2	?	?	?	?	1	0	1
Ischigualastia jenseni	1	?	1	0	2	2	1	3	2	0	?	1	1	1	0	1	0	0	0	?	1	1	1	2	?	?	?	2	1	0	1
Jachaleria	1	?	1	0	2	2	1	3	2	0	0	?	?	1	0	1	0	0	0	?	?	1	1	2	?	?	?	2	?	0	1
Zambiasaurus submersus	?	?	?	?	?	?	?	?	?	?	?	?	?	?	?	1	1	0	?	?	?	?	1	2	?	?	?	2	?	?	1
Placerias hesternus	1	1	0	0	2	2	?	?	2	0	?	1	1	1	?	1	0	1	?	1	1	1	1	2	?	?	?	2	0	0	1
Moghreberia nmachouensis	?	?	?	?	2	2	?	1	2	0	?	?	?	?	?	1	0	?	?	?	1	1	1	2	?	?	?	2	1	0	1
Rastodon procurvidens	0	0	?	0	0	?	?	1	?	0	0	?	?	1	0	1	1	0	0	?	1	0	1	?	?	?	?	2	0	0	?
Bulbasaurus phylloxyron	0	0	0	0	1	2	1	1	2	0	?	?	?	1	0	1	1	0	0	?	1	1	1	?	?	?	?	2	1	0	1
Compsodon helmoedi	0	0	?	0	1	1	1	1	2	0	0	1	1	1	1	0	1	0	1	?	1	?	?	?	?	?	?	?	?	?	?
LPB 1993 3	1	0	?	0	2	2	?	1	2	0	?	?	?	?	?	0	1	0	1	1	?	?	?	?	?	?	?	?	?	?	?
LPB 1993 2	1	?	?	0	2	2	?	1	2	0	?	?	?	?	?	0	1	?	?	1	?	?	?	?	?	?	?	?	?	?	?
LPB 1995 9	1	0	?	0	2	?	?	?	2	0	?	?	?	?	?	?	?	?	1	?	?	?	?	?	?	?	?	?	?	?	?
Pentasaurus goggai	?	?	?	?	?	?	?	?	?	?	?	?	?	?	?	?	?	?	?	?	?	?	1	2	?	?	?	2	0	0	?
Ufudocyclops mukanelai	1	?	1	0	?	2	1	1	?	0	?	?	?	1	?	1	1	0	0	?	1	1	1	2	?	?	?	?	1	0	1
Lisowicia bojani	?	?	?	?	?	1	?	2	2	0	?	?	?	?	?	1	0	1	1	?	?	?	?	?	?	?	?	?	?	?	?

	148	149	150	151	152	153	154	155	156	157	158	159	160	161	162	163	164	165	166	167	168	169	170	171	172	173	174	175	176	177	178
Sinokannemeyeria	3	0	1	2	1	1	?	?	?	0	?	1	1	?	1	2	1	2	0	0	0	0	1	0	?	1	1	1	0	1	0
Stahleckeria potens	3	0	1	2	1	1	0	1	1	1	0	0	1	1	1	2	1	3	1	0	1	0	1	0	0	1	1	1	0	1	0
Eubrachiosaurus browni	?	?	?	?	?	?	?	?	?	?	?	?	?	?	?	?	?	?	?	?	1	0	1	?	?	1	?	0	0	1	0
Sangusaurus parringtonii	3	0	1	2	1	1	1	1	?	1	0	0	1	1	1	2	1	3	?	?	?	?	?	?	?	?	?	?	?	?	?
Ischigualastia jenseni	3	0	1	?	?	?	?	1	?	?	0	0	1	?	1	2	1	2	1	0	1	0	0	1	0	1	1	0	0	1	0
Jachaleria	?	0	?	?	?	?	?	?	?	?	?	?	?	?	1	2	1	2	1	0	0	1	0	?	?	?	1	?	?	?	?
Zambiasaurus submersus	?	?	?	?	?	?	0	?	?	?	?	?	?	?	?	?	1	?	0	?	1	1	1	0	0	1	?	0	1	1	0
Placerias hesternus	3	0	?	?	?	1	0	?	?	1	?	1	?	?	1	2	1	?	0	0	1	1	1	0	0	1	?	0	0	1	0
Moghreberia nmachouensis	3	0	1	2	1	1	0	?	?	?	?	?	?	?	?	?	1	?	0	?	1	1	0	0	?	1	1	1	1	1	0
Rastodon procurvidens	?	0	2	0	0	1	0	0	?	1	?	1	?	?	?	?	1	?	?	?	?	?	?	?	?	?	?	?	?	?	?
Bulbasaurus phylloxyron	?	0	1	2	1	1	?	?	?	?	?	?	?	?	?	?	1	?	?	?	?	?	?	?	?	?	?	?	0	?	?
Compsodon helmoedi	?	?	?	?	?	?	?	?	?	?	?	?	?	?	?	?	?	?	?	?	?	?	?	?	?	?	?	?	?	?	?
LPB 1993 3	?	?	?	?	?	?	?	?	?	?	?	?	?	?	?	?	?	?	?	?	?	?	?	?	?	?	?	?	?	?	?
LPB 1993 2	?	?	?	?	?	?	?	?	?	?	?	?	?	?	?	?	?	?	?	?	?	?	?	?	?	?	?	?	?	?	?
LPB 1995 9	?	?	?	?	?	?	?	?	?	?	?	?	?	?	?	?	?	?	?	?	?	?	?	?	?	?	?	?	?	?	?
Pentasaurus goggai	?	?	1	0	?	1	0	1	?	?	?	?	?	?	?	?	?	?	?	?	?	?	?	0	0	?	?	?	?	1	0
Ufudocyclops mukanelai	3	?	1	2	1	1	0	?	?	?	?	?	?	1	?	2	1	?	?	?	?	?	?	?	?	?	?	?	?	?	?
Lisowicia bojani	?	?	?	?	?	?	?	?	?	0	0	1	1	1	1	1	?	1	1	?	1	0	0	0	0	1	2	0	0	1	0

	179	180	181	182	183	184	185	186	187	188	189	190	191	192	193	194	195	196	197
Sinokannemeyeria	1	?	1	1	0	?	?	?	0	1	1	1	2	1	1	?	1	1	0
Stahleckeria potens	1	?	1	1	0	1	1	1	1	1	1	1	2	1	1	?	0	1	0
Eubrachiosaurus browni	?	?	?	?	0	?	?	?	?	?	?	?	?	?	?	?	?	1	0
Sangusaurus parringtonii	?	?	?	?	0	1	1	1	1	1	1	?	?	?	?	?	0	?	?
Ischigualastia jenseni	1	?	1	1	0	1	1	1	1	1	1	1	2	1	1	?	0	1	0
Jachaleria	1	?	?	?	0	1	1	1	1	1	1	?	?	?	?	?	0	?	?
Zambiasaurus submersus	0	?	?	?	0	1	1	1	1	1	1	?	?	?	?	?	1	1	1
Placerias hesternus	?	?	?	?	0	1	1	1	1	1	1	?	?	?	?	1	1	1	1
Moghreberia nmachouensis	1	?	?	?	0	1	1	1	1	1	1	?	?	?	?	1	1	1	?
Rastodon procurvidens	?	?	?	?	?	?	?	?	?	?	?	?	?	?	?	?	0	?	?
Bulbasaurus phylloxyron	?	?	?	?	?	?	?	?	?	?	?	?	?	?	?	?	1	?	?
Compsodon helmoedi	?	?	?	?	?	?	?	?	?	?	?	?	?	?	?	?	?	?	?
LPB 1993 3	?	?	?	?	?	?	?	?	?	?	?	?	?	?	?	?	?	?	?
LPB 1993 2	?	?	?	?	?	?	?	?	?	?	?	?	?	?	?	?	?	?	?
LPB 1995 9	?	?	?	?	?	?	?	?	?	?	?	?	?	?	?	?	?	?	?
Pentasaurus goggai	1	?	?	?	?	?	?	?	?	?	?	?	?	?	?	?	1	1	1
Ufudocyclops mukanelai	?	?	?	?	?	?	?	?	?	?	?	?	?	?	?	?	?	?	?
Lisowicia bojani	1	?	?	?	0	0	0	1	1	1	1	?	?	?	?	?	?	1	1

Appendix III: Supplementary data of PAPER III (unpublished)

Table 1S. Resting metabolic rate values of extant species.

Species	RMR ($mLO_2\ h^{-1}$)	Mass (g)	RMR ($mLO_2\ h^{-1}\ g^{-0.67}$)
Anas platyrhynchos	253.587	110.000	10.865
Capreolus capreolus	4107.200	6800.000	11.111
Cavia porcellus	76.103	100.000	3.477
Chelodina oblonga	0.812	29.000	0.085
Crocodylus niloticus	12.796	217.000	0.336
Gallus gallus	168.125	88.667	8.289
Lepus europaeus	1031.580	990.000	10.149
Microcebus murinus	9.200	14.600	1.526
Mus musculus	5.045	5.100	1.696
Oryctolagus cuniculus	675.000	450.000	11.263
Pelodiscus sinensis	0.267	5.767	0.083
Pleurodeles waltl	2.336	22.010	0.297
Podarcis muralis	0.093	1.150	0.084
Trachemys scripta	0.740	15.900	0.117
Varanus exanthematicus	2.254	46.000	0.173
Varanus niloticus	1.728	36.000	0.157
Zootoca vivipara	0.085	0.550	0.124

Abbreviations: **RMR**, mass-specific resting metabolic rate.

Table 2S. Initial histological data.

FEMUR			
Species	**OstD**	**OstA**	**OstS**
Anas platyrhynchos	0.002567298	20.64401514	0.496256631
Capreolus capreolus	0.00503404	66.3338	0.682011681
Cavia porcellus	0.0018753	34.15500446	0.497251828
Chelodina oblonga	0.000972828	28.12464156	0.615366523
Crocodylus niloticus	0.000707445	29.69356703	0.474721005
Gallus gallus	0.00251267455	27.73256	0.52401853
Lepus europaeus	0.00485708	49.1568	0.6433817
Microcebus murinus	0.003900548	30.00811295	0.586549866
Mus musculus	0.001222124	29.48473031	0.48045441
Oryctolagus cuniculus	0.00403514	73.277	0.646803938
Pelodiscus sinensis	0.000913358	24.48596176	0.52191737
Pleurodeles waltl	0.00059114268	134.9394709	0.59478267
Podarcis muralis	0.001117739	11.99151273	0.438353062
Trachemys scripta	0.001403736	28.96309753	0.494580499
Varanus exanthematicus	0.001195398	33.36199916	0.462645883
Varanus niloticus	0.001007931	39.69956533	0.478829164
Zootoca vivipara	0.002442651	13.67676453	0.42653396
Moghreberia nmachouensis	0.00316485	82.1627	0.6130401
Oudenodon baini	0.00495632	21.0048	0.5732658
Lystrosaurus sp.	0.00428176	45.2548	0.62009

HUMERUS			
Species	**OstD**	**OstA**	**OstS**
Anas platyrhynchos	0.002567298	20.64401514	0.496256631
Capreolus capreolus	0.00503404	66.3338	0.682011681
Cavia porcellus	0.0018753	34.15500446	0.497251828
Chelodina oblonga	0.000972828	28.12464156	0.615366523
Crocodylus niloticus	0.000707445	29.69356703	0.474721005
Gallus gallus	0.00251267455	27.73256	0.52401853
Lepus europaeus	0.00485708	49.1568	0.6433817
Microcebus murinus	0.003900548	30.00811295	0.586549866
Mus musculus	0.001222124	29.48473031	0.48045441
Oryctolagus cuniculus	0.00403514	73.277	0.646803938
Pelodiscus sinensis	0.000913358	24.48596176	0.52191737
Pleurodeles waltl	0.00059114268	134.9394709	0.59478267
Podarcis muralis	0.001117739	11.99151273	0.438353062
Trachemys scripta	0.001403736	28.96309753	0.494580499
Varanus exanthematicus	0.001195398	33.36199916	0.462645883
Varanus niloticus	0.001007931	39.69956533	0.478829164
Zootoca vivipara	0.002442651	13.67676453	0.42653396
Moghreberia nmachouensis	0.00316485	82.1627	0.6130401
Oudenodon baini	0.00495632	21.0048	0.5732658
Lystrosaurus sp.	0.00428176	45.2548	0.62009

Abbreviations: **OstA**, osteocyte area (μm^2); **OstD**, osteocyte density (osteocyte/ μm^2); **OstS**, osteocyte shape.

Appendix IV: Supplementary data of PAPER IV

Table 1S. Bone and specimen numbers added in the study.

Taxa	Higher taxon	Bones and specimen number
Capreolus capreolus	Synapsida, Mammalia	Humerus MNHN-Histos 2681 Femur MNHN-Histos 2674, 2675
Cavia porcellus	Synapsida, Mammalia	Humerus MNHN-Histos 2508, 2509, 2511, 2516, 2517 Femur MNHN-Histos 2500, 2502, 2504
Lepus europaeus	Synapsida, Mammalia	Humerus MNHN-Histos 2687 Femur MNHN-Histos 2684
Microcebus murinus	Synapsida, Mammalia	Humerus MNHN-Histos 2665 Femur MNHN-Histos 2664
Mus musculus	Synapsida, Mammalia	Humerus MNHN-Histos 2598, 2599, 2600, 2603, 2608, 2609 Femur MNHN-Histos 2588, 2590, 2592, 2594, 2596
Oryctolagus cuniculus	Synapsida, Mammalia	Humerus MNHN-Histos 2693 Femur MNHN-Histos 2690
Anas platyrhynchos	Saurospida, Dinosauromorpha	Humerus MNHN-Histos 2538, 2543, 2544 Femur MNHN-Histos 2527, 2529, 2531, 2533
Chelodina oblonga	Saurospida, Testudines	Humerus MNHN-Histos 2399, 2400, 2402, 2403 Femur MNHN-Histos 2393, 2395, 2397
Pelodiscus sinensis	Saurospida, Testudines	Humerus MNHN-Histos 2568, 2572, 2577, 2578 Femur MNHN-Histos 2557, 2559, 2561, 2563, 2565
Trachemys scripta	Saurospida, Testudines	Humerus MNHN-Histos 2630, 2631, 2632, 2635, 2636, 2638, 2640, 2646, 2647 Femur MNHN-Histos 2619, 2621, 2623, 2625, 2627
Crocodylus niloticus	Saurospida, Crurotarsia	Humerus MNHN-Histos 2471, 2474, 2478, 2479 Femur MNHN-Histos 2463, 2465, 2467
Podarcis muralis	Sauropsida, Squamata	Humerus MNHN-Histos 2453, 2455, 2457, 2459 Femur MNHN-Histos 2452, 2454, 2456, 2458
Varanus exanthematicus	Sauropsida, Squamata	Humerus MNHN-Histos 2433, 2434, 2436, 2437, 2442, 2443 Femur MNHN-Histos 2426, 2428, 2430
Varanus niloticus	Sauropsida, Squamata	Humerus MNHN-Histos 2419, 2420 Femur MNHN-Histos 2410, 2412
Zootoca vivipara	Sauropsida, Squamata	Humerus MNHN-Histos 2492, 2493 Femur MNHN-Histos 2483, 2485, 2487, 2489
Pleurodeles waltl	Urodela, Amphibia	Humerus MNHN-Histos 2364, 2369, 2370, 2376, 2381, 2382, 2386 Femur MNHN-Histos 2363, 2368, 2375, 2379, 2380, 2385

Kannemeyeria simocephalus †	Synapsida, Dicynodontia	Femur NMQR 2674
Moghreberia nmachouensis †	Synapsida, Dicynodontia	Humerus MNHN-Histos 2717, 2718 Femur MNHN-Histos 2714, 2715, 2716
Myosaurus gracilis †	Synapsida, Dicynodontia	Humerus BP1/4269
Lystrosaurus murrayi †	Synapsida, Dicynodontia	Humerus NMQR 3840 Femur NMQR 835
Oudenodon baini †	Synapsida, Dicynodontia	Humerus MNHN-Histos 2695, 2697, 2700 Femur MNHN-Histos 2696, 2699
Tropidostoma †	Synapsida, Dicynodontia	Humerus NMQR 9960 Femur NMQR 9960
Daptocephalus †	Synapsida, Dicynodontia	Femur NMQR 3633
Endothiodon †	Synapsida, Dicynodontia	Humerus SAM-PK-5605

Table 2S. Tests of the correlation between the humeral and femoral predictive (taken one by one and/or in combination with others, for each bone) and RMR in a phylogenetic context, using the R package caper and the pgls function (Orme 2018).

	Femur		Humerus	
	adjusted R^2	**p-value**	**adjusted R^2**	**p-value**
All	0.6697	0.002	0.6484	0.003
with OstD	-	0.060	-	0.386
with OstA	-	0.474	-	0.986
with OstS	-	0.854	-	0.149
with VascD	-	0.022	-	0.019
only OstD	0.3979	0.005	0.2968	0.017
only OstA	0.3209	0.013	0.3643	0.008
only OstS	0.2069	0.044	0.3659	0.008
only VascD	0.4973	0.001	0.4119	0.004

Abbreviations: All, all predictive variables included; **OstA,** osteocyte area; **OstD,** osteocyte density; **OstS,** osteocyte shape; **VascD,** primary osteon density.

Table 3S. Comparison between inference models (built using the R package caper and the pgls function) including different combinations of histological variables. Hypothesis testing for the regression model based on the femur and humerus the R package caper and the pgls function (Orme 2018) and the AIC function (Sakamoto et al. 1986).

	Femur		Humerus	
	R^2	AIC criterion	R^2	AIC criterion
All	0.6697	44.18096	0.6484	45.17998
OstD ex	0.5768	47.53806	0.6777	44.32515
OstA ex	0.6821	42.96247	0.6073	43.18044
OstS ex	0.6962	42.23243	0.6538	46.33979
VascD ex	0.5014	50.16157	0.4563	51.54730
OstS/VascD ex	0.526	48.63139	0.4906	49.78413
OstA/VascD ex	0.3787	52.96215	0.3866	52.75836
OstS/OstA ex	0.6851	42.09183	0.5749	46.89040
OstD/VascD ex	0.2894	55.11007	0.4071	52.21470
OstS/OstD ex	0.5466	47.92034	0.4945	49.66351
OstA/OstD ex	0.6069	45.63932	0.6789	42.40167
only OstD	0.3979	51.64720	0.2968	54.13040
only OstA	0.3209	53.57087	0.3643	52.51468
only OstS	0.2069	56.05439	0.3659	52.47496
only VascD	0.4973	48.75843	0.4119	51.27064

Abbreviations: All, all predictive variables included; **"X" ex,** predictive variable "X" excluded; **OstA,** osteocyte area; **OstD,** osteocyte density; **OstS,** osteocyte shape; **VascD,** primary osteon density.

Table 4S. Comparison between inference models (built using BayesTraits V3.0.1 (Pagel and Meade 2016)) including different combinations of histological variables using the selected model "28" for the femur and the selected model "5" for the humerus (see Tables 4S-5S). The difference between the models were assessed by Bayes Factor.

	Femur			Humerus		
	R^2	log marginal likelihood	log BF	R^2	log marginal likelihood	log BF
All	0.697	-31.1367	0	0.684	-31.8359	0
OstD ex	0.631	-31.1101	-0.0533	0.704	-30.5482	-2.5754
OstA ex	0.697	-30.1441	-1.9852	0.724	-29.9779	-3.7159
OstS ex	0.713	-30.3999	-1.4736	0.649	-31.8436	0.0155
VascD ex	0.510	-30.7481	-0.7772	0.556	-30.6533	-2.3651
OstS/VascD ex	0.578	-29.6947	-2.8842	0.565	-30.1063	-3.4591
OstA/VascD ex	0.442	-30.9802	-0.3131	0.386	-30.5547	-2.5623
OstS/OstA ex	0.693	-29.6738	-2.9258	0.599	-31.5610	-0.5498
OstD/VascD ex	0.410	-30.9277	-0.4182	0.511	-29.8244	-4.0230
OstS/OstD ex	0.591	-30.9280	-0.4176	0.571	-31.8268	-0.0181
OstA/OstD ex	0.556	-29.9633	-2.3469	0.715	-28.6957	-6.2803
only OstD	0.418	-30.5123	-1.2489	0.324	-31.6722	-0.3273
only OstA	0.397	-30.6610	-0.9516	0.437	-30.2425	-3.1868
only OstS	0.273	-31.3274	0.3812	0.424	-29.9325	-3.8066
only VascD	0.496	-31.4446	0.6158	0.415	-32.5315	1.3912

Abbreviations: BF, Bayes Factor (log BF= 2 (log marginal likelihood of Model 1 - log marginal likelihood of Model 2)).

Table 5S. Model checking of the multiple regressions based on femur using MCMC and PGLS methods, using BayesTraits V3.0.1 (Pagel and Meade 2016). The branch length scaling parameters were automatically determined simultaneously in models "10", "23", and "32". The model "28" has been selected in this study for the femur. The RMR values were expressed in $mLO_2\ h^{-1}\ g^{-0.67}$.

Abbreviations: **abs diff**, absolute difference; **CI**, 95% confidence interval; $\mathbf{RMR_{obs}}$, the known mass-specific resting metabolic rate in literature; $\bar{x}\mathbf{RMR_{pred}}$, the predicted arithmetic mean of the mass-specific resting metabolic rate. 0 →

N°	Priors				Evolution parameters				R^2	$\bar{x}RMR_{pred}$ *Capreolus* (RMR_{obs}= 11.11)	Min limit of $CI_{95\%}$	Max limit of $CI_{95\%}$	% abs diff between RMR_{obs} and $\bar{x}RMR_{pred}$
	Beta 2	Beta 3	Beta 4	Beta 5	lambda	kappa	delta	OU					
1	exp 5	exp 5	exp 5	exp 5	0.10000	1.60000	5.00000	0.00000	0.84539	11.95706	11.58300	12.34319	7.61459
2	exp 5	exp 5	exp 5	exp 5	0.55000	1.30000	1.30000	0.30000	0.82509	15.44918	15.05822	15.85030	39.04405
3	exp 5	exp 5	exp 5	exp 5	0.70000	1.30000	5.00000	0.10000	0.82475	14.93292	14.55427	15.32143	34.39766
4	exp 5	exp 5	exp 5	exp 5	0.55000	1.30000	1.30000	0.50000	0.82434	15.65315	15.26546	16.05069	40.87978
5	exp 5	exp 5	exp 5	exp 5	0.55000	1.30000	1.30000	0.70000	0.82399	14.70981	14.34074	15.08838	32.38961
6	exp 5	exp 5	exp 5	exp 5	0.55000	1.00000	1.00000	0.70000	0.82362	15.53826	15.14441	15.94235	39.84571
7	exp 5	exp 5	exp 5	exp 5	0.70000	2.50000	5.00000	0.10000	0.82360	14.68005	14.31023	15.05942	32.12173
8	exp 5	exp 5	exp 5	exp 5	0.80000	1.30000	1.30000	0.70000	0.82324	15.19379	14.81941	15.57763	36.74549
9	exp 5	exp 5	exp 5	exp 5	0.70000	1.30000	1.30000	0.01000	0.82260	15.35673	14.98282	15.73997	38.21193
10	exp 5	exp 5	exp 5	exp 5	0.51941	1.43945	1.46348	0.77172	0.81665	15.31757	14.92442	15.72107	37.85949
11	exp 5	exp 5	exp 5	exp 5	0.70000	1.30000	5.00000	0.00010	0.79574	10.40275	10.12277	10.69047	6.37432
12	exp 5	exp 5	exp 5	exp 5	0.50000	2.50000	1.50000	0.00001	0.79476	13.26735	12.92923	13.61431	19.40734
13	exp 5	exp 5	exp 5	exp 5	0.60000	1.60000	5.00000	0.00000	0.79258	8.80004	8.52968	9.07898	20.79882
14	exp 5	exp 5	exp 5	exp 5	0.70000	1.30000	5.00000	0.00001	0.79179	10.45167	10.16601	10.74535	5.93407
15	exp 5	exp 5	exp 5	exp 5	0.60000	1.00000	5.00000	0.00000	0.78789	12.78469	12.46232	13.11540	15.06336
16	exp 5	exp 5	exp 5	exp 5	0.80000	1.00000	5.00000	0.00000	0.77773	12.40117	12.09207	12.71818	11.61169
17	exp 5	exp 5	exp 5	exp 5	0.30000	1.60000	1.50000	0.00000	0.77098	12.20882	11.90221	12.52333	9.88052
18	exp 5	exp 5	exp 5	exp 5	0.50000	2.30000	5.00000	0.00000	0.76501	7.30891	6.99311	7.63898	34.21914
19	exp 5	exp 5	exp 5	exp 5	0.70000	1.30000	1.30000	0.00100	0.75451	12.59148	12.27314	12.91808	13.32450
20	exp 5	exp 5	exp 5	exp 5	0.40000	4.00000	1.50000	0.00000	0.73962	9.84011	9.56849	10.11944	11.43812
21	exp 5	exp 5	exp 5	exp 5	0.50000	2.50000	1.50000	0.00000	0.73164	10.29287	10.02603	10.56682	7.36321
22	exp 5	exp 5	exp 5	exp 5	0.50000	1.30000	1.30000	0.00010	0.73022	12.25403	11.95527	12.56026	10.28741
23	exp 5	exp 5	exp 5	exp 5	0.63107	1.63673	1.55861	0.00000	0.72030	10.67887	10.41094	10.95369	3.88923
24	exp 5	exp 5	exp 5	exp 5	0.60000	1.60000	1.50000	0.00000	0.71828	10.81190	10.54566	11.08487	2.69190
25	exp 5	exp 5	exp 5	exp 5	0.75000	2.50000	5.00000	0.00000	0.71590	5.99340	5.69693	6.30531	46.05883
26	exp 5	exp 5	exp 5	exp 5	0.75000	2.50000	2.50000	0.00000	0.70998	8.23497	7.97327	8.50525	25.88456
27	exp 5	exp 5	exp 5	exp 5	0.70000	1.30000	1.30000	0.00010	0.70107	11.07630	10.80796	11.35129	0.31234
28	exp 5	exp 5	exp 5	exp 5	0.70000	2.50000	1.50000	0.00000	0.69692	9.60442	9.35240	9.86324	13.55932
29	exp 5	exp 5	exp 5	exp 5	0.75000	3.00000	3.00000	0.00000	0.69251	7.21431	6.93585	7.50394	35.07060
30	exp 5	exp 5	exp 5	exp 5	0.80000	1.60000	1.50000	0.00000	0.69023	10.11545	9.85734	10.38032	8.96007
31	exp 5	exp 5	exp 5	exp 5	0.75000	2.00000	1.30000	0.00000	0.68632	9.98316	9.73240	10.24039	10.15064
32	unif -100 100	unif -100 100	unif -100 100	unif -100 100	0.61970	1.63535	1.50507	0.00000	0.68554	8.85243	8.61040	9.10126	20.32731
33	exp 5	exp 5	exp 5	exp 5	0.75000	2.50000	1.30000	0.00000	0.68192	9.96669	9.71005	10.23012	10.29885
34	exp 5	exp 5	exp 5	exp 5	0.70000	4.00000	1.50000	0.00000	0.67697	9.63627	9.36478	9.91563	13.27269
35	unif -100 100	unif -100 100	unif -100 100	unif -100 100	1.00000	1.00000	1.00000	0.00000	0.60349	7.48741	7.27523	7.70578	32.61260

N°	$\bar{x}$RMR$_{pred}$ *Microcebus* (RMR$_{obs}$= 1.526)	Min limit of CI$_{95\%}$	Max limit of CI$_{95\%}$	% abs diff between RMR$_{obs}$ and $\bar{x}$RMR$_{pred}$	$\bar{x}$RMR$_{pred}$ *Mus* (RMR$_{obs}$= 1.696)	Min limit of CI$_{95\%}$	Max limit of CI$_{95\%}$	% abs diff between RMR$_{obs}$ and $\bar{x}$RMR$_{pred}$	$\bar{x}$RMR$_{pred}$ *Cavia* (RMR$_{obs}$= 3.477)	Min limit of CI$_{95\%}$	Max limit of CI$_{95\%}$	% abs diff between RMR$_{obs}$ and $\bar{x}$RMR$_{pred}$
1	5.52292	5.41920	5.62862	261.92114	0.41767	0.41001	0.42546	75.37347	1.18424	1.16284	1.20603	65.94077
2	5.62021	5.49823	5.74490	268.29695	0.65889	0.64413	0.67400	61.15007	1.56872	1.53416	1.60406	54.88300
3	5.57719	5.45902	5.69792	265.47763	0.64936	0.63490	0.66416	61.71211	1.60587	1.57040	1.64214	53.81450
4	5.54558	5.42771	5.66601	263.40653	0.64480	0.63020	0.65974	61.98111	1.54215	1.50814	1.57693	55.64705
5	5.61809	5.49639	5.74249	268.15809	0.63282	0.61873	0.64725	62.68722	1.57135	1.53653	1.60696	54.80727
6	5.60027	5.48008	5.72310	266.99033	0.65835	0.64340	0.67365	61.18204	1.61293	1.57700	1.64968	53.61148
7	5.64925	5.52765	5.77354	270.20004	0.64229	0.62795	0.65696	62.12915	1.56844	1.53449	1.60314	54.89101
8	5.64995	5.52909	5.77346	270.24601	0.64498	0.63048	0.65980	61.97078	1.59829	1.56273	1.63466	54.03245
9	5.38590	5.27249	5.50174	252.94205	0.71148	0.69591	0.72740	58.04970	1.71367	1.67670	1.75144	50.71425
10	5.55240	5.43293	5.67450	263.85344	0.64539	0.63074	0.66038	61.94620	1.56870	1.53404	1.60415	54.88340
11	6.01199	5.91514	6.11042	293.97049	0.73474	0.72110	0.74864	56.67784	1.72438	1.69374	1.75558	50.40601
12	5.78462	5.68056	5.89058	279.07076	0.75570	0.74033	0.77139	55.44226	1.82300	1.78731	1.85940	47.56970
13	5.85444	5.76609	5.94415	283.64615	0.62276	0.61194	0.63377	63.28086	1.60115	1.57483	1.62792	53.95021
14	5.86518	5.77311	5.95871	284.34966	0.72904	0.71541	0.74292	57.01442	1.75762	1.72805	1.78770	49.45001
15	5.90410	5.79611	6.01411	286.90060	0.77050	0.75478	0.78655	54.56958	1.86682	1.82967	1.90473	46.30936
16	5.80774	5.70696	5.91031	280.58617	0.81562	0.79919	0.83239	51.90926	1.89047	1.85480	1.92684	45.62914
17	5.99937	5.89588	6.10467	293.14350	0.64006	0.62745	0.65292	62.26063	1.61165	1.58155	1.64234	53.64812
18	5.49091	5.40360	5.57963	259.82352	0.52523	0.51617	0.53445	69.03151	1.36290	1.34091	1.38525	60.80249
19	5.97436	5.87798	6.07232	291.50442	0.81871	0.80262	0.83512	51.72705	1.89934	1.86438	1.93494	45.37429
20	5.75796	5.67547	5.84165	277.32375	0.54633	0.53682	0.55600	67.78735	1.41723	1.39433	1.44050	59.24000
21	6.15551	6.07231	6.23985	303.37561	0.67932	0.66730	0.69155	59.94593	1.66322	1.63635	1.69053	52.16520
22	6.29358	6.19363	6.39515	312.42327	0.71867	0.70422	0.73341	57.62579	1.77654	1.74350	1.81021	48.90593
23	6.21748	6.13308	6.30305	307.43662	0.75792	0.74408	0.77201	55.31137	1.84200	1.81206	1.87243	47.02336
24	6.31288	6.22679	6.40016	313.68832	0.74211	0.72838	0.75610	56.24358	1.84405	1.81344	1.87517	46.96442
25	5.72425	5.64986	5.79963	275.11488	0.72086	0.70920	0.73271	57.49675	1.64198	1.61802	1.66629	52.77609
26	5.96742	5.90265	6.03291	291.05008	0.84139	0.82844	0.85454	50.38979	1.83131	1.80621	1.85677	47.33061
27	6.21428	6.12724	6.30256	307.22678	0.80410	0.78908	0.81940	52.58843	1.92584	1.89314	1.95910	44.61211
28	6.17049	6.10223	6.23952	304.35735	0.84347	0.82980	0.85736	50.26738	1.85531	1.82910	1.88189	46.64061
29	5.94520	5.87913	6.01201	289.59349	0.83551	0.82274	0.84847	50.73666	1.75754	1.73424	1.78117	49.45227
30	6.24501	6.17065	6.32027	309.24069	0.87144	0.85653	0.88661	48.61798	1.99163	1.96190	2.02181	42.71980
31	6.25881	6.18754	6.33090	310.14475	0.86844	0.85391	0.88322	48.79463	1.95822	1.92987	1.98699	43.68074
32	7.64293	7.52529	7.76240	400.84702	0.85607	0.83899	0.87349	49.52438	2.03927	2.00224	2.07698	41.34974
33	6.16301	6.09817	6.22854	303.86724	0.88518	0.87099	0.89961	47.80769	1.94569	1.91867	1.97310	44.04100
34	5.95751	5.89519	6.02049	290.40038	0.84403	0.83115	0.85710	50.23423	1.76740	1.74364	1.79149	49.16870
35	7.67464	7.57623	7.77433	402.92543	1.38550	1.35988	1.41161	18.30760	2.40291	2.36393	2.44252	30.89143

N°	$\bar{x}$RMR$_{pred}$ *Lepus* (RMR$_{obs}$= 10.149)	Min limit of CI$_{95\%}$	Max limit of CI$_{95\%}$	% abs diff between RMR$_{obs}$ and $\bar{x}$RMR$_{pred}$	$\bar{x}$RMR$_{pred}$ *Oryctolagus* (RMR$_{obs}$= 11.263)	Min limit of CI$_{95\%}$	Max limit of CI$_{95\%}$	% abs diff between RMR$_{obs}$ and $\bar{x}$RMR$_{pred}$	$\bar{x}$RMR$_{pred}$ *Podarcis* (RMR$_{obs}$= 0.084)	Min limit of CI$_{95\%}$	Max limit of CI$_{95\%}$	% abs diff between RMR$_{obs}$ and $\bar{x}$RMR$_{pred}$
1	9.54865	9.35152	9.74993	5.91535	7.39334	7.24623	7.54342	34.35732	0.03912	0.03837	0.03989	53.42578
2	10.87676	10.6098	11.1505	7.17074	9.30914	9.09052	9.53302	17.34759	0.04292	0.04185	0.04401	48.90737
3	11.02199	10.7538	11.2969	8.60177	9.27562	9.05315	9.50354	17.64525	0.04258	0.04155	0.04363	49.31389
4	10.37189	10.1223	10.6276	2.19618	9.43676	9.20902	9.67014	16.21447	0.04251	0.04149	0.04355	49.39595
5	10.99852	10.7234	11.2801	8.37043	9.06474	8.84531	9.28961	19.51756	0.04220	0.04117	0.04325	49.76519
6	10.33938	10.0834	10.6019	1.87585	9.27030	9.04885	9.49717	17.69244	0.04395	0.04289	0.04505	47.67443
7	10.65705	10.4015	10.9189	5.00595	9.07342	8.85448	9.29777	19.44047	0.04299	0.04193	0.04407	48.82426
8	10.55260	10.3034	10.8078	3.97680	9.56475	9.33452	9.80065	15.07816	0.04270	0.04167	0.04377	49.16277
9	10.62122	10.3719	10.8765	4.65284	9.21315	8.99673	9.43476	18.19990	0.05047	0.04955	0.05141	39.91323
10	10.42732	10.1730	10.688	2.74236	9.53821	9.30572	9.77650	15.31378	0.04259	0.04155	0.04366	49.29214
11	9.93136	9.75751	10.1083	2.14447	8.63074	8.47464	8.78971	23.37089	0.05152	0.05076	0.05230	38.66073
12	10.77485	10.5555	10.9987	6.16662	9.47102	9.27753	9.66854	15.91032	0.05135	0.05038	0.05233	38.87400
13	9.20080	9.04495	9.35933	9.34283	8.15425	8.01505	8.29587	27.60140	0.04809	0.04738	0.04882	42.74555
14	9.53187	9.36432	9.70243	6.08066	8.43984	8.29171	8.59061	25.06581	0.05209	0.05133	0.05287	37.98402
15	10.27298	10.0607	10.4898	1.22157	9.54494	9.34686	9.74721	15.25404	0.05064	0.04971	0.05158	39.71691
16	10.41840	10.2124	10.6285	2.65440	9.19168	9.01374	9.37314	18.39047	0.05385	0.05302	0.05469	35.89030
17	9.75594	9.56236	9.95343	3.87292	8.54616	8.37781	8.71789	24.12180	0.04308	0.04221	0.04396	48.71960
18	8.21846	8.07325	8.36628	19.02199	7.67723	7.54407	7.81274	31.83671	0.04542	0.04474	0.04611	45.93107
19	10.01979	9.83073	10.2125	1.27315	9.06735	8.89831	9.23960	19.49439	0.05305	0.05218	0.05394	36.83933
20	8.03194	7.88957	8.17688	20.85977	7.57859	7.44454	7.71504	32.71255	0.04516	0.04443	0.04590	46.24060
21	8.84816	8.69983	8.99901	12.81746	7.97994	7.84338	8.11887	29.14909	0.04696	0.04615	0.04778	44.09451
22	9.91230	9.72195	10.1064	2.33225	8.72095	8.55698	8.88805	22.56995	0.04589	0.04500	0.04679	45.37495
23	9.30404	9.14886	9.46185	8.32556	8.20554	8.06910	8.34428	27.14608	0.04971	0.04888	0.05057	40.81636
24	9.24114	9.08579	9.39916	8.94527	8.31136	8.17013	8.45503	26.20653	0.04898	0.04812	0.04984	41.69557
25	7.86579	7.75143	7.98184	22.49690	7.99715	7.87364	8.12260	28.99626	0.05294	0.05232	0.05357	36.97602
26	8.04536	7.93455	8.15772	20.72755	8.43539	8.31117	8.56147	25.10527	0.05613	0.05539	0.05688	33.18074
27	9.54149	9.37992	9.70584	5.98592	8.50411	8.35818	8.65258	24.49517	0.05122	0.05033	0.05212	39.02508
28	8.29871	8.17749	8.42172	18.23128	8.12083	7.99671	8.24688	27.89818	0.05379	0.05299	0.05460	35.96585
29	7.59783	7.49399	7.70311	25.13717	8.20627	8.08569	8.32864	27.13959	0.05615	0.05545	0.05685	33.15537
30	8.88871	8.75859	9.02077	12.41783	8.30966	8.18293	8.43835	26.22162	0.05630	0.05549	0.05711	32.97770
31	8.65624	8.52750	8.78692	14.70842	8.20959	8.08573	8.33535	27.11009	0.05435	0.05353	0.05519	35.29566
32	8.10008	7.94746	8.25564	20.18835	6.69085	6.56092	6.82335	40.59444	0.04386	0.04301	0.04473	47.78255
33	8.12422	8.01000	8.24006	19.95058	8.25280	8.13233	8.37507	26.72641	0.05605	0.05523	0.05688	33.27419
34	7.50442	7.40011	7.61020	26.05756	8.17130	8.04837	8.29611	27.45008	0.05658	0.05580	0.05736	32.64667
35	7.78393	7.65987	7.91000	23.30349	6.41859	6.31599	6.52285	43.01175	0.03807	0.03755	0.03859	54.68293

N°	$\bar{x}$RMR$_{pred}$ *Zootoca* (RMR$_{obs}$= 0.124)	Min limit of CI$_{95\%}$	Max limit of CI$_{95\%}$	% abs diff between RMR$_{obs}$ and $\bar{x}$RMR$_{pred}$	$\bar{x}$RMR$_{pred}$ *V. exanthemicus* (RMR$_{obs}$= 0.173)	Min limit of CI$_{95\%}$	Max limit of CI$_{95\%}$	% abs diff between RMR$_{obs}$ and $\bar{x}$RMR$_{pred}$	$\bar{x}$RMR$_{pred}$ *V. niloticus* (RMR$_{obs}$= 0.157)	Min limit of CI$_{95\%}$	Max limit of CI$_{95\%}$	% abs diff between RMR$_{obs}$ and $\bar{x}$RMR$_{pred}$
1	0.13899	0.13585	0.14220	12.09132	0.41240	0.40607	0.41883	138.38289	0.55032	0.54186	0.55891	250.52007
2	0.11889	0.11564	0.12222	4.12467	0.59806	0.58571	0.61067	245.70004	0.77127	0.75564	0.78723	391.25658
3	0.12246	0.11902	0.12599	1.24488	0.58429	0.57221	0.59662	237.73781	0.75777	0.74232	0.77354	382.65451
4	0.12076	0.11742	0.12420	2.61256	0.58988	0.57751	0.60252	240.97377	0.78529	0.76906	0.80187	400.18566
5	0.12165	0.11831	0.12508	1.89877	0.59693	0.58441	0.60972	245.04451	0.75464	0.73926	0.77035	380.66404
6	0.11861	0.11535	0.12195	4.34857	0.58469	0.57247	0.59717	237.97147	0.77338	0.75763	0.78945	392.59802
7	0.11278	0.10967	0.11599	9.04590	0.59858	0.58617	0.61126	246.00104	0.78501	0.76910	0.80125	400.00739
8	0.12223	0.11887	0.12569	1.42415	0.59499	0.58249	0.60775	243.92348	0.78252	0.76654	0.79884	398.42308
9	0.15488	0.15174	0.15810	24.90536	0.40464	0.39656	0.41289	133.89699	0.57255	0.56167	0.58364	264.67945
10	0.11368	0.11059	0.11685	8.32391	0.60238	0.58991	0.61512	248.19833	0.76961	0.75372	0.78584	390.19976
11	0.15161	0.14906	0.15420	22.26576	0.23487	0.23153	0.23827	35.76457	0.35496	0.34999	0.36000	126.09001
12	0.13914	0.13623	0.14210	12.20625	0.28639	0.28118	0.29169	65.54219	0.42918	0.42133	0.43717	173.36150
13	0.14383	0.14136	0.14635	15.99284	0.23222	0.22915	0.23533	34.23128	0.35208	0.34754	0.35667	124.25271
14	0.15238	0.14989	0.15491	22.88409	0.23065	0.22743	0.23391	33.32257	0.35566	0.35078	0.36060	126.53186
15	0.14614	0.14316	0.14918	17.85274	0.29813	0.29270	0.30365	72.32682	0.44234	0.43428	0.45055	181.74650
16	0.15405	0.15144	0.15672	24.23788	0.23567	0.23175	0.23965	36.22471	0.36416	0.35830	0.37013	131.95158
17	0.12225	0.11948	0.12508	1.41491	0.38226	0.37550	0.38915	120.96001	0.52422	0.51485	0.53376	233.89539
18	0.14554	0.14310	0.14801	17.36856	0.21868	0.21626	0.22113	26.40654	0.31473	0.31114	0.31836	100.46339
19	0.14477	0.14218	0.14740	16.74700	0.23438	0.23050	0.23833	35.47994	0.36554	0.35969	0.37149	132.82954
20	0.13290	0.13045	0.13541	7.18138	0.25149	0.24823	0.25480	45.37058	0.36732	0.36253	0.37216	133.95966
21	0.12162	0.11934	0.12394	1.92215	0.25635	0.25248	0.26028	48.17957	0.39025	0.38453	0.39607	148.57000
22	0.12473	0.12202	0.12750	0.58587	0.31257	0.30694	0.31831	80.67796	0.45549	0.44731	0.46382	190.12332
23	0.12872	0.12632	0.13115	3.80257	0.24392	0.24010	0.24779	40.99255	0.37407	0.36826	0.37997	138.26033
24	0.12914	0.12661	0.13172	4.14469	0.25929	0.25517	0.26347	49.87797	0.39314	0.38688	0.39951	150.40951
25	0.14962	0.14763	0.15164	20.66052	0.16428	0.16292	0.16565	5.04245	0.25928	0.25709	0.26150	65.14764
26	0.13180	0.12994	0.13369	6.29233	0.17011	0.16829	0.17196	1.66946	0.29228	0.28919	0.29540	86.16453
27	0.12967	0.12725	0.13214	4.57548	0.23476	0.23099	0.23860	35.70195	0.36862	0.36266	0.37469	134.79174
28	0.12193	0.11992	0.12397	1.67104	0.19748	0.19489	0.20011	14.15250	0.32427	0.32002	0.32857	106.53911
29	0.12968	0.12791	0.13148	4.58380	0.16351	0.16199	0.16505	5.48380	0.27025	0.26775	0.27277	72.13122
30	0.13287	0.13080	0.13497	7.15156	0.18694	0.18441	0.18951	8.05823	0.31553	0.31132	0.31981	100.97756
31	0.12259	0.12055	0.12466	1.13753	0.19575	0.19308	0.19845	13.14842	0.32276	0.31839	0.32720	105.58263
32	0.18600	0.18120	0.19093	50.00345	0.26302	0.25850	0.26761	52.03231	0.36634	0.36009	0.37270	133.33913
33	0.12301	0.12101	0.12504	0.80101	0.18724	0.18481	0.18971	8.23163	0.31536	0.31131	0.31945	100.86361
34	0.12305	0.12119	0.12494	0.76732	0.17623	0.17430	0.17818	1.86704	0.29127	0.28808	0.29450	85.52332
35	0.27657	0.27191	0.28131	123.03971	0.14548	0.14399	0.14699	15.90574	0.25086	0.24828	0.25347	59.78246

N°	$\bar{x}$RMR$_{pred}$ *Crocodylus* (RMR$_{obs}$= 0.336)	Min limit of CI$_{95\%}$	Max limit of CI$_{95\%}$	% abs diff between RMR$_{obs}$ and $\bar{x}$RMR$_{pred}$	$\bar{x}$RMR$_{pred}$ *Anas* (RMR$_{obs}$= 10.8)	Min limit of CI$_{95\%}$	Max limit of CI$_{95\%}$	% abs diff between RMR$_{obs}$ and $\bar{x}$RMR$_{pred}$	$\bar{x}$RMR$_{pred}$ *Pelodiscus* (RMR$_{obs}$= 0.083)	Min limit of CI$_{95\%}$	Max limit of CI$_{95\%}$	% abs diff between RMR$_{obs}$ and $\bar{x}$RMR$_{pred}$
1	0.26055	0.24984	0.27172	22.45544	1.41759	1.36296	1.47440	86.87420	0.06656	0.06547	0.06767	19.80335
2	0.40769	0.39734	0.41831	21.33623	1.42283	1.39587	1.45031	86.82565	0.08166	0.07976	0.08361	1.61048
3	0.44339	0.43223	0.45485	31.96188	1.42758	1.40034	1.45534	86.78169	0.08053	0.07863	0.08247	2.97794
4	0.42893	0.41786	0.44029	27.65741	1.42327	1.39552	1.45158	86.82156	0.07996	0.07808	0.08188	3.66549
5	0.40550	0.39519	0.41609	20.68547	1.41300	1.38602	1.44050	86.91666	0.08097	0.07906	0.08292	2.44357
6	0.41153	0.40089	0.42244	22.47840	1.43827	1.41097	1.46610	86.68269	0.08232	0.08037	0.08431	0.82124
7	0.41134	0.40085	0.42209	22.42141	1.43453	1.40706	1.46254	86.71732	0.08060	0.07870	0.08254	2.89002
8	0.41549	0.40482	0.42644	23.65745	1.44719	1.41968	1.47524	86.60009	0.08180	0.07983	0.08381	1.44670
9	0.51164	0.49883	0.52478	52.27271	1.46544	1.43811	1.49329	86.43110	0.08042	0.07858	0.08231	3.10763
10	0.40540	0.39488	0.41621	20.65563	1.41531	1.38855	1.44258	86.89528	0.07977	0.07793	0.08165	3.89138
11	0.47759	0.46391	0.49167	42.14081	1.23516	1.20412	1.26699	88.56338	0.07670	0.07524	0.07818	7.59327
12	0.58406	0.56979	0.59869	73.82818	1.28867	1.26472	1.31306	88.06790	0.08078	0.07894	0.08266	2.67875
13	0.35099	0.33684	0.36574	4.46162	1.15897	1.11542	1.20422	89.26882	0.07451	0.07330	0.07574	10.22470
14	0.47273	0.45860	0.48730	40.69365	1.23977	1.20752	1.27288	88.52069	0.07500	0.07357	0.07646	9.63600
15	0.59933	0.58458	0.61444	78.37101	1.28643	1.26218	1.31116	88.08859	0.08129	0.07945	0.08318	2.05677
16	0.65897	0.64283	0.67552	96.12210	1.22643	1.20296	1.25036	88.64416	0.08309	0.08122	0.08500	0.10938
17	0.40714	0.39567	0.41894	21.17189	1.21090	1.18171	1.24081	88.78795	0.07787	0.07632	0.07946	6.17678
18	0.23148	0.20755	0.25818	31.10599	0.93684	0.84135	1.04318	91.32553	0.07391	0.07303	0.07480	10.94733
19	0.65702	0.64067	0.67379	95.54170	1.13856	1.11575	1.16183	89.45779	0.08281	0.08096	0.08470	0.23187
20	0.25466	0.23871	0.27168	24.20808	0.92528	0.86896	0.98526	91.43255	0.07480	0.07380	0.07580	9.88336
21	0.35586	0.34259	0.36964	5.90946	0.99660	0.96248	1.03192	90.77223	0.07846	0.07714	0.07980	5.47510
22	0.53197	0.51808	0.54624	58.32510	1.06428	1.04178	1.08727	90.14553	0.08162	0.07990	0.08337	1.66700
23	0.49344	0.47848	0.50887	46.85727	0.99915	0.97320	1.02580	90.74859	0.07977	0.07822	0.08135	3.89257
24	0.49321	0.47875	0.50810	46.78796	1.00097	0.97597	1.02660	90.73180	0.07975	0.07817	0.08136	3.91899
25	0.24906	0.21451	0.28919	25.87377	0.67221	0.57858	0.78099	93.77583	0.07898	0.07810	0.07987	4.83988
26	0.32297	0.30490	0.34211	3.87806	0.80929	0.76575	0.85531	92.50655	0.08255	0.08126	0.08386	0.54607
27	0.60847	0.59209	0.62530	81.09109	0.94543	0.92413	0.96722	91.24601	0.08375	0.08199	0.08556	0.90778
28	0.41347	0.39667	0.43099	23.05714	0.79823	0.76907	0.82851	92.60895	Modèle	0.08093	0.08389	0.72772
29	0.23864	0.21471	0.26523	28.97658	0.68294	0.61628	0.75682	93.67645	0.08264	0.08159	0.08371	0.42894
30	0.59546	0.57718	0.61431	77.21903	0.85152	0.82841	0.87528	92.11554	0.08389	0.08219	0.08562	1.06984
31	0.51512	0.49782	0.53303	53.31008	0.82499	0.80012	0.85062	92.36124	0.08430	0.08270	0.08593	1.56965
32	0.51020	0.49345	0.52752	51.84621	0.99217	0.96397	1.02120	90.81324	0.07560	0.07396	0.07728	8.91253
33	0.45267	0.43494	0.47112	34.72358	0.75487	0.72794	0.78280	93.01042	0.08391	0.08238	0.08547	1.09658
34	0.27929	0.26025	0.29971	16.87906	0.65265	0.60937	0.69901	93.95695	0.08374	0.08258	0.08493	0.89623
35	0.96770	0.93735	0.99903	188.00653	0.65170	0.63390	0.67001	93.96572	0.08741	0.08533	0.08954	5.31186

N°	$\bar{x}$RMR$_{pred}$ *Trachemys* (RMR$_{obs}$= 0.171)	Min limit of CI$_{95\%}$	Max limit of CI$_{95\%}$	% abs diff between RMR$_{obs}$ and $\bar{x}$RMR$_{pred}$	$\bar{x}$RMR$_{pred}$ *Chelodina* (RMR$_{obs}$= 0.085)	Min limit of CI$_{95\%}$	Max limit of CI$_{95\%}$	% abs diff between RMR$_{obs}$ and $\bar{x}$RMR$_{pred}$	$\bar{x}$RMR$_{pred}$ *Pleurodeles* (RMR$_{obs}$= 0.297)	Min limit of CI$_{95\%}$	Max limit of CI$_{95\%}$	% abs diff between RMR$_{obs}$ and $\bar{x}$RMR$_{pred}$
1	0.12683	0.12481	0.12888	25.82919	0.13787	0.13488	0.14093	62.20016	0.14419	0.13036	0.15950	51.44960
2	0.13499	0.13178	0.13829	21.05642	0.15560	0.15176	0.15953	83.05416	0.09452	0.09197	0.09714	68.17514
3	0.13415	0.13104	0.13733	21.55093	0.15846	0.15460	0.16241	86.42450	0.09844	0.09573	0.10123	66.85399
4	0.13447	0.13133	0.13768	21.36284	0.16132	0.15733	0.16541	89.78914	0.09285	0.09028	0.09549	68.73859
5	0.13625	0.13299	0.13959	20.32350	0.15728	0.15351	0.16113	85.03019	0.10233	0.09947	0.10526	65.54590
6	0.13681	0.13358	0.14011	19.99678	0.15516	0.15137	0.15905	82.54137	0.09849	0.09576	0.10130	66.83781
7	0.13307	0.12995	0.13625	22.18345	0.16219	0.15817	0.16631	90.81184	0.09419	0.09167	0.09679	68.28540
8	0.13682	0.13364	0.14008	19.98691	0.16011	0.15620	0.16411	88.35927	0.10152	0.09875	0.10437	65.81850
9	0.12457	0.12166	0.12755	27.15271	0.15224	0.14857	0.15599	79.10175	0.10918	0.10622	0.11222	63.24044
10	0.13698	0.13376	0.14027	19.89502	0.15869	0.15489	0.16259	86.69896	0.09511	0.09251	0.09779	67.97485
11	0.11261	0.11040	0.11487	34.14357	0.14041	0.13722	0.14368	65.19014	0.14660	0.14016	0.15335	50.63872
12	0.12473	0.12182	0.12771	27.05889	0.15080	0.14723	0.15446	77.41248	0.11802	0.11481	0.12132	60.26197
13	0.11610	0.11421	0.11802	32.10524	0.14115	0.13816	0.14420	66.05622	0.16411	0.14802	0.18195	44.74520
14	0.11175	0.10962	0.11391	34.65156	0.13858	0.13550	0.14172	63.03205	0.15657	0.14893	0.16460	47.28427
15	0.12405	0.12119	0.12699	27.45351	0.15128	0.14770	0.15495	77.97576	0.12280	0.11934	0.12637	58.65154
16	0.12046	0.11771	0.12329	29.55297	0.15266	0.14901	0.15640	79.60287	0.12900	0.12543	0.13268	56.56586
17	0.12792	0.12532	0.13057	25.19306	0.14612	0.14287	0.14945	71.90746	0.12843	0.12355	0.13349	56.75910
18	0.12212	0.12066	0.12360	28.58424	0.14421	0.14140	0.14708	69.66101	0.18686	0.10641	0.32815	37.08443
19	0.12191	0.11916	0.12472	28.70781	0.15174	0.14819	0.15537	78.52012	0.14489	0.14057	0.14934	51.21501
20	0.11994	0.11836	0.12154	29.86039	0.14000	0.13737	0.14269	64.70914	0.15685	0.13326	0.18461	47.18953
21	0.11989	0.11784	0.12198	29.88744	0.13799	0.13511	0.14093	62.33777	0.18118	0.16956	0.19361	38.99504
22	0.12667	0.12396	0.12944	25.92353	0.14742	0.14415	0.15075	73.43050	0.13588	0.13142	0.14049	54.24885
23	0.11727	0.11494	0.11966	31.41886	0.14328	0.14003	0.14660	68.56109	0.17493	0.16761	0.18256	41.10178
24	0.11974	0.11737	0.12215	29.97791	0.14505	0.14179	0.14839	70.64660	0.16211	0.15568	0.16880	45.41910
25	0.11783	0.11646	0.11921	31.09466	0.13992	0.13719	0.14271	64.61349	0.47009	0.19918	1.10949	58.27964
26	0.11565	0.11386	0.11748	32.36619	0.14177	0.13879	0.14482	66.79315	0.25282	0.21854	0.29248	14.87562
27	0.12091	0.11834	0.12354	29.29169	0.14624	0.14293	0.14963	72.05213	0.16494	0.15932	0.17075	44.46490
28	0.11678	0.11470	0.11891	31.70576	0.13979	0.13674	0.14292	64.46082	0.24707	0.22990	0.26552	16.81147
29	0.11777	0.11625	0.11931	31.12783	0.13749	0.13477	0.14026	61.75097	0.31562	0.20691	0.48144	6.26804
30	0.11647	0.11408	0.11890	31.89137	0.14109	0.13787	0.14438	65.98868	0.21960	0.21008	0.22955	26.06061
31	0.11663	0.11434	0.11896	31.79592	0.14325	0.14000	0.14656	68.52542	0.23068	0.21926	0.24271	22.32881
32	0.13514	0.13195	0.13841	20.96953	0.11212	0.10870	0.11564	31.90063	0.07730	0.07330	0.08152	73.97266
33	0.11627	0.11411	0.11847	32.00674	0.13938	0.13630	0.14253	63.97715	0.27520	0.25783	0.29374	7.34033
34	0.11645	0.11478	0.11814	31.90065	0.13788	0.13507	0.14074	62.20708	0.27584	0.23101	0.32939	7.12295
35	0.11123	0.10848	0.11404	34.95436	0.13329	0.12951	0.13719	56.81549	0.15798	0.14978	0.16664	46.80694

Table 6S. Model checking of the multiple regressions based on humerus using MCMC and PGLS methods, using BayesTraits V3.0.1 (Pagel and Meade 2016). The branch length scaling parameters were automatically determined simultaneously in models "1", "2", and "3". The model "5" has been selected in this study for the femur. The RMR values were expressed in $mLO_2\ h^{-1}\ g^{-0.67}$.

Abbreviations: **abs diff**, absolute difference; **CI**, 95% confidence interval; $\mathbf{RMR_{obs}}$, the known mass-specific resting metabolic rate in literature; $\bar{x}\mathbf{RMR_{pred}}$, the predicted arithmetic mean of the mass-specific resting metabolic rate.

N°	Priors				Evolution parameters				R^2	$\bar{x}RMR_{pred}$ *Capreolus* (RMR_{obs}= 11.11)	Min limit of $CI_{95\%}$	Max limit of $CI_{95\%}$	% abs diff between RMR_{obs} and $\bar{x}RMR_{pred}$
	Beta 2	Beta 3	Beta 4	Beta 5	lambda	kappa	delta	OU					
1	exp 5	exp 5	exp 5	exp 5	0.52152	1.43549	1.45507	0.76811	0.77599	15.58945	15.16712	16.02353	40.30641
2	exp 5	exp 5	exp 5	exp 5	0.71366	1.79858	1.51148	0.00000	0.68626	10.29899	10.02991	10.57528	7.30821
3	unif -100 100	unif -100 100	unif -100 100	unif -100 100	0.63447	1.76616	1.48912	0.00000	0.66198	10.93141	10.61082	11.26169	1.61631
4	unif -100 100	unif -100 100	unif -100 100	unif -100 100	1.00000	1.00000	1.00000	0.00000	0.57683	8.46276	8.20870	8.72469	23.83436
5	exp 5	exp 5	exp 5	exp 5	0.70000	2.50000	1.50000	0.00000	0.68378	9.60531	9.34754	9.87019	13.55134
6	exp 5	exp 5	exp 5	exp 5	0.70000	2.50000	1.50000	0.000100	0.78481	13.31175	12.96113	13.67185	19.80692

N°	$\bar{x}RMR_{pred}$ *Microcebus* (RMR_{obs}= 1.526)	Min limit of $CI_{95\%}$	Max limit of $CI_{95\%}$	% abs diff between RMR_{obs} and $\bar{x}RMR_{pred}$	$\bar{x}RMR_{pred}$ *Mus* (RMR_{obs}= 1.696)	Min limit of $CI_{95\%}$	Max limit of $CI_{95\%}$	% abs diff between RMR_{obs} and $\bar{x}RMR_{pred}$	$\bar{x}RMR_{pred}$ *Cavia* (RMR_{obs}= 3.477)	Min limit of $CI_{95\%}$	Max limit of $CI_{95\%}$	% abs diff between RMR_{obs} and $\bar{x}RMR_{pred}$
1	3.61005	3.51961	3.70281	136.56919	0.69385	0.67579	0.71240	59.08875	1.25543	1.22507	1.28655	63.89316
2	4.02812	3.96643	4.09077	163.96612	1.15125	1.13031	1.17257	32.11979	1.59918	1.57344	1.62535	54.00676
3	4.39812	4.31569	4.48212	188.21227	1.85373	1.80145	1.90753	9.30019	1.12186	1.10020	1.14396	67.73475
4	3.94651	3.88214	4.01195	158.61813	2.42230	2.37091	2.47480	42.82432	1.67688	1.64626	1.70807	51.77216
5	3.90026	3.84578	3.95552	155.58732	1.09978	1.08089	1.11900	35.15443	1.53118	1.50864	1.55405	55.96267
6	3.30856	3.22905	3.39002	116.81240	0.97313	0.94913	0.99772	42.62228	1.50235	1.46652	1.53906	56.79173

N°	$\bar{x}RMR_{pred}$ *Lepus* (RMR_{obs}= 10.149)	Min limit of $CI_{95\%}$	Max limit of $CI_{95\%}$	% abs diff between RMR_{obs} and $\bar{x}RMR_{pred}$	$\bar{x}RMR_{pred}$ *Oryctolagus* (RMR_{obs}= 11.263)	Min limit of $CI_{95\%}$	Max limit of $CI_{95\%}$	% abs diff between RMR_{obs} and $\bar{x}RMR_{pred}$	$\bar{x}RMR_{pred}$ *Podarcis* (RMR_{obs}= 0.084)	Min limit of $CI_{95\%}$	Max limit of $CI_{95\%}$	% abs diff between RMR_{obs} and $\bar{x}RMR_{pred}$
1	11.32565	11.02489	11.63461	11.59372	9.06347	8.82102	9.31259	19.52883	0.02406	0.02343	0.02470	71.36008
2	9.17806	9.02858	9.33003	9.56681	8.82833	8.67877	8.98046	21.61656	0.03590	0.03530	0.03651	57.26435
3	9.90364	9.70713	10.10413	2.41757	5.95086	5.82744	6.07688	47.16456	0.03255	0.03192	0.03320	61.24417
4	8.10968	7.97884	8.24265	20.09384	7.30217	7.16942	7.43738	35.16677	0.04563	0.04499	0.04629	45.67609
5	8.82466	8.69201	8.95934	13.04893	8.86189	8.72206	9.00397	21.31854	0.03747	0.03686	0.03809	55.39320
6	9.61105	9.36247	9.86622	5.30056	9.15122	8.91663	9.39198	18.74972	0.02958	0.02903	0.03014	64.78565

N°	$\bar{x}$RMR$_{pred}$ *Zootoca* (RMR$_{obs}$= 0.124)	Min limit of CI$_{95\%}$	Max limit of CI$_{95\%}$	% abs diff between RMR$_{obs}$ and $\bar{x}$RMR$_{pred}$	$\bar{x}$RMR$_{pred}$ *V. exanthemicus* (RMR$_{obs}$= 0.173)	Min limit of CI$_{95\%}$	Max limit of CI$_{95\%}$	% abs diff between RMR$_{obs}$ and $\bar{x}$RMR$_{pred}$	$\bar{x}$RMR$_{pred}$ *V. niloticus* (RMR$_{obs}$= 0.157)	Min limit of CI$_{95\%}$	Max limit of CI$_{95\%}$	% abs diff between RMR$_{obs}$ and $\bar{x}$RMR$_{pred}$
1	0.15288	0.14814	0.15777	23.29124	0.72522	0.70799	0.74288	319.20440	0.99609	0.97446	1.01819	534.44916
2	0.16501	0.16166	0.16842	33.06971	0.21323	0.20993	0.21657	23.25282	0.35196	0.34704	0.35695	124.18015
3	0.18495	0.17960	0.19045	49.14951	0.21686	0.21279	0.22100	25.35005	0.39808	0.39163	0.40463	153.55196
4	0.20328	0.19956	0.20708	63.93899	0.14085	0.13926	0.14245	18.58369	0.26028	0.25759	0.26301	65.78596
5	0.15707	0.15413	0.16006	26.66543	0.19545	0.19271	0.19823	12.97817	0.32791	0.32383	0.33203	108.85745
6	0.28181	0.27561	0.28814	127.26286	0.31441	0.30804	0.32091	81.73999	0.49400	0.48492	0.50326	214.65114

N°	$\bar{x}$RMR$_{pred}$ *Crocodylus* (RMR$_{obs}$= 0.336)	Min limit of CI$_{95\%}$	Max limit of CI$_{95\%}$	% abs diff between RMR$_{obs}$ and $\bar{x}$RMR$_{pred}$	$\bar{x}$RMR$_{pred}$ *Anas* (RMR$_{obs}$= 10.8)	Min limit of CI$_{95\%}$	Max limit of CI$_{95\%}$	% abs diff between RMR$_{obs}$ and $\bar{x}$RMR$_{pred}$	$\bar{x}$RMR$_{pred}$ *Pelodiscus* (RMR$_{obs}$= 0.083)	Min limit of CI$_{95\%}$	Max limit of CI$_{95\%}$	% abs diff between RMR$_{obs}$ and $\bar{x}$RMR$_{pred}$
1	0.46026	0.44773	0.47315	36.98360	1.20458	1.17984	1.22984	88.84650	0.10385	0.10117	0.10660	25.11815
2	0.55820	0.53953	0.57751	66.13029	0.72167	0.70175	0.74215	93.31790	0.09570	0.09381	0.09763	15.30081
3	0.63348	0.61159	0.65615	88.53447	0.84609	0.82150	0.87141	92.16586	0.09912	0.09700	0.10129	19.42378
4	1.21502	1.17753	1.25371	261.61435	0.52059	0.50735	0.53418	95.17972	0.09346	0.09112	0.09586	12.60083
5	0.46747	0.44896	0.48673	39.12650	0.67963	0.65491	0.70528	93.70712	0.09507	0.09340	0.09676	14.53893
6	0.78200	0.76226	0.80226	132.73822	1.28312	1.25813	1.30859	88.11930	0.09666	0.09424	0.09913	16.45610

N°	$\bar{x}$RMR$_{pred}$ *Trachemys* (RMR$_{obs}$= 0.171)	Min limit of CI$_{95\%}$	Max limit of CI$_{95\%}$	% abs diff between RMR$_{obs}$ and $\bar{x}$RMR$_{pred}$	$\bar{x}$RMR$_{pred}$ *Chelodina* (RMR$_{obs}$= 0.085)	Min limit of CI$_{95\%}$	Max limit of CI$_{95\%}$	% abs diff between RMR$_{obs}$ and $\bar{x}$RMR$_{pred}$	$\bar{x}$RMR$_{pred}$ *Pleurodeles* (RMR$_{obs}$= 0.297)	Min limit of CI$_{95\%}$	Max limit of CI$_{95\%}$	% abs diff between RMR$_{obs}$ and $\bar{x}$RMR$_{pred}$
1	0.13033	0.12699	0.13375	23.78638	0.18232	0.17760	0.18716	114.49143	0.17196	0.16676	0.17731	42.10204
2	0.11541	0.11311	0.11777	32.50627	0.15580	0.15234	0.15933	83.29280	0.26743	0.25493	0.28054	9.95593
3	0.10828	0.10591	0.11070	36.67897	0.20393	0.19889	0.20910	139.91819	0.09282	0.08774	0.09818	68.74877
4	0.10655	0.10391	0.10926	37.68949	0.16593	0.16131	0.17067	95.20757	0.35216	0.33540	0.36975	18.57090
5	0.11666	0.11455	0.11881	31.77673	0.15555	0.15226	0.15890	82.99617	0.28472	0.26534	0.30552	4.13358
6	0.11872	0.11578	0.12174	30.57294	0.16842	0.16416	0.17280	98.14312	0.20794	0.20169	0.21438	29.98751

Bibliography

Orme D. 2018. The caper package: comparative analysis of phylogenetics and evolution in R.

Pagel M., Meade A. 2016. BayesTraits V3 Manual.

Sakamoto Y., Ishiguro M., Kitagawa G. 1986. Akaike information criterion statistics. D. Reidel Publishing Company.

Dicynodonts represent an emblematic Permian-Triassic (P-Tr) taxa to survive the big crisis at the end of Permian. While they were strongly impacted, they largely diversified during the Middle Triassic. They occupied an important part of the herbivore fauna in their ecosystem. However, the major environmental changing occurring in Late Triassic, and more specifically in Carnian, sharply affected the populations of dicynodont, which finally became extinct at the end of Triassic. The evolution of Triassic dicynodonts and their recovery and extinction conditions are still unclear. This work focused on the Laotian and Moroccan forms and their input to our knowledge on the phylogenetic relationships, paleobiogeography, and paleophysiology of the Triassic dicynodonts.
Previously supposed to be delayed until the Middle Triassic, the post-crisis recovery of dicynodonts would appear to be earlier as supported by the description of two new Laotian species (*Counillonia superoculis* and *Repelinosaurus robustus*) in Early Triassic. Despite their phylogenetic relationships remaining non-consensual, they support the survivorship of multiple lineages across the P-Tr boundary. A high termometabolism was proposed to mainly explain the survivorship of populations beyond the crisis. Paleophysiological models built with histological features to infer metabolism in Permian and Triassic dicynodonts concluded all studied dicynodonts endotherm, and refuted the previous hypothesis. They also highlighted a unique acquisition of the mammalian endothermy in Synapsida occurring at least in middle Permian at the Neotherapsida node.
The geographic situation of the Laotian dicynodonts in the Indochina blocks provide new data on the debate about the collision of the block with the rest of Pangea. Indeed, cconsidering the age and the almost entirely terrestrial lifestyle of dicynodonts, a terrestrial connection between the Indochina Block and Pangea could thus be interpreted at least in late Permian-Early Triassic, most likely via the South and North China blocks.
A new dicynodont postcranial material discovered in Morocco was studied and a taxonomic revision of the Moroccan dicynodonts was made. The species *Moghreberia nmachouensis*, known by most of the remains recovered in the Argana Basin, was considered as valid and clearly distinguished from the North American *Placerias* that was previously supposed to be synonym by many studies. The restudy of the cranial material of *Azarifeneria* did not emphasized significant differences distinguishing it from other Triassic genera. However, a second morphotype could at least be noticed in the postcranial material by its strong robustness. The large size of *Moghreberia* and especially the second big morphotype confirmed an increase of the body size in dicynodonts during the Triassic.

Key words: Dicynodontia, Morocco, Laos, taxonomy, phylogeny, paleobiogeography, endothermy, paleohistology

Les dicynodontes sont des organismes emblématiques de la période du Permien-Trias (P-Tr), du fait de leur survie à la grande crise ayant eu lieu à la fin du Permien. Bien que fortement impactés par cette crise, ils se sont largement diversifiés durant le Trias moyen. Ils représentaient les herbivores dominants de leur écosystème. Cependant, les changements environnementaux majeurs survenus au Trias supérieur, et plus particulièrement au Carnien, ont fortement affecté les populations de dicynodontes, qui ont finalement disparus à la fin du Trias. L'évolution des dicynodontes triasiques ainsi que les conditions de leur résilience et de leur extinction restent peu connues. Ce travail s'est concentré sur les formes laotiennes et marocaines et leur apport à notre connaissance des relations phylogénétiques, de la paléobiogéographie, et de la paléophysiologie des dicynodontes du Trias.
Précédemment supposée retardée au Trias moyen, la résilience post-crise des dicynodontes semble avoir été plus précoce, comme l'atteste l'ajout de deux nouvelles espèces laotiennes (*Counillonia superoculis* et *Repelinosaurus robustus*) datée du Trias inférieur. Bien que leurs relations phylogénétiques restent non consensuelles, elles confirment la survie de plusieurs lignées de dicynodontes à la crise P-Tr. Un thermométabolisme élevé aurait été l'élément déterminant pour expliquer la survie des populations à la crise. Réfutant cette hypothèse, les modèles paléophysiologiques construits à partir de variables histologiques pour inférer le métabolisme de dicynodontes permiens et triasiques ont conclu à une endothermie chez tous les dicynodontes étudiés. Ils ont également mis en évidence une acquisition unique de l'endothermie mammalienne chez les Synapsida au moins au Permien moyen, au niveau du nœud des Neotherapsida.
La situation géographique des dicynodontes laotiens au sein du bloc indochinois apporte de nouveaux éléments sur le débat concernant la collision de ce dernier avec le reste de la Pangée. En effet, du fait de l'âge et du mode de vie presque essentiellement terrestre des dicynodontes, une connexion terrestre entre le bloc indochinois et la Pangée a donc été supposée au moins dès la fin Permien-début Trias, très probablement via les blocs sud- et nord-chinois.
Du matériel post-crânien marocain inédit de dicynodonte a été étudié et une révision taxonomique des dicynodontes marocains a été effectuée. L'espèce *Moghreberia nmachouensis*, connue par la plupart des restes retrouvés au sein du bassin d'Argana, a été considérée valide et clairement distincte du genre nord-américain *Placerias*, auparavant supposé synonyme par plusieurs études. L'étude du matériel crânien d'*Azarifeneria* n'a pas montré de différences significatives le distinguant des autres genres triasiques. Cependant, un second morphotype, au moins, a pu être remarqué dans le matériel postcrânien par sa forte robustesse. La grande taille de *Moghreberia* et surtout celle de ce deuxième grand morphotype ont confirmé une augmentation de la taille corporelle des dicynodontes au cours du Trias.

Mots clés: Dicynodontia, Maroc, Laos, taxonomie, phylogénie, paléobiogéographie, endothermie, paléohistologie.